BAINITE IN STEELS

H.K.D.H. Bhadeshia

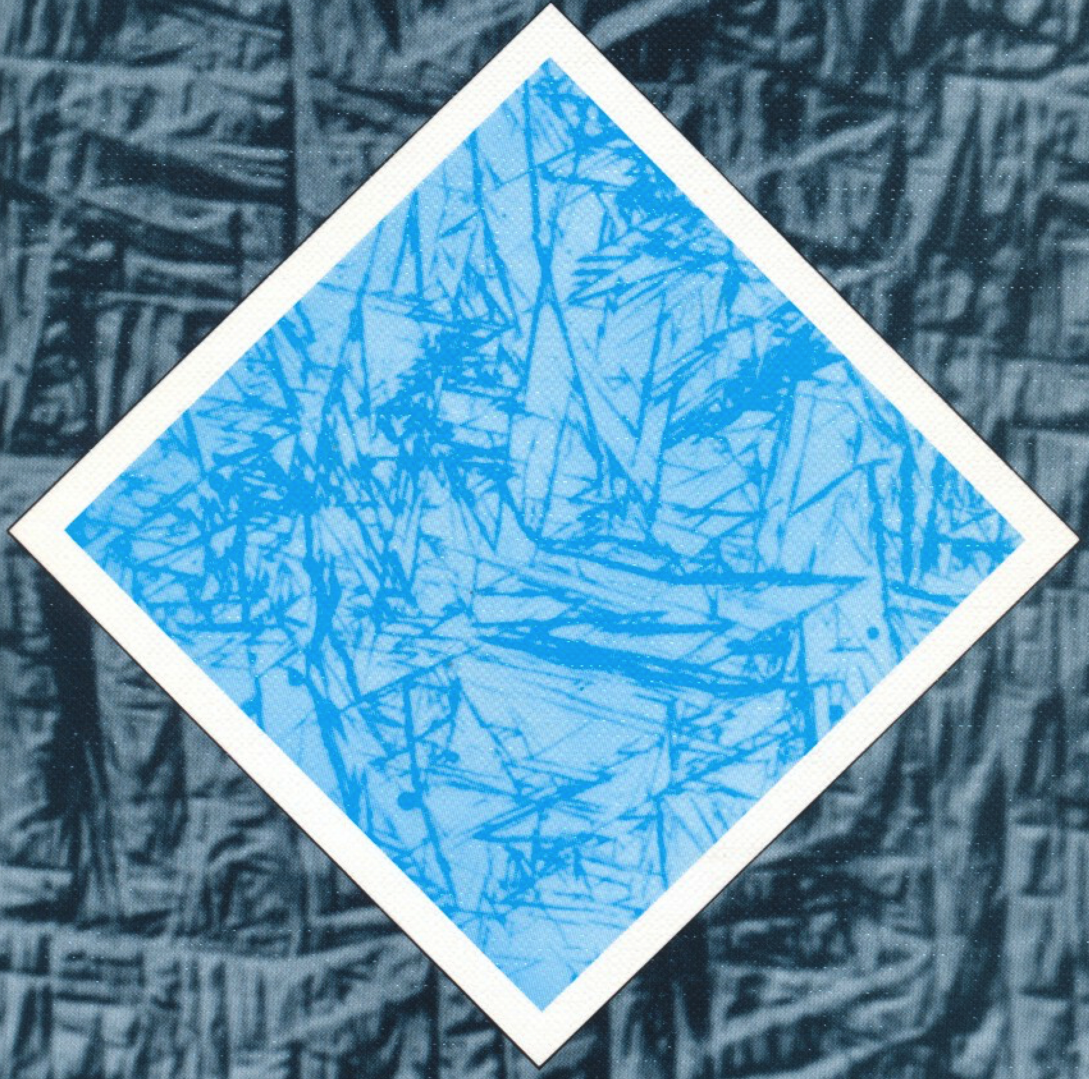

The Institute of Materials

BAINITE IN STEELS

Transformations, Microstructure and Properties

H.K.D.H. BHADESHIA

THE INSTITUTE OF MATERIALS

Book Number 504

Published in 1992 by
The Institute of Materials
1 Carlton House Terrace
London SW1Y 5DB

© 1992 The Institute of Materials

All rights reserved

British Library Cataloguing-in-Publication Data

Bhadeshia, H.K.D.H. (Harshad Kumar Dharamshi Hansraj)
Bainite in steels.
I. Title
620.17

ISBN 0901462 95 0

Typeset by Inforum Typesetting, Portsmouth

Printed and bound in Great Britain by
Cambridge University Press

Contents

Nomenclature

a	Length of an edge crack
Δa_m	Minimum detectable increase in austenite layer thickness
$\overline{A}$	Mean areal intercept in stereology
Ac_3	Temperature at which a sample becomes fully austenitic during heating
Ae_3	Temperature separating the α+γ and γ phase fields for a specific alloy
Ar_3	Temperature at which an austenitic sample begins to transform to ferrite during cooling
A_f	Temperature at which the transformation to austenite is complete
A_i	Atomic weight of element i
A_s	Temperature at which the transformation of austenite begins
A_s	Mean free slip area in statistical theory for plasticity (Kocks, 1966)
$\underline{B}$	Matrix representing the Bain deformation
B_d	Highest temperature at which bainite forms under the influence of an externally applied stress
B_s	Bainite start temperature
B_σ	A temperature below which bainitic transformation is considered to be stress assisted and above which it is considered to be strain induced, during transformation under the influence of an externally applied stress
c	Length of an edge crack, or length of a microcrack nucleus
c_d	Diameter of a penny shaped crack in a spheroidal particle

$c_i^{\alpha\theta}$	Concentration of element i in phase α which is in equilibrium with phase θ
c_o	Carbide thickness
C_i	Constants, with $i = 1, 2, 3 \ldots$
d	Interatomic spacing along a specific crystallographic direction
$\underline{d}$	Vector describing the shear component of an IPS
D_α	Diffusivity of carbon in ferrite
D *or* D_γ	Diffusivity of carbon in austenite
D_i^α	Diffusivity of element *i* in phase α
D_{eff}	Effective diffusion coefficient
$\overline{D}$	Weighted average diffusivity of carbon in austenite
E	Young's Modulus
f_1	Normalised supersaturation
f^*	Attempt frequency for atomic jumps across an interface
G	Growth rate
ΔG_m	Molar Gibbs free energy change on transformation; alternatively, the maximum molar Gibbs free energy change accompanying nucleation
G_N	Function specifying the free energy change needed in order to obtain a detectable rate of nucleation for Widmanstätten ferrite and bainite
G_N^α	Function specifying the critical value of $\Delta G^{\gamma\rightarrow\alpha}$ at the M_s temperature
G^*	Activation free energy for nucleation, or for interfacial motion
G_o^*	Activation free energy to overcome the resistance to dislocation motion without the aid of a chemical driving force
G_1^*	Activation free energy for the growth of an embryo into a nucleus
G_2^*	Activation free energy for the transfer of atoms across the nucleus/matrix interface
G_{dd}	Free energy dissipated in the process of solute diffusion ahead of an interface
G_F	Free energy per unit area of fault plane
G_{id}	Free energy dissipated in the transfer of atoms across an interface
G_{id}'	Free energy term describing the maximum glide resistance of dislocations

G_S	Strain energy per mole
G_{SB}	Stored energy of bainite
G_{SW}	Stored energy of Widmanstätten ferrite
ΔG	General term representing driving force
ΔG_{CHEM}	Chemical driving force
ΔG_{MECH}	Mechanical driving force
ΔG_{STRAIN}	Coherency strain energy during nucleation
$\Delta G^{\gamma\rightarrow\alpha}$	Free energy change for transformation without composition change
h_α	Ledge height at the interface between α and the parent phase
H	Hardness of martensite
H_F	Hardness of tempered martensite when all excess carbon has precipitated
H_o	Hardness of virgin martensite
H_1	A function in the theory of diffusion controlled growth
$\Delta H^{\gamma\alpha}$	Enthalpy change during the γ→α transformation
I_V	Nucleation rate per unit volume
J	Diffusion flux
k	Boltzmann constant
k_A	Constant in the Avrami equation
k_e	Equilibrium solute partitioning coefficient
k_g	Constant relating lath size to strength
k_i	Partitioning coefficient for alloying element i
k_p	Coefficient representing the strengthening effect of cementite particles; alternatively, a solute partitioning coefficient
k_ε	Coefficient in an equation for the strength of tempered martensite
K_I	Stress intensification factor in fracture mechanics
K_{IC}	Critical value of K_I, a measure of the toughness of a material
K_{ISCC}	Threshold value of the stress intensity below which stress corrosion cracks do not grow at a perceptible rate
ΔK	Stress intensity range during fatigue testing
ΔK_o	Threshold value of the stress intensity range during fatigue crack growth studies

Δl_m	Maximum relative length contraction due to isothermal reaustenitisation
$\bar{L}_3$	Mean intercept length in stereology
L_s	Lower bainite start temperature
m	Paris constant in fracture mechanics approach to fatigue
m_i	Mass fraction of element i
M	Mobility of an interface
M_d	Highest temperature at which martensite forms under the influence of an externally applied stress
M_s	Martensite start temperature
n	Time exponent in the Avrami equation
n_A	Number of atoms in an embryo involved in nucleation
n_{Fe}	Number of iron atoms per unit volume of α
n_P	Number of close-packed planes involved in the faulting process during displacive nucleation
N	Number of cycles in fatigue loading
N_v	Number of particles per unit volume
p	Péclet number, a dimensionless velocity
P	Pressure
$\underline{P}$	Matrix representing a homogeneous invariant-plane strain deformation
q	Half the increase in the thickness of austenite during one-dimensional growth
Q	Activation energy
$\underline{Q}$	Matrix representing in inhomogeneous lattice-invariant deformation
r	Radius of a disc; alternatively, the distance ahead of a crack tip; alternatively the tip radius of a growing plate
r_1	Proof stress to ultimate tensile stress ratio
r_2	Ratio of σ_a to σ_s
r_C	Critical distance in fracture mechanics, related to K_{IC}; alternatively, critical tip radius at which the growth of a plate ceases
r_e	Value of r_2 at the endurance limit in fatigue
$\bar{r}$	Mean particle radius at time t
$\bar{r}_o$	Mean particle radius at time zero

R	Universal gas constant; alternatively, the semi-axis of an oblate ellipsoid
R_d	Rate at which growing austenite dilutes
s	Shear component of the IPS shape deformation
$\underline{S}$	Deformation matrix in the crystallographic theory of martensite
S_1,S_2	Functions in the Trivedi model for the growth of parabolic cylinders
S_v	Interfacial area per unit volume
t	Time; alternatively, the thickness of a disc
t_1	Time for isothermal transformation to bainite during austempering of cast iron
t_2	Time to the beginning of carbide precipitation from austenite during austempering
t_a	Time required to reach a given fraction ξ of isothermal transformation
t_c	Time required for a sub-unit to reach a limiting size
t_d	Time required to decarburise a plate of bainite
t_i	Time interval for step i in a series of isothermal heat treatments
t_θ	Time for the precipitation of cementite from ferrite
Δt	Time interval between the nucleation of successive sub-units during sheaf lengthening
T	Temperature
T_c	Critical Zener ordering temperature for carbon atoms in ferrite; alternatively, the temperature below which cementite can in principle precipitate in association with upper bainitic ferrite
T_h	The temperature below which the nucleation of displacive transformations first becomes possible at a detectable rate
T_i	Isothermal transformation temperature
T_F	Temperature at which accelerated cooling is stopped
T_o	Temperature at which γ and α of the same composition have the same free energy
T_{om}	As T_o but forcing the Zener ordering of carbon atoms in the ferrite
T_o'	As T_o but accounting for the stored energy of ferrite
T_M	Melting temperature
T_r	Temperature below which a midrib is found in lower bainite plates
T_R	Temperature at which rolling deformation is stopped

T_t	Transition temperature for impact toughness
T_γ	Isothermal reaustenitisation temperature
$T^{\gamma\alpha}$	Austenite to ferrite transformation temperature
v^*	Activation volume
V	Volume of a sample
V^α	Volume of phase α
V_e^α	Extended volume of phase α
V_d	Diffusion field velocity
V_i	Velocity of an interface calculated on the basis of its mobility
V_k	Velocity of an interface calculated using a solute trapping function
V_I	Volume fraction of inclusions
V_L	Plate lengthening rate
V_m^θ	Molar volume of phase θ
ΔV_m	Change in molar volume on transformation
V_s	Sheaf lengthening rate
ΔV_v	Minimum detectable change in volume fraction
V_α^s	Velocity of steps in the α/parent phase interface
V_τ	Volume per particle
w	Thickness of a bainite sub-unit
w_i	Weight percent of element *i*
w_i^{sol}	Weight percent of element *i*, in solution
W	Width of a fracture toughness specimen for a K_{IC} test
$\bar{x}$	Average mole fraction of carbon in an alloy
x_m	Maximum carbon supersaturation permitted in ferrite, on thermodynamic grounds
x_α	Carbon in α at interface
x_γ	Carbon concentration in austenite
x_γ^I	Carbon concentration in austenite before the start of austenite growth
$x^{\alpha\gamma}$	Mole fraction of carbon in ferrite which is in equilibrium or paraequilibrium with austenite
$x^{\gamma\alpha}$	Mole fraction of carbon in austenite which is in equilibrium or paraequilibrium with ferrite

$x_{T'_o}$	Carbon concentration given by the T'_o curve
x_{Ae_3}	Carbon concentration given by the Ae_3 curve
x^{θ}	Thickness of cementite particle
x_x	Concentration of X in cementite
$\bar{x}_x$	Average concentration of X in cementite
$x_x^{\alpha\theta}$	Concentration of X in ferrite which is in equilibrium with cementite
y	Semi-axis of an oblate ellipsoid
Y	Compliance function in fracture mechanics; alternatively, a constant in the theory of thermally activated dislocation motion
z	Coordinate normal to the interface plane; alternatively, a constant in the theory of thermally activated dislocation motion
z_d	Effective diffusion distance
Z	Position of the interface along coordinate z
α	Allotriomorphic or idiomorphic ferrite which forms by reconstructive transformation
α_1	One-dimensional parabolic thickening rate constant
β	Constant in weld metal inclusion formation theory; alternatively, an autocatalytic factor
γ	Austenite
Γ	Activity coefficient for carbon in austenite
δ_b	Boundary thickness
Δ	Uniform dilatation accompanying transformation; alternatively, the average distance between neighbouring particles in tempered martensite
θ	Cementite
ε_1	Average transverse thickness of dislocation cell structure in martensite
λ	Interledge spacing; alternatively, an intersite jump distance during diffusion
μ	Shear modulus
μ_i	Chemical potential of element i
ν	Poisson's ratio
ρ	Density
ρ_A	Density of atoms in close packed planes

ρ_d	Dislocation density
τ	Incubation time before the growth of an individual particle begins during isothermal transformation, or before a detectable degree of overall transformation. Alternatively, the shear stress resolved along the shear direction
τ_o	Resistance to dislocation motion
τ_μ	Athermal resistance to dislocation motion
κ	Percent planar matching during expitaxial nucleation
ψ	Constant in weld metal inclusion formation theory
σ	Applied stress
σ_a	Cyclic stress amplitude in a fatigue test
σ_C	Critical stress in fracture mechanics, related to K_{IC}; alternatively, solid solution strengthening due to carbon
σ_F	Stress necessary for the propagation of cleavage fracture
σ_{Fe}	Strength of pure annealed iron
σ_g	Strengthening due to grain boundaries
σ_N	Normal stress on the habit plane
σ_P	Work of fracture, per unit area of crack surface
σ_r	Stress as a function of the distance r ahead of the crack tip
σ_s	Saturation value of σ_{iy} in a fatigue test
σ_{ss}	Solid solution strengthening due to substitutional solutes
σ_{iy}	Instantaneous flow stress at any particular stage of a test
σ_y	Yield stress or proof stress in monotonic loading tests
$\sigma^{\theta\alpha}$	θ/α interface free energy per unit area
σ_0	Intrinsic strength of martensite, not including microstructural strengthening
Ω	Volume per atom
Ω_{Fe}	Volume of an atom of Fe in α
Ω_c	Volume of a molecule of Fe_3C less $3\Omega_{Fe}$
ξ	Volume fraction, or volume fraction divided by the equilibrium or some other limiting volume fraction
ξ_a	A specific value of ξ
ζ	Uniaxial dilatation normal to the habit plane

Abbreviations

ASM	American Society for Metals
ASTM	American Society for Testing Materials
BCC	Body centered cubic
BCT	Body centered tetragonal
CE	Carbon equivalent
FATT	Fracture assessed ductile–brittle transition temperature
FCC	Face centered cubic
HAZ	Heat affected zone of welded joints
HREM	High resolution transmission electron microscopy
HSLA	High strength low alloy (steels)
HV	Vickers hardness
IIW	International Institute for Welding
IPS	Invariant-plane strain shape change
KS	Kurdjumov–Sachs
LEFM	Linear elastic fracture mechanics
NW	Nishiyama–Wasermann
p.p.m	Parts per million by weight
SCR	Stress corrosion cracking resistance
SSAW	Self-Shielded Arc Weld
TRIP	Transformation induced Plasticity
TTT	Time–temperature transformation diagram

ULCB	Ultra low carbon bainitic steel
UTS	Ultimate tensile strength

Note The term *residual austenite* refers to the austenite that exists at the reaction temperature during transformation to bainite, whereas the term *retained austenite* refers to the austenite which remains untransformed after cooling the specimen to ambient temperature.

Preface

The versatility of iron has its origins in the nature of its electronic, atomic and crystal structure. There are three allotropic forms of iron, α (ferrite, body-centered cubic), γ (austenite, cubic close-packed) and ε (hexagonal close-packed). The most dense allotrope is ε-iron, which is also the most stable form at high pressures. α-iron undergoes a paramagnetic to ferromagnetic transition on cooling below about 1042 K, the effects of which were at one time incorrectly attributed to the presence of a further allotrope, β-iron.

Austenite is considered to exist in two electronic states separated by a narrow energy gap, the state stable at high temperatures being ferromagnetic (Curie temperature 1800 K). At low temperatures, γ-iron is in the lower energy antiferromagnetic state with a Néel temperature below 80 K.

All this can in principle explain the peculiar behaviour of iron at ambient pressure. Ferrite is stable at low temperatures, whereas austenite is found at intermediate temperatures, only to revert to ferrite at temperatures close to the melting point. It is the two-spin state electronic structure of austenite that gives it an extra entropy which stabilises it above 1185 K. The reversion to ferrite above 1667 K results from its magnetic entropy which builds up rapidly above the Curie temperature and eventually overcomes the two-spin state entropy of austenite.

These descriptions help rationalise the allotropes of iron, but the transformations between the allotropes can occur by many mechanisms, giving rise to a variety of microstructures. The addition of carbon introduces further variants of microstructure, and of substitutional solutes an incredibly rich variety of microstructures. This versatility, and the demonstrated ability of the steel industry to exploit it, is responsible for the amazing success of steels.

The current production of steel in the world is about 780 million tonnes per annum, and if all goes well, is predicted to increase to about 930 million tonnes by the year 2000. New iron alloys are still being designed,

manufactured and marketed with notorious regularity. A recent ingenious example is the inoculated acicular ferrite steel, where controlled *additions* of specific nonmetallic particles lead to the formation of chaotic microstructures capable of hindering the propagation of cleavage cracks. The steel is at the same time, weldable.

There are other examples of *designed* steels, and bainitic alloys are now at the forefront of this new kind of learned metallurgical technology. This has not always been the case; the thrill of discovering bainite led many investigators to suggest that the microstructure should possess outstanding mechanical properties, but time did not bear them out. Extensive research has relatively recently identified the weak links in bainitic microstructures, and this has led to the development of several classes of bainitic steels based on new metallurgical concepts.

I am convinced that further major advances are possible with the help of a fundamental understanding of the mechanism of bainitic transformation and of the relationship between the resulting microstructure and mechanical properties (i.e., good theory). The trouble is that the subject has in recent years been shrouded in controversy, so much so that some textbooks on steels do not dare venture into bainite in any depth. Some of the controversy is of relevance, but its perceived importance is almost certainly exaggerated. A major aim in writing this book was to demonstrate that it is, in spite of the many outstanding difficulties, possible to present a fairly interesting, self consistent and reasonable story on bainite, one which can be utilised in the design of steels and their associated thermomechanical treatments. Apart from its industrial importance, the subject is of considerable interest from an academic point of view. The challenge of bainite is that it is not in any respect, a well-behaved phase transformation.

There has never to my knowledge, been a book published which is dedicated to the subject of the bainite transformation. Nor has there been a major review that addresses the detailed phase transformation issues and the microstructure property relationships for bainite in a coordinated way. There were many occasions during the compilation of this book when I felt a sense of excitement, as the story began to piece together. My hope is that I have been able to convey some of this feeling into the text. I have attempted to write the book in a style which is somewhere between that of a review and a teaching text. The state of the subject is such that it is necessary to preserve the detail, although at the same time I have tried hard to maintain the sort of clarity that typifies textbooks, as opposed to research papers. It is unlikely that there are any modern undergraduate courses in the now broad field of materials science which devote much time to bainite, or for that matter to any other interesting subject! The book should be of greatest use to those in industry and academia who are interested particularly in transformations in steels, or who are curious about phase changes in general.

Acknowledgements

This book has developed out of a long standing interest in the subject of bainite and I am grateful to many friends for their help and advice. In particular, I have benefited enormously from the support of Professor J. W. Christian, Professor M. Cohen, Dr S. A. David, Dr D. V. Edmonds, Dr H. Harada, Professor Sir Robert Honeycombe, Professor D. Hull, Professor C. Humphreys, Professor J. F. Knott, Professor G. B. Olson, Professor C. M. Wayman and Dr M. Yamazaki.

I have over the years enjoyed the privilege of working with many research students who have contributed significantly to my understanding of bainite; J. R. Yang, M. Strangwood, A. Sugden, A. Ali, S. Mujahid, M. Takahashi, G. Rees and S. Babu deserve a special mention in this respect. I should also like to express my gratitude to John Garnham for being so generous with his knowledge on bainitic rail steels, to David Gooch for discussions on creep resistant bainitic steels, to Lars-Erik Svensson for introducing me to the problem of welding metallurgy and hence to 'acicular ferrite', and to Greg Olson for so many inspiring discussions on bainite. In addition, I would like to thank H.–O. Andren, S. S. Babu, G. Barritte, P. Clayton, D. V. Edmonds, M. Faroque, V. Gadgil, B. Josefsson, T. Maki, S. Mujahid, Y. Ohmori, M. Oka, J. Race, G. Rees, M. Takahashi, H. Tamehiro, R. Thomson, B. J. P. Sandvik and M. Umemoto for providing micrographs, as acknowledged in the text. Fig. 1.1 is reprinted with permission from E. C. Bain, *The Alloying Elements in Steel*, American Society for Metals, 1939.

Finally, it is with considerable pleasure that I acknowledge the 'support' of Anika and Maya without whom this project would certainly have failed. I dedicate this book to my parents Narmda and Dharamshi.

1 *Introduction*

We begin with a historical survey of the exciting early days of metallurgical research during which bainite was discovered, covering the period up to about 1960, with occasional excursions into more modern literature. The early research was usually well conceived and was carried out with enthusiasm. Many of the original concepts survive to this day and others have been confirmed using the advanced experimental techniques now available. The thirty years or so prior to the discovery of bainite were in many respects formative as far as the whole subject of metallurgy is concerned. The details of that period are documented in the several textbooks and articles covering the history of metallurgy,[1] but a few facts deserve special mention, if only as an indication of the state of the art for the period between 1920–1930.

The idea that martensite was an intermediate stage in the formation of pearlite was no longer accepted, although it continued to be taught until well after 1920. The β-iron controversy, in which the property changes caused by the paramagnetic to ferromagnetic transition in ferrite were attributed to the existence of another allotropic modification of iron (the β-phase) was also in its dying days. The first evidence that a solid solution is essentially a homogeneous mixture of solvent and solute atoms in a single phase was beginning to emerge (Bain, 1921) and it soon became clear

1 Notable historical works include: 'The Sorby Centennial Symposium on the History of Metallurgy', published by the A.I.M.E. in 1965 (includes an article by Bain himself), the commentary by H. W. Paxton, Metallurgical Transactions *1* (1970) 3479–3500, and by H. W. Paxton and J. B. Austin, Metallurgical Transactions *3* (1972) 1035–1042. Paxton's 1970 article is published along with a reproduction of the classic 1930 paper on the discovery of bainite by Davenport and Bain, and is based on first hand historical knowledge obtained directly from Davenport and Bain.

that martensite consists of carbon dispersed atomically as an interstitial solid solution in a tetragonal ferrite crystal. Austenite was established to have a face-centered cubic crystal structure, which could sometimes be retained to ambient temperature by quenching. Bain had already proposed the physical deformation (now known as the Bain Strain) which could relate the face-centered cubic and body-centered cubic or body-centered tetragonal lattices during martensitic transformation. It had been established using X-ray crystallography that the tempering of martensite led to the precipitation of cementite, or to alloy carbides if the tempering temperature was high enough. Although the surface relief associated with martensitic transformation had been observed, its importance to the mechanism of transformation was not fully appreciated. Widmanstätten ferrite had been observed in steels, and was believed to precipitate on the octahedral planes of the parent austenite; some notions of the orientation relationship between the ferrite and austenite were also being discussed.

This was an era of major discoveries and great enterprise in the metallurgy of steels. The time was therefore ripe for the discovery of bainite. The term 'discovery' implies something new; in fact, microstructures containing bainite must undoubtedly have been encountered prior to the now acknowledged discovery date, but the phase was never clearly identified because of the confused microstructures that followed from the continuous cooling heat treatment procedures common in those days. A number of coincidental circumstances inspired Bain and others to attempt isothermal transformation experiments. That austenite could be retained to ambient temperature was clear from studies of Hadfield's steel (used by Bain to show that austenite has a face centered cubic structure) and nickel- or carbon-rich iron alloys. It was accepted that increasing the cooling rate could lead to a greater amount of austenite being retained. Indeed, it had been demonstrated using magnetic techniques that austenite in low-alloy steels could exist at low temperatures for minutes prior to completing transformation. The concept of isothermal transformation was in fact used widely in industry in the manufacture of patented steel wire, and Bain was aware of this through his contacts at the American Steel and Wire Company. He began to wonder 'whether exceedingly small heated specimens rendered wholly austenitic might successfully be brought unchanged to any intermediate temperature at which, then their transformation could be followed' and he 'enticed' E. C. Davenport to join him in putting this idea into action.

1.1 The Discovery of Bainite

During the late 1920s, in the course of these pioneering studies on the *isothermal* transformation of austenite at temperatures above that at which

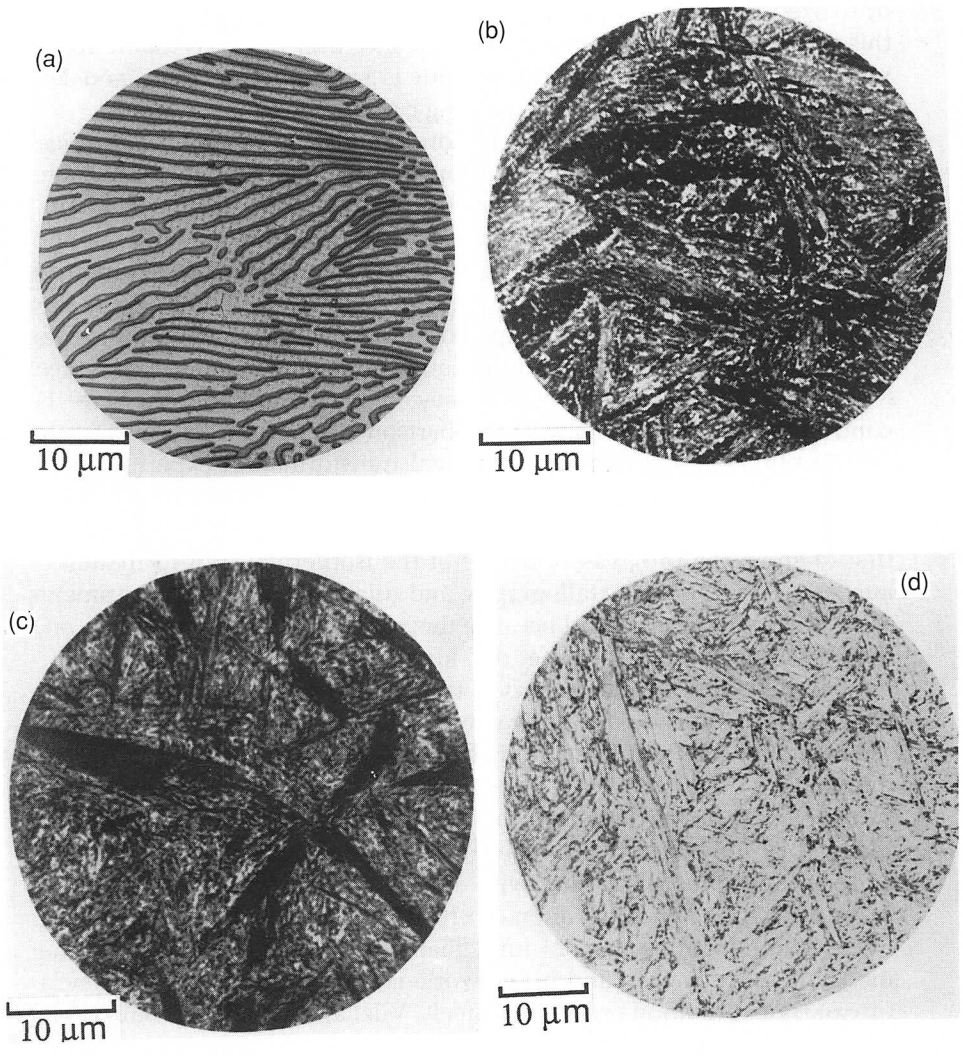

Fig. 1.1 *Mictrostructures in a eutectoid steel. (a) Pearlite formed at 720°C; (b) bainite obtained by isothermal transformation at 290°C; (c) bainite obtained by isothermal transformation at 180°C; (d) martensite. The micrographs were taken by Vilella and were published in the book* The Alloying Elements in Steel *(Bain, 1939). Notice how the bainite etches much darker than martensite, because of the presence of numerous fine carbides.*

martensite first forms, but below that at which fine pearlite is found, Davenport and Bain (1930) discovered a new microstructure consisting of an 'acicular, dark etching aggregate' which was quite unlike the pearlite

or martensite observed in the same steel (Fig. 1.1). They originally called this microstructure 'martensite–troosite' since they believed that it 'forms much in the manner of martensite but is subsequently more and less tempered and succeeds in precipitating carbon'.

The structure was found to etch more rapidly than martensite but less so than troostite (fine pearlite). The appearance of 'low range' martensite–troostite (formed at temperatures just above the martensite-start temperature M_s) was found to be somewhat different from the 'high range' martensite–troostite formed at higher temperatures. The microstructure exhibited unusual and promising properties; it was found to be 'tougher for the same hardness than tempered martensite' (Bain, 1939), and was the cause of much excitement at the newly established United States Steel Corporation Laboratory in New Jersey. It is relevant to note here the contributions of Lewis (1929) and Robertson (1929), who were in fact the first to publish the results of isothermal transformation experiments on eutectoid steel wires (probably because of their relevance to patented steel), but the Davenport and Bain experiments were undoubtedly the first to show the progressive nature of the isothermal transformation of austenite, using both metallography and dilatometry. Their experiments were much more successful because they utilised very thin samples, and their method of representing the kinetic data in the form of time-temperature-transformation curves turned out to be so simple and elegant, that it would be inconceivable to find any contemporary materials scientist who has not been trained in the use or construction of TTT diagrams.

In 1934, the research staff of the laboratory named the microstructure 'Bainite' in honour of their colleague E. C. Bain who had inspired the studies, and presented him with the first ever photomicrograph of bainite, taken at a magnification of ×1000 (Smith, 1960; Bain, 1963).

The name 'bainite' did not immediately catch on. It was used rather modestly even by Bain and his co-workers. In a paper on the nomenclature of transformation products in steels, Vilella, Guellich and Bain (1936) mentioned an 'unnamed, dark etching, acicular aggregate somewhat similar to martensite' when referring to bainite. Hoyt, in his discussion on this paper appealed to the authors to name the structure, since it had first been produced and observed in their laboratory. Davenport (1939) ambiguously referred to the structure, sometimes calling it 'a rapid etching acicular structure', at other times calling it bainite. In 1940, Greninger and Troiano used the term 'Austempering Structures' instead of bainite. The 1942 edition of the book *The Structure of Steel* (and its reprinted version of 1947) by Gregory and Simmons contains no mention of bainite.

The high range and low range variants of bainite were later called 'upper bainite' and 'lower bainite' respectively (Mehl, 1939) and this

terminology remains useful to this day. Smith and Mehl (1942) also used the term 'feathery bainite' for upper bainite which forms largely, if not exclusively, at the austenite grain boundaries in the form of bundles of plates, and only at high reaction temperatures, but this description has not found frequent use. In fact, both upper and lower bainite ferrite consist of aggregates of plates, aggregates which were later designated sheaves of bainite (Aaronson and Wells, 1956).

1.2 The Early Research

Early work into the nature of bainite continued to emphasise its similarity with martensite. Bainite was believed to form with a supersaturation of carbon (Wever, 1932; Wever and Jellinghaus, 1932; Portevin and Jolivet, 1937, 1938; Portevin and Chevenard, 1937). It had been postulated that the transformation involves the abrupt formation of flat plates of supersaturated ferrite along certain crystallographic planes of the austenite grain (Vilella *et al.*, 1936). The ferrite was then supposed to decarburise by rejecting carbon at a rate depending on temperature, leading to the formation of carbide particles which were quite unlike the lamellar cementite phase associated with pearlite. The transformation was believed to be in essence martensitic, 'even though the temperature be such as to limit the actual life of the quasi-martensite to millionths of a second'. Bain (1939) reiterated this view in his book *The Alloying Elements in Steel*. Isothermal transformation studies were by then becoming very popular and led to a steady accumulation of data on the bainite reaction, still variously referred to as the 'intermediate transformation', 'dark etching acicular constituent', 'acicular ferrite', etc.

In many respects, isothermal transformation experiments led to the clarification of microstructures, since individual phases could be studied in isolation. There was, however, room for difficulties even after the technique became well established. For alloys of appropriate composition, the upper ranges of bainite formation were found to overlap with those of pearlite, preceded in some cases by the growth of proeutectoid ferrite. The nomenclature thus became confused since the ferrite which formed first was variously described as massive ferrite, grain boundary ferrite, acicular ferrite, Widmanstätten ferrite, etc. On a later view, some of these microconstituents are formed by a 'displacive' (Buerger, 1951) or 'military' (Christian, 1965a) transformation of the iron atoms (together with any substitutional solute atoms) from austenite to ferrite, and are thus similar to carbon free bainitic ferrite, whereas others form by a 'reconstructive' or 'civilian' transformation which is a quite different kinetic process.

1.2.1 Crystallography

By measuring the crystallographic orientation of austenite using twin vestiges and light microscopy, Greninger and Troiano (1940) were able to show that the habit plane of martensite in steels is irrational; these results were consistent with earlier work on non-ferrous martensites and put paid to the contemporary view that martensite in steels forms on the octahedral planes of austenite. They also found that with one exception, the habit plane of bainite is irrational, and different from that of martensite in the same steel (Fig. 1.2). The habit plane indices also tended to vary with the transformation temperature and the average carbon concentration of the steel. The results seemed to imply some fundamental difference between bainite and martensite. Because the habit plane of bainite seemed to approach the austenite octahedral plane (then thought to be the habit plane of Widmanstätten ferrite) at high temperatures, but the proeutectoid cementite habit at low temperatures, and because it always differed from that of martensite, Greninger and Troiano proposed that bainite from the very beginning grows from austenite as an aggregate of ferrite and cementite. A competition between the ferrite and cementite of the aggregate was thus suggested as the reason for the observed variation of bainite habit, the ferrite controlling at high temperatures and the cementite at low temperatures. The competition between the ferrite and cementite was thus proposed to explain the observed variation of bainite habit plane. The crystallographic results were later confirmed using an indirect and less accurate method (Smith and Mehl, 1942). These authors also showed that the orientation relationship between bainitic ferrite and austenite does not change very rapidly with transformation temperature and carbon content and is within a few degrees of the orientations found for martensite and Widmanstätten ferrite, but differs considerably from that of pearlitic ferrite/austenite. Since the orientation relationship of bainite with austenite was not found to change, Smith and Mehl

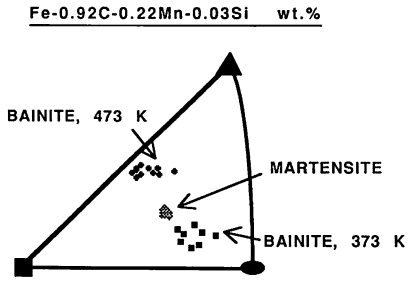

Fig. 1.2 *An example of the results obtained by Greninger and Troiano (1940), showing the irrational habit of bainite, which not only varied with transformation temperature but was also found to be different from the habit plane of martensite in the same steel.*

considered Greninger and Troianos' explanation for habit plane variation to be inadequate, implying that the habit plane cannot vary independently of orientation relationship.

1.2.2 *The Incomplete Reaction Phenomenon*

It was known as long ago as 1939 that in certain alloy steels (such as Fe–1.1Cr–1.1Mo–0.33C wt%) 'in which the pearlite change is very slow', the degree of transformation to bainite decreases (ultimately to zero) with increasing isothermal transformation temperature (Allen *et al.*, 1939). Similarly, the bainite transformation in a Fe–2.98Cr–0.2Mn–0.38C wt% alloy was found to begin rapidly but cease shortly afterwards, with the maximum volume fraction of bainite obtained increasing with decreasing transformation temperature (Klier and Lyman, 1944). At no temperature investigated did the complete transformation of austenite occur solely by decomposition to bainite. The residual austenite remaining untransformed after the cessation of the bainite reaction, reacted by another mechanism (pearlite) only after a further long delay. For another low alloy steel, Cottrell (1945) found that the amount of bainite that formed at 525°C ($<<Ae_3$) was negligible, and although the degree of transformation increased as the isothermal reaction temperature was decreased, the formation of bainite appeared to cease before reaching completion. Other experiments on several chromium-containing steels (0.08–1.28C wt%) revealed that the total dilatometric expansion accompanying the initial rapid formation of bainite increased continuously with decreasing reaction temperature (Fig. 1.3, Lyman and Troiano, 1946). The curve of total expansion versus temperature was found to show an increasing slope as a function of carbon concentration. The odd feature of such results was that the bainite transformation did not seem to reach completion on

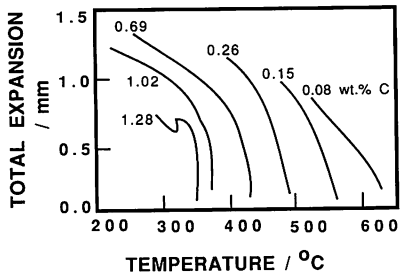

Fig. 1.3 *Temperature dependence of the total dilatometric expansion due to the formation of bainite (Lyman and Troiano, 1946). Transformation to bainite does not begin until in each case, a large undercooling is achieved below the Ae_3 temperature, to a critical temperature B_s. The maximum amount of bainite that forms, increases with undercooling below B_s.*

isothermal heat treatment, even though full transformation to peralite could be achieved at a *higher* transformation temperature. Often, the transformation of austenite at lower temperatures occurred in two stages (Klier and Lyman, 1944), beginning with the bainite reaction which stopped prematurely, and which was followed by the formation of pearlite at a slower rate. As will become apparent later, it is significant that the two reactions may only be separated by a long delay in well-alloyed steels; in plain carbon steels 'the second reaction sets in within a few seconds after the beginning of the bainite reaction' (Klier and Lyman, 1944).

1.2.3 Carbon Redistribution

X-ray and other experiments indicated that the formation of bainite enriches the residual austenite in carbon. Klier and Lyman (1944) took this to imply that the austenite, prior to its transformation to bainite, becomes compositionally unstable and separates into carbon rich and carbon depleted volumes (a process like this would require uphill diffusion). The low carbon regions were postulated to transform into supersaturated bainite of the same composition, by a 'martensite-like' lattice rearrangement, which then rapidly decomposed further, by precipitating iron carbides. A similar suggestion had been made earlier by Kurdjumov (1933) with respect to Widmanstätten ferrite: 'regions of low carbon concentration in the γ crystal result from diffusion within the γ phase, and these regions can at this time transform into the α phase . . .' Entin (1962) seemed to rediscover the idea that bainite grows by martensitic transformation in low carbon regions that develop in austenite prior to its transformation. His emphasis of the concept spurred Aaronson *et al.* (1966) to demonstrate using thermodynamics that an austenitic Fe–C solid solution cannot in fact spontaneously undergo separation into carbon rich and carbon poor regions (i.e., there is no tendency for the solution to undergo spinodal decomposition). The concept nonetheless seems to crop up with notorious regularity in modern literature (e.g., Prado, 1986; Prado *et al.*, 1990).

The proof by Aaronson *et al.* does not of course rule out random fluctuations of composition, of the type associated with any solid solution at dynamic equilibrium. Hence, a more modern variation of the above ideas is that the nucleation of bainite is favoured in regions of austenite where the carbon concentration is relatively low as a consequence of fluctuations (Degang *et al.*, 1989). Indeed, it has been demonstrated by Russell (1971) that carbon free regions of several thousand iron atoms exist at all temperatures in austenite of eutectoid composition. There is however, a conceptual difficulty with any claim that such regions can enhance overall nucleation rates. For every carbon depleted region there must also exist a

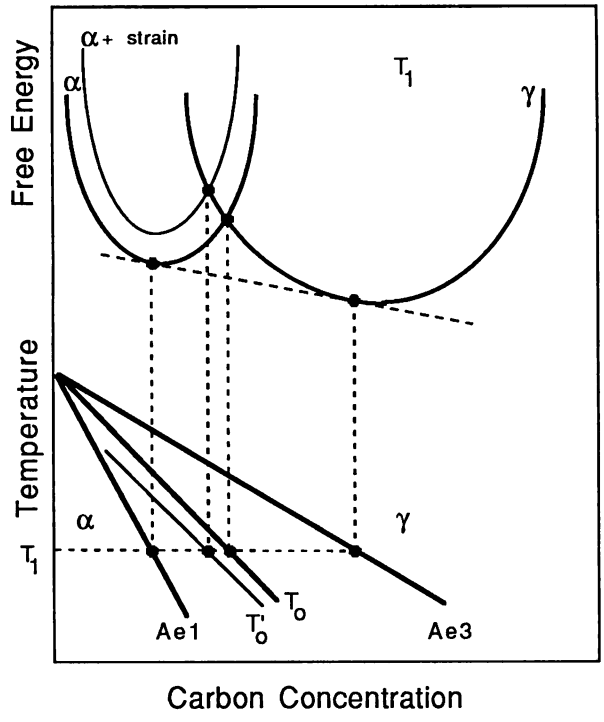

Fig. 1.4 *Schematic illustration of the origin of the T_o curve on the phase diagram. The T'_o curve incorporates a strainenergy term for the ferrite, illustrated on the diagram by raising the free energy curve for ferrite by an appropriate quantity.*

carbon enriched region where the probability of ferrite nucleation is presumably reduced, thereby balancing the effects of the depleted regions. Consequently, there seems no advantage in adopting this microscopic approach. The usual macroscopic thermodynamic model in which the driving forces are calculated for uniform composition should suffice.

1.2.4 Thermodynamics

In a far reaching paper, Zener (1946) attempted to give a rational thermodynamic description of the phase transformations that occur in steels. He assumed the bainite growth is diffusionless, any carbon supersaturation in bainitic ferrite being relieved subsequent to growth, by partitioning into the residual austenite. The atomic *mechanism* of bainite growth was not discussed in detail, but he believed that unlike martensite, there is no strain energy associated with the growth of bainite. Thus bainite should form by diffusionless transformation at a temperature just below

T_o where the austenite and ferrite of the same composition have identical free energy (Fig. 1.4). However, T_o is frequently used in martensite theory for the temperature at which austenite and martensite (i.e. supersaturated tetragonal 'ferrite') have the same free energy; for clarity, we follow Christian and Edmonds (1984) and call this temperature T_{om}. The Bain strain applied to a random interstitial solution of carbon in austenite automatically produces the ordered tetragonal form of ferrite if the carbon atoms are trapped in their original sites, but Zener also supposed that the tetragonal form may be regarded as a result of an ordering of the interstitial atoms into one set of sites of the cubic structure. He derived an equation for the critical temperature T_c at which the cubic and tetragonal forms of ferrite have the same free energy. T_c rises with interstitial solute content, and thus intersects the M_s temperature and also has a joint intersection with the T_o and T_{om} temperatures. Clearly T_{om} lies below T_o at low carbon contents and above T_o at high carbon contents. According to one interpretation (Owen, Wilson and Bell, 1964, martensite formed above room temperature is cubic at carbon contents below the intersection of M_s and T_c (above 2.5 at % carbon in plain iron–carbon alloys) and tetragonal above it. As Zener pointed out, martensite cannot form until the driving

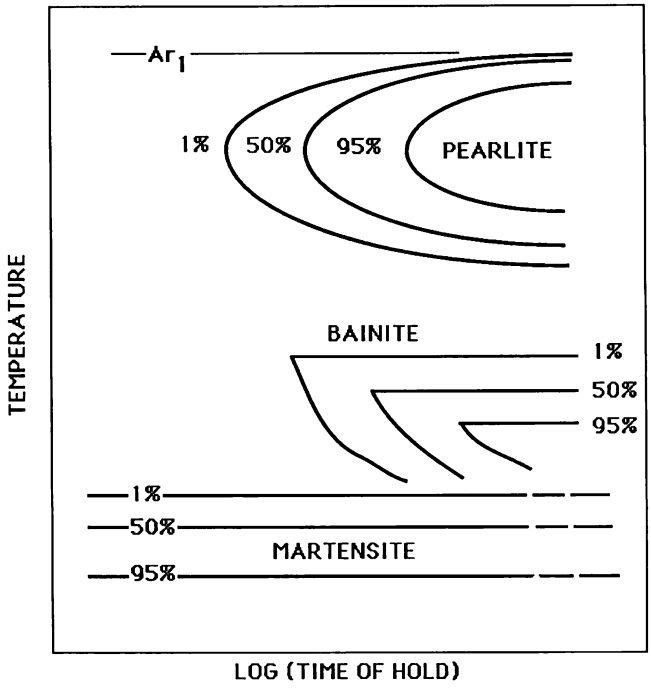

Fig. 1.5 *Schematic TTT diagram (after Zener, 1946) illustrating the flat tops on the bainite C-curves.*

force obtained by supercooling below the T_o or T_{om} temperature is large enough to provide the necessary strain energy.

It is usually assumed that bainite forming first as fully supersaturated ferrite nevertheless has a cubic structure, but it would seem more logical to assume a tetragonal structure unless the temperature of formation is above T_c.

The Zener model failed to provide an explanation of why the strain energy should exist for martensite and not for bainite. On the other hand, it explained the data showing that the degree of transformation to bainite increases with supercooling from zero at an upper limit, which is generally known as the B_s temperature. The carbon that partitions into tte austenite *after* the formation of bainite changes its composition, until it eventually becomes thermodynamically impossible for the austenite to transform without a composition change. For a given alloy composition, a higher undercooling below T_o would allow more bainite to form before transformation without a composition change becomes impossible. Consistent with experimental data, the model also requires the bainite C curve of the TTT diagram to tend asymptotically to infinite time (Fig. 1.5) at a temperature corresponding to the T_o or T_{om} temperature whichever is higher, since the transformation of austenite without a composition change cannot occur above this limit.

The initial plates of bainite, unlike those of many martensites, often grow to a limited size less than that of the parent austenite grain. Zener postulated that this is due to the formation of a layer of cementite around the plate, which stifles any subsequent growth.

1.2.5 *Paraequilibrium*

By 1947, it was evident that the cementite which grows during the bainite transformation in alloy steels differed from that associated with pearlite. The pearlitic cementite was always found to contain a higher than average concentration of some substitutional alloying elements whereas bainitic cementite seemed to have above the same overall substitutional alloy content as the parent material. Hultgren (1947), has cited several references which report magnetic, chemical and X-ray data on extracted carbides which confirm this difference between the two kinds of carbides.

Hultgren was at the time proposing a model for the role of substitutional alloying elements in steels; at high temperatures where diffusion rates are reasonable, these elements can redistribute during transformation if equilibrium demands such redistribution. In these circumstances, the transformation was said to occur under 'orthoequilibrium' conditions. This compares with 'paraequilibrium' transformation in which the substitutional alloying elements are unable to partition during the time scale

of the experiment, although carbon which is a fast diffusing interstitial element, redistributes between the phases and reaches equilibrium subject to this constraint.

The mechanism of pearlite formation was itself not clear in those days, but the transformation was believed to be initiated by the nucleation of cementite. It was suggested that bainite was instead initiated by the nucleation of ferrite (Mehl, 1939; Smith and Mehl, 1942; Mehl, 1948). Hultgren put these ideas together and postulated that the transformation at high temperatures (upper bainite) begins with the nucleation of ferrite of paraequilibrium carbon concentration, so that the residual austenite is enriched with respect to carbon. This bainitic ferrite, unlike the ferrite associated with pearlite, was believed to have a rational Kurdjumov–Sachs or Nishiyama–Wasserman orientation relationship with the parent austenite in which it grows; this was considered to explain the difference in ferrite morphology observed experimentally in pearlite and bainite. Bainitic ferrite was always found to consist of individual plates of sheaves whereas the ferrite in pearlite apparently formed alternating plates of a regularly spaced two-phase lamellar aggregate. The enrichment of austenite with respect to carbon should then eventually lead to the paraequilibrium precipitation of cementite from austenite in a region adjacent to the bainitic ferrite. At the time, pearlitic cementite was thought to bear a rational orientation relation to the austenite grain into which the pearlite colony grows, and Hultgren proposed, without any evidence, that bainiic cementite should be randomly orientated to the austenite in which it precipitated. This process of ferrite and subsequent cementite precipitation then repeated, giving rise to the sheaf of bainite. Hultgren therefore considered upper bainite to be a kind of a reconstructive transformation in essence similar to pearlite but growing under paraequilibrium conditions and different in the orientation relations of the various phases with respect to the parent austenite.

No explanation was offered for the occurrence of paraequilibrium with bainite, nor for the existence of the various orientation relationships. He admitted the possibility that bainite formed at lower temperatures (later known as *lower* bainite) 'forms directly', implying that the bainitic ferrite formed with a supersaturation of carbon, although the mechanism was not discussed.

The model of pearlite formation involving the repeated formation of ferrite and cementite was abandoned when Hillert (1962) demonstrated that a pearlite colony really consists of two interwoven crystals, one of ferrite and the other of cementite. Hillert (1957, 1962) also pointed out an important distinction between pearlite and upper bainite; in the former case, the ferrite and cementite phases grow cooperatively, whereas in the latter case, the plates of bainitic ferrite form first with the precipitation of cementite being a subsequent reaction.

1.2.6 Kinetics

The experiments of Wiester (1932), Hannemann *et al.* (1932–1933) and Forster and Scheil (1936, 1937) indicated that martensite can grow very rapidly in steels, a plate taking a few microseconds to grow right across an austenite grain. Bunshah and Mehl (1953) later demonstrated that the rate of growth of martensite can be as high as $1\,km\,s^{-1}$, i.e., one-third of the velocity of sound. This gave rise to the incorrect impression that martensitic transformation does not involve a 'nucleation and growth process', i.e., it is not a first order transformation in the thermodynamic sense.[2] For example, Smith and Mehl (1942), wondered whether bainitic structures form by a process of nucleation and growth or whether the plates spring fully formed from the matrix lattice 'as they do in the transformation to martensite'. A nucleation and growth model was favoured since the sizes of the reacted regions apparently increased with time at the reaction temperature. This was consistent with the work of Wever and his co-workers (1932), who found that in the bainite transformation range, the austenite decomposes relatively slowly. Furthermore, the progress of the bainite transformation could be represented by means of a C curve on a TTT diagram (Davenport and Bain, 1930), with a well defined incubation period before the beginning of isothermal transformation. Martensitic transformation, on the other hand could not be suppressed by the fastest available quench rates (Troiano and Greninger, 1946); it seemed to form athermally and was represented on the TTT diagram by a family of lines parallel to the time axis (Cohen, 1946). The bainite reaction was found to follow C curve kinetics even below the M_s temperature (Howard and Cohen, 1948).

It is in this context that Ko and Cottrell (1952) attempted to investigate whether bainite is 'a nucleation and growth reaction, or like martensite,

2 The Ehrenfest (1933) classification of phase transformations is based on the successive differentiation of a thermodynamic potential (e.g., Gibbs free energy) with respect to an external variable such as temperature or pressure. The order of the transformation is given by the lowest derivative to exhibit a discontinuity. In a first order transformation the partial derivative of the Gibbs free energy with respect to temperature is discontinuous at the transition temperature. There is thus a latent heat of transformation evolved at a sharp transformation interface which separates the coexisting parent and product phases. The phase change occurs at a well defined interface, the interface separating perfect forms of the parent and product phases. First order transformations involve the nucleation and growth of a product phase from the parent phase. In a second order transformation the parent and product phases do not coexist. Martensite in steels can coexist with austenite, and is then separated from the latter by a well defined interface. It is, like bainite, a first order transformation involving the nucleation and growth of individual plates.

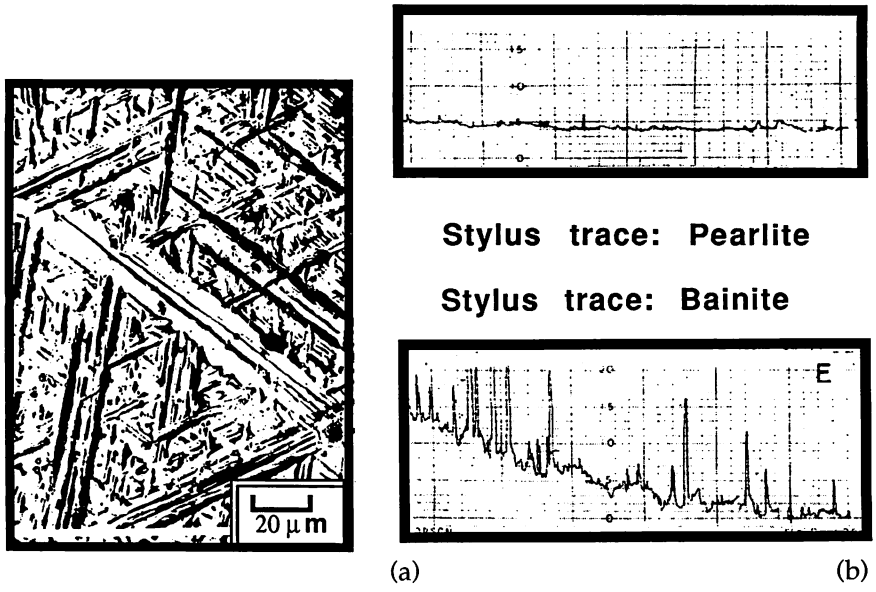

Fig. 1.6 *Surface effects observed during the transformation of pre-polished samples of austenite (Ko and Cottrell, 1952). (a) Surface relief due to the formation of bainite. (b) Line traces obtained by traversing a stylus across the surface of a pearlitic and a bainitic sample. Notice the severe upheavals caused by bainite, which contrast with the negligible relief due to pearlite.*

forms in a fraction of a second'. They also wanted to establish whether the transformation leads to surface relief effects similar to those associated with martensitic transformations. Ko and Cottrell were able to demonstrate, through hot-stage light microscopy, that bainite grows relatively slowly and that its formation causes the shape of the transformed region to change, the shape change being characterised qualitatively as an invariant-plane strain (Fig. 1.6). They also noted that unlike pearlite which is not hindered by austenite grain boundaries (Mehl, 1948), bainite growth terminated at austenite twin or grain boundaries. The transformation was therefore similar to martensite, and Ko and Cottrell attempted to identify any clear differences that may exist between martensite and bainite.

It was known already that martensite first forms at a large undercooling below the T_o temperature, at which ferrite and austenite of identical composition have equal free energy (Zener, 1946; Cohen *et al.*, 1950). Since diffusionless transformation is *thermodynamically* feasible below T_o, the extra undercooling was believed necessary to account for the strain and to a lesser extent, the interface energy associated with the formation of the

martensite plate. Bainite, which can form at more elevated temperatures than martensite, should therefore require a modified mechanism of transformation, a mechanism which has to be consistent with the lower driving force that is available for the transformation of austenite at higher temperatures. Ko and Cottrell postulated that a 'coherent nucleus' can develop either into martensite or into bainite depending on the driving force available for transformation, the nucleus developing into martensite below M_s. At the higher temperatures where bainite occurs, 'coherent growth' can only 'take place when the strain due to the density change is relieved'. They suggested that this could happen if the amount of carbon dissolved in bainite is reduced; this would also lead to a free energy reduction. The removal of carbon from the ferrite could occur by diffusion from bainite or by precipitation within bainite, or by a combination of these processes, depending on the transformation temperature. It is not entirely clear from their description whether they envisaged initially diffusionless growth, followed by carbon diffusion to provide the driving force for further growth, or whether the diffusion and interface migration are coupled so that precipitation within the ferrite (for lower bainite) or carbon rejection to the austenite (for upper bainite) takes place at the moving interface. The former mechanism seems illogical since the extra driving force is only available after a stage of initial growth to martensite which should not be posible (according to their growth condition) above M_s. Provided there is some way of circumventing the difficulty of forming the initial coherent nucleus (of whatever composition), the second type of growth model would allow bainite to form above M_s, and indeed above T_o. In some later work, Ko (1953) distinguished between incoherent ferrite and 'acicular ferrite' which he proposed should be regarded as carbon-free bainitic ferrite.

Kriesement and Wever (1956) pointed out that the appearance of bainite changes continuously between upper and lower bainite, and postulated that the growth of bainite involves the repeated and alternating nucleation and growth of lamellae of cementite and ferrite, from austenite. Unlike pearlite, the growth direction of the macroscopic plate of bainite was supposed to be normal to the plane of the lamellae. Although this particular mechanism has since been shown to be incorrect, they identified clearly the condition necessary for cementite precipitation to occur from residual austenite during the bainite transformation. Cementite precipitates from austenite if the carbon concentration of the latter exceeds that given by the extrapolated $\gamma/(\gamma+\theta)$ phase boundary.

Although many of the characteristics of bainite, especially the morphology and the shape deformation, had been found to be similar to those of martensite, a different microstructural approach was developed by Aaronson (1962). He used the Dubé morphological classification (Dubé *et*

al., 1958; Heckel and Paxton, 1961) for all non-pearlitic forms of ferrite formed from austenite, and he attributed the morphological variations to the dependence of the growth kinetics of an interface and to the nature of the site from which a precipitate crystal develops. In particular, plate morphologies were regarded as the result of the formation of immobile, partly coherent, planar interfaces which can grow normal to themselves only by the lateral migration of 'ledges'. In a later discussion of bainite (Aaronson, 1969), developed the 'microstructural' definition in which bainite is regarded simply as a non-lamellar two-phase aggregate of ferrite and carbides in which the phases form consecutively (as distinct from peralite where they form cooperatively). Aaronson stated that according to this definition, the upper limiting temperature of bainite formation should be that of the eutectoidal reaction (Ae_1), and he denied that the kinetic B_s temperature has any fundamental significance. In those alloy systems where there seems clear evidence for a separate C curve for bainite, the bainitic 'bay' and the apparent upper limit of bainite formation (B_s) were attributed to a special effect of certain alloying elements on the growth kinetics. Aaronson equally dismissed the observation of surface relief as a basis for classifying the various forms of ferrite.

1.3 Bainitic Steels: Industrial Practice

In spite of the early optimism about the potential properties of bainitic steels, major commercial exploitation took many years to become established. The steels were not in general found to be better than quenched and tempered martensitic steels, partly because of the relatively coarse cementite particles associated with bainite and partly because the continuous cooling heat treatments which were popular in industry, could not in practice produce fully bainitic steels. The use of lean alloys gave mixed microstructures whereas heavy alloying led to a considerable quantity of martensite in the final microstructure. It was not until low alloy, low carbon steels containing boron and molybdenum were introduced by Irvine and Pickering (1958) that fully bainitic steels could be produced in commercial quantities using continuous cooling heat treatments. Nonetheless, martensitic steels dominated the high strength steel market, with their better overall mechanical properties and well understood physical metallurgy principles.

It is natural to reduce the carbon concentration even further to produce better bainitic steels, which acquire their strength and toughness via the submicron size grain structure of bainite. However, technology was not in those days sufficiently advanced to cope with the necessarily higher cooling rates required to produce bainite in very low carbon steels, as the steel left the hot-rolling mill. The first system designed to accelerate the cooling

rate of hot sheet steel as it leaves the mill, was at the United Steel Company (UK), probably in an effort to reduce the length of the run-out table which allows the strip to cool to a specified temperature before coiling; the faster cooling was achieved using a laminar water jet system (Adcock, 1962). The first papers discussing the metallurgical benefits of accelerated cooling were presented in 1965 (Morgan *et al.*, 1965). The technology of accelerated cooling designed to produce partially or wholly bainitic microstructures in very low carbon, microalloyed steels has been perfected within the last fifteen years or so, and has resulted in the production of a new class of steels which are the cause of much excitement (DeArdo, 1988).

An area of major success for bainite was in the sector of creep resistant steels, where the so-called 2.25Cr–1Mo steel (Fe–0.1C–2.25Cr–1Mo wt%) was known to be one of the best low-alloy steels in terms of creep strength and microstructural stability (Miller *et al.*, 1940). Of course, the microstructural aspects of the steel may not have been appreciated in those days, but on continuous cooling it transforms into carbide free upper bainite. In most applications, the microstructure is then heavily tempered at 700°C for several hours in order to stress relieve; the tempering treatment and service at elevated temperatures causes the precipitation of a series of metastable alloy carbides, which together with solid solution strengthening by molybdenum, enhance creep resistance. Even today, this particular alloy finds wide applications, especially the energy generation industry (Lundin *et al.*, 1982).

1.4 Summary of the Early Research

By the beginning of the sixties, bainite was generally regarded as a transformation product differing significantly from various forms of proeutectoid ferrite as well as from pearlite and martensite. The results of the early research can be summarised as follows (Fig. 1.7).

Bainite can be obtained by isothermal transformation at all temperatures where the formation of pearlite and proeutectoid ferrite is sluggish, and also at temperatures below the martensite start temperature. Upper bainite, when it forms at relatively high temperatures, was found to consist of sheaves of ferrite plates with cementite particles trapped between the plates, whereas lower bainite also contained fine cementite particles within the bainitic ferrite platelets themselves.

Observations using light microscopy indicated that the lengthening of bainite sheaves occurred at a rate much slower than that at which martensite plates were known to grow. Bainite sheaves were found to have irrational habit planes, the indices of which differed from those of martensite found in the same alloy. The orientation relationship between bainitic ferrite and austenite was on the other hand similar to that

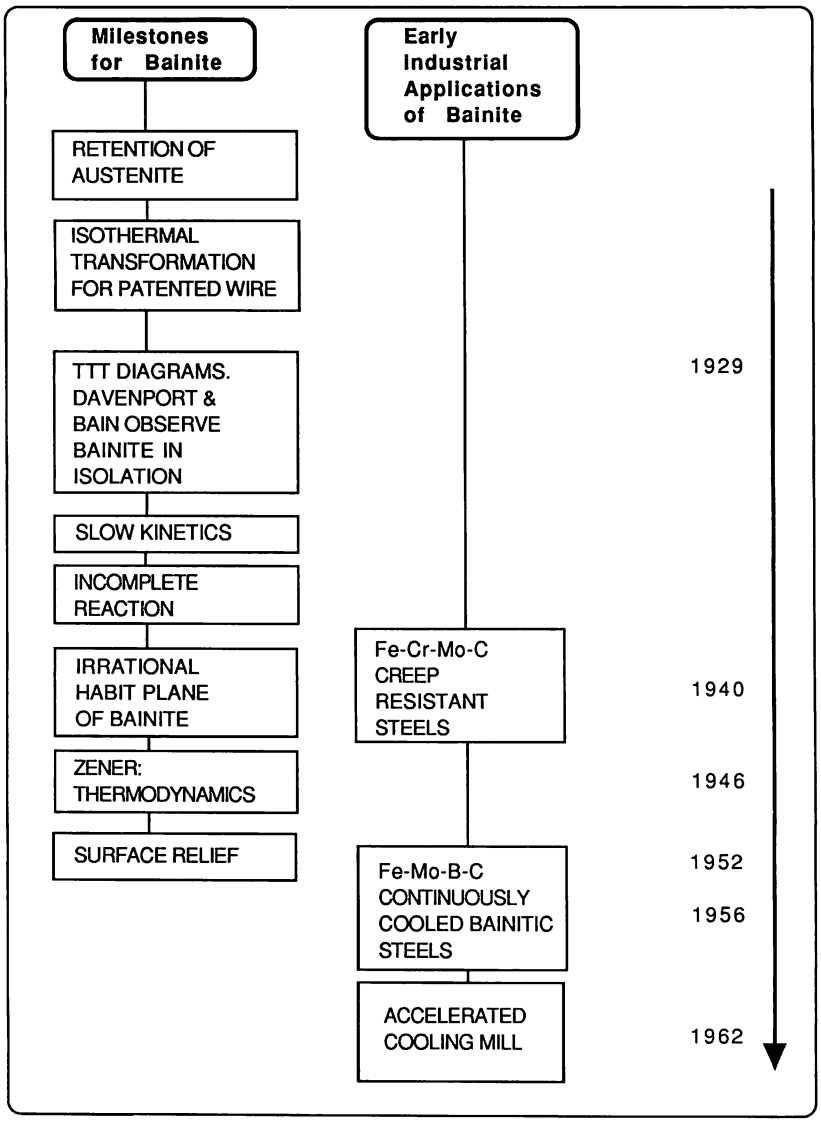

Fig. 1.7 *Flow chart illustrating some of the important milestones in the history of bainite.*

between martensite and austenite. Bainite plates were never found to cross austenite grain boundaries and the formation of bainite was, like martensite, observed to cause the shape of the parent crystal to change. This shape deformation is in present day terminology better described as an invariant-plane strain.

In steels where transformation to bainite could be carried out without interference from other reactions, experiments demonstrated that the degree of transformation to bainite decreases (ultimately to zero) and that the time taken to initiate the reaction increases rapidly with increasing isothermal transformation temperature. This led to the definition of a 'bainitic start' temperature (B_s) above which there is no reaction. This temperature was always found to lie well within the (metastable) $\alpha+\gamma$ phase field. Other reactions could follow the bainitic transformation, but in all cases, the rapid formation of bainite ceased prematurely before the austenite was fully transformed.

The prevailing, albeit rather ill-defined concept of the bainitic reaction as involving a martensitic type interface combined with diffusion controlled growth had already led to the suggestion of bainitic reactions in other (non-ferrous) alloy systems. In particular, the observation of surface relief effects apparently combined with compositional changes in the decomposition of some β-phase copper–zinc alloys had been used in a pioneering paper by Garwood (1954–5) to identify this decomposition as bainitic, and the difficulties in accounting for such a reaction in purely substitutional alloys had been emphasised (Christian, 1962). This remains an interesting and controversial aspect of transformation theory (Wu and Wayman, 1986; Takezawa and Sato, 1986).

The early emphasis on the similarities between bainitic and martensitic transformations still dominated the literature in the 1960s. The contrasting views of Aaronson and co-workers were only beginning to emerge, views which later led to considerable controversy some of which has continued until the present time. Some of the dispute has only been semantic, and thus of marginal importance; Ko's proposal that the term 'bainite' should be extended to include Widmanstätten ferrite forming with a shape change (thus satisfying what Aaronson has termed the shear definition of bainite, but contravening the reaction kinetics definition) falls into this category. The various disputes do, however, also concern mechanisms, and are thus important. It is for example, necessary to establish whether all the observed ferrite particles which occur in steels grow by essentially the same reconstructive transformation mechanism, or whether there are useful mechanistic distinctions to be made between coherent growth of ferrite initially supersaturated with carbon (bainite), coherent growth of Widmanstätten ferrite under paraequilibrium conditions, and incoherent growth of ferrite under local equilibrium conditions. Calculations of microstructure for the purposes of alloy and process design cannot be conducted with confidence in the absence of such detailed information.

2 *Bainitic Ferrite*

One of the key characteristics of the eutectoid decomposition of austenite to pearlite, is that the ferrite and cementite crystals grow cooperatively at a common transformation front with the parent austenite. Their growth rates are coupled, and their compositions are complementary in the sense that the excess solute displaced as the ferrite grows is incorporated into the cementite. All this is in stark contrast to the situation which prevails during the growth of bainite. It is now well established that bainitic transformation occurs in two separable stages, that of the growth of ferrite followed eventually by the precipitation of carbides. This chapter deals in detail with the ferritic component of bainite, focusing on its morphology, crystallography, constitution and kinetics. The term 'ferrite' is in the present context not intended to carry any connotations about its carbon concentration during growth. It simply reflects the fact that little or no excess carbon remains in solid solution in bainitic ferrite, by the time that experimental measurements become possible. The treatment of the carbides associated with the bainite transformation is in the chapter that follows.

2.1 Sheaves of Bainite

2.1.1 Morphology

Both upper and lower bainite consist of aggregates of platelets or laths of ferrite, separated by regions of *residual* phases consisting of untransformed austenite or of phases such as martensite or cementite which form subsequent to the growth of bainitic ferrite (Fig. 2.1). The aggregates of bainitic platelets are called *sheaves* (Aaronson and Wells, 1956), and the individual platelets are sometimes called *sub-units*. The platelets within a given sheaf may not be completely isolated from one another by the residual phases, in which case low misorientation grain boundaries are

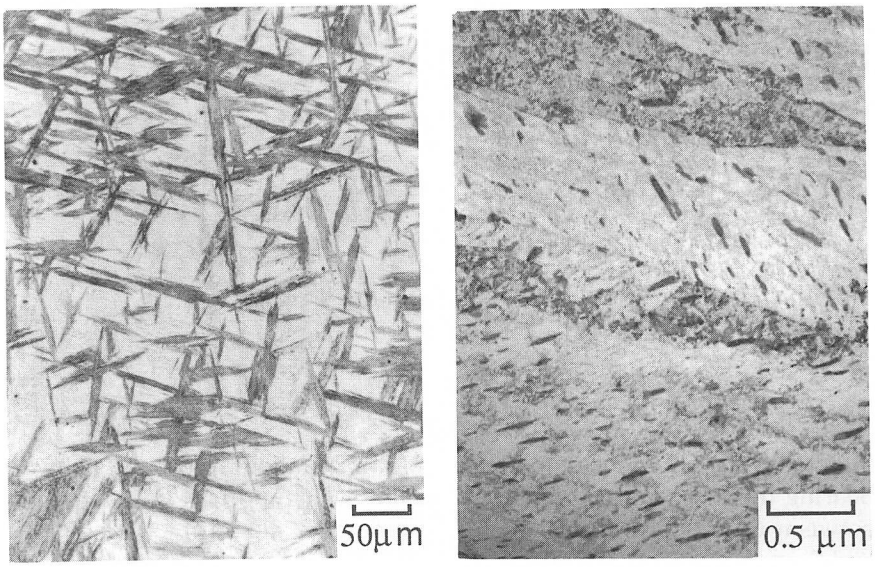

Fig. 2.1 *(a) Light micrograph illustrating sheaves of lower bainite in a partially transformed (395°C) sample of a Fe–0.3C–4Cr wt% alloy. The light etching matrix phase is martensite. (b) Corresponding transmission electron micrograph illustrating a sub-unit of lower bainite.*

formed along the surfaces where the platelets come in contact. This is because within a sheaf, the sub-units all tend to be in a common crystallographic orientation. A possible explanation for the fact that some of the austenite adjacent to the bainitic ferrite remains untransformed at the reaction temperature, is that its carbon concentration increases as a consequence of transformation, to such an extent that the growth of bainite eventually becomes thermodynamically impossible. If the starting carbon concentration of the steel is large, then the formation of bainite ceases at an earlier stage of the reaction, and the volume fraction of the residual phases is then expected to be large.

The cluster of platelets which forms a sheaf is sometimes called a 'packet' of bainite, because on the scale of light microscopy, fully transformed grains of austenite appear to be divided into discrete regions (i.e., packets), within which the traces of the habit planes of bainite are parallel. The term 'packet' has its origins in the description of lath martensite in low alloy, low carbon steels, where laths of martensite are also found to be in parallel formations (e.g. Chilton *et al.*, 1970). The similarity in both morphology and crystallography between lath martensite and upper bainite has been noted in many investigations, but it also appears that

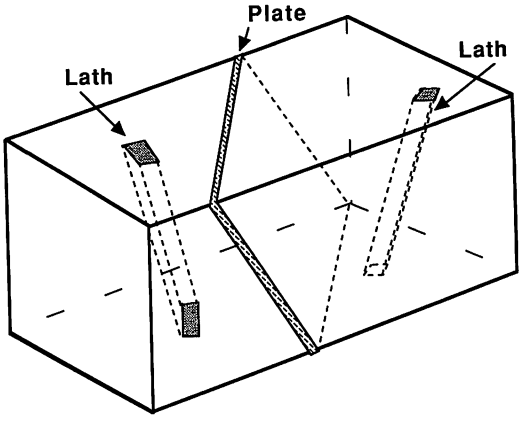

Fig. 2.2 *Schematic representation of a plate and of a lath.*

there may be differences in the detailed crystallography (see below). Bearing the mechanical properties in mind, it is important to distinguish between groups of platelets with the same crystallographic orientation, and those groups in which the platelets have mixed orientations. Matsuda *et al.* (1968, 1972) refer to the former kind of grouping as a *covariant packet*.

Two-surface analysis involves the simultaneous observation of the habit plane trace on two nonparallel surfaces, and other observations on specimens partly transformed to bainite, show that the overall shape of a sheaf on a macroscopic scale is in three dimensions like that of a wedge shaped plate (Oblak *et al.*, 1964; Srinivasan and Wayman, 1968b; Ohmori, 1971a; Bhadeshia and Edmonds, 1980a). The thicker end of the sheaf originates at an austenite grain boundary. The microscopic sub-units within a sheaf themselves have a lenticular plate or lath morphology (Fig. 2.2), whose form is most prominent near the edge or tip of a sheaf where impingement effects are minimal. For the same reason, these features are best observed in partially transformed specimens. The width of a sub-unit near the tip of a sheaf is approximately the same as that near the original nucleation site of the sheaf (i.e., an austenite grain surface), implying that the sub-units grow to a limiting size. In the development of a sheaf, new sub-units are most frequently nucleated near the tips of sub-units which are already present, rather than on their sides. The overall morphology of a sheaf is illustrated in Fig. 2.3.

When the sub-units are in the form of laths, each lath has its longest dimension along the close packed direction of the ferrite which is most nearly parallel to a corresponding close packed direction of the parent austenite (Davenport, 1974). It is not clear why the sub-units sometimes grow in the form of laths (e.g., Oblak *et al.*, 1964; Ohmori, 1971a; Ohmori and Honeycombe, 1971, Davenport, 1974) whereas on other occasions

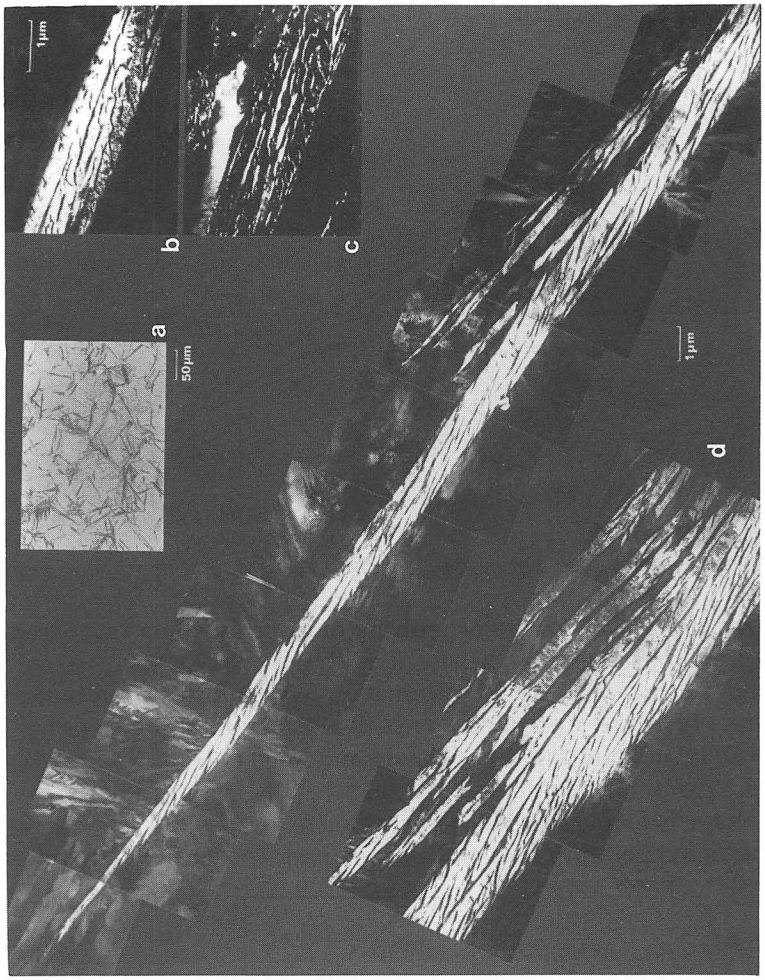

Fig. 2.3 *Transmission electron micrograph of a sheaf of upper bainite in a partially transformed Fe–0.43C–2Si–3Mn wt% alloy. (a) Light micrograph. (b, c) Bright field and corresponding dark field image of retained austenite between the sub-units. (d) Montage showing the structure of the sheaf.*

they form as plates (Srinivasan and Wayman, 1968b, c; Ohmori, 1971b; Bhadeshia and Edmonds, 1980a, Sandvik, 1982a). A qualitative impression from the literature is that the plate morphology tends to form at lower transformation temperatures and larger carbon concentrations.

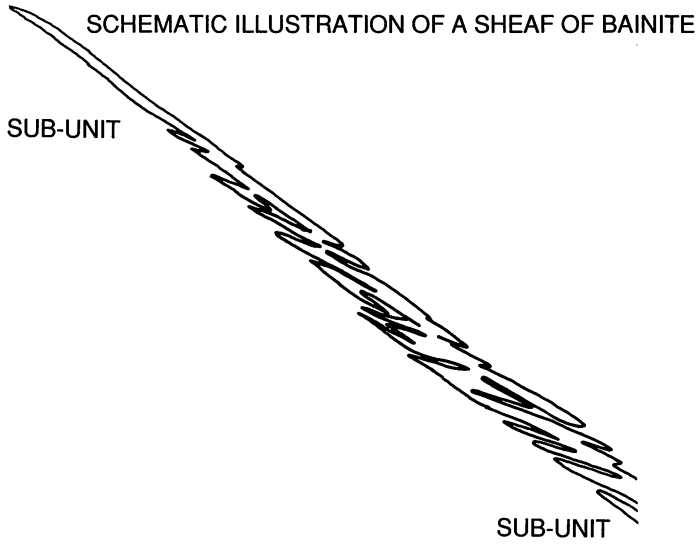

Fig. 2.3 *(e) Corresponding outline of the sub-units near the sheaf tip region.*

This observation is consistent with more extensive data on martensitic transformations (Fig. 2.4), where it is found that an increase in alloy content, a decrease in the transformation temperature, or an increase in the strength of the austenite favours the formation of plates rather than laths (Kelly and Nutting, 1960; Davies and Magee, 1970a, b, 1971; Haezebrouck, 1987). Laverrouz and Pineau's results (1974) indicate that the plate shape is favoured as the strength increases, even though the transformation temperature rises at the same time. The lath to plate transition

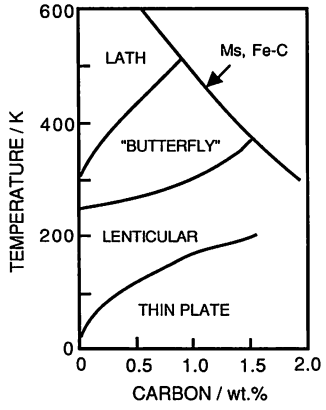

Fig. 2.4 *The martensite morphology as a function of the transformation temperature and carbon concentration of Fe–Ni–C alloys (After Maki and Tamura, 1986).*

can also be induced by increasing the driving force (using a magnetic field) without altering the transformation temperature (Korenko, 1973).[1]

The physical basis for such correlations is not clear, because the variables described are not always independent; for example, alteration of alloy content inevitably changes the transformation temperature. It is probable that the most important factor governing the lath to plate transition is the strength of the austenite and hence the extent to which the shape change is plastically accommodated. Lath martensite has always been associated with extensive plastic accommodation, which (like the sub-units of bainite) stifles the growth of the lath before it encounters any strong obstacles such as grain boundaries.

This hypothesis has been developed in detail by Haezebrouck (1987); he proposed that a plate shape is promoted by rapid radial growth and a high yield stress in the parent phase. Both of these factors favour elastic growth. A high growth rate is equivalent to a high strain rate, whence yielding becomes more difficult. When the particle size is small, the radial growth is expected to be elastic, but the extent to which elastic growth can be sustained as the particle grows depends on the flow behaviour of the austenite. The effect of plasticity is to cause the radial growth to arrest. If plasticity sets in at an early stage of growth, it is assumed that lath martensite is obtained since, consistent with experimental data, the lath ceases growth before encountering a grain boundary. Haesebrouck demonstrated that his model is consistent with all available experimental data (including the Korenko experiment, since an increase in driving force leads to an increase in growth rate, which promotes elastic growth). While the model clearly explains growth arrest, it does not really address the issue of the *shape* transition. A plate to lath transition depends on a change from isotropic to anisotropic radial growth. More work is needed to resolve this perplexing issue.

Returning now to the general characteristics of the bainite morphology, it is found that in some cases, lower bainite sheaves seem to develop with a macroscopically planar interface on just one side of each sheaf (Oblak and Hehemann, 1967; Srinivasan and Wayman, 1968c). The same effect has been found in lath martensite in an iron–nickel–manganese alloy (Sandvik and Wayman, 1983). In other cases, the thickening of sheaves has been observed to occur from both sides of the habit plane (Speich, 1962). The aspect ratio (thickness/length) of such sheaves is known to decrease with the transformation temperature but is not sensitive to the

1 Some early theories where it was suggested that a lowering of austenite stacking fault energy, or the onset of tetragonality in martensite, correlate with the morphological transition from lath to plate seem to lack in generality — see review by Haezebrouck (1987).

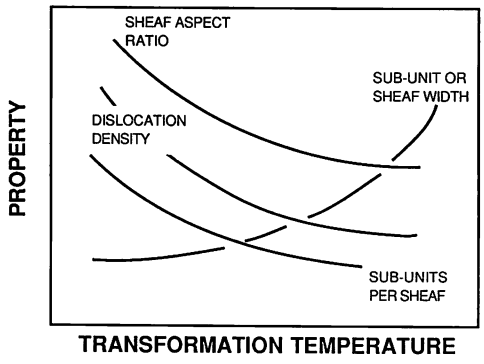

Fig. 2.5 *Qualitative trends in microstructure as a function of the transformation temperature.*

substitutional alloy content, at least for the relatively low alloy steels that have been studied to date (Speich, 1962; Irvine and Pickering, 1965; Hawkins and Barford, 1972). The number of platelets within a sheaf also increases as the transformation temperature is reduced (Sandvik, 1982a), presumably reflecting a reduction in platelet width. The aspect ratio seems to increase slightly as the volume fraction of bainite increases during isothermal transformation (Tomita and Okabayashi, 1985a, b). The sheaf width decreases with transformation temperature (Naylor and Krahe, 1974; Miihkinen and Edmonds, 1987a), although the sub-unit width is not influenced by either the austenite grain size or the bainite sheaf size (Lonsdale and Flewitt, 1978; Miihkinen and Edmonds, 1987a). Similar effects are found with martensite but their detailed explanation is not yet available (Roberts, 1970; Carlson *et al.*, 1979). The microstructural variations with temperature are summarised in Fig. 2.5.

2.1.2 *Stereology*

The 'grain size' of bainite usually has to be characterised by measurements made on *random* planar sections of the microstructure, as observed using a transmission electron microscope with replica or thin foil specimens. In such sections, the ferrite plates appear approximately parallel sided, and the thickness is then measured in a direction normal to the long edges of the plates. The average value of the measurements is taken to represent a 'grain size', which is really an apparent plate thickness. The procedure is useful in characterising any qualitative trends in microstructure, but obviously ignores stereological considerations. For example, if a platelet is represented as a disc of radius r and thickness t with $r >> t$, then the mean intercept length is given by $\overline{L}_3 = 2t$,

and the mean intercept area is given by $\overline{A} = 2rt$ (Fullman, 1953). Note that the intercepts are in this case random with respect to the orientation of the microstructure.[2]

The specific manner in which the grain size of an anisotropic structure is defined is somewhat dependent on the application. For example, in considering the strengthening due to lath boundaries, it is appropriate to examine the dimensions of the available slip planes within individual platelets (Naylor, 1979; Daigne *et al.*, 1982). If it is assumed that there is a random distribution of slip plane orientations with respect to the lath axes, the grain boundary strengthening effect (σ_g) is found to be of the form $\sigma_g = k_g M^{-1}$, where k_g is a constant and M is the mean value of the larger diameter of a slip plane. This behaviour is different from the classical Hall–Petch relation where it is the inverse square root of grain size which matters, as discussed further in Chapter 10.

There is some uncertainty about the influence of carbon on the grain size of bainite. Pickering (1958) found the size to be independent of carbon concentration for bainite produced during continuous cooling transformation, although Davenport (1974) states (without citing evidence) that it is a well known effect that the size decreases with carbon concentration. In fact, the apparent thickness of bainite is in general found to increase with transformation temperature from about 0.2 μm to 2 μm as the transformation temperature changes from 425°C to 570°C respectively, for a Fe–0.22C wt% commercial steel and similar data have been reported for other steels (Ohmori *et al.*, 1971; Kunitake *et al.*, 1972; Kamada *et al.*, 1976; Sandvik and Nevalainen, 1981; Sandvik, 1982a). Whether this reflects a change in the plate aspect ratio is not clear. It is noteworthy that the width of laths of martensite in steels has been reported to decrease as a function of the martensite start temperature, when the latter was varied either by altering pressure (Vyhnal and Radcliffe, 1967) or by altering the carbon concentration (Speich and Warlimont, 1968).[3] This is consistent with the general trend for bainite, where the plate width seems to decrease with transformation temperature.

Bainitic ferrite formed at high temperatures often contains sub-grain boundaries, the sub-grain size becoming finer for bainite formed at lower

2 A lath shape may be represented as a rectangular parallelepiped of dimensions a, b, and c with $a > b > c$. The corresponding mean intercepts are then given by (Myers, 1953; Mack, 1956):

$$\overline{L}_3 = (2abc)/(ab + bc + ca)$$
$$\overline{A} = (2abc)/(a + b + c)$$

3 For reasons not understood, alloys of iron which contain little or no carbon apparently do not show any variation in martensite lath width as a function of the martensite-start temperature (Roberts, 1970).

temperatures (Pickering, 1958). The boundaries are probably a consequence of the recovery (polygonisation) of the dislocation structure introduced during transformation at high homologous temperatures.

2.2 Dislocation Density

There is little doubt, and considerable circumstantial evidence, that bainite has a 'high' dislocation density, although there are few quantitative data to support this. Smith (1984) has shown using transmission electron microscopy, that a Fe–0.07C–0.23Ti wt% alloy the estimated B_s temperature of which is about 650°C, when isothermally transformed to allotriomorphic ferrite at 800°C has a mean dislocation density of $\approx 0.5\times10^{14}$ m^{-2}, whereas when the same alloy is transformed to bainite at 650°C, the dislocation density obtained is $\approx 4\times10^{14}$ m^{-2}. These figures compare very well with data reported by Graf *et al.* (1985); using accurate and detailed transmission electron microscopy, they found that the mean dislocation density of bainite in a Fe–0.11C–1.5Mn wt% steel transformed by continuous cooling is about 1.7×10^{14} m^{-2}, whereas that of allotriomorphic ferrite was found to be 0.37×10^{14} m^{-2}. It is particularly significant that the dislocation density in bainite is found to be higher than that in allotriomorphic ferrite which has formed at a similar transformation temperature (Oblak and Hehemann, 1967).

The relatively high dislocation density associated with bainitic ferrite is often attributed to the fact that it forms by a shear mechanism, on the grounds that this necessitates the deformation of the parent lattice by dislocations, which are then somehow incorporated into the product phase. This reasoning is however, incorrect since the dislocations that are responsible for the transformation and for the lattice-invariant deformation are

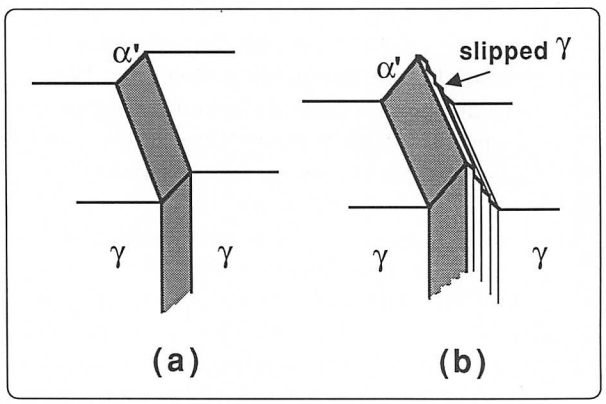

Fig. 2.6 *Schematic illustration of a perfect invariant-plane strain surface relief (a) and one where plastic relaxation of the shape change occurs in the adjacent matrix (b).*

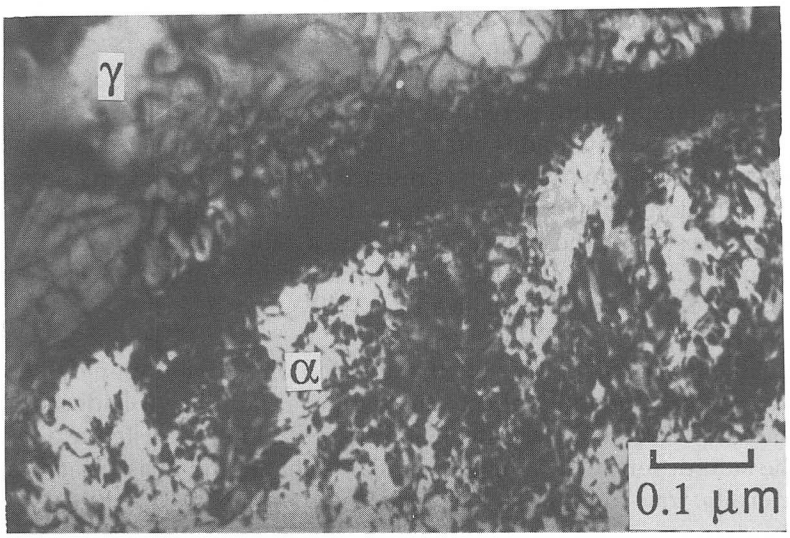

Fig. 2.7 *Intense dislocation debris, at and in the proximity of the bainite/austenite interface.*

located and remain in the interface between the parent and product lattices. Indeed, there are many such transformations where few dislocations are to be found in the product phase (e.g., thermoelastic martensites).

If the shape deformation accompanying displacive transformation is accommodated at least partially by plastic relaxation then the resulting dislocation debris introduced into the austenite can in principle be inherited by any bainite that forms subsequently. The bainitic ferrite may itself undergo plastic relaxation, since the yield stresses of both ferrite and austenite decrease with increasing transformation temperature. Plastic relaxation of the shape change has been observed experimentally (Srinivasan and Wayman, 1968b). When pre-polished samples of austenite are transformed to bainite, the adjacent austenite surface does not remain planar, but instead exhibits curvature which is characteristic of slip deformation (Fig. 2.6). Observations of the transformation using hot-stage transmission electron microscopy have revealed that the growth of bainite is accompanied by the formation of dislocations in and around the bainite (Nemoto, 1974), and direct observations of the austenite/bainitic ferrite interface (Fig. 2.7) also provide evidence of plastic accommodation in both phases (Bhadeshia and Edmonds, 1979a). Sandvik and Nevalainen (1981) have demonstrated that the austenite adjacent to the bainitic ferrite undergoes twinning deformation, and that the density of twins increases as the transformation temperature decreases. The plastic accommodation is also believed to be responsible for the lower residual

stresses in samples which are bainitic compared with those transformed to martensite (Diesburg *et al.*, 1981).

The dislocation density of bainitic ferrite seems to increase as the transformation temperature is reduced (Pickering, 1967), although there are few quantitative data to this effect. X-ray line profile measurements show that the lattice strain (due to the presence of dislocations) increases as the transformation temperature decreases (Fondekar *et al.*, 1970). These can be used to estimate the dislocation density ρ_d; for the low alloy steel used by Fondekar *et al.*, isothermal transformation to bainite at 300, 360 and 400°C gave dislocation densities of 6.3×10^{15}, 4.7×10^{15} and 4.1×10^{15} m^{-2} respectively.

Finally, it is pertinent to note that in addition to dislocation debris, the plastic accommodation effects also induce faulting (Bhadeshia and Edmonds, 1979a) and twinning (Sandvik, 1982a) in the austenite adjacent to the bainitic ferrite, in a manner similar to that found in association with martensitic transformations (Jana and Wayman, 1970).

2.2.1 *Quantitative Estimation of Dislocation Density*

The meagre dislocation density data available for bainitic ferrite are not in themselves sufficient to obtain a reliable quantitative relationship of the density as a function of temperature or other variables. If it is assumed that for low alloy steels, the dislocation density depends mainly on transformation temperature, and that the main effect of temperature (in this context) is in altering the strengths of the parent and product phases, then a general relation could be derived using data on all of the displacive transformations in steels. This seems justified because the magnitudes of the shape deformations involved in the variety of reactions does not vary much.

Hence, if the data reported by Kehoe and Kelly (1970) for martensite are combined with those reported by Smith and Fondekar *et al.*, the following empirical relation, applicable over the range 570–920 K, is obtained for the dislocation density in ferrite as a function of temperature (Fig. 2.8):

$$\log_{10}\{\rho\} = 9.28480 + (6880.73/T) - (1780360/T^2) \qquad (2.1)$$

where ρ is the dislocation density in m^{-2}, and T is the reaction temperature in K (Takahashi and Bhadeshia, 1990). For the martensite, the transformation temperature was taken to be the M_s temperature. Although the dislocation densities of martensite measured by Norström (1976) are also plotted in the Fig. 2.8, those data were not used in deriving the above expression because of uncertainties in the method used to assess the thickness of the thin foil samples used.

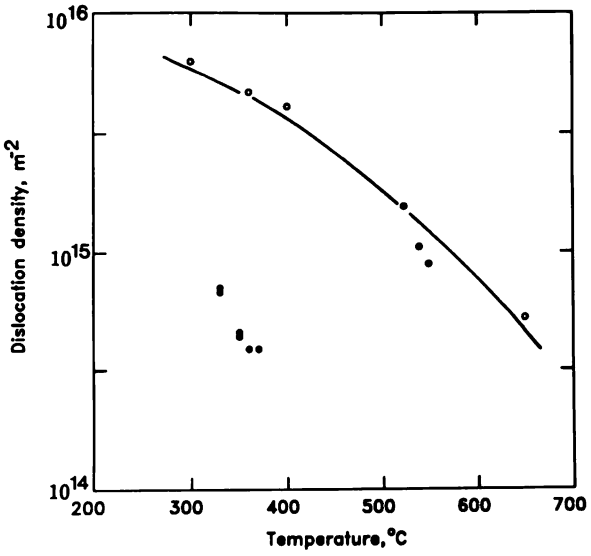

Fig. 2.8 *Changes in the dislocation density of bainitic ferrite (open circles) and martensite (solid circles) as a function of the reaction temperature. The cluster of points which lie below the curve are due to Norström (1976). The other data are due to Smith (1984), Fondekar* et al. *(1970) and Kehoe and Kelly (1970).*

2.3 Chemical Composition

2.3.1 *Substitutional Alloying Elements*

It is generally accepted that there is no long range redistribution of substitutional alloying elements during the growth of bainitic ferrite. See for example, Aaronson and Domain (1966), where some of the electron microprobe analysis results refer to bainitic ferrite. The bulk substitutional alloy content of the bainitic ferrite was found to be identical to that of the parent austenite. A variety of other results using the atom probe technique, on steels containing silicon, nickel, manganese, chromium or molybdenum, confirm that there is no bulk partitioning of substitutional alloying elements during the formation of bainitic ferrite (Bhadeshia and Waugh, 1981, 1982; Stark *et al.*, 1988, 1990; Josefsson and Andren, 1988, 1989). One set of atom probe experiments (Bach *et al.*, 1980) apparently indicated the opposite conclusion, namely that there is a redistribution of chromium and molybdenum during the formation of bainite. These results are however, doubtful since they indicate an enrichment of these alloying elements on both sides of the transformation interface. Indeed, the measured concentrations in both phases sometimes exceeded the average concentrations in the alloy used.

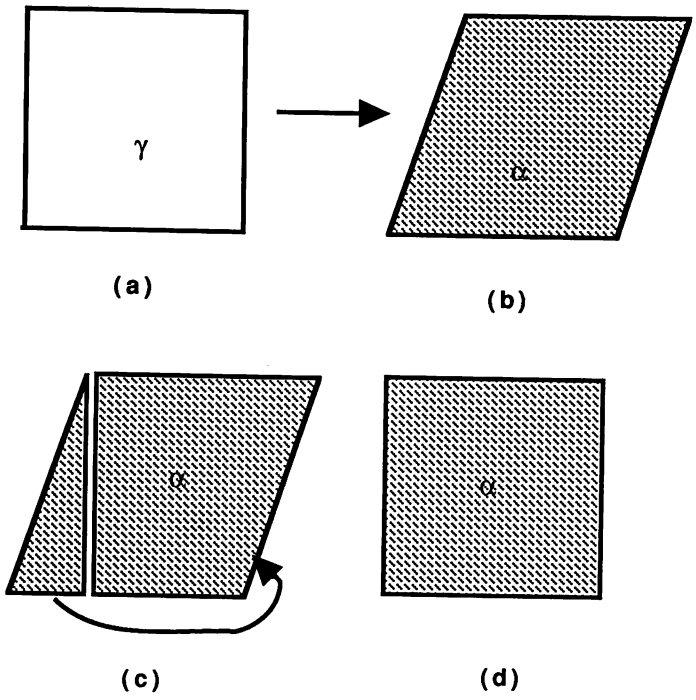

Fig. 2.9 *Schematic illustration of the mass transport necessary to achieve reconstructive transformation, in both pure metals and alloys. Steps (a) to (b) represent displacive transformation, whereas (a) to (d) represent reconstructive transformation. The mass transport illustrated in (c) eliminates the shape change due to the shear.*

The behaviour of the atoms on substitutional sites during transformation is critical in specifying the mechanism of change. The iron and substitutional atoms (X) do not diffuse during displacive transformation, so that the ratio of Fe/X atoms is expected to be constant throughout a transforming crystal, even on the finest conceivable scale.

During reconstructuve transformation, the atoms transfer across the interface in an uncoordinated manner which accomplishes the required lattice change and simultaneously ensures a minimisation of the strain energy. This requires the thermally activated migration (in the interface region at least) of all the atoms, irrespective of whether the transformation occurs in a pure metal or in an alloy (Fig. 2.9). There will normally be a volume change associated with the stress free change of structure, and at sufficiently high temperatures this may be compensated by a flux of vacancies (and an opposite flux of atoms) between the growing precipitate and the dislocations, grain boundaries and (ultimately) the free surface of the parent phase. At temperatures where the rate of diffusion in

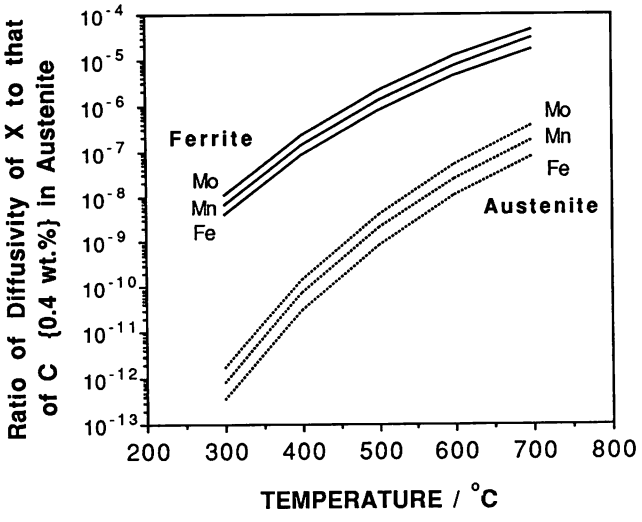

Fig. 2.10 *A comparison of the mobilities of iron and substitution solutes relative to that of carbon (in austenite at a concentration of 0.4 wt%), in FCC and BCC iron, over the bainite transformation temperature range (data from Fridberg* et al., *1969).*

the parent phase is inadequate for such an adjustment, reconstructive growth with minimum strain energy will still be possible if the precipitate has a lenticular (tapered plate) shape, and the reconstruction takes place in such a way that the volume change is simply an expansion or contraction normal to the plane of the lens. This can be achieved by atomic migration entirely within, or in the limit around, the particle. Reconstructive growth is, however, scarcely feasible unless all atoms have some mobility in the incoherent interface, roughly equivalent during the time of growth to a diffusion distance of the order of magnitude of the dimensions of the particle.

This necessary mass flow has been described as 'reconstructive diffusion' and the two classes of transformation have been called 'diffusional' and 'displacive' (Bhadeshia, 1985b) in place of the older divisions, mentioned above, into 'reconstructive' and 'displacive' or 'civilian' and 'military'. Bainite was one of the first transformations for which this wider classification was needed to replace the original division into 'nucleation and growth' and 'martensitic' transformation, (see Christian, 1965a, b, 1975). The term 'diffusional transformation' is avoided here since it refers only to the motion of the Fe+X atoms. If diffusional is used as one main category, there is the apparent paradox that a displacive transformation in which there is segregation of carbon during growth has

to be described as 'non-diffusional' even though the growth rate might be controlled by the diffusion rate of carbon!

In an alloy in which there is some atomic mobility within the parent phase, the reconstruction provides an opportunity for the solvent and solute atoms to redistribute between the two phases. However, in a system such as Fe–C–X, the diffusion rate of carbon in the austenite may be many orders of magnitude greater than that of a substitutional atom in the temperature range of interest (Fig. 2.10) and these very different rates of atomic migration mean that true equilibrium segregation with regard to all components may not be produced at a migrating interface. It is, however, possible to envisage growth under diffusion control with local equilibrium at the interface in the sense that the compositions of the two phases are joined by a tie line of the equilibrium diagram, even though this tie line does not pass through the point representing the initial (or average) composition of the alloy. When these kinetic restrictions apply, the two phases may differ either significantly or negligibly in substitutional solute content. A qualitative analysis for ternary steels was first developed by Hillert (1953), and a simplified quantitative theory in which diffusion cross terms are neglected was developed by Kirkaldy (1958), Purdy *et al.* (1964), and Coates (1972); the effect of the cross terms was later examined by Coates (1973a, b). The theory shows that for the diffusion controlled growth of ferrite from austenite in an Fe–C–X alloy with initial composition near the $\gamma/\alpha+\gamma$ phase boundary (i.e. with a small supersaturation), the tie line selected will have the carbon composition of the austenite at the interface almost equal to that of the bulk alloy so that the activity of carbon is nearly constant in the austenite, thus reducing the driving force for carbon diffusion almost to zero. There will be a concentration gradient of the substitutional solute ahead of the interface (Fig. 2.11), resulting in appreciable partition, and the relatively slow growth rate will be determined by the diffusion rate of this solute. For large supersaturations, the tie line will have the Fe+X composition of the ferrite virtually identical with that of the bulk austenite, partitioning of the substitutional solute will be extremely small, with a relatively fast growth rate. These are referred to as the partitioning local equilibrium (P–LE) and negligible partitioning local equilibrium (NP–LE) growth modes respectively (Purdy *et al.*, 1964; Coates, 1973b), and for a high ratio of the diffusivities, the theory predicts an abrupt transition from one to the other as the supersaturation increases.

In the NP–LE mode, the concentration of X is uniform except for a small 'spike' in the parent phase adjacent to the interface. As the ratio of interstitial: substitutional diffusion rates increases, the width of this spike decreases, and when it becomes of the order of atomic dimensions, the concept of local equilibrium at the interface is invalid and has to be

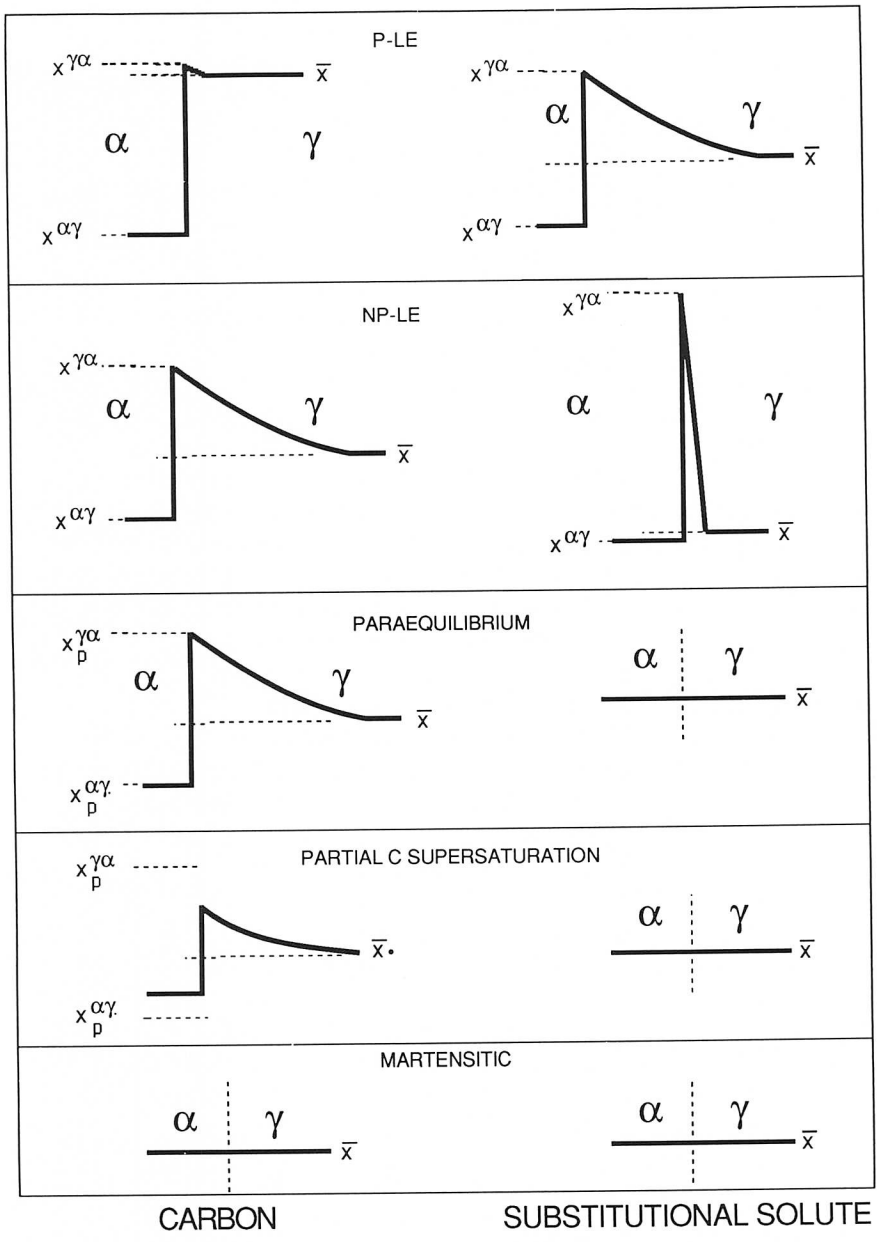

Fig. 2.11 *Schematic illustration of the composition variation expected in the vicinity of the transformation interface, for a variety of growth mechanisms.*

replaced (assuming the growth is nevertheless diffusion controlled) by that of paraequilibrium (Hultgren, 1951; Rudberg, 1952; Aaronson *et al.*, 1966a, b). In conditions of paraequilibrium, there is no redistribution of Fe + X atoms between the phases, the Fe/X ratio remaining uniform right up to the interface. One interpretation of the paraequilibrium limit is that reconstructive transformation occurs with all displacements of the Fe+X atoms taking place in the incoherent interface; another interpretation might be that only displacive transformation can occur. In either case, to quote from Coates, 'the slower diffuser and the solvent participate only in the change of crystal structure'. Paraequilibrium implies that the growth rate is controlled by the interstitial diffusivity, the interface compositions now being given by the tie lines of the pseudo-equilibrium between the two phases under the constraint of a constant Fe/X ratio.

In conclusion, the experimental evidence that bainitic ferrite has the same bulk substitutional content as its parent austenite is consistent with both reconstructive and displacive mechanisms for the change in crystal structure. However, reconstructive transformation with local equilibrium (or indeed any state between local and paraequilibrium) requires some perturbation of the substitutional solute content in the proximity of the interface. Very detailed atom probe experiments which have a chemical and spatial resolution on an atomic scale (Bhadeshia and Waugh, 1981, 1982; Stark *et al.*, 1988, 1990; Josefsson and Andren, 1988, 1989) have all failed to show any evidence of such redistribution of alloying elements (Cr, Mn, Mo, Ni, Si) at the interface between bainitic ferrite and austenite (Fig. 2.12). These experiments were all based on steels where other reactions, such as the precipitation of carbides, do not interfere with the formation of bainitic ferrite. Measurements of the growth rates of grain boundary allotriomorphs of ferrite from austenite in alloy steels under conditions where bulk segregation is not observed (e.g. Kinsman and Aaronson, 1973; Bradley *et al.*, 1977) indicate calculated thicknesses of the spike of much less than 0.1 nm, and although these results are complicated by the effect of grain boundary diffusion, they are in general agreement with the concept that the lattice diffusion rate is inadequate to sustain local equilibrium at the growing interface. Only at temperatures above 600°C, has the segregation of some (though by no means all) substitutional elements been obtained in grain boundary allotriomorphs (Aaronson and Domian, 1966b). Allotriomorphs are agreed to form by reconstructive mechanisms, but the absence of bulk segregation at moderately high transformation temperatures reinforces the belief, derived from the observed shape change, that bainitic ferrite forms at lower temperatures by a displacive rather than a reconstructive mechanism.

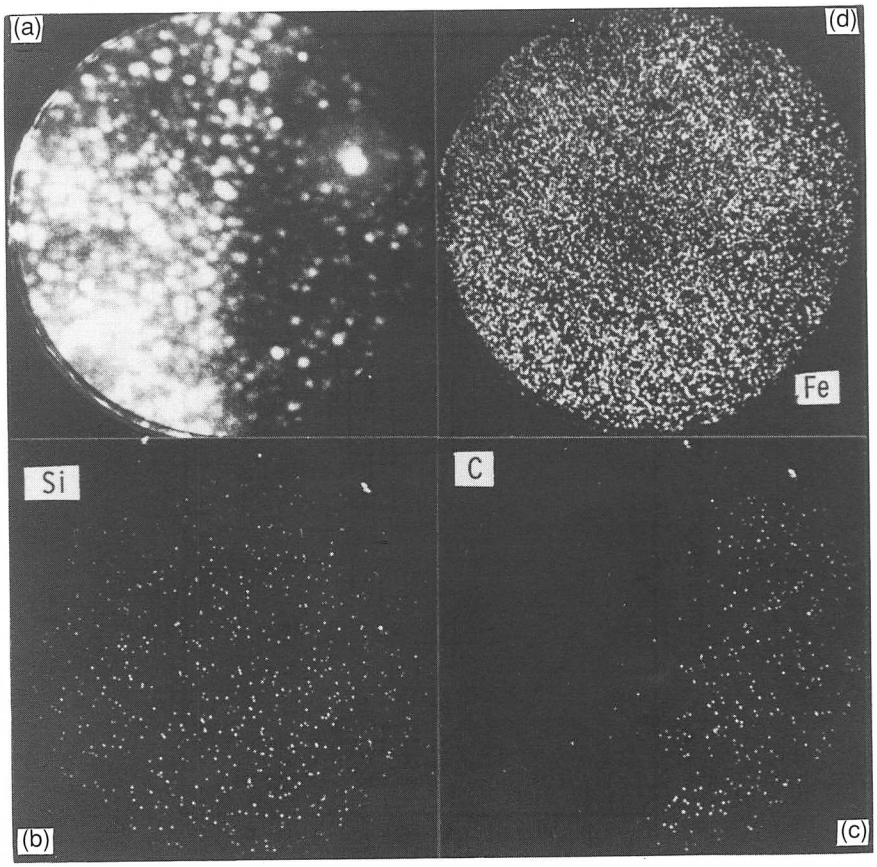

Fig. 2.12 *Imaging atom-probe micrographs, taken across an austenite-bainitic ferrite interface in a Fe–C–Si–Mn alloy. The images confirm quantitative data (Bhadeshia and Waugh, 1982) showing the absence of any substitutional atom diffusion during transformation. (a) Field-ion image; (b) corresponding silicon map; (c) corresponding carbon map; (d) corresponding iron map.*

2.3.2 *Interstitial Alloying Elements*

A particular experimental difficulty with the bainite transformation is that in the case of upper bainite at least, it is almost impossible to say anything about the initial carbon content of the ferrite. This is because the time taken for any carbon to diffuse from the supersaturated ferrite into the austenite can be very small. For the moment we refer to the interstitial content of bainitic ferrite *after* transformation. As will be seen later, the concentration *during* transformation is likely to be different.

Internal friction experiments indicate that the amount of carbon which associates with dislocations in bainitic ferrite increases as the transformation

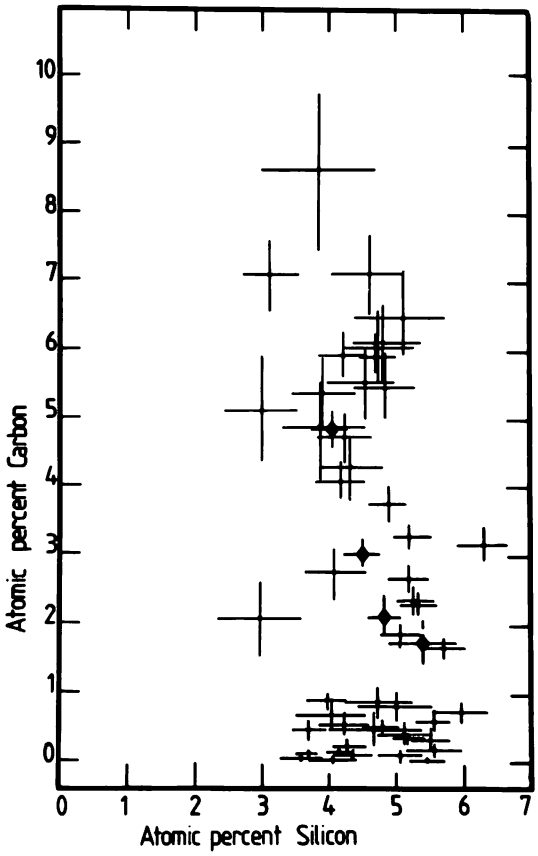

Fig. 2.13 *Atom probe determinations of the carbon and silicon concentrations of bainitic ferrite in an Fe–C–Mn–Si alloy transformed to upper bainite (Bhadeshia and Waugh, 1982). The average carbon concentration in the alloy is 1.93 at.%, so that all concentrations below the level are measurements from bainitic ferrite. Note that they are all significantly larger than would be expected from equilibrium.*

temperature decreases, but is independent of the average carbon concentration in the steel, at least in the range 0.1–0.4 wt%C (Pickering, 1967). This is consistent with the observation that the dislocation density of bainitic ferrite increases with a decrease in transformation temperature. The insensitivity to the alloy carbon concentration is because most of the carbon ends up in the residual austenite. The results also show that at some stage during the evolution of bainitic ferrite, it must have contained a higher than equilibrium concentration of carbon.

These observations have been confirmed directly by using microanalysis on an imaging atom probe, which has demonstrated quantitatively (Fig. 2.13)

that the *post-transformation* carbon content of bainitic ferrite tends to be significantly higher than equilibrium (Bhadeshia and Waugh, 1982; Stark *et al.*, 1988, 1990; Josefsson and Andren, 1988, 1989).

2.4 Crystallography

The properties of bainitic steels are believed to depend on the crystallographic texture that develops as a consequence of transformation from austenite. As an example, the ease with which slip deformation is transmitted across the adjacent platelets of bainitic ferrite must be related to their relative orientation in space. Bainite grows in the form of clusters of platelets called sheaves, with little misorientation between the platelets within any given sheaf. Where they touch, adjacent platelets are separated by low misorientation grain boundaries.

The relative orientations of the bainitic ferrite and its parent austenite are always close to the classic KS (Kurdjumov–Sachs, 1930) and NW (Nishiyama–Wasserman, 1934) relationships (Fig. 2.14), although as will become evident later, they can never be exactly KS or NW. These two rational relations differ only by a relative rotation of 5.25° about the normal to the parallel close-packed planes of the two structures, and the exact relative orientation is found in martensites to be intermediate and irrational, as is predicted by the crystallographic theory. High accuracy is required to compare theory with experiment since the predicted orientation relation is insensitive to input parameters such as lattice spacings or lattice invariant deformation. In the case of bainite, as in that of lath martensite, such precision is difficult to achieve partly because of the

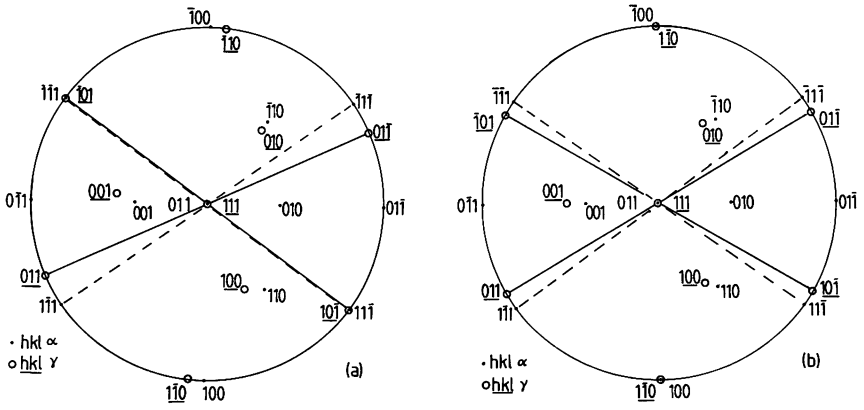

Fig. 2.14 *Sterographic representation of the (a) Kurdjumov–Sachs and, (b) Nishiyama–Wasserman orientation relationships. Note that NW can be generated from KS by a rotation of 5.25° about* $[0\ 1\ 1]_{\alpha}$.

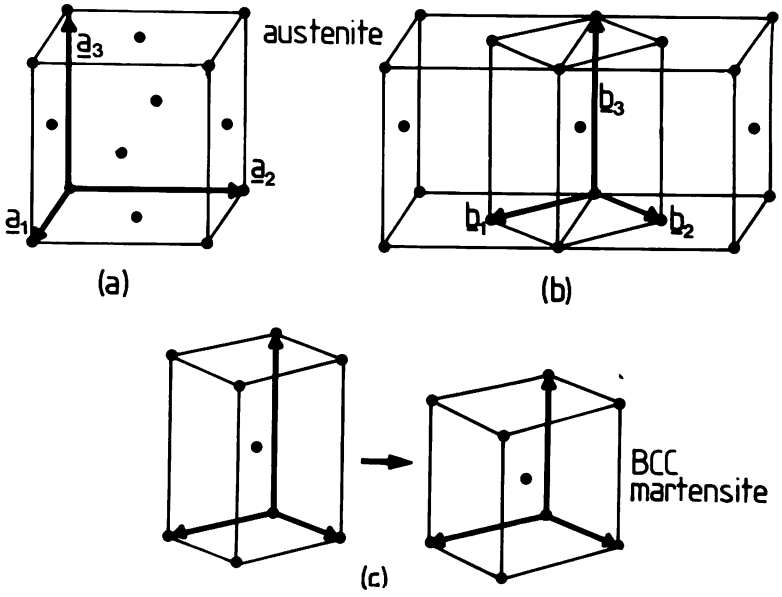

Fig. 2.15 *An illustration of the Bain deformation. (a) Conventional face centered cubic unit cell. (b) Relation between the FCC and body centered tetragonal unit cell representations of austenite. (c) Bain strain deforming the austenite lattice into a body centered cubic lattice.*

experimental difficulties in retaining austenite and partly because of the high dislocation densities.

In spite of these difficulties, it is significant that the experimental data always lie well within the 'Bain region' which encompasses the KS and NW relationships. The Bain strain is the pure part of the lattice deformation which for displacive transformations in steels converts austenite into ferrite or martensite (Fig. 2.15, Bain, 1924). During the Bain strain, no plane or direction is rotated by more than 11° so that any pair of corresponding planes or directions may be made parallel by utilising a lattice deformation in which the Bain strain is combined with a rotation of not more than 11° (Crosky *et al.*, 1980). This defines the Bain region, and for a displacive transformation, it is expected that the experimentally observed orientation relation will lie within this region. This need not be the case for reconstructive transformations, and allotriomorphic ferrite in steels is known to grow into austenite grains with which it has an orientation which is random or outside of the Bain region (King and Bell, 1975). Hence it is very significant that bainitic ferrite always exhibits an orientation which is close to KS or NW, and well within the Bain region.

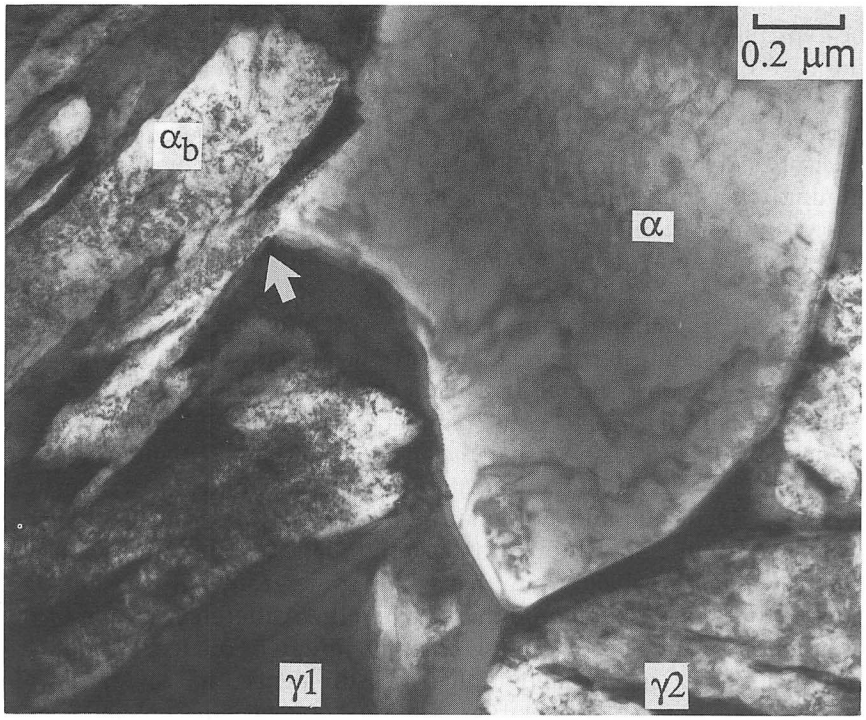

Fig. 2.16 *Transmission electron micrograph showing an allotriomorph of ferrite at an austenite grain boundary. The allotriomorph is related to the austenite grain* γ_1 *by an orientation relationship which is close to KS, but is randomly orientated with respect to the other grain* γ_2*. Consequently, a bainite plate has been able to nucleate from the allotriomorph only on the side where the orientation is suitable.*

There is an interesting consequence of the requirement that bainite must have an orientation with the austenite, which is within the Bain region. It is accepted that allotriomorphic ferrite, during austenite grain boundary nucleation, must also grow with an orientation relationship which is close to KS or NW in order to minimise the activation energy for nucleation. On the other hand, the growth of such ferrite occurs by a reconstructive mechanism, and occurs most rapidly along austenite grain boundaries with which the ferrite has a random orientation. It therefore grows selectively away from its original nucleation sites, so that it has a random orientation with the austenite along a large fraction of its interface with the austenite. It is then found that bainite can only nucleate directly from allotriomorphic ferrite if the latter is in the right crystallographic orientation (within the Bain region), but as expected, not when the orientation is random (Fig. 2.16).

Pickering (1967) has suggested that the crystallography of bainite can be explained if the individual platelets or laths adopt different variants of the NW or KS orientations, such that the ferrite orientations within a sheaf can be generated simply by rotation about the normal to a specific close packed plane of the austenite. In this way, the bainite laths may nucleate side by side in rapid succession, the transformation strains determining the variant and hence the exact sequence. This early work was based on measurements of only ferrite–ferrite orientation relations, since the specimens may have contained only thin films of austenite which are observable only with high resolution microscopy. However, it must be admitted that results from more recent work in which measurements of the direct austenite–ferrite relations have been made are still rather contradictory. There is general agreement that adjacent platelets or laths in bainite all have a $\{1\ 1\ 0\}_\alpha$ plane parallel (or almost parallel) to the same close-packed $\{1\ 1\ 1\}_\gamma$ and that the macroscopic habit plane is near to $\{1\ 1\ 1\}_\gamma$ in upper bainite but is irrational in lower bainite. Most investigators (e.g. Bhadeshia and Edmonds, 1980a; Sandvik, 1982a) find all the platelets within a sheath or 'sub-packet' to have a common orientation, but Sarikaya *et al.* (1986) claim that whilst some groups of adjacent laths have a common orientation, others have either different variants of the orientation relationship, or in lower bainite are twin-related. Similar discrepancies exist in crystallographic measurements on lath martensite where three types of orientation relation between adjacent laths of a packet are reported by some workers (Eterasivili *et al.*, 1979; Sarikaya *et al.*, 1986) and only one common orientation by others (Wakasa and Wayman, 1981; Sandvik and Wayman, 1983).

When there is a common orientation, the platelets within a sheaf have small misorientations; there is also an appreciable spread of orientation within a single platelet because of its high dislocation density. Direct crystallographic analysis indicates that all platelets within a 'sub-packet' have an irrational orientation with the austenite which is rather closer to NW than to KS (Sandvik, 1982). Moreover, the shape deformations of all the platelets are identical, Fig. 2.17, in agreement with earlier work (Srinivasan and Wayman, 1968b; Bhadeshia and Edmonds, 1980a). One further crystallographic observation made by Sandvik is of considerable interest. He found that twins formed in the austenite adjacent to the ferrite, and that the ferrite laths were able to grow through the twins, producing a reorientation of the lattice and also displacing the direction of the twin boundaries in the manner expected for a displacive (shear) transformation.

Similar results for the relative orientations of adjacent platelets were obtained in a careful examination of lath martensite by Sandvik and Wayman, using an iron–nickel-manganese alloy which contained appreciable retained austenite (Sandvik and Wayman, 1983). They found that

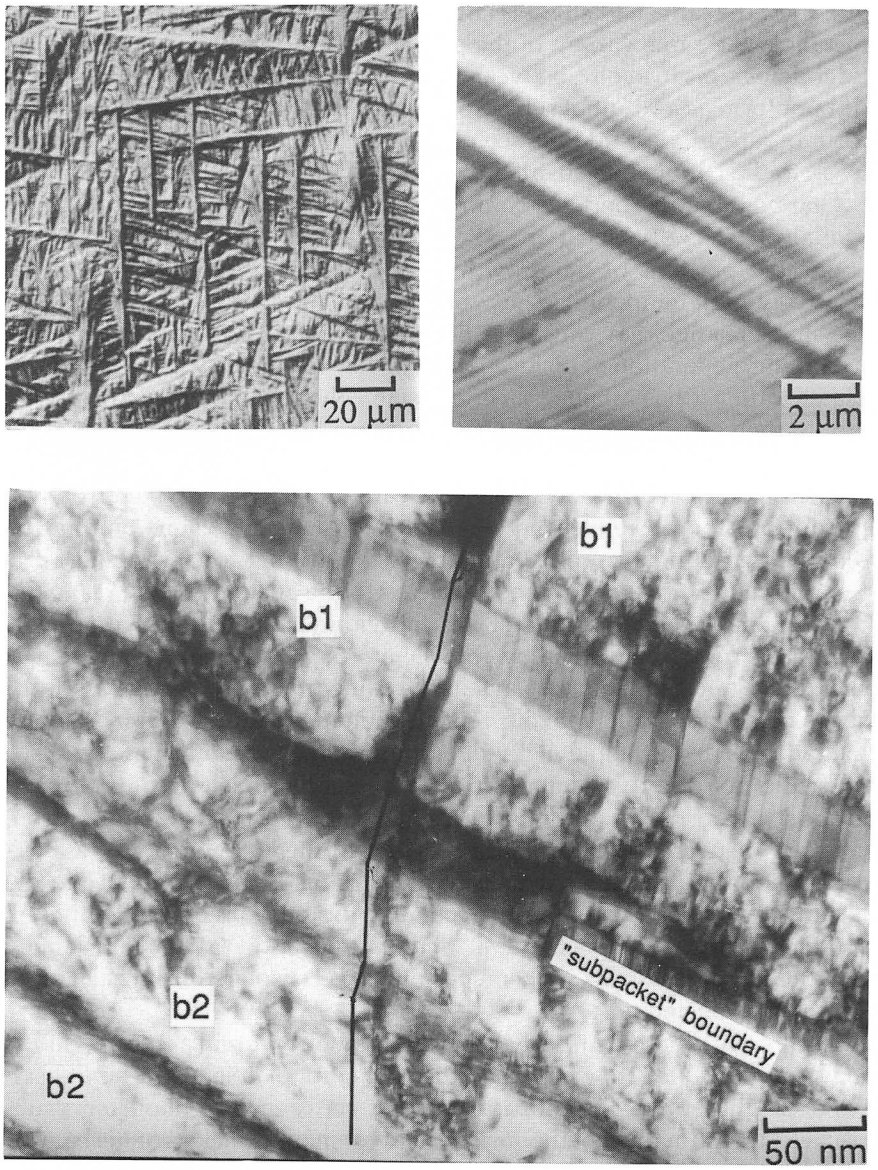

Fig. 2.17 *(a) Nomarski differential interference contrast micrograph showing the general surface displacements due to upper bainite. (b) Higher magnification Nomarski image showing identical surface relief for all the sub-units within a given sheaf. (c) Sandvik's experiment showing the displacement of twin boundaries (parallel to the black line) caused by individual sub-units of bainite. The ferrite variants b1 and b2 belong to separate sheaves.*

although the laths had slight relative misorientations of up to 2°, they all exhibited the same variant of the parent–matrix orientation relation, and thick layers of austenite between adjacent laths indicated that the laths did not form as a result of self accommodation of their shape strains. This form of lath martensite thus seems to be very similar, in substructure at least, to the bainite investigated by Sandvik.

One possible reason for a common orientation might be that the individual platelets of a sheaf are not separate crystals but are continuously connected portions of the growth front of one original nucleus. At the relatively high temperatures at which bainite (and lath martensite) form, the shape change may cause plastic deformation of the structure leading to copious generation of dislocations which stops the forward growth of a platelet after it has attained a certain size. 'Nucleation' of a new platelet would then simply be resumed growth caused by breakaway of a part of the original interface in a region near but not at the tip. In bainite, the growth would resume only after some carbon had been rejected from the ferrite into the austenite and would be most likely where pinning by dislocation debris is minimal and where the driving force is highest due to rapid dispersion of the carbon rejected to the austenite.

An alternative model is that the individual platelets are completely separated from each other by thin layers of austenite, so that each is separately nucleated, but always in the same orientation. In general, the stress field at the tip will favour renucleation in the same variant, whereas that at the side of the platelet will favour another variant (Fig. 2.18). The nucleation of other variants is of course essential if self-accommodating groups are to form, and thus must be suppressed for some reason, perhaps because adjacent sheaves are formed together in a self-accommodating fashion. At present, there is insufficient evidence to determine whether either of these speculative descriptions is valid, although Srinivasan and Wayman, Sandvik, and Sandvik and Wayman all claimed that the individual laths in their specimens were isolated from each other by retained austenite.

As already mentioned, early conclusions about mutual accommodation may have applied to sheaves rather than to platelets in each sheaf. Sandvik measured the misorientations between neighbouring 'sub-packets' (presumably neighbouring sheaves) in one 'packet' of his bainitic alloy and found that these correspond to different variants of his irrational orientation relation in which the same austenite {1 1 1} plane is parallel to a ferrite {1 1 0} plane. The six variants which satisfy this condition lead to four different relative orientations, one of which is only 3° from the original orientation and the others are respectively 8°, 11° and 14° away from a twin orientation. Sandvik comments that the first misorientation is difficult to detect, and that it is difficult to distinguish the remaining three

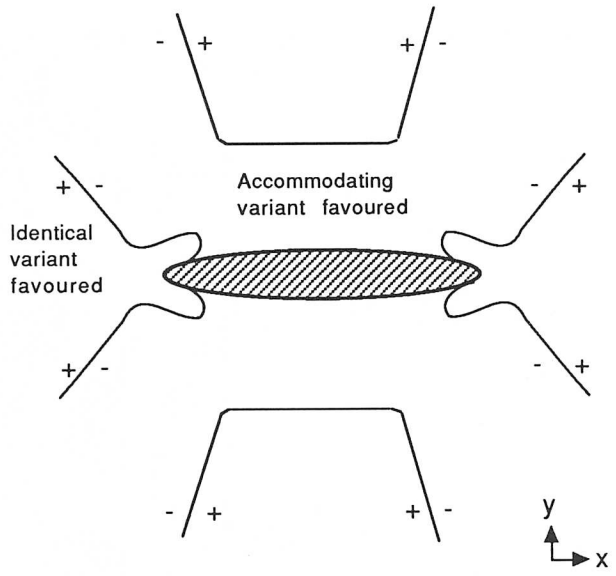

Fig. 2.18 *Stress field contours of a martensitic particle lying in the xz plane with the transformation shear in the x direction. The positive signs represent regions where plates with the same shear direction are favoured, whereas the regions with the negative signs favour the formation of accommodating variants (Olson and Owen, 1976).*

from each other. He also comments that only the variant with orientation relation 14° from a twin relationship gives efficient self-accommodation, and this was observed fairly infrequently. Adjacent sub-packets are thus attributed to random association, although it is not clear why they should then all have the same pair of parallel close packed planes. Sandvik and Nevalainen have also suggested that adjacent sheaves of bainitic ferrite are approximately twin related, and correspond to variants of a near NW orientation. Recent transmission electron microscopy by Josefsson (1989) has confirmed these observations in a Fe–Cr–Mo–C steel.

2.4.1 *Autocatalytic Nucleation*

Autocatalytic nucleation is a term commonly associated with martensitic transformations (Raghavan and Entwisle, 1965; Magee, 1970). The nucleation of martensite in steels is believed to begin at structural imperfections in the parent phase, such as arrays of dislocations. These are the pre-existing defects which, on cooling below the M_s temperature dissociate into suitable partial dislocations in a way which leads to the nucleation of martensite (Olson and Cohen, 1976a–c). The defects are not all identical (they vary in potency) and are stimulated to grow into plates of martensite at

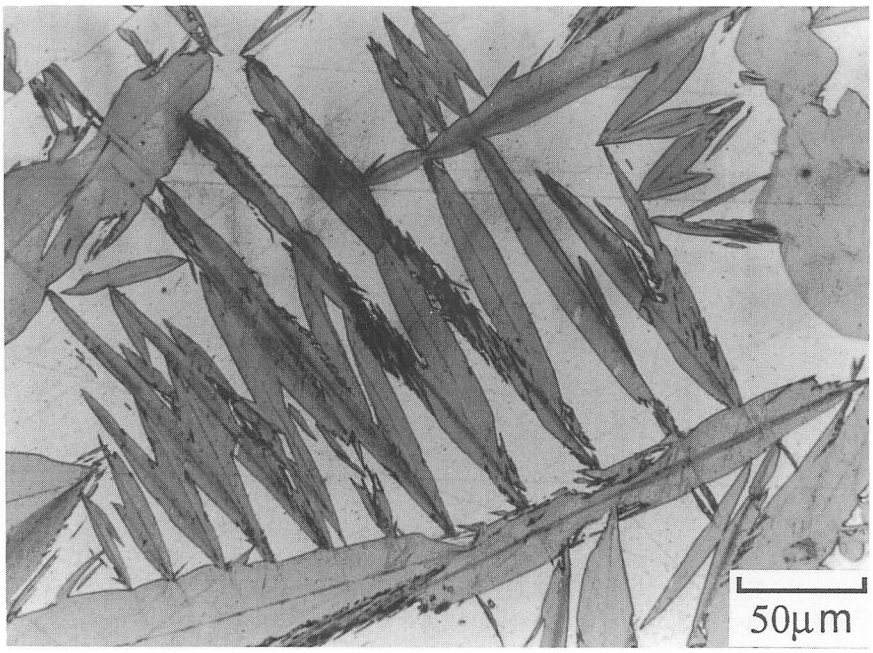

Fig. 2.19 *A burst of autocatalytic martensitic transformation in a Fe–30Ni–0.31C wt% alloy. Such bursts are not observed during bainitic transformation.*

different degrees of undercooling below the M_s temperature. This is the cause of the classical behaviour observed for athermal martensitic reactions, in which the volume fraction of martensite varies only with the undercooling below M_s.

Detailed analysis reveals that the initial number density of pre-existing defects typically found in austenite is not large enough to explain the kinetics of martensitic transformation. The extra defects necessary to account for the faster than expected transformation rates are attributed to autocatalysis: when plates of martensite form, they induce new embryos which are then available for further transformation. Three mechanisms have been proposed for autocatalysis (Olson and Cohen, 1981). In stress assisted nucleation, the activation of less potent defects at a given temperature is induced by the internally generated elastic stresses arising as a consequence of the shape change due to transformation. In strain induced autocatalysis, the creation of new and more potent nucleating defects is induced by some plastic accommodation in the parent phase. Finally, 'interfacial autocatalysis' refers to the nucleation of new martensitic units from the existing martensite/austenite interfaces. Autocatalysis is responsible for the 'bursts' of transformation (Fig. 2.19) that occur in certain

martensitic steels, whence the initial formation of a plate stimulates a disproportionately large degree of further transformation, sometimes causing the emission of audible clicks.

All of these effects arise as a consequence of the severe elastic and plastic disturbance of the austenite in the immediate vicinity of a plate of martensite. It is the shape change due to the martensitic transformation that is the cause of the disturbance. On this basis, autocatalysis should also feature prominently in bainitic transformations which are accompanied by similar shape deformations. There is however, a significant difference in that bainite grows at relatively small driving forces, where defects induced by transformation do not seem to play as crucial a role in stimulating further nucleation. The initial nucleation event is almost always confined to the austenite grain surfaces, which presumably contain the most potent defects for nucleation. Intragranular nucleation of bainite can essentially be ignored except when non-metallic particles may act as nucleation surfaces. The initial formation of a platelet of bainite (or of a lath of martensite) must lead to appreciable elastic and plastic strains, but this does not seem to cause the nucleation of other platelets in different orientations, as happens with plate martensite, and 'bursts' of transformation are not observed. In the case of bainite, this may be because the driving force is only adequate for the formation of a carbon-free nuleus, and thus it may be nmpossible to form in the carbon enriched region around an existing platelet. Whatever the reason, it seems that strain induced autocatalysis does not play an important role in bainite formation. As already discussed, there is some evidence for stress assisted autocatalysis if it is indeed true that adjacent sheaves form in such a way as to help accommodate each other's shape deformation.

The concept of autocatalytic nucleation may be related to that of sympathetic nucleation, defined by Aaronson and Wells (1956) as the nucleation of a precipitate crystal at the interphase boundary of a previously formed crystal of the same phase when the matrix and precipitate differ in composition. Although in discussing sympathetic nucleation, volume strain energy 'can be effectively ruled out' according to Aaronson (1962), it seems clear that many examples of this phenomenon would alternatively be interpreted as autocatalytic nucleation by other workers.

2.4.2 *Phenomenological Theory*

A major feature of martensitic transformations is the shape deformation $\underline{P}$, which on a macroscopic scale has the characteristics of an invariant plane strain. However, an application of the homogeneous deformation $\underline{P}$ to the face centered cubic (FCC) lattice, does not produce the required body centered cubic (BCC) or body centered tetragonal (BCT) lattices. In

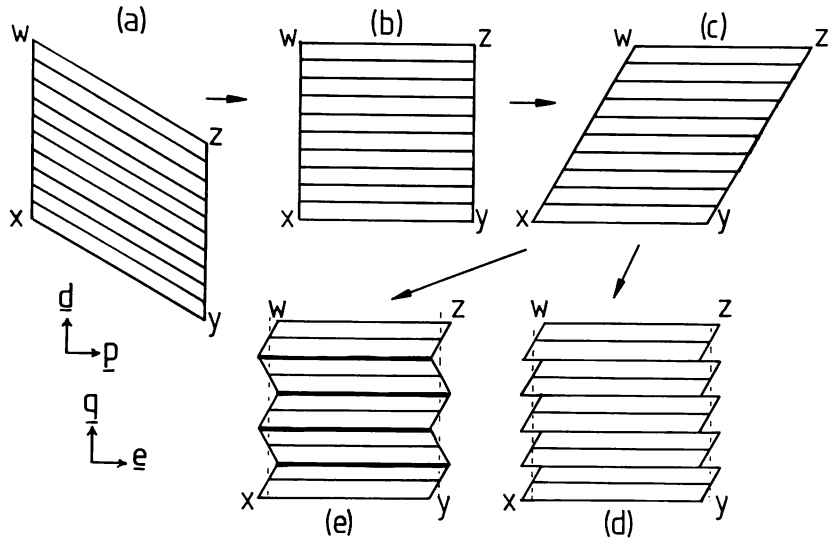

Fig. 2.20 *An illustration of the essential features of the phenomenological theory of martensite crystallography. (a) represents the austenite crystal and (c), (d) and (e) all have a body centered cubic structure. (b) has an intermediate structure between FCC and BCC (or BCT),* p *is the habit plane unit normal and* q *is the unit normal to the plane on which the lattice invariant deformation occurs. Although (c) has the BCC structure, its shape is inconsistent with the observed invariant plane strain. The effect of the inhomogeneously applied lattice invariant deformations (d, e) is to correct the shape change to an IPS, without altering the structure. The bold horizontal lines in (e) are coherent twin boundaries. Note that the vector* e *is normal to* q *but does not lie in the plane of the diagram.*

fact, the homogeneous lattice deformation $\underline{S}$ capable of changing the parent lattice into that of the product is not an invariant plane strain, but a combination of the Bain strain ($\underline{B}$, a pure strain) and an appropriate rigid body rotation $\underline{R}$, which has to be such as to make the deformation $\underline{S}$ an invariant-line strain. Consequently, the observed shape deformation is not reproduced by $\underline{S}$. The anomaly is resolved by the inclusion of an inhomogeneous lattice-invariant deformation $\underline{Q}^{-1}$, which leaves the unit cells unchanged but the shape change produced macroscopically by the combined effects of $\underline{S}$ and $\underline{Q}^{-1}$ is then an invariant plane strain (Fig. 2.20):

$$\underline{P} = \underline{Q}^{-1}\underline{R}\,\underline{B} = \underline{Q}^{-1}\underline{S} \tag{2.2}$$

We have seen that the bainite transformation exhibits crystallographic features and surface relief effects identical to those associated with martensitic reactions. It is then natural to assume that the phenomenological theory of martensite crystallography (Wechsler *et al.*, 1953; Bowles and

Mackenzie, 1954) should be applicable to bainite. The crystallographic theory predicts a unique relationship between the habit plane, shape deformation, orientation relationship, lattice types and lattice invariant deformation. It can only be tested satisfactorily when these variables are not determined in isolation. Much of the early data (reviewed by Bowles and Kenon, 1960) are incomplete in this sense, although consistent with the theory. All of the early measurements of habit planes must now be interpreted to refer to the habit planes of bainite sheaves, rather than of the individual sub-units.

A considerable difficulty in applying the theory to bainite is the lack of accurate structural information relating to the transformation which is needed as input data. Thus if bainite grows with a full supersaturation but the carbon escapes in a very short time, the measured lattice parameters of upper bainitic ferrite will not relate to the initially formed structure, which may even have been tetragonal. A problem exists for lower bainite if appreciable carbide precipitation has taken place before any measurements are possible.

Srinivasan and Wayman (1968b, c) reported the first detailed results on the crystallography of sheaves of lower bainite in a Fe–1.11C–7.9Cr wt% alloy ($B_s \approx 300°C$, $M_s \approx -34°C$) in which large quantities of austenite remained untransformed at ambient temperature. Each sheaf was found to have just one planar face when examined using light microscopy, and this was taken to be the habit plane. The (irrational) habit plane indices being close to $(2\ 5\ 4)_\gamma$ relative to the orientation variant in which $(1\ 1\ 1)_\gamma$ is almost parallel to $(0\ 1\ 1)_\alpha$ and $[\bar{1}\ 0\ 1]_\gamma$ is at a small angle to $[\bar{1}\ \bar{1}\ 1]_\alpha$; this is henceforth called the *standard variant*. The martensite habit plane in the same alloy is close to $(4\ 9\ 4)_\gamma$ and the difference in the two habits and in the exact orientation relations led Srinivasan and Wayman to the conclusion that the mode of displacive transformation is different in bainite and martensite. Their measured habit plane is only about 6° from that found for a different alloy by Sandvik, who pointed out, however, that his result applied to an individual platelet whereas that of Srinivasan and Wayman was for the average 'habit' of a sub-packet or sheaf.

The shear component of the shape deformation, as averaged over the entire sheaf, was measured to be ≈ 0.128, the magnitude of the total shape strain being ≈ 0.129. This is consistent with the earlier data of Tsuya (1956) and Speich (1962). The actual shape strain for an individual sub-unit must of course be larger, and was estimated using crystallographic theory as being ≈ 0.23; this compares with the ≈ 0.28, 0.25 and 0.22 estimated for different alloys by Ohmori (1971a), Bhadeshia (1980a) and Sandvik (1982a) respectively. These values are in good agreement with a measurement of the shear component of the shape strain (0.22) of an individual sub-unit, reported by Sandvik (1982a).

Srinivasan and Wayman showed that their data on lower bainite are indeed consistent with solutions based on the phenomenological theory of martensite. The crystallography was, as expected, inconsistent with the inhomogeneous lattice invariant deformation being twinning, since transformation twinning is not observed in bainitic ferrite. It was found that the sheaf habit plane and orientation relationship could be predicted for an undistorted habit plane if it is assumed that the lattice invariant shear is irrational in both plane and direction. On the other hand, if the habit plane is permitted to undergo a small isotropic contraction, then the lattice invariant shear (for the standard variant) consists of a double shear on the planes $(1\ \bar{1}\ 1)_\gamma$ and $(1\ 0\ 1)_\gamma$ in the common direction $[\bar{1}\ 0\ 1]_\gamma$ (these correspond to $(1\ 0\ 1)_\alpha$, $(1\ 1\ 2)_\alpha$ and $[\bar{1}\ \bar{1}\ 1]_\alpha$ respectively). This double system is equivalent to a single shear on an irrational plane, and is not associated with any of the difficulties encountered in theories which postulate more general combinations of lattice invariant shears. The component planes on which the interface dislocations would glide are those most usually considered as candidates for single lattice invariant shears in the martensite theory. However, at the time of the Srinivasan and Wayman work, it was not fully appreciated that the so-called habit plane of a sheaf (which they measured) may differ from that of a platelet within a sheaf (which Sandvik measured), and it is not yet clear whether the phenomenological theory of martensite should be applied to the sheaf or the platelet. It may be more important to minimise long-range distortions over the whole sheaf, in which case the invariant plane condition would apply to the apparent habit plane of the sheaf, but in cases where there are reasonably thick layers of austenite between the platelets, it seems more logical to apply the theory to the individual platelet.

Hoekstra and his co-workers (1978a, b, 1980) have recently examined the crystallography of bainite in an Fe–0.35C–0.25Si–0.6Mn–4.5Ni–1.3Cr wt% alloy isothermally transformed at 365°C. They used hot-stage light microscopy and a technique for determining the orientation of the austenite using twin vestiges, so that the resulting habit plane data they obtained are assumed to refer to the sheaf habit plane, which was found to be irrational with means indices $\{5\ 6\ 9\}_\gamma$. They observed a small degree of scatter which they attributed to the development of internal stresses during transformation. The orientation of the ferrite was determined using electron diffraction and the habit plane indices with respect to the ferrite were determined using the criterion that a unique orientation relationship and habit plane should emerge from an analysis of three sets of experimental data. It was deduced that the habit with respect to ferrite was $\approx \{2\ 7\ 10\}_\alpha$, with the orientation relation being very close to Kurdjumov–Sachs. On these grounds, it was concluded that the crystallography of bainite in their samples was inconsistent with the pheno-

menological theory of martensite. The analysis (Fig. 5, Hoekstra, 1980) does not however seem correct because the angles made by the habit plane pole to the $\{1\ 1\ 1\}_\gamma \| \{0\ 1\ 1\}_\alpha$ planes and to the $<1\ 0\ \bar{1}>_\gamma \| <1\ 1\ \bar{1}>_\alpha$ directions are not in fact the same for the three sets of data analysed. If the three sheaves are just crystallographic permutations, then the relationship between the habit plane and the orientation relation is uniquely defined in the phenomenological theory of martensite.

2.4.3 *The Shape Change: Further Considerations*

In discussing the application of the phenomenological theory of martensite to bainite, the classical view (Hull, 1954; Bilby and Christian, 1956; Christian, 1962) that the experimentally observed invariant plane strain shape deformation implies a coordinated movement of at least the iron and substitutional atoms was implicitly accepted. Given that there is some confusion in the literature about the interpretation of this shape change, particularly in circumstances where diffusion might accompany transformation, it is worth presenting here, some recent assessments of the significance of the shape change (Christian and Edmonds, 1984; Christian, 1990a). The problem is of major importance since the strain energy associated with the shape deformation when transformation occurs under constraint, cannot be ignored in the thermodynamic and kinetic descriptions of bainitic reactions, irrespective of the mechanism by which the shape change arises.

The intersection of a plate of bainitic ferrite with a free surface causes that surface to tilt about the lines of intersection. This is the description of an invariant plane strain, which is due to the combined effects of the lattice deformation and a lattice invariant deformation. The tilting produced is homogeneous on a macroscopic scale, indicating that the net atomic displacements include common non-random components which accumulate during growth. This is an obvious conclusion, but the term 'net atomic displacements' needs to be deconvoluted in order to assess the degree of diffusion which can be tolerated before the transformation must be regarded as a reconstructive reaction.

Focusing attention on equivalent lattice points which define unit cells (not necessarily primitive) of the two structures containing the same number of atoms, a change in shape will accompany transformation if the new set of lattice points can be related to the original set by a homogeneous deformation. It is then possible to specify (in a localised region at least) how particular vectors, planes and unit cells of one structure (defined by an imaginary labelling of the individual atoms) are derived from *corresponding* vectors, planes and unit cells of the other structure. This is termed a lattice correspondence and it defines the pure lattice

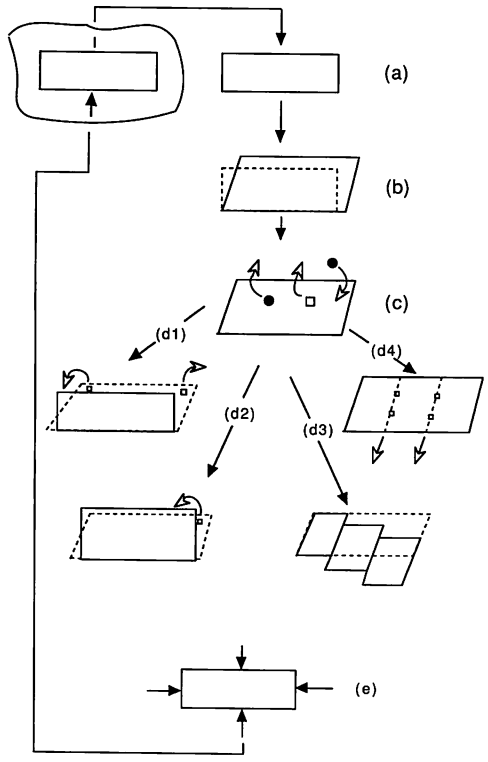

Fig. 2.21 *Schematic diagram illustrating the virtual operations required to form a particle in a constraining matrix (after Christian and Edmonds, 1984).*

deformation which carries the original lattice points, or some fraction of those points into points of the new lattice.

When interstitial atoms are present, they may move over large distances without affecting the correspondence; this is sometimes expressed by stating that there is an atomic correspondence for the solvent and substitutional solute atoms but not for the interstitials. A further relaxation of the condition is to allow the solvent and substitutional solute atoms to be displaced during transformation among the sites specified by the lattice correspondence, but not to create new sites or destroy any specified sites; in this way the lattice correspondence is preserved but there is no longer an atomic correspondence. Thus, a systematic shape change implies a lattice correspondence even if accompanied by some diffusion of atomic species. As will become evident later, the existence of this correspondence (and the shape change) requires an interface which is at least semi-coherent.

The detailed implications of the shape change on the mechanism of growth can be illustrated using the virtual operations illustrated in Fig. 2.21

(Christian and Edmonds, 1984). A region of the matrix is first removed (leaving behind an equivalent hole) and then allowed to undergo unconstrained transformation with the help of a homogeneous lattice deformation which is not in general an invariant-plane strain (Fig. 2.21a, b). The particle is then allowed to have any required composition by transferring suitable numbers of solute atoms between interstitial sites in the particle and the matrix, and/or by interchanging atoms of substitutional species in the particle with atoms in the matrix (operation c, Fig. 2.21).

A number of further operations are now possible before the particle is reinserted into the hole in the matrix, in order to reduce the strain energy:

(i) The volume and shape of the particle may be made equal to that of the hole, by transferring atoms over long distances from the particle to sinks within the matrix or at its surface (operation d_1, Fig. 2.21). The strain energy then vanishes.
(ii) The total number of atoms in the particle may be conserved but its shape may nevertheless be adjusted by the creation and removal of atom sites. The strain energy is effectively that of a hole in the matrix filled with a compressible fluid of different natural volume. For a plate shaped particle, the minimum in strain energy for this case corresponds to an IPS with a zero shear component, with the expansion or contraction being normal to the habit plane (operation d_2, Fig. 2.21). A plate shaped particle will give the lowest strain energy if the volume change is appreciable, but there will only be a *preferred* habit plane if there is appreciable anisotropy of either the elastic propeties or the surface energy of the interface.
(iii) The shape of the particle may be changed by conservative plastic deformation. The lowest strain energy for a plate shaped particle then occurs if the plastic deformation converts the lattice deformation into a shape deformation which is an IPS on the habit plane, as in the theory of martensite crystallography (operation d_3, Fig. 2.21).
(iv) The shape of an epitaxially coherent particle (which has interfacial dislocations with Burgers vectors which have an edge character and which lie in the interface plane) may be changed by the removal or addition of particular planes of atoms, e.g., by dislocation climb from one surface to another, again giving lowest strain energy for an IPS on the habit plane of a plate precipitate. If there is no reconstruction of the atom sites, the shape change may retain an appreciable shear component (operation d_4, Fig. 2.21).

Particles of type d_1 and d_2 both require long range diffusion or mass transport, and there is no obvious reason why large scale redistributions of solute atoms cannot at the same time occur between the product and parent phases, if demanded by thermodynamic equilibrium. In d_1 there is not shape change, whereas d_2 will lead to surface rumpling due to the

volume change accompanying transformation; both of these kinds of transformation are therefore reconstructive. Shear stresses and strains are not transferred across the interface, which behaves in some respects as a liquid-like layer. Since there is no continuity of planes or vectors, the interface can be displaced only as a result of individual atomic migration and its velocity will depend on atomic mobility.

It could also be argued that in case d_4, the need to have sufficient atomic mobility for interfacial dislocations to climb means that in reality, other diffusion processes might also occur which remove the shear component of the shape deformation (Christian, 1962).

This leaves only the martensitic type change d_3 as a likely candidate for an IPS shape change, but step c (Fig. 2.21) ensures that the shape change cannot be taken to imply diffusionless transformation. It is easy to see how interstitial atoms can partition between the phases during growth without affecting the IPS shape change. There may also be an interchange of substitutional atoms (of the type necessary to induce ordering in equiatomic random alloys), but it is likely that the migration of these atoms can only occur over a few interatomic distances — otherwise, any longer range diffusion would destroy the shape change and its associated strain energy at the same time. It is therefore to be concluded that one implication of the observation of an invariant plane strain shape change with a significant shear component is that any diffusion of solvent or substitutional atoms during transformation must be absent or minimal. Further implications of the shape change become clear when its relationship with the interfacial structure is considered. The interface in cases d_3 and d_4 is semicoherent because for coherency $\underline{S} = \underline{P}$, an equation which is rarely satisfied in general, and not satisfied for the FCC to BCC or BCT transformation in steels. For the 'epitaxial semicoherency' illustrated in d_4, coherent patches on the invariant plane are separated by interface dislocations whose motion with the interface requires climb and hence diffusion of atoms in substitutional sites. The semicoherent interface may alternatively be glissile; the interface dislocations then glide conservatively as the interface moves and growth does not require diffusion and hence has a high mobility even at very low temperatures (case d_3). For ferrous bainites, the mobility of the solvent and substitutional atoms is negligible, and the experimental observation of a shape deformation with a significant shear component gives strong evidence that the bainitic-ferrite/austenite interface is semi-coherent and glissile.

2.4.4 *The Shape Change and The Superledge Mechanism*

The lattice correspondence that is implied by the IPS shape deformation is a relationship between the lattices of the parent and product phases, independent of the orientation of the actual interface between the

enclosed particle and the matrix. It follows that all the interfaces surrounding an enclosed particle of bainitic ferrite must be semicoherent (Christian, 1990a). It is not tenable to consider some interface orientations to be incoherent ('disordered') while semi-coherency is maintained on other interface orientations, as is sometimes implied in the superledge mechanism of bainitic growth (Aaronson *et al.*, 1970). This mechanism considers that the growth of bainitic ferrite plates occurs by the propagation of macroscopic ledges on the habit plane. The model requires at least two differently oriented macroscopic interfaces around an enclosed bainitic ferrite particle, the invariant plane and the superledge. Macroscopic interfaces like these can only exist if the distortion due to the coherency between the parent and product lattices is within an elastically tolerable range — i.e., if the shape deformation across the interface is a close approximation to an IPS. Thus, the presence of two different orientations of macroscopic interface means that there are two invariant planes between the parent and product crystals, a situation only possible if the net shape deformation is zero, in contradiction with experimental evidence.

All interface orientations other than the invariant plane of the observed IPS shape deformation (which is also the habit plane of the bainitic ferrite) must be small coherent steps in the semi-coherent habit plane interface. The small steps are in forced *coherency* with the matrix, and have the characteristics of transformation dislocations which can glide and climb conservatively (also called coherency dislocations, Olson and Cohen, 1979). Coherency implies that all the corresponding planes and lines are continuous across the step; thus, these transformation dislocations are not lattice discontinuities. There is therefore no difficulty in these transformation dislocations climbing and gliding conservatively even when the Burgers vector is not parallel to the line vector.[4]

The strain energy associated with the small steps is tolerable only because of their small size. It is therefore considered that large steps (or 'superledges') are most improbable because of their high strain energy (Christian, 1990a).

2.4.5 *The Structure of the Interface*

It has already been pointed out that any atomic height steps in the bainitic-ferrite/austenite interface are in effect transformation dislocations, with strain fields whose character can be specified by assigning a

4 The terms transformation dislocation and coherency dislocation are identical. They are distinct from the adjectives 'interface', 'intrinsic', 'misfit' and 'anti-coherency', all of which are used to describe dislocations which form an intrinsic part of the boundary structure (Olson and Cohen, 1979; Christian, 1990a).

Burgers vector to each such dislocation. The motion of these steps (or coherency dislocations) which are in forced coherency, leads to phase change: there is continuity of planes and vectors across the steps so that regions of the parent lattice are homogeneously deformed into that of the product as the steps are displaced. Since the energy of the step varies with the square of the magnitude of its Burgers vector, the step is restricted to atomic height, which is another way of stating that superledges are impossible on a bainitic-ferrite/austenite interface. The anticoherency or interface dislocations cause the lattice invariant deformation as the interface is displaced.

There are no decisive direct observations of the structure of the bainitic-ferrite/austenite interface, but general conclusions can nevertheless be deduced using other experimental data and theoretical considerations. The observation of an invariant plane strain shape change accompanying the growth of bainitic-ferrite, when combined with the negligible mobility of the solvent and substitutional solute atoms, provides strong evidence that the structure of the transformation interface must be glissile. The number of iron and substitutional solute atoms is conserved during growth. Since they are not required to diffuse during transformation, the interfacial mobility is expected to be high even at low temperatures.

A semi-coherent interface containing a single array of anticoherency dislocations is considered to be glissile when the dislocations are able to move conservatively as the interface migrates. The dislocations must therefore all be pure screw dislocations, or have Burgers vectors which do not lie in the interface plane. The interface plane is the irrational invariant plane or habit plane of the bainite plate. A glissile interface also requires that the glide planes (of the anticoherency dislocations) associated with the ferrite lattice must meet the corresponding glide planes in the austenite lattice edge to edge in the interface along the dislocation lines (Christian and Crocker, 1980).

If more than one set of anticoherency dislocations exist, then these should either have the same line vector in the interface, or their respective Burgers vectors must be parallel (Christian and Crocker, 1980). This condition ensures that the interface can move as an integral unit. It also implies that the deformation caused by the anticoherency dislocations, when the interface moves can always be described as a simple shear (caused by a resultant anticoherency dislocation which is a combination of all the anticoherency dislocations) on some plane which makes a finite angle with the interface plane, and intersects the latter along the line vector of the resultant anticoherency dislocation.

Obviously, if the anticoherency dislocation structure consists of just a single set of parallel dislocations, or of a set of different dislocations which can be summed to give a single glissile anticoherency dislocation,

then it follows that there must exist in the interface, a line which is parallel to the resultant anticoherency dislocation line vector, along which there is zero distortion. Because this line exists in the interface, it is also unrotated. It is an *invariant-line* in the interface between the parent and product lattices. When full coherency is not possible between the two structures (as in the case for the FCC to BCC transformation), then for the interface to be glissile, the transformation strain relating the two lattices must be an invariant-line strain, with the invariant-line lying in the interface plane.

An interesting consequence of the restriction that the transformation strain must be an invariant-line strain is that models of the ferrite/austenite interface as a single array of anticoherency dislocations are not possible for any orientation between Nishiyama–Wasserman and Kurdjumov–Sachs if the most densely packed planes of the two structures are regarded as exactly parallel (Knowles and Smith, 1982; Christian, 1990a). This is because for realistic values of the lattice parameters, it is not possible to obtain a transformation strain which is an invariant-line strain if the planes are exactly parallel. If it is assumed that the interface contains just one set of anticoherency dislocations then the predicted orientation relation always has the most densely packed planes of the two structures at a small angle (about 0.5°) to each other — such a small deviation is unfortunately very difficult to detect experimentally.

2.4.6 *The Crystallography of a Lath of Bainite*

It has already been noted that the sub-units of a bainite sheaf may adopt the morphology of a plate or of a lath, where the latter is idealised as a parallelepiped of dimensions a, b, and c, with $a > b > c$. There is a general tendency for the lath shape to be adopted when the transformation occurs at relatively high temperatures. The crystallography of such laths has been characterised in detail and to a high level of accuracy, by Davenport (1974), as follows:

Growth direction	$[\bar{1}\,0\,1]_\gamma \parallel [\bar{1}\,\bar{1}\,1]_\alpha$
Habit plane (area = ab)	$(2\,3\,2)_\gamma \approx (\bar{1}\,5\,4)_\alpha$
Face of area = ac	$(1\,0\,1)_\gamma$
Orientation relationship (KS)	$[\bar{1}\,0\,1]_\gamma \parallel [\bar{1}\,\bar{1}\,1]_\alpha$
	$(1\,1\,1)_\gamma \parallel (0\,1\,1)_\alpha$

where the crystallography is, for consistency, stated in the standard variant described earlier. Hence, the major growth direction of each lath corresponds to the parallel close packed directions from the α and γ lattices. This is consistent with less direct trace analysis results which indicated that the major growth direction of the laths lies along $\langle\bar{1}\,\bar{1}\,1\rangle_\alpha$

(Goodenow and Hehemann, 1965; Oblak and Hehemann, 1967; Ohmori and Honeycombe, 1971). The habit plane indices are significantly different from earlier data which indicated a $\{1\ 1\ 1\}_\gamma$ habit (Greninger and Troiano, 1940; Oblak and Hehemann, 1967; Ohmori, 1971b; Ohmori and Honeycombe, 1971) but those analyses were either of insufficient precision or were concerned with the apparent habit planes of sheaves (Davenport, 1974). Davenport also demonstrated that sets of two groups of laths with a common growth direction, but with virtually orthogonal habit planes, tended to form in close proximity. There is as yet, no detailed analysis available which can predict these results.

Sandvik (1982a) has reported measurements carried out using single surface trace analysis, of the habit planes of individual sub-units. The mean habit plane is found to be close to $(0.373\ 0.663\ 0.649)_\gamma$ for an orientation relationship in which $(1\ 1\ 1)_\gamma \parallel (0\ 1\ 1)_\alpha$ and $[\bar{1}\ 0\ 1]_\gamma$ is approximately 4° from $[\bar{1}\ \bar{1}\ 1]_\alpha$ (such an orientation is close to the Nishiyama–Wasserman orientation relationship). The habit plane was not found to vary significantly with transformation temperature. Using data from high resolution observations of the displacements of austenite twins by the shape deformation due to transformation, he was able to show that the shear component of the shape strain of a sub-unit is about 0.22. Sandvik also showed that the observed shape strain direction and magnitude are close to the corresponding parameters for the classic $\{2\ 2\ 5\}_\gamma$ and $\{3\ 10\ 15\}_\gamma$ martensites in steels.

2.5 Microstructure of Bainite: The Midrib

Recent work by Okamoto and Oka (1986) indicates that in certain circumstances, high carbon steels transform to plates of lower bainite which do not have a homogeneous microstructure. When observed using light microscopy, what appears macroscopically an individual plate of lower bainite is seen to have a black line running centrally along its axis (Fig. 2.22). Transmission electron microscopy reveals that this line corresponds to a centrally located, coplanar thin plate of martensite which is sandwiched between regions of lower bainite. The lower bainite containing the midrib is actually found to evolve in two stages, from thin-plate martensite which forms first by the isothermal transformation of austenite, and which then stimulates the growth of the adjacent bainite regions.

Okamoto and Oka deduced that at relatively high transformation temperatures, the steels react to give lower bainite without a midrib, but as the transformation temperature is reduced to below a certain temperature T_r, this is replaced by the lower bainite with a thin plate martensite midrib, which then gives way to just the thin plate martensite; at a sufficiently low

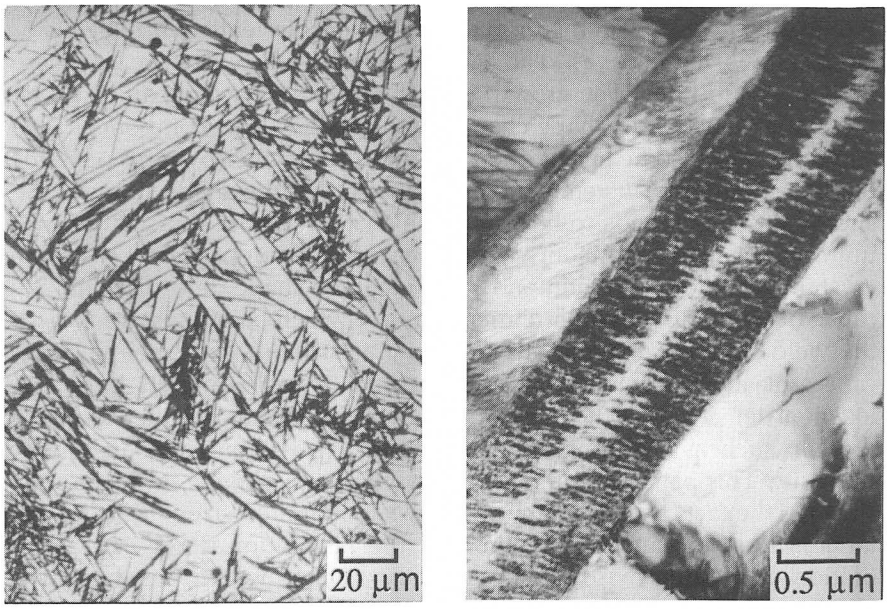

Fig. 2.22 *Optical and transmission electron micrographs of the midrib associated with lower bainite in a plain carbon steel. (Okamoto & Oka, 1986).*

temperature (below the conventional M_s temperature), ordinary martensite with a lenticular plate morphology forms by the athermal transformation of austenite.

It was noted above that both the lower bainite containing the midrib, and thin plate martensite isothermally form in the temperature range $T_r \rightarrow M_s$. Okamoto and Oka demonstrated that the difference between these two temperatures diminishes as the carbon concentration of the steel decreases, until at about 1wt% C, it becomes zero. Consequently, neither of these phases have been reported to occur in lower carbon steels.

The terminology 'thin plate martensite' has its origins in work done on nickel rich Fe–Ni–C alloys, where the martensite transformation temperatures are well below –100°C (Maki *et al.*, 1973, 1975). The martensite then tends to form as extremely thin, parallel-sided plates in preference to much thicker lenticular plates, especially as the carbon concentration is increased. Because of their very large aspect ratios, the thin plates are elastically accommodated in the austenite matrix. Their interfaces therefore remain glissile. The plates can therefore thicken as the temperature is reduced, or indeed become thinner as the temperature is raised.

2.6 Summary

Bainitic ferrite grows in the form of clusters of thin lenticular platelets or laths, known as sheaves. The individual platelets within a sheaf are known as sub-units. The growth of each sub-unit is accompanied by an invariant plane strain shape change with a large shear component. The sub-units are to some extent separated from each other by films of residual phases such as austenite or cementite, so that the shape strain of the sheaf as a whole tends to be much smaller than that of an isolated sub-unit. The platelets within any given sheaf tend to adopt almost the same crystallographic orientation and have identical shape deformations. Because of the relatively high temperatures at which bainite grows (where the yield stresses of ferrite and austenite are reduced), the shape strain causes plastic deformation which in turn leads to a relatively large dislocation density in both the parent and product phases; other kinds of defects, such as twinning and faulting are also found in the residual austenite. This plastic accommodation of the shape change seems responsible for the fact that each sub-unit grows to a limited size which may be far less than the austenite grain size; the dislocation debris stifles the motion of the otherwise glissile interface. Consequently, the sheaf as a whole grows by the repeated 'nucleation' of new sub-units, mostly near the tips of those already existing.

The bainitic-ferrite/austenite orientation relationship is always found to lie well within the Bain region; this and other features of the transformation are broadly consistent with the phenomenological theory of martensite crystallography. The growth of bainitic ferrite undoubtedly occurs without any redistribution of iron or substitutional solute atoms, even on the finest conceivable scale at the transformation interface. Although some excess carbon is retained in solution in the bainitic ferrite after transformation, most of it is partitioned into the residual austenite, and in the case of lower bainite, also precipitated as carbides within the ferrite. This redistribution of carbon could of course occur after the diffusionless growth of bainitic ferrite, and the subject is discussed in more detail in Chapters 5 & 6. All of the observed characteristics of bainitic ferrite suggest strongly that it grows by a displacive transformation mechanism.

3 *Carbide Precipitation*

An important characteristic of bainitic microstructures, especially relevant to their mechanical properties, is the nature and extent of carbide precipitation. Indeed, the carbides are probably largely responsible for the commercial failure of many of the early bainitic steels. Thus, conventional bainitic alloys have in the past been unable to compete against the well established quenched and tempered martensitic alloys, which tend to have much finer dispersions of carbide phases. These issues are discussed further in Chapter 10, which deals with the mechanical properties of bainitic steels. The purpose here is to examine the carbide precipitation reactions themselves and to relate the observations to the transformation mechanism of bainite.

3.1 Upper Bainite

The carbide phase associated with upper bainite precipitates from carbon enriched residual austenite and is almost always cementite (Wever and Mathieu, 1940; Lyman and Troiano, 1946; Hultgren, 1947, 1951; Austin and Schwartz, 1952, 1955). There are, however, many notable exceptions. In steels containing relatively large concentrations of silicon ($\approx$ 2wt%), transition carbides such as κ precipitate first from the austenite, but when given the opportunity, they tend eventually to transform into cementite (Houllier *et al.*, 1971). κ has a hexagonal lattice, with $a = 6.9$ and $c = 4.8$ Å. Schissler *et al.* (1975) reported a new carbide of orthorhombic lattice ($a = 6.5$, $b = 7.7$ and $c = 10.4$ Å), which precipitates from the residual austenite during the bainite reaction in a Fe–1.15C–3.9Si wt% alloy transformed isothermally at 420°C. The addition of about 1 wt% Mn to the alloy changed this to another new carbide, also with an orthorhombic lattice, but with the lattice parameters $a = 14.8$, $b = 11.4$ and $c = 8.5$ Å. Sandvik (1982b) has reported the formation of plate-shaped 'c' carbides during the

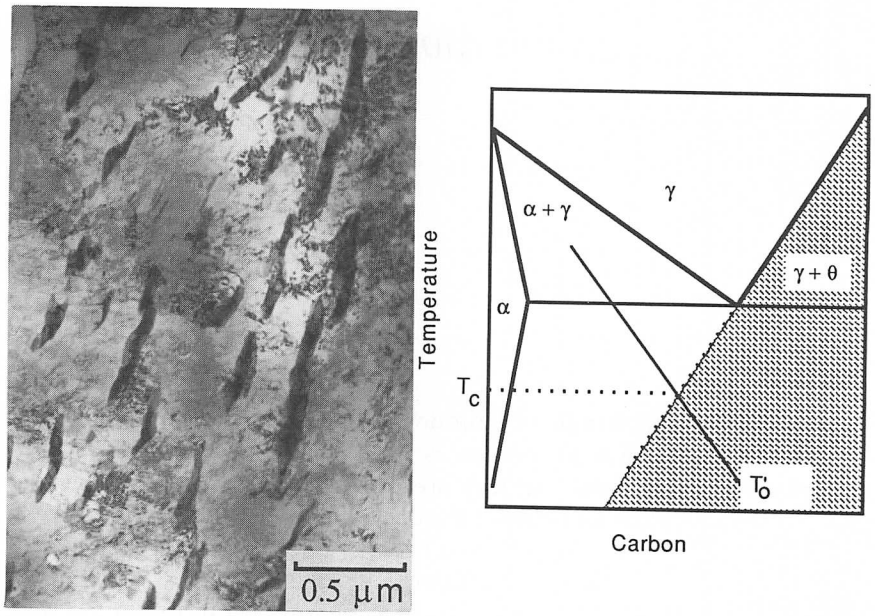

Fig. 3.1. *(a) Transmission electron micrograph illustrating the distribution of cementite particles between the ferrite platelets in upper bainite. AISI 4340 steel, isothermally transformed to upper bainite. (b) Schematic illustration of the thermodynamic condition which has to be satisfied before cementite may precipitate from the residual austenite.*

ageing of mixtures of bainitic ferrite and austenite in high silicon steels. Upper bainitic ferrite does not itself contain any carbide precipitates (Fig. 3.1a).

As a consequence of transformation to bainite, the austenite that is trapped between platelets of upper bainite becomes enriched in carbon. If the carbon concentration of the residual austenite (i.e., x_γ), exceeds the value given by the extrapolated $\gamma/(\gamma+\theta)$ phase boundary, then cementite precipitation from the enriched austenite lying adjacent to the platelets of bainitic ferrite, becomes thermodynamically possible (Kriesement and Wever, 1956). This is illustrated in Fig. 3.1b, where the shaded area represents austenite which is unstable to the precipitation of cementite. If it is additionally assumed that bainite growth stops when the carbon concentration of the austenite exceeds the T_o' phase boundary, then subject to kinetics, carbide precipitation is expected to accompany the growth of upper bainite if the transformation temperature is below T_c (Fig. 3.1b).

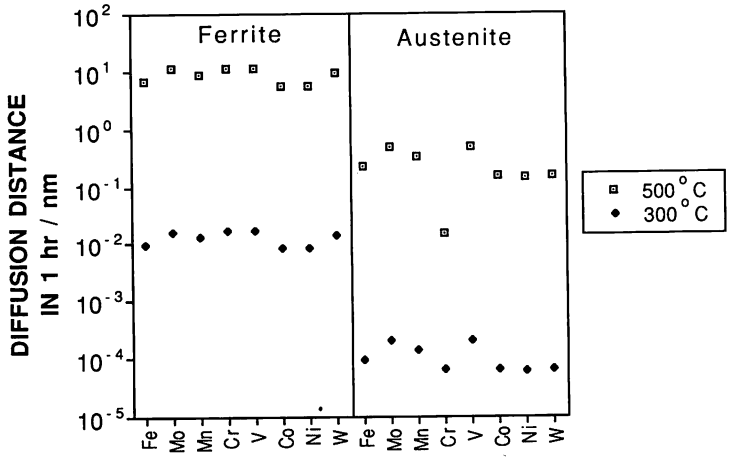

Fig. 3.2 *A* $2(Dt)^{0.5}$ *estimate of the diffusion distances for iron and some substitutional solutes in iron, as a function of temperature, with* $t = 1$ *hour.*

The carbide precipitation reaction discussed above is clearly a secondary process, since it is peripheral to the formation of bainitic ferrite. Of course, the formation of cementite or other carbides leads to a reduction of the carbon concentration in the residual austenite, thereby permitting the growth of a further amount of ferrite (designated α). The mechanism of this secondary ferrite reaction is not fully established, but in view of the very small diffusion coefficients of iron and substitutional atoms at the temperatures involved (Fig. 3.2), and the absence of an incoherent interface or grain boundary to start the process, it is unlikely to involve reconstructive transformation. Sandvik (1982b) has proposed that the decomposition of the residual austenite involves the displacive formation of a triclinic carbide, close to cementite in structure, and the subsequent formation of a small amount of *bainitic* ferrite. Nakamura and Nagakura (1986), in a study of the second stage of martensite tempering, suggested that cementite and ferrite form directly from austenite, the cementite nucleating on the ferrite/austenite boundaries and growing by rapid diffusion along this boundary. They also proposed that the secondary ferrite, which they called bainite, grows martensitically, from the carbon depleted austenite. Regions of secondary ferrite were observed to be twinned, and this was taken to indicate the formation of self-accommodating crystallographic variants of bainitic ferrite.

The sequence of reactions can be summarised as follows (the α refers to the secondary ferrite which forms as the carbides precipitate from residual austenite):

$$\begin{aligned} \gamma \quad &\rightarrow \gamma + \alpha_{b,\ \text{SUPERSATURATED}} \\ &\rightarrow \alpha_{b,\ \text{UNSATURATED}} + \gamma_{\text{ENRICHED}} \\ &\rightarrow \alpha_{b,\ \text{UNSATURATED}} + \alpha + \theta \end{aligned} \tag{3.1}$$

This contrasts with the cooperative growth of cementite and ferrite during the formation of pearlite in plain carbon steels:

$$\gamma \quad \rightarrow \alpha + \theta \tag{3.2}$$

When pearlite grows in substitutionally alloyed steels, the austenite, ferrite and cementite may coexist in equilibrium over a range of temperatures, with the equilibrium compositions of all the phases changing with transformation temperature

$$\gamma \quad \rightarrow \alpha + \theta + \gamma' \tag{3.3}$$

The composition of the residual austenite (γ) is then expected to differ from that of the original austenite, in general with respect to both substitutional and interstitial solutes. The reaction stops when all the phases are homogeneous and of equilibrium composition, before all the austenite has transformed.

In planar sections, the cementite particles in upper bainite appear parallel to the traces of habit planes of the bainitic ferrite platelets. Using transmission electron microscopy and extraction replicas, Fisher (1958) showed that these particles are in the form of irregular ribbons in three dimensions particularly when bainite forms at high temperatures. Carbide precipitation also occurs at the austenite grain boundaries and this may influence mechanical properties, especially toughness in high strength steels (Pickering, 1958). The precipitation of cementite from supersaturated austenite probably first occurs at the austenite grain boundaries, so that those carbides can be expected to be relatively coarse. When high carbon steels (> 0.45C wt%) are isothermally reacted in the bainite temperature range, thin films of 'proeutectoid' cementite are known to precipitate at the austenite grain surfaces, independently of any bainitic reaction (Stickels, 1974). The growth rate of the films, which are detrimental to toughness, can be retarded by lowering the isothermal transformation temperature.

3.2 Lower Bainite

Lower bainite also consists of a non-lamellar aggregate of ferrite and carbides. There are however, two kinds of carbides. Like upper bainite, there is some precipitation of carbides from the enriched austenite occurs between the bainite platelets. In addition, there is usually a fine dispersion of plate-like carbides (ε-carbide or cementite) within the lenticular

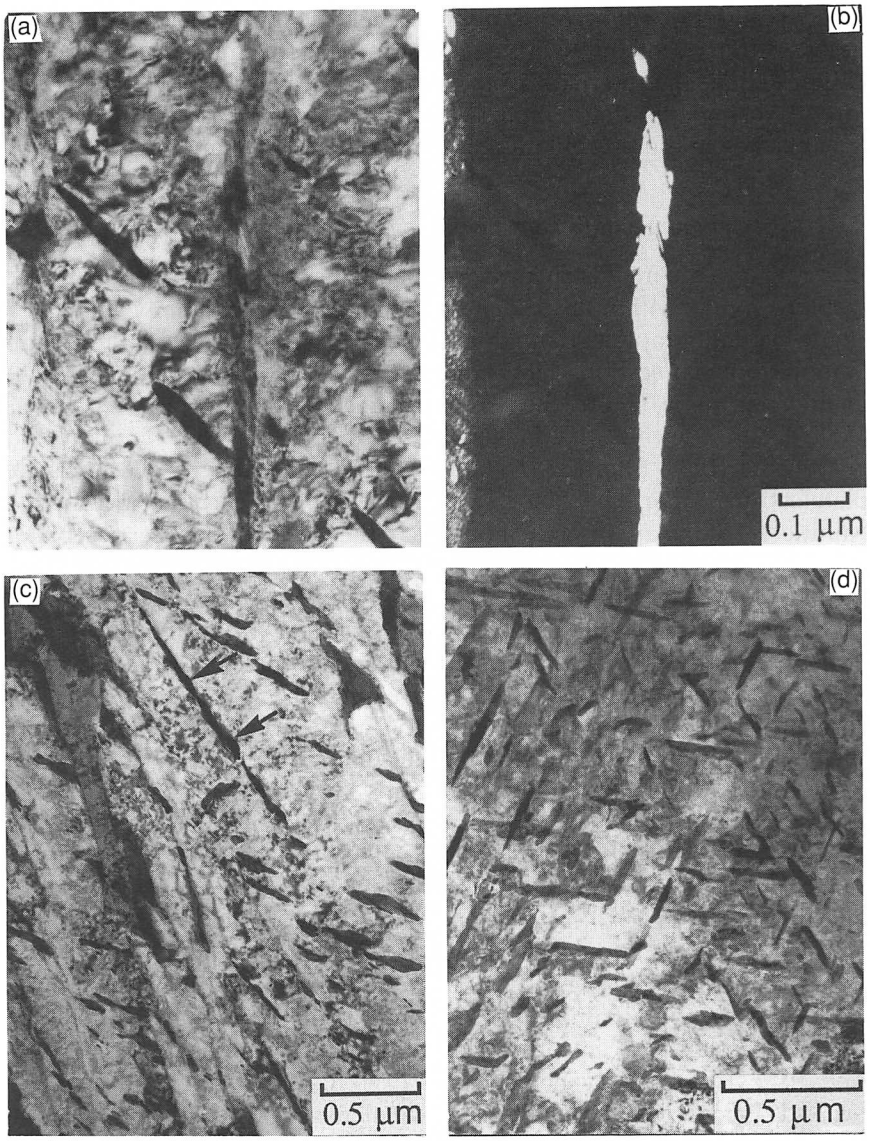

Fig. 3.3 *(a–c) Fe–0.3C–4.08Cr wt% (a) Lower bainite obtained by isothermal transformation for a short time period (435°C, 10min). Shows particles of cementite within the platelets but not between the platelets. (b) Corresponding dark field image showing the films of austenite between the bainitic ferrite platelets. (c) The same sample after prolonged heat treatment (435°C, 30 min) at the isothermal transformation temperature, causing the precipitation of carbides between the ferrite platelets. (d) Typical multi-variant carbide precipitation in tempered martensite (415°C, 50 min, AISI 4340 steel). After Bhadeshia (1980a).*

ferrite plates. As will become apparent later, the mechanism of precipitation is different for the two types of sites. The striking feature of lower bainite is that the internal carbides within the bainitic ferrite in general form in a single crystallographic variant, whereas the tempering of martensite leads to the precipitation of many variants of cementite (Fig. 3.3).

3.2.1 *Precipitation within Lower Bainitic Ferrite*

In contrast to the microstructure obtained after tempering martensite, the carbides found within any given bainitic ferrite plate usually occur in a single crystallographic orientation. When the carbide is cementite, examination of planar sections shows that the particles have their longest axes inclined at some 60° to the 'growth direction' of the ferrite platelets (ASTM, 1955; Irvine and Pickering, 1958; Speich, 1962; Shimizu and Nishiyama, 1963; Shimizu *et al.*, 1964). The sharp edges of the ferrite platelets are reported to be free of carbides. The carbides within the bainitic ferrite may or may not touch the sides of the ferrite plates (Bhadeshia, 1980a). The angle quoted must of course vary as a function of the plane of section; it has been shown that for lower bainitic ferrite which has a habit plane with approximate indices $(0.761\ 0.169\ 0.626)_\gamma$ the cementite precipitates on $(1\ \bar{1}\ 2)_\alpha$ so that the true angle between the α and cementite habit plane normals is approximately 57° (Bhadeshia, 1980a). Similar results have been obtained for the angle between the lower bainite sheaf and cementite habit plane normals (Ohmori, 1971a). In some cases, the carbides have been found to form on several different variants of the $\{1\ 1\ 2\}_\alpha$ plane, although a particular variant generally tends to dominate (Srinivasan and Wayman, 1968b; Lai, 1975; Bhadeshia and Edmonds, 1979a). In fact, a re-examination of published micrographs sometimes reveals the presence of several variants which were not noticed in the original publication (see for example, Fig. 5, Degang *et al.*, 1989).

Early experiments using Curie point measurements and dilatometry gave indirect indications that the carbide precipitation associated with lower bainite is not always cementite (Wever and Lange, 1932; Allen *et al.*, 1939; Antia *et al.*, 1944). Austin and Schwartz (1952) first identified the presence of ε-carbide in lower bainite. Since then, several investigators have reported the detection of ε-carbide in association with lower bainite (Matas and Hehemann, 1961; Deliry, 1965; Pomey, 1966; Oblak and Hehemann, 1967; Hehemann, 1970; Lai, 1975; Huang and Thomas, 1977; Sandvik, 1982a)).

Matas and Hehemann interpreted these results to suggest that the initial carbide in hypoeutectoid steels is ε-carbide, which is then replaced by cementite on holding at the isothermal transformation temperature. The rate at which the ε-carbide converts to cementite increases with temperature, but also depends on the steel composition; a high silicon

Table 3.1 Compositions of steels (wt%) in which ε-carbide has been found in lower bainite. The carbon concentration quoted for the alloy studied by Dubensky and Rundman represents an estimate of the concentration in the austenite matrix of an austempered ductile cast iron.

C	Si	Mn	Ni	Cr	Mo	V	Reference
0.87	–	–	–	–	–	–	Austin and Schwartz, 1952, 1955
0.95	0.22	0.60	3.27	1.23	0.13		Matas and Hehemann, 1961
0.60	2.00	0.86	–	0.31	–	–	Matas and Hehemann, 1961
1.00	0.36	–	0.20	1.41	–	–	Matas and Hehemann, 1961
0.58	0.35	0.78	–	3.90	0.45	0.90	Matas and Hehemann, 1961
1.00	2.15	0.36	–	–	–	–	Deliry, 1965
0.60	2.00	0.86	–	0.31	–	–	Oblak and Hehemann, 1967
0.60	2.00	–	–	–	–	–	Hehemann, 1970
0.41	1.59	0.79	1.85	0.75	0.43	0.08	Lai, 1975
0.54	1.87	0.79	–	0.30	–	–	Huang and Thomas, 1977
0.85	2.55	0.3	–	–	–	–	Dorazil and Svejcar, 1979
0.74	2.40	0.51	–	0.52	–	–	Sandvik, 1982a
1.3	3.09	0.17	–	–	–	–	Dubensky and Rundman, 1985
0.40	2.01	–	4.15	–	–	–	Miihkinen and Edmonds, 1987a

concentration (≈ 2wt%) in the steel considerably retards the reaction. This is consistent with the fact that silicon is known to retard the formation of cementite during the tempering of martensite (Owen, 1954; Gordine and Codd, 1969; Hobbs *et al.*, 1972).

The detection of ε-carbide in lower bainite is important in that it implies the existence of a rather high carbon supersaturation in bainitic ferrite, perhaps to a level of the order of 0.25wt% (Roberts *et al.*, 1957). However, ε-carbide is not always found as a precursor to the precipitation of cementite in lower bainite. Bhadeshia and Edmonds (1979a) failed to detect ε-carbide in a high silicon medium carbon steel (Fe–3.0Mn–2.02Si–0.43C wt%) even during the early stages of the lower bainite transformation. The steels in which ε-carbide has been observed during the formation of lower bainite are listed in Table 3.1.[1]

These observations can be rationalised in terms of a theory of tempering due to Kalish and Cohen (1970), who showed that it is energetically favourable for carbon atoms to remain segregated at dislocations when compared with their presence in the ε-carbide lattice (Bhadeshia, 1980a). If the dislocation density is high, then sufficient carbon can be tied up at

1 ε-carbide has been reported in bainite produced by continuous cooling transformation, in a Fe–0.15C–0.94Mo–2.12Cr wt% steel (Baker and Nutting, 1959) and in a Fe–0.34C–1.25Mn–1.39Ni–0.34Mo wt% alloy isothermally transformed to bainite (Fondekar *et al.*, 1970). In both cases, the evidence quoted is rather indirect. A recent detailed study by Yu (1989) on steels very similar to those used by Baker and Nutting has not revealed any ε-carbide.

the dislocations so that the ε-carbide stage is missed in the precipitation sequence. In such cases, cementite precipitation occurs directly. Kalish and Cohen estimated that a dislocation density of 2×10^{12} cm^{-2} should prevent ε-carbide precipitation in steels containing up to 0.20 wt% carbon. This theory can be applied to bainite if it is considered that after the formation of supersaturated ferrite, there commence two competitive reactions which tend to reduce the carbon supersaturation of the ferrite. The two reactions are the partitioning of carbon into the residual austenite and the precipitation of carbides in the bainitic ferrite. The reactions interact in that the partitioning process reduces the amount of carbon that is available for precipitation, and vice versa. Judging from available data (Table 3.1), and if steels containing a large amount of nickel are excluded, then it seems that there is sufficient carbon for the precipitation of a detectable amount of ε-carbide if the average carbon content of the steel is above approximately 0.55 wt%. Otherwise, the partitioning of carbon into the residual austenite depletes the bainitic ferrite too rapidly to permit any significant precipitation of ε-carbide. It is believed that nickel enhances the precipitation of ε-carbide (Miihkinen and Edmonds, 1987a) and this is consistent with the lower carbon concentrations ($\approx$ 0.4 wt%) at which ε-carbide forms during the bainite transformation in these steels. Rao and Thomas (1980) have demonstrated a similar effect of nickel in martensitic steels; they found ε-carbides and cementite to be the dominant carbides during the tempering of martensite in Fe–0.27C–4Cr–5Ni and Fe–0.24C–2Mn–4Cr wt% steels respectively. The other substitutional elements may also have some effect on these phenomena, but this has not been systematically studied. If lower bainite containing ε-carbide is tempered, the ε-carbide transforms to cementite and the reaction is accompanied by a volume contraction, which can be monitored accurately using dilatometry (Hehemann, 1970).

Finally, η-carbide (Fe_2C) has also been observed in lower bainitic ferrite obtained by transforming the austenite matrix of a high silicon cast iron (Franetovic *et al.* 1987a, b). This carbide has previously only been reported in tempered martensite (Hirotsu and Nagakura, 1972; Nagakura *et al.* 1983) and so reinforces the conclusion that the carbides precipitate from carbon supersaturated lower bainitic ferrite. Like ε-carbide, tentative results indicate that the overall carbon concentration of the parent austenite has to exceed some critical concentration before the η-carbide can be detected readily in lower bainite (Franetovic *et al.* 1987a, b).

3.2.2 *Precipitation between Lower Bainitic Ferrite Platelets*

As discussed earlier, there are in fact two separable carbide precipitation reactions associated with the lower bainite transformation (see for example,

Hehemann, 1970; Bhadeshia, 1980a). The first, which in general is faster, has been discussed above and involves the precipitation of carbides from supersaturated ferrite. In the second, more sluggish reaction, carbides are precipitated between the bainitic ferrite platelets by the decomposition of the carbon-enriched residual austenite into a mixture of cementite and ferrite. The second reaction is therefore identical to the precipitation of carbides from austenite during the upper bainite transformation.

Since some of the carbon in the alloy is tied up in the form of carbides within the ferrite, the volume fraction of residual austenite trapped between bainite platelets is less for lower bainite (Hehemann, 1970). Hence, the decomposition of this austenite into cementite and ferrite leads to a smaller volume fraction of inter-plate cementite. An important consequence of this is that lower bainite often has a higher toughness than upper bainite, even though it usually is stronger than upper bainite. The precipitation reactions for lower banite can be summarised as follows:

Case 1: High dislocation density

$$\begin{aligned}\gamma \quad &\rightarrow \gamma + \alpha_{b,\ \text{SUPERSATURATED}} \\ &\rightarrow \theta_{\text{IN FERRITE}} + \alpha_{b,\ \text{UNSATURATED}} + \gamma_{\text{ENRICHED}} \\ &\rightarrow \alpha_{b,\ \text{UNSATURATED}} + \alpha + \theta_{\text{BETWEEN FERRITE PLATES}} + \theta_{\text{IN FERRITE}}\end{aligned} \tag{3.4}$$

Case 2: Low dislocation density

$$\begin{aligned}\gamma \quad &\rightarrow \gamma + \alpha_{b,\ \text{SUPERSATURATED}} \\ &\rightarrow \varepsilon\text{-carbide}_{\text{IN FERRITE}} + \alpha_{b,\ \text{UNSATURATED}} + \gamma_{\text{ENRICHED}} \\ &\rightarrow \alpha_{b,\ \text{UNSATURATED}} + \varepsilon\text{-carbide}_{\text{IN FERRITE}} + \alpha + \theta_{\text{BETWEEN FERRITE PLATES}} \\ &\rightarrow \alpha_{b,\ \text{UNSATURATED}} + \theta_{\text{IN FERRITE}} + \theta_{\text{BETWEEN FERRITE PLATES}} + \alpha\end{aligned} \tag{3.5}$$

Recent *in situ* observations using hot-stage transmission electron microscopy, of the precipitation of carbides within lower bainite indicate that the lower bainitic ferrite remains supersaturated with carbon some time after the completion of the ferrite growth (Kang *et al.*, 1990).

A new carbide, which is for convenience designated κ-carbide, has been discovered in high carbon steels transformed to lower bainite (Deliry, 1965; Pomey, 1966). It occurs as a transition carbide, precipitating at a late stage of the transformation, from the carbon enriched residual austenite. Its crystal structure is discussed later. The carbide has a high solubility for Si and on continued holding at the isothermal transformation temperature, transforms to χ-carbide which in turn eventually gives way to the more stable cementite. Similarly, the transition carbide discovered in high silicon transformer steels by Konoval *et al.* (1959), with an orthorhombic lattice (parameters a = 8.8, b = 9.9 and c = 14.4 Å), has been reported to precipitate from lower bainitic ferrite in Fe–1.15C–3.9Si wt% alloy (Schissler *et al.*, 1975).

3.3 Kinetics of Carbide Precipitation

3.3.1 Partitioning and Distribution of Carbon

The carbon concentration of bainitic ferrite during transformation is of major importance in determining the kinetics of carbide precipitation. The transformation, however, occurs at relatively high temperatures and any excess carbon in the ferrite can be removed by the precipitation of carbides within the ferrite or by the diffusion of carbon into the residual austenite. The two mechanisms of carbon removal usually take place simultaneously, although one or the other may dominate depending on temperature. Both events can be rapid because of the high mobility of carbon in iron.

The partitioning of excess carbon from supersaturated ferrite into austenite lowers its chemical potential. This process of carbon partitioning was simulated experimentally by Matas and Hehemann (1960, 1961), with the help of tempering experiments on mixtures of martensite and retained austenite. Single crystals of austenite (Fe–1.23Cr–0.60Mn–0.13Mo–3.27Ni–0.22Si–0.95C wt%) were cooled below the M_s temperature ($\approx$ 350K) to obtain two microstructures, one containing 50% martensite and the other 90% martensite in a matrix of austenite. The crystals were then tempered at 405 K to allow the carbon to diffuse from martensite into austenite. The tempering treatments caused rapid precipitation of ε-carbide in the martensite, thereby lowering the carbon concentration of the martensite to 0.22wt%, a value consistent with that quoted by Roberts *et al.* (1957) for the equilibrium between martensite and ε-carbide. Continued holding at the tempering temperature led to further reductions in martensite carbon concentration, the carbon diffusing into the residual austenite. The rejection of excess carbon into austenite occurred more rapidly for the sample containing less martensite, presumably because the larger amount of residual austenite provided a bigger sink for carbon.

An increase in the carbon concentration of residual austenite has also been reported in more recent experiments involving lath martensites (Rao and Thomas, 1979; Barnard *et al.*, 1981). The experiments were interpreted to imply the partitioning of carbon during the formation of lath martensite, but since the martensite start temperatures of the steels used were rather high, it is likely that the carbon diffused into the austenite after the formation of the lath martensite, in the manner discussed above (Bhadeshia, 1983b).

The distribution of carbon in the residual austenite is not in general homogeneous after isothermal transformation to bainite (Fig. 3.4). The austenite is enriched to a greater extent in the immediate vicinity of

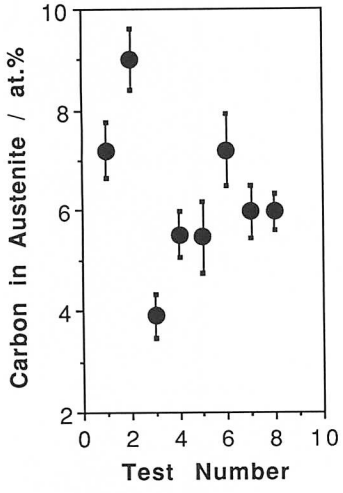

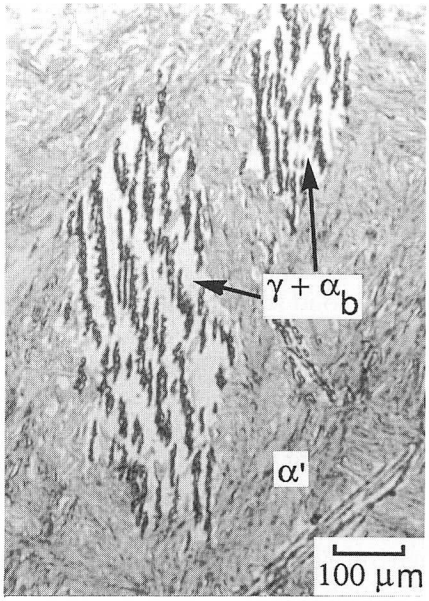

Fig. 3.4 *The non-uniform distribution of carbon in the residual austenite associated with bainitic ferrite. (a) Direct measurements of the carbon concentration using an atom probe; Fe–0.39C–2.05Si–4.08Ni wt%, isothermally transformed at 340°C for 10 h (Bhadeshia and Waugh, 1981). (b) Rim of austenite retained around a sheaf of bainite in Fe–0.81C–1.98Si–3Mn wt% steel, where the carbon concentration is expected to be largest.*

bainite platelets or in the regions trapped between the platelets (Schrader and Wever, 1952; Matas and Hehemann, 1961). Carbon causes an expansion of the austenite lattice parameter, and in some cases, two lattice parameters have been observed for the retained austenite, corresponding to different levels of carbon in the austenite within a single specimen (Matas and Hehemann, 1961). In many cases, the austenite which is relatively poor in carbon decomposes martensitically on cooling to ambient temperature. Any subsequent measurement of the carbon concentration of austenite (x_γ) using an X-ray method would then be expected to lead to an overestimation of x_γ if it is assumed that the carbon is distributed uniformly in the residual austenite that existed at the isothermal transformation temperature. For example, for upper bainite in a high silicon steel, X-ray measurements indicated that the carbon concentration of the austenite retained at ambient temperatures was about 1.7 wt%, whereas volume fraction data gave an average concentration of 1.35 wt% for the residual austenite which existed at the bainitic transformation temperature (Houllier *et al.* 1971).

3.3.2 *Kinetics of Precipitation from Residual Austenite*

The incomplete reaction in silicon and some other alloy steels strongly suggests that the precipitation of carbides during the bainite reaction occurs after the formation of bainitic ferrite. Carbide formation can therefore lag behind that of bainitic ferrite. The extent of this lag depends both on temperature and on alloy composition; for steels which transform rapidly, the lag may not be detectable.

Using a chemical technique which separates precipitated carbon from that in solid solution, together with dilatometry, it is possible to show that during the formation of bainitic ferrite at high temperatures, the amount of carbide formed is proportional to the amount of bainitic ferrite at any stage of the reaction (Vasudevan *et al.*, 1958). On the other hand, for lower transformation temperatures, the carbide precipitation reaction is found to lag significantly behind the formation of bainitic ferrite. The steel used to establish these results contained only small concentrations of substitutional solutes and it is likely that an increase in alloy content would in general lead to changes in the relative kinetics of all the essential reactions.

With lower bainite, it is necessary to distinguish between the carbides within the bainitic ferrite (which precipitate rather rapidly), and those which form by the decomposition of the carbon enriched residual austenite which is trapped between the ferrite plates. Transmission electron microscopy studies on an Fe–4.08Cr–0.3C wt% alloy have shown that of the two reactions which lead to carbide formation in lower bainite, the precipitation of cementite from the residual austenite is a comparatively slow process (Bhadeshia, 1980a). Isothermal transformation at 435°C for 10 min (a time long enough to allow the bainite transformation to reach completion) gave cementite within the lower bainitic ferrite, but the regions between the ferrite platelets remained as untransformed austenite (Fig. 3.3). It was necessary to hold the alloy at the transformation temperature for a period of 30 min before cementite began to precipitate from the residual austenite. The slow rate of this precipitation reaction might indicate that, in contrast to the precipitation within ferrite, it is a reconstructive transformation. However, as suggested by Sandvik, both transformations might be displacive so far as the iron atoms are concerned and the difference may be ascribable simply to the difference in the diffusion rates of carbon in ferrite and austenite.

The most striking evidence that the formation of carbides from residual austenite lags behind the formation of bainitic ferrite, and behind the precipitation of carbides within the ferrite, is found in steels containing relatively large amounts of silicon. For example, no carbide formation accompanies the formation of upper bainite in Fe–0.31Cr–0.86Mn–2.00Si–

0.60C wt% alloy, even after holding at the isothermal transformation temperature for several hours (Matas and Hehemann 1961). Similar results have been reported by Houllier *et al.*, (1971), Sandvik (1982b) and by many other researchers.

Silicon is usually present in steels as an aftermath of the deoxidation reactions involved in the steelmaking process. However, it is clear that the effect of relatively large deliberate additions of silicon on the upper bainite reaction is to retard the formation of cementite from austenite, thereby giving a microstructure of just bainitic ferrite and austenite (Entin, 1962; Deliry, 1965; Pomey, 1966; Hehemann, 1970; Houllier *et al.*, 1971; Bhadeshia and Edmonds, 1979a; Sandvik, 1982a, b). Silicon in cast irons has long been known to favour the formation of grey cast iron, which contains large amounts of graphite instead of the cementite found in low silicon white cast irons. The precipitation of cementite during the tempering of martensite is significantly retarded by the presence of silicon (Bain, 1939; Allten and Payson, 1953; Owen, 1954; Keh and Leslie, 1963; Gordine and Codd, 1969; Hobbs *et al.* 1972) and the phenomenon has been used in the design of one of the most successful ultra high strength steels (commercial designation 300M, reviewed by Pickering, 1979).

The effect of silicon is generally reconciled with the fact that its solubility in cementite is very small. It intuitively seems reasonable that high silicon steels consequently form a poor environment for the precipitation of cementite. The need for silicon to diffuse away from the cementite/ferrite interface could explain the retardation of its growth (Owen, 1954). During the tempering of martensite in high silicon steels, the retardation of cementite growth allows transition carbides to persist for longer periods. It was at one time thought that the effect is really due to the stabilisation of the transition carbides which have a high solubility for silicon, rather than the retardation of cementite growth (Reisdorf, 1963; Gordine and Codd, 1969) but recent work shows that the transition carbides are not particularly enriched with respect to silicon (Barnard *et al.* 1981).

Aluminium in solid solution is also believed to retard tempering reactions (Alten, 1954; Langer, 1968; Bhat, 1977). In all respects, aluminium seems to behave in a similar way to silicon, with respect to both the bainite and martensite transformations, although detailed data, for example on its solubility in carbides, are not available.

The fact that carbide precipitation from residual austenite lags behind that from bainitic ferrite is also established for steels containing little or no silicon or aluminium. In an Fe–0.3C–4.08Cr alloy isothermally transformed to lower bainite at 435°C for 10 min, the phase between the cementite containing ferrite platelets, is found to be austenite, whereas if

the sample is held at the transformation temperature for 30 min, the austenite is replaced with cementite (Bhadeshia, 1980a). Heavily alloyed, low carbon steels also show this effect: in a Fe–0.06C–0.27Si–1.84Mn–2.48Ni–0.2 wt% alloy, no cementite could be detected long after the cessation of the bainite transformation at 460°C. It was only after a mixture of bainitic ferrite and carbon enriched austenite (obtained by isothermal transformation at 460°C) was annealed at 600°C for 2 h did cementite formation eventually occur (Yang and Bhadeshia, 1987). A similar effect can be found in copper containing steels, when cementite formation only ocurs after annealing the mixture of bainitic ferrite and retained austenite at an elevated temperatue (Thompson *et al.*, 1988). It is well known that the upper bainite which forms in Fe–2.5Cr–1Mo–0.1C wt% steel (used in vast quantities in the power generation industry) is essentially free of carbides, the regions between the bainitic ferrite consisting of mixtures of martensite and retained austenite. For these steels, it is known that an increase in the average carbon concentration accelerates the precipitation of cementite in association with the upper bainitic microstructure (Wada and Eldis, 1982). It is likely that this is a general result in the sense that an increase in carbon concentration should lead to a corresponding increase in the driving force for cementite precipitation from austenite.

3.3.3 *Kinetics of Precipitation within Bainitic Ferrite*

It is particularly interesting that the precipitation of cementite from martensite or lower bainite can occur at temperatures below 400 K, in time periods too short to allow any substantial diffusion of iron atoms. The long range diffusion of carbon atoms is of course necessary, but because carbon resides in interstitial solution, it can be very mobile at temperatures as low as –60°C (Winchell and Cohen, 1962).

Thus, the formation of cementite in these circumstances must differ from the normal diffusional decomposition reactions which become very sluggish at low temperatures. For this reason, it has been believed for some time that the cementite lattice may be generated by the deformation of the ferrite lattice, combined with the necessary diffusion of carbon into the appropriate sites. The ways in which the ferrite lattice could be deformed to produce the right arrangement of iron atoms needed to generate the cementite or ε-carbide structures have been considered phenomenologically by Andrews (1963), Hume-Rothery *et al.*, (1942) and the subject has been reviewed by Yakel (1985). The models are not however sufficiently developed to predict transformation kinetics apart from suggesting that if the diffusion of iron is not necessary, then the precipitation reaction may be relatively rapid.

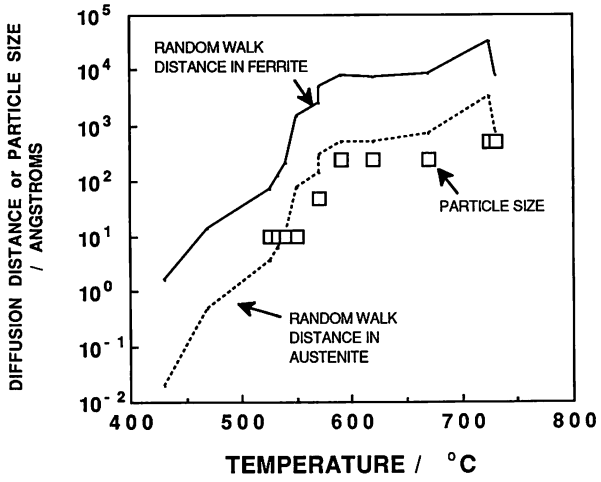

Fig. 3.5 *Correlation of a random walk distance for molybdenum atoms versus carbide particle size. The points represent experimental molybdenum carbide particle size data due to Stark and Smith (1987) whereas the curves represent calculated values of the random walk distance (in austenite and ferrite)* $2(D_{Mo}\,t)^{0.5}$ *for all of the particular heat treatments used in their experiments. The work revealed no such carbide precipitation when the ferrite examined was bainitic, all of the positive observations being from the ferrite that grew by reconstructive transformation. Carbides enriched in substitutional solute content are unable to precipitate in bainite due to the lack of atomic mobility.*

The lack of atomic mobility over the temperature range where bainite grow manifests itself in two ways as far as the precipitation of carbides is concerned. If the formation of a carbide particle necessitates the diffusion of iron or substitutional solute atoms, then its size will be restricted by the distance through which these atoms can diffuse during the time scale of the experiment. This is emphasised by recent atom probe experiments in which the transformation of a Fe–Mo–C alloy was studied over a wide range of temperatures with the carbide type, size and composition being characterised at a very high spatial and chemical resolution (Stark and Smith, 1987). Fig. 3.5 shows that the measured particle sizes correlate rather well with the random walk distance $2(D_{Mo}\,t)^{0.5}$, which is related to the available atomic mobility.

The second effect of atomic mobility on carbide precipitation is related to the mechanism by which the ferrite itself grows. The crystallographic change from $\gamma \rightarrow \alpha$ may occur without any diffusion. However, if the transformation mechanism is reconstructive, then mass transport is essential during growth even when there is no composition difference between the parent and product phases, because the mass transport occurs in a way

which minimises the strain energy associated with the lattice change. As pointed out earlier, this transport is called reconstructive diffusion. The transformation can then only proceed at a rate consistent this diffusion, so that substitutional solutes like molybdenum may at the same time have an opportunity to precipitate. It is not surprising that the ferrite in which the molybdenum carbides were observed to precipitate by Stark and Smith, was always that which grew by a reconstructive transformation mechanism, the carbides never being found in association with bainitic ferrite.

Table 3.2 Crystal structures of carbides in bainite or in tempered bainite. The designation κ is used for the new carbide discovered by Deliry (1965) and Pomey (1966). The ratio of iron+other metal atoms to carbon is designated Fe,M/C. The lattice parameters are stated in units of Ångstroms. The actual lattice parameters in any particular alloy must also depend on its detailed chemical composition.

Carbide	Crystal System	Fe,M/C	Reference
κ	Hexagonal a = 6.9 c = 4.8	1.37	Deliry, 1965 Pomey, 1966
ε	Hexagonal a = 2.735 c = 4.339	2.4–3	Jack, 1950, 1951 Hofer *et al.*, 1949
χ	Monoclinic a = 11.563 b = 4.573 c = 5.058 β = 97.44°	2.2 or 2.5	Hägg, 1934
η	Orthorhombic a = 4.704 b = 4.318 c = 2.830	2	Hirotsu and Nagakura, 1972
Fe_3C	Orthorhombic a = 4.525 b = 5.087 c = 6.743	3.0	
M_7C_3	Orthorhombic a = 4.526 b = 7.010 c = 12.142	7/3	Morniroli *et al.* (1983)
$(Fe,Si)C_x$	Orthorhombic a = 8.8 b = 9.0 c = 14.4		Knoval *et al.* (1959)
$(Fe,Si)C^x$	Orthorhombic a = 6.5 b = 7.7 c = 10.4		Schissler *et al.* (1975)
$(Fe,Si,Mn)C_x$	Orthorhombic a = 14.8 b = 11.4 c = 8.5		Schissler *et al.* (1975)
$M_{23}C_6$	Cubic F a = 10.621	23/6	
M_6C	Cubic F a = 11.082	6	
'c'	Triclinic a = 6.38 b = 5.05 c = 4.59 α = 90.0 β = 70.1 γ = 84.7		Sandvik 1982b

3.4 Crystallography of Carbide Precipitation in Bainite

Some of the details of the crystal structures of the carbides found in bainite or in tempered bainite are presented in Table 3.2; a comprehensive review has recently been published by Yakel (1985).

During typical isothermal heat treatments of the type used to generate bainite, the steel is not held at temperature for periods long enough to permit the long-range diffusion of substitutional atoms, so that only ε-carbide, η-carbide or cementite precipitate within bainitic ferrite, and only cementite or κ-carbide precipitate from the carbon enriched austenite between the ferrite platelets. The other carbides which do require long range diffusion form during tempering or during prolonged holding at the isothermal transformation temperature. Shackleton and Kelly (1965) reported that on rare occasions, $M_{23}C_6$ and M_7C_3 could be found in as-transformed bainite, but the heat treatment they used was not fully specified and the observations have not been verified subsequently. The crystal system of M_7C_3 is conventionally reported as hexagonal (a = 13.982, c = 4.506 Ångstroms) but there is evidence that it is better regarded as ordered orthorhombic (Morniroli *et al.* 1983).

3.4.1 Cementite: Orientation Relationship

Shackleton and Kelly (1965) conducted a very detailed and extensive study of the orientation relationships that exist between ferrite and carbides in bainite. The carbides within lower bainitic ferrite were always found to exhibit the orientation relationships observed for cementite that forms during the tempering of supersaturated martensite. As with martensite, the most frequently observed orientation relationship, also called the tempering or Bagaryatski (1950) relationship, was found to be

$$\{0\ 0\ 1\}_\theta \parallel \{2\ 1\ 1\}_\alpha$$
$$<1\ 0\ 0>_\theta \parallel <0\ \bar{1}\ 1>_\alpha$$

The next most frequently observed α/θ orientation relationship which is also consistent with the tempering of martensite, was found to be

$$\{0\ 0\ 1\}_\theta \parallel \{\bar{2}\ \bar{1}\ 5\}_\alpha$$
$$<1\ 0\ 0>_\theta \text{ within } 2.6° \text{ of } <3\ \bar{1}\ 1>_\alpha$$
$$<0\ 1\ 0>_\theta \text{ within } 2.6° \text{ of } <1\ 3\ 1>_\alpha$$

For the cementite that precipitates during the formation of upper bainite, Shackleton and Kelly showed that the large number of observed orientation relationships could all be rationalised if it is assumed that the cementite precipitates from austenite with the Pitsch (1962) γ/θ relationship

$\{0\ 0\ 1\}_\theta \parallel \{\bar{2}\ 2\ 5\}_\gamma$
$\langle 1\ 0\ 0\rangle_\theta$ within 2.6° of $\langle\bar{5}\ 5\ \bar{4}\rangle_\gamma$
$\langle 0\ 1\ 0\rangle_\theta$ within 2.6° of $\langle(\bar{1}\ 1\ \bar{0}\rangle_\gamma$

The α/θ relationships can be generated from the γ/θ relationship by allowing the ferrite to be a variant of the Kurdjumov and Sachs α/γ orientation relationship.

These results have been confirmed subsequently (e.g., Pickering, 1967; Bhadeshia, 1980a) and are important in understanding the mechanism of the bainite transformation; they suggest that in lower bainite the carbides precipitate from ferrite which is supersaturated with respect to carbon, since the same θ/α orientations are found during the tempering of martensite.

The θ/α orientation relationship found by Isaichev (1947) has also been reported for the cementite within lower bainitic ferrite (Ohmori, 1971a; Huang and Thomas, 1977). It is in fact quite close to the Bagaryatskii relationship (the two are difficult to distinguish experimentally) and in terms of rational indices, the Isaichev orientation relationship can be written

$$\langle 0\ 1\ 0\rangle_\theta \parallel \langle 1\ \bar{1}\ \bar{1}\rangle_\alpha$$
$$\{1\ 0\ 3\}_\theta \parallel \{1\ 0\ 1\}_\alpha$$

3.4.2 *The Habit Plane of Cementite*

Using single surface trace analysis, Shackleton and Kelly showed that for the tempering orientation relationship, the habit plane of cementite in lower bainitic ferrite is in the vicinity of the zone containing $\{1\ \bar{1}\ 2\}_\alpha$ and $\{0\ \bar{1}\ 1\}_\alpha$ (corresponding to $\{1\ 0\ 1\}_\theta$ and $\{1\ 0\ 0\}_\theta$ respectively). The results are vague because of the irregular shape of the cementite particles and because of the inaccuracies in the technique used. The long dimension of the cementite laths was found to be approximately $\langle 1\ \bar{1}\ \bar{1}\rangle_\alpha$ (corresponding to $\langle 0\ 1\ 0\rangle_\theta$). Note that for these data, the crystallographic indices have justifiably been quoted with respect to both the α and θ lattices since some of the trace analyses were carried out using diffraction information obtained simultaneously from both lattices. The results are qualitatively consistent with the habit plane of cementite containing the direction of maximum coherency between the ferrite and cementite lattices, i.e., $\langle 0\ 1\ 0\rangle_\theta \parallel \langle 1\ \bar{1}\ \bar{1}\rangle_\alpha$ (Andrews, 1963).

For some alloys, the observation of streaks in electron diffraction patterns has been interpreted to indicate that in those cases, the habit plane of the cementite within lower bainitic ferrite is approximately $\{0\ 0\ 1\}_\theta \parallel \{2\ 1\ 1\}_\alpha$ (Srinivasan and Wayman, 1968c). However, similar streaking has been observed for a case where the cementite habit plane is

$\{2\ 0\ 1\}_\theta$; the streaking may therefore be due to faulting on the $\{0\ 0\ 1\}_\theta$ planes (Ohmori, 1971a).

For upper bainite, the carbides precipitate from austenite; it is not therefore surprising that the particles do not exhibit a consistent set of habit plane indices with respect to ferrite, although those with respect to the cementite lattice are always found to be close to $\{1\ 0\ 1\}_\theta$ with a long direction close to $<0\ 1\ 0>_\theta$ (Shackleton and Kelly, 1965).

3.4.3 *Three Phase Crystallography*

Crystallographic information can be interpreted in much greater detail if the data are obtained *simultaneously* from austenite, ferrite and cementite. The first such experiments were reported by Srinivasan and Wayman (1968b, c) and subsequent (contradictory) data were given by Bhadeshia (1980a). The two sets of data, referred to the standard variant of the austenite ferrite relation defined above, and using *rational approximations* to the measurements are as follows:

(Srinivasan and Wayman, 1968b, c)

$$[1\ 1\ 1]_\gamma \parallel [0\ 1\ 1]_\alpha\ [1\ 0\ 0]_\theta$$
$$[\bar{1}\ 0\ 1]_\gamma \parallel [\bar{1}\ \bar{1}\ 1]_\alpha \parallel [0\ 1\ 0]_\theta$$
$$[1\ \bar{2}\ 1]_\gamma \parallel [2\ \bar{1}\ 1]_\alpha \parallel [0\ 0\ 1]_\theta$$

(Bhadeshia, 1980a)

$$[1\ 1\ 1]_\gamma \parallel [0\ 1\ 1]_\alpha$$
$$[0\ \bar{1}\ 1]_\gamma \parallel [\bar{1}\ \bar{1}\ 1]_\alpha$$

$$[0\ \bar{1}\ 1]_\alpha \parallel [1\ 0\ 0]_\theta$$
$$[1\ \bar{1}\ \bar{1}]_\alpha \parallel [0\ 1\ 0]_\theta$$
$$[2\ 1\ 1]_\alpha \parallel [0\ 0\ 1]_\theta$$

For the first set of data, the habit plane of the cementite within the lower bainitic ferrite is found to be $(1\ 1\ 2)_\alpha$, corresponding to $(1\ 0\ 1)_\gamma$ Srinivasan and Wayman noted that this is one of the planes for the lattice invariant deformation for lower bainite as predicted using the phenomenological theory of martensite and implied that this may somehow explain the presence of just one crystallographic variant of cementite in lower bainite, as compared with the many found when martensite is tempered. When the lattice invariant deformation is slip, as is the case for bainite, it is incredibly difficult to establish any microstructural evidence in its support (although Ohmori, 1989, has claimed that the cementite traces in lower bainite can often be seen to be parallel to the traces of transformation twins in adjacent and approximately parallel plates of martensite). Srinivasan and Wayman interpreted the presence of the carbide on the appropriate planes to lend support to proposed mode of

lattice invariant deformation in bainite. It was pointed out that the results may not be generally applicable, because they found that for a Fe–3.32Cr–0.66C wt% alloy the cementite habit plane seemed to be $\{0\,0\,1\}_\theta$ unlike the case for the more heavily alloyed sample.

Unfortunately, the second set of data above (Bhadeshia, 1980a) is not in agreement with the Srinivasan and Wayman hypothesis, and they noted themselves that the cementite habit plane in another Fe–Cr–C alloy containing less chromium and carbon was $(0\,0\,1)_\theta$ rather than $(0\,1\,0)_\theta$. Thus, although the lattice invariant deformation may be linked to the nucleation of cementite under some circumstances, it does not provide a consistent explanation in others. It also does not explain why multiple variants of carbides are observed in martensites. Further experimental results are highly desirable to ascertain whether the single dominant variant of cementite formed in lower bainite does have different crystallographic relations with the ferrite in different alloys.

3.4.3.1 Interphase Precipitation

An alternative view is that the cementite of lower bainite nucleates and grows at the austenite/ferrite interface, a process which is well established in the high temperature precipitation of carbides and is described as 'interphase precipitation' (Honeycombe and Pickering, 1972). The carbon that is necessary to sustain the growth of cementite can be absorbed from the adjacent austenite and it is then not necessary for the ferrite to be supersaturated. It is argued that during nucleation, the cementite should adopt an orientation which provides good lattice matching with *both* α and γ. If it happens to be the case that there is only one orientation in space which allows good matching with both the adjacent phases, then the theory indicates that only one crystallographic variant of cementite should precipitate for a given variant of ferrite.

It seems intuitively reasonable that a particle at the transformation interface should attempt to lattice match simultaneously with both the adjacent phases. However, the experimental evidence quoted in support of the model (reviewed by Honeycombe, 1984) does not seem adequate. For example, during the interphase precipitation of $M_{23}C_6$ in chromium rich steels, the carbide (which has a face centered cubic lattice) adopts a cube-cube orientation with the austenite, and a Kurdjumov–Sachs orientation with the ferrite. However, $M_{23}C_6$ in austenite always precipitates in a cube-cube orientation with austenite, even in the absence of any ferrite. Suppose that the carbide precipitates in austenite, and that the austenite then transforms to ferrite, then it follows that the ferrite is likely to adopt a rational Kurdjumov–Sachs orientation with the austenite, and *consequently* with the $M_{23}C_6$, the final three phase crystallography having nothing to do with simultaneous lattice matching between all three phases.

During interphase precipitation, the $M_{23}C_6$ could be completely oblivious of the ferrite, even though it may be in contact with the phase, but the good three phase crystallography would nevertheless follow simply because the $M_{23}C_6$ has a cube-cube orientation with the austenite. To test unambiguously, the theory requires a system where the particles which form at the interphase interface are able to adopt many different variants of an orientation relation with the austenite. It is suggested that interphase precipitation of Mo_2C is an example suitable for further work.

Given a Bagaryatskii orientation relationship between lower bainitic ferrite and its internal cementite particles, and a Kurdjumov–Sachs orientation relationship between the ferrite and austenite, it can be shown (Bhadeshia, 1980a) that the three phase crystallography expected on the basis of the lattice matching arguments is

$$[1\ 0\ 0]_\theta \parallel [0\ \bar{1}\ 1]_\alpha \parallel [1\ 1\ 1]_\gamma$$
$$[0\ 1\ 0]_\theta \parallel [1\ \bar{1}\ \bar{1}]_\alpha \parallel [\bar{1}\ 0\ 1]_\gamma$$

The experimental data for lower bainite clearly do not agree with these orientation relations, the cementite 'making no effort' to lattice match with the austenite.[2] This conclusion remains valid even if the α/γ orientation relationship turns out to be of the Nishiyama–Wasserman type.

There is another way of verifying this conclusion. Aaronson *et al.* (1978) have modelled the growth of cementite which nucleates at the α/γ interface. In this model, the penetration of the cementite into the adjacent ferrite or austenite is determined by the rate at which either of these phases transform into cementite. The growth of the cementite is treated in terms of a one-dimensional diffusion controlled growth process. With the Zener approximation of a linear concentration gradient in the parent phase, the penetration of cementite in ferrite (G_α) and in austenite (G_γ) are given by

$$G_\alpha \approx 0.5t^{-0.5}D_\alpha{}^{0.5}(\bar{c}^\alpha - c^{\alpha\theta})/[2(c^{\theta\alpha} - c^{\alpha\theta})(c^{\theta\alpha} - \bar{c})]^{0.5} \qquad (3.6)$$

$$G_\gamma \approx 0.5t^{-0.5}D_\gamma{}^{0.5}(\bar{c}^\gamma - c^{\gamma\theta})/[2(c^{\theta\gamma} - c^{\gamma\theta})(c^{\theta\gamma} - \bar{c})]^{0.5} \qquad (3.7)$$

where for example, D_α is the diffusivity of carbon in ferrite, $\bar{c}$ is the average carbon concentration in the parent phase (α or γ), $c^{\gamma\theta}$ represents

2 Huang and Thomas (1977) have expressed the three phases crystallography of lower bainitic ferrite, the cementite within this ferrite, and austenite as follows:

$$(1\ 0\ 0)_\theta \parallel (5\ \bar{4}\ 5)_\gamma\ 5.77^\circ \text{ from } (1\ 0\ 1)_\alpha$$
$$(0\ 1\ 0)_\theta \parallel (1\ 0\ \bar{1})_\gamma \parallel (1\ 1\ \bar{1})_\alpha$$

The three phase relationship is not however based on direct experimental evidence. The angle quoted has been corrected from the original paper.

the concentration of carbon in the austenite which is in equilibrium with cementite and t represents the time after the nucleation event. If it is assumed that $c^{\theta\alpha}$ or $c^{\theta\gamma}$ are much greater than $\bar{c}$, $c^{\alpha\theta}$ or $c^{\gamma\theta}$, the ratio of growth rates is given by

$$G^{\alpha}/G^{\gamma} = [D_{\alpha}{}^{0.5}(\bar{c}^{\alpha} - c^{\alpha\theta})]/[D_{\gamma}{}^{0.5}(\bar{c}^{\gamma} - c^{\gamma\theta})] \quad (3.8)$$

Note that the left hand side of this equation could be replaced by the corresponding ratio of particle dimensions in the two parent phases. Aaronson *et al.* made the further assumption that the carbon concentrations of the austenite and ferrite before the onset of cementite formation are given by $c^{\gamma\alpha}$ and $c^{\alpha\gamma}$ respectively. This in turn implies a number of further assumptions which are not consistent with experimental data: that carbide formation does not begin until the formation of all bainitic ferrite is complete, that there is no supersaturation of carbon in the bainitic ferrite and that the bainite transformation does not obey the incomplete-reaction phenomenon.

On the basis of these assumptions, the cementite in bainite essentially grows by drawing on the richer reservoir of carbon in the austenite, and should therefore penetrate to a far greater extent into the austenite than into the ferrite. Contrary to this conclusion, direct observations (Fig. 3.3) prove that in the rare cases where a cementite particle in lower bainite happens to be in contact with the transformation interface, the cementite is confined to the ferrite (Bhadeshia, 1980a).

Aaronson *et al.* also concluded that since the model predicts that the interphase growth of cementite occurs into both bainitic ferrite and austenite, the debate about whether the carbides nucleate in α or γ is irrelevant. This is not justified because it assumes that the carbides nucleate at the interphase interface, whereas it is more likely that the carbides which precipitate within the lower bainitic ferrite nucleate and grow from the supersaturated bainitic ferrite.

3.4.4 *Relief of Strain Energy*

The evidence, therefore, seems to suggest that the occurrence of a single crystallographic variant of carbide in lower bainite cannot be explained in terms of either the interphase precipitation model or the lattice invariant shear arguments. A possible alternative explanation is that the variant which forms is one that is best suited towards relieving the elastic strains associated with the austenite to lower bainite transformation (Bhadeshia, 1980a). The observation that carbide precipitation modifies the surface relief of lower bainite supports this conclusion, particularly since freshly formed plates (apparently without carbide precipitation) exhibit perfect invariant plane strain relief (Clark and Wayman, 1970).

If this explanation is accepted, then it begs the question as to why multiple variants of carbides occur during the tempering of martensite. However, an examination of a large number of published micrographs in the literature indicates that even in tempered martensite, there is usually one dominant variant and in many cases, just one variant of carbide present. Examples can be found in standard textbooks such as that by Honeycombe (Fig. 8.3, 1981), or in the latest of research articles (Speich, Fig. 3, 1987).

3.4.5 Epsilon-Carbide

The orientation relationship between ε-carbide in tempered martensite was deduced by Jack (1950, 1951) as

$$(1\ 0\ 1)_\alpha \parallel (1\ 0\ \bar{1}\ 1)_\varepsilon$$
$$(2\ \bar{1}\ 1)_\alpha \parallel (1\ 0\ \bar{1}\ 0)_\varepsilon$$
$$(0\ 1\ 1)_\alpha \parallel (0\ 0\ 0\ 1)_\varepsilon$$
$$(\bar{1}\ \bar{1}\ 1)_\alpha \parallel (1\ \bar{2}\ 1\ 0)_\varepsilon$$

which also implies that

$$(1\ 0\ 1)_\alpha \approx 1.37^\circ \text{ from } (1\ 0\ \bar{1}\ 1)_\varepsilon$$
$$[1\ 0\ 0]_\alpha \approx 5^\circ \text{ from } [1\ 1\ \bar{2}\ 0]_\varepsilon$$

The first reported crystallographic results for ε-carbide in lower bainite seem to be those of Lai (1975), who observed that $\langle 1\ 0\ 0\rangle_\alpha \parallel \langle 1\ 1\ \bar{2}\ 0\rangle_\varepsilon$ and therefore concluded that the orientation relationship was that found in tempered martensite. However, although his data are consistent with the tempered martensite orientation relationship within the limits of experimental error, they are incomplete since a minimum of two pairs of parallel vectors need to be stated in order to specify the relationship between two crystals. A more detailed study by Huang and Thomas (1977) has subsequenly confirmed that the ε-carbide found in lower bainite does indeed obey the same orientation relationship with bainitic ferrite as is found during the tempering of martensite.

The ε-carbides are found to occur in the form of plates which are approximately 6–20 nm thick and 70–400 nm long (Huang and Thomas). The carbide/ferrite interface tends to be ragged, but on a more macroscopic scale, single surface trace analysis suggests that the carbide particles grow along $\langle 1\ 0\ 0\rangle_\alpha$ directions on $\{0\ 0\ 1\}_\alpha$ habit planes (Lai).

Huang and Thomas concluded that the ε-carbides precipitate at the austenite/bainitic ferrite interface, on the grounds that the observed orientation between the bainitic ferrite and ε-carbide could be generated by assuming a Kurdjumov–Sachs α/γ orientation, and a relationship between ε-carbide and austenite in which

$$(1\ 1\ 1)_\gamma \parallel (0\ 0\ 0\ 1)_\varepsilon$$
$$(1\ \bar{1}\ 0)_\gamma \parallel (1\ \bar{2}\ 1\ 0)_\varepsilon$$

However, neither this orientation relationship nor the three phase crystallography has been verified experimentally, and furthermore, it is not established that the proposed three phase crystallography is unique, so that the explanation for the occurrence of the single variant of carbide is also unjustified.

Subsequent work by Sandvik (1982a) experimentally verified the above three phase crystallography for ε-carbide in bainitic ferrite, but the precipitation observed was obtained by prolonged ageing of bainite and was believed to have formed at the interface between bainite and small regions of austenite twins which were left untransformed within the bainite. The observed ε-carbide habit plane, $(1\ 0\ 1)_\alpha \parallel (0\ 0\ 0\ 1)_\varepsilon$ was also found to be different from that noted by Lai. More work is needed to clarify the crystallography of ε-carbide precipitation in bainite.

3.4.6 Eta-Carbide

η-carbide is a transition Fe_2C carbide in the orthorhombic crystal system. It is usually associated with the tempering of martensite (Hirotsu and Nagakura, 1972; Nagakura *et al.* 1983) where the martensite/carbide orientation relationship is found to be as follows:

$$(1\ 1\ 0)_\eta \parallel \{0\ 1\ 0\}_\alpha$$
$$[0\ 0\ 1]_\eta \parallel \langle 1\ 0\ 0\rangle_\alpha$$

The carbide has recently been found in lower bainitic ferrite in the austenitic matrix of a high-silicon cast iron (Franetovic *et al.* 1987a, b), where electron diffraction confirms that

$$[0\ 0\ 1]_\theta \parallel \langle 1\ 0\ 0\rangle_\alpha \parallel \langle 0\ \bar{1}\ 1\rangle_\gamma$$

This information is consistent with the η-carbide/martensite orientation relationship stated earlier and lends further support to the hypothesis that the carbides within lower bainitic ferrite precipitate in a manner analogous to the tempering of martensite.

Franetovic *et al.* also deduced, from an examination of the zone axes of their diffraction patterns, that

$$[0\ 1\ 0]_\theta \parallel \langle 0\ 1\ 2\rangle_\alpha \parallel \langle \bar{1}\ 1\ 1\rangle_\gamma$$

However, the zone axes of the three superimposed patterns could be far from parallel and this particular set of data is doubtful. Indeed, if the parallelisms are assumed then the Nishiyama–Wasserman orientation

relationship implied between the austenite and ferrite lattices does not follow. More research is needed to fully establish the three phase crystallography of η-carbide, austenite and bainitic ferrite.

3.4.7 *Chi-Carbide*

χ-Carbide is another transition carbide which is metastable with respect to cementite. It is found during the tempering of martensite, where high resolution electron microscopy has demonstrated that what at first sight appears to be faulted cementite in fact consists of interpenetrating layers of cementite and χ, described as 'microsyntactic intergrowth' (Nagakura *et al.*, 1981; Nakamura *et al.*, 1985). The $\{2\ 0\ 0\}_\chi$ planes are found to be parallel to the $\{0\ 0\ 1\}_\theta$ planes of slightly different spacing (0.57 and 0.67 nm respectively). Thus, the faults in the cementite really correspond to regions of χ, each a few interplanar spacings thick, and this intimate mixture of cementite and χ consequently has a non-stoichiometric overall composition expressed by $Fe_{2n+1}C_n$, where $n \geq 3$.

Similar observations have recently been reported by Ohmori (1986), but for cementite in both tempered martensite and lower bainite, in a Fe–0.7C wt% steel (Fig. 3.6). High resolution electron microscopy (HREM) revealed that the cementite particles (in both cases in the same crystallographic orientation with the matrix) contained regions of χ-carbide, lending yet more support to the analogy between tempered martensite and lower bainite. This is also consistent with Ohmori's qualitative observation that the particles of cementite within the bainitic ferrite increase in size during transformation, as if growing from carbon supersaturated ferrite.

Ohmori (1986) has also claimed that the mechanism of precipitation in the lower bainite was different from that in tempered martensite, on the grounds that the cementite in the lower bainite contained a smaller amount of χ-carbide. A difficulty with this conclusion is that the amount of material examined in an HREM experiment is negligible, and is unlikely to be representative. The heat treatments utilised in producing lower bainite and martensite are also different, so that good comparisons are difficult to make.

Direct observations on martensite tempering, by Nakamura *et al.* (1985), indicate that the mechanism by which the mixed χ/cementite particles are replaced by cementite can be complicated and site dependent. One of the cementite layers in the mixed particle tends to grow into the surrounding matrix, at the expense of the mixed particle which dissolves. This dissolution is found to occur more rapidly for mixed particles which happen to be located at grain boundaries, presumably because such boundaries provide easy diffusion paths.

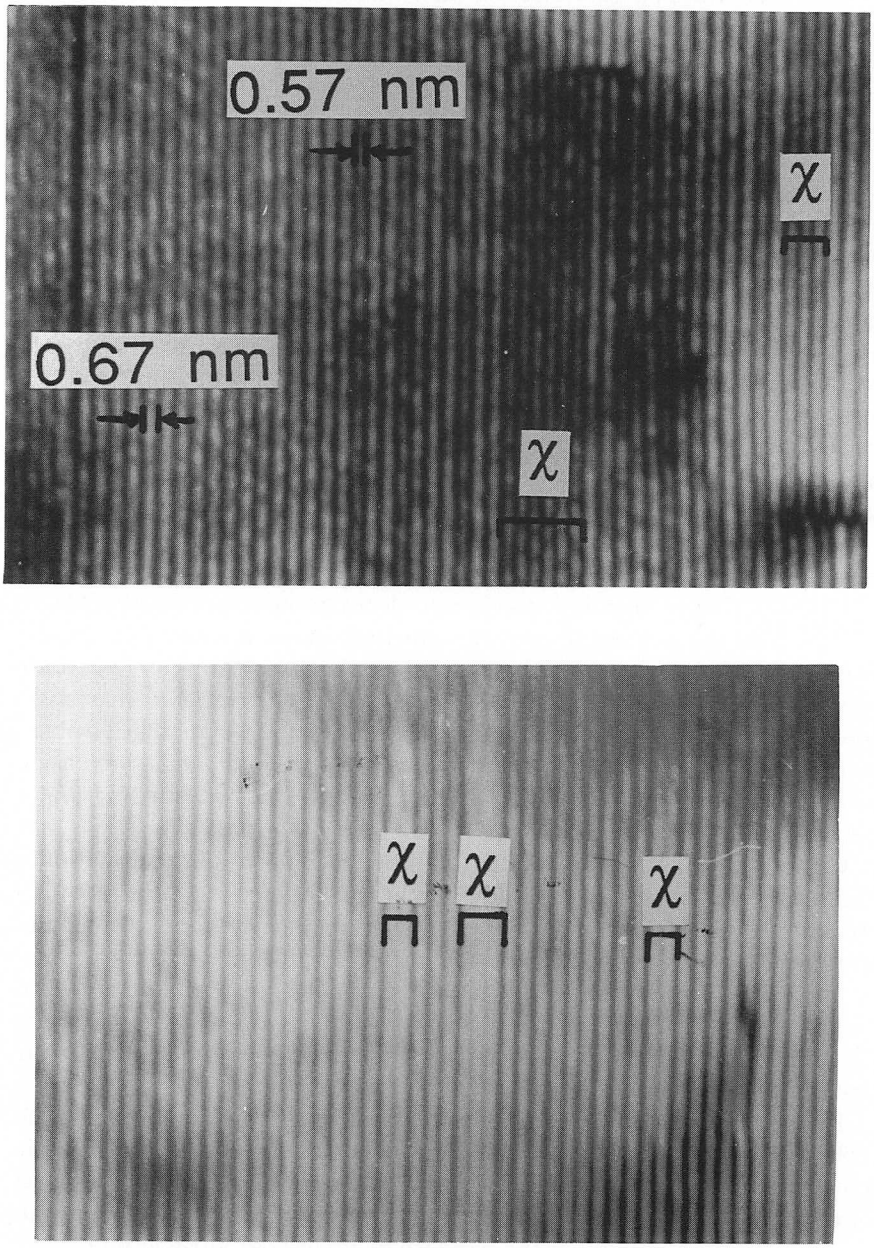

Fig. 3.6 *Lattice resolution transmission electron micrographs showing the intergrowth of layers of cementite and χ-carbide (Ohmori, 1986). (a) Carbide particle which precipitated in lower bainitic ferrite. (b) Carbide particle formed during the tempering of martensite.*

It is interesting that the mechanism involves the dissolution of both the cementite and χ in the mixed particles. This might be expected if it is assumed that the original particle forms by displacive transformation; the accompanying strain energy could then provide the driving force for its replacement by more globular cementite particles forming by reconstructive growth. Also, the boundaries between the χ and cementite layers are coherent and would not be expected to be very mobile, in which case, the cementite layers would be kinetically hindered from growing into the adjacent χ layers.

3.5 Chemical Composition of Bainitic Carbides

It has long been established, using magnetic, chemical and X-ray methods on extracted carbides, that the cementite associated with upper bainite in alloy steels has a substitutional solute content which is close to, or slightly higher than that of the steel as a whole, and far from what would be expected from considerations of chemical equilibrium (see for example, Hultgren, 1947, 1953).[3] Tsivinsky *et al.* (1959) reported that in steels containing chromium and tungsten, a significant degree of partitioning of Cr and W was found to occur to the cementite from austenite during the growth of pearlite, but not during the growth of bainite. Recent work is in broad agreement with the early data; Chance and Ridley (1981) found that for upper bainite in a Fe–0.81C–1.41Cr wt% alloy, the partition coefficient k_{cr}, defined as (wt% Cr in θ)/(wt% Cr in α) could not be distinguished from unity. Results like these have been interpreted to imply that there is no significant redistribution of substitutional alloying elements during the growth of bainitic cementite. Chance and Ridley suggested that the reason why segregation is found in pearlite but not in bainite (for the same transformation temperature) is that there is a fast diffusion path along the incoherent interface for pearlite.

3.6 Summary

The growth of upper bainite leads to the partitioning of carbon into the residual austenite. If the transformation conditions render the austenite thermodynamically unstable with respect to carbide precipitation, then it

3 The determination of the chemical composition of cementite must be conducted on specimens which have been held at the isothermal transformation temperature for short periods of time. Otherwise, diffusion after transformation has been shown to significantly influence the results, as the cementite and ferrite tend towards equilibrium (Hultgren, 1947).

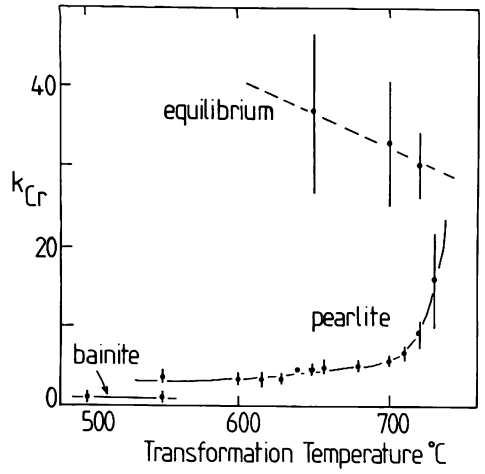

Fig. 3.7 *Partitioning coefficient of chromium between cementite and ferrite, as a function of transformation temperature (after Chance and Ridley). For the pearlite, the partitioning coefficients are measured in the pearlite at the pearlite/austenite interface.*

eventually decomposes by precipitation of cementite and more ferrite. In some alloys, cementite formation is preceded by that of transition carbides such as κ or c-carbide. In lower bainite, some of the carbon precipitates from supersaturated ferrite and the rest is partitioned into the remaining austenite. The quantity of carbides that precipitate from the austenite between the platelets of bainitic ferrite is therefore smaller when compared with upper bainite. Every carbide precipitation reaction that is found in tempered martensite has also been observed in lower bainite with exactly identical crystallographic and morphological characteristics. However, the exception is that the carbide particles in any given lower bainitic platelet tend to precipitate in a single crystallographic orientation whereas the tempering of martensite usually leads to the precipitation of several crystallographic variants. The reasons for this difference are not yet understood, but a possible explanation is that the self-stress of a lower bainite plate favours precipitation of a particular carbide variant.

The carbide precipitation reactions for both upper and lower bainite are secondary events which occur after the growth of bainitic ferrite. In some alloys, especially those containing relatively large concentrations of silicon or aluminium, the carbide precipitation reaction can be so sluggish that for practical purposes, the bainite consists of a mixture of only bainitic ferrite and carbon enriched residual austenite.

The mobility of atoms over the range of temperatures within which bainite grows is extremely small. This, and other observations, suggests

that the precipitation of carbides occurs by a displacive mechanism in which only the interstitial elements diffuse. This is consistent with the fact that there is no change in substitutional solute content when bainitic carbides precipitate, and with the crystallographic characteristics of the carbides with respect to the matrix.

4 *Microstructural Changes During the Tempering of Bainite*

4.1 Introduction

Tempering is a term historically associated with the heat treatment of martensite in steels. It describes how the microstructure and mechanical properties change as the metastable sample is held isothermally at a temperature below Ae1. The processes that occur during the tempering of martensite can be categorised into several stages. Stage 1 primarily influences any carbon that may be in solid solution; the excess carbon first tends to segregate to defects or cluster within the solid solution. It eventually precipitates, either as cementite for low carbon steels, or as transition carbides for relatively high carbon alloys. The carbon concentration that remains in solid solution may be quite large if the precipitate is a transition carbide. Further annealing leads to stage 2, in which almost all the excess carbon is precipitated, and the carbides all convert into the stable cementite form. Any retained austenite may also decompose during this stage. Continued tempering then leads to the spheroidisation of carbides, extensive recovery of the dislocation structure, and finally to the recrystallisation of the ferrite plates into equiaxed grains.

The description presented above is rather idealised. Many of the reactions ascribed to stage 1 can occur *during* the formation of the martensite when the martensite start temperature is high (such effects are known as *autotempering*). Bainite forms at even high temperatures, so that autotempering phenomena should be further exaggerated. The redistribution of carbon from supersaturated ferrite into the residual austenite, and the precipitation of carbides during the bainite reaction, occur very rapidly and could be classified as autotempering effects (Fig. 4.1). The purpose of this Chapter is to deal primarily with the tempering effects which occur after a bainitic microstructure is reheated; the *in situ* tempering phenomena are described elsewhere in the text.

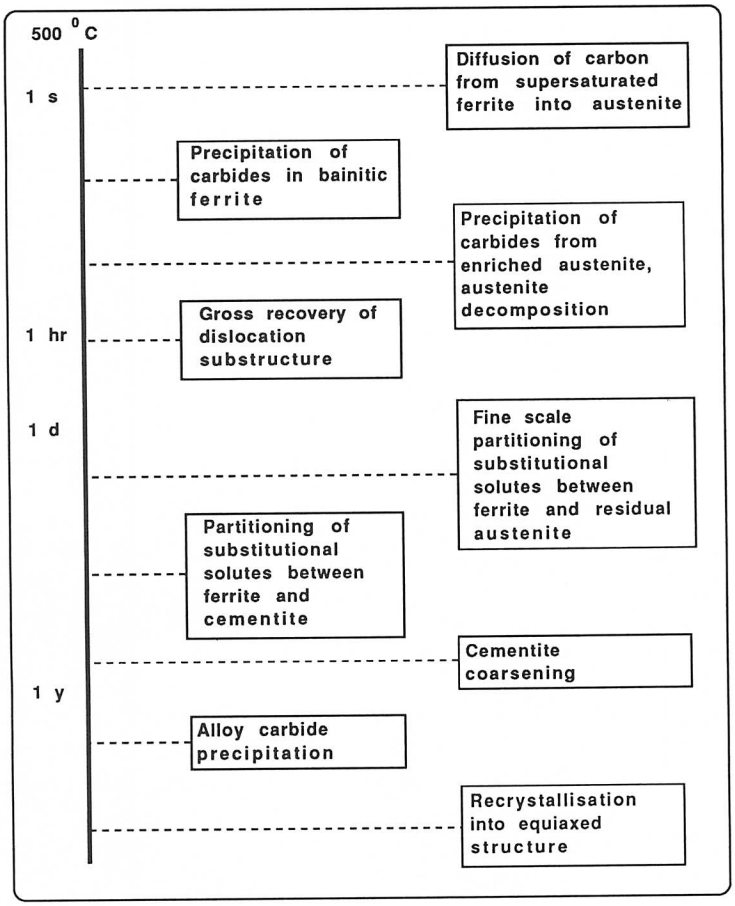

Fig. 4.1 *The time scales associated with a variety of tempering phenomena for bainite.*

The extent and the rate of change of the microstructure and properties during tempering, is intuitively expected to scale with the degree to which the virgin sample deviates from equilibrium. Bearing this in mind, there are a number of essential differences between the tempering behaviour of bainite and that of martensite.

Bainitic ferrite is only slightly supersaturated with carbon in solid solution. Most of the carbon in ordinary bainitic steels is tied up in the form of cementite precipitates, which tend to be coarse when compared with the carbides associated with tempered martensite. Consequently, in alloy steels, the kinetics of secondary hardening reactions for bainite are found to be slower than in martensite, because the cementite particles take longer to dissolve (Woodhead and Quarell, 1965). Secondary hardening

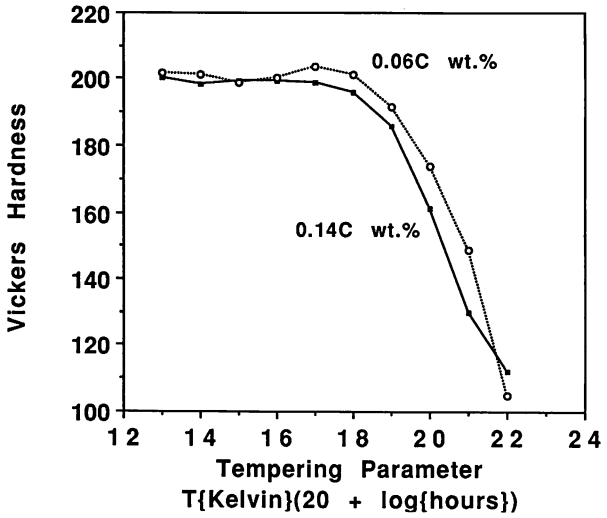

Fig. 4.2 *Diagram illustrating the change in hardness of two bainitic steels containing different carbon concentrations, as a function of a time–temperature tempering parameter (after Irvine and Pickering, 1957). The substitutional alloy concentrations of the steels illustrated are slightly different.*

involves the replacement of cementite with substitutional solute rich alloy carbides which are thermodynamically more stable.

When compared with martensite, bainite grows at relatively high temperatures where the microstructure undergoes some recovery during transformation. The extent of this recovery is much larger than would be associated with autotempered martensite. Consequently, when low carbon steel bainitic microstructures[1] are annealed at temperatures as high as 700°C(1 hr), there is only a slight increase in recovery, and little change in the morphology of the ferrite platelets or the number density of the carbide particles (Irvine *et al.*, 1957; Bush and Kelly, 1971). More rapid softening occurs only when the plate-like structure of ferrite changes into equiaxed ferrite. Whether this change is due simply to grain growth or to recrystallisation has not been investigated. In the former case it is the excess surface energy which constitutes the driving force, whereas during recrystallisation, it is the stored energy due to defects such as dislocations or due to elastic strains in the lattice which provides the major component of the driving force for the reaction. During the change to a more equiaxed microstructure, the cementite spherodises and coarsens

1 Typical composition: Fe–0.002B–0.17Si–0.52Mn–0.52Mo–0.1C, wt%. Without the boron, the formation of allotriomorphic ferrite would precede that of bainite, so that a mixed microstructure would be obtained.

considerably. Continued tempering then causes much smaller changes in hardness with time.

In marked contrast with martensitic steels, small variations in the carbon concentation (0.06–0.14wt%) have little effect on the bainite tempering curve (Fig. 4.2). Carbon has a very potent solid solution strengthening effect. Thus, the strength of martensite drops sharply as the carbon precipitates during tempering. For bainitic microstructures, the carbon is not in solid solution but is precipitated as coarse carbides which contribute little to strength (Irvine and Pickering, 1957; Irvine *et al.* 1957). It is not therefore surprising that the tempering response is rather insensitive to the average carbon concentration.

4.2 Tempering Kinetics

There is no complete model for the kinetics of bainite tempering reactions, certainly not of the kind that could be used in alloy and heat-treatment design. Fig. 4.2, illustrates an empirical method of rationalising tempering data using a time–temperature parameter, useful in the sense that it permits interpolation between experimentally established heat treatment conditions, together with the possibility of estimating anisothermal heat treatments which are more common in industrial practice.

The method has its origins in some pioneering work by Holloman and Jaffe (1945), who proposed that for a given isothermal heat treatment, the effectiveness of that treatment should be related to the product

$$t \exp\{-Q/RT\} \tag{4.1}$$

where Q is an effective activation energy and the other terms have their usual meanings. The product is in effect the integral of the curve of $\exp\{-Q/RT\}$ versus time. To estimate the period required to achieve the same metallurgical effect at another temperature simply involves the assumption that the product $t \exp\{-Q/RT\}$, once evaluated, is constant irrespective of temperature. The product is often called the *kinetic strength* of the heat treatment and provides a rough method for combining the influence of time and temperature. The fundamental justification of the concept of kinetic strength is rather difficult, especially in circumstances where the driving force varies with temperature. The mechanism of the metallurgical process concerned may also vary with temperature. Nevertheless, in the absence of more rigorous solutions, it is worth noting that the kinetic strength as defined above, and other empirical parameters (e.g., Fig. 4.2) have had many useful applications, for example in the representation of creep data, in weld microstructure calculations (Alberry and co-workers, 1977, 1979, 1983; Ashby, Easterling and Ion, 1982, 1984,

1987), and in the rationalisation of martensite tempering data (Hollomon and Jaffe, 1945). Irvine and Pickering have demonstrated its usefulness in representing the hardness of tempered bainite.

4.3 Tempering of Steels Containing Austenite

The decomposition of retained austenite during the heat treatment of martensite in quenched steels occurs during the 'second stage' of the tempering process. Appreciable quantities of retained austenite are usually only present in quenched steels which have carbon concentrations in excess of about 0.4 wt%. The conventional wisdom is that the decomposition of the austenite involves the formation of bainite. More recent work has demonstrated that the decomposition occurs by a reconstructive mechanism in which the formation of a mixture of ferrite and carbides does not generate surface relief effects of the kind associated with bainitic transformation (Kennon and Burgess, 1978). The austenite transformation begins at the interfaces with tempered martensite regions, perhaps simply involving the growth of those regions at the expense of the austenite.

For steels which are intended to have a predominantly bainitic microstructure, the alloy composition is usually chosen to generate a mixture of bainitic ferrite and carbides, with little or no austenite being retained to ambient temperature. On the other hand, when the precipitation of cementite is adequately retarded by the presence of elements such as silicon, relatively large quantities of austenite can be retained to ambient temperature. The austenite is usually present in two forms, as thin films between the bainitic ferrite sub-units, and as larger blocks between different crystallographic variants (sheaves) of bainite. All the austenite is enriched in carbon but the films, because they are isolated between ferrite platelets, might contain abnormally large concentrations of carbon.

4.3.1 Redistribution of Substitutional Solutes

The mechanism of bainitic transformation does not permit the diffusion of substitutional atoms, which may consequently be trapped in the product phase. Given the opportunity, they should tend to redistribute in a manner which leads to a reduction in the overall free energy. It is found that when a mixture of bainitic ferrite and austenite is tempered at relatively low temperatures, the substitutional species are able to partition between the phases before the austenite begins to decompose to more stable phases. The partitioning is necessarily on a very fine scale, and can only be detected using atomic resolution techniques. Fig. 4.3 illustrates one such experiment, in which a mixture of bainitic ferrite and austenite was annealed at 328°C for 11 days. There is clear evidence for the

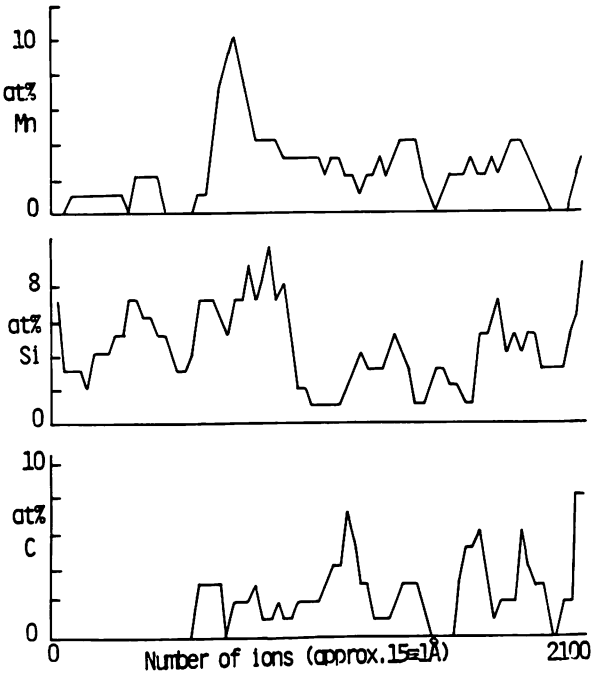

Fig. 4.3 *A field ion microscope/atom-probe experiment on an alloy Fe–0.43C–2.24Si–2.82Mn wt%, heat treated at 328°C for 11 days. This produces a mixture of bainitic ferrite and austenite with the reaction stopping after the first few minutes at temperature, the subsequent holding simply leading to an annealing of the microstructure. The diagram illustrates the composition profile obtained across the austenite/bainitic ferrite interface, which is identified by the point where significant levels of carbon begin to be detected. (Stark* et al., *1990).*

diffusion of manganese into the austenite at the interface, accompanied by a corresponding depletion zone in the ferrite.

4.3.2 *Decomposition of Austenite*

When the carbon concentration in all the regions of untransformed austenite is larger thac or equal to that given by the T'_o curve, tempering can only lead to further transformation by a mechanism involving the diffusion of carbon. The austenite may decompose into a mixture of ferrite and carbides if its carbon concentration exceeds that given by the extrapolated $\gamma/(\gamma + \text{carbide})$ phase boundary (Fig. 3.1b). The larger regions of austenite tend to form colonies of pearlite with a fine interlamellar spacing, whereas the films of austenite decompose during tempering into

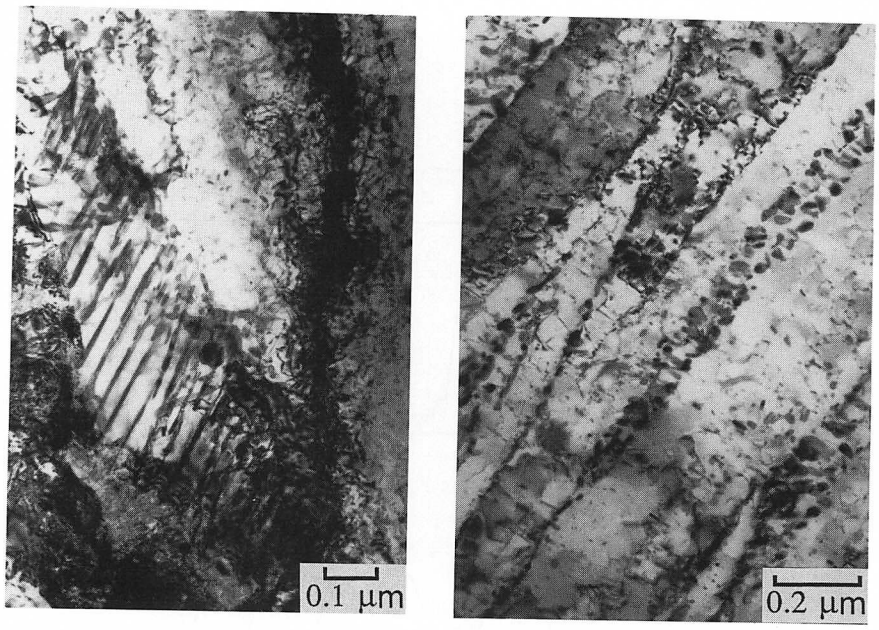

Fig. 4.4 *Transmission electron micrographs illustrating the effect of tempering a mixture of bainitic ferrite and retained austenite, in a Fe–3Mn–2Si–0.4C wt% alloy, at 500°C for 60 min. The austenite is supersaturated with respect to carbides. (a) The larger blocks of austenite tend to decompose into pearlite. (b) Arays of discrete carbide particles form between the sub-units of bainitic ferrite when the films of austenite decompose. The micostructure prior to tempering consisted of just bainitic ferrite and residual carbon enriched austenite.*

discrete particles of cementite in a matrix of ferrite (Fig. 4.4). The films are probably too thin to present an opportunity for the establishment of a cooperative growth process of the kind associated with pearlite colonies. The carbide formation condition might not be satisfied at high temperatures above T_c (Fig. 3.1b), in which case the austenite could still transform to ferrite although not by a bainitic mechanism. The decomposition of austenite by a reconstructive mechanism requires the diffusion of iron and substitutional atoms, and consequently tends to be sluggish in the temperature range where bainite forms.

The tempering process discussed above is in many respects equivalent to the prolonged heat treatment of austenite at temperatures below B_s. Continued holding at the isothermal transformation temperature after the growth of bainitic ferrite ceases, effectively tempers the microstructure and causes the decomposition of any residual austenite, albeit at a much slower rate as the microstructure attempts to approach equilibrium. The

quantity of residual austenite at the point where bainite growth ceases is larger at high temperatures, so that pearlite colonies eventually develop and consume the austenite. For example, in a Fe–3Mn–2Si–0.4C wt% alloy transformed isothermally at a temperature (452°C) close to B_s, the formation of upper bainite was found to finish in a matter of minutes, whereas it took more than 30 h for the development of a small amount of pearlite from the residual austenite (Fig. 4.5, Bhadeshia and Edmonds, 1979a). If a Fe–4Cr–0.3C wt% alloy is isothermally transformed at 478°C, the bainitic transformation stops within some 30 min but continued holding of the same specimen for some 40 days causes the residual austenite to undergo extremely slow reconstructive transformation into two different products (Bhadeshia, 1981b, 1982b). The first of these is alloy pearlite which nucleates at the austenite grain boundaries and develops as a separate transformation. In the other, the original bainite/austenite interfaces move to produce epitaxial reconstructive transformation (Fig. 4.5). The interfaces degentrate into a series of perturbations having an extremely irregular morphology. The perturbations have exactly the same crystallographic orientation as the original bainite (i.e., they are contiguous with the

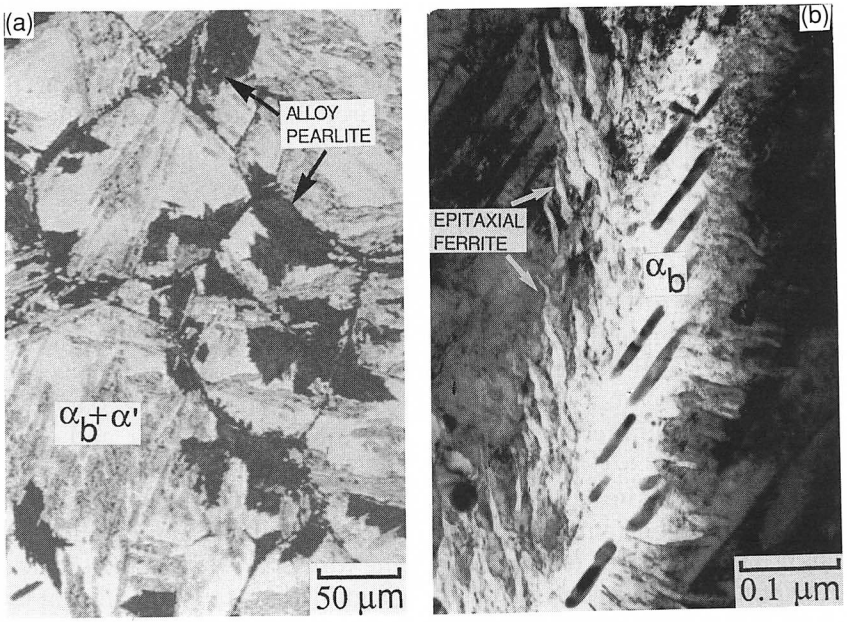

Fig. 4.5 *The non-bainitic decomposition of residual austenite during prolonged holding at the isothermal transformation temperature (below B_s). (a) Pearlite colonies; (b) ferrite growing epitaxially from bainite plates.*

bainitic ferrite) and they grow with the same substitutional alloy content as the parent austenite; this further transformation is not accompanied by an IPS shape change. It is incredible that the perturbations took 43 days to grow to a length comparable to the hickness of the original bainite plates (which completed transformation in a matter of seconds). Reconstructive growth is bound to be much slower than displacive transformation at low homologous temperatures.

4.4 Coarsening of Cementite

Coarsening reactions are driven by the need to minimise the total interfacial area per unit volume of sample. The rate equation for a coarsening process controlled by the diffusion of solute through the matrix is given by (Greenwood, 1956; Lifshitz and Slyozov, 1961; Wagner, 1961)

$$\bar{r}^3 - \bar{r}_o^3 = (8\sigma^{\theta\alpha} D_{eff} V_m^{\theta} t) \;/\; 9RT \qquad (4.2)$$

where V_m^{θ} is the molar volume of cementite, $c^{\alpha\theta}$ is the concentration of carbon in ferrite which is in equilibrium with cementite, $\bar{r}^3$ is the mean particle radius at time t and $\bar{r}_o^3$ is the mean particle radius at time zero, the moment when the coarsening reaction is purported to start. $\sigma^{\theta\alpha}$ is the cementite/ferrite interface energy per unit area ($\approx 690 \mathrm{J/m^2}$, Li *et al.*, 1966) and D_{eff} is an effective diffusion coefficient for carbon in ferrite. Since there is no change in precipitate volume fraction during coarsening, the diffusion of carbon is coupled to that of iron in such a way that the total volume remains constant. D_{eff} is then given by (Li *et al.*, 1966)

$$D_{\mathrm{eff}} = n_{\mathrm{Fe}} D^{\alpha}_{\mathrm{Fe}} D^{\alpha}_{\mathrm{c}} \Omega_{\mathrm{Fe}} [\Omega_{\mathrm{Fe}} + (n_{\mathrm{c}}/n_{\mathrm{Fe}})\Omega_{\mathrm{c}}] / [(n_{\mathrm{Fe}} D^{\alpha}_{\mathrm{Fe}} \Omega_{\mathrm{Fe}}^2) + (n_{\mathrm{c}} D^{\alpha}_{\mathrm{c}} \Omega_{\mathrm{c}}^2)] \qquad (4.3)$$

where n_{Fe} and n_{c} are the numbers of iron or carbon atoms per unit volume of ferrite respectively, D^{α}_{Fe} and D^{α}_{c} are the respective diffusivities of iron and carbon in ferrite, Ω_{Fe} is the volume per atom of ferrite and Ω_{c} is the volume of a molecule of Fe_3C less $3\Omega_{\mathrm{Fe}}$. It has been shown that equation 4.3 describes to a fair accuracy, the coarsening kinetics of cementite during the tempering of both upper and lower bainite in a Fe–0.67C–0.73Mn–0.27Si wt% commercial steel (Deep and Williams, 1975). The agreement with theory was found to be best for the higher tempering temperatures, the theory underestimating the coarsening rates at lower temperatures. The discrepancy was attributed to grain boundary diffusion contributing significantly to the net flux at low temperatures.

A model which deals with the coarsening of cementite under conditions where both grain boundary and lattice diffusion are important has been presented by Venugopalan and Kirkaldy (1977). It takes account of

the simultaneous coarsening of carbide particles and ferrite grains, allows for the multicomponent nature of alloys steels and works remarkably well in predicting the mean particle size, ferrite grain size and strength of tempered martensite; it has yet to be applied to bainite.

Coarsening theory also suggests that the time-independent particle size distribution (normalised with respect to the mean particle radius) should be skewed towards large particles, with a sharp cut off at a normalised radius of 1.5. However, measured distributions for cementite in bainite are not found to fit this behaviour, the distributions instead being skewed towards smaller particle sizes. Deep and Williams point out that this behaviour is also found for cementite in tempered martensite.

4.5 Secondary Hardening and the Precipitation of Alloy Carbides

Secondary hardening is usually associated with the tempering of martensite in steels containing strong carbide forming elements like Cr, V, Mo, Nb, etc. The formation of these alloy carbides necessitates the long range diffusion of substitutional atoms and their precipitation is consequently sluggish. Hence, cementite (or one of the transition iron carbides) has a kinetic advantage even though it may not be the most thermodynamically stable of all the possible carbides in an alloy steel. It is important to note, however, that in substitutionally alloyed steels, the 'iron carbides' only have a kinetic advantage if the substitutional solutes do not have to diffuse during the nucleation and growth processes.

This stage of tempering is accompanied by a drop in the hardness, but the alloy carbides, when they eventually form at the expense of cementite, often pose formidable obstacles to dislocation motion and lead to an increase in hardness with tempering time. This is the phenomenon commonly referred to as *secondary hardening*. Eventually, the usual growth and coarsening reactions make even these carbides less effective in hindering dislocation motion and the hardness then drops monotonically with tempering time. Although the strengthening effects discussed here and elsewhere are of considerable commercial importance, there are other applications of the phenomenon. For example, the exact manner in which bainitic cementite transforms to alloy carbides is of considerable practical interest in the power generation industry, where alloy steels with a microstructure which contains a substantial amount of bainite are used for long periods at elevated temperatures (approximately 560°C for periods up to 30 years).

There is in principle no reason why tempering reactions in bainite in alloy steels should be different with respect to secondary hardening in martensitic microstructures. The early work of Irvine *et al.* (1957) did not reveal any pronounced peaks in the tempering curves for bainite,

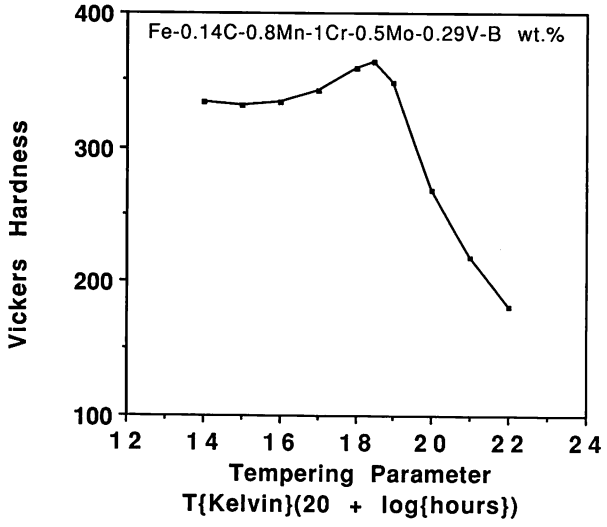

Fig. 4.6 *An illustration of a secondary hardening peak in a vanadium containing bainitic steel (after Irvine and Pickering, 1957).*

perhaps because of the low Mo concentration in the steels used. Secondary hardening peaks were subsequently observed during the tempering of a vanadium containing bainitic steel though no such peaks were found to Cr or Mo containing bainitic steels (Fig. 4.6, Irvine and Pickering, 1957). An unexplained observation was that for the Mo containing steels, the carbide formed on tempering bainite is initially cementite, which then transforms to $(Fe,Mo)_{23}C_6$, whereas on tempering martensite in the same steels the ultimate carbides are found to be Mo_2C.

Later work revealed clear evidence of secondary hardening in low carbon bainitic steels containing up to 2.95wt% Mo, 2.12wt%Cr and also in vanadium containing bainitic steels (Baker and Nutting, 1959; Irvine and Pickering, 1957). Whether or not secondary hardening *peaks* are observed in the tempering curves, all of these data are consistent with the existence of such hardening during the tempering of bainite, because the tempering resistance of the steels was improved.

Finally, since the bainite reaction can occur at relatively high temperatures, it should in principle be possible to design a steel in which the bainite secondary hardens during the period of the heat treatment required to generate much of the microstructure. The bainite start temperature of such a steel would be expected to be around 650°C, and the alloy chemistry would have to be engineered to avoid interference from any diffusional transformation products such as pearlite or allotriomorphic ferrite.

4.6 Changes in the Composition of Cementite

We have already noted that the cementite that is precipitated from austenite during the formation of upper bainite in alloy steels has a substitutional solute content which is similar to that of the parent phase. In general, the composition of bainitic cementite deviates considerably from that demanded by equilibrium with ferrite or with austenite. Consequently, before any alloy carbides are precipitated, the cementite during tempering tends towards its equilibrium composition. The exact manner in which the cementite composition alters must depend on the steel composition, starting microstructure and tempering conditions. There is as yet no complete theory capable of relating all of these variables and the work reviewed below should be interpreted with caution; many of the experiments deal with mixed microstructures (e.g. bainite and allotriomorphic ferrite) produced by continuous cooling transformation. They also do not distinguish between the bainitic cementite which precipitates from austenite and that which grows from any lower bainitic ferrite. The detailed steel composition will also determine the equilibrium composition of the cementite, since the chemical potential of an element is in general a function of the concentrations of all the elements in solution.

Most of the chemical data have been obtained using either direct chemical analysis of extracted carbides, or energy dispersive X-ray analysis techniques associated with transmission electron microscopy. These techniques are not well suited for the analysis of carbon or nitrogen concentrations, and the problem is usually circumvented by assuming stoichiometry. It is however likely that carbon and nitrogen can to some extent substitute for each other in many cases where carbo-nitrides may in fact form, and indeed, the thermodynamic stabilities of these phases may then be significantly altered. Nitrogen concentrations in wrought steels tend to be very small (<40 p.p.m.) since it is detrimental to toughness, but much higher concentrations are often unavoidable in weld deposits. Using atom probe field ion microscopy, a technique which can easily detect and quantify the concentration of light elements, it has been shown that M_2C carbides found in a tempered bainitic weld deposit have the average chemical composition $(Cr_{0.41}\ Mo_{0.59})_2(C_{0.96}N_{0.04})$ (Josefsson *et al.*, 1987; Josefsson, 1989).

Some of the first data on the tempering of bainite were obtained by Baker and Nutting (1959). A Fe–0.15C–2.12Cr–0.94Mo wt% commercial steel was normalised to give a mixed microstructure of allotriomorphic ferrite and bainite, and the bainitic cementite chemical composition was measured using an X-ray fluorescence method, as a function of time at the tempering temperature. The cementite was found to become richer in Cr,

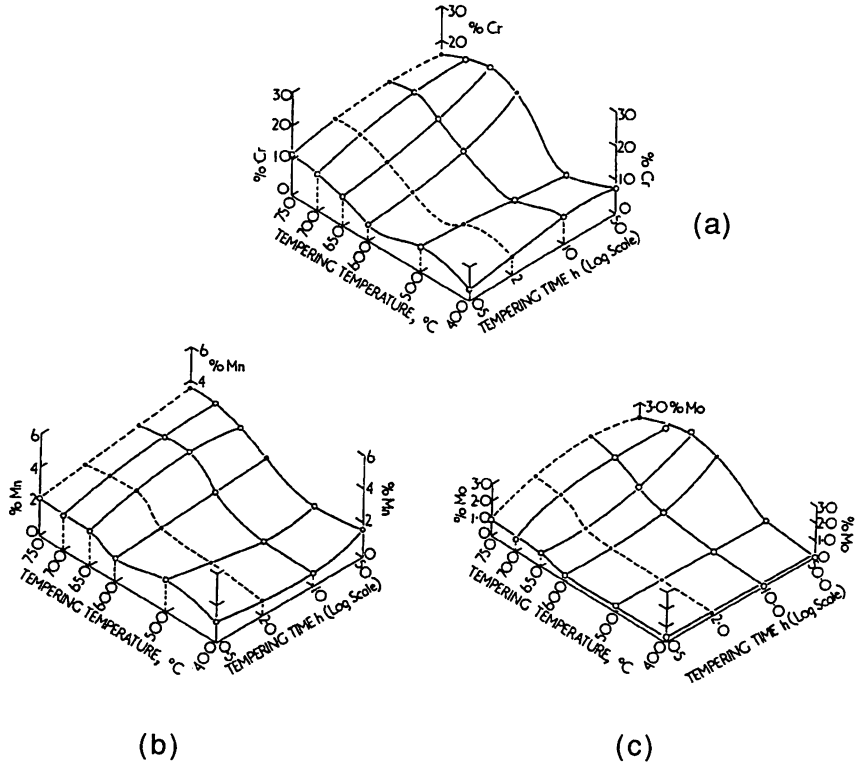

Fig. 4.7 *Diagrams showing the concentrations of Cr, Mn, and Mo in extracted carbides, as a function of the tempering time and temperature. The starting microstructure was bainitic. (Barker and Nutting, 1959).*

Mo and Mn, the degree of enrichment being highest for Cr, with its concentration eventually reaching some 20wt% (Fig. 4.7).

The enrichment diminishes as alloy carbide formation begins, until the cementite eventually starts to dissolve. This is illustrated by some recent research on a bainitic steel of composition similar to that used by Baker and Nutting. The data obtained after ageing the samples at 565°C (Thomson, 1990) seem to suggest that not only does the concentration of Cr in cementite level off, but it begins to drop as M_2C and other carbides precipitate at the expense of cementite (Fig. 4.8). This is not unexpected, since a dissolving particle of cementite will contain a chromium depleted zone in the cementite near the moving ferrite/austenite interface.

4.6.1 Remanent Life Prediction

The study of changes in the chemical composition of carbides during the tempering of bainite has assumed new significance in recent years. Where

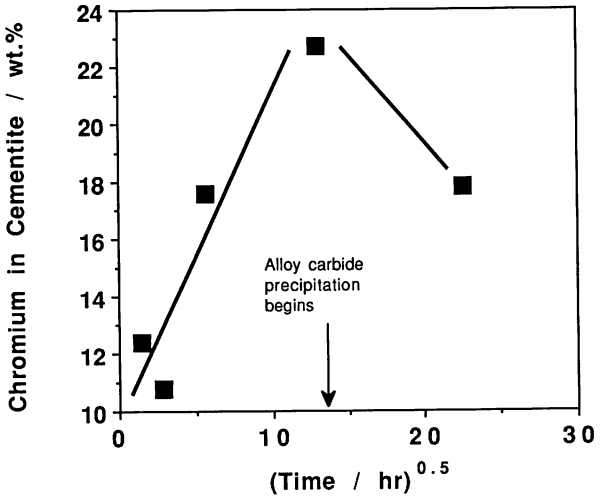

Fig. 4.8 *Plot of the mean chromium concentration in cementite found in a tempered bainitic microstructure aged at 565°C, in a '2.25Cr–1Mo' power plant steel (Thomson, 1990).*

creep resistant bainitic steels are in service at elevated temperatures over time periods covering many years, it is important for safety reasons to know accurately, the time–temperature history of the steel at any stage during service. The thermal history of the steel can be related to the amount of creep life remaining in that steel, before the accumulated damage becomes intolerable. This remaining creep life is in the power generation industry called the *remanent life.*

Accurate prediction of remanent life permits safe and anticipated plant closure or the timely replacement of components. Unfortuantely, power plant temperatures fluctuate considerably and are difficult to record over long periods of time and for the large number of components involved (Fig. 4.9). As a consequence, the life assessment of power plant has to be made on a very conservative basis, which leads to considerable expense due to wastage in terms of premature closure of plant which has not really exhausted its safe life. Any method which gives an accurate measure of the thermal history experienced by the steel during service can lead to large savings by enabling more accurate assessments of the remaining creep life. At first sight, the obvious thing to do would be to monitor the temperature everywhere using strategically located thermocouples, but this is impractical over the large time span involved and in the harsh environment of the power station.

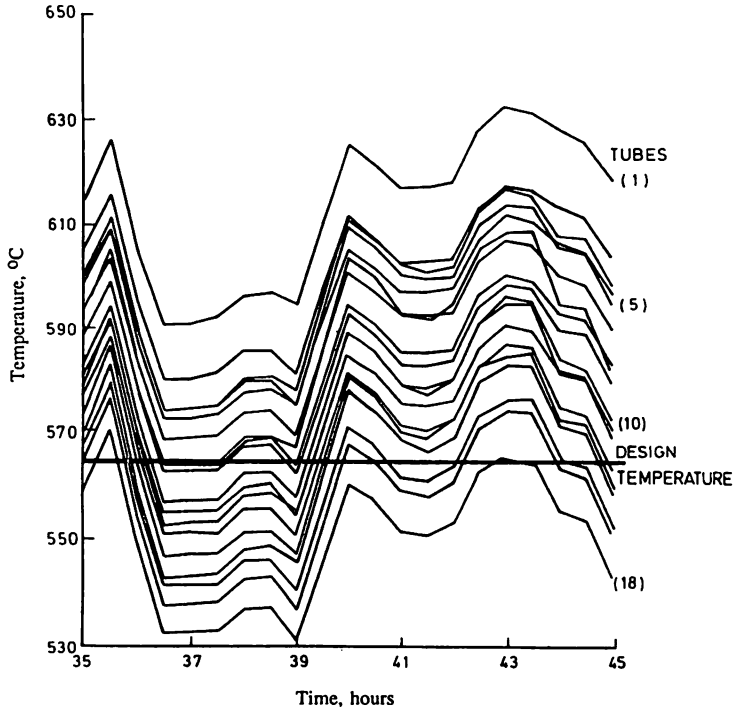

Fig. 4.9 *Illustration of the variation in the temperature at different locations on a particular component ('reheater drum')of a 500 MW power station (Cane and Townsend, 1984).*

The microstructure of the steel, and especially the chemical composition of the cementite, changes during service. These changes can be utilised to assess the effective thermal history experienced by the steel since its implementation. The microstructure is in this context, an *in situ* time–temperature recorder since the cementite phase can be monitored at any stage during service. The monitoring would consist of removing a few cementite particles by extraction replica techniques, and measuring their compositions using a microanalytical technique on a transmission electron microscope. The interpretation and extrapolation of such data relies on the existence of theory capable of relating the cementite composition to heat treatment. The theory itself is discussed in a later section, after a brief introduction to the published data.

The method involving the use of cementite composition for thermal history assessment was first applied to pearlitic cementite in Fe–Cr–Mo–V low alloy steels where it was found that the Cr and Mn concentrations varied approximately with $t^{1/3}$, where t is the time at tempering tempera-

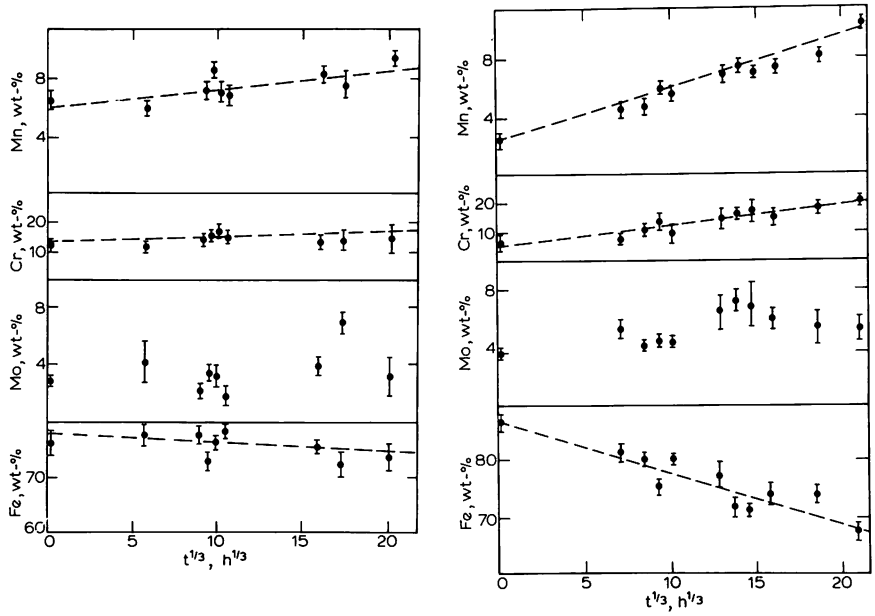

Fig. 4.10 *Changes monitored during the tempering of bainitic steels of the type used in the power generation industry. The alloying element concentrations in cementite are plotted as a function of time at 550°C. (a) Service exposed material. (b) Reheat-treated material (after Afrouz* et al., *1983).*

ture (Carruthers and Collins, 1981).[2] This relationship has not been theoretically justified.

Afrouz *et al.* (1983) reported similar results on a bainitic Fe–0.1C–0.84Cr–0.48Mo–0.48Mn–0.02V wt% alloy. The alloy was normalised to give a microstructure of allotriomorphic ferrite and 20% bainite, was then tempered in an unspecified way, and held at 565°C for 70000 h at a stress of ≈ 17MPa. This service exposed material was then examined after further tempering at 550°C for a range of time periods. As expected, the chromium and manganese concentrations of the cementite (M_3C) increased with time, the manganese possibly showing signs of saturation during the later stages of ageing, and the data for molybdenum exhibiting considerable scatter (Fig. 4.10).

2 The technique normally used is energy dispersive X-ray analysis on thin samples in a transmission or scanning transmission electron microscope. In most cases it does not allow the detection of light elements such as carbon, and since carbides contain substantial amounts of carbon, the absolute values of the reported concentrations may represent an overestimation of the actual levels.

Afrouz *et al.* also reaustenitised (reheat treated) the service exposed material so that after oil quenching, a fresh fully bainitic microstructure was obtained; it is likely that both upper and lower bainite were present. This was then tempered at 693°C for an hour to give coarse M_3C particles at the lath boundaries and within the bainite, and subsequently held at 550°C for a variety of time periods. The change in M_3C composition was monitored during the latter tempering treatment (Fig. 4.10). The starting composition of the carbide is of course leaner than that of the service exposed material and the rate of enrichment was found to be higher for the reheat treated samples (Fig. 4.10). In both cases, the composition changed approximately as $t^{1/3}$, the slope being greater for the reheat treated material.

The results are interesting and provide a clear method for assessing the thermal history experienced by creep resistant steels. The details of these experiments are revealing; the fact that the service exposed material changes composition at a slower rate than the reheat treated sample, implies that a $t^{1/3}$ relationship cannot hold for prolonged ageing. In addition, the starting composition of the service exposed M_3C seems rather low considering that it has been held at 565°C for 70000 h. The reasons for these discrepancies are not clear. We note that the service exposed material was tempered under a low level of stress but comparisons of stressed and unstressed samples shows no significant influence of stress on the kinetics of composition change (Carruthers and Collins, 1981; Afrouz *et al.*, 1983). During tempering, Afrouz *et al.* also reported the precipitation of M_7C_3 and subsequently M_6C carbides. This may influence the diffusion of carbide forming elements into the cementite, but there is no systematic study of such phenomena.

4.6.2 *Theory for Carbide Enrichment*

The process by which carbide particles enrich during tempering has recently been analysed theoretically (Bhadeshia, 1989). The method is similar to the one employed in determining the time required to decarburise supersaturated plates of ferrite, as discussed in detail in Chapter 6. The kinetics of cementite composition change are given by

$$t_c^{0.5} = x^{\theta}(\bar{x}_x - x_x)\,\pi^{0.5} \,/\, 4D^{0.5}(x_x^{\alpha\theta} - \bar{x}_x) \qquad (4.4)$$

where t_c is the time required for the carbide to reach a composition x_x (the subscript represents a substitutional solute), and x^{θ} is the thickness of the cementite plate. D is the diffusion coefficient for the solute in the matrix (assumed to be identical to the corresponding diffusivity in the particle) and $x_x^{\alpha\theta}$ is the concentration of the substitutional solute in the ferrite which is in equilibrium with the cementite.

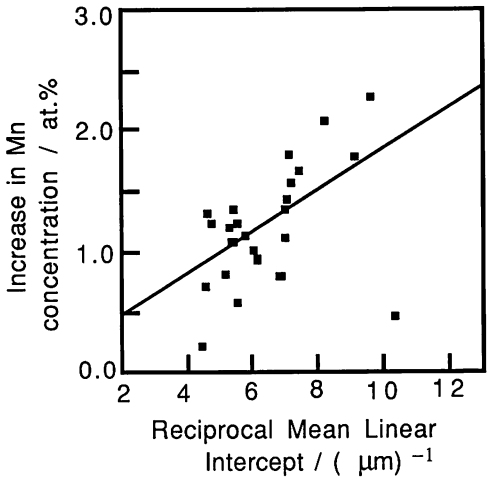

Fig. 4.11 *Size dependence of the cementite chemical composition, for particles extracted from a bainitic microstructure aged for 4 weeks at 565°C (Wilson, 1991).Detailed analysis shows that the scatter in the data are a consequence of the microanalysis technique.*

The equation demonstrates that the time dependence of concentration should in fact be $t^{1/2}$ rather than the $t^{1/3}$ generally assumed. It has been demonstrated that the published experimental data are in fact consistent with the parabolic relation. The theory assumes the absence of soft impingment effects, but a finite difference model can then be used. The time exponent then varies with time, since the boundary conditions for the diffusion process also do so. A further important point is that the carbide composition should depend on its size (Fig. 4.11).

4.7 Sequence of Alloy Carbide Precipitation

Cementite is not the equilibrium carbide in many alloy steels, but it is nevertheless kinetically favoured because its formation can occur by a mechanism which does not necessitate the long range diffusion of substitutional solutes. The actual equilibrium carbide depends naturally on the precise steel composition, and the change from cementite to the equilibrium carbide may occur via a number of other transition carbides. Baker and Nutting's study (1959) on the Fe–2.12Cr–0.94Mo–0.15C wt% alloy showed that in the case of bainite, Mo_2C is the first alloy carbide to form (Fig. 4.12) and that it precipitated independently of the cementite, in the form of needles. Later work has shown that the Mo_2C in fact contains substantial amounts of other elements and is better represented as M_2C (Woodhead and Quarrel, 1965; Murphy and Branch, 1971). Similarly, the

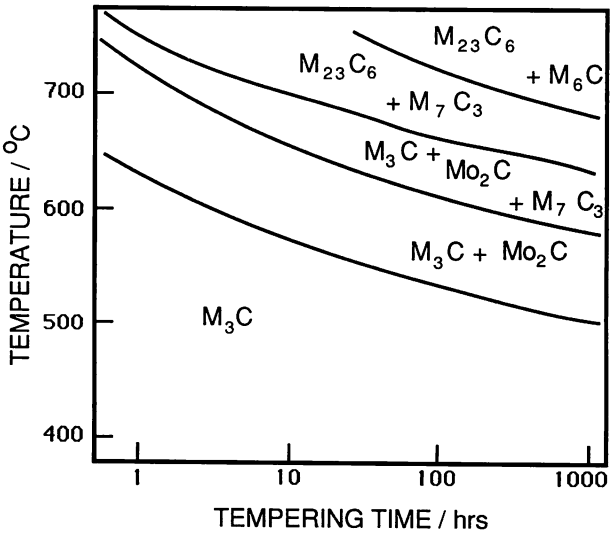

Fig. 4.12 *Carbide stability diagram for a 2.25Cr–1Mo steel (Modified from Baker and Nutting, 1959).*

Cr_7C_3 that Baker and Nutting referred to, is here called M_7C_3 to indicate that other metal atoms are likely to be incorporated into the carbide structure. Soon after the precipitation of M_2C, M_7C_3 starts to form, perhaps at the interface between the Cr-enriched cementite and ferrite. Mo_2C then beings to dissolve, giving way to $M_{23}C_6$, and both $M_{23}C_6$ and M_7C_3 are eventually replaced by the equilibrium carbide M_6C. Enhanced chromium concentrations are known to accelerate the formation of $M_{23}C_6$ and this can be of crucial importance in determining the sensitivity of the microstructure to severe hydrogen attack (Ritchie *et al.*, 1984; Spencer *et al.*, 1989).

Baker and Nutting indicated that with the exception of M_2C, new transition carbides precipitated at the positions of preexisting carbides. The sequence of changes can be summarised as follows:

$$\begin{array}{l} \theta \rightarrow \theta + M_2C \rightarrow M_{23}C_6 \rightarrow M_6C \\ \qquad\quad \downarrow \\ \qquad\quad M_7C_3 \rightarrow \quad \rightarrow M_6C \end{array} \qquad (4.5)$$

Baker and Nutting (1959) also reported the presence of ε-carbide in the Fe–Cr–Mo–C bainite, but the evidence presented was rather indirect and has not been confirmed by subsequent work. A later study by Pilling and Ridley (1982) on a similar set of Fe–Cr–Mo–C alloys containing lower carbon concentrations (0.018–0.09 wt%) revealed a somewhat different precipitation sequence

$$\theta \rightarrow \begin{array}{l} M_2C \rightarrow M_{23}C_6 \rightarrow M_6C \\ + \\ M_7C_3 \rightarrow \qquad \rightarrow M_7C_3 \end{array} \tag{4.6}$$

The explanation for the differences between these two studies is not clear. An analysis based on the thermodynamic stability of carbides as a function of alloy chemistry and temperature could in principle explain the results, because there is some evidence to suggest that small chemical composition differences can significantly alter the tempering behaviour. Yu (1989) has shown that an increase in silicon concentration from zero to about 0.6 wt% stabilises M_6C (which is absent in silicon-free 2.25Cr1Mo steels) since silicon has a relatively high solubility in that carbide. It was also found to accelerate the precipitation of M_2C. An increase in the manganese concentration from 0–0.8 wt% was found to accelerate M_7C_3 precipitation.

Baker and Nutting also studied the precipitation sequences in initially martensitic or ferritic microstructures. With martensite, the sequence was found to be essentially similar to that in bainite. The ferrite, on the other hand, contained M_2C precipitates, which presumably formed during its growth. Subsequent ageing led to the dissolution of M_2C, which was replaced by M_6C particles. This difference between bainite and ferrite has not been explained in detail, but must be related to the mechanism of transformation. The ferrite forms by a reconstructive transformation mechanism, and the atomic mobility inherent in the process could also permit the simultaneous precipitation of alloy carbides. The growth of bainite and martensite is displacive, precluding the formation of alloy carbides during transformation.

That the starting microstructure can have a profound effect on the tempering sequence has been confirmed recently by Lee (1989). Using steels with the nominal composition Fe–1Cr–0.5Mo–0.15C wt%, they not only demonstrated detailed differences between bainitic, ferritic and pearlitic initial microstructures, but also showed that in a given microstructure, the carbide type is sensitive to position. For example, M_2C carbides dominated that microstructure within the tempered bainite plates, whereas mixtures of cementite, M_2C, M_7C_3 and $M_{23}C_6$ could be found at the bainite grain boundaries. This may have something to do with the fact that far less carbon is available within the upper bainite plates, whereas the regions at the plate boundaries are the sites for the precipitation of cementite during the growth of upper bainite. Consequently, more carbon is available (in the form of cementite, or dissolved in carbon enriched austenite) in the proximity of the plate boundaries to stimulate the formation of a variety of alloy carbides. Given that carbide precipitation sequences are sensitive to the initial microstructure, the

kinetics of tempering are also expected to vary similarly. Thus, Lee demonstrated that in their steels, the equilibrium carbide M_6C formed first in bainitic rather than pearlitic or ferritic regions of the microstructure.

Collins (1989) recently reported microanalytical data on alloy carbides generated during the tempering of bainite in commercial steels of nominal composition Fe–1Cr–1Mo–0.75V–(B, Ti) wt% which also contained a variety of trace impurities. Casts with essentially the same chemical composition were known to give quite different creep properties. It was discovered that they also exhibited different carbide precipitation sequences, attributed to differences in unspecified impurity concentrations. After normalising to produce bainitic microstructures, and after tempering heat treatments (details unspecified, but the usual stress relief temper involves several hours at 700°C) the casts all contained mixtures of TiC and V_4C_3, with both kinds of precipitates containing some molybdenum in solid solution. In fact, the measured compositions of individual particles were found to vary continuously between TiC and V_4C_3, and Collins interpreted this to indicate that the TiC carbides form first, with V_4C_3 nucleating on extant TiC particles. Consequently, microanalysis of what appeared to be individual particles gave an intermediate chemical composition. With prolonged ageing at 575°C, the TiC was found to dissolve, and a M_2C type carbide (rich in Mo) began to precipitate. This process was believed to occur by the *in situ* transformation of TiC to M_2C. Collins also pointed out that since the stabilities of V_4C_3 and M_2C are not very different at temperatures around 600°C, tempering below about 610°C gives the following order of carbide stability

$$M_2C > V_4C_3 > TiC$$

whereas at higher temperatures, the V_4C_3 may be more stable than M_2C. Consequently, caution should be exercised in assessing creep properties using data derived from creep tests which have been 'accelerated' by elevating the test temperature since the actual sequence of carbide precipitation might then change.

4.8 Changes in the Composition of Alloy Carbides

Most of the experimental data on alloy carbide composition changes during the tempering of bainite come from experiments on steels used in the power generation industry. Changes in the chemical composition after precipitation are usually complicated by phase transformations involving the precipitation of other more stable particles, and these effects need much further investigation before any clear rationalisation can be attempted. Pilling and Ridley's (1982) careful investigations on the Fe–Cr–Mo–C alloys discussed earlier, revealed that the compositions of

the chromium based M_7C_3 and $M_{23}C_6$ carbides remain essentially constant during prolonged annealing at 700°C. The M_2C and M_6C carbides on the other hand, became richer in molybdenum. The enrichment of M_2C was found to occur even during the period when its volume fraction was decreasing, the dissolving particles providing a source of molybdenum for the coarser M_2C particle and for the more stable M_6C precipitates. The molybdenum concentrations in these carbides were found to increase as the average carbon concentration of the steel decreased (with a fixed average Mo concentration), presumably because the amount of molybdenum approaches the stoichiometrically required quantity.

It is not surprising that changes in alloy carbide chemistries, as induced by tempering, are found to be less striking than those observed for cementite. The growth of the alloy carbides involves considerable long range substitutional atom diffusion and there is therefore a greater opportunity for the carbide to be closer to equilibrium when it first forms. The observed cases where the alloy carbide does not form with the equilibrium composition, but is nevertheless enriched with substitutional solute, are very interesting from a fundamental viewpoint. The growth process must then be non-equilibrium with solvent trapping as the interface advances.

4.9 Precipitation Hardening with Copper

There has recently been considerable interest in the use of low carbon, copper bearing, high strength, low alloy steels for applications in heavy engineering, where strength toughness and weldability are prime requirements. The normal microstructure of such steels consists of allotriomorphic ferrite and pearlite. However, when the steels are required in the form of thick plates, other hardenability enhancing elements are added in order to obtain relatively uniform microstructures throughout the plates, after water quenching from the austenite phase field. In these circumstances, the microstructure is upper bainitic with the platelets of bainitic ferrite separated by thin films of retained austenite and martensite (Thompson *et al.*, 1988). Fine particles of copper are also found within the bainitic ferrite and these are known to contribute significantly to the strength of the steel. The microstructural characterisation of these steels is still at an early stage, and it is not established whether the copper also precipitates in the austenite and martensite regions. The stage at which the copper precipitates in the bainitic ferrite, and the crystallography of precipitation also needs investigation, along with the micromechanisms of strengthening.

A potential disadvantage which has been noticed in quenched and tempered copper precipitation strengthened steels is their tendency

towards stress relief cracking following welding (Wilson *et al.*, 1988). Although the steels are generally very weldable, the copper particles are taken into solid solution in some regions of the heat affected zone during welding. Subsequent stress relief heat treatment causes the copper to reprecipitate in these regions, thereby hindering the sort of creep/recovery processes that are necessary for the annealing of stresses.

4.10 Summary

There are significant differences in the tempering behaviour of bainite and martensite, the most prominent being that there is little carbon in solid solution in bainite by the time tempering heat treatments are envisaged. This has the consequence that bainitic microstructures are much less sensitive to tempering, since there is hardly any loss of strength due to the removal of the small quantity of dissolved carbon. Major changes in strength occur only when the bainite plate microstructure coarsens or recrystallises into one consisting of equiaxed grains of ferrite. Minor changes in strength are due to cementite particle coarsening and a general recovery of the dislocation substructure. Bainitic steels containing strong carbide forming elements tend to exhibit secondary hardening phenomena rather like those observed in martensitic steels, although the exact sequence of precipitation can vary for reasons which are as yet unresolved. In almost all cases, new carbides nucleate on existing less stable carbides, with the exception of M_2C which tends to nucleate in isolation, perhaps heterogeneously on dislocations. While the chemical compositions of the alloy carbides are close to those expected from equilibrium thermodynamics, that of bainitic cementite deviates strongly from equilibrium, perhaps because the cementite grows by a displacive transformation mechanism.

5 *Thermodynamics of the Bainite Transformation*

5.1 Equilibrium and Deviations from Equilibrium

Equilibrium is said to exist in a system when it reaches a state in which no further change is perceptible, no matter how long one waits (Pippard, 1981). This could happen if the system sinks into a very deep free energy minimum. As to whether this represents the lowest free energy state, it is impossible to say, and a question more of philosophy rather than immediate practical consequence. It is more realistic to refer to the state of metastable equilibrium, which represents a local minimum in free energy but does not exclude the existence of further lower minima. The thermodynamic laws governing metastable equilibria are exactly identical so that there are no obvious difficulties.

A bainitic microstructure is far from equilibrium. As an example, the free energy change accompanying the formation of bainite in an Fe–0.1C wt% alloy at 540°C is ≈ -580 J/mol, whereas that accompanying the formation of an equilibrium mixture of allotriomorphic ferrite and austenite at the same temperature is ≈ -1050 J/mol. Consequently, the excess energy of bainite could in this case be said to be ≈ 470 J/mol, or ≈ 0.04 in units of RT_M, where R is the Gas Constant and T_M the absolute melting temperature. This is about an order of magnitude larger than the stored energy due to severe cold deformation of pure metals ($\approx 0.003\ RT_M$) but is small in comparison with that of some highly metastable materials such as rapidly quenched liquids which solidify as highly supersaturated solutions $\approx 1\ RT_M$, or multilayered structures with an excess energy of $\approx 0.1\ RT_M$ (Turnbull, 1981).

In spite of the large deviations from equilibrium, we shall see that the concepts of equilibrium, metastable equilibrium and indeed, constrained equilibrium, can nonetheless be useful in interpreting the mechanism and consequences of the bainite transformation.

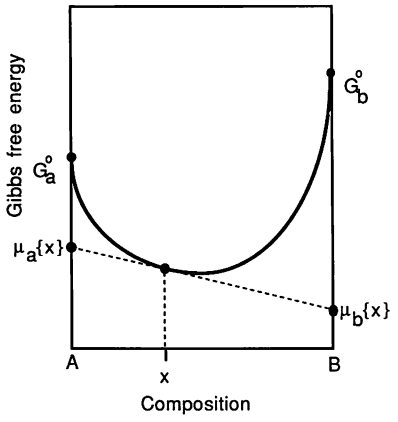

Fig. 5.1 *Illustration of the concept of a chemical potential. The chemical potentials for a solution of composition x are given by the intercepts on the vertical axes of the tangent drawn at x to the curve representing the solution free energy. The potentials clearly vary with chemical composition.*

It is useful when considering the thermodynamics of solid solutions to define the concept of a chemical potential. The molar Gibbs free energy of a binary solution containing A and B atoms (mole fractions x_A and x_B, respectively) can be written

$$G_M = x_A\mu_A + x_B\mu_B \tag{5.1}$$

where μ_i represents the chemical potential of element i in a solution of concentration x_i. It is evident that from this equation (illustrated in Fig. 5.1) that the chemical potential μ_A of A can be interpreted simply, to represent the average free energy of a mole of A atoms *in a solution* of composition x_A. Equilibrium is said to exist between homogeneous phases when the chemical potential of each component is the same in all the phases present. It is defined by the equation

$$\mu_i^\gamma = \mu_i^\alpha \tag{5.2}$$

for $i = 1, 2, 3 \ldots$, where μ_i is the chemical potential of component 'i'. In the study of the kinetics of transformations, the concept of equilibrium in terms of phases which are *homogeneous* is rather restrictive. It is then useful to consider equilibrium to exist locally. For example, it is a reasonable approximation that during diffusion controlled transformation, the compositions of the phases in contact at the interface are such as to allow equilibrium to exist locally even though the phases may not be homogeneous. As long as the phases are not too inhomogeneous (as is the case with some artificial multilayered structures or during spinodal

decomposition) classical equilibrium thermodynamics can be applied locally.

A form of constrained equilibrium which arises in substitutionally alloyed steels is *paraequilibrium*, in which the ratio of iron to substitutional solute atoms remains the same everywhere, but subject to this constraint, the carbon atoms achieve equality of chemical potential in the parent and product phases (Fig. 2.11). Either the substitutional solute atoms, or the iron atoms are then said to be trapped by the advancing transformation interface, the criterion for trapping requiring that the chemical potential of that species increases on transfer across the interface.

Transformation may also be diffusionless, but such transformation is thermodynamically only possible below the T_o temperature, where the parent and product phases of the same composition have equal free energy (Fig. 1.4).

The concepts of local equilibrium, paraequilibrium and diffusionless transformation are relatively easy to visualise and formulate, and hence are very popular. However, between local and paraequilibrium, there could exist an infinite number of states in which the substitutional elements partially partition between the phases. Similarly, between paraequilibrium and diffusionless transformation there can exist an infinite number of states in which the degree of partitioning of carbon may be different from equilibrium. On the other hand, such states would have to be stabilised by some other rate controlling factor such as interface inetics; oζrwise, they should tend to degenerate towards equilibrium, because any small perturbation in composition at the interface, which leads to a reduction in free energy, would tend to grow. We shall see that the stabilisation of such nonequilibrium states is at least in principle feasible for solid state transformations in steels.

Before these concepts can be utilised in assessing the mechanism of the bainite reaction, it is necessary to consider additional terms which raise the free energy of the product phase. For example, the effect of including the stored energy terms is to change the temperature at which composition invariant transformation becomes thermodynamically possible from T_o to T_o'.

5.2 Stored Energy due to Transformation

Much of the stored energy of bainite comes from the strain energy due to the invariant plane strain shape change accompanying transformation. If the shape of a platelet of bainite is approximated by that of an oblate ellipsoid of semi-axes R, R and y, with $R>>y$, then Christian (1958) has shown that the molar strain energy G_s which is a consequence of the shape change is given by

$$G_s = \frac{\mu V_m}{1-\nu}\left[\frac{2}{9}(1+\nu)\Delta^2 + \frac{\pi y}{4R}\zeta^2 + \frac{(1-\nu)\pi y}{3R}\Delta\zeta\right] + 0.5\mu V_m \frac{(2-\nu)\pi y}{4(1-\nu)R} s^2 \quad (5.3)$$

where μ and ν are the shear modulus and Poissons' ratio respectively of the matrix austenite, V_m is the molar volume of the austenite, Δ is the uniform dilatation accompanying transformation, ζ is the additional uniaxial dilatation normal to the habit plane and s is the shear component of the shape change. Although the Δ term has in the past been used to explain the crystallography of bainite, direct measurements of the shape change have not revealed any significant uniform dilatation. Calculations indicate that the strain energy term due to the shape change is about 400 J mol^{-1} for bainite (Bhadeshia, 1981a), this being smaller than the corresponding term for martensite, which is about 600 J mol^{-1} (Christian, 1979b). The smaller value for bainite is because the aspect ratio (y/R) for bainite platelets is usually found to be considerably smaller than that for martensite. The shear and dilatational components of the shape change are in fact rather similar for martensite and bainite. There is some uncertainty about the stored energy term for bainite. The value mentioned above is for an isolated sub-unit, but as discussed earlier, it may be more appropriate to consider the sheaf as a whole, in which case the stored energy would be smaller since the shear component of the shape deformation reduces when averaged over the sheaf. Recent claims that much larger values of the strain energy are associated with the shape deformation of bainite, are incorrectly based on the use of a very large value (0.36) of the shear component of the shape strain, unjustified by experimental results (Mou and Hsu, 1988; Hsu, 1990).

There are some further complications in the use of equation 5.3 for the bainite transformation. Bainite platelets do not form in isolation, but grow in sheaves which themselves have a plate like morphology on a macroscopic scale; the shear component of the shape change as averaged over the whole sheaf is much smaller than that of an individual platelet (Srinivasan and Wayman, 1968b, c; Tsuya, 1956; Speich, 1962). The effect of such three-dimensional formations of platelets on the stored energy term has not been investigated. Bainite forms at relatively high temperatures where both the austenite and ferrite have low yield strengths. Consequently, the strain energy due to the shape change can be reduced by plastic relaxation. The plastic deformation causes an increase in dislocation density, but since it is driven by the shape change, the strain energy calculated on the basis of an elastically accommodated shape change should be an upper limit (Christian, 1979b). Another complication, which should lead to a reduction in stored energy per unit volume as transformation proceeds, is that new sheaves may grow adjacent to those already existing, in a mutually accommodating manner (Hehemann, 1970). As the

transformation proceeds, carbides grow diffusionally either from austenite or from the bainitic ferrite; these may grow in such a way as to anneal the transformation strains.

In martensitic reactions, transformation twinning can contribute ≈ 100 J mol^{-1} of stored energy (Christian, 1979b); this term does not arise for bainite where the lattice invariant shear is always found to be slip. Also, the contribution from the bainite/austenite interface is very small during the growth stage (Bhadeshia and Edmonds, 1980a).

5.3 Thermodynamics of Growth

5.3.1 Substitutional Solutes during Growth

The fact that there does not seem to be any bulk partitioning of substitutional alloying elements during the growth of bainite, does not rule out the possibility of growth involving local equilibrium at the interface. At sufficiently large undercoolings, the negligible partitioning local equilibrium mode of transformation is consistent with the lack of any bulk partitioning, although the maintenance of local equilibrium at the interface requires in general that the two phases are different in composition (Hillert, 1953; Kirkaldy, 1958; Purdy *et al.* 1964; Coates, 1973a, b). This means that in the immediate proximity of the interface, the compositions of the phases are likely to be different. However, the atom probe experiments described in Chapter 2, which reveal directly the absence of any substitutional alloying element partitioning at the bainitic ferrite/austenite interface even on the finest conceivable scale, prove that the growth of bainite in alloy steels cannot be treated in terms of local equilibrium or in terms of any intermediate state between local and paraequilibrium. The atom probe experiments have now been carried out for a wide range of steels and it is established that Mn, Ni, Si, Cr and Mo do not redistribute during transformation.

It is instructive to contrast the role of substitutional solute atoms during the displacive growth of bainitic ferrite, with their role in the diffusional formation of pearlite. Whereas the substitutional lattice is frozen during the growth of bainite, pearlite growth (involving the movement of an incoherent interface) always seems to involve the diffusion of substitutional solute atoms. There are no experiments in which pearlite has been reported to grow by a paraequilibrium mechanism (Ridley, 1984, Al-Salman and Ridley, 1984). Elements such as chromium, molybdenum, silicon and cobalt have been shown to partition at the reaction front. In the case of manganese and nickel, the bulk substitutional concentrations of the parent and product phases have been found to be similar during transformation at high undercoolings, although this

is because of negligible-partitioning local equilibrium transformation rather than paraequilibrium (Hillert, 1982; Ridley, 1984). The results seem logical since during diffusional transformations, a degree of mass transport is essential to achieve the change in crystal structure without necessitating the shape deformations characteristic of martensitic transformations (see for example, Bhadeshia, 1985b). Given the fact that such mass transport occurs, solute elements have an opportunity to redistribute amongst the phases. The general observation that alloying elements have a larger effect on the overall transformation kinetics of diffusional reactions (i.e., on their TTT curves) when compared with the overall kinetics of displacive reactions is consistent with the above observations. In both cases, the alloying elements will influence the thermodynamics of transformations, but for diffusional reactions, their movement will additionally retard kinetics.

5.3.2 *Interstitial Solutes during Growth*

It remains to consider the role of carbon in the growth of bainite. This is difficult to resolve directly because if the bainite is supersaturated during growth, the relatively high temperatures at which it grows provides an opportunity for much of the excess carbon to diffuse rapidly into the residual austenite before any experimental measurements can be conducted. The time involved may typically be less than a second (Bhadeshia, 1988b); the time does of course increase as the temperature is reduced but the excess carbon can then precipitate in the form of carbides within the bainitic ferrite. If attempts are made to drastically reduce the transformation temperature by alloying, then bainite ceases to form, leaving martensite as the only displacive transformation product of austenite (Bhadeshia 1981a).

There are however, indirect methods of determining the carbon concentration of bainitic ferrite during growth. If bainitic ferrite initially has the same composition as the parent austenite, the transformation should in principle go to completion since there is no diffusion necessary. In practice, the whole of the austenite grain does not transfoIm instantaneously because of kinetic restrictions (e.g., heterogeneous nucleation and the fact that the plates reach a limiting size). Even if the first plate of bainite forms without any diffusion, it has an opportunity to reject its excess carbon into the remaining austenite during the progress of the reaction as a whole. This is a reflection of the fact that at the temperatures where bainite typically forms, the time required for partitioning is not large when compared with that for the reaction to terminate. Because the austenite becomes enriched with carbon, a stage is eventually reached when it is thermodynamically impossible for further bainite to form by

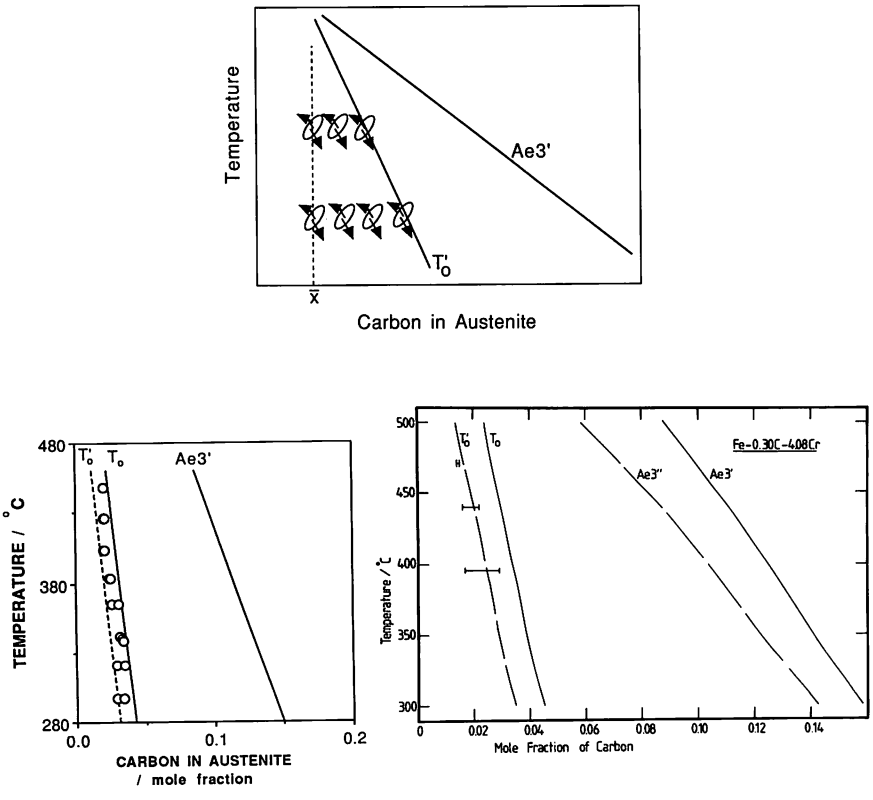

Fig. 5.2 *(a) Schematic illustration of the incomplete-reaction phenomenon. A plate of bainite grows without diffusion, then partitions its excess carbon into the residual austenite. The next plate thus grows without diffusion from carbon enriched austenite, and the process continues until such transformation becomes impossible at the T_o' curve. For paraequilibrium growth, the transformation should proceed until the carbon concentration reaches the Ae3' curve. (b) Experimental data on the incomplete reaction phenomenon for Fe–0.43C–3Mn–2.12Si wt% alloy (Bhadeshia and Edmonds, 1979a). (c) Similar data for Fe–0.3C–4.08Cr wt% alloy.*

diffusionless transformation. At this point, the composition of the austenite is given by the T_o' curve of the phase diagram (Fig. 5.2). If the alternative hypothesis is that paraequilibrium exists during all stages of transformation, then the reaction would stop when the carbon concentration of the austenite is given by the Ae3″ curve. the Ae3′ curve is the $(\alpha+\gamma)/\gamma$ paraequilibrium phase boundary, and the Ae3″ curve is obtained when this is modified to account for the stored energy of transformation. The reaction is found experimentally to stop when the average carbon

concentration of the austenite is close to the T_o' curve rather than the Ae3″ boundary (Fig. 5.2).

The reaction therefore remains incomplete in the sense that there is no equilibrium between the austenite and ferrite and that the volume fraction of bainitic ferrite does not satisfy the lever rule. Note that the difference in carbon concentrations between the T_o' and *Ae3″* curves at the temperatures where bainite typically forms is very large, so that the experiments mentioned above are a sensitive indication of the failure of the transformation to reach paraequilibrium. This 'incomplete reaction phenomenon' explains immediately why the degree of transformation to bainite is zero at the B_s temperature and increases with undercooling below B_s in steels where other reactions do not overlap with the formation of bainitic ferrite; the T'_o curve has a negative slope on a temperature/carbon concentration plot, so that the austenite can tolerate more carbon before diffusionless transformation becomes impossible, as the temperature is reduced.

The experimental evidence for the incomplete reaction phenomenon manifests itself in many forms. The carbon concentration of the residual austenite at the point where the reaction stops can be measured using X-ray techniques, lattice imaging using high resolution transmission electron microscopy, field ion microscopy/atom probe methods, quantitative metallography and dilatometry. It is always found that the concentration is far below that required by equilibrium or paraequilibrium, and is on the whole consistent with that given by the T_o' curve of the phase diagram. The experimental evidence has been reviewed by Christian and Edmonds (1984). Another effect is that in dilatometric experiments, the length change due to transformation is zero above the B_s temperature, even though that temperature may be well within the $\gamma+\alpha$ phase field. The maximum length change then increases with undercooling below the B_s temperature. Numerous examples of such data can now be found in the literature (e.g., Vandermeer, 1983 and Fig. 5.3).

The incomplete reaction phenomenon supports the hypothesis that the growth of bainitic ferrite is diffusionless, with carbon being subsequently partitioned into the residual austenite. There is as yet no reasonable alternative explanation of this phenomenon.

Hsu and Yiwen (1984) have published a thermodynamic analysis of bainitic reactions in Fe–C alloys, and reached the conclusions that not only is the formation of bainitic ferrite by a displacive mechanism impossible, but so is the growth of bainite without a composition change. Experimental measurements on Fe–C alloys are notoriously difficult because of their high rates of transformation. Hsu and Yiwen's conclusions are based on an estimation of the bainite start temperature of Fe–C alloys, by the empirical extrapolation of the Steven and Haynes (1956) equation well outside of its range of applicability. By doing this, they incorrectly

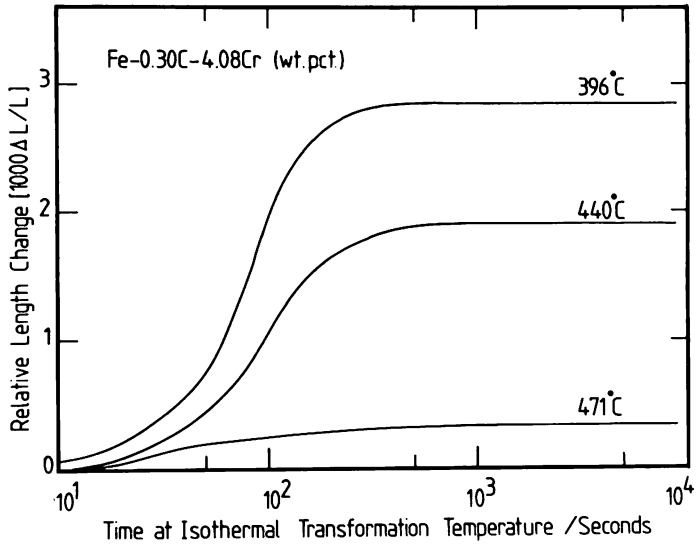

Fig. 5.3 *Dilatometric length change data illustrating the incomplete reaction phenomenon for a Fe–0.3C–4.08Cr wt% alloy (Bhadeshia, 1981b).*

concluded that the B_s temperature of Fe–C alloys lies in all cases above the T_0 curve. Experimental measurements (Kinsman and Aaronson, 1970) of B_s temperatures for hypoeutectoid Fe–C alloys are always found to be well below the T_0 curve. Kinsman and Aaronson's B_s measurements on hypereutectoid steels do exceed the T_0 curve, but those data are not reliable since cementite from austenite reduced its carbon concentration. Some careful measurements by Oka and Okamoto (1986), of the B_s temperatures of Fe–C alloys with carbon concentrations exceeding 0.6 wt%, have recently been shown (Takahashi and Bhadeshia, 1990) to be in agreement with the hypothesis that the bainite grows by a displacive transformation mechanism without any diffusion.

Hsu and Yiwen's (1984) thermodynamic analysis also contains a number of inconsistencies. Values of thermodynamic parameters, such as the carbon–carbon interaction energies, reported in the literature for particular solution models have been used in other models; parameters like these are model dependent and should not be applied arbitrarily. The carbon–carbon interaction energy in ferrite was reported by Shiflet *et al.* (1978) to be negative, based on an incorrect formulation of the McLellan and Dunn (1969) quasichemical solution model (Bhadeshia, 1982c). The negative value was nonetheless used by Hsu and Yiwen, even though the quasichemical models are not designed to handle attractive interactions between the interstitial species.

5.3.3 *Further Consequences of the Incomplete Reaction Phenomenon*

We have already emphasised that the bainite reaction stops well before the austenite reaches its equilibrium composition (or volume fraction). The transformation is kinetically favoured at low temperatures, but does not lead to the largest free energy change during the decomposition of austenite. There is however, no reason why the austenite that remains untransformed after the cessation of the bainite reaction, cannot continue to decompose by other mechanisms of transformation. If these transformations are reconstructive, then the rates of transformation must be very small given that atomic mobilities tend to be very small at the temperatures where bainite grows.

There is much historical evidence to support the notion that more sluggish reactions involving the growth of pearlite can occur after bainitic transformation ceases in alloy steels (Allen *et al.*, 1939; Klier and Lyman, 1944; Lyman and Troiano, 1946). More recent results support these data. Bhadeshia and Edmonds (1979a) found that if an Fe–3.0Mn–2.12Si–0.43C wt% alloy is transformed to upper bainite at 452°C, the reaction ceases in a matter of minutes, but if the specimen is nevertheless held at the transformation temperature for some 32 h, the residual austenite begins to transform to pearlite. If a Fe–4.08Cr–0.3C wt% alloy is isothermally transformed to lower bainite at 478°C, the reaction is found to stop within about 30 min, but prolonged holding at the transformation temperature (43 days) causes the residual austenite to undergo extremely sluggish reconstructive transformation to two different products (Bhadeshia, 1981b, 1982b). One of these is alloy pearlite which nucleates at the austenite grain boundaries and develops as a separate reaction (Fig. 4.5a). The other involves the original lower bainite/austenite interfaces, which degenerate into a series of perturbations having an extremely irregular morphology. The perturbations are found to be in the same crystallographic orientation as the original plates (i.e., they are continguous with the bainite) and they grow with the same substitutional alloy content as the parent austenite. The extent of growth, within the period of 43 days at temperature is found to be comparable to the thickness of the bainite plates, which took just a few seconds to form. Consistent with the shape deformation which accompanies the growth of bainite, these results also emphasise the glissile character of the austenite/bainite interface. The interface clearly has a very high mobility even at low homologous temperatures. Furthermore, the shape of the original plates is clearly not determined by any interface energy minimisation criterion, since that shape is not preserved as the system is allowed to approach equilibrium.

The two stage decomposition of austenite discussed above, is more difficult to establish for plain carbon steels since the reaction rates are

always very large, with the pearlite reaction setting in a few seconds after the growth of bainite (Klier and Lyman, 1944). There is nevertheless indirect evidence for the two stage decomposition in plain carbon steels. Ohmori and Honeycombe (1971) found that the microhardness of bainite in a plain carbon steel, in a mixed microstructure of bainite and pearlite obtained by isothermal transformation, is lower than that of lamellar or degenerate pearlite even though the two products formed at the same isothermal reaction temperature. This can be explained on the basis of a two stage reaction, since the bainite which forms first, enriches the remaining austenite with carbon. When the enriched austenite subsequently decomposes to pearlite, the latter contains a higher volume fraction of hard cementite.

Another consequence of the incomplete reaction phenomenon is that the growth of austenite from bainite does not occur without a large superheat, as discussed in the Chapter 9 which deals with the reverse transformation from bainite to austenite.

5.4 Summary

The thermodynamic description of the bainite reaction depends to a large extent on its mechanism of transformation and on the behaviour of solute species during transformation. By far the largest contribution to the stored energy of bainite is due to the invariant plane strain shape deformation accompanying growth. The contributions from interfacial area are by comparison negligible (at least during the growth stage). The dislocation density of bainite probably arises from the plastic deformation driven by the shape change. Its energy is therefore included in the calculation of the stored energy of an elastically accommodated shape change.

The substitutional solutes do not partition during the bainite reaction, their primary effect on transformation being via their influence on the relative thermodynamic stabilities of the austenite and ferrite phases. Since the elements could lower their chemical potentials by partitioning, their kinetically forced transfer across the transformation interface raises the free energy of bainite.

The evidence relating to the incomplete reaction phenomenon indicates that carbon also does not partition during growth.

6 *Kinetics of the Bainite Transformation*

Thermodynamic theory is an essential prerequisite to the understanding of any transformation. It defines the bounds of what is spontaneously possible in nature. It does not, however, reveal much about the rate at which a reaction takes place, and usually is unable to specify the exact path (mechanism) that the reaction is likely to adopt in achieving the change from the initial to the final states. Within the context of these limitations, thermodynamic theory is far more rigorously defined than kinetic theory. Whereas phase diagram calculation (which relies on thermodynamics) is now commercially established, there are but a handful of examples in metallurgy where kinetic concepts are sufficiently advanced to enable the prediction of microstructures.

The bainite reaction has always faced some unique paradoxes as far as its kinetics are concerned. It was clear from the very beginning that the transformation exhibited many of the features commonly observed in martensitic transformations in steels. And yet, most of the early scientists felt uneasy about the fact that the reaction proceeded at a comfortably observable rate, whereas martensite growth was known to be limited only by the speed of sound in the metal. The notion of a slow, diffusionless transformation was not established in those days. It was in this context that Oblak and Hehemann (1967) suggested that the apparently slow growth rates of bainite sheaves, as measured on a macroscopic scale, may be attributed to a sub-unit mechanism. A sheaf of bainite is then supposed to grow by the repeated nucleation of sub-units, each of which forms relatively rapidly by martensitic growth to a limited size.

Any recognition that bainite grows like martensite begs further questions; for example, how is bainite to be distinguished from martensite? Zener achieved the distinction by assuming the bainite to grow below T_o (i.e., diffusionless), and asumming without justification that the strain energy associated with bainite is zero. The strain energy of martensite

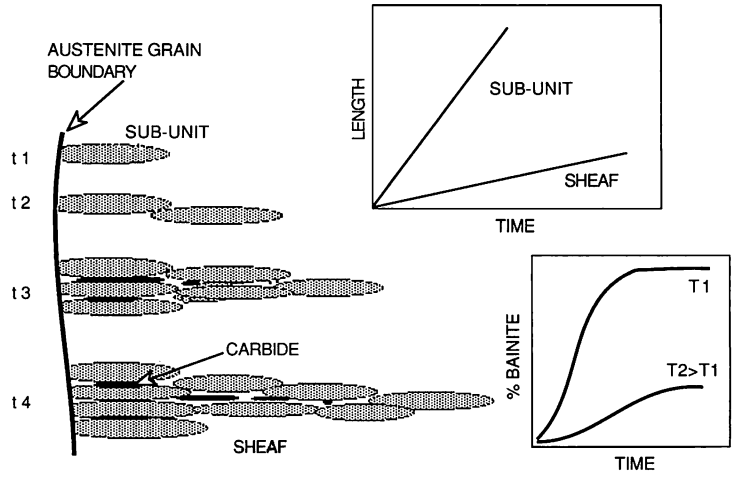

Fig. 6.1 *Schematic illustration of the microstructural features relevant in the kinetic description of a bainitic microstructure.*

would then depress its transformation temperature below that of bainite.

These are just two examples of the interesting ideas stimulated by a consideration of the kinetics of bainite, ideas which led, in the good tradition of science, to the design of ingenious experiments. Bainite grows in a regime where easy solutions are not available. Quantities such as atomic mobility and driving force adopt intermediate values whose interpretation is rarely clear cut. Fig. 6.1 illustrates the essential features of the problem at a variety of scales. It is necessary to understand the nucleation and growth of an individual sub-unit, the sequential formation of sub-units in the form of a sheaf, and the combined effect of many sheaves to generate the overall transformation kinetics important in the calculation of time–temperature transformation diagrams. In most cases, the formation of bainitic ferrite is accompanied by that of carbides, either from supersaturated bainitic ferrite or from the carbon enriched residual austenite. Carbide precipitation kinetics are dealt with in Chapters 3 & 7, but the knowledge available in this area is limited.

6.1 Experimental Observations on the Thermodynamics of Nucleation

Many phase changes do not simply happen the moment that the equilibrium transformation temperature is reached. Nucleation is necessary in all cases where the formation of a new phase involves the creation of an interface between the parent and product phases. The existence of the interface raises the free energy per atom of the product phase. Because

interfacial area scales with the square of the particle dimension, whereas the volume free energy change with the cube, the formation of a particle below a critical dimension is not thermodynamically favoured even though the parent phase may be supersaturated. This critical dimension is in most practical circumstances very small indeed. The direct observation of nucleation is therefore almost impossible. The contribution of interfacial energy to the overall energy balance rapidly becomes smaller as the particle grows, leading to an acceleration in the growth rate and making it difficult to freeze in any embryos. There are nevertheless, macroscopic parameters which can be used to monitor nucleation phenomena, and it is these which are addressed in this section.

6.1.1 The Free Energy Change During Nucleation

We begin with a diagrammatic illustration of the thermodynamic parameters important in nucleation and growth theory. Detailed descriptions of Gibbs free energy diagrams for phase changes can be found elsewhere (e.g., Hillert, 1975b), their purpose here being to serve as an aid to the visualisation of the thermodynamics of transformations.

The equilibrium state is defined by the minimisation of free energy. For austenite of composition $\bar{x}$ (Fig. 6.2), a decrease in free energy can be achieved by decomposing into a mixture of ferrite and carbon enriched austenite. Furthermore, the largest free energy decrease is obtained if it decomposes into a mixture consisting of ferrite and austenite of compositions $x^{\alpha\gamma}$, $x^{\gamma\alpha}$ respectively. These correspond to the values drawn by constructing a tangent which is common to the ferrite and the austenite (Fig. 6.2). Any other pair of compositions will always lead to a smaller free energy decrease. $x^{\alpha\gamma}$ and $x^{\gamma\alpha}$ are therefore the equilibrium compositions at the specified temperature for austenite of composition $\bar{x}$. The free energy change accompanying the equilibrium decomposition of a mole of austenite is clearly, $\Delta G^{\gamma\rightarrow\gamma'+\alpha}$ (Fig. 6.2a).

It is sometimes convenient to define the free energy change with respect to the amount of ferrite that forms. Since the mole fraction of the ferrite that forms is generally less than that of the parent austenite, the free energy change defined in this manner, and referred to as ΔG_2, must be larger (Fig. 6.2). It is in fact given by dividing $\Delta G^{\gamma\rightarrow\gamma'+\alpha}$ by $(\bar{x} - x^{\alpha\gamma})/(x^{\gamma\alpha} - x^{\alpha\gamma})$, which is the mole fraction of ferrite and is designated ΔG_2 in Fig. 6.2.

In the above case, there is clearly a significant change in the composition of the austenite that remains untransformed. Nucleation on the other hand, only involves the formation of a minute amount of product phase. So small is the quantity, that the overall composition of the parent phase is hardly affected even when nucleation involves the partitioning of solutes. The

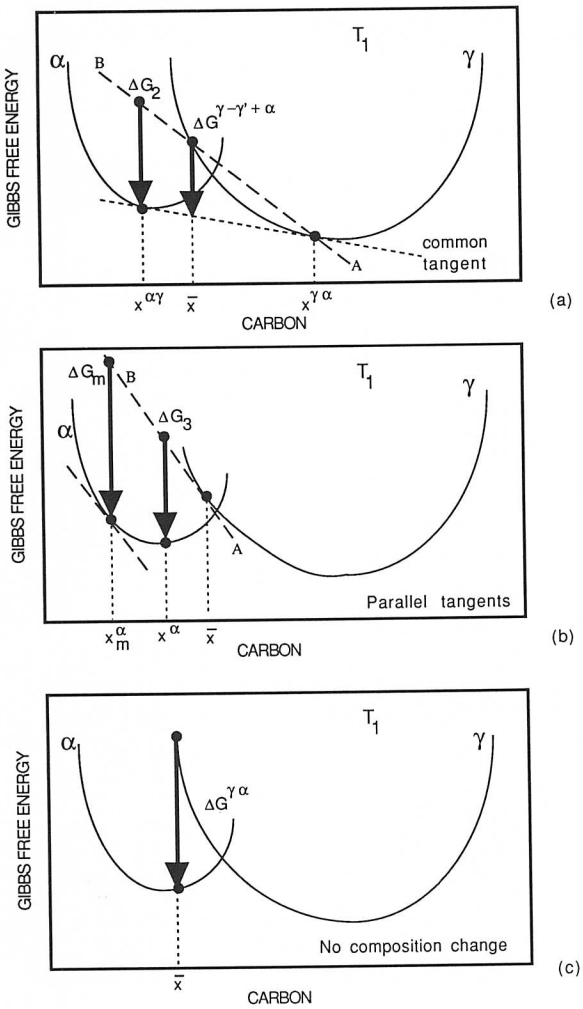

Fig. 6.2 *Free energy diagrams illustrating the chemical free energy changes during the nucleation and growth of ferrite from austenite of composition* $\bar{x}$.

chemical free energy change accompanying the formation of a mole of nuclei is then obtained in a manner similar to ΔG_2, but the construction on the free energy diagram has to take into account that the composition of the residual austenite (x_γ) is nearly identical to that of the original austenite ($\bar{x}$). These two points therefore move closer together and in the limit, the construction line AB becomes tangential to the austenite free energy curve at the composition $\bar{x}$. The free energy change for the formation of a mole of ferrite nuclei of composition x_α is thus given by ΔG_3, as illustrated in Fig. 6.2b.

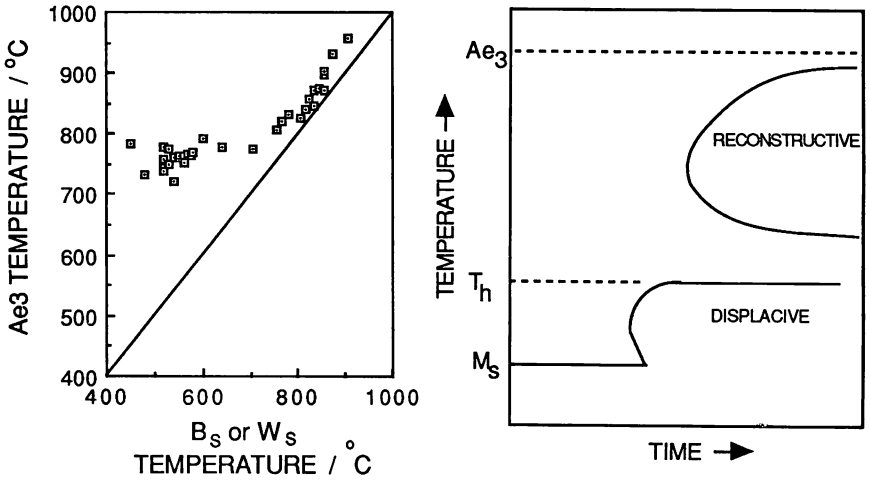

Fig. 6.3 *(a) Diagram illustrating the variation of the Widmanstätten ferrite start and bainite start temperatures as a function of the Ae3 temperature of the steel concerned (Ali, 1990). (b) Schematic TTT diagram illustrating the two C curves and the T_h temperature.*

The procedure just described, is equivalent to removing a mole of material of suitable composition from a very large amount of parent phase, and then transforming the material into the structure of the product phase. A larger free energy change can in fact be obtained by choosing an appropriate ferrite nucleus composition, using the parallel tangent construction shown in Fig. 6.2b. This maximum possible free energy change is designated ΔG_m.

Finally, the driving force $\Delta G^{\gamma\rightarrow\alpha}$ for diffusionless nurleation and growth is given by the distance on the free energy axis, between the austenite and ferrite free energy curves at the composition of interest (Fig. 6.2c).

6.1.2 *The Transformation Start Temperature*

It turns out that there are certain features of bainite nucleation that can be usefully explored in terms of the driving forces to reveal information about rate phenomena. One of these features is the observation that the Widmanstätten ferrite start (W_s) and bainite start (B_s) temperatures are much more sensitive to alloy chemistry when compared with the Ae3 temperature, which is the highest temperature at which α-ferrite and austenite can coexist in equilibrium. This immediately indicates that the effect of solute additions on the nucleation of Widmanstätten ferrite and bainite is more than just thermodynamic (Fig. 6.3a).

The problem has been investigated using data from time–temperature transformation diagrams, and from direct metallographic measurements of the transformation start temperatures (Bhadeshia, 1981a; Ali, 1990). Although there is a lot of fine detail in TTT diagrams, they can be considered to consist essentially of two C curves. In steels where the transformation kinetics are very rapid, the C curves overlap to such an extent that the TTT diagram *appears* to contain just one C curve.

We now present an interpretation of the two C curves which helps reveal the mechanism of bainite and Widmanstätten ferrite nucleation. The lower one has a characteristic flat top and represents the highest temperature (T_h) at which ferrite can form by a displacive transformation mechanism (Fig. 6.3b). Bearing this in mind, the temperature T_h could represent either the Widmanstätten ferrite start or bainite start temperature, an issue which has to be resolved experimentally or with the help of certain thermodynamic criteria discussed below. Further characterisation is necessary to define the role of carbon at the nucleation stage. Whereas the low temperatures involved ensure the absence of substitutional solute partitioning, the same cannot be said of carbon, which can in principle, redistribute during nucleation.

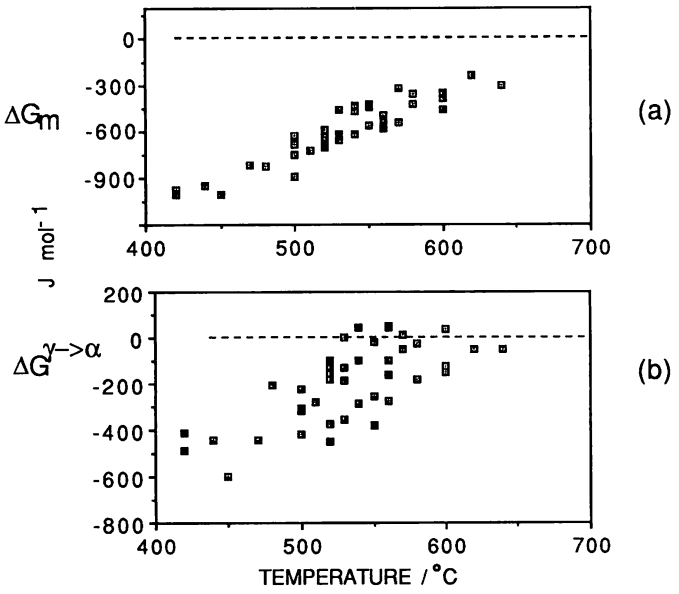

Fig. 6.4 *Curves representing the free energy change necessary in order to obtain a detectable degree of transformation to Widmanstätten ferrite or bainite. (a) The free energy change calculated assuming the partitioning of carbon occurs during the nucleation of ferrite. (b) The free energy change calculated assuming that the ferrite nucleus inherits the composition of the parent austenite.*

A transformation start temperature is usually defined as the highest temperature at which a phase is observed to form at a detectable rate. In the present context, T_h is identified as the transformation start temperature. By calculating the maximum driving force ΔG_m available for nucleation at T_h as a function of the alloy chemistry, it can be deduced that both Widmanstätten ferrite and bainite nucleate by the same mechanism, since in a plot of ΔG_m versus T_h, the data are all found to fall on the same general curve (Fig. 6.4a). Furthermore, if the driving force is calculated assuming no partitioning of carbon, then in some cases, the free energy change is found to be positive during transformation (Fig. 6.4b), so that the nucleation process must involve the redistribution of carbon.

The curve plotted in Fig. 6.4a can be regarded as a *universal* nucleation function (designated G_N) applicable to all low alloy steels. Its purpose would be to enable the prediction of the temperature T_h. It gives the free energy needed in a steel before a detectable amount of Widmanstätten ferrite or bainite transformation is achieved, and hence defines the maximum temperature to which the lower C curve of the TTT diagram can extend. This universal nucleation function is found experimentally to be given by (Ali and Bhadeshia, 1990)

$$G_N = 3.637T - 1537 \qquad \text{J mol}^{-1} \tag{6.1}$$

where T is the absolute temperature. For very low alloy steels, where transformations occur at relatively high temperatures, G_N approaches zero, which is its maximum value. This simply means that the formation of Widmanstätten ferrite is then governed only by the need to satisfy the thermodynamic conditions for growth rather than nucleation.

6.1.3 *Evolution of the Nucleus*

Given that the nucleation process is identical for Widmanstätten ferrite and bainite, the growth conditions for these two phases must determine which of these phases evolves from the nucleus. If at T_h, the available driving force is insufficient to sustain the diffusionless growth of bainite, then $T_h = W_s$. A further undercooling is then necessary before the B_s temperature is reached. On the other hand, if sufficient driving force is available at T_h to account for both diffusionless transformation and the stored energy of bainite, then Widmanstätten ferrite does not form in the steel concerned.

The rules for predicting W_s and B_s can therefore be stated formally in terms of the thermodynamic quantities discussed earlier. Thus, Widmanstätten ferrite forms below the Ae3 temperature when

$$\Delta G^{\gamma\rightarrow\gamma'+\alpha} < -G_{SW} \tag{6.2}$$

$$\Delta G_m < G_N \tag{6.3}$$

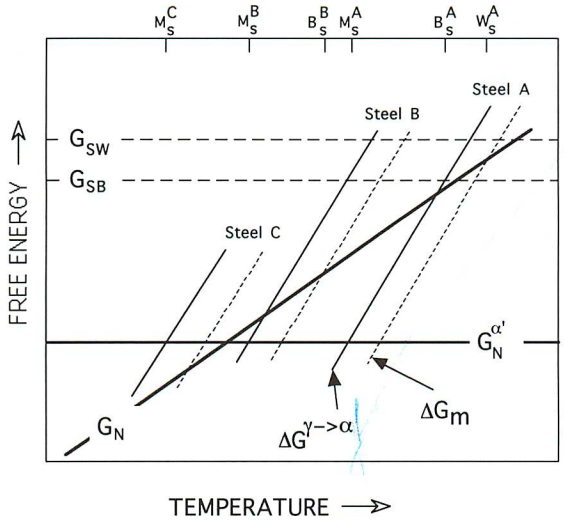

Fig. 6.5 *Free energy curves for a low (A), medium (B) and high (C) alloy steel showing the conditions necessary for the nucleation and growth of Widmanstätten ferrite, bainite and martensite.*

where G_{SW} is the stored energy of Widmanstätten ferrite (about 50 J mol^{-1}). The first condition ensures that the chemical free energy change available for transformation at any temperature exceeds the stored energy of the transformation product, and the second that enough free energy is available to ensure a detectable nucleation rate.

Bainite is expected to form below the T_o' temperature when

$$\Delta G^{\gamma\rightarrow\alpha} < -G_{SB} \tag{6.4}$$

$$\Delta G_m < G_N \tag{6.5}$$

where G_{SB} is the stored energy of bainite (about 400 J mol^{-1}) and the conditions are again for the growth and nucleation processes respectively. There is no inconsistency in assuming that carbon partitions during the nucleation stage but that its growth is diffusionless. The free energy available for interfacial motion in fact becomes larger with particle size. This is because the surface to volume ratio increases with particle size, so that the amount of energy used up in the creation of new interface per unit of transformation decreases.

The conditions just described are illustrated schematically in Fig. 6.5. The diagram includes an additional function $G_N^{\alpha'}$, representing the critical value of the free energy change $\Delta G^{\gamma\rightarrow\alpha}\{M_S\}$ needed before the athermal, diffusionless nucleation and growth of martensite becomes possible. The value is experimentally found to be relatively insensitive to solute

concentration in low alloy steels (Bhadeshia, 1981c, d) and is consequently plotted as a horizontal line.

It is well known that all of the three displacive transformations (Widmanstätten ferrite, bainite and martensite) do not necessarily occur in all steels. In some alloys, only martensite is ever observed (e.g. Fe–28Ni–0.4C wt%), whereas in others only bainite and martensite are found (e.g., Fe–4Cr–0.3C wt%). The model presented above is able to explain these observations. Steels A, B and C in Fig. 6.5 are supposed to contain increasing quantities of austenite stabilising elements, as reflected in their respective free energy curves (the driving force decreases with alloy content at constant temperature). In steel A, all three transformations are expected as the isothermal transformation temperature is progressively reduced. The situation is different for steel B; at the temperature where Widmanstätten ferrite nucleation becomes possible, it is also possible to satisfy the growth condition for bainite (equation 5.4), so that any nuclei evolve into bainite. Widmanstätten ferrite is therefore not to be found in steel B. A further increase in the alloy concentration can eliminate both the Widmanstätten ferrite and bainite reactions, since their nucleation is suppressed to temperatures below that at which martensite can form, as illustrated by Steel C.

The nucleation condition for bainite (equation (5.5)) becomes redundant for any steel in which the Widmanstätten ferrite transformation precedes bainite, because ΔG_m varies approximately linearly and monotonically with temperature. There is only one intersection of the ΔG_m and G_N curves. Hence, if the condition for Widmanstätten ferrite nucleation is satisfied, then so is it for bainite. Recent work has shown that whilst this is true for most steels, there are certain alloys for which the ΔG_m curve

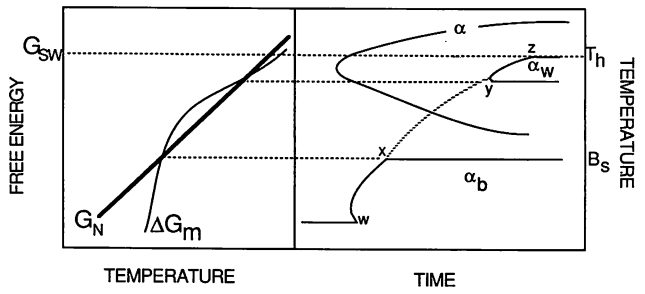

Fig. 6.6 *(a) Free energy curves for the nucleation of Widmanstätten ferrite and bainite in a low alloy steel for which the ΔG_m and G_N curves exhibit a double intersection. (b) Calculated TTT diagram for the same steel, showing how Widmanstätten ferrite and bainite form separate C curves. The Widmanstätten ferrite and bainite C curves would ordiarily be just one curve, joined by the line 'wxyz'. After Ali and Bhadeshia (1991).*

intersects the G_N function at two points, Fig. 6.6a (Bhadeshia and Svensson, 1989c; Ali, 1990). Thus, Widmanstätten ferrite can form at high temperatures, but the reaction becomes stifled within an intermediate temperature range, until after a further undercooling, the nucleation of bainite becomes possible. The usual single C curve for the displacive formation of bainite and Widmanstätten ferrite then splits into a high temperature segment for Widmanstätten ferrite and a lower temperature segment for bainite (Fig. 6.6b).

The 'universal' function G_N has so far been presented as being effective in predicting some of the key features of bainitic reactions, but it is nevertheless, empirical. It can however, be interpreted further, by realising that G_N decreases linearly with T_h. This simple form is consistent with a key experimental observation, that the Widmanstätten ferrite and bainite start temperatures are depressed to a much larger extent than the Ae3 temperature as the concentration of austenite stabilising elements is increased. According to G_N (eq. 5.1), a larger driving force is needed to achieve a given nucleation rate if the transformation temperature is depressed by alloying. Assuming that the form of the relationship between G_N and T_h can be justified theoretically, the model provides a clear explanation of the fact that the B_S and W_S temperatures are more sensitive to alloy concentration than is the Ae_3 temperature, which can be determined from just the thermodynamic effect on the austenite to ferrite transformation. The next section therefore deals with the interpretation of G_N.

6.2 The Nucleation Mechanism

The empirical observations documented in the previous sections, particularly that the driving force needed for nucleation (G_N) varies directly with the transformation start temperature (T_h), can be interpreted further to reveal the mechanism of nucleation. Solid state nucleation theory is usually an adaptation of the classical Becker–Döring model of homogeneous or heterogeneous nucleation (Christian, 1975, 1986). In the model, a new phase arises during a thermal fluctuation, and might survive to grow into a fully fledged particle if it is able to overcome an activation energy barrier due to the need to create the defective interface region between the parent and product phases. By balancing the work done in creating new surface area as the particle grows, against the chemical free energy as the volume of the particle increases, it can easily be demonstrated that the height of the activation barrier varies as the inverse square of the driving force.

The activation barrier is the essence of all nucleation theories for first order transformations. It is detected experimentally by the fact that the

transformations do not occur instantaneously as the driving force for reaction becomes negative. An activation barrier can of course arise for many reasons other than nucleation although its variation with driving force is then expected to be different. A popular model for martensitic nucleation is that embryos of martensite are already present in the parent phase when it is supercooled below the M_s temperature. It is the mobility of the embryo/austenite interface which prevents the embryos from developing instantaneously into sizeable plates. The nucleation process below M_s is therefore not one involving heterophase fluctuations (as in the Becker–Döring model), but it consists instead of the thermally activated motion of the embryo/austenite interface to a point where this interface is able to accelerate to a relatively large velocity. This process is often called 'operational nucleation' since the activation energy detected experimentally is for the transfer of atoms across the interface and hence describes its mobility (Magee, 1970; Olson and Cohen, 1976a–c). As will be seen later, a model like this reveals a different dependence of the activation energy on the chemical driving force, and this can in practice be used to distinguish between the proposed mechanisms of nucleation.

Finally, the homogeneous nucleation of bainite can almost certainly be ruled out since the phase is always observed to nucleate at austenite grain surfaces or intragranularly at nonmetallic inclusions of the kind present in most steels.

6.2.1 *Dependence of The Activation Energy on Driving Force*

6.2.1.1 *Classical Theory*

Classical nucleation theory is based on the occurrence of random phase fluctuations in the parent phase, successful nucleation amounting to the survival and continued growth of the fluctuation into a product phase particle. The fluctuations in the context of classical theory involve the uncoordinated transfer of atoms across the embryo interface, and in this sense must be regarded as a reconstructive nucleation process. This does not of course mean that such a nucleus cannot in principle develop into a particle which grows by a displacive transformation mechanism. Full discussions of the classical nucleation theory can be found in many textbooks and reviews (e.g., Christian, 1975). The purpose here is to introduce the relationship between the driving force and the activation energy for nucleation.

The free energy change ΔG accompanying the formation of an embryo containing n_A atoms is given by

$$\Delta G = n_A \Delta G_{CHEM} + n_A \Delta G_{STRAIN} + C_0 \sigma^{\alpha\gamma} (n_A)^{2/3} \qquad (6.6)$$

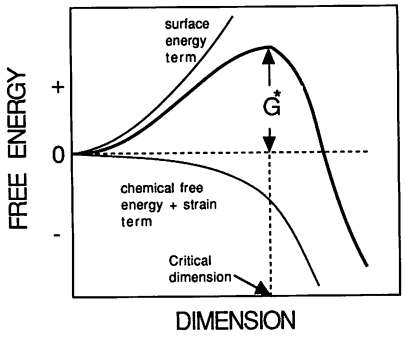

Fig. 6.7 *An illustration of the activation energy barrier according to classical nucleation theory.*

where ΔG_{CHEM} is the chemical free energy change per atom (product minus parent) ΔG_{STRAIN} is the coherency strain energy accompanying nucleation, $\sigma^{\alpha\gamma}$ is the effective interfacial energy per unit area of embryo/matrix interface, and C_0 is a constant. The first term on the right hand side of the equation is negative below the equilibrium transformation temperature, whereas the other terms are positive. It follows that ΔG goes through a maximum to form a barier whose height is the activation energy G^* (Fig. 6.7). It can easily be demonstrated by differentiating equation (6.6) that

$$G^* \propto (\Delta G_{CHEM})^{-2} \tag{6.7}$$

6.2.1.2 Preexisting Embryo Model

The pre-existing embryo model has its origins in martensite nucleation theory, based on the existence of a glissile interface at all stages of the evolution of the martensite phase. It is therefore a displacive nucleation mechanism. As discussed earlier, the activation energy detected experimentally would in this model be interpreted to be that controlling the mobility of the preexisting embryo/matrix interface. Martensitic nucleation is considered to occur by the spontaneous dissociation of defects (the pre-existing embryos) which are present in the austenite at temperatures above M_S, and which become activated as the austenite is cooled to temperatures below M_S (Olson and Cohen, (1976a–c). The embryonic defect is in fact supposed to consist of a closely spaced group of faults derived from the dissociation of other defects already present in the austenite (Fig. 6.8). As the temperature and fault energies fall, the embryo develops athermally into a thin plate of martensite, which might subsequently thicken by some self-reproducing mechanism such as the pole mechanism proposed by Christian. Thermally activated nucleation then

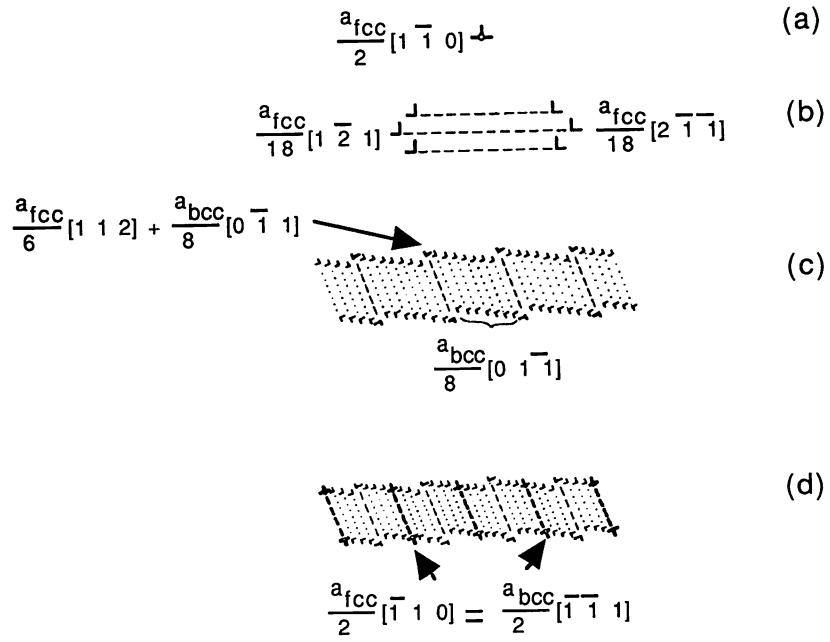

Fig. 6.8 *The Olson and Cohen model for the development of a semicoherent body centered cubic embryo from a perfect screw dislocation (a) in a face centered cubic austenite. (b) Three- dimensional dissociation of dislocation over a set of three close packed planes. The structure thus produced is not yet body centered cubic. (c) Relaxation of fault to a body centered cubic structure, involving the introduction of partial dislocations in the interface. (d) Addition of perfect screw dislocations which cancel the long range strain field of the partial dislocations introduced in (c).*

corresponds to the attempts by the embryo/matrix interface to overcome an interface friction stress. The model differs from the traditional concept of nucleation in which the embryos develop by heterophase fluctuations. Thus, the preexisting embryos simply need to go unstable (i.e. to begin rapid growth) in order to give the appearance of a nucleation phenomenon, when in fact the kinetics are controlled by the mobility of the embryo/matrix interface.

The Olson and Cohen nucleation model is based on the dissociation of defect clusters to cause faulting on the close-packed planes, leading eventually to the formation of a region of the product phase (Fig. 6.8). The structural change is achieved by the passage of transformation dislocations in the embryo/matrix interface, which have to move against any resistance provided by the lattice. In normal circumstances, the creation of faults also opposes the dissociation process, but the fault energy becomes negative at a low enough temperature when transformation is

favoured. It is this negative fault energy (in effect a driving force for transformation) which pushes the transformation dislocations against the resistance of the lattice. The free energy G_F per unit area of fault plane is given by

$$G_F = n_P \rho_A (\Delta G_{CHEM} + G_{STRAIN}) + 2\sigma\{n_P\} \tag{6.8}$$

where ΔG_{CHEM} is the chemical free energy difference between the parent and product phases, G_{STRAIN} is the strain energy, and σ is the embryo/matrix interfacial energy per unit area, a function of n_P which is the number of close packed planes involved in the faulting process. ρ_A is the density of atoms in the close packed planes (moles per unit area).

For a fault embryo bounded by an array of n_P dislocations each of Burgers vector b, the force per unit length of dislocation array required to move the array is $n_P \tau_o b$. τ_o is the magnitude of the shear stress representing the resistance of the lattice to the movement of dislocations at a specified velocity. A fault energy G_F exerts a force per unit length on the array of $-G_F$ (since the friction opposes the faulting). The limiting condition whereby a defect is rendered unstable and develops into a growing martensite plate is given by

$$G_F = -n_P \tau_o b \tag{6.9}$$

This model of martensite nucleation can now be explored further to deduce the relationship between the chemical driving force and the activation energy, G^* for interfacial motion. The theory of thermally activated plastic deformation (involving the conservative glide of dislocations) can be used for this purpose since the chemical driving force can be thought of as a stress acting on the transformation interface. Suppose that in the absence of an applied stress, the activation energy for a dislocation to glide from one equilibrium position to another is given by G_o^*. The application of a shear stress τ reduces the height of this barrier to a value G^* (Conrad, 1964; Dorn, 1968)

$$G^* = G_o^* - (\tau - \tau_\mu) v^* \tag{6.10}$$

where v^* is an 'activation volume' and τ_μ is the athermal resistance to dislocation motion, a resistance which never vanishes irrespective of temperature (Fig. 6.9). On combining the last three equations, and utilising the fact that the stress τ is not externally applied but has its origin in the driving force for transformation (i.e. substituting $\tau = \tau_o$), G^* can be obtained explicitly as a function of the chemical driving force

$$G^* = G_o^* + [\tau_\mu + (\rho_A / b) G_{STRAIN} + (2\sigma / n_P b)] v^* + (\rho_A v^* / b) \Delta G_{CHEM} \tag{6.11}$$

It follows that the activation energy G* is expected to be directly proportional to the driving force ΔG_{CHEM}, a result which contrasts sharply with

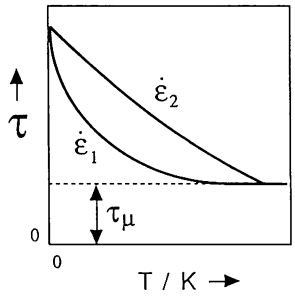

Fig. 6.9 *Temperature dependence of the applied stress necessary for plastic deformation at two different strain rates (after Conrad, 1964). The strain rate* $\dot{\varepsilon}_2$ *is larger than* $\dot{\varepsilon}_1$.

the inverse square relationship expected from classical nucleation theory based on heterophase fluctuations.

We now proceed to demonstrate that the experimentally observed linear relationship between G_N and T_h is consistent with the martensitic nucleation theory discussed above (Bhadeshia, 1981a). It is expected that the nucleation rate I_v will vary with temperature as follows

$$I_v \propto \nu \exp\{-G^*/RT\} \tag{6.12}$$

where ν is an attempt frequency, R is the universal gas constant and T is the absolute temperature. Thus

$$-G^* \propto \beta T \tag{6.13}$$

where

$$\beta = R \ln\{I_V/\nu\} \tag{6.14}$$

In the derivation of the function G_N, the temperature T_h is for each steel, the top of the lower C curve of the TTT diagram, corresponding to a temperature where some fixed detectable nucleation rate is obtained. It follows that the term β is a constant for all steels, and indeed is negative since the attempt frequency should be larger than the actual rate. It follows that

$$G_N \propto \beta T \tag{6.15}$$

precisely the relationship observed experimentally. These results and the analysis discussed earlier, indicate that the nucleation of Widmanstätten ferrite and bainite occurs by a displacive mechanism, but that unlike martensitic nucleation, it involves the partitioning of carbon. However, much further work remains to be done to verify that the experiments are consistent with the detailed predictions of the theory, rather than just the form of the predicted relationships.

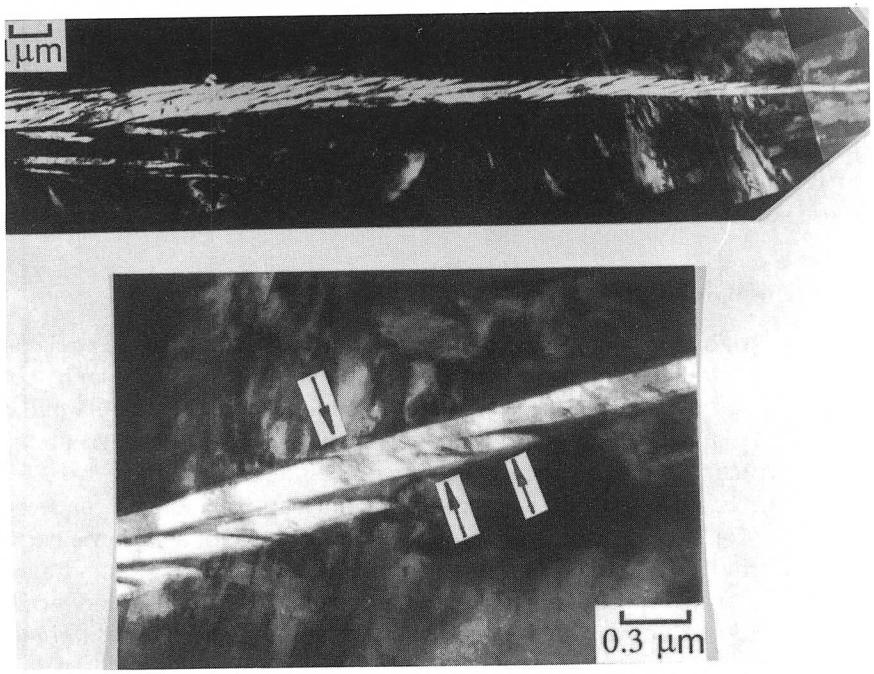

Fig. 6.10 *Transmission electron micrograph ofa sheaf of bainite in a partially transformed sample. A region near the tip of the sheaf in (a) is enlarged in (b). The arrows in (b) indicate possible sub-operational embryos which are much smaller than the fully grown sub-units seen in (a). After Olson* et al. *(1989).*

The pre-existing embryo model predicts that during thermal nucleation, the time for 'nucleation' should be much larger than during growth. The nucleation event consists of a relatively slow activation of the embryo to a point where it becomes unstable and develops rapidly into a large plate. Hence, the size distribution of bainite sub-units should include a population of very fine platelets below the operational nucleus size required for rapid growth to the final size. Fig. 6.10 shows a bainite sheaf in a partially transformed Fe–0.43C–2.12Si–0.43C wt% alloy. In addition to the fully growth sub-units (a few μm in length, Fig. 6.10a) the arrows in the higher magnification view of Fig. 6.10b illustrate another population of much smaller (submicron) particles which are believed to represent these sub-operational embryos.

6.3 The Bainite Start Temperature: Other Models

Zener's original model for the bainite reaction assumed that the transformation is martensitic, but without the strain energy that accompanies the formation of martensite. He was therefore able to explain why bainite is observed to form at temperatures above M_s but below T_o. All other models for the reaction do not explicitly recognise a bainite start temperature. Nor do they recognise that the isothermal transformation diagrams for steels contain a separate C curve for bainite, any appearance of a separate curve being attributed to rather ill-established phenomena such as solute drag.

In an internal report published by Hillert in 1960, Widmanstätten ferrite, bainite and martensite were treated as being continuous, with no difference in transformation mechanism apart from changes in the degree of carbon supersaturation in the ferrite as the undercooling below the equilibrium transformation temperature increases. A slightly revised version of that model has recently been stated by Purdy and Hillert (1984). It is still argued that the three transformations are continuous, but that upper bainite can be distinguished from Widmanstätten ferrite by a larger dislocation density in the former phase. Both upper and lower bainite are considered to grow with nonequilibrium compositions but with some carbon diffusion during growth, the main distinction between these two products being the presence of internal carbides within the lower bainite. Only martensite is recognised to be a truly diffusionless transformation.

A different conclusion was reached by Radcliffe *et al.* (1963) whose analysis of published data led them to the conclusion that the growth of bainite occurs at a rate controlled approximately by the diffusion of carbon in the austenite ahead of the interface. Consequently, they considered that there are no essential differences between Widmanstätten ferrite and bainite in the sense that they are both displacive transformations during which carbon redistributes during growth. Although these and other

similar conclusions are still widely quoted, they all suffer from the fact that the experimental growth rate data were obtained using light microscopy, a technique which does not have the resolution to distinguish the platelets within a sheaf. The data thus refer to the growth rates of sheaves rather than of bainite plates. In any case, the theory for the diffusion controlled growth of plates was not well developed in those days, and more modern assessments show clearly that both bainite sheaves and individual platelets grow at rates much faster than expected from diffusion controlled growth, (section 6.6.2).

A general inconsistency with the models which claim continuity in the Widmanstätten ferrite, bainite and martensite reactions is that bainitic transformation can be shown to cease when the temperature is raised above B_S. It has ben demonstrated using hot-stage light microscopy, thattransformation to upper or lower bainite ceases when the specimen is rapidly reheated to a temperature above B_S after partial transformation to bainite, even when the specimen is held at temperatures greater than B_S for prolonged periods of time.

6.4 Empirical Equations for the Bainite Start Temperature

The most popular empirical equation expressing the bainite start temperature as a function of steel chemistry is due to Steven and Haynes (1956). They rigorously determined the B_S temperatures for a range of wrought steels covering the composition ranges (wt%)

Carbon	0.1–0.55	Nickel	0.0–5.0
Silicon	0.1–0.35	Chromium	0.0–3.5
Manganese	0.2–1.7	Molybdenum	0.0–1.0

and found that

$$B_S, {}^{o}\mathrm{C} = 830 - 270w_C - 90w_{Mn} - 37w_{Ni} - 70w_{Cr} - 83w_{Mo} \qquad (6.16)$$

where w_i is the wt% of element i which is in solid solution in austenite.

Bodnar *et al.* (1989) determined the continuous cooling transformation diagrams for a series of Fe–Ni–Cr–Mo–C steels of the type used in the power generation industry, and found that the upper temperature at which bainite formed as a function of cooling rate was insensitive to the rate of cooling. This is in fact expected when no other transformation precedes bainite, since its C curve in TTT diagrams has long been known to have a flat top (Zener, 1946), a reflection of the thermodynamic limit to the highest temperature at which bainite can form. However, allotriomorphic ferrite did in fact form prior to bainitic reaction in some of their samples, giving rise to difficulties in fundamental interpretation of the data which are nevertheless useful for practical applications of the

steels studied. The data do not represent true B_S temperatures, but temperatures at which the bainite begins to form during continuous cooling at a variety of rates. Not surprisingly, the equation they derived differs significantly from that of Steven and Haynes

$$\text{"}B_S\text{"}, ^{\circ}\text{C} = 844 - 597w_C - 63w_{Mn} - 16w_{Ni} - 78w_{Cr} \qquad (6.17)$$

for the composition range (wt%)

Carbon	0.15–0.29	Nickel	0.21–3.61
Silicon	0.01–0.23	Chromium	1.13–2.33
Manganese	0.02–0.77	Molybdenum	0.44–1.37

6.5 The Nucleation Rate

An implication of the linear dependence of the activation energy for nucleation on the driving force is that the nucleation rate per unit volume is expected to vary as follows

$$I_V = B_1\exp\{-G_1^*/RT\} = B_1\exp\{-(B_2 + B_3\Delta G_m)/RT\} \qquad (6.18)$$

where ΔG_m is the chemical free energy change available for nucleation, and B_i are positive constants with typical values $B_2 = 29710\ \text{J mol}^{-1}$ and $B_3 = 3.77$ (Bhadeshia, 1982b). This equation needs to be modified slightly if the notion that the nucleation rate is a constant at the top of the bainite C-curve (for any steel) is to be preserved (Rees, 1991)

$$I_V = B_1\exp\{-(B_2 + B_3\Delta G_m/B_4)/RT\} \qquad (6.19)$$

where the constant B_4 originates in the nucleation function G_N.

The applicability of equation (6.19) to bainite and Widmanstätten ferrite has to a limited extent been confirmed from an analysis of time–temperature transformation diagrams, and of overall transformation kinetics, although it is too early to claim that the model should be applicable to all steels, including those in which carbide precipitation reactions accompany the formation of bainite.

There is another model by Hawkins and Barford (1972) who used quantitative metallography and found that the nucleation rate I_v of sheaves can be represented empirically by an Arhenius relationship with a *constant* activation free energy G^*

$$I_V = B_5\exp\{-G^*/RT\} \qquad (6.20)$$

in which both the activation energy and B_5 are constant. The nucleation rate thus increases with transformation temperature. By contrast, classical nucleation theory involves two activation events, one determined by the increase in free energy as new surface is created, and the other by the

barrier to the transfer of atoms across the embryo/matrix interface, with activation free energies G^*_1 and G^*_2 respectively. The nucleation rate is then given by

$$I_V \approx B_6 \exp\{-(B_7 \Delta G_m)^{-2} + G^*_2)/RT\} = B_6 \exp\{-(G^*_1 + G^*_2)/RT \quad (6.21)$$

where B_6 can be insensitive to temperature. F^*_1 decreases as the driving force for nucleation increases ($G^*_1 \propto (\Delta G_m)^{-2}$) whereas G^*_2 does not change with temperature. At a low enough temperature, G^*_1 may become negligible and the two equations then become identical, with $G^* = G^*_2$. This prompted Hawkins and Barford to suggest that it is G^*_2 which controls the nucleation process for bainite, or in other words, the transfer of atoms across the nucleus/matrix interface determines the activation free energy for nucleation. Although the form of the equation used, based on classical nucleation theory, appears to contradict that of the pre-existing embryo theory, their experimental data are in fact consistent with the linear relationship between driving force and activation energy. Since ΔG_m varies approximately linearly over the usual temperature range of interest, the pre-existing embryo model also predicts an increase in nucleation rate with the isothermal transformation temperature. It has the additional advantage that it permits the effect of alloy chemistry to be included, whereas the Hawkins and Barford model does not seem to do so.

In steels of reasonable purity, including most modern commercial steels, bainite inevitably nucleates at the austenite grain surfaces. It then grows into the austenite grain with which it has an orientation within the 'Bain region'. On the other hand, in steel weld deposits, which frequently contain relatively large quantities of nonmetallic inclusions, the formation of intragranularly nucleated bainite (often called *acicular ferrite* in the welding industry) is quite common, and regarded as beneficial to mechanical properties. There has been considerable interest in replicating this effect for wrought steels by deliberately inoculating them with suitable particles, the idea being to induce the formation of acicular ferrite in the vulnerable heat affected zone of welded steel plates, thereby leading to an improvement in properties. This intragranular nucleation behaviour needs much further experimental characterisation and is not yet understood in the depth required to calculate the kinetics of the acicular ferrite reaction.

6.6 Growth Rate

The rate at which an interface moves depends both on its intrinsic mobility (related to the process of atom transfer across the interface) and on the ease with which any alloying elements partitioned during transformation move ahead of the moving interface. The two processes are in series so that the interface velocity as calculated from the interface mobility always

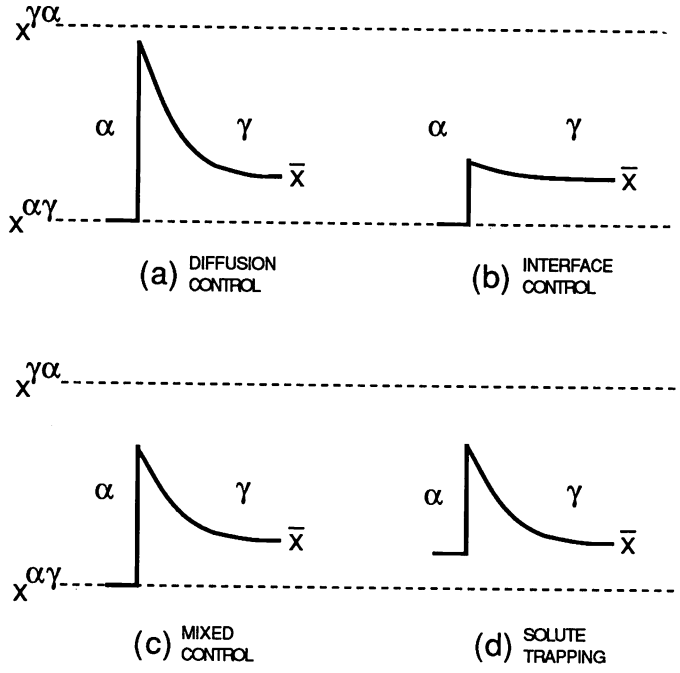

Fig. 6.11 *Carbon concentration profiles at a moving α/γ interface. The terms $x^{\alpha\gamma}$, $x^{\gamma\alpha}$ and $\bar{x}$ refer to the equilibrium concentrations in the ferrite and austenite respectively, and the average concentration in the alloy as a whole. (a) Diffusion control. (b) Interface control. (c) Mixed control. (d) Solute trapping (discussed later).*

equals the velocity calculated from the diffusion of solute ahead of the interface. Both of these processes dissipate the free energy available for interface motion. In this sense, interface motion is always under mixed control. Nevertheless, a process is said to be diffusion controlled when most of the free energy is used up in driving the diffusion of solute in front of the boundary. Interface controlled growth occurs when most of the free energy is dissipated in the process of atom transfer across the interface. The compositions of the phases at the moving interface during diffusion controlled growth are given approximately by a tie line of the phase diagram, and other circumstances are illustrated in Fig. 6.11.

6.6.1 Theory for the Lengthening of Plates

Particle dimensions during diffusion controlled growth vary parabolically with time when the extent of the diffusion field in the matrix increases with particle size. The growth rate then decreases with time because the solute has to diffuse over ever increasing distances. The diffusion controlled lengthen-

ing of plates or needles can however occur at a constant rate because solute can be partitioned to the sides of the plates or needles.

There is good reason to suppose that if there is any partitioning of interstitial elements during displacive transformation, then growth should be diffusion controlled. The shape change characteristic of displacive transformations implies the existence of a high mobility glissile interface so that the amount of the available driving force dissipated in interfacial processes must be rather small. Iron and any substitutional solute atoms do not diffuse during bainite growth and there is no reconstructive diffusion during transformation.

Trivedi (1970) has given a solution for the problem of the diffusion controlled growth of plates. The shape of the plate is taken to be that of a parabolic cylinder and is assumed to be constant throughout growth. A parabolic cylinder describes the shape generated when a parabola is translated along the direction normal to its plane. The plate lengthening rate (V_L) at a temperature T for steady state growth is obtained by solving the equation

$$f_1 = \frac{x_r - \bar{x}}{x_r - x^{\alpha\gamma}}$$

$$f_1 = \pi^{0.5}\exp\{p\}\ \mathrm{erfc}\{p^{0.5}\}[1 + (r_c/r)f_1S_2\{p\}] \tag{6.22}$$

where the Pèclet number p, which is a dimensionless velocity, is given by

$$p = V_L r/2\overline{D} \tag{6.23}$$

The weighted-average diffusion coefficient $\overline{D}$ for carbon in austenite is given by integrating D (the diffusivity at a specific concentration) over the range $\bar{x}$ to x_r, and then dividing the integral by this range. x_r is the carbon concentration in the austenite at the plate tip. It may differ significantly from the equilibrium carbon concentration $x^{\gamma\alpha}$ because of the Gibbs–Thompson capillarity effect which allows for the change in equilibrium concentration as a function of interface curvature (Christian, 1975); x_r decreases as interface curvature increases, and growth ceases at a critical plate tip radius r_c when $x_r = \bar{x}$. For a finite plate tip radius (r)

$$x_r = x^{\gamma\alpha}[1 + (\Gamma/r)] \tag{6.24}$$

where Γ is the capillarity constant (Christian, 1975) given by

$$\Gamma = (\sigma V_m/RT)[(1 - x^{\gamma\alpha})/(x^{\alpha\gamma} - x^{\gamma\alpha})]/[1 + [d(1n\ \Gamma)/d(1n\ x^{\gamma\alpha})]] \tag{6.25}$$

σ is the interfacial energy per unit area, Γ is the activity coefficient of carbon in austenite, and V_m is the molar volume of ferrite. This assumes that the ferrite composition is unaffected by capillarity, since $x^{\alpha\gamma}$ is always very small. The critical plate tip radius r_c can be obtained by setting $x_r = \bar{x}$. The function $S_2\{p\}$ depends on the Pèclet number, varying from about 10

to about 0.05 as p changes from 0.05 to 10. It corrects for the variation in composition due to changing curvature along the interface and has been evaluated numerically by Trivedi.

As pointed out earlier, Trivedi's solution for diffusion controlled growth assumes a constant shape (parabolic cylinder), but the solution is not really shape preserving. The capillarity effect implies that x_r varies over the surface of the parabolic cylinder, and this should lead to a deviation from the parabolic shape. Trivedi claims that the variation in x_r has a negligible effect provided the tip radius is greater than $3r_c$.

The Trivedi equation, and in fact all other models of plate growth which account for capillarity effects, each provide a relation between velocity and tip radius but do not allow these quantities to be fixed (Fig. 6.12). Additional theory is needed to enable the choice of a particular tip radius, and hence to fix V_L. Small tip radii favour fast growth due to the point effect of diffusion, but this is opposed by the capillarity effect since the driving force for growth tends towards zero as $r \rightarrow r_c$. Zener proposed that the plate should tend to adopt a tip radius which allows V_L to be maximised but there is no fundamental justification nor experimental evidence to support this hypothesis. Recent work on the dendritic growth of solid from liquid (formally an almost identical problem) has conclusively demonstrated that the dendrites do not attain a radius consistent with the Zener maximum velocity hypothesis, the actual tip radius being determined by a shape stability criterion (Glicksman *et al.*, 1976; Langer and Muller–Krumbhaar, 1978). If these results can be extrapolated to solid state transformations, and it is doubtful that they can since the shape for displacive transformation products is determined by strain energy minimisation, then any calculated velocities would be less than those given by the Zener hypothesis. In the absence of reliable data on plate tip radii, the Zener hypothesis provides an upper limit for V_L.

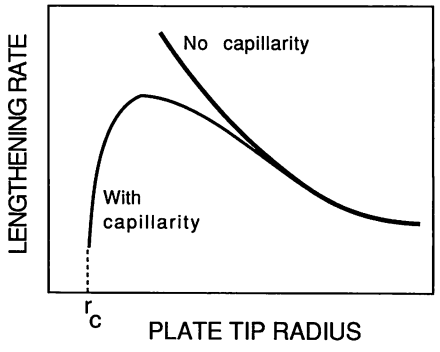

Fig. 6.12 *Schematic illustration of the variation in velocity as a function of the plate tip radius.*

The shape of ferrite plates is sometimes more needle-like (lath) than plate-like. Trivedi has obtained a steady state solution for the diffusion controlled growth of paraboloids of revolution (i.e., needles)

$$f_1 = p \exp\{p\}\, Ei\{p\}[1 + r_c/r)f_1 R_2\{p\}] \tag{6.26}$$

where the function $R_2\{p\}$ corrects for the variation in composition due to the changing curvature of the interface and has been numerically evaluated by Trivedi. The tip radius r_c is twice as large as that for plates.

Finally, we note that Trivedi has also given a slightly more elaborate theory to take account of any free energy dissipated in interface processes. In this, a second set of functions ($S_1\{p\}$ for plates and $R_1\{p\}$ for needles) is introduced to allow for the variation in dissipation due to the changing orientation of the interface. The current evidence suggests that the dissipation in any interface processes can be neglected given the glissile nature of the transformation interface.

6.6.2 *Growth Rate of Sheaves of Bainite*

In wrought steels, sheaves of bainite normally nucleate at the austenite grain surfaces and then propagate towards the grain interiors by the successive formation of individual sub-units, each of which grows to just a limited size. New sub-units form mainly near the tips of existing platelets; the nucleation of sub-units in adjacent positions occurs at a much lower rate. This means that the overall shape of the sheaf on a macroscopic scale is plate-like in three dimensions. Since coordinated movements of atoms cannot in general be sustained across austenite grain boundaries, the growth of a given sheaf is confined strictly to a single austenite grain. Bainite plates are also stopped by austenite twin boundaries (Ko and Cottrell, 1952; Speich, 1962). The grain in which bainite grows is the one with which it has an orientation within the Bain region as previously defined; this contrasts with the C. S. Smith theory of grain boundary nucleation for reconstructive transformations which states that the new phase will grow into the grain with which it has a random (incoherent boundary) orientation.

Most direct observations of bainite growth are of limited resolution and refer to the growth of *sheaves* of bainite. Typical thicknesses of 'plates' of bainite observed in such studies (e.g., Speich, 1962) are in the range 1–5μm, far greater than that of a sub-unit as observed using transmission electron microscopy, at about 0.2μm. In the discussion that follows, observations using light microscopy are interpreted as referring to sheaf growth, even though the original papers may not make any explicit distinction between the sheaf and sub-unit. If it is assumed that a sub-unit reaches its limiting size in a time period t_c, and that the time interval Δt

elapses before another sub-unit nucleates at the tip of the original sub-unit, then the lengthening rate, V_s, of a sheaf is given by

$$V_S = Vt_C/(t_C + \Delta t), \tag{6.27}$$

where V is the average lengthening rate of a sub-unit (Ali and Bhadeshia, 1989).

Several direct observations have shown that the bainite sheaves lengthen at a constant rate (Speich and Cohen, 1960; Goodenow *et al.*, 1963; Hawkins and Barford, 1972). For a given transformation temperature, the measured rates are found to exhibit a significant degree of scatter, attributed to small variations in growth rate in radial directions within the habit plane of a given sheaf, giving rise to a noncircular habit plane. An increase in carbon, nickel or chromium concentration leads to a decrease in the lengthening rate. From measurements of the thickening rates of sheaves, Speich and Cohen concluded that the aspect ratio (thickness/length) was independent of sheaf size, the thickening rate being proportional to the lengthening rate and similar results have been reported by Hawkins and Barford (1972). This does not imply that the thickening and lengthening processes for sheaves are coupled, because thickening was found to continue at the same rate, even when lengthening stopped. For an integral plate of martensite which is elastically accommodated, radial growth will continue until some obstacle is encountered, but thickening is expected to come to a halt only when a condition of thermoelastic equilibrium is reached (Olson and Cohen, 1977). In this, a balance is reached between the available chemical driving force, and the increasing elastic strain energy as the plate thickens (equation 5.3). As pointed out in Chapter 2, it may be more important to minimise long range distortions over a whole sheaf of bainite rather than for an individual sub-unit. The thickening of a sheaf continuing after its lengthening has been halted, would then be a situation analogous to the thermoelastic equilibrium described for martensite, but the analogy should not be carried much further. The thickening in the case of bainite proceeds by the formation of new sub-units. Furthermore, whilst a plate of thermoelastic martensite would begin to revert to austenite with little hysteresis on heating, the formation of bainite sub-units involves considerable plastic accommodation and a rapid redistribution of carbon. In that sense, the bainite is not as reversible as the martensite.

The observations described above, and other findings, were interpreted originally to refer to the growth of individual bainite plates rather than sheaves. Speich considered that the thickening process involves the planar motion of the broad face of the plate at a rate controlled by the diffusion of carbon in the austenite, and the observed *constant* thickening rate was then explained by the periodic precipitation of carbides such that the effective diffusion distance for carbon remained approximately

constant. The observations really refer to sheaf growth, the rate of thickening depending perhaps on the nucleation of other adjacent sub-units.

The ratio of the thickening to lengthening rate (when these are independent of time) determines the aspect ratio of a sheaf whose growth has not been limited by impingement with obstacles such as grain boundaries. The activation energy Q of a growth process may be defined as (Kaufman *et al.*, 1962)

$$Q = -R[d(\ln\{V_s\})/d(1/T)] \tag{6.28}$$

This phenomenological relation makes no specific assumptions about the temperature dependence of growth rate, so that the activation energy Q cannot be physically interpreted without further justification. The activation energy for lengthening is found to be smaller than that for thickening, so that the aspect ratio of a sheaf is expected to decrease with temperature, as confirmed experimentally. There is however, no satisfactory theoretical treatment of the kinetics of sheaf thickening and it is also not established that the rate of thickening is constant, as claimed by Speich and Cohen (1960) and Speich (1962). Goodenow and Hehemann (1962) found that the thickening rate decreases with increasing thickness.

Recent critical assessments (Bhadeshia, 1985a; Ali and Bhadeshia, 1989) of the published kinetic data (Oblak and Hehemann, 1967; Hillert, 1960; Speich and Cohen, 1960; Goodenow *et al.*, 1963; Rao and Winchell, 1967; Townsend and Kirkaldy, 1968; Simonen *et al.*, 1973; Nemoto, 1974) for the lengthening of plates of Widmanstätten ferrite and sheaves of bainite in plain carbon steels demonstrate that for bainite, the measured sheaf growth rates are much larger than would be indicated by carbon

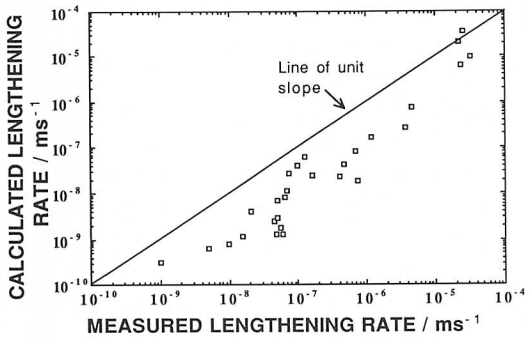

Fig. 6.13 *A comparison of published data on the lengthening rate of bainite sheaves (Oblak and Hehemann, Goodenow* et al., *Rao and Winchell, Simonen* et al., *and Nemoto) against the lengthening rate expected if growth occurs under paraequilibrium conditions and is controlled by the diffusion of carbon in the austenite ahead of the interface. After Ali and Bhadeshia, (1989).*

diffusion controlled growth, and that there is no special nickel-atom/interface interaction in Fe–Ni–C alloys as has been suggested in the past by Rao and Winchell (1967) and Purdy and Hillert (1984). The experimental data are compared against calculations assuming diffusion controlled growth (Trivedi solution) in Fig. 6.13.

6.6.3 Growth Rate of Individual Sub-Units of Bainite

In many steels, martensite is found to grow at a speed which is limited by that of sound in the alloy. Although much faster than expected from carbon diffusion controlled growth, the lengthening rate of individual sub-units of bainite is undoubtedly far less than this limiting velocity. While the shape change accompanying transformation indicates that the bainite/austenite interface is glissile, the rate at which the interface moves is relatively slow, especially if it is accepted that the growth is diffusionless. Goodenow and Hehemann (1962) suggested that the slow growth of bainite is associated with the damping of interface dislocation motion at the high temperatures at which bainite forms but such effects should not be significant unless the growth rate is a large fraction of the speed of sound in the steel. There may also be a dissipation of energy associated with the movement of carbon atoms in compliance with the interface stress field.

The growth rate of individual sub-units of bainite has been measured using hot-stage photoemission electron microscopy, which is a high resolution technique using bulk samples. Electrons are excited from the surface of the sample using incident ultraviolet radiation, and it is these electrons which form the image. The technique is sufficiently powerful to resolve individual sub-units of bainite. Fig. 6.14 illustrates a series of photoemission electron micrographs taken at 1 s intervals, showing the growth of bainite sub-units at 380°C in a Fe–0.43C–3Mn–2.02Si wt% alloy. The measured growth rate of the arrowed sub-unit is 75 $\mu m\ s^{-1}$. Plate lengthening by a paraequilibrium mechanism would give a maximum rate of 0.083 $\mu m\ s^{-1}$, a value which is many orders of magnitude smaller than obtained experimentally. The sub-units clearly lengthen at a rate much faster than is expected from carbon diffusion control.

6.6.4 Solute Drag

Solute drag can be defined formally as a process which involves the dissipation of free energy due to diffusion *within the interface*. A good picture of the process can be imagined by comparison with the drag on individual dislocations as a consequence of the segregation of solute atoms to dislocation cores. Solute drag theory has been developed in

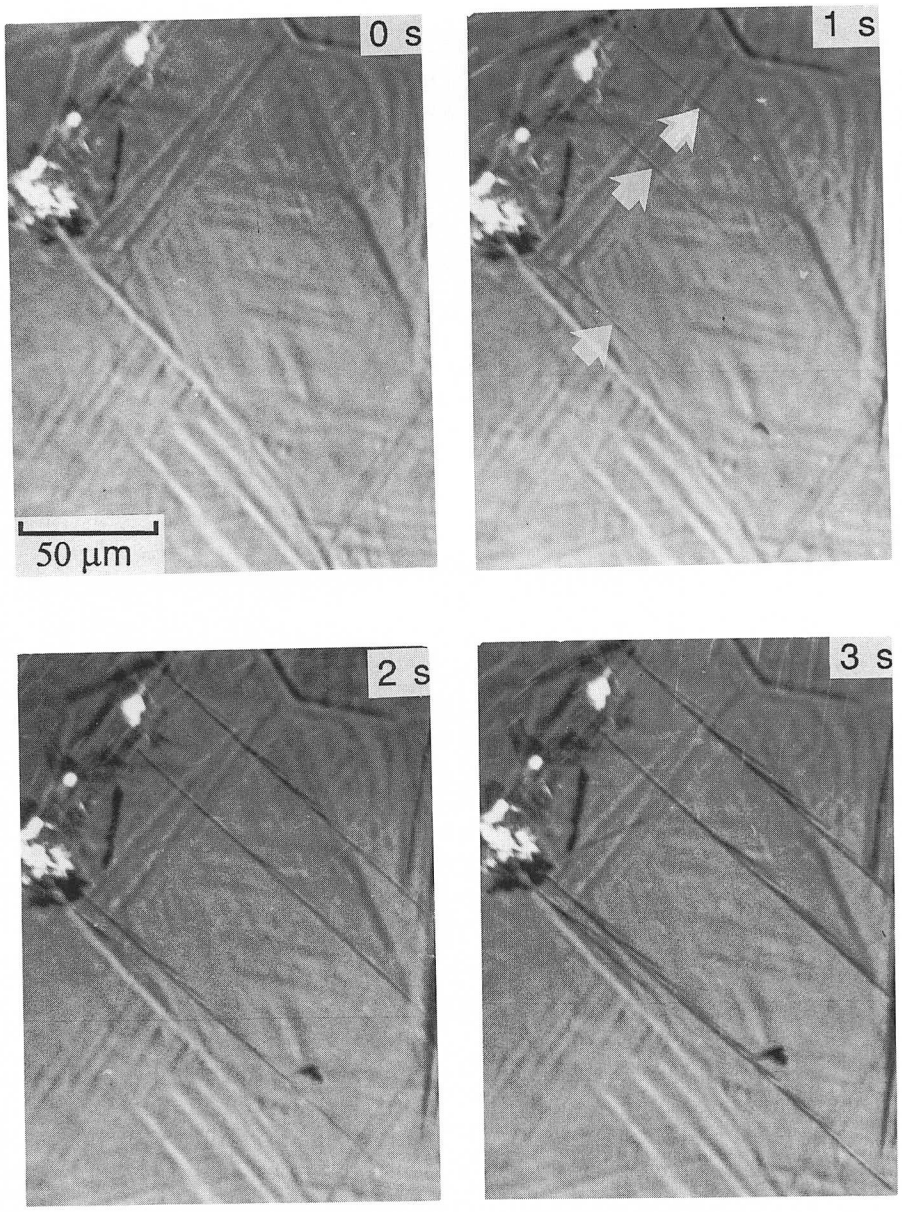

Fig. 6.14 *Photoemission electron microscope observations on the growth of individual sub-units in a bainite sheaf (Bhadeshia, 1984). The pictures are taken at 1s intervals during transformation at 380 Centigrade in a Fe–0.43C–2.02Si–3Mn wt% alloy. The micrograph at 0s is fully austenitic, the relief being a residue from a previous experiment.* *Continued overleaf.*

Fig. 6.14 *Photoemission electron microscope observations on the growth of individual sub-units in a bainite sheaf (Bhadeshia, 1984). The pictures are taken at 1 s intervals during transformation at 380 Centigrade in a Fe–0.43C–2.02Si–3Mn wt% alloy. The micrograph at 0 s is fully austenitic, the relief being a residue from a previous experiment.*

considerable detail for grain boundaries but satisfactory models are not available for interphase interfaces. There is certainly no model which can predict the extent of drag expected due to the segregation or desegregation of the solute to a moving transformation interface, especially when the growth process involves at the same time the long range partitioning of solute between the phases on either side of the interface. The situation is made worse by the fact that clear experiments have yet to be defined to prove the existence of any drag phenomena at α/γ interfaces (Bhadeshia, 1983a).

There is on the other hand, a considerable body of evidence that suggest firstly the absence of any chemical segregation to the bainitic ferrite/austenite interface, and secondly that the growth rate of bainitic ferrite is too large to invoke any free energy dissipations due to solute drag phenomena. The latter have already been discussed earlier in the section on growth rate, and the discussion below is therefore confined to the evidence on segregation.

Recent atomic resolution experiments using a field-ion microscope with an atom probe to obtain directly the compositions at the bainitic ferrite/austenite interfaces support this conclusion. The experiments reveal that elements such as Mn, Ni, Si, Mo, and Cr not only do not partition between

the phases, but that they also do not segregate to the transformation interface (Bhadeshia and Waugh, 1981, 1982; Stark *et al.*, 1988, 1990; Josefsson and Andren, 1988, 1989; Josefsson, 1989). This work has been challenged on the grounds that if the formation of bainite involves a ledge mechanism of diffusional growth, then the observations are unlikely to correspond to actual ledges where the transfer of atoms is supposed to take place. The criticism does not however seem to be justified on the following grounds. Since a finite deformation can have at most only one invariant plane, any macroscopic interface other than the habit plane of the plate must be forced elastically into coherence. The stresses required to achieve this become very large as the dimensions of the second interface increase. The second interface cannot be semi-coherent since this would imply that there is no appreciable shape deformation. This argument seems to preclude the formation of superledges on bainitic plates (Christian, 1990a).

Further atom probe experiments by Stark and Smith (1987) have revealed that for steels containing up to 2 wt% Mo, there is no clustering of molybdenum atoms in the austenite, and that there probably is no association of carbon and molybdenum atoms in austenite. There have in the past been suggestions that such clusters, by interacting with the transformation interface, may give rise to a solute drag effect since the stability of the clusters may be different in the ferrite (Sharma and Purdy, 1973).

It is interesting that in no case has solute segregation been found to occur to the austenite/bainitic ferrite interface during transformation. This could be related to the semi-coherent nature of the interface, but an important factor is the lack of atomic mobility at the temperatures where bainite forms. It is natural to expect, from a thermodynamic point of view, some segregation of misfitting atoms to an interface, which may after all contain dislocations which can accommodate such atoms. However, for bainite the segregation does not happen during transformation because the solute atoms would then have to diffuse along with the moving interface to maintain the segregation, and this is not possible at the low transformation temperatures. When the bainite reaction stops, segregation could occur at the stationary interfaces, but any such effects could then easily be masked by the process of solute redistribution between the phases as the system approaches equilibrium during annealing. Gadgil *et al.* (1989) have obtained very clear evidence using the imaging atom probe, to show the segregation of molybdenum to an austenite/δ-ferrite interface in a duplex stainless steel sample annealed at temperatures in excess of 1050°C, showing that such interfaces can indeed accommodate excess solute. They also found that as a consequence of the segregation, the regions in the austenite and ferrite in the immediate vicinity of the interface were depleted of molybdenum, as would be expected from a

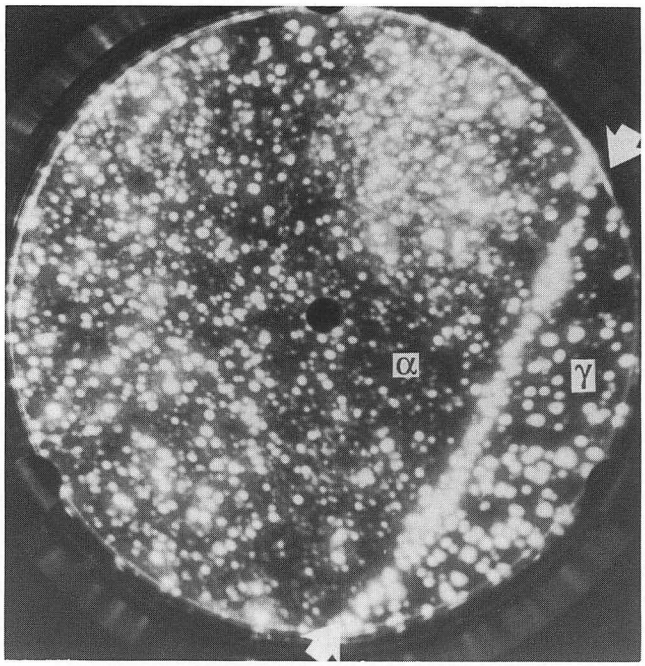

Fig. 6.15 *Direct experimental evidence illustrating that it is in some circumstances possible for the austenite/ferrite interface to accumulate an excess concentration of solute (in this case Mo). The image is from a sample of duplex stainless steel in which the transformation from ferrite to austenite occurs at very high temperatures (1050°C for one hour). After Gadgil* et al., *(1989).*

true segregation phenomenon (Fig. 6.15). It should be noted that the nature (degree of coherency) of the interface illustrated has not been characterised.

6.7 Partitioning of Carbon from Supersaturated Bainitic Ferrite

If bainitic ferrite grows with a non-equilibrium concentration of carbon, then given the opportunity, the carbon should tend to partition into the residual austenite where it has a lower chemical potential. This tendency for excess carbon to redistribute after transformation should also apply to steel microstructures containing mixtures of martensite and austenite. However, martensite forms at relatively low temperatures, where the time taken to redistribute the carbon is large compared with that taken to transform most of the austenite. Consequently, the redistribution process does not hinder the progress of martensitic transformation, as it does for bainite.

The time t_d required to decarburise the supersaturated ferrite is expected to at least be comparable to that required for a sub-unit to complete its growth. If t_d is small compared with the kinetics of carbide precipitation from ferrite, then the transformation would be classified as upper rather than lower bainite, an aspect discussed further in Chapter 7.

Kinsman and Aaronson (1967) considered the kinetics of the partitioning of carbon from bainitic ferrite of the same composition as the parent phase. For a plate thickness w, it is reasonably assumed that the flux of carbon is one dimensional, along a coordinate z normal to the α/γ interface, with origin at the interface and z being positive in the austenite. A more recent version of the calculation (Bhadeshia, 1988) begins with the conservation condition

$$0.5w(\bar{x} - x^{\alpha\gamma}) = \int_0^\infty [x_\gamma\{z, t_d\} - \bar{x}]\, dz \tag{6.29}$$

where $\bar{x}$ is the average mole fraction of carbon in the alloy and $x^{\alpha\gamma}$ and $x^{\gamma\alpha}$ are the paraequilibrium carbon concentrations in α and γ respectively. These equilibrium concentrations should strictly allow for the stored energy of bainitic ferrite. Since the diffusion rate of carbon in austenite is slower than in ferrite, the rate of decarburisation will be determined by the diffusivity in the austenite, and the concentration of carbon in austenite at the interface remains constant for times $0 < t < t_d$, after which it steadily decreases as the austenite becomes homogeneous in composition. The function x_γ is given by

$$x_\gamma = \bar{x} + (x^{\gamma\alpha} - \bar{x})\ \mathrm{erfc}\{z/2(\overline{D}\, t_d)^{0.5}\} \tag{6.30}$$

On integrating equation (6.30) we get

$$t_d^{0.5} = w(\bar{x} - x^{\alpha\gamma})\pi^{0.5} \,/\, 4\overline{D}^{\,0.5}(x^{\gamma\alpha} - \bar{x}) \tag{6.31}$$

By substituting different levels of starting carbon concentrations in the ferrite, the time dependence of the average ferrite concentration can also be determined. The analysis indicates that plates of bainitic ferrite do not generally decarburise within a matter of milliseconds as is popularly believed, but could take substantially longer time periods depending on the transformation temperature and alloy chemistry, Fig. 6.16.

The analytical equation presented above has limitations in the sense that it does not allow for the coupling of fluxes in the austenite and ferrite. It is based on the assumption that the diffusivity in the ferrite is so large, that any concentration gradients within the ferrite are rapidly eliminated. This assumption must fail as the carbon concentration in the austenite at the interface rises (i.e., as the transformation temperature or the

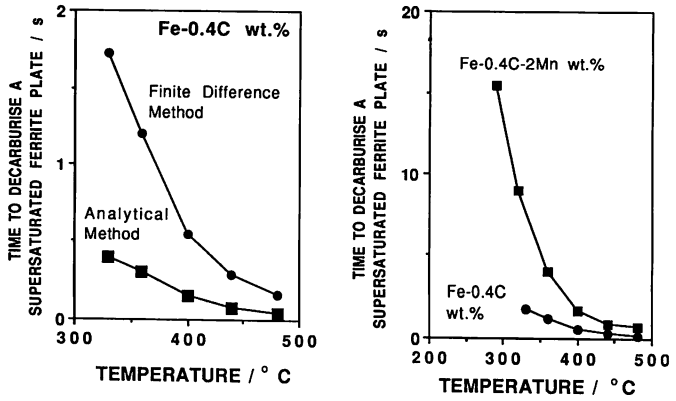

(a) (b)

Fig. 6.16 *(a) Diagram illustrating how the time required to decarburise a plate of bainite (thickness 0.2 μm) in an Fe–0.4C wt% alloy varies with temperature. The calculations have been carried out in two ways, the analytical and finite difference methods. (b) The effect of adding an austenite stabilising substitutional alloying element on the decarburisation time (After Mujahid and Bhadeshia, 1992).*

concentration of austenite stabilising substitutional elements is reduced) because of the need to satisfy the mass conservation condition at the interface

$$D_\alpha \, (\partial x^\alpha / \partial z) = \overline{D} \, (\partial x^\gamma / \partial z) \qquad (6.32)$$

where D_α is the diffusivity of carbon in the ferrite, x^α is the concentration of carbon in the ferrite at the interface, and z is a coordinate defined to be normal to the austenite ferrite interface. The concentration gradients in equation (6.32) are both to be evaluated at the position of the interface (i.e., z=0). The diffusivity of carbon in ferrite is much larger than in austenite, so that the composition x^α in the ferrite at the interface will almost always deviate from equilibrium ($x^{\alpha\gamma}$) in order to maintain compatibility with equation (6.32). It will only reach the equilibrium value towards the end of the partitioning process. As $x^{\gamma\alpha}$ increases, the concentration gradients in the ferrite must also increase, and the partitioning process becomes to an increasing extent limited by diffusion within the ferrite. As a consequence, the diffusion time as predicted by the finite difference method becomes larger than that estimated by the approximate analytical equation when the transformation temperature or austenite stability is reduced (i.e. $x^{\gamma\alpha}$ increased), as illustrated in Fig. 6.16. Typical concentration profiles that develop during the partitioning process are illustrated in Fig. 6.17.

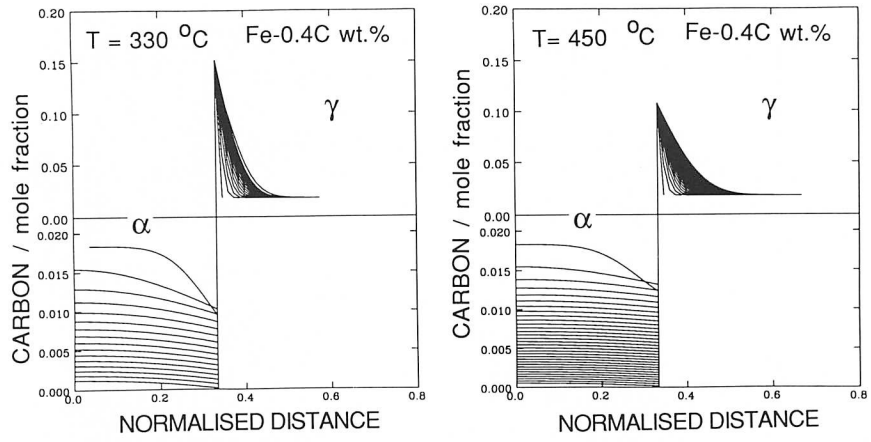

Fig. 6.17 *The concentration profiles that develop in ferrite and austenite during the partitioning of carbon from supersaturated bainite (Fe–0.4C wt%, plate thickness 0.2 μm). (a) 330°C, the time interval between the concentration contours in each phase being 0.094 s. (b) 450°C, the corresponding time interval is 0.007 s (Mujahid and Bhadeshia, 1992).*

6.8 Growth of Ferrite with Partial Supersaturation

Martensite nucleates and grows without any diffusion — it can after all, form at temperatures close to 0K. This contrasts with equilibrium transformation at elevated temperatures close to the Ae_3 temperature, where atomic mobility permits the long range diffusion of atoms. Between these limiting cases, there exist in principle an infinite set of non-equilibrium transformation modes with varying degrees of solute trapping and solute partitioning. These non-equilibrium modes can be classified further into two regimes, one where substitutional solutes are mobile, and the other where only the interstitials are able to diffuse. It is this latter mode which is relevant for the displacive transformations considered here; the upper limit of this mode would correspond to displacive transformation by a paraequilibrium mechanism, with increasing deviations from paraequilibrium as the transformation temperature is reduced and the degree of carbon trapping increases.

Thus, only some of the carbon may redistribute during transformation, the rest being trapped by the advancing interface. The interface compositions cannot then be determined from a knowledge of the phase diagram and the capillarity effect, as is done for diffusion controlled growth. The actual interface compositions for ferrite could lie anywhere between the limits $x^{\alpha\gamma}$ and $\bar{x}$, and for austenite between $\bar{x}$ and $x^{\gamma\alpha}$.

The product phase is then said to grow with a *partial supersaturation* because its solute content is in excess of paraequilibrium, but is less than

that of the parent phase. Bainite has often been considered to form with only a partial supersaturation with respect to carbon (Hillert, 1960; Christian, 1962; Pickering, 1967). All experimental measurements of the carbon content of bainitic ferrite are consistent with at least some partitioning during growth. However, measurements like these cannot indicate the conditions during growth because the carbon, which has a very large diffusivity in iron, can redistribute before any experimental measurements can be conducted.

Although this section deals at length with the problem of ferrite plates growing with a partial supersaturation, it must be emphasised that there is no reliable evidence to support these ideas. The work should be treated as a hypothesis which requires further theoretical and experimental study. The problem itself is nevertheless challenging and has implications far beyond the metallurgy of steels — non-equilibrium transformations occur in many areas of materials science, such as rapid solidification processing.

6.8.1 Stability

There are no conceptual difficulties in thinking of a transformation as either being diffusionless, or an equilibrium transformation. On the other hand, an intermediate mode of reaction requires some justification. Although thermodynamics may prevent it from developing into a diffusionless transformation (the temperature may be above T_o), an increase in the degree of partitioning would be accompanied by a reduction in free energy so that the reaction might tend to collapse towards equilibrium.

In Fig. 6.18, x_m represents the maximum permitted level of carbon supersaturation in ferrite which precipitates from austenite of composition $\bar{x}$. Any higher supersaturation cannot be sustained from a thermodynamic point of view because the driving force for transformation would then

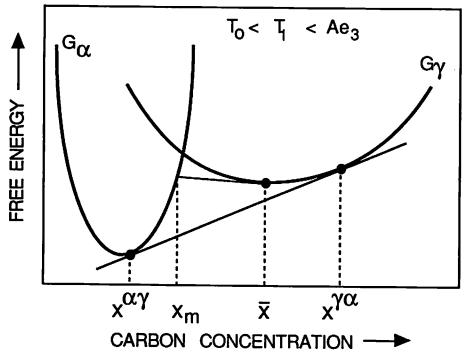

Fig. 6.18 *Schematic austenite and ferrite free energy curves illustrating the unstable nature of any assembly in which the ferrite forms with only a partial supersaturation of carbon.*

be positive. It is evident that growth involving partial supersaturation (such as that indicated by the interface tie-line $x_m \rightarrow \bar{x}$) would be *unstable* to perturbations in the interface compositions. Since any diffusion field is by its very nature subject to random perturbations, opportunities must arise for the field to adjust toward lower free energy states. It follows that the assembly should tend irreversibly to cascade towards the equilibrium partitioning of carbon (tie line $x^{\alpha\gamma} \rightarrow x^{\gamma\alpha}$), especially since the carbon has a high mobility in iron. Experimental evidence supports this conclusion since the growth of Widmanstätten ferrite is found to be consistent with the (para) equilibrium partitioning of carbon, irrespective of the undercooling below the equilibrium transformation temperature. These considerations do not, however, rule out the *theoretical* possibility of growth involving varying degrees of partitioning as a function of undercooling, since the instability problem discussed above can be dismissed on the grounds that some other physical phenomenon could provide the necessary stabilising influence on interfacial velocity (Christian and Edmonds, 1984).

There are in fact a number of different processes occurring in series as the ferrite grows. Each of these processes is responsible for the dissipation of a proportion of the available driving force, and the variation in interface velocity and this dissipation constitutes a physical law (an 'interface response function') representing that process. The actual velocity of the interface depends on the simultaneous solution of all the interface response functions, a procedure which at the same time fixes the composition of the growing particle for a specified transformation temperature. The problem can be illustrated with the help of an electrical analogy (Fig. 6.19); the resistors in series represent the variety of hurdles in the process of transformation (e.g., diffusion in the parent phase, the transfer of atoms across the interface, solute drag, etc.). The potential drop across each resistor is the driving force dissipated in each process, and the current, which is the same through each resistor, represents the interface velocity. The relationship between the current and potential is different for each resistor, but the actual current is obtained by a simultaneous solution of all such relations (Fig. 6.19).

The driving force available for transformation can similarly be partitioned into that dissipated in the diffusion of carbon ahead of the interface, a quantity dissipated in the transfer of atoms across the interface, and into any other process which might be significant in determining the motion of the interface. There might exist many such processes, but to solve for the set of three unknowns (the austenite composition at the interface, supersaturation and velocity) it is necessary to have available at least three interface response functions. If the tip radius of the plate is considered to be an additional variable, then the number of unknowns is four. However, for displacive transformations the radius is determined by the minimisation of the strain energy due to the shape change accompanying transformation

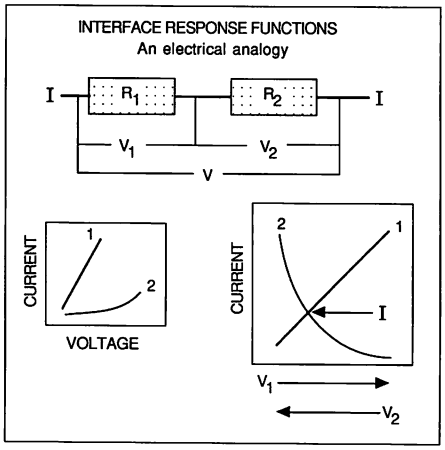

Fig. 6.19 *An electrical analogy illustrating the dissipations caused by the different processes which occur in series as the transformation interface moves. The resistors represent the series of hurdles to be overcome to achieve transformation, the voltage the driving force and the current the interface velocity. The way in which voltage (driving force) is dissipated as a function of current (velocity) across each resistor is different, since each resistor represents a separate physical process. There is but one interface, so all these physical processes must yield the same velocity, as indicated by the same current passing through all the resistors.*

(Olson *et al.* 1988, 1989). The necessary three interface velocity functions are, therefore, the diffusion field velocity, the velocity determined by interface mobility and a carbon trapping function. Each of these are now discussed in detail. They all give different velocities for a given level of free energy dissipation, but the correct velocity corresponds to their simultaneous solution. For that solution, the available free energy is partitioned to different degrees between the three processes, such that they all give the same velocity.

6.8.2 The Interface Response Functions

As mentioned earlier, the process of structural change across the interface, and the diffusion of solute ahead of the interface, both dissipate a proportion of the net free energy ΔG that is available for interfacial motion. The law relating interface velocity to a particular process leading to the dissipation of free energy is the interface response function, and we begin by introducing the different functions.

6.8.2.1 The Interface Mobility (Martensitic Interface)

Considerable experimental data exist for martensitic transformations, and can be exploited if it is assumed that bainite is identical to martensite in

interface structure and interface mobility, except that for bainite there is some partitioning of interstitial solute. This partitioning increases the available free energy change, thereby allowing transformation to happen above the martensite start temperature. Interfacial and elastic energy quantities are thus assumed to be identical to estimates available for martensitic transformation (Olson *et al.*, 1989, 1990).

The theory for thermally activated dislocation motion can be adapted to represent the motion of the α/γ interface, using dislocation models of interfacial structure (Grujicic *et al.*, 1985a–c). The velocity V_i for the motion of the interface is then given by the classical relationship:

$$V_i = V_o \exp\{-G^*/kT\}, \tag{6.33}$$

where G^* is a free energy of activation, and the pre-exponential factor V_o can be taken to be 30 ms^{-1} based on experimental data from single-interface martensite transformations (Grujicic *et al.*, 1985b); k is the Boltzmann constant and T the absolute temperature. We then exploit the dislocation model of the interface to extrapolate slip dislocation theory by converting the chemical driving force into a mechanical force on the interface. The activation energy G^* can then be expressed as a function of the net interfacial driving force G_{id} through the relation (Kocks *et al.*, 1975)

$$G^* = \int_{G_{id}}^{G_{id}'} v^* \, dG \tag{6.34}$$

where G_{id}' is the maximum glide resistance presented by obstacles to interfacial motion, and v^* is the activation volume swept by the interface during a thermally activated event. For a wide range of obstacle interactions, the function $G^*\{G_{id}\}$ can be represented by

$$G^* = G_o^*[1 - (G_{id}/G_{id}')^y]^z \tag{6.35}$$

where G_o^* is the total activation free energy necessary to overcome the resistance to dislocation motion without the aid of an interfacial driving force. The constants y and z define the shape of the force–distance function and for solid solution interactions in the Labusch limit (i.e., where the hardening is largely due to the overall effect of a lot of strain centres, rather than strong dislocation interactions with individual centres), it may be assumed that $y = 0.5$ and $z = 1$ (Nabarro, 1982).[1]

1 The relationship between the activation energy and driving force is here non-linear, compared with eq. 5.11 of the nucleation theory presented earlier. It simply is a better approximation to the problem, the linear relation of eq. 5.11 sufficing for most purposes.

Analysis of kinetic data for the interface controlled barrierless nucleation of martensite gives

$$G_o^* = 0.31\ \mu\Omega \tag{6.36}$$

where μ is the shear modulus of the matrix and Ω is the volume per atom. Based on the behaviour of Fe–Ni–C alloys (Olson, 1984), G_{id}' is taken to be

$$G_{id}' = 1.22 \times 10^{-3}\mu \tag{6.37}$$

6.8.2.2 The Interface Mobility (Absolute Reaction Rate Theory)

An alternative, empirical model is sometimes used to represent the interface mobility as defined by the process of atom transfer across the interface, for the purposes of displacive transformations (Hillert, 1960; Agren, 1989). The model is based on chemical rate theory, one of the asumptions of which is that the 'reaction' consists of the repetition of unit steps involving the interaction of a small number of atoms. This approach seems justified for a solidification process, but as pointed out by Christian (1975), the assumptions of chemical rate theory are unlikely to be applicable to displacive transformations involving the coordinated movement of large numbers of atoms.

If the activation free energy (per mole) for the process of atom transfer is G^*, the theory can be used to show that (Christian, 1975):

$$V_i = \delta_b f^* \exp\{-G^*/RT\}\ [1 - \exp\{-G_{id}/RT\}] \tag{6.38}$$

where δ_b is the thickness of the interface, and f* is an attempt frequency for atomic jumps across the interface. For *small undercoolings* below the equilibrium transformation temperature, the equation simplifies to

$$V_i = M\ G_i \tag{6.39}$$

where M is a mobility, estimated by Hillert (1975a) for reconstructive transformations to be

$$M = 0.035 \exp\{-17700/T\}\ m^4 J^{-1} s^{-1} \tag{6.40}$$

There are obvious difficulties with the application of this model to displacive reactions: it represents the uncoordinated transfer of atoms across the interface. The relationship is applicable only at small undercoolings below the equilibrium transformation temperature but the equation is nonetheless extrapolated to low temperatures, and the parameters for the equation have not been fully justified for displacive transformations.

6.8.2.3 The Diffusion Field Velocity

The calculation of the diffusion field velocity requires amongst other things, a knowledge of the compositions of the phases at the transforma-

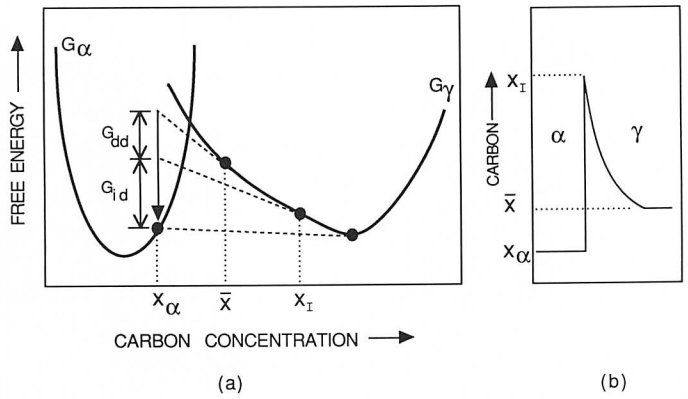

Fig. 6.20 *(a) Constant temperature free energy curves showing the quantities G_{dd} and G_{id} for the case where the interface compositions are as illustrated in (b). Note that the net free energy available for interfacial motion* after *allowing for strain energy and interface energy contributions is ΔG, which is the sum of the two dissipations G_{dd} and G_{id}.*

tion interface. The compositions are illustrated in Fig. 6.20, on a free energy diagram as a function of the amount G_{dd} of free energy dissipated in the diffusion of solute ahead of the interface. It is however, important to note that the concentrations x_α and x_I are not independent, and that the choice of either fixes the value of the other.

The Trivedi solution to the diffusion controlled growth of plates represented as parabolic cylinders has already been discussed. That solution is probably the most advanced method currently available; nevertheless, there are other approximations which are sometimes more convenient to use. One such method is due to Ivantsov (1947), in which the growth of a parabolic cylinder shaped particle is treated without the inclusion of interface mobility and capillarity effects. The velocity V_d for steady state growth of ferrite of constant composition x_α in a steel of composition $\bar{x}$, transformed at a temperature T, and as a function of the diffusion of carbon in the austenite ahead of the interface can be approximated by

$$(\bar{x} - x_I)/(x_\alpha - x_I) = (\pi p)^{0.5}\exp\{p\}\ \mathrm{erfc}\{p\}^{0.5}\} \qquad (6.41)$$

where x_I is the carbon concentration in the austenite at the interface, and p is the Pèclet number.

6.8.2.4 Solute Trapping Law

It has long been established that under suitable conditions, the transformation interface may move at a rate which is higher than would be consistent with the equilibrium partitioning of solute. The martensitic transformation in steels is a classic example of such non-equilibrium interfacial motion, since neither the interstitial nor substitutional atoms diffuse during the

nucleation and growth process. Similarly, paraequilibrium transformation in substitutionally alloyed steels, involves the redistribution of interstitial elements, but the substitutional atoms remain configurationally frozen. In both of these examples, some of the atoms are forced into the growing crystal as a consequence of a lack of atomic mobility; these noncompliant substitutional atoms experience an increase in their chemical potentials on transfer across the interface, and are said to be trapped (Baker and Cahn, 1969, 1971). When it is the solute atoms whose chemical potential increases on entering the growing phase, the phenomenon is called *solute trapping*, in contrast to *solvent trapping* where it is the host species whose chemical potential increases due to transformation. The trapping phenomenon is illustrated in Fig. 5.12, in the context of the equilibrium modes of transformation. Most of the driving force in diffusion controlled growth is dissipated in the diffusion of solute in the matrix ahead of the growing particle, and the compositions of the phases at the interface are given approximately by a tie line of the phase diagram. When interfacial processes become rate limiting, concentration gradients in the matrix phase are diminished, as illustrated in Fig. 5.12b, and the majority of the available driving force is then dissipated in the transfer of atoms across the boundary. Mixed control is illustrated in Fig. 5.12c; it is important to note that in none of these three cases can the transformation be classified as non-equilibrium and that both the phases are expected eventually to achieve their equilibrium volume fractions as given by the lever rule of the phase diagram. Solute trapping is illustrated in Fig. 5.12d, where the composition of the growing phase deviates from equilibrium.

Aziz (1982, 1983) has developed a model for solute trapping during rapid solidification processing. A transition from diffusion controlled to diffusionless solidification is predicted as the interface speed exceeds the maximum speed with which solute atoms can diffuse across the interface and are thus pinned down in the product phase. Consequently, when the growth velocity V exceeds the diffusion speed D/λ, where λ is an intersite jump distance and D is the solute diffusivity in the matrix phase, the solute atoms cannot keep up with the advancing interface and are engulfed into the product phase whether they like it or not. The model relates interfacial velocity to the partitioning coefficient k_p, which is the ratio of the solute concentration in the (homogeneous) product phase to the solute concentration in the parent phase at the interface. In the context of transformations in steels, the partitioning ratio is defined by the equation

$$k_p = x_\alpha / x_I, \tag{6.42}$$

and $k_p = k_e$ when the two concentration terms represent the respective equilibrium concentrations of the phases concerned; k_e is thus the equilibrium partitioning coefficient.

The model is based on chemical reaction rate theory, and as pointed out earlier, its assumptions are unlikely to be applicable to displacive transformations involving the coordinated motion of large numbers of atoms. Although the Aziz model is here being considered in the context of displacive transformations, it is the substitutional atoms which participate in such coordinated atomic displacements. The interstitial carbon is in most cases, sufficiently mobile to be treated as a species which is *diffusing* across the interface, i.e., the carbon atoms undergo an uncoordinated transfer across the boundary. Consequently, the Aziz model, which relies on diffusive fluxes across the interface, may be utilised as a solute trapping function for the redistribution of carbon during the displacive transformation of austenite.

There are two basic mechanisms of interface displacement, one involving propagation by the displacement of steps, and the other by the displacement of all elements of the boundary; this latter mechanism is called 'continuous' motion. Aziz (1982, 1983) has derived slightly different trapping models for the two cases. The step model only permits transformation below the T_o temperature, of the austenite in the vicinity of the interface, where it is thermodynamically possible to get composition invariant transformation in those regions. This is in general too restrictive, and inapplicable for transformations at temperatures above the T_o temperature, of the type being considered here. Goldman and Aziz (1987) have proposed another model for stepped growth, the 'aperiodic step model', in which the steps are assumed to pass at random intervals, and which also restricts transformation to below the T_o temperature of the parent phase at the interface. The interesting point is that for that case, the trapping law they found turns out to be the same as for the continuous growth model, the only one which is suitable for transformation above T_o. The trapping model then gives a velocity function of the form

$$V_k = (D\{x_I\}/\lambda)[(k_p - k_e)/(1 - k_p)] \tag{6.43}$$

where λ, the intersite jump distance is taken to be about 0.25 nm and $D\{x_I\}$ is the carbon diffusivity in austenite of composition x_I. The $D\{x_I\}/\lambda$ is the diffusion velocity of carbon, and trapping becomes significant as the actual interface velocity approaches this value. Note that the carbon atoms execute jumps across a glissile semi-coherent interface, so that it is appropriate in the present context to approximate the diffusion coefficient in the Aziz equation as the volume diffusivity calculated for the composition of the austenite at the interface.

This third velocity relation (equation 6.43) as obtained using solute trapping theory, is a smooth function of x_α and x_I. Note that as x_α approaches $\bar{x}$, the diffusion field velocity diverges (tends towards infinity) and the interfacial dissipation then imposes the condition that $x_I = \bar{x}$ such

that the trapping velocity V_k also tends towards infinity in the full trapping limit.

6.8.3 Calculated Data on Transformation with Partial Supersaturation

We now consider the results from the two main models for growth involving a partial supersaturation of carbon, that due to Olson *et al.* (1987, 1989, 1990) and, due to Hillert (1960, 1975a) and Agren (1989).

Olson *et al.* in their later work utilised three interface response functions, the diffusion field velocity (Ivantsov model, with a plate-tip radius fixed at 1.5 nm via strain energy considerations), the glissile-interface mobility function and the Aziz solute trapping function. It was consequently possible to solve uniquely for the interfacial velocity and phase compositions as a function of transformation temperature. Some of their results are presented in Fig. 6.21a, for a Fe–0.4C wt% alloy, illustrating how the predicted level of supersaturation varies with the transformation temperature for both the nucleation and growth processes. With a variety of assumptions about the strain energy of transformation and about the nucleation behaviour, the data can be favourably compared with published TTT diagrams for the Fe–0.4C wt% alloy, on the basis that martensitic transformation is diffusionless at all stages of transformation. Recent work by Malecki (1990) has extended the calculations to cover Fe–0.71C and Fe–1.2C wt% alloys, with results similar to those reported by Olson *et al.* Malecki did, however, report significant discrepancies between the

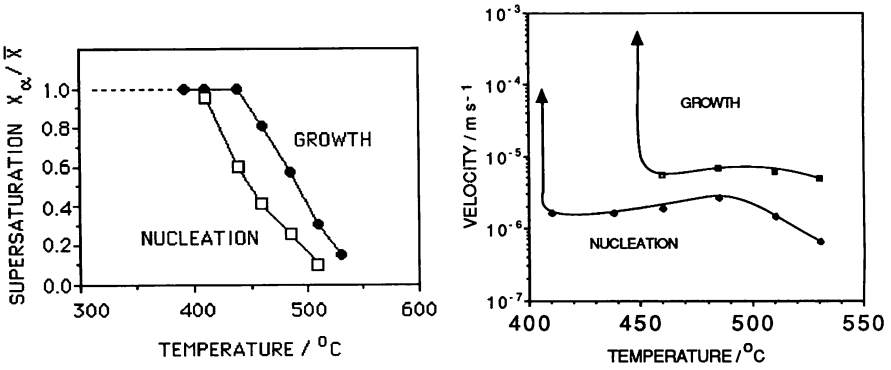

Fig. 6.21 *(a) Plot of calculated normalised supersaturation ($x_\alpha/\bar{x}$) of carbon in ferrite versus the isothermal transformation temperature, for a Fe–0.4C wt% alloy, with the data obtained by the simultaneous solution of the interfacial mobility, diffusion field velocity and trapping velocity functions. (b) The interfacial velocities during the 'nucleation' and growth processes.*

calculated and actual incubation times on TTT diagrams in the region where bainitic transformation accelerates in a narrow temperature range above the M_s temperature — i.e., the model is unable to predict the acceleration in bainite kinetics at temperatures just above M_s, as noted first in the work by Howard and Cohen (1948), and discussed in detail in the section on TTT diagrams.

The Olson *et al.* model is consistent with the notion that the nucleation process for martensite and bainite involves simply the growth of preexisting embryos, the activation energy for nucleation being related to the interfacial mobility, and the ('operational') nucleation event being identified by the point at which the embryo begins to grow rapidly. An interesting prediction which follows from the fact that the interface velocities during the 'nucleation' stage were found to be much smaller than during growth (Fig. 6.21b), is that the time during nucleation is much larger than during growth. The size distribution of bainite sub-units should therefore include a population of very fine platelets below the 'operational nucleus' size required for rapid growth to the final size. Fig. 5.10 shows a bainite sheaf in a partially transformed sample. In addition to the fully grown sub-units (few μm in length), there is another population of much smaller submicron particles which may well represent the suboperational embryos.

The model by Hillert and Agren is based on rather different considerations when compared with that of Olson *et al.*. The interface mobility function used relies on absolute reaction rate theory, which is not appropriate for glissile interfaces. The radius of curvature at the plate tip is treated as a free variable, so that the curvature which yields the maximum diffusion field velocity is taken to represent the actual diffusion field velocity. Stored energy terms arising primarily from the displacive mode of transformation are neglected. To solve for the three unknowns (austenite and ferrite compositions and the interfacial velocity), a solute drag function due to Hillert and Sundman (1976) is utilised in addition to the interface mobility and diffusion field velocity response functions. The model predicts that as the driving force is increased, there is a gradual transition from diffusion controlled to diffusionless growth, although the plate morphology is then lost because diffusionless growth occurs with the interface curvature becoming zero (i.e., a flat interface!).

6.8.4 Summary

Within their specific limitations, the models discussed above are both consistent with an increase in the amount of carbon trapped in the ferritic phase as the transformation temperature is reduced. In this sense they establish the possibility that the transition from bainite to martensite is a gradual one. Nonetheless, there remain numerous difficulties with the

concept of growth with partial supersaturation in the context of bainite in steels. The models all predict that the degree of supersaturation rises with undercooling; this is inconsistent with the fact that the bainite reaction stops when the carbon concentration of the residual austenite approaches the T_o curve. At first sight, the consequence of increasing supersaturation with undercooling would be to change the terminal carbon concentration of the austenite from the Ae_3'' down to T'_o at full supersaturation as the transformation temperature is reduced. On the other hand, for a given transformation temperature, one might expect the level of supersaturation to decrease as the transformation progresses (since the austenite becomes enriched in carbon). The terminal carbon concentration may then always be expected to be given by the Ae_3'', irrespective of transformation temperature.

A further difficulty is that at a given transformation temperature, it is predicted that for growth involving partial supersaturation, the terminal carbon concentration of the austenite cannot be less than a value x^{γ}_{m}, where x^{γ}_{m} is determined by the tangent to the austenite free energy curve, the tangent being chosen such that it intersects the ferrite free energy curve at the average alloy carbon concentration $\bar{x}$. This is again inconsistent with experimental measurements (Bhadeshia and Waugh, 1981, 1982).

It is pertinent to note that the models for growth involving partial supersaturation are not as yet fully developed. They do not for example take account of stored energy or plate aspect ratio variations as a function of temperature, nor do they predict the stifling of the growth of individual platelets of bainite.

If partial supersaturation is not possible, then some explanation is needed as to why there is an abrupt transition for paraequilibrium growth for Widmanstätten ferrite, and diffusionless growth for bainite. An abrupt transition may be expected if in addition to the requirement that diffusionless transformation is only permitted below T'_o, it is also necessary to consider the relative kinetics of interface motion and of the partitioning of carbon from the supersaturated ferrite behind the advancing interface, into the residual austenite. If the kinetics of the latter process are comparable to the rate at which the interface advances, then the diffusion fields of the two phenomenologically different processes must overlap, and growth should tend to reduce towards equilibrium partitioning. This is a distinct possibility at high temperatures (still below T'_o) because the decarburisation of ferrite is then very rapid. It is necessary to construct a model of plate growth which accounts for diffusion processes which begin immediately behind the transformation interface to consider this problem in detail. It provides for the moment, a possible explanation for a relatively abrupt transition from paraequilibrium growth of Widmanstätten ferrite to the diffusionless growth of bainite.

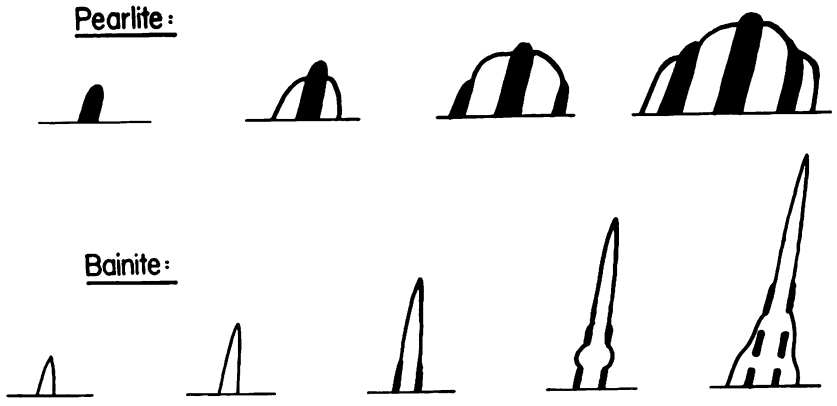

Fig. 6.22 *Hultgren's interpretation of the cooperative and noncooperative growth modes of pearlite and bainite respectively.*

6.9 Cooperative Growth of Ferrite and Cementite

During the eutectoid decomposition of austenite, pearlite colonies grow in such a way that the ferrite and cementite maintain a common transformation front with the parent phase. Their growth rates must therefore be equal and this is the meaning of the term 'cooperative growth'. In the days when pearlite was thought to involve the simultaneous and alternating precipitation of ferrite and cementite, Hultgren (1947) proposed that a difference between pearlite and bainite growth is that in the latter case the cementite and ferrite do not grow cooperatively (Fig. 6.22). While the details mechanisms illustrated in Fig. 6.22 are now known to be incorrect, the conclusion is still valid. It is widely recognised that the precipitation of cementite can lag behind that of ferrite during bainitic transformation.

Recent work has attempted to re-emphasise Hultgren's ideas, by adopting a very generalised definition of bainite as the product of a non-lamellar, non-cooperative mode of eutectoid decomposition. It is in addition assumed that both pearlite and bainite grow by reconstructive transformation in which the transformation interfaces move by a ledge mechanism (Lee *et al.*, 1988). It is claimed that the transition from pearlite to bainite can be correlated with the point where the cementite and ferrite can no longer grow at the same rate from austenite. Lee *et al.* developed a model for fixing the criteria controlling the transition from cooperative to non-cooperative transformation for the case where the pearlite/austenite interface is displaced by a ledge mechanism. In this theory, the two product phases cease to grow at the same rate when

$$h_\alpha/\lambda_\alpha \neq h_\theta/\lambda_\theta \tag{6.44}$$

where h and λ represent the height and interledge spacing respectively for the phase identified by the subscript. As long as this ratio is identical, the two phases can maintain a common growth front with the austenite, so that the transformation product would be pearlite. The ledges, which move in a direction parallel to the transformation front, would then be shared, i.e., the ledges have to be able to travel across the transformation front irrespective of the nature of the underlying product phase whether it be ferrite or cementite. In fact, cooperative growth fails when

$$(h_\alpha v_\alpha^s)/\lambda_\alpha \neq (h_\theta v_\theta^s)/\lambda_\theta \tag{6.45}$$

where v^s represents the step velocity for the phase concerned. It would seem intuitively that the ledge velocity must change when the ledge moves from the ferrite to the cementite phase, since the equilibrium compositions with the austenite must also change.

Whatever the details of the model for predicting the breakdown of cooperative growth, it is doubtful whether such a criterion can be used as an essential difference between bainite and pearlite. It ignores completely the nature of the transformation interfaces (glissile versus sessile) and indeed, the detailed mechanisms of transformation.

6.10 Overall Transformation Kinetics

6.10.1 Isothermal Transformation Kinetics

Most attempts at predicting the behaviour of steels require a way of calculating the degree of transformation as a function of time, temperature, composition and other variables. The necessary detailed information on the nucleation and growth kinetics of the phases involved is rarely available, so that the problem of obtaining a quantitative description of overall transformation kinetics is complex indeed. The subject has been reviewed thoroughly by Christian (1975), but to illustrate some of the difficulties involved, we present here a brief derivation of a particular rate equation, based on the classical work of Johnson, Mehl and Avrami.

For the isothermal, homogeneous, nucleation of a phase α from the parent phase γ, the volume v_τ of an individual particle of α nucleated at a time $t = \tau$ is given by some function f

$$v_\tau = f\{G_1, G_2, G_3, (t-\tau), \bar{x}\} \tag{6.46}$$

with $t = 0$ at the moment the specimen reaches the isothermal transformation temperature T. G_1, G_2 and G_3 are the growth rates of the particle along three mutually perpendicular directions. The growth rates are assumed to be independent of time. Particles nucleated at different positions are allowed notionally to grow through other particles in their path

and if nucleation continues in regions which have already transformed, then during a time period $d\tau$ the change in *extended* volume V_e^α is

$$dV_e^\alpha = v_\tau I_v (V^\alpha + V_\gamma)\, d\tau \tag{6.47}$$

where V^α and V^γ are the total volumes of the α and γ phases respectively, and I_v is the nucleation rate per unit volume of γ. The total extended volume as a function of time is therefore given by

$$V_e^\alpha = V \int_0^t f_1 I_v\, d\tau \tag{6.48}$$

where V is the total volume of the sample. Of course, the actual change in the volume of α is given by

$$dV^\alpha = v_\tau I_v V^\gamma\, d\tau \tag{6.49}$$

so that

$$dV^\alpha = dV_e^\alpha (1 - \xi) \tag{6.50}$$

or

$$dV_e^\alpha = -V\, 1n\{1 - \xi\} \tag{6.51}$$

where $\xi = (V^\alpha / V)$. It follows that

$$-1n\{1 - \xi\} = \int_0^t f_1 I_v\, d\tau \tag{6.52}$$

If it is now assumed that the growth is isotropic and that the nucleation rate is constant, than equation (6.52) can be integrated to give a relationship of the form:

$$\xi = 1 - \exp\{-k_A t^n\} \tag{6.53}$$

where k_A and n characterise the kinetics of the reaction as a function of time, temperature and other variables. Christian (1975) has shown that this exponential law (often called the *Johnson–Mehl–Avrami equation*) is valid for linear growth under most circumstances, and approximately valid for the early stages of diffusion controlled growth, even when nucleation is not homogeneous. Hence, a knowledge of n and k_A alone does not in general give very useful information about the mechanism of transformation. Clear interpretations of empirical fits to the equation are therefore difficult and usually ambiguous.

Nevertheless, if equation 6.35 is obeyed for whatever values of n and k_A (fortuitously or otherwise), it can provide an economic way of representing large quantities of data, and can at the very least, permit interpolation

between experimental results. There are, however, many instances where the constants in the equations are not found to be well-behaved. Radcliffe *et al.* studied overall transformation kinetics for the bainite reaction in an essentially plain carbon steel, and showed that the data were not consistent with the form of the Avrami equation. Small discrepancies were observed at small values of ξ with larger deviations occurring at larger values. The exponent n obtained exhibited considerable scatter, its value ranging from approximately 1.8–4.0. Similar results have recently been reported by Okamoto and Oka (1986) for the formation of lower bainite in high carbon steels. All this emphasises that an empirical application of equation 6.53 not only makes it difficult to draw any fundamental conclusions about the bainite reaction, but that the procedure is not very useful since the variations in the rate constants cannot be predicted.

A particular problem for most steels is that during kinetic experiments, it is impossible to avoid the simultaneous formation of bainitic ferrite and carbides, the rates of the two reactions being recorded simultaneously. The reactions have separate transformation mechanisms. There is as yet no model capable of rationalising their simultaneous effects on transformation behaviour. The activation energies derived by examining the variation of k_A (equation 6.53) as a function of temperature (e.g., White and Owen, 1961; Barford, 1966) are thus of doubtful significance. The experiments have nevertheless demonstrated that there is a clear change in the overall transformation kinetics when the upper bainite transformation gives way to the formation of lower bainite, indicating that carbide precipitation can have a significant influence on the progress of the bainite reaction.

Bhadeshia (1982b) has proposed a model for the overall transformation kinetics of upper bainite in steels where the precipitation of cementite from the residual austenite is retarded by the addition of alloying elements such as silicon. The model is consistent with the fact that the activation energy for the nucleation of bainite varies linearly with the driving force and allows the nucleation rate to vary as the transformation proceeds. The transformation is limited by the point where the carbon concentration of the enriched austenite makes the diffusionless growth of bainite thermodynamically impossible (i.e. the reaction stops at T_o'). The model is designed for the sub-unit mechanism of bainite growth, in which each sub-unit grows to a limited size before its growth is stifled, so that each sub-unit is responsible for the transformation of a fixed volume of austenite at any transformation temperature. The effect of alloy chemistry is reflected in the thermodynamic driving force for nucleation, and in determining the T_o' and other phase boundaries. An autocatalytic factor β allows each sub-unit to stimulate the formation of others; it is interesting that β is found to be smaller than that normally associated with martensitic transformations,

consistent with the fact that bursts of bainitic transformation do not occur. The model is complicated in form but is consistent with many of the real characteristics of the bainitic reaction, and is currently being developed for the intragranular nucleation of acicular ferrite.

6.10.2 Austenite Grain Size Effect

A case where the use of the Avrami equation has been used with limited success involves the formation of bainite in an alloy of nominal composition Fe–1C–1.4Cr wt% (Umemoto *et al.*, 1980). Significantly, isothermal transformation experiments were carried out at a temperature below 'B_F' where the reaction could transform all the austenite, in order to avoid the complications associated with the incomplete reaction phenomenon.[2] Dilatometry was used to follow the progress of the transformation via measurements of length changes, which presumably were assumed to be proportional to volume fraction changes. This is not valid when the maximum degree of isothermal transformation expected is less than 100%, but is likely to be a reasonable approximation given that the experiments were carried out below the practical B_F temperature (Takahashi and Bhadeshia, 1988). An analysis of the experimental data on the basis of the Avrami equation indicated a nearly constant time exponent ($n \approx 4.8$) with the temperature dependence of k_A being given by an empirical activation energy of $49\,\mathrm{kJ\,mol^{-1}}$.

Following a procedure used by Barford and Owen (1961), Umemoto *et al.* investigated the effect of austenite grain size (the mean lineal intercept $\bar{L}_3$) on the kinetics of the bainite transformation below B_F. This involves the use of different austenitising temperatures to alter the austenite grain size, following by cooling to a temperature of 1000°C for 15 min (i.e., a temperature within the austenite phase field) before quenching to the isothermal transformation temperature. The intermediate hold is designed to avoid any differences in quenching stresses that might develop between samples austenitised at different temperatures. In this way, the austenite grain size was varied between 80→600 μm. The rate of the bainite reaction was found to decrease with an increase in grain size, consistent with an increase in bainitic hardenability with grain size as reported first by Barford and Owen for different steels.

2 The bainite finish temperature does not really exist and in general has no fundamental significance. However, for steels in which carbide precipitation can occur at a rate consistent with the formation of bainitic ferrite, it is feasible for all of the austenite to transform fully to a mixture of bainitic ferrite and carbides. In these circumstances, it may be appropriate to identify a practical B_F temperature.

Umemoto *et al.* were able to rationalise the grain size results using an equation that they developed for the pearlite transformation (Umemoto *et al.*, 1980)

$$\xi = 1 - \exp\{-k_A t^n/(\bar{L}_3)^m\} \tag{6.54}$$

where m ideally takes on values of 1, 2 or 3 depending on whether grain surface, edge or corner nucleation dominates. The equation is based on the assumption that the nucleation rate can be written as

$$I_V = C_4(S_V)^m t^{C_5} \tag{6.55}$$

where C_4 and C_5 are constants, and S_V is the austenite grain boundary area per unit volume of the sample. The grain size $\bar{L}_3 = S_V^{-1}$, and raising it to the power $-m$ gives the number density of surface, edge and corner nucleation sites.

Analysis of kinetic data revealed that m tends to be less than unity (about 0.65) for bainite, a result attributed to a contribution to the overall rate from intragranular nucleation events. This is consistent with the observation that pearlitic transformation is much more sensitive to the austenite grain size with m>1.5 (Umemoto *et al.*, 1980). Given that bainite sheaves effectively propagate by the sub-unit mechanism, and that the vast majority of sub-units form away from the austenite grain surfaces, it is not surprising that the transformation should be less sensitive to the austenite grain structure, and indeed to elements such as boron which alter transformation kinetics bay a modification of the austenite grain boundary energy.

Not all studies of the influence of grain size on the transformation kinetics of bainite give a decrease in the reaction rate as the grain size increases. Graham and Axon (1959) found the opposite result for lower bainite in a Fe–0.97C wt% alloy, which when austenitised to take all the cementite into solution, gave an increase in the rate with grain size. The result was attributed to a lessening of physical constraint as the austenite grain size increased, a behaviour analogous to the increase in M_S temperature experienced as the γ-grain size of richly alloyed Fe–Ni–C steels is increased. These contradictory results might be explained if it is supposed that factors such as physical constraint of this type only become prominent when the driving force for transformation is small. The grain size effect needs further investigation over a wider range of chemical compositions.

6.10.3 Anisothermal Transformation Kinetics

Methods of using isothermal transformation data to predict the kinetic behaviour during continuous cooling experiments are of vital importance in industry, where most heat treatments are, for reasons for economy, anisothermal. In many cases, such as during the manufacture of large

quantities of steel plate, the heat treatment is an integral part of the thermomechanical processing as the ingot cools from elevated temperatures. The very large physical dimensions of many of them also make isothermal heat treatments impracticable.

A popular way of utilising isothermal transformation data in the design and assessment of anisothermal reactions is enshrined in the *additive reaction rule* proposed by Scheil (1935), which has been reviewed in detail by Christian (1975). The method is based on the assumption that the time required to reach a given stage ξ_a of reaction during continuous cooling is given by dividing the cooling process into a series of isothermal steps, and adding the contributions from each isothermal stage. The fractional contribution from each stage is calculated as the ratio of the actual time spent, at that temperature to the time required to reach the specified extent ξ_a at that temperature. When the sum of such contributions reaches unity, ξ_a of reaction is obtained by continuous cooling transformation

$$\int_{t=0}^{t} [dt/t_a\{T\}] = 1 \tag{6.56}$$

where $t_a\{T\}$ is the isothermal time to stage ξ_a, and t is the time to ξ_a for the non-isothermal reaction. The rule will only work if the reaction rate depends solely on ξ and T, and although this is very unlikely, there are many examples where the rule has been used empirically with success. Reactions for which the additivity rule is justified are called isokinetic (Avrami, 1939; Cahn, 1956) and imply that the fraction transformed at any temperature depends only on time and a single function of temperature. For example, since nucleation and growth rates are both dependent on temperature, a reaction can only be isokinetic if these two rates are proportional to each other as a function of temperature.

Umemoto *et al.* (1982) demonstrated that the additivity rule could in practice be used to predict the continuous cooling transfomation behaviour for the Fe–1C–1.4Cr wt% steel and concluded that this is a consequence of the sub-unit mechanism of bainite sheaf growth, in which the sub-units grow rapidly to a limited size. Presumably, this allows the kinetics of the transformation to be regarded as being nucleation limited, and if the nucleation rate is time independent, then there would be just one function of temperature in the equation of volume fraction of transformation as a function of time and temperature.

6.10.4 *Time–Temperature Transformation (TTT) diagrams*

Time–temperature transformation diagrams have served an incredibly useful purpose in representing the transformation characteristics of

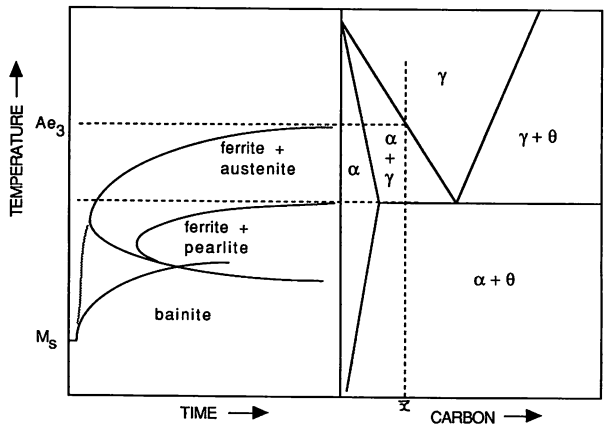

Fig. 6.23 *Schematic illustration of the relationship between a TTT diagram for a Fe–0.4C wt% steel and the Fe–C phase diagram. The TTT diagram for this particular steel is very difficult to measure experimentally due to the fast reaction kinetics. Measured diagrams for this alloy usually are unable to resolve the separate C curves.*

steels, and in revealing the role of alloying elements in influencing the microstructure of steels. The C curve characteristic associated with any reaction represented on such a diagram is usually attributed to the balancing contributions from the driving force and diffusion processes, whose combined effects determine the overall reaction kinetics. The driving force is small in the vicinity of the transformation start temperature and increases with undercooling whereas diffusion becomes increasingly sluggish as the temperature is reduced. The diagrams can to a limited extent be related to the phase diagram, since the latter gives the limiting temperatures for some of the transformations. Relationships like these are obviously not straightforward for multicomponent steels (Fig. 6.23). The phase diagram does not contain any information about transformations which deviate significantly from equilibrium, like bainite or martensite.

As has previously been discussed, the detailed interpretations of overall kinetics are very complicated and not fully understood. Nevertheless, for the decomposition of austenite, most diagrams can be divided into two C curves, the one at higher temperatures representing reconstructive transformation to ferrite or pearlite, and that at lower temperatures were atomic mobility is diminished, representing displacive reactions such as Widmanstätten ferrite and bainite. The martensite start temperature is generally represented as a horizontal line parallel to the time axis (Cohen, 1940).

There are two major effects of alloying additions on the transformation kinetics as reflected on TTT diagrams. Solute additions which decrease

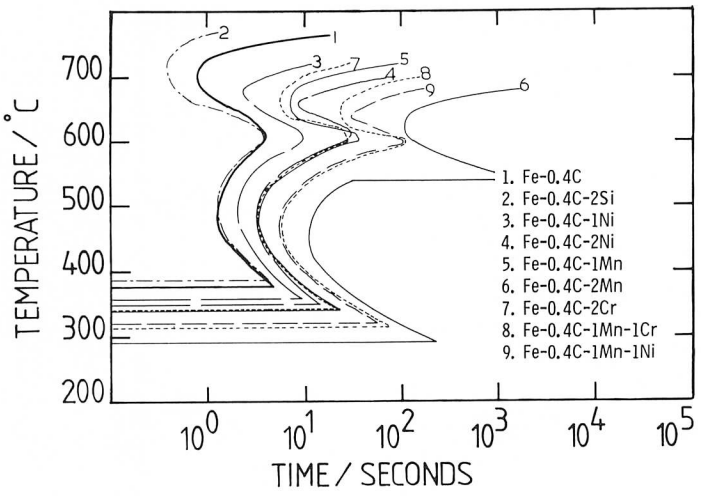

Fig. 6.24 *Calculated TTT diagrams showing the reaction initiation C curves for a series of steels.*

the driving force for the decomposition of austenite retard the rate of transformation, and cause both of the C curves to be displaced to longer times, and depress the martensite start temperature (Fig. 6.24). However, this retardation is always more pronounced in the case of the C curve for reconstructive reactions. This is presumably because in contrast to displacive reactions, *all* the atoms have to diffuse during reconstructive growth and this diffusional drag enhances the effect of solute additions on the upper C curve relative to the lower C curve.

It is sometimes argued that multiple substitutional solute additions lead to effects which are not found in ternary steels. This idea partly owes its origin to empirical models of hardenability, in which the critical cooling rate to obtain martensite is expressed as a function of alloying elements, and equations involving products of solute concentrations often give better correlations when compared with expressions which are linear in concentration. Other studies (Llopis, 1977) have revealed that the overall transformation kinetics of steels containing Cr or Ni were faster than of a steel containing both elements, but the mechanism of such interactions needs further investigation, especially since comparisons have not been made where the total alloy concentration has been kept constant.

As the austenite stabilising elements are reduced in concentration, transformation kinetics become more rapid and it is then experimentally very difficult to distinguish the two C curves as separate entities. For plain carbon and very low alloy steels, experimentally determined diagrams appear to consist of just a single C curve over the entire transformation

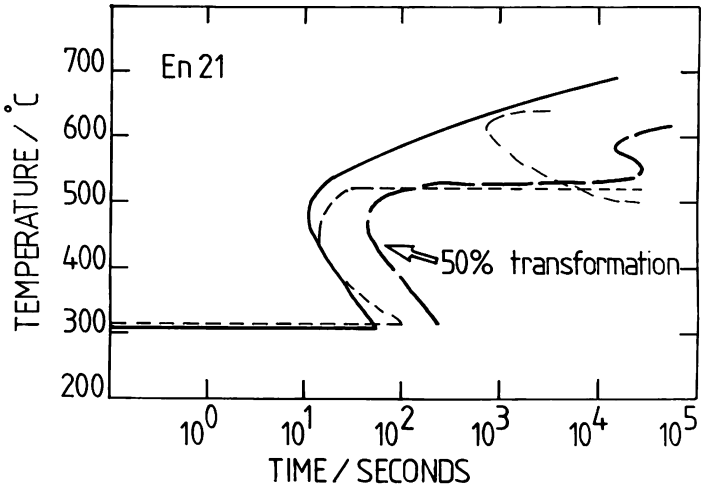

Fig. 6.25 *Time–Temperature Transformation diagram for Steel En21 (BISRA, 1956). The continuous line represents the beginning of transformation — the separation of its two constituent C curves becomes more distinct as the extent of reaction increases (50% transformation curve). The other dashed curve represents a calculated TTT diagram for the same steel, again representing the first detectable degree of reaction. It illustrates how the reconstructive and displacive reaction C curves can overlap to give the impression of a single overall C curve (Bhadeshia, 1982c). It is interesting that the bay at intermediate temperatures in the 50% transformation curve coincides with the intersection point of the two calculated C curves.*

temperature range. This is because the separate reconstructive and displacive reaction C curves overlap to such an extent that they cannot easily be distinguished using conventional experimental techniques (e.g., Hume-Rothery, 1966). Careful experiments have demonstrated that this interpretation is correct; Brown and Mack, (1973) and Kennon and Kaye (1982) have shown that in the TTT diagram for a Fe–0.8C–0.787Mn wt% steel, what is usually identified as a single C curve (ASM, 1977) really consists of two overlapping C curves, one due to pearlite and the other due to bainite formation. In some steels the extent of overlap of the reconstructive and displacive reaction C curves decreases as the volume fraction of transformation increases, because any solute partitioning during transformation has a larger influence on the reconstructive C curve (Fig. 6.25). When the two curves can be distinguished clearly, the lower C curve is found to exhibit a flat top (Zener, 1946) which can be identified with the Widmanstätten ferrite-start or bainite start temperature, whichever is the larger in magnitude (Bhadeshia, 1981a).

Within the two C curve general description of TTT diagrams, it is possible to identify finer features the details of which can be rather

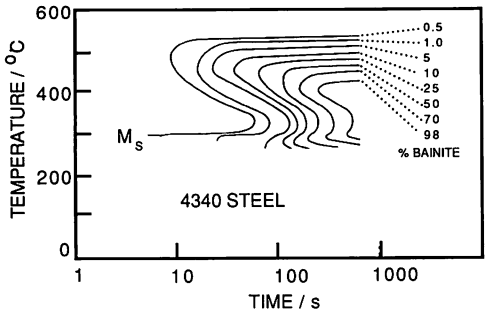

(a)

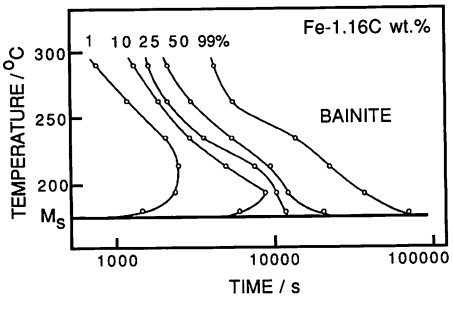

(b)

Fig. 6.26 *(a) TTT diagram for a Fe–0.39C–0.70Mn–1.7Ni–0.76Cr–0.2Mo–0.28Si–0.22Cu wt% alloy austenitised at 900°C for 15 min. Note the acceleration in the rate of transformation as the M_S temperature is approached (data from Babu* et al., *1976). (b) Similar data for a plain carbon steel (Howard and Cohen, 1948).*

complex. For example, it is known that where experimental conditions permit, the upper and lower bainite reactions each seem to exhibit their individual C curve characteristics (Schaaber, 1955; White and Owen, 1961; Barford, 1966; Kenon, 1978; Bhadeshia and Edmonds, 1979a). Recent work by Oka and Okamoto (1986, 1988) has confirmed earlier observations that in some alloys, there is an acceleration of overall rate of isothermal transformation just above the classical M_S temperature, due to the formation of isothermal martensite (Howard and Cohen, 1948; Schaaber, 1955; Radcliffe and Rollason, 1959; Smith *et al.*, 1959; Brown and Mack, 1973a, b; Babu *et al.*, 1976).[3] The martensite is found to be in the

3 Mutui *et al.* (1977) failed to detect any acceleration in the kinetics of bainitic transformation at temperatures just above the martensite start temperature in AISI 4340 steel, in contradiction to the work of Babu *et al.*. This may have something to do with the more bulky samples used in the former study, but the matter warrants further investigation.

form of very thin plates which can easily be distinguished from bainite. Although the overall rate of martensitic transformation appears isothermal, the individual plates are known to grow extremely rapidly, the isothermal character being largely attributable to the nucleation process (Smith *et al.*, 1959). The stress caused by bainitic transformation seem to trigger off the formation of isothermal martensite. The rate eventually decreases as the transformation temperature is reduced below the M_S temperature, giving the appearance of a C curve with the peak transformation rate located below M_S (Fig. 6.26).

6.10.5 Continuous Cooling Transformation (CCT) Diagrams

As emphasised earlier, steels are usually not isothermally heat treated in order to generate the required microstructure, the more common industrial practice involving continuous heating and cooling treatments. A mapping of the microstructures obtained during such heat treatments forms the continuous cooling transformation (or CCT) diagram (Fig. 6.27). Like TTT diagrams, CCT curves are constructed on temperature/time plots. The necessary data are acquired by monitoring transformation (e.g., using dilatometry) as the sample cools under controlled conditions. For a given steel and austenite grain structure, there should exist just one TTT diagram, but several different CCT diagrams are necessary to represent different kinds of cooling conditions. For example, the CCT diagram for a constant cooling rate from the austenitisation temperature is likely to be very different from one generated by testing samples cooled naturally. It follows that in order to fully specify a CCT diagram, it is necessary to plot the actual cooling curves on the CCT diagram (Fig. 6.27). The plotting

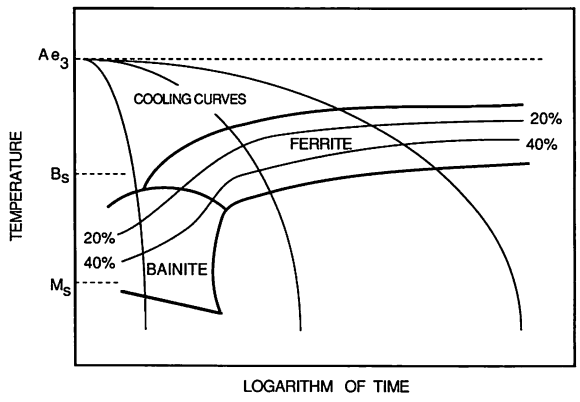

Fig. 6.27 *A schematic CCT diagram illustrating the cooling curves, constant volume percent contours and transformation temperatures.*

of the cooling curves must begin at the highest temperature where transformation becomes possible (i.e., the Ae_3 temperature). It is a common (though incorrect) practice to start the plots from the Ac_3 temperature. This leads to difficulties because the Ac_3 temperature is of course, a function of the heating rate and the ambient temperature microstructure. The popularity of this practice may be related to the difficulty in measuring the Ae_3 temperature, but the problem could be circumvented by approximating the Ae_3 temperature with a mean of the Ac_3 and Ar_3. From these discussions it is evident that a full description of a CCT diagram requires a specification of the steel composition, the austenitisation conditions (including the austenite grain size), the nature of the cooling conditions used in generating the continuous cooling transformation data, and the heating rate used in estimating the Ac_3 temperature. The diagrams are therefore specific to particular processes and lack the generality of TTT diagrams.

The CCT diagram is usually divided into microstructure domains as illustrated in Fig. 6.27, which shows the bainite and ferrite regions. Mixed microstructures are obtained when a domain boundary is intersected by a cooling curve. Like TTT diagrams, CCT plots also have constant volume

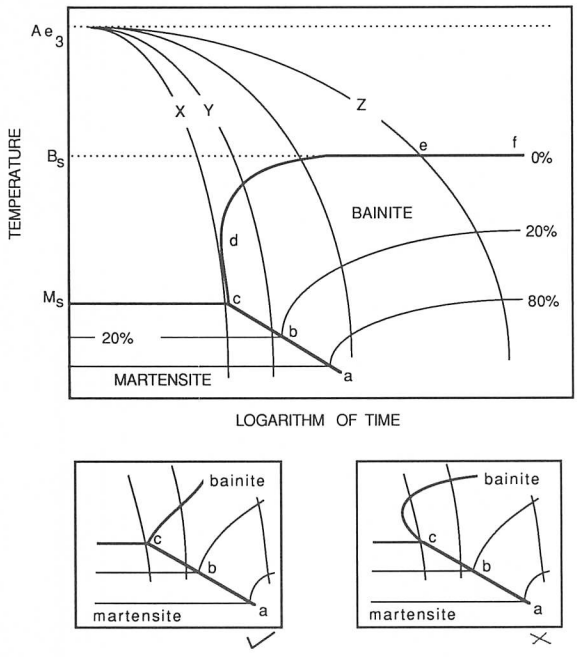

Fig. 6.28 *Schematic CCT diagrams illustrating the continuity of constant volume percent contours across microstructure domain boundaries, and the correct way in which the zero percent curves of different domains must meet at the point c.*

fraction contours, which must be continuous across the domain boundaries in order to ensure that there is no sudden change in volume fraction as the boundary is crossed (e.g., points *a*, *b* on Fig. 6.28). The constant volume fraction contours do not therefore refer to any particular product phase, but to the volume fraction of austenite which has transformed, either to a single microstructure or to a mixture of phases. The zero percent martensite and bainite curves must therefore meet in a specific way which does not allow a double intersection with the cooling curve (Fig. 6.28b, c). It is for this reason that the cooling curve *X* which leads to a fully martensitic microstructure, intersects the 0% transformation curve at just one point in Fig. 6.28, avoiding an intersection with the region marked cd. Cooling curve *Y* on the other hand, produces a mixed microstructure with less than 20% of bainite, the remainder of the austenite transforming to martensite during cooling. Note that the temperature at which martensitic transformation begins (as represented by the line *abc*) is progressively depressed with increasing prior transformation to bainite, since bainitic transformation in general leads to an enrichment of carbon in the residual austenite. Another notable feature is that the bainite curve asymptotically approaches the B_S temperature (along *ef*) as the cooling rate decreases.

The C curve which represents bainitic reaction on TTT diagram is now well established to exhibit a characteristic flat top. This can however, become confused in CCT diagrams, as illustated by numerous examples of published data (e.g., Kunitake, 1971; Schanck, 1969; Lundin *et al.*, 1982) and as shown schematically in Fig. 6.29. Any transformation occurring

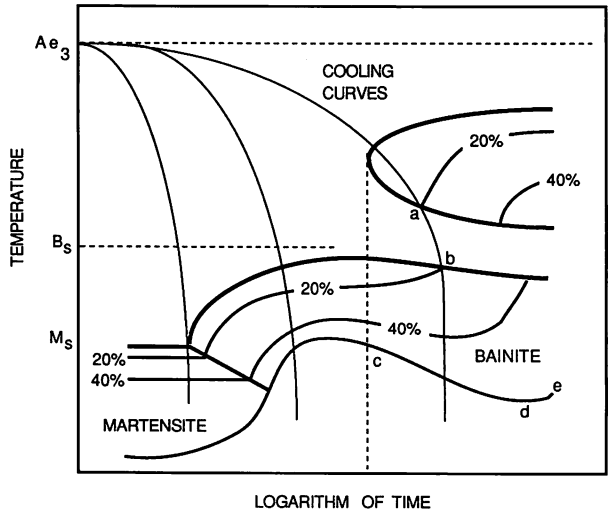

Fig. 6.29 *Schematic illustration of a TTT diagram in which the bainite region is strongly influenced by the initial formation of ferrite during continuous cooling transformation.*

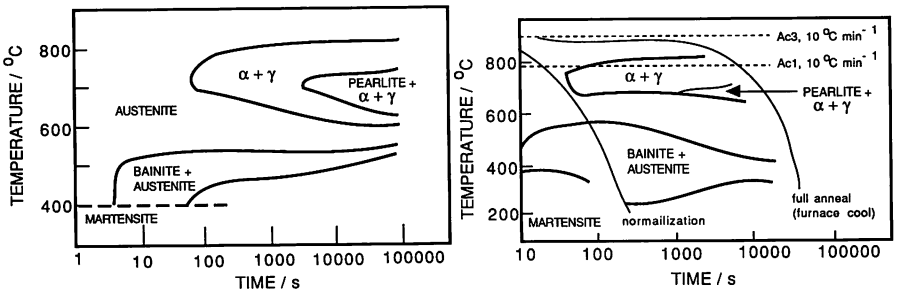

Fig. 6.30 *Corresponding TTT and CCT diagrams (Lundin* et al., *1982) for a 2.25Cr1Mo steel. The CCT diagram also illustrates the terminology sometimes used in describing air cooling from the austenitisation temperature (i.e., normalising) and furnace cooling (i.e., annealing).*

prior to bainitic reaction during cooling from the austente phase field, can change the chemistry and microstructure of the residual austenite and consequently alter the kinetics of any subsequent bainitic reaction. The main changes in the bainite region are reflected in the region beyond the vertical line *c* in Fig. 6.29. The temperature at which the bainite first forms is depressed by the fact that ferrite formation increases the carbon concentration of the residual austenite. Because the ferrite and bainite domains are separated by a significant time gap, the continuity of constant volume fraction contours is interrupted, but the contours must still be plotted so that their loose ends are connected by a cooling curve as illustrated by ab in Fig. 6.29. Finally, although the formation of bainite is retarded by the prior formation of allotriomorphic ferrite as the cooling rate decreases, the temperature range over which bainite forms is eventually reduced since very slow cooling rates give ample opportunity for transformation, as illustrated by the rising curve *de* in Fig. 6.29.

All of the features described above can be found in actual TTT and CCT diagrams, as illustrated by the experimentally measured diagrams for a classic '2.25Cr–1Mo' steel which is used widely in the bainitic condition for power plant applications (Fig. 6.30). This particular steel is discussed later in the chapter dealing with mechanical properties.

6.10.6 Boron, Sulphur and the Rare Earth Elements

We have already noted (Chapter 1) that the early commercial development of bainitic steels relied on the effect of boron on the transformation characteristics of low carbon steels. The boron retards the heterogeneous nucleation of allotriomorphic ferrite to a greater degree than that of

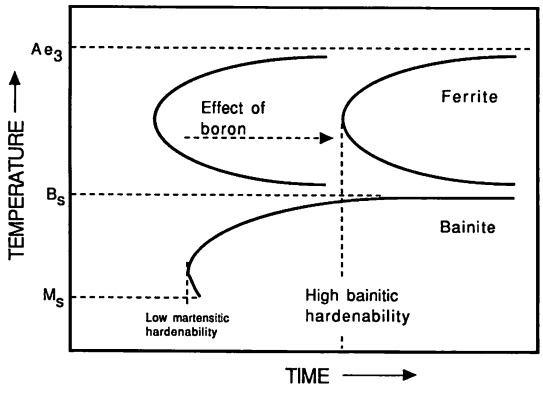

(a)

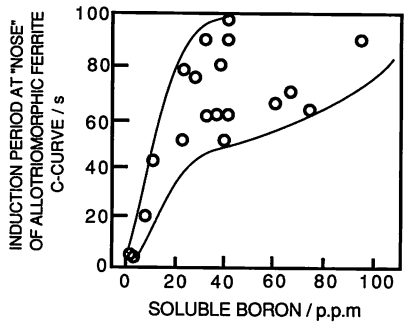

(b)

Fig. 6.31 *(a) The effect of boron and its analogues (the rare earth elements) on the TTT diagram, showing a pronounced effect on the allotriomorphic ferrite transformation but only a minor retardation of bainitic reaction. (b) Change in the incubation time for the allotriomorphic ferrite reaction as a function of the soluble boron concentration. (After Pickering, 1978).*

bainite (Fig. 6.31). This in turn permits boron containing steels to be cooled continuously, to fully bainitic microstructures. The use of elements such as manganese to achieve this purpose is not appropriate since they significantly improve the martensite hardenability, so that mixed microstructures of bainite and martensite are obtained.

Boron retards nucleation by segregating to austenite grain boundaries, thereby reducing their interface energy per unit area, and hence increasing the activation energy for heterogeneous nucleation. For typical commercial steels, a boron addition of $\approx$0.002 wt% is sufficient, although the exact amount must depend on the amount of austenite grain surface per unit volume. Too large an addition is detrimental because it leads to the formation of borides at the austenite grain boundaries and these are known to

enhance the nucleation of ferrite. The boron should be present in solution in the steel; it is not effective as an oxide or nitride. Hence, boron containing steels are usually deoxidised with aluminium. Titanium is sometimes added to tie up any nitrogen. Carbon also tends to segregate to austenite grain boundaries; in low carbon steels, niobium or titanium additions have the effect of tying up the carbon in the form of carbides, so that the boron is not displaced from the austenite grain boundaries (Tamehiro *et al.*, 1987a, b). In the absence of such high temperature carbide forming elements, the displaced boron tends to precipitate as $M_{23}(CB)_6$, thereby loosing its hardenability effect, and in fact making the situation worse since such precipitates tend to stimulate the nucleation of allotriomorphic ferrite.

The amount of effective boron in a steel is also influenced by the presence of non-metallic inclusions, a factor of importance in steel welds or in inoculated steels where such inclusions are added deliberately to induce the precipitation of desirable forms of bainite. For example, MnS and Al_2O_3 particles seem to act as heterogeneous nucleation sites for BN and $M_{23}C_6$ during fabrication (Saeki *et al.*, 1986). This in turn reduces the amount of free boron available for segregation to the ferrite nucleation sites (Dionne *et al.*, 1988).

An interesting study by Umemoto *et al.* (1986b) has revealed that quite small concentrations of sulphur ($\approx$ 0.005 wt%) can in some circumstances lead to an enhancement in the nucleation rate of bainite. It seems that when the austenitisation temperature is sufficiently low, the sulphur tends to precipitate at the austenite grain boundaries in the form of iron rich sulphides. These in turn appear to promote the nucleation of bainite.

There has been considerable recent interest in the addition of traces of the 'rare-earth' elements (cerium, neodymium, lanthanum and yttrium) to steels in order to enhance their hardenability (Jingsheng *et al.*, 1988). Attention has been focused on cerium additions of up to 0.134 wt%, where it is found that the transformation kinetics for allotriomorphic ferrite formation are retarded to a greater extent than for bainite formation. The mechanism is believed to be similar to that of boron, involving segregation to the austenite grain boundaries. The effect of cerium is reduced drastically if the phosphorous content exceeds $\approx$ 0.02 wt%, although the mechanism of this interaction is not yet established.

A further indirect role of elements such as yttrium arises from their ability to getter sulphur, especially if the presence of sulphides influences the nucleation frequency of ferrite (Abson, 1987).

6.11 Superhardenability

In steels which ordinarily have a reasonable degree of hardenability with respect to martensitic transformation, it has been established that the

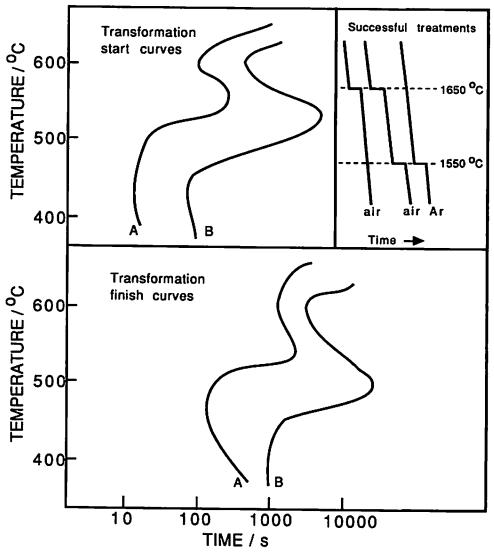

Fig. 6.32 *An illustration of the superhardenability effect (Mostert and van Rooyen, 1982). Curves A and B represent steels which were cast using melt temperatures of 1550 and 1650°C respectively. The steels have similar compositions but their aluminium concentrations ae 0.03 and 0.09 wt% respectively.*

hardenability can be enhanced significantly by superheating the melt to a temperature of about 1650°C during steelmaking, and by ensuring a relatively high concentration of aluminium of about 0.03–0.05wt% (Brown and James, 1980). The transformation C curves on the TTT diagram are shifted to longer times as a consequence of this heat treatment (Fig. 6.32), and an increase in hardenability is registered in Jominy tests. This phenomenon is dubbed the *superhardenability effect*.

The strength of the superhardenability effect increases with the baseline hardenability of the steel used, and with the aluminium concentration up to about 0.06 wt% before it saturates (Mostert and van Rooyen, 1982). Superhardenability is not influenced by prolonged holding at the austenitisation temperature, as is the case with hardenability increments produced using boron additions. Some of the samples used in the experiments were cast in air, the others being cast in argon, and tests were carried out for both superheated (1650°C) and conventional melts (1550°C), at varying concentrations of aluminium. The superheated melts were held at 1650°C for a few minutes and then cooled to 1500°C, where alloying additions were made before casting.

There is a speculative explanation of the effect, in which it is proposed that the superheat causes the breakdown of clusters of alloying atoms in

the liquid and this in turn influences hardenability (Sachs *et al*, 1980). This is however inconsistent with the fact that there is no effect of holding a superheated melt at a lower temperature before casting, since the latter treatment should allow any clustering to return. It also appears that superheating is not necessary when the melting is carried out under an inert atmosphere.

The superhardenability effect may have something to do with the presence of non-metallic inclusions such as manganese oxysulphides or titanium oxides in the steel. These have the ability to enhance the nucleation rate of ferrite, and therefore to reduce hardenability (Chapter 10). Aluminium is a sronger oxidising element than Mn, Si, or Ti. It forms alumina which is relatively ineffective as a heterogeneous nucleation site for ferrite. The preferential formation of alumina would therefore lead to an increase in hardenability. This hypothesis explains several features of the superhardenability effect

(i) The need to add aluminium.
(ii) The fact that a superheat is not needed when an inert gas cover is used during steelmaking. This would lead to a reduction in the oxygen concentration and hence the number density of oxides which are proposed to be nucleation sites.
(iii) An inclusion effect is not expected to fade during prolonged austenitisation, consistent with experimental data.
(iv) The inclusion effect would be expected to be most prominent in steels which have a reasonable hardenability, i.e., where any enhancement of nucleation kinetics would have a noticeable outcome.

The potentially potent influence of inclusions is well established in welding metallurgy (Chapter 10). Controlled experiments are now needed, in which the trace element concentrations (Al, Ti, O, N, S, B) are carefully monitored.

6.12 The Effect of Chemical Segregation

Most commercial steels have some degree of chemical heterogeneity in the finished product. Thermomechanical treatments of the kind commonly used in the manufacture of the steel are in general inconsistent with the achievement of thermodynamic equilibrium. The chemical segregation can have a profound effect on the development of microstructure, as manifested in the development of bands of transformation (Fig. 6.33). The bands are parallel to the chemical segregation, and arise because the microstructure begins to form from those regions where the segregation favours transformation. The 'banding' is caused by rolling deformation which flattens the solidification microstructure parallel to

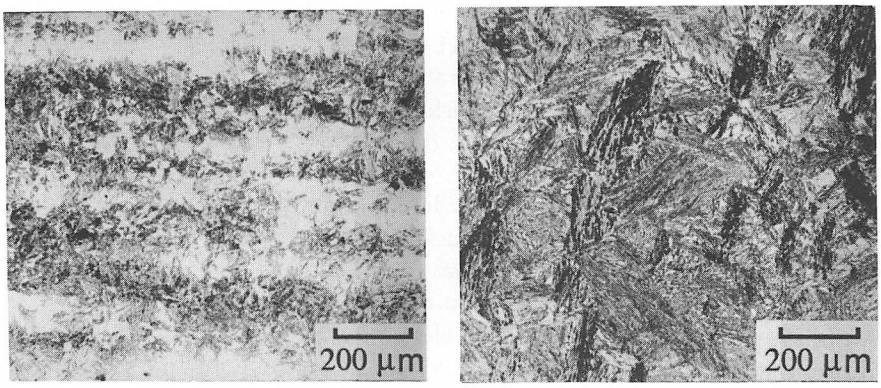

Fig. 6.33 *(a) Optical micrograph illustrating the banded microstructure obtained in a heterogeneous steel (300M) after isothermal transformation to bainite; (b) corresponding optical micrograph for the sample which was homogenised prior to isothermal transformation to bainite (Khan and Bhadeshia, 1990a).*

the rolling plane. In the discussion that follows, substitutional solutes which stabilise austenite are referred to as the X-elements.

Before reviewing the limited work on the role of segregation on transformation kinetics, it is worth noting that the scale of segregation is usually of the order of the spacing of secondary dendrite arms that grow during solidification. It typically repeats at distances of a few tens of micrometres. The peak segregation levels are usually within a factor of two of the mean concentrations in the alloy concerned. It is consequently not necessary to worry about coherency strains caused by composition induced lattice parameter variations; such strains are important in the theory of spinodal decomposition (or artificial multilayered structures) where the concentration gradients that develop tend to be much larger.

It is the segregation of the substitutional solutes which is the real cause of banding. Carbon diffuses very rapidly and should be homogeneously distributed in the austenite prior to transformation. There is a minor, second order effect in which the variations substitutional concentration lead to a corresponding non-uniform distribution of carbon as the carbon attempts to achieve equality of thermodynamic activity in the inhomogeneous austenite (Kirkaldy *et al.* 1962). The interesting point about banding is that while the carbon is homogeneously distributed in the austenite, the preferential growth of ferrite in the X-depleted regions leads to the gross partitioning of carbon into the X-enriched regions where the ferrite does not grow. The carbon enriched bands are therefore a consequence of solid state transformation and are only indirectly related to the solidification process which is the root cause of the segregation of substitutional elements.

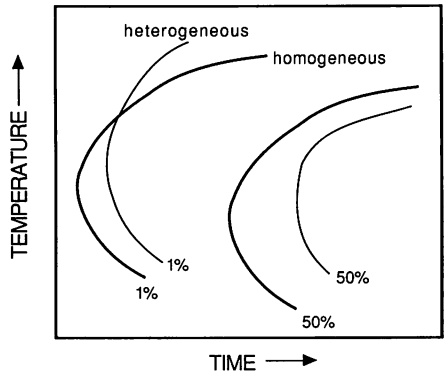

Fig. 6.34 *An illustration of the effect of chemical segregation on the bainite C curves of TTT diagrams.*

An early indication of the role of chemical segregation specifically on bainite reaction kinetics is due to Davenport (1939), who compared the isothermal transformation kinetics of steels containing banding with those which had been homogenised by prolonged annealing at high temperatures within the austenite phase field. Davenport believed that in heterogeneous steels, the initiation of transformation must occur in the regions which are relatively poor in austenite stabilising elements. The initial C curves of TTT diagrams for such steels should therefore be more representative of such X-depleted regions. On the other hand, the C curves representing larger amounts of reaction should reflect the local chemistry of the X-enriched regions. His experiments did not in fact confirm this hypothesis, because in many cases, the bainite reaction initiation C curve for the unhomogenised steel was found to be displaced to longer times when compared with the corresponding curve for homogenised steel.[4]

The essential features for bainite in heterogeneous steels are summarised in Fig. 6.34. It is evident that during the early stages of reaction, the bainite reaction is faster in the heterogeneous sample at high transformation temperatures, but not as the undercooling below the B_S temperature increases. For larger degrees of reaction, the transformation is always found to be slower in the heterogeneous samples. Experiments by Grange (1971) are consistent with these observations. The fact that the C curves of

4 Davenport's original diagrams (his Figures 30–32) did not state the bainite start temperatures, which were calculated by the present author in order to identify the C curves for bainite. The calculations used the method given by Bhadeshia (1988a); thus, the B_S temperatures were found to be 485, 497 and 479°C for steels S.A.E. 4640, 4140 and T–1335 respectively.

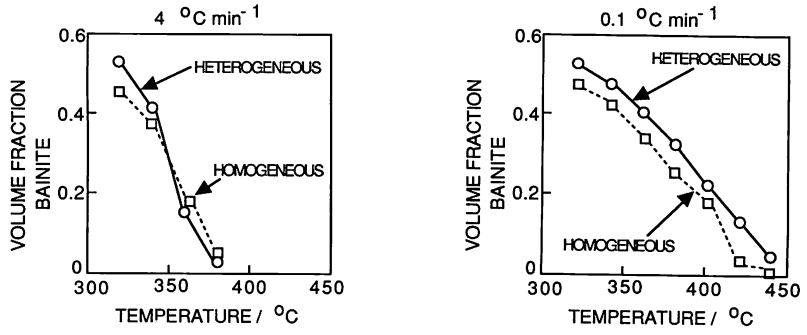

Fig. 6.35 *Experiments on homogenised and heterogeneous steel samples in which bainitic transformation was obtained by continuous cooling. (a) 4°C per min. (b) 0.1°C per min. The slower cooling conditions permit a more uniform distribution of carbon in the residual austenite, in which case the heterogeneous sample transforms to a greater extent relative to the homogenised sample, at all temperatures.*

the homogeneous and heterogeneous samples cross is difficult to understand on the intuitive reasoning that transformation should always be easier in the X-depleted regions of the heterogeneous steels.

The peculiar behaviour illustrated in Fig. 6.34 has been investigated theoretically and confirmed experimentally (Khan and Bhadeshia, 1990a). It can be explained as follows. At temperatures above the bainite start temperature of the homogeneous steel, the segregated sample will transform in the X-depleted regions. This thermodynamic advantage is maintained at small undercoolings, the heterogeneous steel continuing to transform relatively rapidly in the X-depleted regions.

At larger undercoolings, the homogeneous steel is able to transform faster because bainite can nucleate uniformly in all regions, whereas it forms preferentially in the X-depleted regions of the heterogeneous alloy. The carbon that is partitioned during bainite sheaf formation is to some extent localised around the bainite platelets. The X-depleted regions in the segregated sample therefore become enriched with carbon at a faster rate when compared with the homogeneous sample where the bainite is more uniformly disturbed. This causes a retardation of the transformation in the heterogeneous steel. The effect is only of importance at large undercoolings because the volume fraction of bainite that can form then becomes greater than the volume fraction of X-depleted regions. Khan and Bhadeshia demonstrated using very slow cooling experiments (Fig. 6.35) and computer modelling, that if an opportunity is provided for carbon to distribute evenly throughout the residual austenite during the development of the bainitic microstructure, the extent of transformation is always larger for the heterogeneous samples when compared with those which are homogenised.

To summarise, in most industrial circumstances involving continuous cooling transformation of austenite to bainite, reaction may begin at a higher temperature in segregated steels, but both the extent and rate of subsequent transformation should be larger in homogenised steels.

6.13 Martensitic Transformation in Partially Bainitic Steels

The microstructure obtained after the heat treatment of many commercial steels consists of a mixture of bainite and martensite. The bainite forms first and some of the austenite that remains may transform martensitically. It is therefore necessary to be able to estimate the kinetics of martensitic transformation of the carbon enriched residual austenite. Its transformation may also be influenced by the transformation strains and defects introduced by prior bainitic reaction. It cannot therefore be assumed that the theory describing the martensitic transformation of fully austenitic samples applies, although it could serve as a good starting point.

Any kinetic assessment of transformations which are thermodynamically of first order, must consider both the nucleation and growth phenomena. On the other hand, because martensite plates grow very rapidly, and to a size limited only by impingement, it may as a first approximation be assumed that the volume of material transformed by each plate or lath of martensite is a constant value $\overline{V}$. The growth part of the problem may then be neglected, since each nucleus will transform a constant volume $\overline{V}$ of the parent phase.

It has been known for some considerable time, that the progress of the athermal martensitic transformation in an austenitic sample, can be described empirically by an equation of the form

$$1 - f = \exp\{-C_1(M_S - T_Q)\} \tag{6.57}$$

where f is the volume fraction of martensite, T_Q is a temperature to which the sample is cooled below M_S and C_1 is a constant obtained originally by fitting to experimental data (Koistinen and Marburger, 1959).

Magee (1970) demonstrated that this relationship can be justified theroetically if it is assumed that the number of new plates of martensite that form per unit volume of austenite (i.e., dN) as the temperature is decreased below M_S is proportional to the accompanying change in the driving force $\Delta G^{\gamma\alpha}$ for diffusionless transformation

$$dN = -C_2 d(\Delta G^{\gamma\alpha}) \tag{6.58}$$

where C_2 is a proportionality constant. Note that $\Delta G^{\gamma\alpha}$ is given by $G^{\alpha'} - G^{\gamma}$, where $G^{\alpha'}$ and G_{γ} are the Gibbs free energies of unit volumes of

martensite and austenite respectively. The change in the volume fraction of martensite is therefore given by

$$df = \overline{V}\, dN_V \tag{6.59}$$

where dN_V is the change in the number of new plates of martensite formed per unit volume of sample, given by $dN_V = (1-f)dN$. On combining these equations, and substituting $[d(\Delta G^{\gamma\alpha})/(dT)]dT$ for $d(\Delta G^{\gamma\alpha})$, Magee showed that

$$df = -\overline{V}(1-f)\, C_2[d(\Delta G^{\gamma\alpha})/dT]dT \tag{6.60}$$

which on integration between the limits M_S and T_Q gives

$$1n\{1-f\} = \overline{V}C_2[d(\Delta G^{\gamma\alpha})/dT]\,(M_S - T_Q)$$

or

$$1 - f = \exp\{\overline{V}C_2[d(\Delta G^{\gamma\alpha})/dT]\,(M_S - T_Q)\}. \tag{6.61}$$

The integration procedure used above assumes that the term $[d(\Delta G^{\gamma\alpha})/dT]$ is constant with temperature. The form of this equation is similar to that of the empirical relation used by Koistinen and Marburger, so that

$$C_1 = -\overline{V}C_2[d(\Delta G^{\gamma\alpha})/dT]. \tag{6.62}$$

The assumption that C_1 is approximately constant is reasonable given the narrow temperature range over which martensitic transformation occurs. C_1 is usually derived by fitting to experimental data and typically has a value of about 0.004. The Koistinen and Marburger equation turns out to be a reasonable representation of the kinetics of martensitic reaction in partially bainitic steels, after generalising the definition of f to be the ratio of volume fractions of martensite and the austenite prior to any martensitic transformation (Khan and Bhadeshia, 1990b). However, as pointed out by Magee, difficulties might arise because the equation dors not account for autocatalysis.

6.13.1 *Autocatalysis*

Detailed analysis reveals that the initial number density of the defects responsible for the nucleation of martensite is not large enough to explain the kinetics of martensitic transformation (Shih *et al.*, 1955; Pati and Cohen, 1951; Olson and Cohen, 1981). The extra defects necessary to account for the faster than expected transformation rates are attributed to autocatalysis: when plates of martensite form, they induce new embryos which are then available for further transformation. It has been proposed that the number of autocatalytic sites generated per unit volume at

different temperatures can be calculated by integrating the following equation (Lin, 1987)

$$dN = dN_i + d(f'p) \tag{6.63}$$

where N_i is the number of original nucleation sites per unit volume of sample, which remain after the formation of some martensite, and is given (Magee, 1970) by

$$N_i = (1-f')N_i^0 p \tag{6.64}$$

where N_i^0 is the number of original nucleation sites per unit volume of austenite. The term p represents the number of autocatalytic sites generated per unit volume of sample. It is assumed that this autocatalytic factor is related linearly to the volume fraction of martensite and hence to f'

$$p = C_3 + C_4 f' \tag{6.65}$$

then it follows that

$$dN = (-N_i^0 + C_3 + 2C_4 f')df'. \tag{6.66}$$

Since $\overline{V}$ is assumed to be constant, $df'/\overline{V} = (1-f')dN$ so that

$$\int_0^f df'/[\overline{V}(1-f')] = \int_0^f (-N_i^0 + C_3 + 2C_4 f')df'. \tag{6.67}$$

Integration gives

$$p = N_i^0 - \ln\{1-f\}/(f\,\overline{V}). \tag{6.68}$$

It is found experimentally that

$$p - N_i^0 = C_5 + C_6(M_S - T_Q) \tag{6.69}$$

where C_5 and C_6 are constants defining the best fit line between the variables. On setting $M_S - T_Q = 0$, it can be demonstrated that $C_5 = 1/\overline{V}$. It follows that

$$-(\ln\{1-f\})/f = 1 + \overline{V}C_6(M_S - T_Q) \tag{6.70}$$

or

$$-(\ln\{1-f\})f = 1 + C_7(M_S - T_Q) \tag{6.71}$$

where $C_7 = \overline{V}C_6$. This equation represents an alternative kinetic model for the development of martensitic transformation as a function of undercooling below the M_S temperature. It has been used to rationalise martensite transformation kinetics in both directly quenched (fully austenitic)

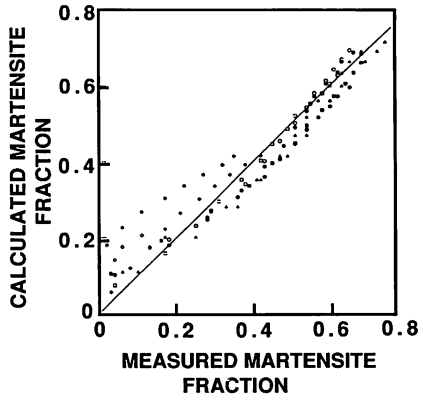

Fig. 6.36 *Comparison of experimental results with those calculated by fitting equation (6.71) to the experimental data.*

samples as well as those partially transformed to ainite and then quenched to ambient temperature.

Given that the data could all be explained using the same equation, it can probably be concluded that the defects generated by bainitic transformation do not contribute significantly to the autocatalytic nucleation of martensite. Although a reasonable fit has been demonstrated between experimental data and the theory (Fig. 6.36), there are some difficulties and assumptions which require justification. The model tends to overestimate the fraction transformed when the amount of martensite is small. That may be due to the assumption of a constant value of $\overline{V}$ at all stages of transformation. More work is needed to deduce $\overline{V}$ for martensitic transformation in low alloy steels. It is also assumed that all nucleation sites have the same activation energy. Magee (1971) demonstrated that there is in fact a distribution of effectiveness of nucleation sites.

6.14 Summary

Both the individual platelets (sub-units) and the sheaves of bainite lengthen at rates much faster than expected from the theory of carbon diffusion controlled paraequilibrium transformation. It must therefore be concluded that they grow with a supersaturation of carbon, the ferrite probably inheriting the composition of the parent austenite. Any excess carbon in the ferrite is, in a matter of seconds, able to partition into the residual austenite or precipitate as carbides.

There is little doubt of the possibility of growth involving a partial supersaturation of carbon in ferrite. The experimental evidence in

support of this idea is, however, lacking and the necessary theory is in some important respects incomplete.

It appears that carbon must partition during the nucleation of bainite. The nucleation probably occurs by a displacive mechanism akin to martensite, but the initial nucleation sites are confined largely to the austenite grain surfaces, and the role of autocatalysis is not as prominent for bainite as it is for martensite. The activation energy for nucleation varies linearly with the driving force (within the limits of experimental error). This relationship is inconsistent with classical theory based on heterophase fluctuations, but it readily explained by a pre-existing embryo model in which the nucleation event is identified with the onset of unstable growth. The activation energy detected experimentally would therefore represent the interfacial mobility in that interpretation.

The least developed (and most urgently required) kinetic theory for bainite is that dealing with overall transformation behaviour. It is currently impossible to make accurate predictions of alloying element and temperature effects. A qualitative result is that bainitic transformation is less sensitive to the austenite grain size when compared with bainite. This may be a consequence of the fact that sheaf growth involves mostly the formation of sub-units at sites away from the austenite grain surfaces.

Except at temperatures close to B_S, homogeneous steels transform more rapidly than those containing chemical segregation. The martensitic decomposition of austenite left untransformed after the growth of bainite can, within experimental error, be described adequately by the theory for the martensitic decomposition of fully austenitic samples.

7 *The Transition from Upper to Lower Bainite*

Although there have been many attempts to generalise the definition of bainite, the most appropriate description remains that the microstructure consists of a non-lamellar mixture of ferrite and carbides, which can be classified further into upper and lower bainite. This latter distinction is valuable both from the point of view of phase transformation theory, and because the mechanical properties of upper and lower bainite are quite different. The two microstructures can also be clearly distinguished, controlled and exploited to suit specific applications.

Lower bainite is usually obtained by transformation at relatively low temperatures, although both phases can sometimes be found in the same microstructure. Both upper and lower bainite tend to form as aggregates (sheaves) of small platelets or laths (sub-units) of ferrite. The essential difference between upper and lower bainite is with respect to the carbide precipitates. In upper bainite, the bainitic ferrite is free of precipitation, any carbides growing from the regions of carbon enriched residual austenite which are trapped between the sub-units of ferrite. By contrast, lower bainitic ferrite contains a fine dispersion of plate-like carbides (e.g., ε-carbide or cementite) within the bainitic ferrite plates.

7.1 The Matas and Hehemann Model

The transition between upper and lower bainite is generally believed to occur over a narrow range of temperatures. As already emphasised, there are circumstances where both 'phases' can grow simultaneously during isothermal transformation near the transition temperature (Pickering, 1967). The first clear indication of the mechanism of the transition emerged from the work of Matas and Hehemann (1961), whose experiments on several steels (containing 0.38–1.0 wt% C) indicated a narrow transition temperature range centred around 350°C, irrespective of steel

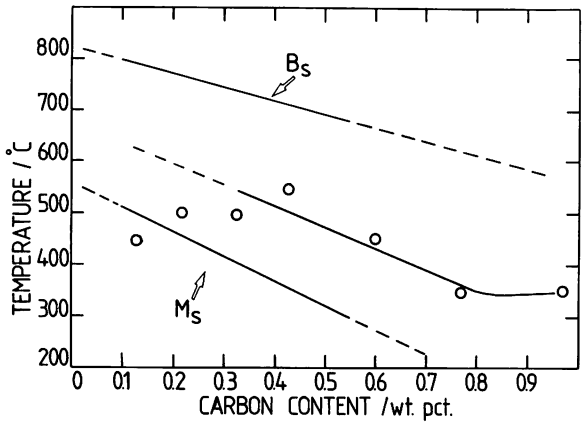

Fig. 7.1 *The lower bainite start temperature relative to the bainite and martensite start temperatures. (After Bhadeshia, 1980a; data due to Pickering, 1967).*

composition. Upper and lower bainite were distinguished by the degree of carbon enrichment in the retained austenite, which was found to be less for lower bainite. The difference between upper and lower bainite was suggested to be related to the competing kinetics of carbide precipitation in ferrite and carbon diffusion from ferrite. In their model, both upper and lower bainite were assumed to form with a supersaturation of carbon, but with the former, almost all of the excess carbon is rejected into the residual austenite; with lower bainite, carbon precipitates rapidly in the supersaturated ferrite, so that the amount that diffuses into the residual austenite is reduced. The apparently constant transition temperature was explained by suggesting that ε-carbide will, for some reason, not precipitate from ferrie at temperatures above about 350°C. The ε-carbide was envisaged as a precursor to the formation of cementite.

While the Matas and Hehemann model is intuitively reasonable, their belief that the transition temperature, L_s, is constant for all steels is not consistent with other experimental results (Pickering, 1967; Matsuda, 1970; Llopis, 1977; Bhadeshia, 1980a; Oka and Okamoto, 1986). The transition temperature can in fact be as high as 500°C and is found to vary with the carbon concentration (Fig. 7.1). The model also requires the initial carbide phase in lower bainite to be ε-carbide, which might then convert to cementite on further tempering. Later work has shown that it is possible to obtain lower bainite containing the appropriate cementite particles, without any ε-carbide as a precursor (Bhadeshia and Edmonds, 1979a). Others have reported lower bainite containing η-carbide (Fe_2C) in a high silicon cast iron, and there is no reason to suppose that precipitation temperature and behaviour of η-carbide should be similar to that of

ε-carbide (Franetovic *et al.* 1987a, b). It is also difficult to explain (as the model requires) why ε-carbide should not precipitate from ferrite at temperatures above 350°C.

Pickering (1967) found that L_S rises initially and then decreases to about 350°C, becoming independent of the carbon concentration beyond about 0.8 wt%C. His explanation of the transition is essentially the same as that of Matas and Hehemann (1961), that the transition to lower bainite occurs when the rate of carbon diffusion from ferrite is slow, so that the carbides have an opportunity to precipitate. This is consistent with the initial rise in transition temperature with carbon concentration, since as the transformation temperature drops due to a reduction in driving force, so does the diffusivity of carbon. The model does not, however, account for any changes in the kinetics of carbide precipitation as a function of carbon concentration. Similar results have been obtained for more heavily alloyed steels, where the peak in the experimental transition curve is found to shift to lower carbon concentrations (Llopis, 1977). Pickering suggested that for high carbon steels (where the transition was claimed to be insensitive to carbon concentration), the cementite precipitates directly from the austenite, as its carbon concentration x_γ exceeds the concentration $x^{\gamma\theta}$ which is given by the extrapolated γ / (γ + Fe_3C) phase boundary; this does not however explain the formation of carbides within the bainitic ferrite.

To summarise, a plausible model for the transition from upper to lower bainite could be constructed from the assumption that there is no fundamental difference in transformation mechanism between these two forms of bainite, if the bainitic ferrite is when it forms, supersaturated with carbon. The excess carbon may eventually partition into the residual austenite or precipitate from the ferrite in the form of carbides. If the latter process is dominant, then lower bainite is obtained. Upper bainite is obtained only when the carbon partitions relatively rapidly into the residual austenite, before the carbides have an opportunity of precipitate (Fig. 7.2). This essentially amounts to the Matas and Hehemann model, but without the constraint that the transition temperature is limited to a narrow temperature range around 350°C.

The model also implies that upper bainite should cease to form at carbon concentrations which are large enough; this is indeed found to be the case in a Fe–7.9Cr–1.1C wt% alloy which has a B_S temperature of 300°C (Srinivasan and Wayman, 1968a), and in a Fe–4.08Cr–0.3C wt% alloy which has a B_S temperature of 490°C. Ohmori and Honeycombe (1971) have shown that in a series of high purity Fe–0.16–0.81C wt% alloys, lower bainite is not obtained when the carbon concentration is less than about 0.4 wt%. A thorough piece of work by Oka and Okamoto (1986) on high purity, high carbon Fe–0.85–1.8C wt% steels has shown the

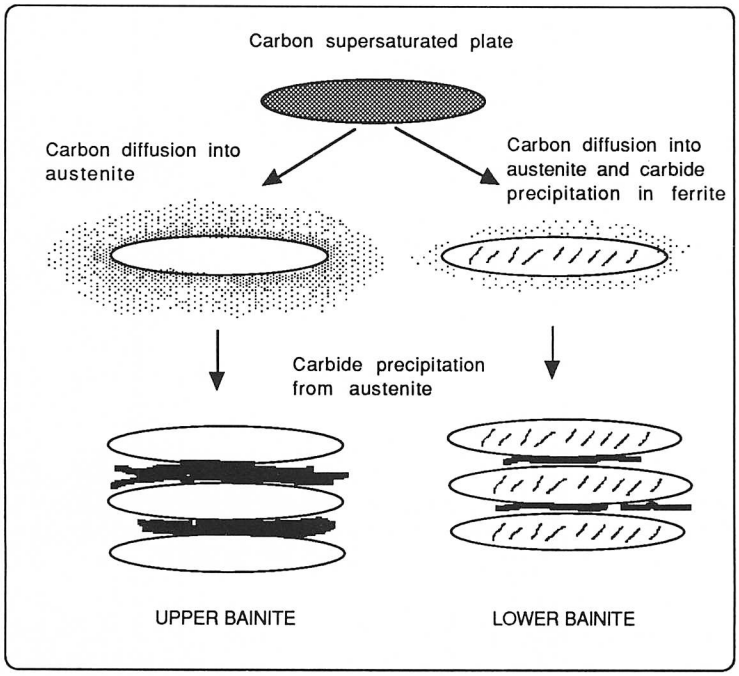

Fig. 7.2 *Schematic representation of the transition from upper to lower bainite.*

absence of upper bainite in all cases. The formation of pearlite was in each case found to give way directly to that of lower bainite.

The model illustrated in Fig. 7.2 has recently been formulated in quantitative terms, by comparing the time required to decarburise supersaturated ferrite against cementite precipitation kinetics (Takahashi and Bhadeshia, 1990). These aspects are discussed below, but further work is needed before these ideas can be developed for alloy steels.

7.2 Quantitative Model

7.2.1 Time to Decarburise Supersaturated Ferrite

The detailed theory for the partitioning of carbon from an initially supersaturated plate of ferrite has been presented earlier. If it is assumed that the diffusivity of carbon in ferrite is very large when compared with that in austenite, and that local paraequilibrium is established during the partitioning of carbon between the austenite and ferrite, then the time t_d required to decarburise a supersaturated bainitic ferrite plate of a specified thickness can be calculated (equation 5.28), and some results for

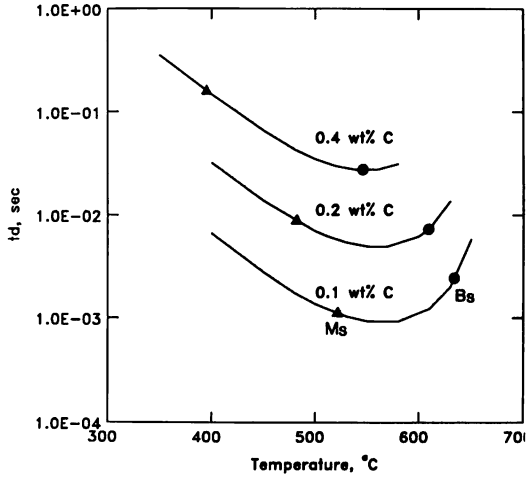

Fig. 7.3 *Calculated time for the decarburisation of supersaturated ferrite plates (of thickness 0.2 μm) in plain carbon steels with 0.1, 0.2 and 0.4 wt% carbon respectively. The calculated martensite start and bainite start temperatures are also indicated.*

plain carbon steels are presented in Fig. 7.3. For each of the steels considered, the time t_d is found to go through a minimum as a function of the transformation temperature. This is because the diffusion coefficient of carbon decreases with temperature (leading to an increase in t_d), while at the same time, the amount of carbon that the austenite can tolerate, rises with falling temperature. The decarburisation time also increases as the average carbon concentration of the steel rises. Given that an increase in carbon concentration should accelerate the precipitation of carbides in the ferrite, the combination of these two effects should lead to an increase in L_S, as reported by Pickering (1967) and Llopis and Parker (1977) for low carbon concentrations.

7.2.2 *Kinetics of Cementite Precipitation*

It is not yet possible to estimate the rate of cementite precipitation from supersaturated ferrite as a function of time, temperature and chemical composition. However, for plain carbon steels, and in some cases for alloy steels, martensite tempering data can be adapted to derive reasonable functions for the purpose of predicting the transition from upper to lower bainite (Takahashi and Bhadeshia, 1990).

When martensite contains an excess concentration of carbon in solid solution, the carbon will tend to precipitate in the form of carbides during tempering. Prolonged annealing can also lead to recovery, recrystallisation and the coarsening of cementite precipitates. Hence to derive a

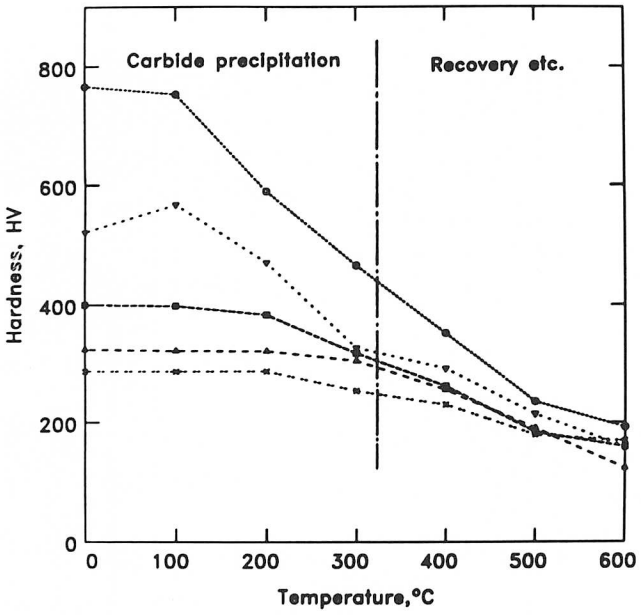

Fig. 7.4 *Hardness curves for iron–carbon martensite samples which were tempered for 1 hour at the temperatures indicated (data due to Speich, 1969). The data to the left of the vertical line largely represent changes due to the precipitation of carbides, rather than recovery or coarsening processes.*

function representing precipitation alone, it is necessary to focus on the early stages tempering.

Speich (1969) reported that the change in hardness of martensite in plain carbon steels after an hour of tempering at temperatures above 320°C, includes significant contributions from recovery, recrystallisation and coarsening of cementite particles (Fig. 7.4). Hence, the data representing hardness changes during tempering below 320°C can be used to derive a function which expresses the change in the volume fraction of cementite precipitation as a function of time and temperature. An Avrami type equation for overall transformation kinetics can then be used to represent the tempering reaction

$$\xi\{t\} = 1 - \exp\{-k_A t^n\} \tag{7.1}$$

where $\xi\{t\}$ is the volume fraction of cementite normalised by its equilibrium volume fraction at the reaction temperature, t is the time, and k_A and n are rate constants determined from the experimental data. Since it is assumed that $\xi\{t\}$ is related at any time to the hardness of the martensite, $H\{t\}$ it follows that

$$\xi\{t\} = (H_0 - H\{t\})/(H_0 - H_F) \tag{7.2}$$

H_0 is the hardness of the as-quenched virgin martensite, H_F is its hardness when all the carbon has precipitated, but before any significant recovery, recrystallisation or coarsening has occurred. Implicit in this relation is the assumption that the amount of carbon precipitated is linearly related to the change in hardness during the early stages of tempering.

Using the values of hardness for plain carbon martensite tempered for 1 h at 320°C, reported by Speich, H_F can be expressed empirically as a function of the initial hardness and average carbon concentration $\bar{x}$ (mole fraction), as follows

$$H_F = H_0\,[1 - 1.731\,(\bar{x})^{0.34}] \tag{7.3}$$

This equation is valid for plain carbon steels containing less than 0.4 wt% carbon, the value of H_F becoming constant thereafter. The hardness H_0 of plain carbon martensite before tempering can also be deduced from the data reported by Speich

$$H_0 = 1267(\bar{x})^{0.9} + 240 \tag{7.4}$$

where the hardness of martensite in pure iron is 240 HV (Leslie, 1982). This equation reflects empirically, the hardness of virgin martensite in plain carbon steels as a function of the carbon in solid solution; there is however, evidence to suggest that the effect of carbon tends eventually to saturate, so that H_0 should not exceed a maximum value of about 800 HV irrespective of the carbon concentration (Bhadeshia and Edmonds, 1983a, b). Consequently, the maximum value of H_0 should not in such calculations exceed 800 HV. Having established all the data necessary to estimate the amount of cementite precipitated, it remains to evaluate the terms k_A and n of the Avrami equation in order to calculate the time t_θ for the formation of a specified fraction of cementite as a function of time, temperature and carbon concentration. This can easily be done by empirically fitting the Avrami equation to experimental data on the tempering of martensite.

There are more elaborate theories available for the change in the strength of low carbon martensite due to the precipitation of cementite, so that the difference $(H_0 - H_F)$ can be evaluated independently of the empirical approach discussed above. The change can be expressed in terms of the decrease in solid solution strengthening as carbon is absorbed during the growth of cementite, and a lesser increase in strength as the cementite particles precipitation harden the martensite. Thus, the yield strength of martensite, σ_y, is expressed as a combination of the intrinsic yield strength, the effect of the dislocation cell structure, and precipitation hardening by cementite (Daigne *et al.*, 1982)

$$\sigma_y = \sigma_0 + k_\varepsilon \varepsilon_1^{-1} + k_p \Delta^{-1},\ \text{MPa} \tag{7.5}$$

where σ_0 is the intrisinc strength of martensite (including solid solution strengthening due to carbon), ε_1 is the average transverse thickness of the cell structure, and Δ is the average distance between a particle and its two or three nearest neighbours. The data needed to evaluate the equation are fairly well established so that a comparison of the calculated strength versus the strength after tempering can give a good idea of the extent of cementite precipitation. When this is done, the relation between hardness and the amount of the precipitation (thus the decrease in solute carbon) is found not to be linear as was assumed in the empirical approach, but the predicted changes in hardness are found to be remarkably consistent with those measured by Speich for the early stages of tempering, justifying the assumption that much of the hardness change can be attributed to the precipitation of carbon rather than due to other annealing effects such as tempering.

7.2.3 *Quantitative Estimation of the Transition Temperature*

Following the gist of the Matas and Hehemann proposal, a comparison of the time t_d required to decarburise a plate of ferrite, with the time interval t_θ necessary to obtain a detectable amount of cementite precipitation in the ferrite should give a good indication of whether upper or lower bainite is expected during isothermal transformation. If $t_d<t_\theta$ then it may be assumed that upper bainite is obtained, and vice versa (Fig. 7.5). A weakness of this theoretical model is that the two processes, of decarburisation and precipitation, should really be coupled. A disposable parameter in the model as it stands is the 'detectable amount' of cementite precipitation, which has to be fixed by comparison with experimental data.

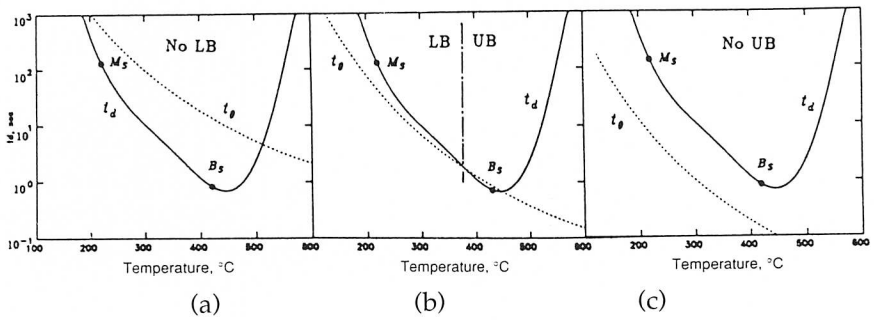

Fig. 7.5 *Illustration of how differences in the relative variation of the decarburisation time t_d and the precipitation time t_θ can lead to: (a) a steel which is incapable of transforming to lower bainite; (b) a steel which should, under appropriate conditions, be able to transform to upper or lower bainite; (c) a steel in which bainitic transformation always leads to the formation of lower bainite. The abbreviations LB and UB refer to lower and upper bainite respectively.*

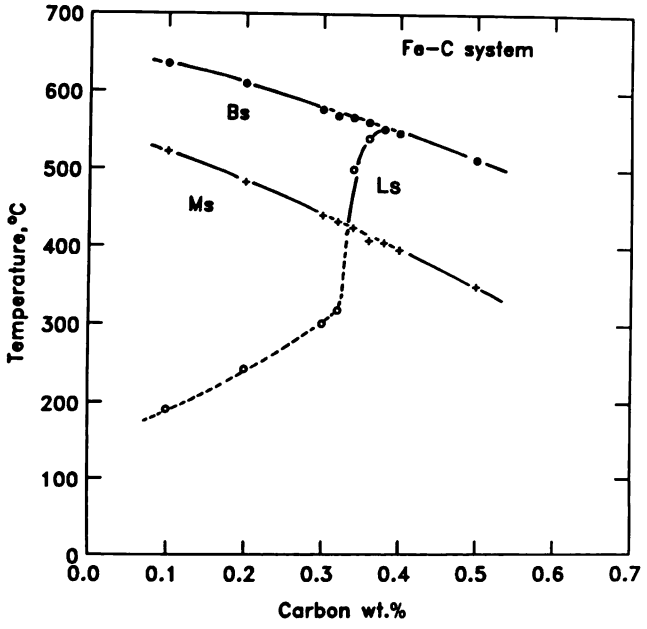

Fig. 7.6 *Calculated lower bainite transformation start temperatures for plain carbon steels, as a function of transformation temperature. The calculated martensite start and bainite start temperatures are also presented. (After Takahashi and Bhadeshia, 1990.)*

Some calculated data on the plain carbon steels illustrated in Fig. 7.5, are presented in Fig. 7.6. They indicate that lower bainite should not be observed in plain carbon steels with carbon concentrations less than 0.32 wt%. Furthermore, only lower bainite (i.e., no upper bainite) is expected in steels with carbon concentrations exceeding 0.4 wt%. Steels containing between 0.32 and 0.4 wt% of carbon should exhibit both upper and lower bainite, depending on the reaction temperatures. Finally, it should be noted that at low temperatures where t_θ and t_d both become very large, the times required for precipitation or redistribution of carbon exceed that to complete transformation, consistent with the fact that untempered martensite can be obtained at temperatures near M_S, with the degree of autotempering of the martensite decreasing as M_S is reduced.

7.2.4 *Comparison of Theory and Experimental Data*

The general behaviour indicated by the calculations for plain carbon steels, is found to be that observed experimentally. Some interesting work by Oka and Okamoto (1986) proves that there is no upper bainite in plain carbon steels with more than 0.8 wt% of carbon; the only bainite observed

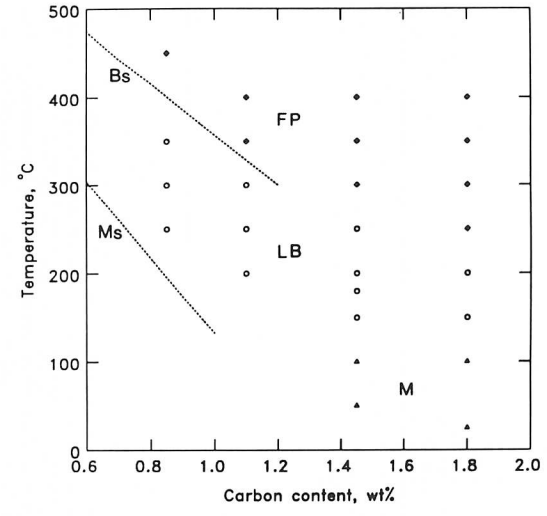

(a)

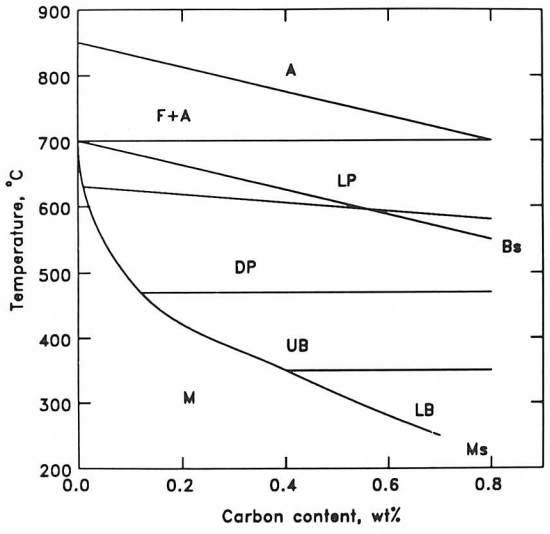

(b)

Fig. 7.7 *(a) Experimental data (Oka and Okamoto, 1986) illustrating the temperatures at which fine nodules of pearlite (FP), classical lower bainite (LB) and martensite (M) were obtained by isothermal transformation of plain carbon steels. The lines represent calculated bainite start and martensite start temperatures (Takahashi and Bhadeshia, 1990). (b) The effect of carbon concentration on the temperature range where each microstructure is formed (Ohmori and Honeycombe, 1971). The terminology is as follows: A austenite, F ferrite, LP lamellar pearlite, DP: degenerate pearlite, UB upper bainite, LB lower bainite, M martensite.*

in their experiments was classical lower bainite at all temperatures above the M_S temperature (Fig. 7.7a).

Ohmori and Honeycombe (1971), in a study of plain carbon steels, showed that during isothermal transformation above the M_S temperature, only upper bainite could be obtained in samples containing less than 0.4C wt% (Fig. 7.7b). This is consistent with theory, although their observation that upper bainite can be obtained in steels with a carbon concentration up to about 0.85C wt% is not consistent with the theory, nor with the data reported by Oka and Okamoto (1986).

7.3 Mixed Microstructures Obtained By Isothermal Transformation

According to the analysis presented above, only lower bainite is expected in steels with more than 0.32 wt% of bulk carbon content. However, the calculations are for ferrite plates whose carbon concentration is initially identical to that of bulk alloy, since the model assumes that bainite growth is diffusionless, with carbon redistribution occurring after the growth event. As a consequence of the redistribution, which is expected to be substantial when t_d is smaller than t_θ, there is an enrichment in the carbon concentration of residual austenite as the bainite transformation proceeds. Consequently, any bainite which grows from enriched austenite will inherit a higher than bulk concentration of carbon. This leads to the possibility of the transformation beginning with the growth of upper bainite, but with the enriched austenite then decomposing to lower bainite at the later stages of transformation. There is then a real possibility of obtaining a mixture of upper and lower bainite in steels containing less than 0.32 wt% carbon, especially if carbide precipitation from the austenite is relatively sluggish, and therefore does not act to relieve any carbon enrichment in the austenite.

The maximum carbon concentration that can be tolerated in residual austenite before the bainite reaction ceases is expressed approximately by the T_0' curve. Therefore if the carbon concentration in residual austenite at T_0' curve (i.e., $x_{T_0'}$) is greater than 0.32 wt%, lower bainite can be expected to form during the later stages of reaction. However, the formation of cementite from the residual austenite also becomes possible if $x_{T_0'} > x^{\gamma\theta}$, where $x^{\gamma\theta}$ is a point on the γ / ($\gamma + \theta$) phase boundary, since the austenite will then be supersaturated with respect to the cementite. The fact that a curve showing the carbon concentration in austenite which is in equilibrium with cementite in plain carbon steels crosses the T_0' curve at 0.4 wt% of carbon concentration (560°C), leads to the identification of three regimes for bainite on the Fe–C phase diagram (Fig. 7.8). In steels with more than 0.4 wt% of the initial bulk carbon content (region *B*), lower bainite is to be expected from the earliest stages of transformation. For

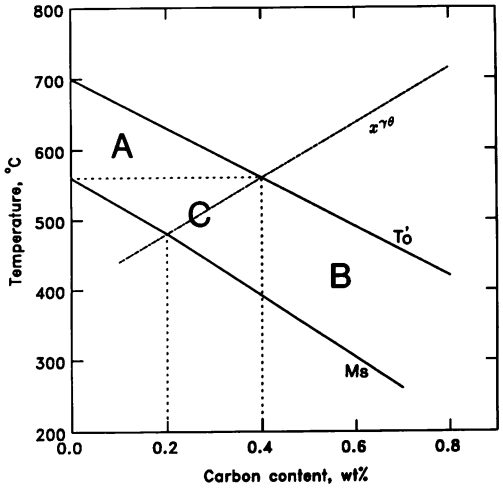

Fig. 7.8 *Identification of regimes A, B and C, in which the progress of isothermal transformation can lead to changes in the nature of the transformation product. The line marked* $x^{\gamma\theta}$ *is the calculated* $\gamma/(\gamma + \theta)$ *phase boundary.*

steels whose composition lies in region *A*, lower bainite is expected to be absent during isothermal transformation at all temperatures above M_S, and this behaviour is valid for any stage of transformation since the austenite cannot be supersaturated with cementite as far as regime *A* is concerned. The behaviour in the region marked *C* should be more complex. The residual austenite for these steels (region *C*) may at some stage of transformation contain enough carbon to precipitate cementite. If the kinetics of cementite precipitation from austenite are rapid, then lower bainite may not be obtained in steels with an average carbon concentration less than 0.32 wt%, but otherwise, a mixed microstructure of upper and lower bainite might arise.

7.4 Other Consequences of the Transition

There are some other characteristic differences between upper and lower bainite, caused by the fact that lower bainite forms at a higher undercooling below B_S when compared with upper bainite. Sub-unit growth during the bainite transformation ceases when the interface is blocked by plastic accommodation induced defects (Bhadeshia and Edmonds, 1979a). For a given defect density, lower-bainite sub-units should be longer than those of upper bainite, since the driving force for transformation increases with undercooling. At lower transformation temperatures the matrix is able to support higher strains without plastic deformation so that the defect

density in the matrix itself would be lower. Step quenching experiments in which an alloy is first partially transformed to lower bainite and then up-quenched into the upper bainite transformation range are consistent with this since they show that the growth of lower bainite ceases following the up-quench (Goodenow and Hehemann, 1965). This also appears to be the case when specimens partially transformed to lower bainite experience an increase in temperature within the lower bainite transformation range (White and Owen, 1961).

7.5 Comparison with the Tempering of Martensite

From the above discussions, it is evident that a plausible model for the transition from upper to lower bainite can be constructed from the assumption that there is no fundamental difference in transformation mechanism between these two forms of bainite, and that bainitic ferrite when it grows is supersaturated with carbon. The excess carbon may eventually partition into the residual austenite or precipitate from the ferrite in the form of carbide. When the latter process is dominant, lower bainite is obtained. Upper bainite is obtained only when the carbon partitions relatively rapidly into the austenite.

Hence, lower bainite in effect 'autotempers' to give the classical carbide morphologies, and should have characteristics which are similar to those of tempered martensite. When high carbon martensite is tempered, the first carbide to form is usually a transition carbide such as ε-carbide, which is eventually replaced by the thermodynamically more stable cementite. Similarly, when lower bainite forms in high carbon steels, ε-carbide forms first, and subsequently transforms into cementite during prolonged holding at the isothermal transformation temperature (Matas and Hehemann, 1961).

The chances of obtaining ε-carbide (instead of cementite) in lower bainite increase as the transformation temperature is reduced for the same steel (see Table II, Matas and Hehemann, 1961). As the transformation temperature is reduced, and the time required to decarburise a supersaturated plate of bainite increases, a high carbon concentration can persist in the ferritic matrix for a time period long enough to allow the formation of ε-carbide, which does not form if the carbon concentration is less than about 0.25 wt%, (Roberts *et al.*, 1957). This effect also explains the result that a medium carbon Fe–0.43C–3Mn–2Si wt% steel transforms to lower bainite containing cementite particles, although when quenched to martensite, gives ε-carbide on tempering (Bhadeshia and Edmonds, 1979a, 1983a). Some of the carbon is in the former case, lost to the austenite by diffusion, thereby preventing the formation of ε-carbide.

7.6 Summary

A comparison between the time required to decarburise supersaturated ferrite plates with the time required to precipitate cementite within thhe plates appears to be a reasonable way of rationalising the transition from upper to lower bainite. If the decarburisation process dominates, upper bainite is predicted whereas relatively rapid carbide precipitation within the ferrite leads to the formation of lower bainite.

Some of the predictions of this method are in agreement with reported experimental data. It is found, for example, that lower bainite cannot form in plain carbon steels containing less than about 0.3 wt% carbon. Similarly, upper bainite is predicted and found to be absent in plain carbon steels containing more than 0.4 wt% carbon, although contradictory results have also been reported in the literature.

More experimental work is needed to verify some of the detailed predictions of the theory for the transition temperature, and to resolve some of the discrepancies between experimental data reported in the literature. More work is also needed from a theoretical point of view, to develop fully the kinetics of cementite precipitation from supersaturated ferrite, and to couple the processes of cementite precipitation with the simultaneous redistribution of carbon into the residual austenite. In the mean time, the model provides a working hypothesis for the transition temperature.

8 *The Effect of Stress on Transformation*

A displacive transformation can justifiably be regarded as a mode of deformation of the parent phase, with the additional characteristic that the crystallographic structure of that phase is altered in the deformed region (Table 8.1). For this reason, the permanent strain caused by the transformation is called *transformation plasticity*. Since a phase transformation can be triggered either by cooling below a certain transformation start temperature, or by the application of a stress in appropriate circumstances, or by a combination of these factors, the deformation that is described as transformation plasticity can be obtained at stresses which are much smaller than the conventional yield stress of the parent phase, as measured in the absence of transformation.

Just as a combination of a plane and a direction constitutes a deformation system for slip or twinning, the habit plane and displacement vector of the invariant plane strain accompanying transformation completely describe the deformation system responsible for transformation plasticity. There will in general be 24 of these systems per austenite grain, and they may operate simultaneously to varying extents. Of course, unlike ordinary slip, the different deformation systems within an austenite grain cannot intersect (except in special circumstances where intervariant transformations are possible), so that the ordinary notion of work hardening does not apply. Work hardening nevertheless manifests itself via a different mechanism, in which the stability of the austenite increases as it becomes more finely divided. Given the large number of transformation variants available per grain, the Taylor criterion leads to the conclusion that transformation plasticity can lead to, or accommodate any externally imposed, arbitrary shape change assuming that sufficient parent phase is available. It follows that polycrystalline samples can remain intact at grain boundaries when transformation plasticity is the sole mode of deformation. Furthermore, the transformation plasticity can lead to

Table 8.1 Characteristics of slip, mechanical twinning and displacive transformation.

	Slip deformation	Twinning deformation	Displacive transformation
Permanent change in shape	Yes	Yes	Yes
Invariant plane strain shape change	Yes	Yes	Yes
Changes crystallographic orientation	No	Yes	Yes
Changes lattice type	No	No	Yes
Can lead to a density change	No	No	Yes

anisotropic shape changes even in polycrystalline samples transformed without applied stress, if the samples are crystallographically textured in their parent phase.

8.1 The Mechanical Driving Force

Given that displacive transformations in steels are accompanied by fairly large shape strains, it is natural to expect an interaction between any applied stress and the progress of the transformation, in a manner which is related uniquely to the transformation mechanism. The total driving force can in these circumstances be partitioned into a 'mechanical driving force' and the more usual chemical driving force (Patel and Cohen, 1953; Christian, 1990b). The physical reasoning behind this idea is that the movement of a glissile interface is a combined deformation and transformation process. The work done by the external stress may be added to the chemical free energy change in order to obtain the total free energy difference. The mechanical driving force is assumed to be given by the work done (ΔG_{MECH}) by the external stress system in producing the macroscopic shape deformation

$$\Delta G_{MECH} = \sigma_N \xi + \tau s \tag{8.1}$$

where σ_N is the normal stress on the habit plane and τ is the component of the shear stress on the habit plane, parallel to the direction along which the shear displacements of the shape deformation occur (Fig. 8.1).[1] The strains ξ and s have been previously defined as the dilatational and shear components of the shape deformation. Given a free choice of some 12 to 24 crystallographic variants of the transformation product in a grain of austenite, the work done by the shear stress is always expected to be positive, whereas that due to the dilatational component depends on the sign of σ_N. For steels, this latter component is however, always much

1 As pointed out by Delaey and Warlimont (1975), the Patel and Cohen treatment assumes incorrectly that it is the maximum shear stress on the habit plane that interacts with the shape deformation, rather than the component of the shear stress resolved parallel to the shear displacements of the shape strain.

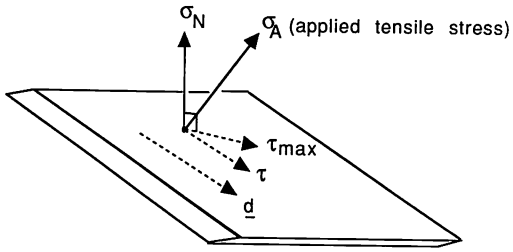

Fig. 8.1 *Resolution of the applied stress σ_A. The normal stress σ_N, and the shear stress τ both act on the habit plane. The vector $\underline{d}$ is the direction along which the shear displacements of the shape deformation lie. τ_{MAX} is the maximum shear stress on the habit plane, but τ is given by resolving τ_{MAX} along $\underline{d}$. Note that $\underline{d}$ differs slightly from the displacement vector of the invariant-plane strain, which includes a dilatational component in addition to the shear.*

smaller, so that any observed stress effects usually reflect the dominant role of the shear component. The exception is when τ is small or zero, as would be the case when the stress is a pressure.

It follows from the Patel and Cohen analysis (equation 8.1), that since the shear stress remains positive irrespective of whether the sample is pulled in tension, or uniaxially compressed, and since the shear component of the shape change is large, a uniaxial stress will always cause an increase in the transformation temperature for displacive transformations in steels. Hydrostatic stress, on the other hand, has no deviatoric components and consequently only interacts with the dilatational component of the shape change. Thus, hydrostatic compression is expected to lead to a decrease in the transformation temperature (Fig. 8.2).

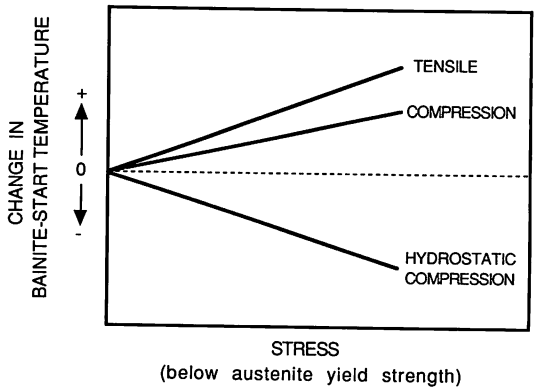

Fig. 8.2 *An indication of how the bainite start temperature should vary as a function of the nature and magnitude of the applied stress.*

A reservation to the analysis described above is that shear stresses, unlike pressures, can not strictly be considered as state variables so that their use in thermodynamic equations is uncertain (Christian, 1982). This difficulty is, however, unimportant in the analysis as long as irreversible processes such as diffusion or dislocation motion do not act to relieve any shear stresses during the time scale of the experiment. What this means in practice is that in the absence of transformation, the state of the system is not altered if the shear stress is changed and then restored to its original value.

A second complicating factor could arise if the stress influences the very nature of the transformation product, either by stimulating the formation of a metastable phase or by decoupling groups of self-accommodating variants which would form in the absence of stress (Christian, 1982). This would lead to a modification of the chemical driving force term, and as discussed later, there is some evidence to show that there are significant microstructural changes when bainite grows under the influence of an externally applied stress.

Assuming that the interaction of the applied stress is with the macroscopic shape deformation, the stress must tend to favour the growth of those particular variants for which ΔG_{MECH} is maximised. Hence, for a tensile stress, plates which have their habit planes inclined at approximately 45° to the tensile axis will tend to be favoured.[2] This assumes however, that the applied stress interacts solely with the growth process whereas its interaction with nucleation events could lead to a different criterion for variant selection (Christian, 1982). Indeed, efforts at predicting the martensitic transformation texture from the crystallographic texture of the parent austenite, are apparently more successful if it is assumed that variant selection depends on the Bain strain rather than on the macroscopic shape deformation (Ray and Jonas, 1990). The IPS deformation is unlikely to have developed at the nucleation stage, where the particle might be too small to sustain the lattice invariant deformation that is necessary to convert the effects of the lattice deformation into what is macroscopically an invariant plane strain. On the other hand, since the Bain strain is necessary to accomplish the lattice change, the texture prediction work indicates that variant selection may depend on the interaction of the applied stress with the nucleation process.

8.2 The B_d Temperature

The highest temperature at which martensite forms during the cooling of austenite is the M_S temperature. This can be raised by the application of a

2 The angle will not be exactly 45° because the displacement vector of the IPS is not quite parallel to the habit plane whenever there is a volume of change accompanying transformation.

suitable stress (Patel and Cohen, 1953). The maximum temperature at which martensite grows under the influence of stress is called the M_d temperature. There are no similar experiments for bainite, but it is possible to piece together a lot of circumstantial evidence to show that the behaviour of bainite is probably similar to that of martensite. Goodenow *et al.* (1969) showed that the transformation stresses associated with the growth of lower bainite stimulated the growth of upper bainite at temperatures just above B_S, showing that stress can indeed raise the bainite start temperature. It should in principle be possible to define a B_d temperature. Early work by Cottrell (1945) gives some support to the B_d concept. He found that the maximum volume fraction of bainite obtainable by isothermal transformation of unstressed samples, can be increased with the application of a tensile stress during transformation, but that the effect of the applied stress diminished as the bainite start temperature was approached. Drozdov *et al.* (1962) demonstrated that at a high enough transformation temperature above B_S (at which the austenite is still metastable), no amount of deformation causes the austenite to transform to bainite, a result which can be interpreted easily if it is assumed that the temperature concerned was higher than B_d.

These concepts are illustrated schematically in Fig. 8.3, which is based on similar ideas for martensitic transformations; the details have yet to be established experimentally for bainite. The net driving force available for transformation, ΔG, is given by

$$\Delta G = \Delta G_{CHEM} - \Delta G_{MECH} \tag{8.2}$$

The model for the influence of stress assumes that the critical driving force needed to trigger bainitic transformation at zero stress (i.e. $\Delta G_{CHEM}\{B_S\}$) remains constant over the temperature range of interest. The application of a tensile or compressive stress assists the transformation by boosting the overall driving force ΔG with the term $-\Delta G_{MECH}$, so that the B_S temperature rises continuously with the magnitude of the applied stress.

It is convenient to define a temperature B_σ, beyond which the austenite can no longer elastically support the applied stress prior to transformation. Clearly, beyond B_σ, the notion of using τ in the thermodynamic equations becomes highly dubious since the austenite inevitably undergoes plastic deformation prior to transformation. The deformation induced defects might then influence the progress of transformation, perhaps by providing additional nucleation sites, although this kind of stimulation does not seem prominent in bainitic transformations where the predominant site for sheaf nucleation is almost always an austenite grain boundary. Following the terminology established for martensitic transformations, the region below B_σ is said to represent *stress assisted*

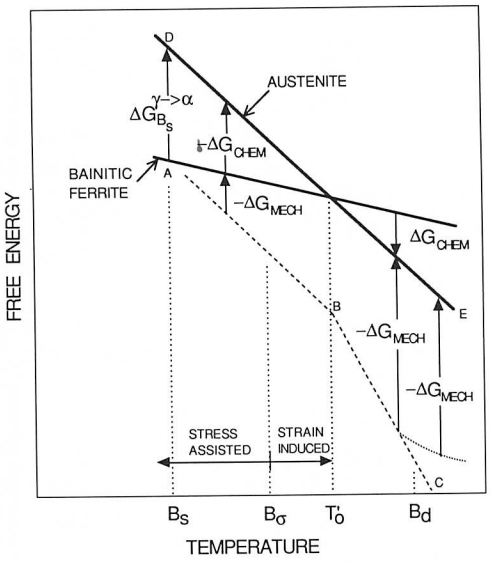

Fig. 8.3 *Illustration of the stress modified B_s, B_σ and B_d temperatures.*

transformation, whereas *strain induced* transformation describes the regime where the yield stress of the parent phase is exceeded.

As the stress is increased further, beyond the yield stress of the austenite, the bainite start temperature continues to rise. When the T_0' temperature is reached, the chemical driving force actually opposes transformation so that the mechanical component has to be larger than $\Delta G_{CHEM}\{B_S\}$. Of course, as the temperature rises, the yield stress of the austenite decreases, until it is no longer able to support a stress large enough to stimulate bainitic transformation; that temperature corresponds to B_d (Fig. 8.3).

8.3 General Observations

8.3.1 Externally Applied Stress

There are many independent observations which suggest that stress has a large effect on the progress of the bainite reaction. It is well known in the context of thermomechanical processing, that deformation accelerates the rate of the bainite reaction (Cottrell, 1945; Jepson and Thompson, 1949; Drozdov *et al.*, 1962; Duckworth, 1966; Dubrov, 1969; Freiwillig *et al.*, 1976; Mutui *et al.*, 1977; Tsuzaki *et al.*, 1989). There is also good evidence that the rate of reaction under stress increases with the rate of deformation (Drozdov *et al.*, 1962; Mutui *et al.*, 1977). The degree of transformation to bainitic ferrite at any temperature is limited by the incomplete reaction

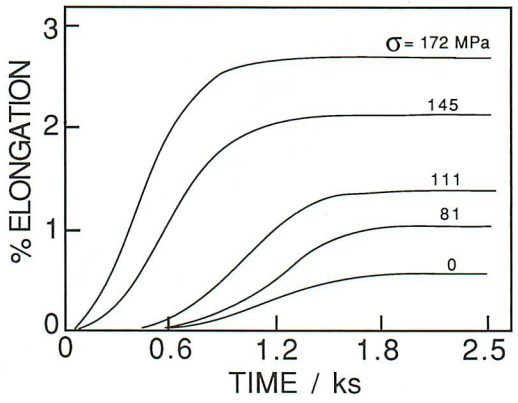

Fig. 8.4 *The overall kinetics of bainitic transformation as a function of an externally applied tensile stress. Assuming that the degree of transformation is related to the elongation, the data show an increase in the rate of reaction as a function of the magnitude of the applied stress (after Umemoto* et al., *1986).*

phenomenon, but the application of a tensile stress during transformation has been shown to stimulate further reaction beyond the limiting value (Cottrell, 1945). The rate of reaction is also found to accelerate under the influence of a tensile stress as long as the stress exceeds a threshold value whose magnitude decreases with increasing temperature, although the significance of the threshold stress is not clear (Porter and Rosenthal, 1959). Umemoto *et al.* (1986) have demonstrated an acceleration of transformation even when the applied tensile stress was rather small (Fig. 8.4).

8.3.2 *Internally Generated Stress*

The stress influencing transformation need not be applied externally; internal stresses generated due to other transformations also have an effect. Early studies indicated an acceleration in the rate at which upper bainite forms in specimens which are first transformed partially at a lower temperature (Lange and Mathieu, 1938; Jellinghaus, 1952). Martensite is the first phase to form on cooling a steel below the M_S temperature, but after the initial burst of martensitic transformation and a suitable incubation period, the austenite undergoes accelerated decomposition to bainite (Howard and Cohen, 1948). This is because the austenite is deformed by the martensitic transformation. Supporting evidence is found in magnetometric studies, which have revealed that isothermal reaction below the M_S temperature leads first to the formation of the usual athermal martensite, followed by a small amount of isothermal martensite, and then some of the residual austenite begins to transform at an accelerated rate to bainite

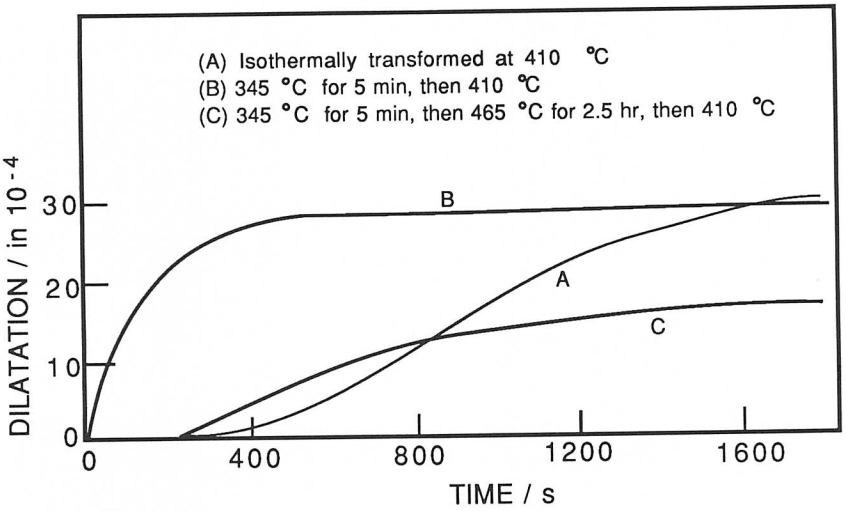

Fig. 8.5 *The influence of internal stresses on the rate of transformation at 410°C, in a Fe–0.31C–0.3Si–0.76Mn–3.07NI–1.22Cr–0.49Mo wt% alloy. Curve A represents isothermal transformation to upper bainite; curve B is for a sample which was first partially transformed to lower bainite and then to upper bainite, showing an acceleration of reaction rate at 410°C due to the internal stresses generated by the presence of lower bainite; curve C shows how annealing above the B_s temperature removes the stresses, and their accelerating influence on transformation kinetics (Goodenow* et al., *1969).*

(Ericsson *et al.*, 1976). Similar results have been obtained by Radcliffe and Rollason (1959) and it has also been demonstrated that the upper bainite reaction is accelerated by initial partial (displacive) transformation to lower bainite (Fig. 8.5). Their experiments also clearly illustrate the 'flat tops' of the bainite C curves as highlighted first by Zener (1946).

Another revealing observation is that both the nucleation and growth rates of bainite are accelerated by the proximity of a free surface (Ko, 1953; Hawkins and Barfod, 1972). The observation emphasises the role of the shape deformation of bainite, since any shape change can be accommodated better at a free surface, where the degree of physical constraint is smaller. In the absence of such mitigating circumstances, the matrix sometimes cannot tolerate the large displacements associated with the formation of bainite. it then relaxes by plastic deformation, which is driven by the shape change due to transformation (Christian, 1979b).

8.3.3 Plastic Deformation and Mechanical Stabilisation

Deformation does not always accelerate transformation; it is well established for martensitic transformations that severe deformation causes the

mechanical stabilisation of the austenite. Mechanical stabilisation is due to the work hardening of the austenite as its defect density increases. The defects interfere with the motion of glissile transformation interfaces. There are no systematic studies of mechanical stabilisation for bainitic reactions. It has been reported that during the continuous cooling transformation of a low alloy steel into a mixed microstructure, the decomposition of austenite to bainite was retarded when the austenite was deformed prior to transformation (Vlad, 1985). This could be interpreted as mechanical stabilisation, but there is unfortunately an alternative explanation for these particular experiments, an explanation which is consistent with the reported data. The deformation accelerates the formation of allotriomorphic ferrite, thereby causing an exaggerated enrichment of the residual austenite with carbon, and therefore a retardation of both the bainite and martensite reactions.

Better evidence comes from experiments using hot rolled samples, which have demonstrated that the austenite which is deformed to a larger extent, tends to transform to bainite at a lower temperature during continuous cooling (Fig. 8.6). This effect can only be interpreted in terms of mechanical stabilisation because the alloy used had sufficient hardenability to avoid the growth of allotriomorphic ferrite or other interfering transformation products during cooling.

Perhaps the most convincing evidence for the mechanical stabilisation of bainite comes from studies of ausformed bainite. Samples of deformed austenite gave smaller maximum volume fractions of bainitic ferrite when compared with those transformed without any prior deformation. This is in spite of the fact that the deformed austenite transformed initially at a

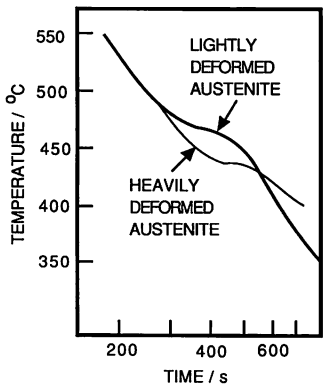

Fig. 8.6 *Plots of temperature versus time, for samples undergoing bainitic transformation during cooling. The deviations from linearity indicate the onset of transformation. The reaction is retarded in the austenite deformed to a greater degree before transformation, indicative of mechanical stabilisation. (Data from Davenport, 1977).*

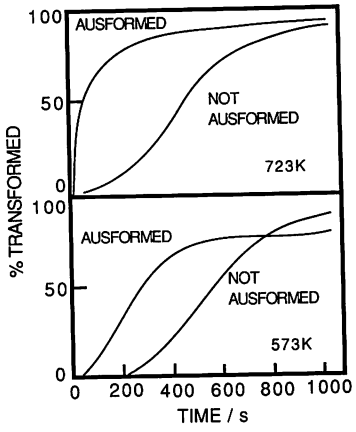

Fig. 8.7 *The effect of ausforming on the kinetics of the bainite reaction in a Fe–0.59C–2.01Si–1.02Mn wt% alloy (data from Tsuzaki et al.,* 1989).

higher rate (Fig. 8.7). This effect did not appear during transformation at higher temperatures, presumably because the total volume fraction of bainite that can form is then reduced. Stabilisation therefore only manifests itself when the 'easy' regions of austenite are exhausted, i.e., those regions left unchanged by the inhomogeneous deformation. The non-uniformity of stabilisation is reflected in the microstructure that develops. The sheaves of bainite that do form are found to be aligned along specific directions within individual austenite grains, in contrast with the usual bainitic transformation where sheaves grow in many different orientations (Fig. 8.8).

As is often the case with martensite plates in ausformed alloys, sheaves of bainite are sometimes found to be curved on a macroscopic scale. This is because of deformation induced lattice curvature present in the parent austenite grains prior to transformation (Fig. 8.8).

Finally, it is worth mentioning two important experiments by Bhattacharyya and Kehl (1955). They first demonstrated that a tensile stress has little effect on transformation if it is applied after more than about 30% of bainite has formed. The effect was attributed to the fact that the overall strength of the microstructure rises during transformation relative to the applied stress. An alternative explanation could be that it becomes difficult to stimulate variants favoured by the applied stress once many nuclei have been activated. Any favoured variants that do form will have a limited scope for development as the amount of austenite decreases.

In the second experiment, Bhattacharya and Kehl showed that the removal of stress after some transformation has occurred, does not decrease

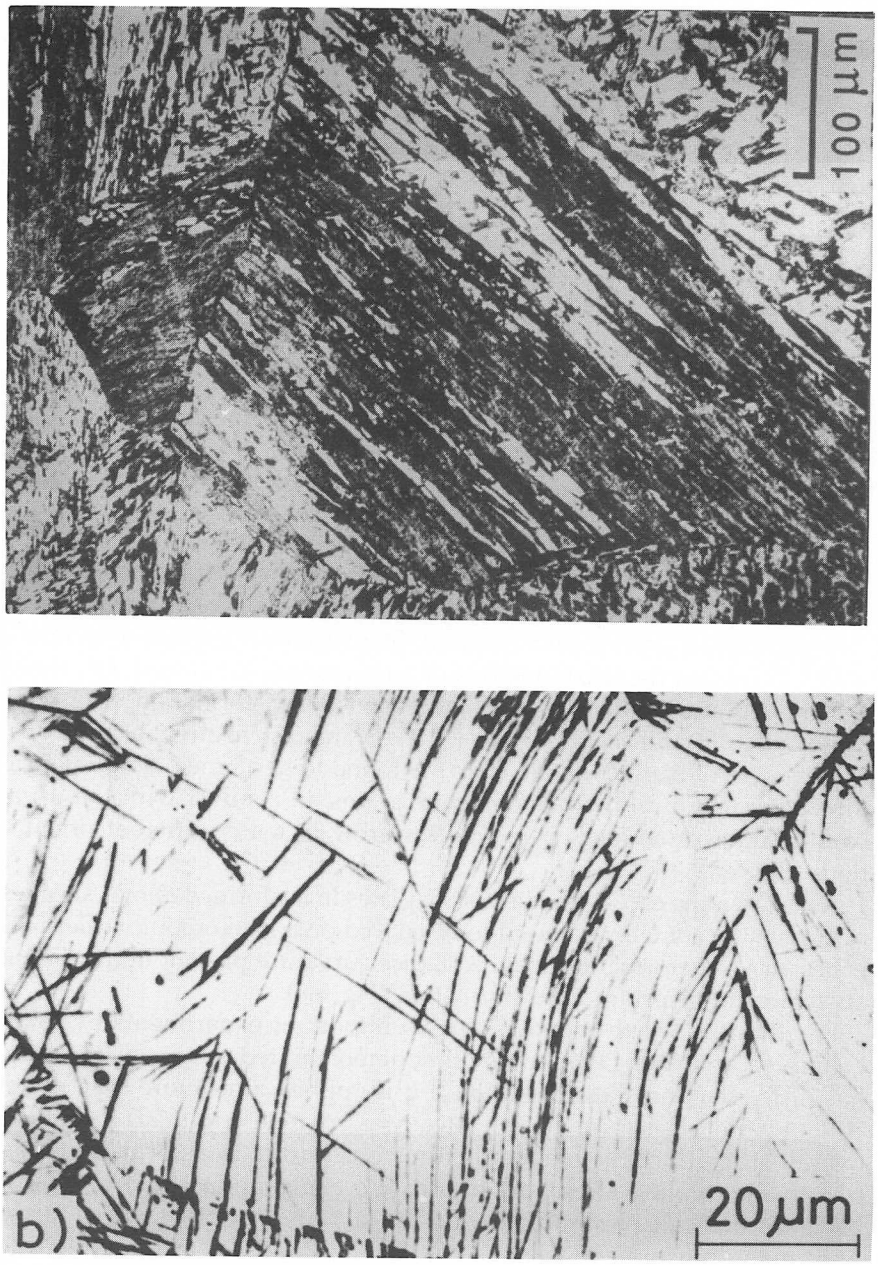

Fig. 8.8 *Optical micrographs illustrating the microstructure of an ausformed bainitic steel. (a) Alignment of sheaves of bainite in individual austenite grains. (b) Curved bainite sheaves reflecting the deformation-induced misorientations within the austenite grains. (After Tsuzaki et al.,* 1989).

the rate of reaction. This might suggest that the primary influence of stress is in these experiments to stimulate nucleation rather than growth.

8.4 The Effect on Microstructure

An applied stress will tend to favour the development of crystallographic variants which comply with that stress. This is analogous to the selective operation of a few of the available slip systems in a crystal under stress; it is the systems with the largest Schmid factor which are favoured. Assuming that variant selection is similarly controlled by the interaction of the applied stress with the shape deformation, the stress should cause an alignment of the plates at roughly 45° to the tensile axis. This alignment has been observed in many experiments involving martensitic transformations (*see* for example, Bhadeshia, 1982a). The observations are more difficult for bainite, partly because of the rapid rate of reaction under the influence of stress. The experiments have to be conducted at high temperatures. Further transformation may occur as the sample cools to ambient temperature, confusing the interpretation of the microstructure. Nonetheless, good evidence for microstructural alignment has been reported for bainite platelets especially at relatively large stresses

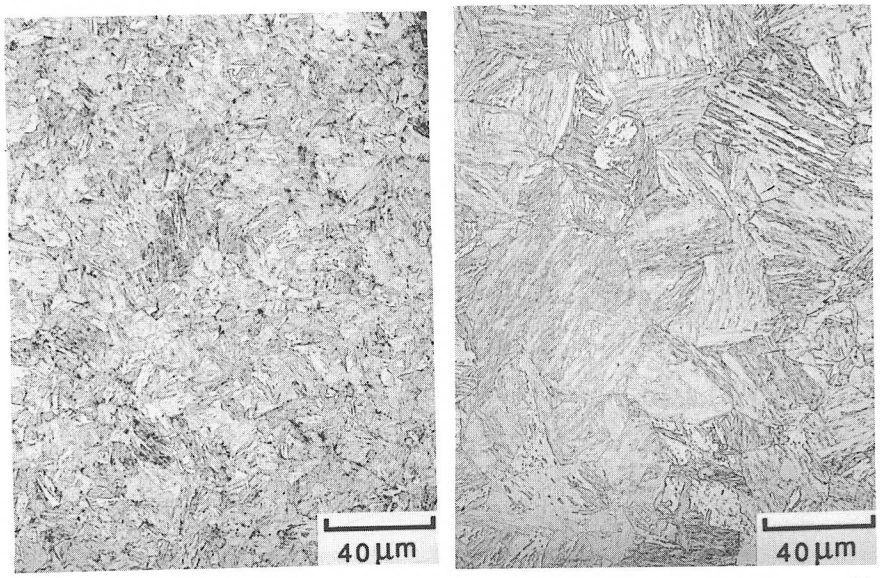

(a) (b)

Fig. 8.9 *Light micrographs of bainitic microstructures generated in a Fe–0.12C–0.27Si–0.84Mn–0.14Ni–1.48Mo–2.86Cr wt% alloy, by isothermal transformation at 400°C under the influence of stress. (a) Zero stress; (b) 95 MPa. (After Bhadeshia* et al., *1991).*

(Bhattacharyya and Kehl, 1955; Umemoto *et al.*, 1986). All of these observations are based on polycrystalline samples, but that does not substantially alter the conclusions. There are so many variants available per austenite grain, that there is a high probability of a plate orientation lying close to the optimum orientation with respect to the stress.

There are more subtle effects of stress on microstructure, even in the absence of any obvious plate alignment, at stress levels as small as 45 MPa. Variant selection leads to the development of a less chaotic microstructure (Jepson and Thompson, 1949; Dubrov, 1969; Bhadeshia *et al.*, 1991). Without stress, each grain of austenite transforms into many different orientations of bainite. Significantly fewer variants develop per austenite grain under the influence of stress, so that the selected orientations can grow unhindered and form thick packets of bainite plates. The sheaves are therefore found to be longer, and their number density per grain smaller when variant selection operates (Fig. 8.9).

A further effect on microstructure is when the austenite has been plastically deformed prior to transformation. Heterogeneous nucleation then occurs not only at the original austenite grain boundaries, but apparently also intragranularly on slip bands or other deformation heterogeneities (Dubrov, 1969).

8.5 The Effect of Hydrostatic Pressure

There is general agreement that the application of hydrostatic pressure causes a retardation of the bainite reaction (Jellinghaus and Friedewold, 1960; Radcliffe *et al.*, 1963; Nilan, 1967). The effect on the time–temperature transformation diagram is illustrated in Fig. 8.10. The observed retardation is not in itself a feature unique to bainite. All transformations which are accompanied by a reduction in density are expected to be retarded by hydrostatic pressure since it opposes a

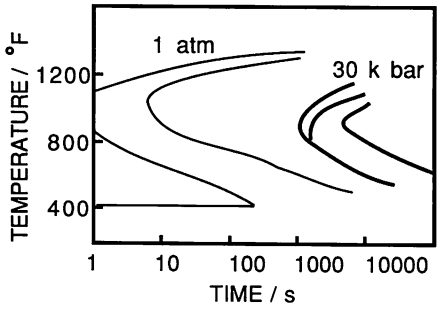

Fig. 8.10 *Isothermal transformation diagrams of Fe–0.82C wt% at 1 atmosphere and at 30kbar pressure (after Nilan, 1967).*

volume expansion. The effect of hydrostatic pressure is two fold: it reduces the diffusion coefficients by decreasing the available free volume (although the details remain to be established), and it influences the free energy change for transformation. If ΔG_m is the molar Gibbs free energy change for a reaction, then since

$$(\partial G/\partial P)_T = V$$

it follows that

$$\Delta G_m\{P\} - \Delta G_m\{1\} = \int_1^P \Delta V_m \, dP \tag{8.3}$$

where ΔV_m is the change in molar volume on transformation, V is the volume and P is the pressure. The way in which the free energy change for transformation is influenced by the pressure determines how the transformation temperature changes as a function of pressure. An alternative way of expressing this relationship is the Clausius–Clapyeron equation, whence the change in transformation temperature is given by

$$dT^{\gamma\alpha} = T^{\gamma\alpha}\Delta V_m \,/\, \Delta H^{\gamma\alpha} \tag{8.4}$$

where $\Delta H^{\gamma\alpha}$ is the enthalpy change on transformation at the transition temperature $T^{\gamma\alpha}$. The equation is approximate in that its derivation depends on the assumption that the enthalpy change does not vary with temperature. With typical values of all the parameters, the variation in transition temperature with pressure should be approximately –0.01 K per MPa (Denis *et al.*, 1985).

Radcliffe *et al.* also found that the bainite transformation could be suppressed completely by the application of hydrostatic pressure ($\approx$ 15 kbar) but Nilan, using similar steels could obtain conventional bainite at the maximum pressures he used (34 kbar). Why these experiments are contradictory is not clear, but Nilan concluded that the transformations at high pressures do not differ substantially from those at ambient pressure.

8.6 Mechanical Stability of Retained Austenite

In steels where the precipitation of carbides during the bainite reaction is relatively sluggish, the residual austenite becomes enriched in carbon and a large proportion is retained on cooling to ambient temperature. The austenite, if it decomposes under the influence of stress, can be detrimental to the steel concerned since the resulting high carbon, untempered martensite is expected to be very brittle. There is ample evidence that the austenite retained to ambient temperature after isothermal formation of

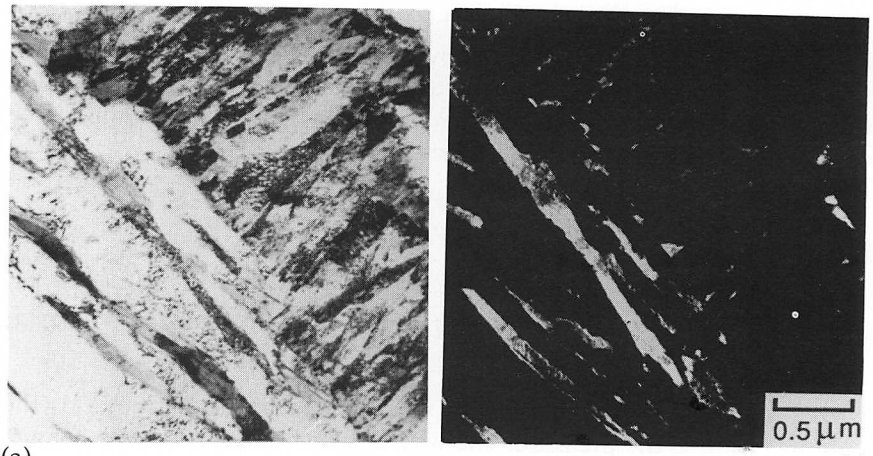

(a) (b)

Fig. 8.11 *Electron micrographs illustrating the effect of applied stress (850 MPa) on a sample which initially had a microstructure of bainitic ferrite and retained austenite (Bhadeshia and Edmonds, 1983a). The larger regions of austenite transform to martensite but the films are preserved. (a) Bright field image showing a large region of stress induced martensite; (b) corresponding austenite dark field image. Note that the sample was tempered prior to stressing in order to distinguish the martensite which forms during cooling from the bainite transformation temperature, from that which is induced by stress.*

bainitic ferrite, especially the larger blocky austenite, can decompose to martensite even at relatively small stresses, Fig. 8.11 (Horn and Ritchie, 1978; Kar *et al.*, 1979; Bhadeshia and Edmonds, 1983a, b: George *et al.*, 1985). The mechanical stability of any retained austenite is therefore important in obtaining good toughness in bainitic steels.

Miihkinen and Edmonds (1987b) have shown that for high silicon steels in which the bainite reaction is allowed to proceed until it stops, the mechanical stability of the retained austenite decreases as the isothermal transformation temperature is increased. The mechanical stability was defined as the ratio of retained austenite content after 2% plastic deformation in a tensile test, to the original content. Given that the bainite reaction in such steels ceases when the carbon concentration of the residual austenite x_γ approaches x_{To}, and that x_{To} increases with decreasing temperature, the austenite on the basis of its composition is theoretically expected to be more stable as the bainite formation temperature is reduced (Bhadeshia and Edmonds, 1983a, b). Furthermore, if the T_o curve can be shifted to higher carbon concentrations by modifying the substitutional alloy content then the stability of the austenite is expected to increase, and this has also been confirmed experimentally.

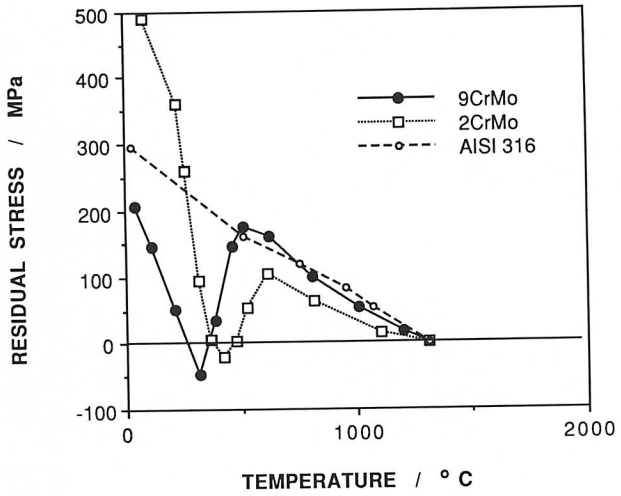

Fig. 8.12 *Plot of residual stress versus temperature for a martensitic (9CrMo), bainitic (2CrMo) and austenitic steel (AISI 316). (After Alberry and Jones.)*

8.7 Transformation under Constraint: Residual Stresses

Residual stresses are mostly introduced unintentionally during fabrication. They are of particular importance in welded structures which as a consequence become susceptible to hydrogen embrittlement and other detrimental phenomena. Jones and Alberry (1977a, b) conducted a series of experiments to illustrate the role of transformations in steels, on the development of residual stress. Using bainitic, martensitic and stable austenitic steels, they demonstrated that transformation plasticity during the cooling of a uniaxially constrained sample from the austenite phase field, acts to relieve the build up of thermal stress as the sample cools. By contrast, the non-transforming austenitic steel exhibited a continuous increase in residual stress with decreasing temperature, consistent with the degree of thermal contraction. On the other hand, with the steels which transformed to bainite or martensite, the transformation strain compensated for any thermal contraction strains that arose during cooling. Significant residual stresses were therefore found to develop only after transformation was completed, and the specimens approached ambient temperature (Fig. 8.12).

The interpretation of experimental data of the kind illustrated in Fig. 8.12 is very difficult. The predominant view amongst those involved in residual stress calculations, that the volume change during transformation gives the major contribution to transformation plasticity is almost certainly incorrect for displacive transformations such as bainite. The

shape change due to transformation has a shear component which is much larger than the dilatational term. Admittedly, this shear component should on average cancel out in a fine grained polycrystalline sample containing plates in many orientations. However, the very nature of the stress effect is to favour the formation of selected variants in which case, the shear component rapidly begins to dominate the transformation plasticity.

8.8 Anisotropic Strain due to Transformation Plasticity

During their attempts to study the isothermal transformation of austenite using dilatometry, Davenport and Bain (1930) had already noticed that 'the volume change (due to transformation) is not necessarily uniformly reflected in linear change in all dimensions'. They even found that the thickness of flat disc specimens actually decreased as the volume increased! These results were stated without interpretation; recent work has demonstrated that in polycrystalline samples which are crystallographically textured, anisotropic transformation plasticity can be detected even in the absence of an applied stress (Bhadeshia *et al.*, 1991). When an unstressed polycrystalline sample of austenite is transformed, the shear components of the individual shape deformations of the large

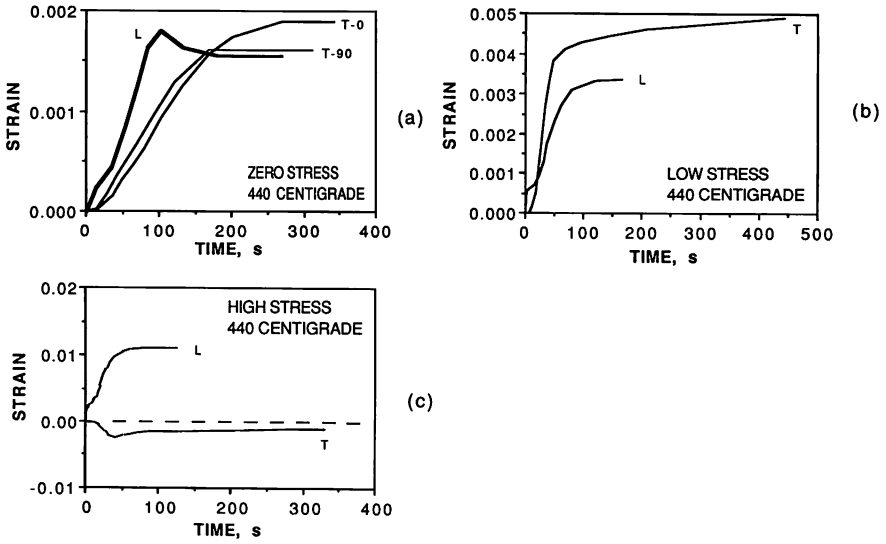

Fig. 8.13 *Dilatometric curves showing the dimensional changes during transformation to bainite in a cylindrical sample. T–0 and T–90 refer to the strains monitored along orthogonal transverse directions, and L to the strain along the longitudinal direction. (a) Transformation in the absence of an applied stress; (b) transformation under the influence of a tensile stress of about 45 MPa. (c) 90 MPa. (Bhadeshia et al.*, 1991).

number of variants which form along any dimension should tend to cancel out on a macroscopic scale. Similarly, the dilatational component of the IPS shape deformation should tend to average out so that the volume expansion appears to be isotropic. Transformation plasticity (the major component of which comes from the large shear strain of the IPS) should not therefore appear in a random polycrystalline sample, and furthermore, the volume change would be reflected in a constant expansion along any direction. If on the other hand, the sample is not random, i.e. it is crystallographically textured, then the possibility of the individual shape deformations cancelling out over large distances is correspondingly reduced. Transformation will then lead to anisotropic strains even in the absence of any applied stress (Fig. 8.13).

8.9 Summary

There is little doubt that the bainite reaction is significantly influenced by both externally applied stress, and any generated internally by prior transformation or heat treatment. This interaction with stress is related uniquely to the displacive mechanism of transformation, and the associated invariant plane strain shape deformation with its large shear component. As an example, the stress assisted transformation can lead to anisotropic dimensional changes whose magnitudes and senses are impossible to explain on the assumption of a reconstructive transformation mechanism. Transformation plasticity is readily detected during the growth of bainite under the influence of stress, the magnitude of the observed effect being far in excess of that expected from volume change criteria alone.

There is considerable circumstantial evidence that the response of bainite to stress is similar to that of martensite. The bainite start temperature is raised by the application of a tensile stress, lowered by hydrostatic compression, and there exists a B_d temperature beyond which bainitic reaction will not occur whatever the magnitude of the stress. The microstructure of bainite responds to the applied stress, with clear evidence that certain crystallographic variants are favoured by the stress. Consequently, the number of different sheaves per austenite grain decreases, leading to the formation of large packets of parallel sheaves, a microstructure which might be detrimental to toughness. Much research remains to be done in order to establish the criteria determining variant selection during stress influenced transformation. Bainite also shows characteristics similar to those associated with the mechanical stabilisation of martensite, when the austenite is deformed prior to the growth of bainite.

The bainite reaction is found to accelerate under the influence of stress; whether this is predominantly a consequence or enhanced nucleation or

growth remains to be resolved. The extent to which the rate of reaction is accelerated increases with the rate of application of stress. On the other hand, heavy deformation of austenite prior to transformation causes mechanical stabilisation, another phenomenon associated uniquely with displacive transformations.

The primary effect on microstructure during transformation under stress is that of variant selection, which at low stresses reduces the number of sheaves per austenite grain. Variant selection does not lead to an obviously aligned microstructure until larger stresses are applied, in which case the sheaves probably form on habit plane variants which are most parallel to the planes of maximum shear stress. Although deviations from the random microstructures that form in the absence of applied stress are often not easily detectable, especially at low stresses, they reveal themselves unambiguously in the form of anisotropic dimensional changes during transformation.

The response of bainitic transformation to stress is therefore essentially similar to that of martensite, although there are some important exceptions related to the fact that bainite forms at higher temperatures. The lower yield stresses of both the parent and product phases then make irreversible processes such as plastic deformation by lattice dislocations or the partitioning of carbon, much more probable during the course of the transformation. This rules out the possibility of conservatively reversing the motion of the interface by reversing the stress, so that phenomena like shape memory effects or rubber elasticity are extremely unlikely with bainite.

9 *Reverse Transformation from Bainite to Austenite*

Most commercial processes rely to some extent on heat treatments which cause the steel to revert into the austenitic condition. This includes the processes involved in the manufacture of wrought steels, and in the fabrication of steel components by welding. It is consequently quite important to study the process of austenite formation in low alloy steels, especially given the increasing tendency of steel manufacturers and users to rely on microstructure and property prediction models. Phase transformation theory plays a key role in such models.

The reverse transformation of low temperature ferrite into austenite differs in many ways from the more usual case where the parent phase, which is stable at elevated temperatures, transforms on cooling below the equilibrium temperature. This is highlighted by an examination of the temperature dependence of the reaction kinetics for the two cases. The vast majority of transformations exhibit classical C curve kinetic behaviour, in which the overall transformation rate goes through a peak as a function of supercooling below the equilibrium temperature. This can be interpreted to be a consequence of two opposing effects; diffusion coefficients decrease with temperature, whereas the driving force for transformation increases as the undercooling increases. The kinetics of austenite growth from ferrite on the other hand, depend on the degree of *superheating* above an equilibrium transformation temperature. Both the diffusion coefficient and the driving force increase with superheating, so that the overall rate of transformation rises indefinitely as the temperature is raised, Fig. 9.1.

This kinetic behaviour leads to several interesting effects. It is a common feature of reconstructive transformations that they can be suppressed by cooling rapidly into a temperature regime where the rate of transformation becomes unreasonably small, when compared with the time scale of the experiment or the service life of the component concerned. Hence,

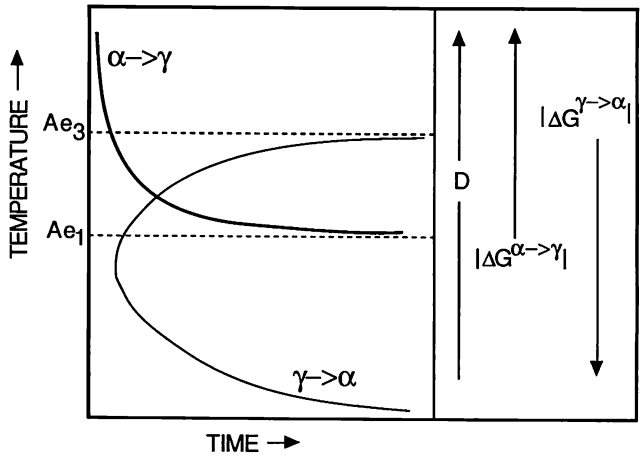

Fig. 9.1 *The TTT curves for the γ→α reaction, and for the reverse α→γ transformation.*

austenite can in many steels (e.g., 18/8 stainless steel) be retained by rapid cooling, even though it ceases to the thermodynamically stable phase at ambient temperature. It should be impossible to similarly retain the ferrite phase to high temperatures in the γ-phase field during a heating experiment, since atomic mobility always increases with temperature.

In steels which are lightly alloyed, rapid cooling from the austenite phase field does not always lead to the retention of the austenite. The austenite instead decomposes by a mechanism which does not require diffusion (martensitic). When the α→γ transformation occurs during heating, the temperatures involved are usually high enough to permit the rapid reconstructive transformation. It is therefore rare for the austenite to grow by a martensitic mechanism.

In compendiums of time–temperature transformation TTT diagrams for steel, the kinetics of austenite decomposition are usually presented as a function of alloy chemistry and the amount of austenite grain surface per unit volume (i.e. the austenite grain size). The number of variables to be considered when presenting similar data for the reverse transformation to austenite is much larger, since the initial microstructure can vary widely. It may consist of a mixture of any of the usual transformation products of austenite. The degree of sophistication with which it is necessary to specify the characteristics of the starting microstructure remains to be determined but factors such as particle size, the distribution and chemistry of individual phases, homogeneity of the microstructure, the presence of nonmetallic inclusions, etc. should all be important.

There are two particular examples where a detailed knowledge of austenitisation could be exploited to considerable advantage. During fusion welding, an optimum microstructure is required immediately after deposition from the liquid state. The luxury of homogenisation or other thermomechanical treatments is simply not available or practical. The welding process itself dissipates heat into the surrounding metal, with regions in the immediate proximity to the fusion surface being heated to very high temperatures, high enough to cause austenitisation. There is considerable interest in the development of computer models for the physical metallurgy of welded joints. A lack of knowledge and detail about the reaustenitisation process currently prevents the development of such models. Another example where austenitisation theory could be usefully applied is in the development of new wrought steels (Fe–Ni–Ti), where attempts are being made to utilise microstructures which have only been on partially austenitised.

There is clearly a lot of work to be done on all aspects of the formation of austenite, but the discussion in this chapter is confined to the austenitisation of bainitic microstructures.

9.1 Heating a Mixture of Austenite and Upper Bainitic Ferrite

When an iron–carbon alloy is heated to a temperature within the $\alpha+\gamma$ phase field until equilibrium is established between allotriomorphic ferrite and austenite, a small rise or fall in temperature leads to the growth or

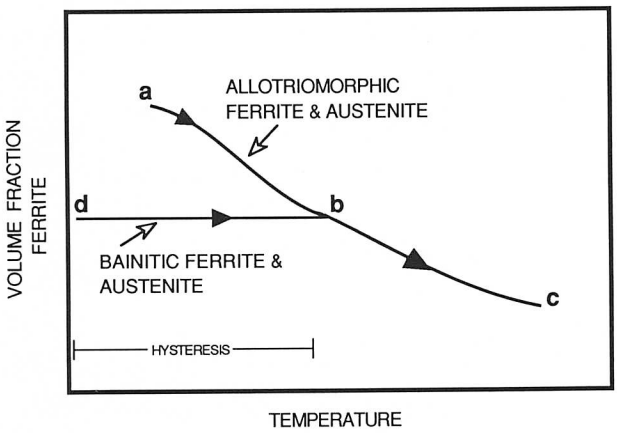

Fig. 9.2 *The growth of austenite when mixtures of ferrite and austenite are heated. An equilibrium mixture of allotriomorphic ferrite and austenite begins to transform immediately the temperature is raised, whereas a large hysteresis is apparent when a mixture of bainitic ferrite and austenite is heated.*

dissolution respectively, of the austenite, until the volume fractions once again satisfy the lever rule (Tsuzaki *et al.*, 1988). The transformation of austenite into allotriomorphic ferrite is in this sense reversible, and exhibits little or no hysteresis. On the other hand, for martensite in steels, a large difference is found between the M_S obtained during quenching, and the austenite start temperatue (A_S) recorded during heating. This is because the martensite tempers (or autotempers) and because its growth involves the dissipation of some work in the form of irreversible plastic deformation. A large hysteresis effect is also found experimentally when a mixture of bainitic ferrite and austenite is heated (Fig. 9.2).

If carbides precipitate from the austenite during the bainite reaction then a considerable hysteresis is expected during the reverse transformation, since the process would require the nucleation of austenite. On the other hand, a large hysteresis effect is not expected if reverse transformation begins from an *equilibrium* mixture of bainitic ferrite and austenite. But bainitic ferrite is never in equilibrium with the residual austenite at any temperature below B_S. Any increase in temperature cannot therefore cause an immediate reversal of transformation.

The problem can be investigated in steels with transform to bainite without any precipitation of carbides. The microstructure obtained by isothermal transformation below B_S is then a mixture of bainitic ferrite and carbon enriched residual austenite. The mixture can be heated to an isothermal austenitisation temperature where the austenite can grow without there being a need to nucleate it Fig. 9.3.[1]

Experiments like these have shown that the austenite in low alloy steels grows by a reconstructive process, and that there is a large difference between the B_S and A_S (austenite start) temperatures. In fact, austenite growth only begins with the Ae_3 temperature of the *residual austenite* is reached. The degree of austenitisation then increases from zero at the A_S temperature, at 100% at the austenite-finish or A_f temperature, which is the Ae_3 temperature of the alloy as a whole. If bainite was simply the product of equilibrium or paraequilibrium transformation then by analogy with allotriomorphic ferrite, a rise in temperature above the

1 This idea has been verified experimentally for bainite in specific alloys by Yang and Bhadeshia (1989b). It is not generally true that there is no need for austenite to nucleate when a mixture of austenite and ferrite is heated to a temperature where the ferrite to austenite transformation becomes thermodynamically possible. The experiments of Kessler and Pitsch (1965) showed that when a mixture of martensite and retained austenite in an interstitial free alloy was heated, the plates of martensite did not shrink by the backwards movement of the austenite/martensite interface, but new, small plates of austenite grew within each of the original martensite plates.

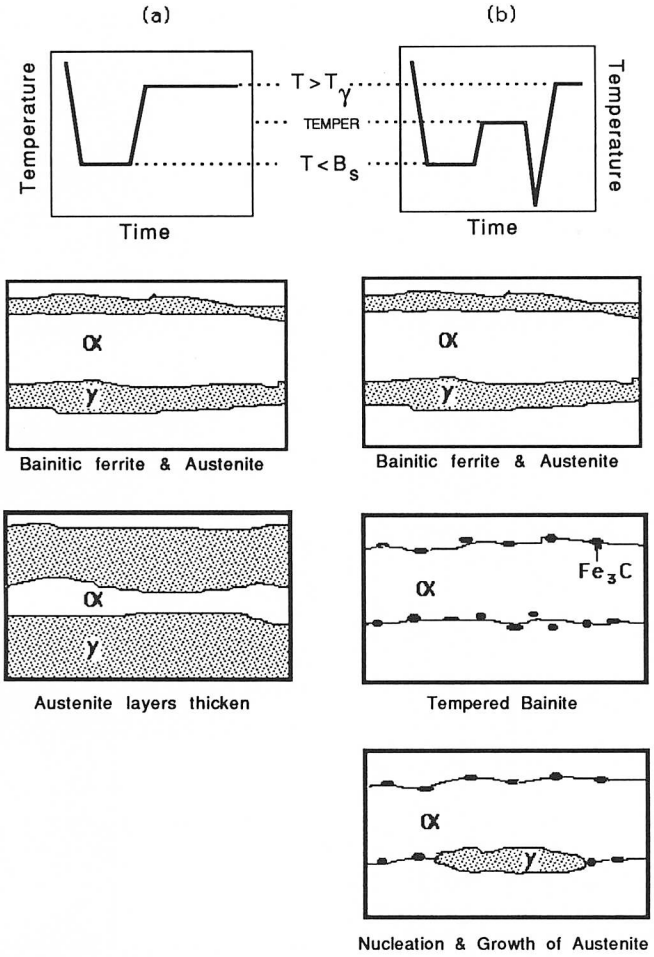

Fig. 9.3 *(a) The mixture of bainitic ferrite and austenite is generated by isothermal transformation at a temperature below B_s; this microstructure is then reheated to an elevated temperature in an experiment designed to allow the growth of austenite to be studied. (b) In this, an intermediate tempering treatment is included to remove any austenite left untransformed after bainite formation. Reheating to an elevated temperature then requires the austenite to nucleate before it can grow.*

isothermal transformation temperature should lead immediately to a reversal of reaction with little hysteresis.

The observed austenitisation behaviour can be understood as follows (Yang and Bhadeshia, 1987, 1988). When carbide precipitation can be avoided, bainitic transformation stops when the carbon concentration of the residual austenite reaches the T_o' curve of the phase diagram

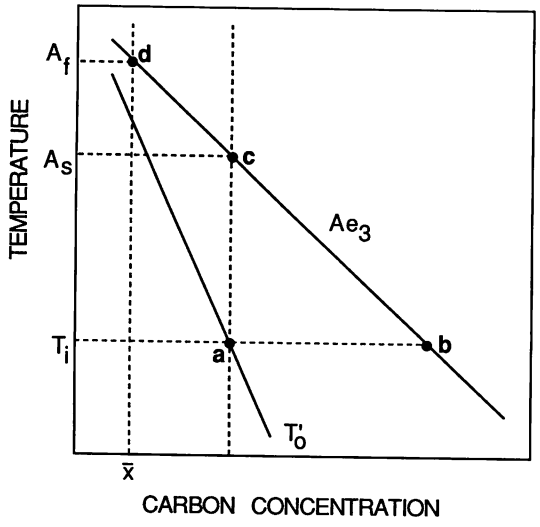

Fig. 9.4 *Schematic phase diagram illustrating the theory for austenite growth when the initial microstructure is a mixture of bainitic ferrite and carbon enriched residual austenite.*

(Fig. 9.4). It follows that the carbon concentration x_γ^I of the austenite when the formation of bainitic ferrite ceases at T_i, is given by

$$x_\gamma^I = x_{T_0'}\{T_i\} \tag{9.1}$$

as indicated by the point **a** in Fig. 9.4. Furthermore, we note that

$$x_\gamma^I << x_{Ae_3}\{T_i\} \tag{9.2}$$

where $x_{Ae_3}\{T_i\}$ is marked **b** in Fig. 9.4.

Thus, although the formation of *bainite* ceases at T_i, because the carbon content of austenite is far less than the equilibrium concentration (i.e., $x_\gamma^I << x_{Ae_3}\{T\}$), the driving force for austenite to transform by a *reconstructive* mechanism to ferrite is still negative. This remains the case until the temperature T is high enough (i.e., $T=A_S$) to satisfy the equation

$$x_\gamma^I = x_{Ae_3}\{A_S\} \tag{9.3}$$

Hence, austenitisation will first occur at a temperature A_S, as indicated by the point **c** in Fig. 9.4, and as observed experimentally. This is a consequence of the mechanism of the bainite reaction, which does not allow the transformation to reach completion. If this were not the case, then the lever rule demands that the temperature need only be raised infinitesimally above T_i in order for the reverse $\alpha \rightarrow \gamma$ transformation to be thermodynamically possible.

The theory predicts that at any temperature T_γ greater than A_S, the $\alpha_b \rightarrow \gamma$ transformation should cease as soon as the residual austenite carbon concentration (initially x_γ^I) reaches the Ae_3 curve, i.e., when

$$x_\gamma = x_{Ae_3}\{T_\gamma\} \tag{9.4}$$

The equilibrium volume fraction of austenite at the temperature T_γ, is then given by

$$V_\gamma\{T_\gamma\} = \bar{x}/x_{Ae_3}\{T_\gamma\} \tag{9.5}$$

assuming that the carbon concentration of ferrite is negligible and that $x_{Ae_3}\{T_\gamma\} > \bar{x}$. When $x_{Ae_3}\{T_\gamma\} = \bar{x}$, the alloy eventually becomes fully austenitic (point **d**, Fig. 9.4), and if this condition is satisfied at $T_\gamma = A_f$, then for all $T_\gamma > A_f$, the alloy transforms completely to austenite.

This model explains why the degree of $\alpha_b \rightarrow \gamma$ transformation increases from zero at A_S (the Ae_3 temperature of the *residual austenite*) to 100% at A_f (the Ae_3 temperature of the alloy as a whole). The behaviour is a direct reflection of the fact that the carbon concentration of the residual austenite after the bainite reaction has ceased is far below equilibrium. This in turn povides further support for the incomplete reaction phenomenon and its implication that the growth of bainite is diffusionless. Finally, it should be noted that the model discussed above assumes that the carbon concentrations of both phases are uniform at all stages.

9.1.1 *One-Dimensional growth from a mixture of austenite and bainitic ferrite*

As discussed earlier, when austenitisation is from a starting microstructure which is mixture of ferrite and austenite, the transformation kinetics are relatively easy to interpret since austenite nucleation need not be considered.

Since both bainite and acicular ferrite are in the form of thin plates, the movement of the planar austenite/ferrite interfaces can, during the early stages of reverse transformation, be modelled in terms of one-dimensional growth, assuming for simplicity that the growth is diffusion controlled. All the redistribution of carbon must occur within the austenite during its growth, since the quantity of carbon in the ferrite is by comparison negligible. Microanalysis experiments have demonstrated that the austenitisation process in low alloy steels can involve the diffusion of substitutional solutes during austenite growth (Yang and Bhadeshia, 1987, 1988, 1989b). The extent of the substitutional solute partitioning is known to decrease with an increase in the transformation temperature T_γ (and hence, the driving force), although the data reported are of insufficient spatial resolution to enable the identification of the compositions at the transformation interface. It could be assumed that local equilibrium exists at the interface for low T_γ, with a tendency towards zero bulk partitioning, (i.e., negligible partitioning

local equilibrium or paraequilibrium) as T_γ increases to beyond the Ae_3 temperature of the alloy concerned. This makes a full analysis difficult since there exist an infinite set of possibilities, between the limits of local equilibrium and paraequilibrium, that the system might choose to adopt as a function of transformation temperature. With the theory currently available, the compositions of the phases at the interface could not then be deduced.

If local equilibrium is achieved at least approximately at the transformation interface, then the growth rate calculated assuming carbon diffusion controlled motion of the γ/α interface, using the equilibrium carbon concentrations may give a good guide to the factors influencing the kinetics of transformation. This forms the basis of the model presented below, and amounts to assuming that the effect of substitutional solute gradients in influencing the flux of carbon is zero (Kirkaldy, 1958). There is a further implicit assumption that the tie line (of the equilibrium phase diagram) which determines the interface compositions passes through the bulk composition of the alloy. This is unlikely in substitutionally alloyed steels (Hillert, 1953; Kirkaldy, 1958; Purdy *et al.*, 1964; Coates, 1973a, b), but might nevertheless be a good approximation for dilute alloys. Finally, any effects due to soft impingement (overlap of diffusion fields) are not included in the analysis.

One-dimensional diffusion controlled growth leads to a parabolic thickening of layers of austenite trapped between the bainitic ferrite or acicular ferrite plates. The increase in the half-thickness of austenite can therefore be described as (see for example, Christian, 1975; Bhadeshia, 1985b)

$$q = \alpha_1 t^{1/2} \tag{9.6}$$

$$dq = 0.5\ \alpha_1 t^{-1/2}\ \ dt \tag{9.7}$$

where q is the increase in the half-thickness of the austenite layer, of starting thickness a_o, and α_1 is the one-dimensional parabolic thickening rate constant.

The geometry assumed for the thickening of austenite layers is based on the shape of the bainite or acicular ferrite plates. If c is the largest dimension of such a plate, idealised as a rectangular parallelepiped with sides of length a, b and c, with $c = b >> a$, then when both of the sides of a ferrite plate are penetrated by the growing austenite, the total area of the γ/α interface which advances into the plate of ferrite is $2c^2$. This reduces the thickness of the plate by $\Delta a/2$ from either side. If the minimum detectable change in volume fraction is ΔV_v, then it follows that

$$\Delta V_v = 2\, N_v c^2 \int_0^{\Delta a_m/2} dq \tag{9.8}$$

where N_v is the initial number of particles of austenite per unit volume, and Δa_m is the minimum detectable thickness increase. It follows that

$$\Delta V_v = 2\, N_v c^2 \int_0^{\tau} 0.5\, \alpha_1 t^{-1/2}\, dt \tag{9.9}$$

where τ is the time taken to achieve the minimum detectable degree of transformation. After integration, equation (9.9) becomes

$$\Delta V_v = 2\, \alpha_1 N_v\, c^2 \tau^{1/2} \tag{9.10}$$

so that

$$\tau = [\Delta V_v / (2\, \alpha_1 N_v\, c^2)]^2 \tag{9.11}$$

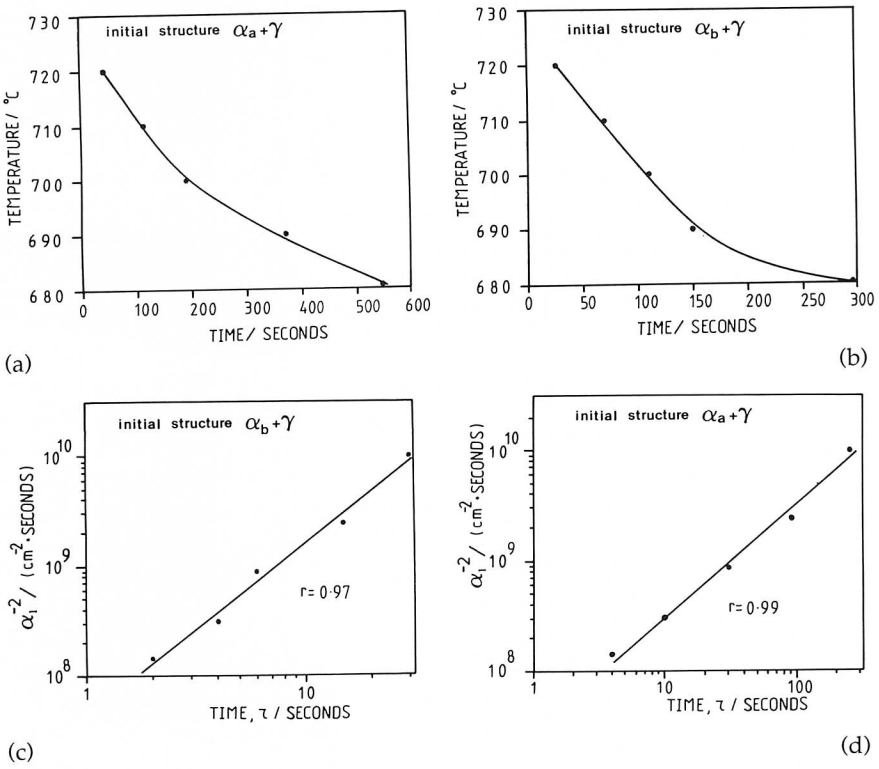

Fig. 9.5 *(a) TTT diagrams for the growth of austenite from equivalent mixtures of bainitic ferrite/austenite, and acicular ferrite/austenite. (b) Illustration of the linear relationship between the time* τ *taken for a constant volume fraction of austenite growth, versus* $(\alpha_1)^{-2}$*, where* α_1 *is the one-dimensional parabolic thickening rate constant for austenite growth (Yang and Bhadeshia, 1989b).*

However

$$2N_v c^2 = S_v = 2 \,/\, \bar{L}_3$$

so that

$$\tau = [\Delta V_v / (\alpha_1 S_v)]^2 \tag{9.12}$$

where S_v is surface area of γ/α boundary per unit volume, and $1/\bar{L}_3$ is the mean number of intercepts of γ/α boundary per unit length of test line (DeHoff and Rhines, 1968). It is clear from equation (9.12) that the value of τ is dependent not only on the parabolic rate constant α_1 but also the surface area of γ/α interface per unit volume S_v for a specific amount of austenitisation.

For the same starting microstructure and a fixed degree of transformation, τ should decrease rapidly as the isothermal austenitisation temperature increases, due to the concomitant increase in α_1. The analysis also indicates that the morphology of the starting microstructure will effect τ, because S_v must depend on the detailed nature of the initial microstructure. This explains experimental observations of the different rates at which mixtures of (α_b+γ) and (α_a+γ) austenitise (Fig. 9.5a). The distribution of plates in an acicular ferrite microstructure is such that S_v is smaller than that of a bainitic microstructure, so that it austenitises at a slower rate. The analysis also shows that for a given quantity of austenitisation, and a fixed initial microstructure, τ is proportional to $(\alpha_1)^{-2}$, and this relationship has been verified experimentally (Fig. 9.5c).

9.12.1 Estimation of the Parabolic Thickening Rate Constant

The parabolic rate constant α_1 can be deduced by analogy with already existing theory for the $\gamma \rightarrow \alpha$ transformation (Zener, 1949; Dubé, 1948; Bhadeshia, 1985). Fig. 9.6 shows the carbon concentration profiles in α and γ before and during austenite growth. The austenite must become more dilute in carbon as it grows, the rate of interface motion being determined by the diffusion of carbon in the austenite behind the interface. In Fig. 9.6, the term x_γ^I is the carbon concentration in the austenite before the start of austenitisation; it is given by $x_\gamma^I = x_{T_o^{\gamma}}$. The carbon concentration of γ at the γ/α interface during austenitisation is $x^{\gamma\alpha}$, and the carbon concentration of γ far away from the interface remains x_γ^I. It is assumed that the carbon concentration of α remains the same, $x^{\alpha\gamma}$, before and during austenitisation. The coordinate z is defined to lie along the normal to the γ/α interface.

During austenitisation the flux of carbon in the austenite, towards the γ/α interface, at the position of interface can be expressed as

$$J = -D\{x^{\gamma\alpha}\}\,(\partial x / \partial Z) \tag{9.13}$$

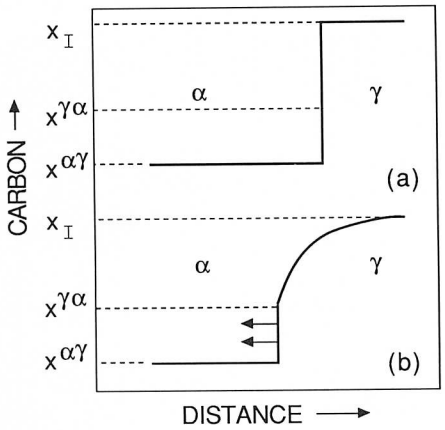

Fig. 9.6 *The distribution of carbon, (a) before austenitisation from a mixture of bainitic ferrite and austenite, and (b) during austenite growth.*

The rate at which the carbon concentration of austenite is diluted can then be written as

$$R_d = V_d\,(x_\gamma^I - x^{\alpha\gamma}) \tag{9.14}$$

where V_d is the velocity of interface (the diffusion field velocity).

Given that the position of Z the interface along the coordinate z is defined by the equation

$$Z = \alpha_1 t^{1/2},$$

it follows that

$$V_d = dZ/dt = 0.5\,\alpha_1 t^{-1/2} \tag{9.15}$$

Consequently, the rate at which the carbon concentration of austenite is diluted is given by

$$R_d = 0.5\,\alpha_1 t^{-1/2}(x^{\mathrm{I}}{}_\gamma - x^{\alpha\gamma}) \tag{9.16}$$

Making the approximation that the concentration dependence of the carbon diffusivity can be accounted for by replacing the diffusion coefficient by its weighted average diffusivity $\overline{D}$, conservation of mass at the interface requires that

$$0.5\alpha_1 t^{-1/2}(x^{\mathrm{I}}{}_\gamma - x^{\alpha\gamma}) = -\overline{D}/\partial x/\partial Z\,|_{z=Z} \tag{9.17}$$

where z is the coordinate normal to the interface plane and Z is the position of the interface along the coordinate z. The concentration gradient $(\partial x/\partial z)$ in equation (9.17) is evaluated at the position of the interface, i.e. at $z=Z$. Equation (9.17) simply states that the rate of dilution of the austenite, per

unit of time, equals the carbon flux towards the γ/α interface. From Fick's laws, the differential equation for the matrix is given by

$$\partial x/\partial t = \partial(\overline{D}\,\partial x/\partial Z)/\partial Z \tag{9.18}$$

subject to the boundary condition $x = x^{\gamma\alpha}$ at $z = Z\{t\}$, and $x = x_\gamma^I$ at $t = 0$, and equation (5.17). It can be solved (Zener, 1949; Dubé, 1948; Atkinson, 1967; Bhadeshia, 1985) to give an implicit relation for α_1 as a solution of the form

$$f_1 = (x_\gamma^I - x^{\gamma\alpha})/(x_\gamma^I - x^{\alpha\gamma}) = H_1\{\overline{D}\} \tag{9.19}$$

where

$$H_1\{\overline{D}\} = (0.25\pi/\overline{D})^{0.5}\,\alpha_1\,\mathrm{erfc}\{0.5\,\alpha_1/(\overline{D}^{0.5})\}\,\exp\{\alpha_1^2/4\overline{D}\} \tag{9.20}$$

9.2 Anisothermal Transformation

Heat treatments are rarely isothermal in commercial practice so that it becomes necessary to consider the nucleation and growth of austenite during continuous heating treatments. It should in principle be possible to approximately derive the continuous heating transformation behaviour from time–temperature transformation diagrams for austenitisation. For example, the continuous heating curve could be treated as a series of small isothermal steps, each occurring at a successively higher temperature, with a time interval t_i associated with each step (where i is the subscript identifying the step number). If the time necessary to reach a specified increment of transformation is written as τ_i for the isothermal transformation temperature T_i, then the simplest approximation is to assume Scheil's rule. In this, the specified increment of transformation is achieved during continuous heating when the sum

$$\sum_{i=1}^{n} t_i/\tau_i = 1 \tag{9.21}$$

As discussed earlier, the adoption of this additivity rule carries with it the assumption that the reaction concerned in isokinetic (Avrami, 1939), whence the fraction transformed at a fixed temperature is dependent only on the time and on a single function of temperature. This is unlikely to be true except in special cases where for example, nucleation is stifled by site saturation. The problem has not been studied in any detail for austenitisation.

9.3 Heating a Mixture of Cementite and Bainitic Ferrite

The earliest reported work on austenisation from bainite containing cementite seems to be that of Nehrenberg (1950); the morphology of

austenite which grew from high temperature transformation products, such as pearlite, was found to be approximately equiaxed in shape. On the other hand, the austenite particles formed by the transformation of martensite or bainite, were in the form of layers which grew between the ferrite plates, along the plate grain boundaries. Some more recent research contradicts these results; during the austenitisation of a Fe–1V–0.2 wt% carbon steel martensite and bainite as the starting microstructure, the austenite was found to nucleate and grow predominantly at the prior austenite grain boundaries (Law and Edmonds, 1980). The reasons for these differences are not understood, but may have something to do with retained austenite in the starting microstructure, as discussed below. An alternative explanation could be that the experiments were done at different degrees of superheat, large superheats permitting nucleation to occur at reasonable rates at all sites, whereas low superheats favouring nucleation predominantly at the high energy prior austenite grain boundaries. The work on the vanadium steel also indicated that the nucleation rate of austenite tends to decrease as the starting microstructure is changed from martensite to bainite, or from bainite to allotriomorphic ferrite.

Whether the austenite grows in an equiaxed or an acicular morphology is of practical importance, not because of the detailed difference in morphology, but because when it grows in the form of layers between ferrite plates, the steel is found to exhibit a *memory effect*. In the memory effect, the original austenite grain structure is regenerated when the transformation is completed, both with respect to shape and crystallography (Sadovskii, 1956; Kimmins and Gooch, 1983). When the memory effect operates, the austenite grain structure cannot be refined by repeated cycling into the austenite phase field followed by transformation. This can be a disadvantage in many commercial applications. The creep ductility of bainitic and martensitic steels of the type used in the power generation industry is improved by grain refinement (Kimmins and Gooch, 1983).[2] The memory effect prevents the achievement of a fine austenite grain structure even when the austenitising temperature used is relatively low.

The memory effect has been shown to be a direct consequence of the existence of retained austenite in the starting bainitic or martensitic microstructure (Kimmins and Gooch, 1983). The austenitisation heat treatment causes the films of austenite to grow, and those originating from the same prior austenite grain then coalesce to regenerate the original austenite grain structure. In these circumstances, the austenitisation process does not require the nucleation of new austenite grains, although if the

2 Note that creep in these materials, for typical circumstances, is not controlled by grain boundary diffusion or sliding.

superheating is large enough, then the nucleation of new grains may follow in adition to the growth of the retained austenite.

The memory effect vanishes if the bainitic microstructure is first annealed at a sufficiently high temperature to remove the retained austenite, and then reheated into the austenite phase field. Furthermore, the austenite then grows with an equiaxed morphology. These results are consistent with other experiments on the reverse transformation of heavily tempered bainite (i.e., not containing any residual austenite), in which, allotriomorphs of austenite were found to nucleate at the prior austenite grain boundaries during austenitisation heat treatments (Wada and Eldis, 1982).

Any austenite present in the initial microstructure may decompose during heating to the austenitisation temperature, so that slow heating from ambient temperature also destroys the memory effect. Very rapid heating to the austentisation temperature can reduce the memory effect by inducing the nucleation of new austenite grains (Kimmins and Gooch, 1983).

It is interesting to note that the memory effect does not exist when the starting microstructure is allotriomorphic ferrite (Kimmins and Gooch, 1983). This is probably because the ferrite allotriomorphs usually grow into both the adjacent austenite grains, thereby destroying the prior austenite grain structure. With martensite and bainite, the plate growth is restricted entirely to the grain in which they nucleate, so that there exist sharp discontinuities in crystallographic orientation at the position of the prior austenite grain boundaries. Indeed, it is for this reason that the prior austenite grain boundaries are good sites for the nucleation of new grains of austenite when the initial microstructure is bainitic or martensitic. If the steel contains residual impurities such as arsenic, phosphorus or tin, which tend to segregate to the prior austenite grain boundaries, then the memory effect is enhanced (Kimmins and Gooch, 1983), presumably because the segregation reduces the grain boundary energy, thereby making heterogeneous nucleation less likely.

There are some additional aspects of the austentisation of tempered bainitic microstructures in alloy steels which need further investigation. Wada and Eldis (1982) have pointed out the large variations in the reported Ac_1 temperatures for Fe–Cr–Mo–C alloys of nominally similar compositions and heat treatments. In their experiments, microstructures of bainitic ferrite and carbides obtained by tempering a steel at different temperatures, were found to exhibit significantly different Ac_1 temperatures for the same heating rate. Unfortunately, the initial microstructures were not characterised; it is likely that the carbide type and distribution was influenced by the different tempering treatments. Indeed, the interpretation of the dilatometric experiments needs to be studied carefully,

since it is possible that carbide transitions might lead to the same kind of dimensional change as is associated with austenite growth (Wada and Eldis, 1982).

9.4 Summary

The current knowledge of the transformation of bainite into austenite during elevated temperature heat treatment, although not very advanced, is of importance in two respects. It forms the basis for further research essential to the modelling of microstructural development in steels, and it provides important clues on the mechanism of bainitic transformation and of solid state phase changes in general.

The simplest experiments have dealt with the growth of austenite from an initial microstructure of bainitic ferrite and carbon enriched residual austenite. They demonstrate that unlike allotriomorphic ferrite, there is

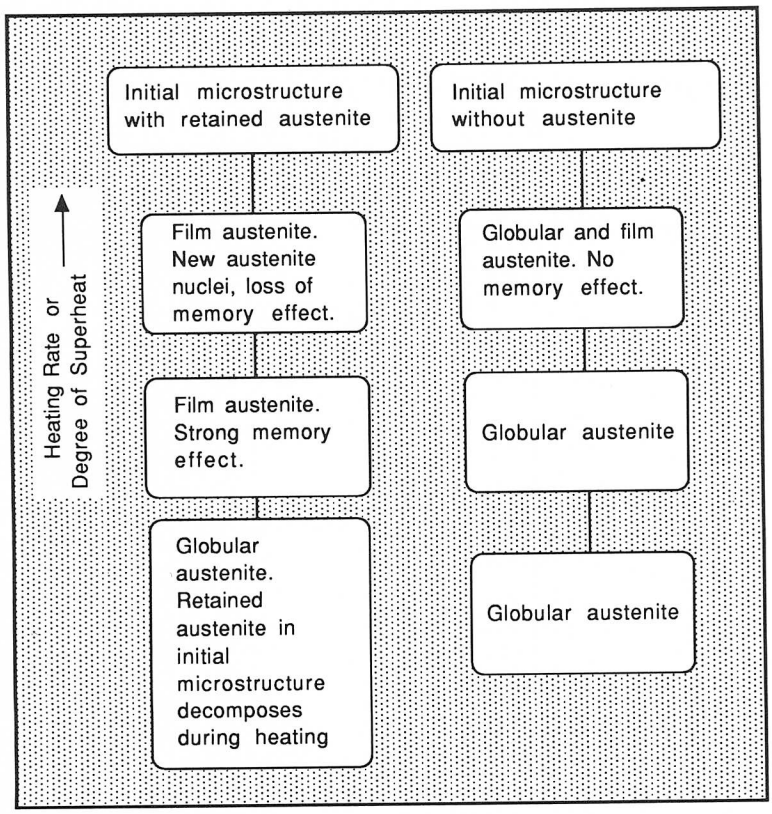

Fig. 9.7 *Summary of the effects of heating rate and starting microstructure on the morphology of austenite and on the tendency for a memory effect.*

a large temperature hysteresis before austenite growth commences during heating, a consequence of the fact that the composition of the austenite at the completion of bainitic transformation is far from equilibrium (or paraequilibrium).

The nucleation of austenite from bainitic microstructures which are free of retained austenite, is favoured at the prior austenite grain boundaries, rather than at the ferrite plate boundaries. Transformation at large driving forces enables the austenite to form even at the less potent plate boundary sites. When nucleation is absent, and the retained austenite grows during elevated temperature heat treatment, the original austenite grain structure is regenerated, giving the so-called memory effect. This memory can be destroyed by tempering prior to austenitisation. Alternatively, the memory effect may be absent even in samples containing retained austenite, if the austenite decomposes during slow heating to the austenitisation temperature (Fig. 9.7).

For low alloy steels which are not very rapidly heated (this includes most commercial steels and processes), the austenite grows by a reconstructive mechanism with diffusion of substitutional solutes. The extent of substitutional solute partitioning decreases with the superheat above the equilibrium transformation temperature, but cannot as yet be predicted theoretically.

10 *Acicular Ferrite*

10.1 General Characteristics and Morphology

'Acicular ferrite' (α_a, Fig. 10.1) is a phase most commonly observed due to the transformation of austenite during the cooling of low alloy steel arc weld deposits (see for example, the recent reviews by Grong and Matlock, 1986; Abson and Pargeter, 1986). It is also found in wrought steels which have deliberately been inoculated with nonmetallic inclusions. Acicular ferrite is of considerable commercial importance because it provides a tough and strong microstructure. It forms at relatively low temperatures, in a range where diffusion and reconstructive transformations are sluggish, and where the transformation mechanism tends to be displacive.

The term *acicular* means shaped and pointed like a needle. Indeed, the shape of acicular ferrite is sometimes stated to be rod-like, but there is in fact no evidence to support this. In two-dimensional sections, the acicular ferrite always appears like a section of a plate rather than that of a rod. Hence it is now generally recognised that the ferrite particles have in three-dimensions the morphology of thin, lenticular plates. The true aspect ratio of such plates has never been measured but in random planar sections, they are typically about 10 μm long and approximately 1 μm wide, so that the true aspect ratio is likely to be much smaller than 0.1.

An arc weld deposit typically contains some 10^{-18} m^{-3} inclusions of a size greater than 0.05 μm, distributed throughout the microstructure, although there is a tendency for some of the larger particles to be pushed towards and consequently trapped along the solidification-cell boundaries during the advance of the solid/liquid interface (Sugden and Bhadeshia, 1988). The mean particle size of the inclusions important in influencing the microstructure is of the order of 0.4 μm. It is the interaction of the liquid weld metal with any surrounding gases, together with the use of strong deoxidising elements such as silicon, aluminium and

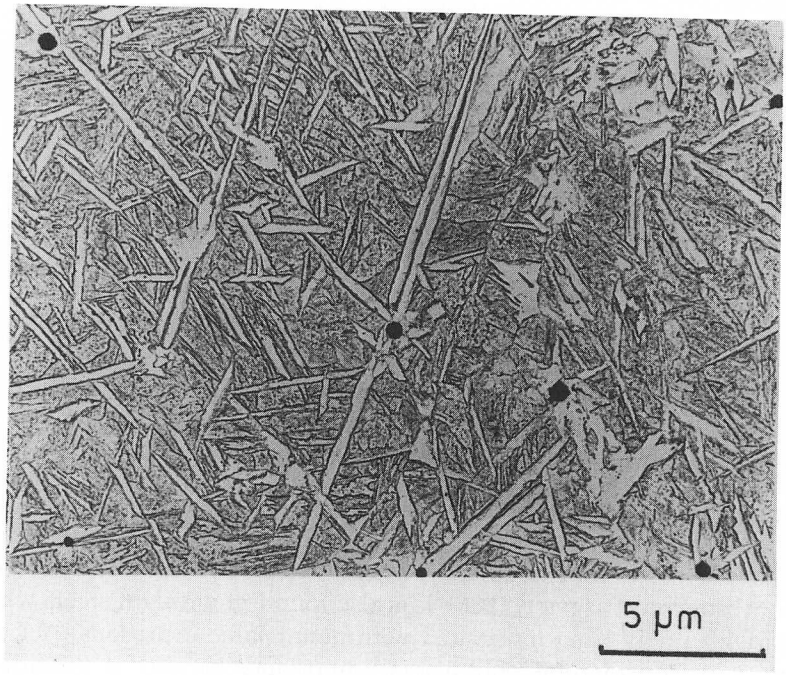

Fig. 10.1 *Replica transmission electron micrograph of acicular ferrite plates in a steel weld deposit. (After Barritte, 1982).*

titanium, together with protective slag forming compounds which causes the entrapment of complex multiphase nonmetallic inclusions (Fig. 10.2) in the solid at the advancing δ-ferrite/liquid interface. The inclusions have two major effects on the steel: they serve the desirable role of promoting the intragranular nucleation of acicular ferrite plates, leading to an improvement in toughness without a loss of strength, but they also are responsible for the nucleation of voids during ductile fracture, or the nucleation of cleavage cracks during brittle fracture. Achieving a proper balance between these conflicting factors is very difficult without a basic understanding of the mechanisms controlling these interactions. The microstructure of the *inclusions* is particularly important from the point of view of developing a clear understanding of its role in stimulating the nucleation of ferrite. As an example, it has been reported that the nonmetallic particles found in some submerged arc weld deposits consist of titanium nitride cores, surrounded by a glassy phase containing manganese, silicon and aluminium oxides, with a thin layer of manganese sulphide (and possibly, titanium oxide) partly covering the surface of the inclusions (Barbaro *et al.*, 1988). This detailed sequence of inclusion

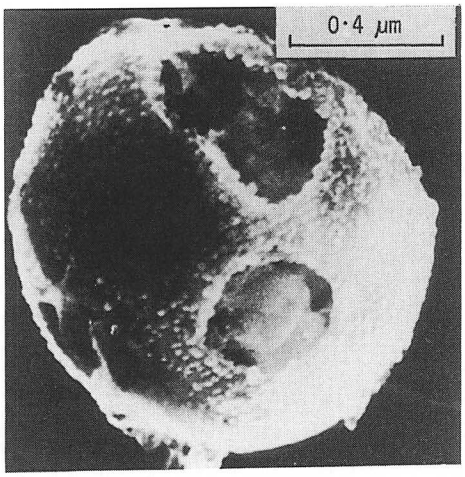

Fig. 10.2 *Scanning transmission electron micrograph of a nonmetallic inclusion in a steel weld metal. The inclusion surface is very irregular, and it features many phases. (Barritte, 1982).*

formation is not understood and seems to contradict (admittedly simplistic) thermodynamic arguments. For example, titanium oxide is supposed to be thermodynamically more stable than titanium nitride, and yet the latter is the first to grow from the liquid phase.

The inclusions may therefore be oxides or other compounds but they can in some circumstances influence the subsequent development of microstructure during cooling of the weld deposit. Acicular ferrite plates, during the early stages of transformation nucleate on inclusions present in the large columnar austenite grains which are typical of weld deposits (Ito and Nakanishi, 1976). The formation of a plate on an inclusion may stimulate others to nucleate autocatalytically, so that a one–to–one correspondence between the number of active inclusions and the number of acicular ferrite plates is not expected (Ricks *et al.*, 1982).

The shape change accompanying the growth of α_a has been characterised qualitatively as an invariant plane strain (Fig. 10.3). The transformation occurs at relatively high temperatures where the ferrite and austenite are weak. The shape change is therefore plastically accommodated, generating dislocations in the process. These are the dislocations which give acicular ferrite its large dislocation density, typically at 10^{14} m^{-2}, contributing approximately 145 MPa to its strength. Other measurements indicate that the stored energy of acicular ferrite is, like bainite, about 400 J mol^{-1} (Strangwood and Bhadeshia, 1987; Yang and Bhadeshia, 1987). Consistent with the observed surface relief effect, microanalysis experiments indicate that there is no bulk partitioning of substitutional alloying elements during

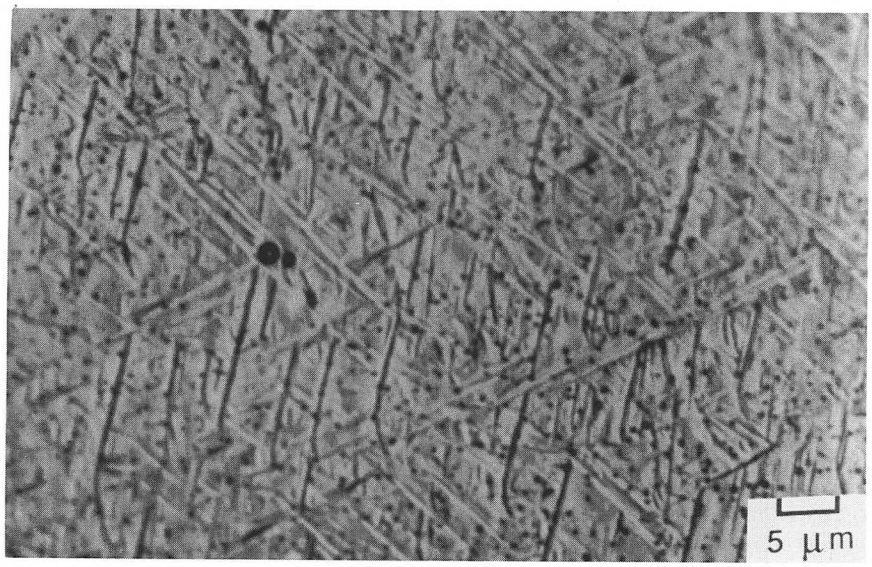

Fig. 10.3 *Nomarski interference contrast micrograph from a surface relief experiment in which a sample was metallographically polished and then transformed to acicular ferrite in an inert protective atmosphere (Strangwood and Bhadeshia, 1987).*

the formation of acicular ferrite (Strangwood, 1987). However, work of a higher spatial and chemical resolution is needed to verify the absence of local effects in the vicinity of the transformation interface.

Plates of acicular ferrite have never been found to cross austenite grain surfaces. The orientation relationship between acicular ferrite and the austenite grain in which it grows is *always* found to be one in which a close packed plane of the austenite is (within the limits of experimental error) parallel or nearly parallel to the most densely packed plane of α_a. Corresponding close packed directions within these planes are found to be within a few degrees of each other (Strangwood and Bhadeshia, 1987).

There is indirect evidence, that like bainite, the size of the acicular ferrite plates increases with transformation temperature. For example, in a series of welds containing substantial quantities of acicular ferrite, Horii *et al.* (1988) found that the apparent plate thickness changed from about 1 to 2μm as the weld heat input was increased (i.e., the cooling rate was decreased). The apparent plate lengths were also observed to increase with welding heat input. Since the measurements reported do not represent the true (stereologically sound) dimensions of the plates, it is not clear whether the observations indicate any changes in plate aspect ratio. The results could be further complicated by possible variations in the austenite grain size with heat input.

10.2 Mechanism of Growth

The acicular ferrite transformation exhibits the incomplete reaction phenomenon, an important characteristic of bainite. The degree of reaction tends towards zero as the transformation temperature rises towards the B_S temperature (Yang and Bhadeshia, 1987; Strangwood and Bhadeshia, 1987). At a given temperature, the transformation stops as the residual austenite carbon concentration x_γ reaches the T'_o curve. The evidence all indicates that the growth of acicular ferrite is diffusionless, with carbon partitioning into austenite after the transformation event.

The experimental data to date indicate that acicular ferrite is essentially intragranularly nucleated bainite. Consistent with this, Ito *et al.* (1982) have shown that as the oxygen concentration (related to the inclusion content) of a weld is increased, a microstructure containing bainite is replaced by one containing acicular ferrite. The detailed morphology of acicular ferrite differs from that of conventional bainite because the former nucleates intragranularly at inclusions within large austenite grains whereas in wrought steels which are relatively free of non-metallic inclusions, bainite nucleates initially at γ/γ grain surfaces and continues growth by the repeated formation of sub-units, to generate the classical sheaf morphology typical of bainite (Yang and Bhadeshia, 1986). Acicular ferrite does not normally grow in sheaves because the development of sheaves is stifled by hard impingment between plates nucleated independently at adjacent sites (Yang and Bhadeshia, 1986). Indeed, conventional bainite or acicular ferrite can be obtained under identical isothermal

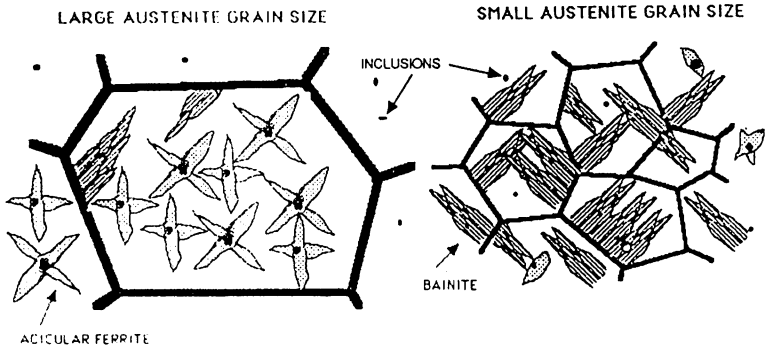

Fig. 10.4 *The effect of austenite grain size in determining whether the microstructure is predominantly acicular ferrite or bainite. A small grain sized sample has a relatively large number density of grain boundary nucleation sites and hence bainite dominates the microstructure, whereas a relatively large number density of intragranular nucleation sites leads to a microstructure consisting predominantly of acicular ferrite.*

transformation conditions in the same (inclusion rich) steel. To generate bainite, the austenite grain size has to be small in order to ensure that most of the nucleation events occur at the austenite grain surfaces. Subsequent growth then swamps the interiors of the austenite grains, preventing the development of acicular ferrite. When the austenite grain size is large, the number density of intragranular nucleation sites (inclusions) is relatively large, so that acicular ferrite is obtained in preference to bainite (Fig. 10.4).

There is in addition, a lot of circumstantial evidence which suggests that a reduction in austenite grain size leads to a replacement of acicular ferrite with bainite (e.g., Imagumbai *et al.*, 1985). When steels are welded, the austenite grains in the heat affected zone coarsen, the degree of coarsening depending on the amount of heat input during welding. It follows that when steels containing appropriate inclusions are welded, the amount of acicular ferrite that forms in the heat affected zone increases at the expense of bainite, as the heat input (and hence the austenite grain size) is increased (Fig. 10.5a). Eventually, at very large heat inputs, the cooling rate decreases so much that larger quantities of Widmanstätten ferrite are obtained and there is a corresponding reduction in the amount of acicular ferrite. Without the inclusions, the acicular ferrite content is always very small (Fig. 10.5b).

An interesting experiment which supports the hypothesis that acicular ferrite is simply intragranularly nucleated bainite, was carried out by Harrison and Farrar (1981). They demonstrated using a vacuum remelting technique that the removal of inclusions caused the formation of bainitic

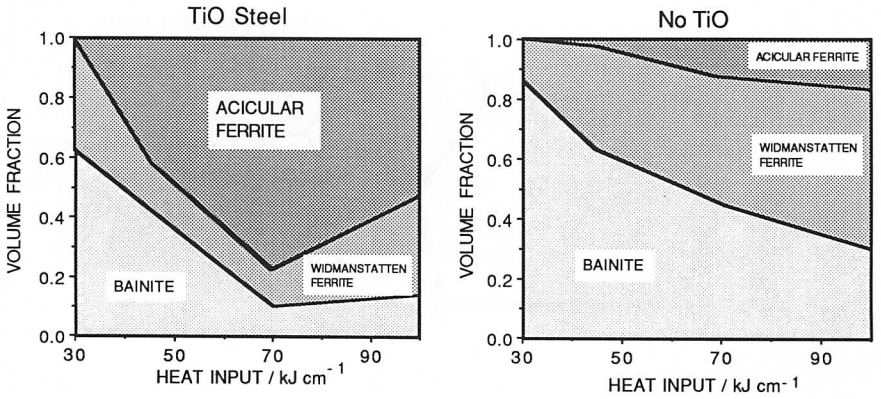

Fig. 10.5 *Changes in the microstructure of the heat affected zone of welds, as a function of the heat input during welding. (a) Steel containing titanium oxide particles. (b) Ordinary steel without inclusion inoculation. (After Chijiiwa* et al., *1988.)*

ferrite in a high hardenability reheated weld deposit which originally transformed to acicular ferrite under identical conditions of heat treatment. Consequently, the transition from acicular ferrite to bainite was in their experiments, induced by the removal of intragranular nucleation sites. The removal of the inclusions also led to a somewhat coarser austenite grain size during reheating; the fact that bainite was obtained in spite of the concomitant reduction in the austenite grain boundary nucleation sites, reinforces the point that inclusions are vital for the initiation of the acicular ferrite transformation. It is therefore clear why acicular ferrite is not usually obtained in the vast majority of wrought steels which are relatively free of inclusions. The fact that most traditional heat treatment practices aim to achieve a small austenite grain size also does not help.

Acicular ferrite is sometimes considered to be intragranularly nucleated Widmanstätten ferrite, on the basis of the observation of 'steps' at the transformation interface, which are taken to imply a ledge growth mechanism (Ricks *et al.*, 1982). A step mechanism is a mechanism for interfacial motion, and does not necessarily say much about the mechanism of transformation. Even martensite may grow by a coherent step mechanism (Christian and Edmonds, 1984). The observations are in any case rather weak; perturbations of various kinds can always be seen on transformation interfaces between ferrite and austenite. Such perturbations do not however necessarily imply a step mechanism of growth. Evidence that the residual austenite is enriched in carbon is sometimes quoted in support of the contention that α_a is Widmanstätten ferrite but as pointed out above, the enrichment can occur during or after the transformation event.

10.3 Nucleation and The Role of Inclusions

With the assumption that classical theory applies to the nucleation of acicular ferrite, it is established theoretically that inclusions are less effective in nucleating ferrite when compared with austenite grain surfaces (Ricks *et al.*, 1982). The essential reasons for this behaviour are firstly, that the inclusions present a convex curved interface in the austenite so that a larger amount of interfacial area has to be created between the nucleus and parent phase per unit volume of nucleus. The second reason is that the energy of the interface between the ferrite and the inclusion is likely to be larger than would be the case when ferrite nucleates on austenite grain surfaces. Both of these factors lead to a larger activation energy for nucleation. Experiments confirm that austenite grain boundaries are indeed more potent heterogeneous nucleation sites when compared with non-metallic inclusions, since ferrite formation first begins at the austenite grain boundaries, although it is notable that this ferrite is not *acicular* ferrite but allotriomorphic ferrite. Larger inclusions are expected to be

more effective as nucleants since the curvature of the inclusion/nucleus interface will then be reduced; this is again generally consistent with experimental observations. However, the tendency to quote a minimum particle size below which nucleation does not occur should be avoided. It is the *activation energy* for nucleation which increases as the inclusion size decreases. The activation energy also depends on other factors, such as the driving force for transformation. Thus, for a specific steel, the size below which inclusions cease to be significant nucleation sites must vary with transformation conditions.

Because of the complexity of the inclusions, and the difficulty in conducting controlled experiments with welds, the nucleation potency of inclusions is not clearly understood. A popular idea is that those inclusions which show the best 'lattice matching' with ferrite are most effective in nucleating the ferrite, and it has even been suggested that there may exist reproducible orientation relationships between inclusions and the ferrite plates that they nucleate (Mills *et al.*, 1987). The lattice matching is expressed in terms of a mean percentage planar misfit κ. To calculate κ, it is assumed that the inclusion is facetted on a plane $(hkl)_I$, and that the ferrite deposits epitaxially with its plane $(hkl)_\alpha \parallel (hkl)_I$, with the corresponding rational directions $[uvw]_I$ and $[uvw]_\alpha$ being inclined at an angle ϕ to each other. The interatomic spacings (d) along three such directions within the plane of epitaxy are examined to obtain (Bramfitt, 1970)

$$\kappa = (100/3) \sum_{j=1}^{3} | d_j^I \cos\phi - d_j^\alpha | \; / \; d_j^\alpha \qquad (10.1)$$

Data calculated in this manner, for a variety of inclusion phases, are presented in Table 10.1. A description of the relationship between two crystals with cubic lattices requires five degrees of freedom, three of which are needed to specify the relative orientation relationship, and a further two in order to identify the interface plane, i.e., the plane of contact between the two crystals. As far as the interface plane is concerned, Mills *et al.* considered nine different kinds of epitaxy, confined to planes of low crystallographic indices: {001}, {011} & {111}. The orientation relationships considered are listed in Table 10.1: the Bain orientation implies $\{100\}_\alpha \parallel \{100\}_I$ and $\langle 100\rangle_\alpha \parallel \langle 011\rangle_I$. The cube orientation occurs when the cell edges of the two crystals are parallel (i.e., they are in an identical orientation in space).

To enable the lattice matching concept to be compared with experiments, it is necessary not only to obtain the right orientation relationship, but the inclusion must also be faceted on the correct plane of epitaxy. Experiments however, demonstrate that the ferrite/inclusion orientation relationship tends to be random (Dowling *et al.*, 1986). The fact that the

Table 10.1 Some misfit values between different substrates and ferrite. The data are from a more detailed set published by Mills *et al.* (1987), and include all cases where the misfit is found to be less than 5%. The inclusions all have a cubic-F lattice and the ferrite is body centered cubic (cubic-I).

Inclusion	Orientation	Plane of Epitaxy	Misfit %
TiO	Bain	{100}	3.0
TiN	Bain	{100}	4.6
γ-alumina	Bain	{100}	3.2
Galaxite	Bain	{100}	1.8
CuS	Cube	{111}	2.8

inclusions, which form in the liquid steel, are randomly orientated in space, and that the orientation relationship of acicular ferrite with the parent austenite is always found to be of the KS/NW type, necessarily implies that the inclusion/ferrite orientation relation also has to be random (Fig. 10.6). A contrary view is due to Kluken *et al.* (1991), who claim that the δ-ferrite grains sometimes nucleate on inclusions in the melt. The acicular ferrite should then bear an orientation relationship with the inclusions since it will be related to the δ-ferrite via the austenite. Textural measurements have been cited in support of this hypothesis (Kluken *et al.*, 1990).

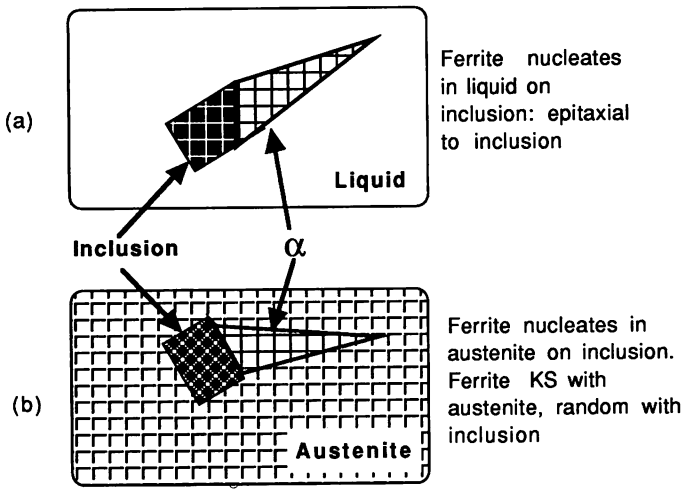

Fig. 10.6 *Schematic illustration of the orientation relationship that might develop between acicular ferrite and an inclusion. (a) When ferrite nucleates on an inclusion, with both phases surrounded by liquid, it is possible for the ferrite to adopt a favoured relationship to the inclusion since it is not limited by the liquid. (b) The inclusion is assumed to be randomly orientated to the austenite, since it nucleates in the liquid, whereas the austenite grows from the fusion boundary. Consequently, the acicular ferrite, which has a KS/NW type orientation relationship with the austenite, must also be randomly orientated to the inclusion.*

Table 10.2 List of ceramics which were found to be chemically active in experiments designed to test for ferrite nucleation at ceramic/steel diffusion bonds.

Chemically Active	Chemically Inactive
TiO_2	TiO, Ti_2O_3, TiC, TiB_2, TiN
$Al_2Si_2O_7$	Al_2O_3
MnO_2	MnO
SiC, Si	Si_3N_4, SiO_2
CoO, V_2O_5	ZrO_2, FeS, Y_2O_3

Other ways in which inclusions may assist the formation of acicular ferrite include stimulation by thermal strains, chemical heterogeneities in the vicinity of the inclusion/matrix interface, and the inclusions may act simply as inert sites for heterogeneous nucleation. Chemical reactions are also possible at the inclusion/matrix interface, as revealed by experiments in which pure ceramics were diffusion bonded to steels (Strangwood and Bhadeshia, 1988). The diffusion bonded composite samples were then subjected to heat treatments in which the steel transforms from austenite to ferrite. By comparing ferrite formation events at the ceramic/steel interface with those within the bulk of the steel, it was possible to identify the mechanism by which the ceramics influence ferrite nucleation. Chemical reactions, the details of which depended on the particular ceramic tested, were found to be powerful stimulants for ferrite nucleation (Table 10.2). Although these experiments reveal a possible mechanism for the interaction between nonmetallic particles and ferrite nucleation, only allotriomorphic ferrite (rather than acicular ferrite) could be studied because of the high alloy content of the steels used. The results may not therefore be directly applicable to weld deposits. For example, Ti_2O_3 is widely believed to be a good nucleant for acicular ferrite, but is found in the context of the diffusion bonding experiments to be chemically inert.

10.3.1 Aluminium and Titanium Oxides

While the theory capable of ranking different kinds of nonmetallic inclusions in terms of their effectiveness in nucleating acicular ferrite does not exist, there is considerable circumstantial evidence that titanium oxides (TiO, Ti_2O_3, TiO_2) are very potent in this respect, and that Al_2O_3 is not. Titanium nitride also appears to be effective in nucleating acicular ferrite, but is less stable at high temperatures when compared with Ti_2O_3. The problem is complicated by the fact that most welds, and indeed, wrought steels contain aluminium, which in general is a stronger oxide former than titanium. Consequently, it is the alumina which forms first from the

melt, followed by titania, which often forms as a thin coating on the alumina particles. Thus, there has to be sufficient oxygen available to first tie up the aluminium, and then to combine with the titanium (Horii *et al.*, 1986, 1988). The concentration of oxygen required therefore depends on the level of aluminium, which should be minimal in steels designated for acicular ferrite microstructures. This is the reason why Ringer *et al.* (1990) were unable to detect titanium oxides in titanium containing steels which had low oxygen concentrations and enough aluminium to combine with that oxygen.

In order to simplify the problem of oxide (or nitride) formation, it is usual to assume that the stronger oxide former is the first to react with oxygen, followed by the weaker oxide forming element using notions based on the free energy change accompanying the oxidation of the free element. This can lead to difficulties. As emphasised earlier, titanium oxide is supposed to be thermodynamically more stable than the titanium nitride, and yet the latter is often the first to form from the liquid phase

$$Ti + O_2 = TiO_2 \quad \Delta G^\circ = -920000 - 50.2T \text{ J mol}^{-1} \tag{10.2}$$

$$Ti + N = TiN \quad \Delta G^\circ = -340000 - 50.2T \text{ J mol}^{-1} \tag{10.3}$$

where ΔG° is the standard free energy of formation (Kubachewski and Evans, 1950).

These apparent contradictions could be attributed to kinetic effects, but they could also arise because the stabilities of the variety of oxides are assessed using free energy data which are standardised on reaction of each metallic element with one mole of oxygen, the oxide and the pure element having unit activities. It is unlikely that this method correctly represents the real situation where the activities of all the reactants and products are expected to be far from unity. The ranking of the oxides with respect to stability can change as a function of the actual concentrations of the reactants. Nevertheless, in the absence of any suitable model capable of predicting the reactivities of the variety of elements in liquid solution with oxygen, the best working hypothesis must assume that they react in accordance with an intuitive order of oxidising potential. For welds, this usually means that aluminium has the first 'bite' at the available oxygen, followed by titanium, as was assumed by Horii *et al.* (1988) in their study of submerged arc weld deposits.

As stated earlier, excessive aluminium can tie up the available oxygen and prevent the titanium from forming oxides. A further advantage of minimising the aluminium content is that lower oxygen concentration can then be used to achieve the same titanium effect, thereby reducing the inclusion content in the steel. Any free nitrogen, which may combine with the titanium to form a nitride, should also be controlled, perhaps by

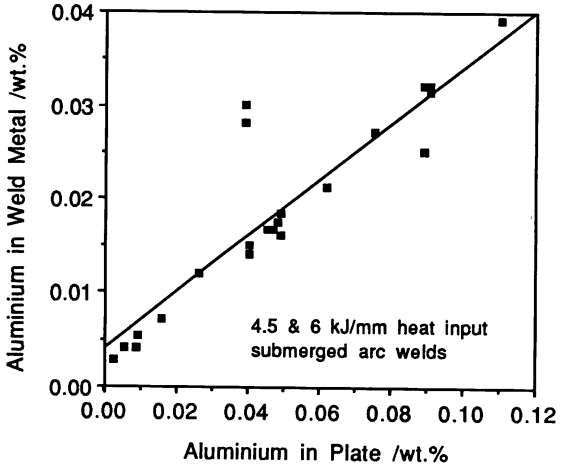

Fig. 10.7 *A plot of the aluminium concentration in the weld metal versus that in the steel, illustrating the incorporation of trace elements from the base plate into the weld fusion zone during high heat input welding (Horii* et al. *1988).*

adding boron as a nitrogen gettering agent. Their experiments also reveal that trace elements like calcium, and rare earth elements like cerium, at the concentrations used conventionally for inclusion shape control in wrought alloys, have no detectable influence on the development of the acicular ferrite microstructure (Horii *et al.*, 1986, 1988). Such elements may be incorporated from the fused base plate into the weld deposit, especially during high heat input welding which leads to considerable dilution effects (Fig. 10.7).

One difficulty as far as welds are concerned, is that the small amount of aluminium that remains in solid solution, as opposed to that which combines with oxygen, does not seem to correlate well with the total aluminium or oxygen concentration (Thewlis, 1989a, b). For reasons which are not clear, small concentrations of dissolved aluminium seem to promote the formation of Widmanstätten ferrite, which is a nuisance when attempts are being made to design microstructures which are essentially acicular ferrite. The effect manifests itself in the as-deposited microstructure of self-shielded arc welds (SSAW), which usually contain abnormally small volume fractions of acicular ferrite, but exaggerated quantities of Widmanstätten ferrite (Abson, 1987; Grong *et al.*, 1988). In The SSAW process, the pool has little or no protection against oxidation by any shielding gas; it is instead, deoxidised by aluminium powder present in the welding electrode. As a consequence, the deposit ends up with more than 0.5 wt% of aluminium and only about 120 p.p.m. of oxygen. The lack of acicular ferrite in such welds has been attributed to the low oxygen

concentration, but on the other hand, it is the Widmanstätten ferrite which forms first, leaving little untransformed austenite available for subsequent decomposition into acicular ferrite. The propensity to form Widmanstätten ferrite in self-shielded arc welds correlates with their large concentration of aluminium in solid solution.

A possible mechanism for the effect of aluminium in promoting Widmanstätten ferrite is as follows. A large concentration of soluble aluminium is only possible when the overall aluminium concentration is large, in which case the aluminium oxide will be in the form of γ-alumina particles instead of galaxite. They will not then be effective in nucleating acicular ferrite, so that grain boundary nucleated Widmanstätten ferrite can grow without hindrance.

It has been reported that the mean size of non-metallic inclusions in welds increases with the overall aluminium concentration (Thewlis, 1989a), but the observed variations are in fact rather small. Evans (1990) has demonstrated that very large changes in aluminium concentration at constant oxygen concentration causelnegligible variations in the mean inclusion diameter. The factors controlling inclusion size are not understood, and although inclusions are sometimes regarded as a panacea for improved weld microstructure, their ability to nucleate cleavage and ductile failure must also be appreciated. These contradicting requirements call for a compromise level of inclusions, but it seems likely that current weld deposits contain excessive oxygen concentrations, well beyond the levels needed to induce the intragranular nucleation of ferrite. For example, oxygen concentrations less than 120 p.p.m. are established to be adequate in producing an acicular ferrite microstructure in suitably alloyed wrought steels. The presence of inclusions surplus to requirements is likely to become a more prominent problem in the near future, as strength levels increase and toughness consequently becomes more sensitive to the presence of nonmetallic particles.

The character of inclusions alters as the aluminium concentration rises, the oxide particles being predominantly $MnOSi_2$ at low Al content, and then changing to a mixed (spinel) oxide (Al_2O_3MnO) and finally to γ-Al_2O_3 (Thewlis, 1990). It is believed that the aluminium to oxygen ratio should be such as to favour the formation of galaxite which has a good lattice match with ferrite (Table 10.1), although the ratio itself is difficult to estimate for multicomponent systems containing strong deoxidising elements other than aluminium.

10.3.2 Sulphur

It is sometimes argued that manganese sulphide (MnS) is a prerequisite for the intragranular nucleation of ferrite. It is in this respect, interesting

to examine a recent attempt (Ochi *et al.*, 1988) at inducing the intragranular nucleation of allotriomorphic ferrite using non-metallic inclusions. The steel concerned had a relatively high sulphur concentration (≈ 0.07 wt%) in order to precipitate a fine dispersion of MnS particles. A small vanadium addition (0.1 wt%) then led to the precipitation of vanadium nitride on the sulphides, nitrides which were shown to be the sites for the subsequent formation of vanadium carbides. The carbides were then demonstrated to provide the intragranular nucleation sites for ferrite

$$MnS \rightarrow VN \rightarrow V_4C_3 \rightarrow \alpha$$

This particular sequence of events has been thoroughly demonstrated by Ochi *et al.*, although the reason why vanadium carbide is effective in nucleating ferrite is not clear. Whether a similar sequence can be of use in nucleating acicular ferrite remains to be seen, although high levels of sulphur are usually not tolerated in steel weld deposits.

Yamamoto *et al.* (1987) claim that it is the MnS, which grows on the titanium oxide long after solidification, that is really responsible for the nucleation of acicular ferrite. Consistent with this, their microanalysis data indicated that the oxide particles usually contain about 10 wt% of manganese, and that the lack of sulphur (< 0.001 wt%) in the steel reduced the degree of acicular ferrite formation. A contradictory result has been reported by Chijiiwa *et al.* (1988), that a reduction of sulphur concentration from 0.005–0.001 wt% tends to decrease the amount of allotriomorphic ferrite and promote the formation of acicular ferrite. Ringer *et al.* (1990) also found that Ti_2O_3 particles without any surrounding MnS films can nevertheless be effective in the intragranular nucleation of ferrite. They also failed to detect any manganese depletion in the austenite near the particles. Following an assessment of the literature on inclusions in weld deposits, Abson (1987) concluded that the presence of MnS at the surface of oxide particles inhibits the nucleation of ferrite, and furthermore, that the addition of elements which getter sulphur makes the inclusions more effective. The work by Umemoto *et al.* (discussed in the chapter on Kinetics) indicates that small concentrations of sulphur can significantly enhance the nucleation of bainite.

There are clearly considerable difficulties in interpreting the experimental data, but the notion that manganese sulphide is potent in nucleating ferrite is attractive from a commercial point of view, because sulphur is in any case, a common impurity in steels. However, in normal circumstances, it precipitates in the solute enriched interdendritic regions of the solidification microstructure. These regions which are rich in manganese and hence have a relatively low tendency to transform to ferrite. The ability of any MnS to act as the heterogeneous nucleation site for ferrite is then reduced by the locally large concentration of austenite stabilising

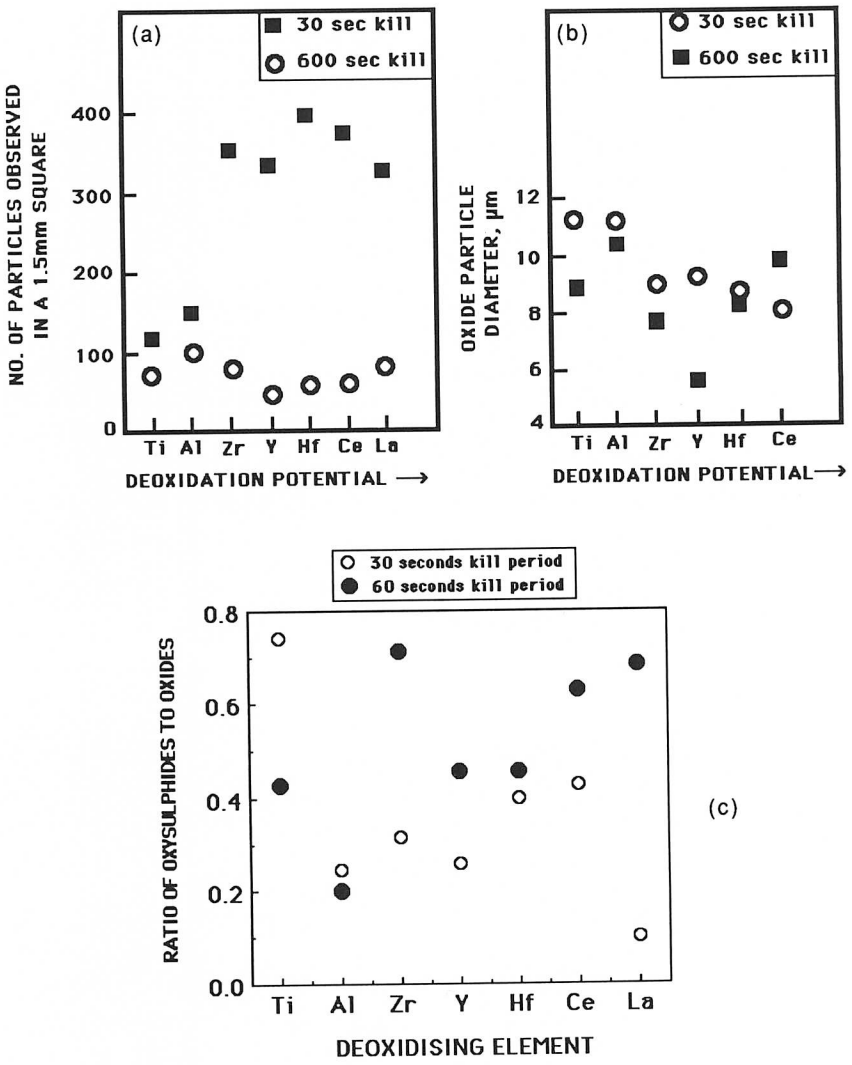

Fig. 10.8 *The effects of a variety of deoxidising elements on the nature of oxide and oxysulphide precipitation in steel (Ueshima* et al., *1989). (a) Number density of oxide particles; (b) size of oxide particles; (c) propensity of the oxide to stimulate the solid-state nucleation of sulphide.*

elements in the interdendritic regions. To overcome this dificulty, Ueshima *et al.* (1989) systematically studied methods of producing more uniform distributions of MnS particles, by inducing the sulphide to itself nucleate on oxide particles which form in the liquid phase and are trapped more or less uniformly by the advancing solidification front.

High purity melts, each containing 0.004 wt% of sulphur, were deoxidised using one of Al, Tn, Zr, La, Ce, Hf or Y. Of these, aluminium and titanium additions were found to be the most uniformly dispersed and insensitive to the killing time within the range 30–600 s (Fig. 10.8).[1] All of the deoxidising elements studied were able to promote MnS nucleation (Fig. 10.8), but Ti_2O_3 and zirconia were particularly effective, with aluminium being the least potent in this respect. The MnS precipitated during solid state transformation over a temperature range estimated to be 1050–1400°C. Whilst these results do not help resolve the role of sulphides in stimulating ferrite nucleation, they establish potential methods of controlling the sulphide size, distribution and precipitation. Ueshima *et al.* estimated, using diffusion theory, that the formation of MnS would lead to a manganese depleted zone in its close proximity, a zone in which the tendency to form ferrite would be enhanced. There are however, contradictory experimental data which suggest the absence of such zones (Barritte *et al.*, 1982). Direct confirmation of the role of sulphides as ferrite nucleating agents is now needed, but even if the role is found to be positive, great care will have to be exercised to avoid the potent grain boundary embrittling effect of sulphur.

10.3.3 Phosphorus

Phosphorus is another impurity element which is never knowingly added to steels because of its well known tendency to reduce the toughness of embrittling boundaries. Its concentration is usually kept below 50 p.p.m., but in welds its average concentration can be around 100 p.p.m. Solidification induced segregation can locally raise the concentration to approximately 500 p.p.m. Recent work by Grong and co-workers has indicated that such segregation can lead to kinetic effects which greatly influence the development of acicular ferrite microstructure in weld deposits (Kluken and Grong, 1989b; Kluken *et al.*, 1990).

The thermodynamic effect of phosphorus is to raise the Ae_3 temperature by about 460°C per wt%, over the concentration range of interest (Bastien, 1957), although the consequences of such a large effect are not for some reason, as powerful as they should be in comparison with the role of other elements on the Ae3 temperature (Kirkaldy *et al.*, 1962).

1 In 'killed' steel, the oxygen concentration in the molten steel is reduced by the addition of metallic elements which have a strong affinity for oxygen. The resulting oxides usually float off into the slag, although very fine particles are retained. The killing time is the interval between the addition of the deoxidising element and the solidification of the steel.

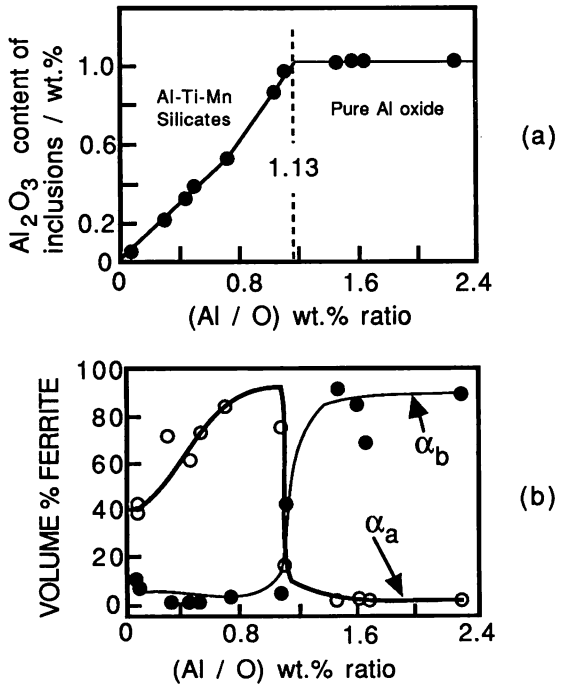

Fig. 10.9 *(a) Variation in the volume fraction of acicular ferrite as a function of the precipitated-Al to oxygen ratio; (b) variation in the inclusion chemistry with the same ratio.*

During weld solidification, the phosphorus segregates between the δ-ferrite dendrites and cells. When solidification is complete the δ-ferrite begins to transform to austenite (which nucleates heterogeneously at the δ/δ grain boundaries). Kluken and Grong suggest, that in these circumstances the austenite grain boundaries coincide with the phosphorus rich regions, and that for some reason this stimulates the formation of acicular ferrite. On the other hand, when the austenite grain boundaries do not coincide with the phosphorus rich regions, ferrite plates are supposed to grow from the grain boundaries and consume most of the austenite before the acicular ferrite has a chance to develop by intragranular nucleation and growth.

This hypothesis is then used to explain why the acicular ferrite content of welds decreases suddenly as the ratio of the precipitated aluminium to oxygen concentrations reaches a value of 1.13 (Fig. 10.9a). Beyond the limiting value, the nonmetallic inclusions become pure γ-alumina (Fig. 10.9b), and these are supposed to be very effective in stimulating the growth of austenite directly from the melt, ahead of the δ-ferrite/liquid

interface. Hence, the austenite grains, which now nucleate independently, have grain boundaries which are not coincident with those of the δ-ferrite (and the phosphorus rich regions), thereby leading to extensive Widmanstätten ferrite formation during subsequent cooling.

The hypothesis is inconsistent with the acknowledged role of phosphorus in raising the driving force for the transformation of austenite. If the austenite grain boundaries coincide with the phosphorus rich regions then grain boundary nucleated transformation products such as allotriomorphic and Widmanstätten ferrite and bainite would be favoured. A second difficulty is the assumption that the austenite grain boundaries coincide with those of δ-ferrite when the austenite does not nucleate directly from the melt, but at the δ/δ boundaries. It is well known that the temperature isotherms change position during cooling, so that the fastest growth direction of the austenite does not coincide with that of the δ-ferrite, and the grains in fact grow across the δ/δ boundaries (Dadian, 1987). The assumption that the austenite is restricted to the δ-ferrite crystal with which it has a reproducible orientation relationship is also incorrect since the δ–>γ transformation is reconstructive, and hence is not confined by the grain boundaries of the parent phase. In spite of these difficulties, the effect illustrated in Fig. 10.9 is remarkable and needs to be investigated further.

10.3.4 Nitrogen, Titanium and Boron

Nitrogen is not often a deliberate alloying addition to low alloy steels and weld deposits. It is picked up from the environment and from impurities in the consumables used in the manufacturing process. Although the concentration of nitrogen is generally kept rather low (about 20–120 p.p.m.) it is known to have a potent detrimental effect on the toughness of the steel. The mechanism of embrittlement is believed to be associated with strain age hardening and solid solution hardening effects, both of which increase the yield stress of the weld, and consequently cause a decrease in the toughness (Lancaster, 1986; Keown *et al.*, 1976; Judson and McKeown, 1982; Oldland, 1985).

The effect of nitrogen on the development of microstructure, especially in weld deposits, has until recently been difficult to understand, especially in the context of alloys containing titanium and boron. Some studies (Mori *et al.*, 1981) suggest that nitrogen has no detectable influence on the acicular ferrite content of welds, whereas others (Okabe *et al.*, 1983; Ito and Nakanishi, 1975) indicate significant changes on the introduction of nitrogen. Given that weld nitrogen concentrations are rarely out of the range 40–200 p.p.m., the nitrogen is hardly expected to have any significant thermodynamic effect on the stability of the parent and product

phases. Any effect must therefore largely be kinetic, perhaps via some interaction with the inclusion phases.

These contradictions have recently been resolved in a series of careful experiments by Horii *et al.* (1986, 1988) and Lau *et al.* (1987, 1988), who studied titanium/boron/nitrogen phenomena in submerged arc welds. Their conclusion is that without boron, nitrogen is not expected to influence the development of microstructure. Boron is added with the intentOon of improving hardenability, so that acicular ferrite is promoted at the expense of less desirable phases such as allotriomorphic and Widmanstätten ferrite. Titanium, which is a strong oxide and nitride forming element, has the function of protecting the boron from oxidation during transfer across the arc. It also prevents boron from combining with nitrogen to form boron nitride. Boron is only effective in improving hardenability if it remains in solid solution in the austenite, since it is a misfitting atom it segregates to the austenite grain surfaces. This reduces the austenite grain boundary energy thereby making the boundaries less potent heterogeneous ferrite nucleation sites. Boron in the form of nitrides or carbides at the austenite grain surfaces can in fact reduce hardenability since the particles seem to induce the nucleation of ferrite. An excess of soluble boron tends to combine with carbon to form boron carbides which are known to be detrimental towards toughness (Dan and Gunji, 1984; Habu, 1978).

It is now recognised that for a given oxygen and boron concentration, the aluminium and titanium concentration (and that of any other oxide former) has to be large enough to combine with all the available oxygen. Furthermore, there has to be enough titanium left over to combine with any nitrogen so as to leave the boron free to segregate to the austenite grain surfaces. If these conditions are not satisfied, then nitrogen renders the boron useless and causes a deterioration in microstructure.

A method for making rational decisions during the design of titanium and boron containing deposits could therefore be based on a methodology in which the oxidation reactions are phenomenologically carried out in a sequence consistent with the thermodynamic stability of the elements (Fig. 10.10). The difficulties of doing this are illustrated by the work of Kluken and Grong (1989a), whose ideas are reproduced below in a more explicit manner. The total volume fraction V_I of inclusions is given approximately by (Franklin, 1969)

$$V_I \approx 0.05 w_o + 0.054(w_S - w_S^{sol}) \tag{10.4}$$

where w_i represents the concentration of element 'i' in units of weight percent and w_S^{sol} the soluble sulphur concentration, usually assumed to be about 0.003 wt%. The mass fraction of the inclusions is then given by

$$m^I = V_I \rho_I / \rho_S \tag{10.5}$$

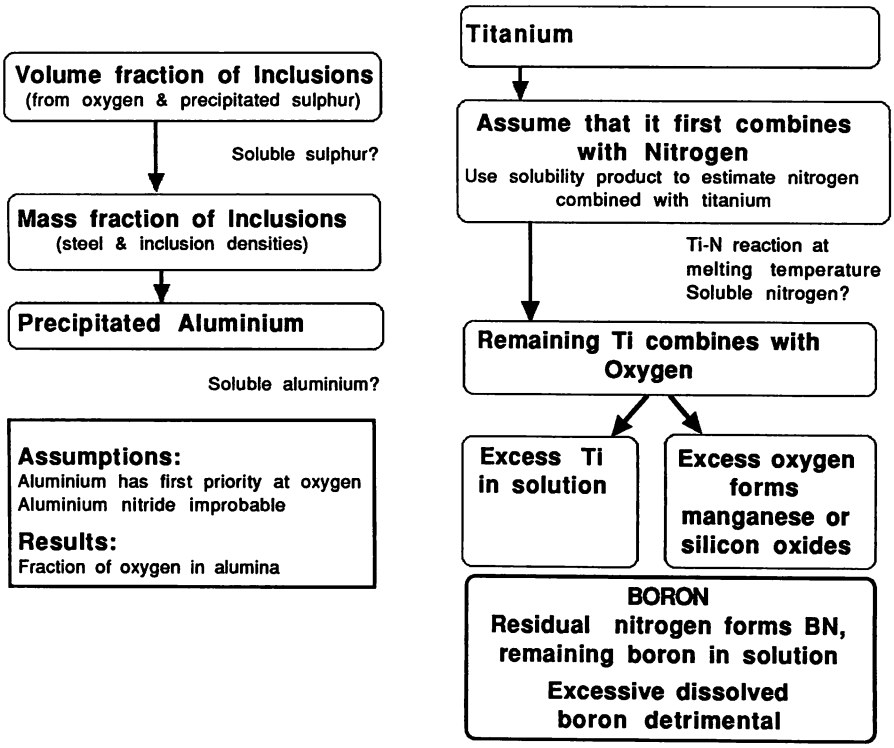

Fig. 10.10 *Flow charts illustrating the procedure for the estimation of inclusion microstructure. The assumptions and difficulties associated with the method are placed outside of the main boxes.*

where ρ_S and ρ_I are the steel and inclusion densities respectively (approximately 7.8 and 4.2 g cm^{-3} respectively). It follows then that the concentration of Al in the inclusions is given by

$$w_{Al}^{I} = (w_{Al}^{T} - w_{Al}^{sol})/m^{I} \tag{10.6}$$

where w_{Al}^{T} and w_{Al}^{sol} represent the total and soluble aluminium concentrations respectively. This relationship assumes that none of the aluminium is present in the form of aluminium nitride, an assumption which is known to be reasonable for most welds. The nitrides however, cause difficulties when considering the next stage in the calculation of inclusion composition, since titanium nitrides are well established to be present in many weld deposits. Lau *et al.* assumed that the titanium reacts first with oxygen, and that any residual titanium can then proceed to combine with nitrogen. In the absence of active oxygen, the amount of titanium present

as nitride can be estimated by first calculating the amount of nitrogen in solution using tried and tested solubility products (Matsuda and Okumura, 1978)

$$\log\{[w_{Ti}^{sol}][w_N^{sol}]\} = (8000/T) + 0.32 \tag{10.7}$$

assuming that the concentration of dissolved Ti is known. The temperature for which the calculation is done can to a good approximation be assumed to be close to the melting temperature of the steel. The quantity of titanium in the inclusion, present in the form of nitride (i.e. w_{Ti}^{I-N}), is then given by

$$w_{Ti}^{I-N} = A_{Ti}(w_N^T - w_N^{sol})/(m_I A_N) \tag{10.8}$$

where A_i represents the atomic weight of element 'i'. It follows then that the amount of titanium in the inclusions, tied up as oxide (i.e. w_{Ti}^{I-O}) is given by

$$w_{Ti}^{I-O} = (w_{Ti}^T - w_{Ti}^{IN}m^I - w_{Ti}^{sol})/m_I. \tag{10.9}$$

The amount of sulphur in the inclusion is calculated in a similar way

$$w_s^I = (w_s^T - w_s^{sol})/m^I. \tag{10.10}$$

Assuming that the sulphur is incorporated in the inclusion in the formm of manganese sulphide, the concentration of Mn in the inclusion as MnS is given by

$$w_{Mn}^{I-S} = A_{Mn}w_s^I/A_s. \tag{10.11}$$

The next step involving the calculation of the SiO_2 and MnO contents of the inclusion requires some assumption about the relative proportions of these two phases. If

$$\psi = \text{wt\% } SiO_2 \text{ / wt\% MnO} \tag{10.12}$$

and

$$\beta = [(A_{Mn}/A_o) + 1]\,\psi \,/\, \{[(A_{Si}/2A_o) + 1] + [(A_{Mn}/A_o) + 1]\psi\} \tag{10.13}$$

then

$$w_{Si}^I = \beta A_{Si}(w_o^T - m^I w_o^{I-A1} - m^I w_o^{I-Ti})/(2m^I A_o) \tag{10.14}$$

where w_o^{I-A1} and w_o^{I-Ti} are the concentrations of oxygen in the inclusion, tied up as alumina and titania respectively. It follows that

$$w_{Mn}^{I-O} = (1-\beta)\,A_{Mn}(w_o^T - m^I w_o^{I-A1} - m^I w_o^{I-Ti})/(m^I A_o) \tag{10.15}$$

The calculations presented above cannot be carried out wethout a knowledge of the Al, Ti and S concentrations in solid solution, and as already

pointed out, are subject to numerous approximations, including the implicit assumptions that the oxidation state of the titanium is known. Titanium compounds such as TiN, TiC and TiO have similar lattice parameters and crystal structures. Therefore, they are difficult to distinguish using diffraction methods. Common microanalytical techniques (such as energy dispersive X-ray analysis) clearly identify the presence of titanium, but unless windowless dectors are used, they cannot detect light elements such as oxygen. Even when oxygen is analysed, the results are difficult to quantify because absorption corrections for X-rays are difficult due to the shape and unknown thickness of the particles. The oxidation state of titanium, and the factors controlling it remains to be established. Lau *et al.* assumed that the Ti is in the form of TiO_2 whereas Kluken and Grong took it to be combined as Ti_2O_3. Abson (1987) on the other hand, assumes that in weld deposits, the titanium oxide is TiO. The major weakness, however, is the method for the partitioning of oxygen between the different metallic elements. It can for example, easily be demonstrated that manganese and silicon oxides are found in systems where no oxygen is expected to remain after combining with Al and Ti.

The sequence of reactions outlined above should in principle determine the microstructure of the inclusions, with the compounds which form first being located near to the cores of the particles (Fig. 10.11). Thus, the elements which are least reactive should be concentrated at the inclusion surface. This is consistent with the fact that the nonmetallic particles found in some submerged arc weld deposits consist of titanium nitride cores, surrounded by a glassy phase containing manganese, silicon and aluminium oxides, with a thin layer of manganese sulphide partly covering the surface of the inclusions (Barbaro *et al.*, 1988). Similarly, in a weld containing negligible quantities of aluminium or titanium (<5 p.p.m), the inclusion core was found to consist of $MnO–SiO_2$ whereas the addition of some 40 p.p.m. of aluminium led to the presence of some alumina in the core (Es-Souni and Beaven, 1990). On the other hand, both these investigations suggested that in welds containing titanium in addition to Al, Mn and Si, some titanium oxide (or other titanium compounds — the detailed chemistry could not be resolved) could be found at the particle surfaces, a result which is inconsistent with the strong deoxidising potential of titanium, and one which suggests that the titanium oxide formed at a late stage in the inclusion growth process. This conclusion seems unlikely; an alternative explanation is that the main body of the inclusions (consisting of manganese and silicon oxides) nucleates and grows on the titanium compound, but that the degree of wetting with the substrate is small so that the other oxides do not succeed in engulfing the titanium compounds.

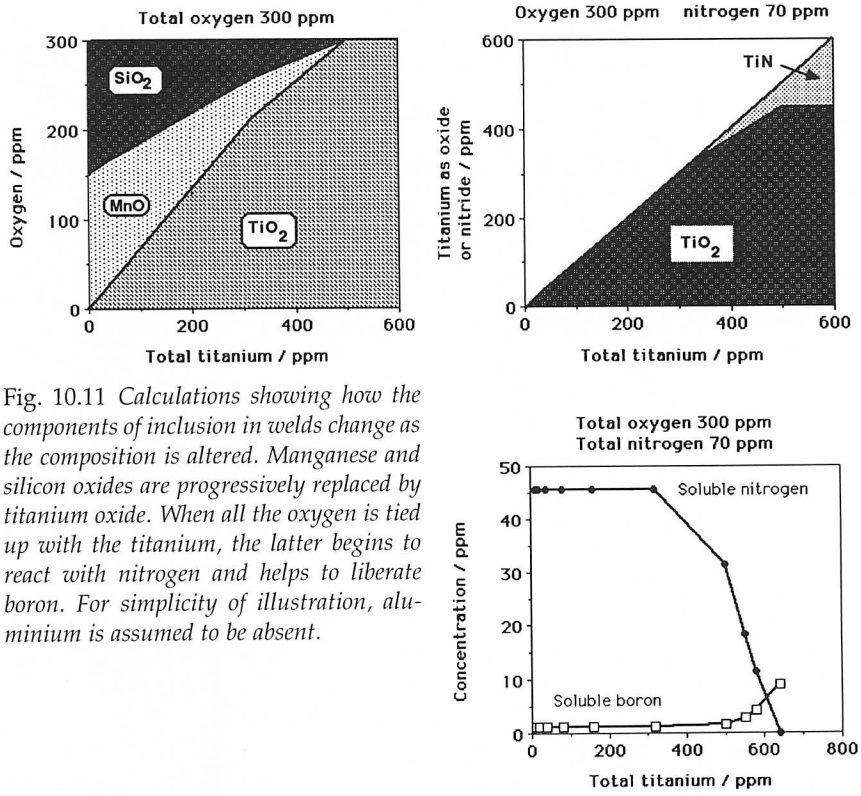

Fig. 10.11 *Calculations showing how the components of inclusion in welds change as the composition is altered. Manganese and silicon oxides are progressively replaced by titanium oxide. When all the oxygen is tied up with the titanium, the latter begins to react with nitrogen and helps to liberate boron. For simplicity of illustration, aluminium is assumed to be absent.*

10.3.5 Stereological Effects

Although the plates of acicular ferrite which form at the beginning of the transformation might be expected to nucleate heterogeneously on the nonmetallic inclusions, subsequent plates can form autocatalytically. As pointed out earlier, it follows that a one–to–one correspondence between plates of acicular ferrite and inclusions is not to be expected. However, it is difficult to establish this using metallography. By analogy with the procedure used by Chart *et al.* (1975) for aluminium alloys, if the volume of a typical plate of acicular ferrite is taken to be 10^{-16} m^3, and that of a spherical inclusion 4×10^{-20} m^3, then of all the grains examined, only 7.4% can be expected to display the nucleating particle. Furthermore, the intercept of the particle in the section concerned may be much smaller then its diameter. The calculation presented by Chart *et al.* is valid when the grains of the major phase are approximately spherical. It is necessary to allow for the anisotropy of shape in the case of acicular ferrite. If the acicular ferrite which contains an inclusion of radius r = 0.2 μm, is

assumed to be of the shape of a square plate of side 10 μm and thickness t = 1 μm, then the ratio of the mean linear intercepts of the two phases is given by $4r/6t$ (Myers, 1953; Mack, 1956). This means that about 13% of all plates observed may be expected to show the nucleating particles, assuming that the entire section of the acicular ferrite plate is observed in the sample.

The calculation also assumes that each plate contains just one inclusion, and more importantly, that each observed inclusion is responsible for nucleating the plate in which it is found (i.e., it has not been incorporated accidentally into the plate during the growth process). If the volume fraction of acicular ferrite in the sample examined is large then it is not safe to assume that the observation of a particle in the plate implies that the particle is a nucleating centre. Recent work by Barbaro *et al.* (1989) claims that many of the acicular ferrite plates nucleate autocatalytically, since the number of nucleating inclusions in any acicular ferrite 'colony' was found to be less than the number of plates in that colony. The conclusion is however not safe since the percentage of plates containing inclusions was around 7–11%. On the other hand, given that there is an invariant plane strain shape deformation accompanying transformation, it is very likely that some degree of autocatalysis does occur during the acicular ferrite transformation. By examining the orientation relationships between adjacent plates in clusters of acicular ferrite plates, it has been possible to demonstrate that such plates have a similar orientation in space (Yang and Bhadeshia, 1989a). Furthermore, the proportion of plates having similar orientations is found to be larger than expected from a knowledge of the austenite/ferrite orientation relationship. This could be taken as evidence for autocatalytic nucleation.

10.4 The Effect of Inclusions on the Austenite Grain Size in Welds

It is widely recognised that a larger austenite grain sized microstructure has a correspondingly better chance of transforming to acicular ferrite since the number density of grain boundary nucleation sites is reduced. However, it is not yet possible to predict the austenite grain size of steel welds and indeed, there is considerable confusion on the factors controlling the size. It has naturally been assumed, by extrapolation from grain growth theory, that the non-metallic inclusions which are common in steel welds control the grain size by Zener pinning the boundaries. This analogy is however, not justified since the austenite grains form by the *transformation* of δ-ferrite grains which evolve during solidification, whereas Zener pinning deals with the hindrance of grain boundaries during grain growth. The driving force for grain growth typically amounts to just a few Joules per mole, whereas that for transformation

from δ-ferrite to austenite increases indefinitely with undercooling below the equilibrium transformation temperature. Pinning of δ/γ interfaces cannot then be effective. A mechanism in which inclusions pin the columnar austenite grain boundaries is also inconsistent with the *shape* of these grains, since the motion of the δ/γ interfaces along the steepest temperature gradients is clearly not restricted; if pinning were effective, the austenite grains that evolve should be isotropic.

There is evidence to support the conclusion that the columnar austenite grain size is not influenced by for example, the oxygen content of the weld (Bhadeshia *et al.*, 1985, 1986a). Experiments to the contrary (Harrison and Farrar, 1981) really refer to the *reheated* weld metal, where the grain size is related to a coarsening reaction driven by γ/γ surface energy. On the other hand, there is some good evidence that low weld oxygen concentrations correlate with large columnar austenite grain sizes (Fleck *et al.*, 1986). There is a plausible explanation for these contradictory results. When the initial austenite grain size is very fine, the columnar grain structure may coarsen during cooling after solidification (North *et al.*, 1990). The coarsening process would certainly be expected to be influenced by the presence of inclusions. Further work is needed urgently to clarify these issues.

The columnar austenite grain size must to some extent correlate with the grain size in the parent plate at the fusion boundary, since solidification occurs by epitaxial growth of those grains (Davies and Garland, 1975). However, the relationship cannot be simple, since during solidification, those grains with their <100> directions most parallel to the direction of steepest temperature gradient grow rapidly, stifling the grains which are not suitably oriented. Consequently, the crystallographic texture of the parent plate, and the plane of that plate on which the weld is deposited, must influence the final austenite grain structure. Clear differences in the austenite grain structure were found between three welds deposited on mutually perpendicular faces of the same sample, in a recent experiment designed to illustrate the influence of texture on the grain size (Babu and Bhadeshia, 1991). More systematic and quantitative work is now called for.

10.5 Influence of Other Transformation Products

In weld deposits, acicular ferrite is one of the last transformation products to form after the growth of allotriomorphic and Widmanstätten ferrite. As a consequence, it is bound to be influenced by prior transformation products. Indeed, its volume fraction during continuous cooling transformation of such welds can in many cases be estimated simply by calculating the volume fractions of allotriomorphic and Widmanstätten ferrite, and assuming that

the remainder of the austenite transforms to acicular ferrite (Bhadeshia *et al.*, 1985). For the same reason, it is found that in wrought alloys with mixed microstructures, the amount of acicular ferrite decreases with the austenite grain size, as grain boundary nucleated phases such as allotriomorphic ferrite become more dominant (Barbaro *et al.*, 1988). The dependence of the volume fraction of acicular ferrite on the austenite grain size becomes less pronounced as the cooling rate (from the austenite phase field) is increased, since at slow cooling rates, much of the austenite is consumed during the higher temperature formation of allotriomorphic ferrite.

This dependence of the acicular ferrite content on the austenite grain size, in a mixed microstructure of acicular ferrite and allotriomorphic ferrite, can for isothermal reaction be expressed precisely using the relationship

$$\ln\{1-\xi\} \propto S_v \tag{10.16}$$

where ξ is the volume fraction of allotriomorphic ferrite divided by its equilibrium volume fraction at the temperature concerned and S_v is the amount of austenite grain surface per unit volume of sample. If a number of reasonable assumptions are made (Bhadeshia *et al.*, 1987) the proportionality can be applied to continuous cooling transformation in low carbon, low alloy steels, in which case, $(1-\xi)$ is approximately equal to the volume fraction of acicular ferrite, thus relating the latter to the austenite grain size.

An interesting observation reported by Dallum and Olson (1989) is that in samples containing mixtures of allotriomorphic ferrite, Widmanstätten ferrite and acicular ferrite, a relatively small austenite grain size leads to a coarser acicular ferrite microstructure. They attributed this to a reduction in the α_a nucleation rate, caused by some unspecified interaction with the prior transformation products (α and α_w). An alternative explanation could be that with a smaller austenite grain size, the volume fractions of α and α_w that form are correspondingly larger, thereby causing a higher degree of carbon enrichment in the residual austenite and hence a significant reduction in the acicular ferrite nucleation rate. A reduction in the nucleation frequency would then permit the fewer plates to grow to larger dimensions before hard impingment with other plates in the vicinity.

Effects like these are of considerable importance in the development of mixed microstructures, but the coarsening of acicular ferrite without any change in shape *per se* is unlikely to lead to any drastic changes in the strength of weld deposits (Bhadeshia and Svensson, 1989a, b). This is because the mean slip distance in a plate does not change very much as the plate becomes larger. Of course, it remains to be demonstrated whether toughness is sensitive to small variations in the size and distribution of acicular ferrite.

10.5.1 Some Specific Effects of Allotriomorphic Ferrite

We now proceed to consider a particular role of allotriomorphic ferrite formation in influencing the development of acicular ferrite in mixed microstructures. The effect is especially prominent in chromium and molybdenum containing steels. At relatively high concentrations of chromium (>1.5wt%) or molybdenum (>0.5wt%), the columnar austenite grains of steel weld deposits transform into bainite instead of acicular ferrite. The bainite is in the form of classical sheaves emanating from the austenite grain surfaces, often with layers of austenite left untransformed between the individual platelets of bainitic ferrite. This is in spite of the presence of non-metallic inclusions, which usually serve to intragranularly nucleate the plates of acicular ferrite. The effect is probably a consequence of the fact that as the amount of allotriomorphic ferrite decreases with increasing solute concentrations, the austenite grain boundaries are freed to nucleate bainite (Fig. 10.12). The observations of Sneider and Kerr (1984) could be interpreted to support this conclusion. In welds containing a

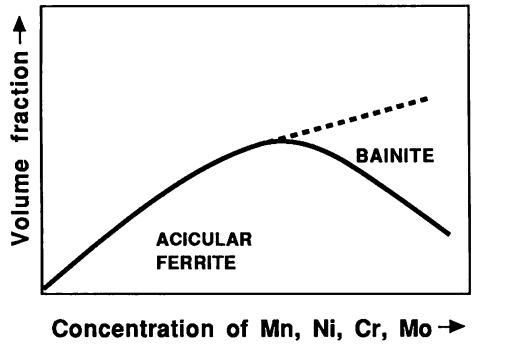

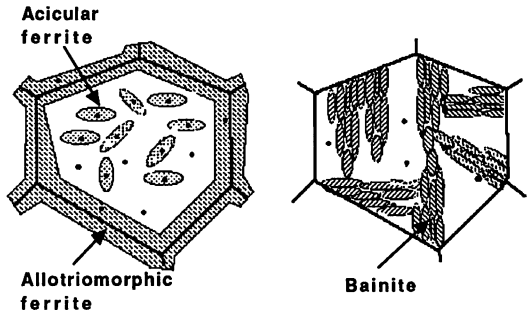

Fig. 10.12 *Schematic illustration of the mechanism by which the presence of allotriomorphic ferrite at the austenite grain surfaces induces a transition from a bainitic to acicular ferrite microstructure.*

variety of chromium concentrations, with microstructures which are predominantly acicular ferrite, the amount of bainite increased directly as the volume fraction of allotriomorphic ferrite decreased. In addition, bainite was not found when the allotriomorphic ferrite volume fraction was greater than 0.08, presumably because in their welds, that quantity was sufficient to completely cover the austenite grain surfaces, and prevents the grain boundary nucleation of bainite at a lower transformation temperature.

It may not in fact be necessary to entirely cover the austenite grain surfaces with allotriomorphic ferrite, because the ferrite will tend to form at the most potent nucleation sites, thereby disabling the most active areas of the grain surfaces.

Some interesting quantitative data have also been reported by Evans (1986); he found that as the chromium or molybdenum concentration of low carbon weld deposits is increased, the amount of allotriomorphic ferrite decreases. The volume fraction of acicular ferrite goes through a maximum as a function of concentration. The volume fraction of the remainder of the microstructure, which is described as 'ferrite with aligned second phase' therefore increases the concentration (Fig. 10.13). This is the terminology used in the welding industry to describe a microstructure in which parallel plates of ferrite are separated by regions of residual phase such as retained austenite. It really refers to packets of parallel plates of Widmanstätten ferrite or to sheaves of bainitic ferrite. There is some evidence (Bhadeshia *et al.*, 1986b) that in typical welds

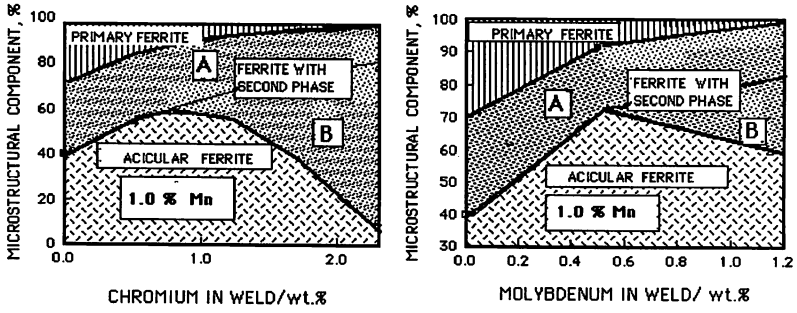

Fig. 10.13 *Changes in the as-deposited microstructure of steel welds as a function of chromium or molybdenum concentration (after Evans). Notice that in each case, the fraction of acicular ferrite goes through a maximum as the Cr or Mo concentration increases. The region labelled 'ferrite with aligned second phase' by Evans has been subdivided schematically into regions A and B, to represent the Widmanstätten ferrite and bainite microstructures respectively. The maximum occurs because at large alloy concentrations acicular ferrite is progressively replaced by austenite grain boundary nucleated bainite.*

deposits of the type studied by Evans, the fraction of Widmanstätten ferrite decreases to very small values (0.04–0.1) as the chromium or molybdenum concentration increases, so that most of the increase in the volume fraction of the 'ferrite with aligned second phase' can be ascribed to an increase in the volume fraction of bainite (Fig. 10.13). The fact that bainite is obtained when the austenite grain boundaries are free from other transformation products is also consistent with the observation that Fe–2.25Cr–1Mo wt% weld deposits used in the power generation industry are well known to have an almost fully bainitic microstructure (variously referred to as conventional bainite or granular bainite) in the as-deposited condition, with classical sheaves in which the platelets of bainitic ferrite are partially separated by films of retained austenite or martensite (Klueh, 1974b; Wada and Eldis, 1982; Kar and Todd, 1982; Lundin *et al.*, 1986; Vitek *et al.*, 1986; McGrath *et al.*, 1989). The large alloy concentration in this steel prevents the growth of allotriomorphic ferrite under normal heat treatment conditions.

It appears therefore, that at relatively large concentrations of chromium and/or molybdenum, acicular ferrite is in increasing proportions, replaced by classical bainite, until eventually, the microstructure becomes almost entirely bainitic. This effect cannot be attributed to any drastic changes in the austenite grain structure, nor to the inclusion content of the weld deposits (Babu and Bhadeshia, 1990). It turns out in fact, that the Cr and Mo alloys have highlighted a more general condition associated with welds containing high concentrations of alloying additions. Several cases have been reported in the literature, where a similar transition from an acicular ferrite microstructure to one containing a greater amount of bainite is found to occur as the concentration of elements other than Cr or Mo is increased so that the amount of allotriomorphic ferrite is reduced. Horii *et al.* (1988) found that in a series of low alloy steel welds, when the manganese or nickel concentrations exceeded about 1.5 and 2.9 wt% respectively, the weld microstructure was found to exhibit significant quantities of bainite. Interestingly, in the case of the nickel containing steels, the toughness nevertheless improved since nickel in solid solution has a beneficial intrinsic effect on the toughness of iron. It apparently increases the stacking fault energy of body centered cubic iron; since the dislocations in such iron are three-dimensionally dissociated, the change in stacking fault energy reduces the stress required for plastic flow at low temperatures, relative to that necessary for cleavage fracture (*see* Leslie, 1982).

To summarise, many experiments have indirectly revealed that the cause for the transition from a predominantly acicular ferrite microstructure to one containing substantial amounts of bainite, may be related to the reduction in the coverage of austenite grain boundaries by layers of

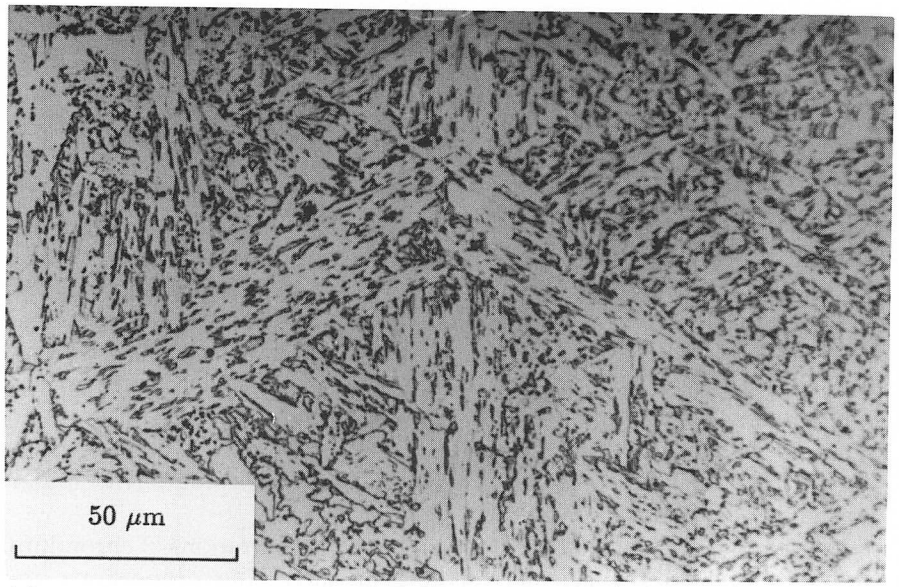

(a)

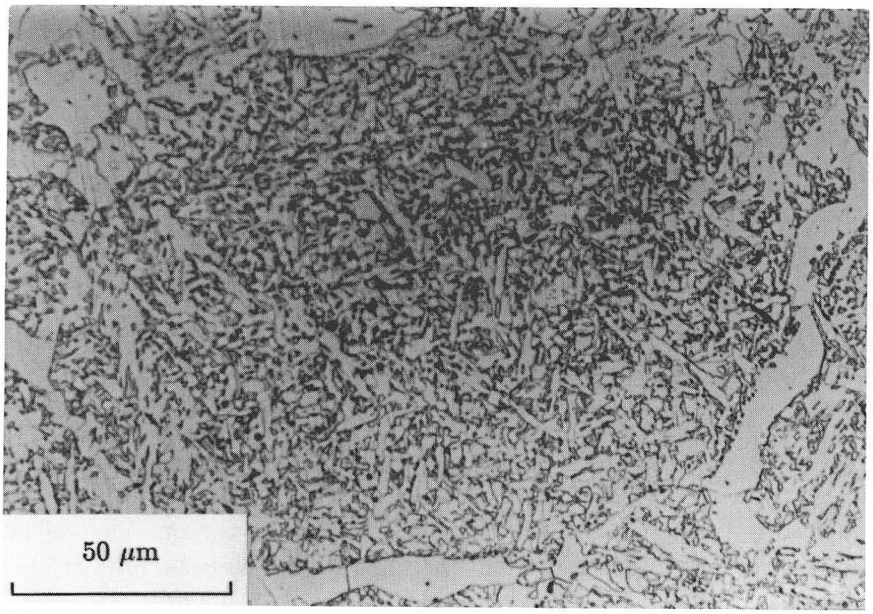

(b)

Fig. 10.14 *The change from a bainitic microstructure (a) to one which is predominantly acicular ferrite (b), induced by the introduction of a thin layer of allotriomorphic ferrite at the austenite grain surface. Both the acicular ferrite and bainite were otherwise obtained by isothermal transformation under identical conditions. (After Babu and Bhadeshia, 1990.)*

allotriomorphic ferrite, as the solute concentration exceeds a certain value (Babu and Bhadeshia, 1990). Below that concentration, the steel hardenability is low enough to ensure that the austenite grain surfaces are completely covered by uniform layers of allotriomorphic ferrite, thereby rendering them useless for bainite nucleation, and consequently allowing the development of acicular ferrite by intragranular transformation. As the concentration of austenite stabilising elements in increased, some of the austenite grain sufrace is left bare and becomes available for the nucleation of bainite sheaves as soon as the temperature falls within the bainite transformation range.

These ideas have been verified directly in experiments on Cr containing steels, which demonstrated that the microstructure can be changed from bainite to acicular ferrite simply by introducing thin layers of allotriomorphic ferrite at the austenite grain surfaces (Fig. 10.14). It appears that the allotriomorphic ferrite/austenite boundaries, even when the α/γ orientation is appropriate, cannot develop into bainite because the adjacent austenite is enriched in carbon, to an extent which drastically reduces its bainite start temperature. A transformation-free zone is therefore found ahead of the allotriomorphic ferrite/austenite interfaces.

10.6 The Effect of Stress on the Acicular Ferrite Transformation

Welded fabrications are prone to the development of residual stresses whose magnitudes may approach the yield stress of the steel concerned. It is likely that these stresses have an effect on the development of microstructure during the cooling of the weld to ambient temperature. A recent of the influence of applied stresses on the formation of acicular ferrite is due to Dallum and Olson (1989). They carried out experiments in which the stress was generated in restrained steel samples during cooling from the austenite phase field. The level of stress therefore varied from zero at the austenitisation temperature to a maximum at ambient temperature, although neither the stress nor the kinetics were recorded. Other tests involving compression were also carried out.

Dallum and Olson concluded that stress has little influence on the volume fraction of acicular ferrite obtained in the final microstructure. This result is probably not generally true. The isothermal formation of acicular ferrite under the influence of an externally applied compressive stress certainly leads to an acceleration of transformation, and major changes in the morphology of the acicular ferrite as it responds to stress (Fig. 10.15). The results also demonstrate the displacive character of the transformation, since anisotropic transformation strains were registered.

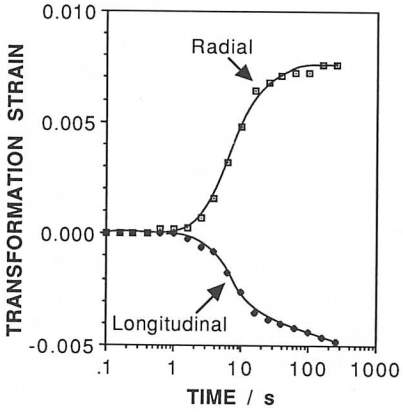

(a)

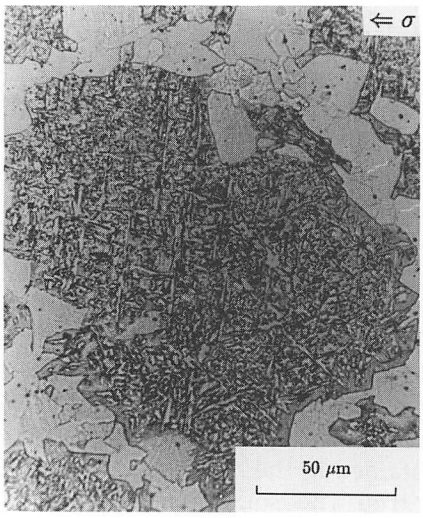

(b)

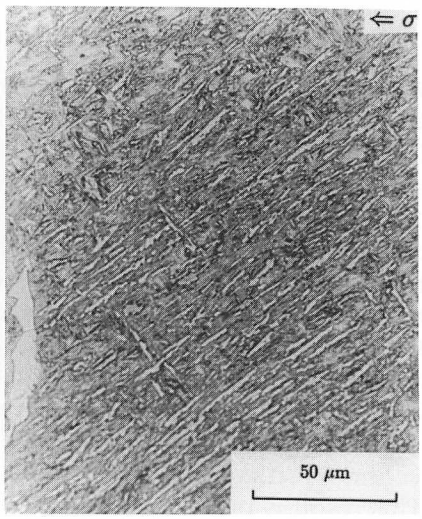

(c)

Fig. 10.15 *(a) Dilatometric data monitored along orthogonal directions, showing the displacive character of the acicular ferrite reaction. (b) The microstructure obtained in the absence of stress. (c) The aligned microstructure generated by the formation only of those acicular ferrite variants which are favoured by the applied stress (100 MPa). The transformation conditions for (b) and (c) are otherwise identical. (After Babu).*

10.7 Inoculated Acicular Ferrite Steels

We have seen that acicular ferrite in weld deposits is essentially, intragranularly nucleated bainite; its detailed morphology differs from that of conventional bainite because it nucleates from point sites (inclusions). This gives rise to a microstructure in which the adjacent ferrite platelets tend to radiate in many directions from each nucleation site. Such clusters of nonparallel platelets lead to an enhancement of toughness since, unlike bainite, any propagating crack frequently encounters plates in different crystallographic orientations.

Conventional bainite and acicular ferrite can be obtained under identical isothermal transformation conditions in the same (inclusion rich) steel. In the former case, the austenite grain size has to be small in order that nucleation from grain surfaces dominates the subsequent growth which then swamps the interiors of the austenite grains. For the same reason, acicular ferrite is not usually obtained in relatively clean wrought steels.

However, significant attempts have recently been made in industry, to inoculate steels with oxide particles in order to induce the formation of acicular ferrite for improved toughness (Nishioka and Tamehiro, 1988). The attempts are driven by the need to develop alloys for the offshore oil and gas industries, steels which are required for service in hostile deep and cold environments. For the Arctic regions, the temperatures at which good toughness is demanded have fallen from about –40°C to as low as –80°C. In some cases, the steels have to be amenable to high heat input welding, of the kind used in shipbuilding, so that the microstructure of the steel in its fabricated condition must be regenerated within the expected heat affected zones due to the welding process. All these stringent requirements call for unprecedented combinations of strength and toughness, both before and after welding operations are carried out. Some of the requirements can be made using thermomechanically processed, rapidly cooled bainitic steels, although welding seems to induce less desirable microstructures in the heat affected zones.

The problem can in principle be resolved rather elegantly and in a way which takes advantage of the coarsening of the austenite grain structure in the heat affected zones of weld deposits. Tamehiro and co-workers have developed low alloy steels containing titanium oxides and nitrides, in which these phases help nucleate acicular ferrite during cooling of the heat affected zone after welding. A typical composition of such a steel would be given by Fe–0.08C–0.2Si–1.4Mn–0.012Ti–0.002Al–0.002N wt%. Small additions of boron are also sometimes made, primarily to reduce the formation of grain boundary allotriomorphic ferrite in any heat affected zone microstructure, and to fix free nitrogen which can lead to a reduction in toughness via a strain hardening mechanism.

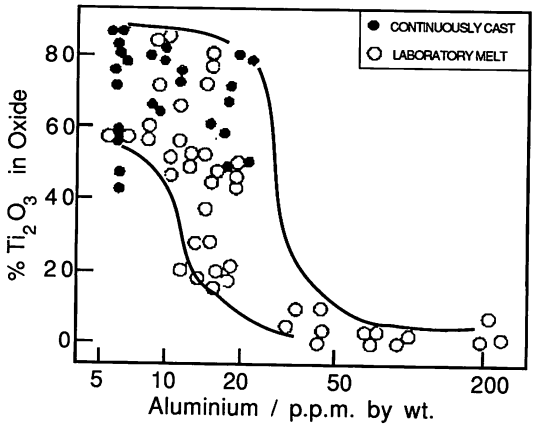

Fig. 10.16 *The effect of aluminium concentration on the proportion of Ti_2O_3 in the total oxide content of the steel (Chijiiwa* et al., *1988).*

The oxide particles effective in stimulating nucleation seem to have a diameter of about 2 μm, and are introduced during steel making. They are believed to be Ti_2O_3, although each inclusion is usually a complex combination of the titanium compounds and phases such as MnS, Al_2O_3, (Mn,Si)O, etc., in both crystalline and amorphous conditions. It appears that the aluminium concentration of the steel has to be minimal (< 30 p.p.m.) during steelmaking since the formation of Ti-oxides is otherwise prevented (Imagumbai *et al.*, 1985; Nishioka and Tamehiro, 1988). Chijiiwa *et al.* (1988) have shown that the amount of titanium oxide as a proportion of the total oxide content, decreases as the aluminium concentration increases (Fig. 10.16). The titanium oxides were distinguished from the other oxides using microprobe analysis, although it is not clear how the fraction of titanium oxide can be determined using this technique, since the particles are not in general of a single phase. The titanium oxide particles are in most cases found to coexist with MnS, Al_2O_3, (Mn,Si)O, etc., in both crystalline and amorphous conditions.

We have seen that the effect of dissolved aluminium is to favour the formation of Widmanstätten ferrite at the expense of acicular ferrite. The aluminium effect is particularly clear in the work by Imagumbai *et al.* (1985), who measured the microstructure of a large number of wrought steels together with the soluble aluminium concentration and the oxide particle densities. They demonstrated that there is a strong effect of dissolved aluminium on the microstructure, with the volume fraction of acicular ferrite obtained decreasing drastically at concentrations greater than about 70 p.p.m. (Fig. 10.17a). The mechanism of this effect is unknown, and a further difficulty is that the dissolved aluminium

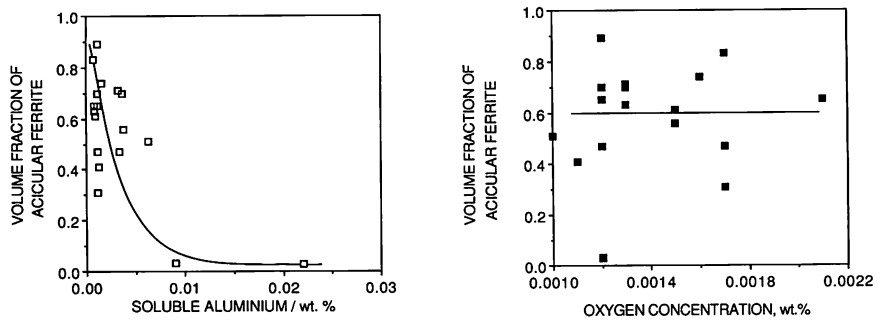

(a) (b)

Fig. 10.17 *(a) The volume fraction of acicular ferrite as a function of the soluble aluminium concentration; (b) the volume fraction of acicular ferrite as a function of the total oxygen concentration. (Data from Imagumbai* et al., *1985.)*

concentration is very difficult to control. In addition, there appears to be very little correlation between the total aluminium concentration and that in solution, even when the chemistry of all the other elements is kept constant (Thewlis, 1989a, b).

An interesting result is that the effect of inclusions in enhancing the formation of acicular ferrite was found to saturate at about 120 p.p.m. of oxygen, although this limiting value must of course depend on the heat treatment and the details of the other phases present in the steel (Fig. 10.17b). For example, it is obvious that the austenite grain size has to be large to prevent grain boundary nucleated transformations from swamping the intragranular formation of acicular ferrite, irrespective of the level of oxygen concentration. The most critical region of the heat affected zone of welds is that nearest the fusion surface, where the austenite grain structure is very coarse, and in this respect, the inoculated steels are ideal since the coarse grains readily transform to acicular ferrite. It is interesting to note (as pointed out by Imagumbai *et al.*) that the oxygen concentration of these steels ($\approx$120 p.p.m.) is comparable with that of normal fully killed steel, which usually contains aluminium oxides. Thus, any detrimental effect of inclusions in helping fracture is not exaggerated for the inoculated steels.

To optimise the properties of the acicular ferrite steels, their nitrogen concentrations also have to be controlled, since titanium can form TiN which is not as useful as the oxide in developing the acicular ferrite microstructure. While TiN particles may contribute to intragranular nucleation, they are not as stable as the corresponding oxide particles. Consequently, the tend to dissolve in the most critical region of the heat affected zone of a weld, the region adjacent to the fusion boundary. With titanium oxide as

the primary inoculant, experimental measurements indicate that the procedure is very successful in enhancing the toughness of the critical regions of the HAZs of welds under both laboratory and commercial conditions.

It is worth emphasising that the design of such steels also requires that the alloy chemistry be adjusted to avoid the prior formation of phases such as allotriomorphic ferrite, Widmanstätten ferrite, etc., so as to leave enough untransformed austenite available for the formation of an effective quantity of intragranularly nucleated acicular ferrite. As discussed by Nishioka and Tamehiro, this can be accomplished by the careful use of microalloying elements such as Nb, Mo and B, thereby avoiding a large rise in the carbon equivalent of the steel. It also seems that the silicon concentration has to be kept rather small (≈ 0.2 wt%) in order to avoid the formation of large oxide particles (Imagumbai *et al.*, 1985).

Prior to the advent of the oxide inoculated wrought steels just discussed, high strength low alloy steels (e.g. Krishnadev and Ghosh, 1979) were sometimes called 'acicular ferrite HSLA' steels. This is because they exhibited a microstructure of heavily dislocated laths; this microstructure is more like the low carbon bainite in which adjacent laths are in the same crystallographic orientation in space and it is probably not useful to call it an acicular ferrite microstructure, given that the latter nowadays carries the implication of intragranular, heterogeneous nucleation.

10.7.1 Some Difficulties with the Inclusion Nucleation Model

A closer examination of the data presented by Imagumbai *et al.* (1985) reveals a number of difficulties if it is accepted that the inoculated acicular ferrite steels derive their microstructure via intragranular nucleation on titanium oxide particles. For example, the metallographically determined oxide particle density shows a strong *negative* correlation with the total titanium concentration of the steel (Fig. 10.18), and indeed, with the soluble aluminium concentration. On the other hand, the oxide particle density correlates strongly with the total oxygen concentration (Fig. 10.18). If the metallographic data are correct, these correlations suggest that the relationship between the particles controlling nucleation, and their number density cannot be straightforward. It is possible that titanium oxide may not be the dominant phase in each particle, a conclusion which would raise questions about the role of the other components in influencing intragranular nucleation. The evidence on the microstructure of the inclusions in wrought steels in fact appears to be rather limited. Nishioka and Tamehiro (1988) have presented one electron diffraction pattern to indicate the presence of Ti_2O_3. Homma *et al.* (1987) have confirmed, using X-ray diffraction on electrolytically extracted particles, that the crystallographic structure of the titanium oxide is indeed that of Ti_2O_3.

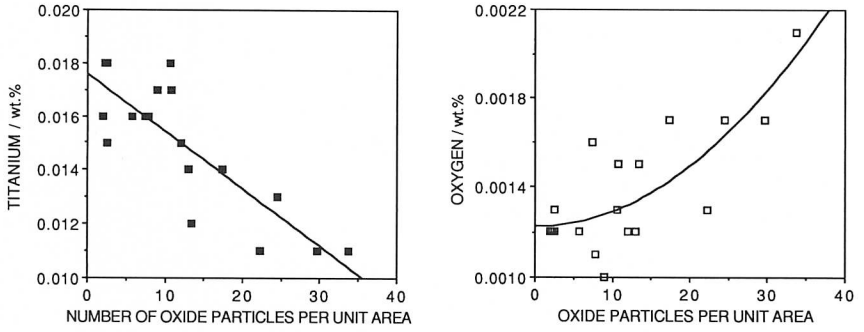

(a) (b)

Fig. 10.18 *Quantitative data on Ti_2O_3 particles in a wrought acicular ferrite steel (Imagumbai* et al.*, 1985). (a) The oxide particle density as a function of the total oxygen concentration. (b) The oxide particle density as a function of the titanium concentration.*

Much further work is needed to clarify these issues. Although there are numerous publications on inoculated steels many of them share a lot of experimental data as far as the microstructure is concerned, and the details of the methods used in obtaining the data are not often stated.

10.7.2 Steelmaking Technology for Inoculated Alloys

The inoculated steels, if they can be reliably manufactured in large quantities, could represent a major and very exciting advance in the technology of steels. For this reason, details of the manufacturing process are shrouded in secrecy. It is probable that there are major difficulties in obtaining the right oxide and the correct particle number density and distribution in the final steel, since there are many steel companies which have failed to reproduce the steels now marketed by Nippon Steel.

Nevertheless, it is possible to gleam a few simple rules from the published literature. The correct precipitate seems to be titanium oxide (Ti_2O_3), since TiN is not sufficiently stable at high temperatures to ensure acicular ferrite formation in the heat affected zones of welds. The steelmaking involves deoxidation with titanium, whereas other strong deoxidisers such as Al, Ca or the rare earth elements are avoided. The oxygen concentration in the molten steel should be between 60 and 120 p.p.m., depending on application. Very high toughness levels demand a small inclusion (and hence oxygen) content. The steel must be otherwise clean, and must not contain large quantities of sulphur.

10.8 Summary

It is ironic that bainite when it was first discovered was referred to as acicular ferrite (Davenport and Bain, 1930), and that the terms acicular ferrite and bainite were often used interchangeably for many years after 1930 (*see* for example, Bailey, 1954). There is growing evidence that the microstructure which in modern terminology is identified as acicular ferrite, consists simply of intragranularly nucleated bainite as far as the mechanism of transformation is concerned. Conventional bainite grows in the form of sheaves of parallel platelets originating at the austenite grain surfaces. Acicular ferrite platelets on the other hand, emanate in many different directions from point sites (non-metallic inclusions) on which they nucleate heterogeneously. The development of sheaves is in the case of acicular ferrite stifled by impingment between plates nuleating from adjacent inclusions.

The transformation has otherwise been verified to exhibit many of the known characteristics of the bainite reaction: the incomplete reaction phenomenon, no substitutional element partitioning during transformation, an invariant plane strain shape deformation accompanying growth, the large dislocation density, the reproducible orientation relationship within the Bain region, etc. Any factor which increases the number density or potency of intragranular nucleation sites relative to austenite grain boundary sites also favours a transition from a bainitic to an acicular ferrite microstructure. The transition can in practice be obtained by increasing the austenite grain size, by decorating the grain boundaries with thin, inactive layers of allotriomorphic ferrite, by increasing the inclusion content or by rendering the boundaries impotent with the help of segregating elements such as boron. It is also recognised that these microstructural factors can only be useful if enough austenite is left untransformed at the relatively low temperature below which acicular ferrite formation becomes possible – i.e., the volume fraction of the grain boundary nucleated phases must be minimal at that temperature.

11 *Other Morphologies of Bainite*

Upper and lower bainite are well established terms describing microstructures which can be readily distinguished using standard experimental methods, and whose mechanisms of formation can be understood theoretically. There are, however, a number of other descriptions of steel microstructures which include the word 'bainite'. As will be seen in the discussion that follows, these morphological descriptions can to varying degrees be useful in communicating the form of the microstructure. But this must be done with care, avoiding the natural tendency to imagine a particular mechanism of transformation, simply because someone has chosen to coin the terminology.

11.1 Granular Bainite

Of all the unusual descriptions of bainitic microstructures, granular bainite is probably the most useful and frequently used nomenclature. During the early 1950s, continuously cooled low carbon steels were found to reveal microstructures which consisted of 'coarse plates and those with an almost entirely granular aspect', together with islands of retained austenite and martensite, Fig. 11.1 (Habraken, 1956, 1957, 1965; Ridal and McCann, 1965; Habraken and Economopolus, 1967). Habraken and coworkers called this granular bainite and the terminology became popular especially because many industrial heat treatments involve continuous cooling rather than isothermal transformation. The energy generation industry in particular uses enormous quantities of bainitic microstructures generated by allowing large steel components to cool naturally (Chapter 12). Granular bainite is supposed to occur only in steels which have been cooled continuously; it cannot be produced by isothermal transformation.

The coarse ferrite plates referred to earlier, do not really exist. They are in fact, sheaves of bainitic ferrite with very thin regions of austenite

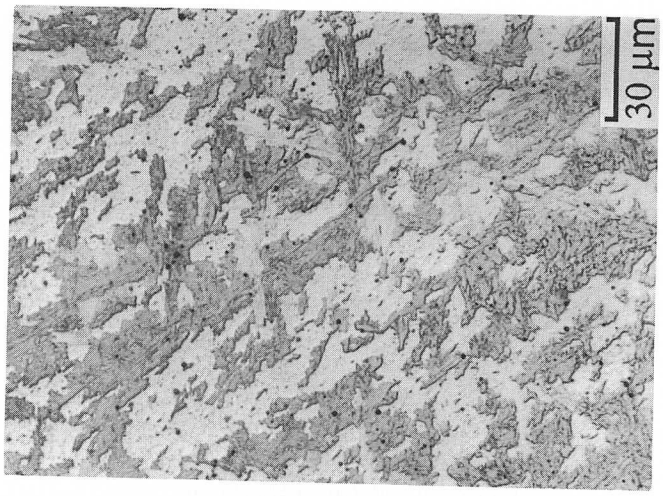

(a)

(b)

Fig. 11.1 *Granular bainite in a Fe–0.15C–2.25Cr–0.5Mo wt% steel. (a) Light micrograph. (b) Corresponding transmission electron micrograph. (After Joseffson, 1989.)*

between the sub-units because of the low carbon concentration of the steels involved (Leont'yev and Kovalevskaya, 1974; Josefsson and Andren, 1989). Hence, on an optical scale, they give the appearance of coarse plates (Fig. 11.1a). Many of the original conclusions were reached from microstructural observations (including those using replicas for transmission electron microscopy) which were not of sufficient resolution to establish the fine structure within the sheaves of bainite. Indeed,

evidence of this interpretation of so-called coarse plates appeared in the literature as early as 1967 when thin foil TEM observations were made by Habraken and Economopolus (their Fig. 16), revealing the fine bainitic ferrite platelets within the sheaves.

A characteristic (though not unique) feature of granular bainite is the lack of carbides in the microstructure. Instead, the carbon that is partitioned from the bainitic ferrite stabilises the residual austenite, so that the final microstructure contains both retained austenite and some high carbon martensite. Consistent with observations on conventional bainite, there is no redistribution of substitutional solutes during the formation of granular bainite (Tenuta–Azevedo and Galvao–da–Silva, 1978).

The extent of transformation to granular bainite is found to depend on the undercooling below the bainite-start temperature (Habraken and Economopolus, 1967). This is a reflection of the fact that the microstructure, like conventional bainite, exhibits an incomplete reaction phenomenon.

The evidence therefore does not indicate that granular bainite is different from ordinary bainite as far as the mechanism of transformation is concerned. The difference in morphology arises because it is generated by continuous cooling transformation in relatively low carbon steels. The continuous cooling treatment allows the transformation to proceed to a large extent by the time ambient temperature has been reached. The low carbon concentration ensures that any films of austenite or regions of carbide that might exist between sub-units of bainite are minimal, making the identification of individual platelets within sheaves rather difficult using light microscopy.

Finally, it is interesting that in an attempt to deduce a mechanism for the formation of granular bainite. Habraken (1965) proposed that the austenite prior to transformation dehomogenises into regions which are rich in carbon, and those which are relatively depleted. These depleted regions are then supposed to transform into granular bainite. The idea is the same as that of Klier and Lyman (1944) and has been shown to be thermodynamically impossible in steels (Aaronson *et al.*, 1966a).

11.2 Inverse Bainite

In conventional bainite, ferrite is the dominant phase, any carbide precipitation occurring as a secondary event. In the so-called 'inverse bainite' which is found in hypereutectoid steels, cementite is the first phase to form (Hillert, 1957). It consist of a central, presumably plate like spine of cementite which grows directly from austenite (Hehemann, 1970) and which then becomes surrounded by a layer of ferrite (Fig. 11.2). The term 'inverse' reflects the fact that unlike conventional bainite, cementite is the first phase to precipitate from austenite.

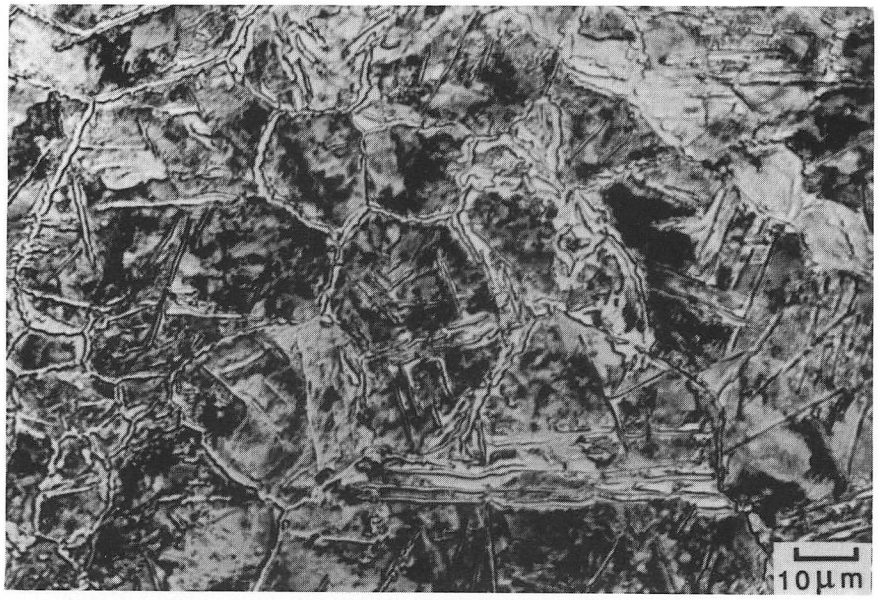

(a)

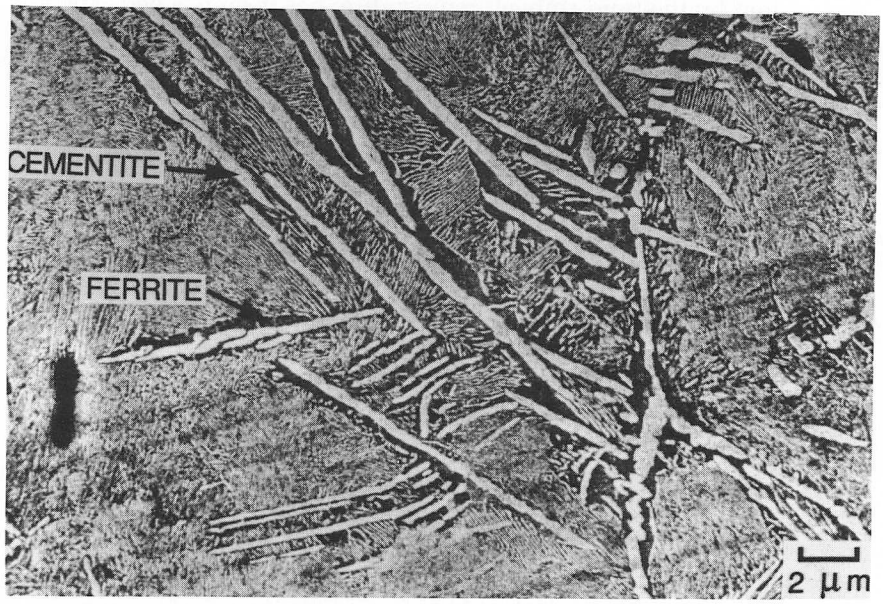

(b)

Fig. 11.2 *Inverse bainite in a hypereutectoid steel. (a) Light micrograph. (b) Transmission electron micrograph. (After Farooque and Edmonds.)*

The mechanism of the transformation is virtually unknown; there is no evidence that the growth of the ferrite involves a coordinated movement of atoms, and no crystallographic or chemical composition data. Judging from the shape alone, the ferrite probably forms by a reconstructive transformation mechanism. It certainly seems premature to classify the transformation as bainite.

11.3 Columnar Bainite

'Columnar bainite' is a description of a non-lamellar aggregate of cementite and ferrite, the overall shape of which is like an irregular and slightly elongated colony (Fig. 11.3). The distribution of cementite particles within the colony is rather peculiar, the majority of needle shaped particles being aligned to the longer dimension of the colony. This latter region is surrounded by a layer of different microstructure, in which the relatively coarser cementite particles meet the austenite/ferrite interface edge on (Nilan, 1967). The structure is normally observed in hypereutectoid steels (Greninger and Troiano, 1940; Vilella, 1940; Jellinghaus, 1957; Speich and Cohen, 1960) but has been found in lower carbon steels transformed at high pressures (Nilan, 1967). It may be relevant to point out that the

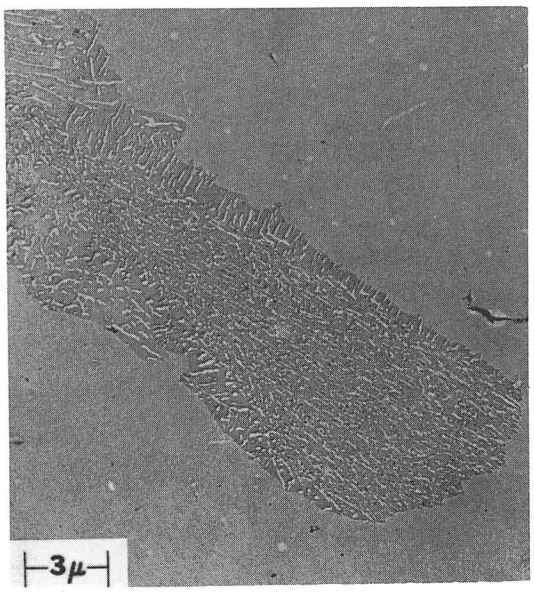

Fig. 11.3 *Electron micrograph, obtained using a replica technique, showing a colony of 'Columnar Bainite' in an Fe–0.82C wt% following isothermal transformation at 288°C and at a pressure of 30 kbar (after Nilan, 1967).*

eutectoid composition is shifted to lower carbon concentrations by hydrostatic pressure.

The microstructure can be obtained at transformation temperatures comparable to those associated with conventional bainite, but there is no invariant plane strain surface relief accompanying the growth of 'columnar bainite'. It is probable that columnar bainite is more akin to pearlite than bainite, but further investigations are clearly necessary in order to make any sensible decisions about the mechanism of growth.

11.4 Pearlitic Bainite

In steels containing strong alloy carbide forming elements, it is possible to obtain alloy pearlite, in which the carbide phase is an alloy carbide (such as M_7C_3) instead of cementite. The alloy pearlite can form at temperatures above B_S, or somewhat below that temperature but only after holding at the transformation temperature for very long time periods (usually many days). On the scale of light microscopy, the pearlite etches as dark nodules (Fig. 11.4), but the colonies tend to have crystallographic facets rather

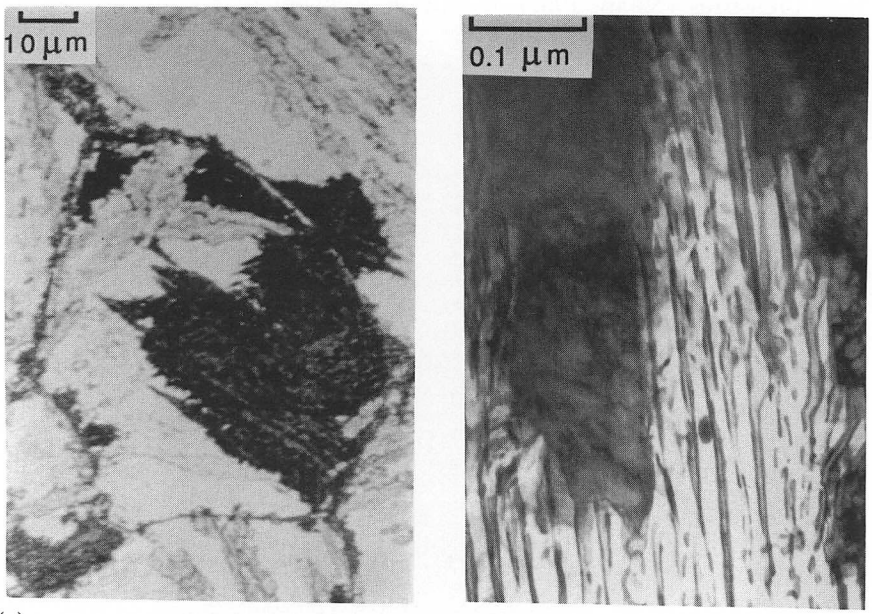

(a) (b)

Fig. 11.4 *Microstructure of the so-called 'pearlitic bainite', which is really just a pearlite with alloy carbide (in this case M_7C_3) instead of cementite. (a) Light micrograph. (b) Transmission electron micrograph.*

than the nicely rounded colonies of normal pearlite. This is probably a reflection of the orientation dependence of the interfacial energy of the alloy carbide.

Because of this faceting, transmission electron microscopy observations can be misleading. The crystallographically faceted nodules of pearlite at a high resolution give the appearance of parallel ferrite plates with intervening carbides, a microstructure on that scale similar to upper bainite. The terminology 'pearlitic bainite' given to this transformation product is extremely misleading. There is gross partitioning of substitutional solutes during the transformation, there is no surface relief effect, the carbide and ferrite phases grow cooperatively, and there is no reason to associate this microstructure with bainite.

11.5 Grain Boundary Lower Bainite

Bainite nucleation in most steels occurs heterogeneously at the austenite grain boundaries. At very high undercoolings above the M_S temperature, the nucleation rate of lower bainite can be so large, that large segments of the grain surface become almost entirely decorated by lower bainite sub-units (Fig. 11.5). At these temperatures, the rate at which carbon partitions from supersaturated ferrite is also very slow, so that the sub-units are able to form in arrays without any intervening austenite (Bhadeshia and Edmonds, 1979a). These layers of sub-units have the overall form of allotriomorphs, but there is no doubt that they form individually.

The microstructure has recently caused some concern in the context of 300 M, which is an ultra high strength steel used in the quenched and

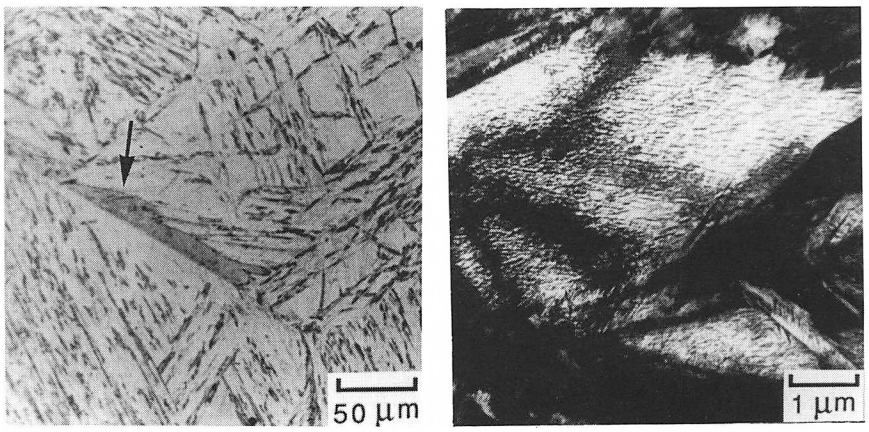

Fig. 11.5 *The microstructure of grain boundary lower bainite. (a) Light micrograph. (b) Transmission electron micrograph.*

tempered condition (Padmanabhan and Wood, 1984). The alloy has a very high hardenability — 10 cm diameter sections can be made martensitic by air cooling from the austenitisation temperature. However, optical microscopy revealed the suprising presence of allotriomorphs, which turned out to be the grain boundary lower bainite described above.

11.6 Summary

Granular bainite is basically, ordinary bainite generated by continuous cooling transformation of low carbon steels. The mechanism of inverse bainite is unclear, but it involves the formation of cementite as the primary phase. It is not clear whether the ferrite, when it eventually forms and engulfs the cementite, forms by a reconstructive or displacive mechanism.

Whilst there is some doubt about the mechanism of inverse bainite, the terms columnar- and pearlitic-bainite are undoubtedly misnomers and are best avoided. Columnar bainite is simply an aggregate of cementite and ferrite which grows by a reconstructive transformation mechanism. Pearlitic bainite is simply a crystallographically facetted alloy pearlite.

At high supersaturations, arrays of lower bainite sub-units can rapidly decorate the austenite grain surfaces, giving the appearance of allotriomorphs. This 'grain boundary lower bainite' is much harder than allotriomorphic ferrite, and can therefore be readily distinguished.

12 *Mechanical Properties*

12.1 Introduction

Many years elapsed after the work of Davenport and Bain before the commercial exploitation of bainitic steels. This is attributable to the difficulties in obtaining fully bainitic microstructures throughout sizeable samples of steel. It has long been recognised that the influence of bainite on the mechanical behaviour of a steel is difficult to understand because of the inability to attain fully bainitic microstructures at all transformation temperatures, a consequence of the incomplete reaction phenomenon (Hehemann *et al.*, 1957). Isothermal transformation to bainite was considered impractical on a commercial scale, continuous cooling from the austenitising temperature being the preferred heat treatment. In most cases, continuous cooling at a rate greater than $\approx 50 Ks^{-1}$ during transformation was also believed impractical. Hence, lean steels gave mixed microstructures of allotriomorphic ferrite and bainite, whereas more heavily alloyed steels transformed only partially to bainite, the residual austenite undergoing martensitic transformation on further cooling. It was not until low alloy, low carbon steels, containing small amounts of boron and molybdenum to suppress proeutectoid ferrite formation, were developed that the potential for significant commercial exploitation became realistic (Irvine and Pickering, 1957).

Boron is effective in retarding proeutectoid ferrite formation but has a negligible effect on the bainite reaction, allowing bainitic microstructures to be obtained over a wider range of cooling rates. The segregation of boron to the austenite grain boundaries leads to a reduction in their energy, thereby making them less favourable as sites for the heterogeneous nucleation of ferrite. The reason why the effect is more pronounced for allotriomorphic ferrite than for bainite has not been investigated, but it may be associated with the fact that for bainite, which

grows in the form of sheaves of small platelets, the vast majority of platelets nucleate autocatalytically after the initial formation of some platelets at the austenite grain boundaries (Chapter 6). Boron thus increases the bainite hardenability. The level of other alloying additions can, in the presence of boron, be kept low enough to avoid the formation of martensite. Steels of typical composition Fe–0.0033B–0.52Mn–0.54Mo–0.11Si–0.10C wt% were found to yield virtually fully bainitic microstructures with very little martensite during normalising (i.e., air cooling from the austenitising temperature), and permitted the characterisation of the mechanical properties of bainite in isolation, without interference from other phases. It is as well to note that in many investigations of mechanical properties, it has not been recognised that the microstructures studied were not fully bainitic.

In the discussion that follows, attention is restricted to cases where the microstructure has been characterised thoroughly, and where it plays a significant role in determining the mechanical properties. Consequently, the effect of traces of impurity elements (e.g. S and P) on the mechanical properties are not included. A full quantitative description of the relationship between microstructure and properties is not yet possible. For this reason, in addition to well established but incomplete quantitative models, qualitative relationships which seek to explain mechanical properties as a function of microstructure are also reviewed.

12.2 The Strength of Bainite

The strength of bainite can in principle be factorised into components consisting of the intrinsic strength of pure annealed iron (σ_{Fe}), substitutional solid solution strengthening contributions (σ_{SS}), strengthening due to carbon in solid solution (σ_C), and a variety of microstructural components including dislocation strengthening, particle effects and grain size effects. Thus

$$\sigma = \sigma_{Fe} + \Sigma_i \sigma^i_{ss} + \sigma_C + k_\varepsilon(\bar{L}_3)^{-1} + k_P\Delta^{-1} + C_{10}\rho_d{}^{0.5} \qquad (12.1)$$

where ρ_d is the dislocation density and Δ the average distance between a cementite particle and its two or three nearest neighbours. From measurements done on martensite, k_ε is approximately 115 MPa m^{-1}; assuming that the cementite particles are spherical and of a uniform size, k_P is given approximately by 0.52 V_θ MPa m^{-1}, where V_θ is the volume fraction of cementite (Daigne *et al.*, 1982). Dislocation theory for body centered cubic metals gives $C_{10} = 0.38\mu b \approx 7.34$ MPa m (Keh and Weissmann, 1963). The carbon and substitutional solutes are listed separately, because their solid solution strengthening contributions vary differently with concentration. For carbon, the strengthening varies with the square root of concentration

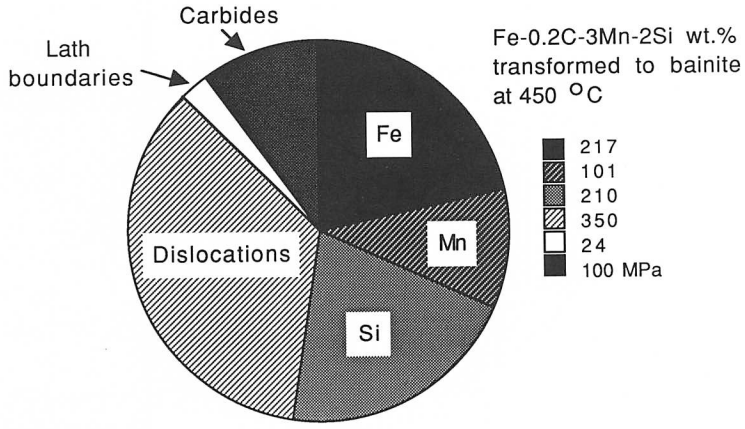

Fig. 12.1 *The tensile yield strength of bainite at 25°C. Estimated contributions to the strength of bainite in a Fe–0.2C–3Mn–2Si wt% alloy.*

(Speich and Warlimont, 1968; Christian, 1971), whereas for the substitutional solutes there is a direct relationship (Leslie, 1982). The purpose of presenting this equation is to illustrate the form of the relationships, but in practice, it is very difficult to decipher the microstructural contributions because parameters such as grain size and particle spacing cannot be varied independently.

It is proposed to concentrate here on the influence of microstructure on strength. The other terms, such as an explanation of the intrinsic strength of pure iron, are well established and dealt with fully in a variety of reviews and textbooks (e.g., Leslie, 1982; Christian, 1983). Fig. 12.1 illustrates the magnitudes of the terms involved, with some typical data for a fully bainitic microstructure.

12.2.1 Hardness

For fully bainitic microstructures, the hardness increases approximately linearly with carbon concentration, by approximately 190 HV per wt% (Irvine and Pickering, 1965). This contrasts with a change of about 950 HV per wt% of carbon for untempered martensite, where most of the carbon is in interstitial solid solution. The austenitising temperature does not influence the hardness unless it is not high enough to dissolve all the carbides (Irvine and Pickering, 1965). Unfortunately, the microstructures obtained are often mixed, in which case the hardness depends on the transformation temperature and composition. This is because the stability of the residual austenite to martensitic transformation changes with its

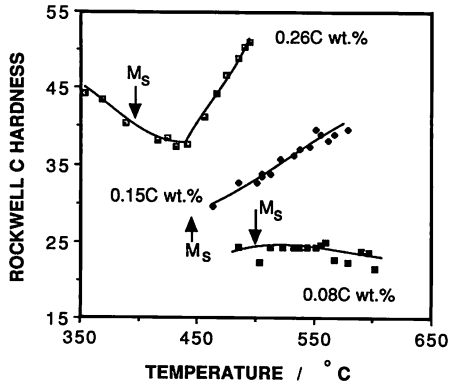

Fig. 12.2 *Variation in hardness as a function of the isothermal transformation temperature. (After Lyman and Troiano, 1946.)*

carbon concentration, the limiting value depends on the transformation temperature via the T_O' curve of the phase diagram.

In high alloy steels where reconstructive transformations are sluggish below B_S, the residual austenite which remains after partial transformation to bainite, decomposes to a mixture of untempered, high carbon martensite and retained austenite on cooling to ambient temperature. In low alloy steels the residual austenite may transform to some form of degenerate pearlite. These secondary transformations have for a long time been known to influence the hardness of the microstructure; Lyman and Troiano (1946) found that for a series of Fe–Cr–C alloys the hardness for the 0.08 wt% C alloy was insensitive to the isothermal transformation temperature (Fig. 12.2). The low carbon concentration ensures that the microstructure is almost fully bainitic for all of the temperatures studied. With higher carbon alloys, the hardness first decreases with the transformation temperature as the volume fraction of bainite increases at the expense of residual phases like martensite and degenerate pearlite.[1] Continuous cooling transformation experiments by Ohmori *et al.* (1971) confirm these trends. The hardness was found to increase with cooling rate, presumably because the proportion of martensite (in a mixed martensite + bainite microstructure) increases with cooling rate.

It is interesting that the *microhardness* of bainite, in a mixed microstructure of bainite and pearlite obtained by isothermal transformation, is

1 This happens even though the dislocation density of bainitic ferrite increases as the transformation temperature decreases (Smith, 1984). The reduction in the quantity of hard phases (martensite, pearlite) appears to more than compensate for the increase in the dislocation density.

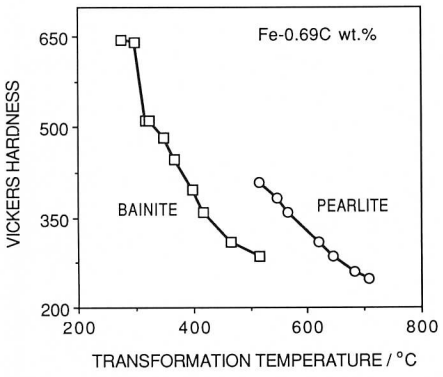

Fig. 12.3 *Microhardness data from plain carbon steels transformed isothermally to a mixture of bainite and pearlite (after Ohmori and Honeycombe, 1971).*

found to be lower than that of the pearlite, Fig. 12.3 (Ohmori and Honeycombe, 1971). This remains true even when the pearlite and bainite have been generated at the same temperature. This behaviour is easy to explain once it is realised that the pearlite grows from carbon enriched austenite and hence contains a much larger fraction of cementite than the bainite.

The hardness of bainite is found to be independent of the prior austenite grain size, even though the latter influences the bainite sheaf thickness (Kamada *et al.*, 1976). This is not unexpected given that the bainite sub-unit size is hardly influenced by the austenite grain size (Chapter 2). Since the sub-units are much smaller they exert an overriding influence on strength. This conclusion is consistent with the observation that the hardness of fully bainitic microstructures is not sensitive to the austenitising temperature (Irvine and Pickering, 1965; Kamada *et al.*, 1976).

12.2.2 *Tensile Strength*

Although there is some direct evidence that bainitic ferrite retains an excess concentration of carbon even after annealing (Bhadeshia and Waugh, 1981, 1982; Stark *et al.*, 1988), the majority of dislocations in bainite are believed to be mobile, since sharp yield points are not observed during tensile tests. The main effect of carbon on strength is through carbide precipitation. Cementite is the usual carbide; it precipitates in a rather coarse form without substantial coherency strains. Matrix dislocations have to bypass the cementite particles because they are unable to cut through them. All this means that the effect of carbon on the strength of bainite is rather small, approximately 400 MPa per 1 wt% of carbon (Irvine *et al.*, 1957).

Plates of bainitic ferrite are typically 10 μm in length and about 0.2 μm in thickness. This gives a rather small mean free path for dislocation glide,

especially since the probability of the slip plane lying parallel to the plate is rather small. The effective grain size of the plate is in fact within a factor of two of the plate thickness. There is only one other process, that of mechanical alloying (Benjamin, 1970), which can give such a small grain size in bulk materials. Thus, the main microstructural contribution to the strength of bainite is from the extremely fine grain size of bainitic ferrite (Irvine *et al.*, 1957).

There have been many attempts at an analysis of the grain size contribution to the strength of bainite, most of them being based on the Hall–Petch relationship. This predicts a linear relationship between the strength and the reciprocal of the square root of 'grain size'. Although most data on bainite can be fitted to the Hall–Petch relation (Siriwardene, 1955; Pickering, 1967), the results are difficult to interpret because the platelet size cannot be altered without influencing other variables such as the dislocation density and the number density of carbide particles.

The Hall–Petch relationship relies on a description of macroscopic yielding in which a dislocation pile-up generates a large enough stress concetration to stimulate a dislocation source in an adjacent grain, thereby transmitting deformation across grains. If the grain size is large, then the number of dislocations that can participate in the pile-up increases, and the larger stress field of the pile-up makes it easier to stimulate distant sources. Hence, the yield strength decreases. This is an unlikely description of events when the grain size is very fine. The slip plane dimensions are then too small to allow the existence of pile-ups, and yielding is determined instead by the stress necessary to expand a dislocation loop across a slip plane (Langford and Cohen, 1969, 1970, 1975). The yield stress is then expected to vary with the inverse of the grain size. The strength of heavily cold deformed iron and of martensitic samples have been interpreted using such a relationship (Langford and Cohen, 1969, 1970, 1975; Naylor, 1979; Daigne *et al.*, 1982). The changeover from the Hall–Petch to the Langford–Cohen relation should occur when the slip plane dimensions become $\approx 1\,\mu m$.

An attempt has been made to separate the effect of bainite grain size and particle strengthening using multiple regression analysis (Gladman, 1972). The results indicate that carbides do not contribute significantly to the strength of bainite; this is probably a reasonable conclusion, but it has been pointed out that the analysis includes empirical constants which are difficult to justify (Honeycombe and Pickering, 1972).

12.2.3 *Effect of Austenite Grain Size*

We have already seen that the hardness of bainite is insensitive to the austenite grain structure. There have, nevertheless, been many investiga-

tions on the role of the austenite grain size and the bainite packet (sheaf) size on the strength. Indeed, these two features must be related to each other, but both of them are much coarser than the lath boundaries. Hence, even though Hall–Petch plots seem to show a dependence on the austenite and packet sizes, this dependence is probably fortuitous. Experiments have demonstrated that for martensite, the strength does not depend on the austenite grain size in low carbon steels (Brownrigg, 1973). Whether this applies to bainite depends on the effectiveness of the low misorientation boundaries that exist between neighbouring platelets within a sheaf, in hindering dislocation motion. If there are films of austenite, or carbides separating the platelets within a sheaf, then they should be much more formidable barriers than implied by the small crystallographic misorientations between the sub-units. Since this is the case for most bainitic steels, it is unlikely that the austenite grain size or the packet size have any significant effect on strength. This does not of course mean that they do not influence mechanical properties such as toughness, as will be discussed later.

It has also been proposed that the gradual yielding behaviour typical of bainitic steels is one of the factors which makes the proof stress insensitive to the austenite grain size (McEvily and Magee, 1968). A similar observation has been reported for lath martensite (Brownrigg, 1973). The main effect of changing the austenite grain size seems to be to reduce the bainite packet size, so that the yield stress must therefore also be insensitive to the packet size (Gladman *et al.*, 1975; Brozzo *et al.*, 1977). The gradual yielding behaviour is discussed later in this Chapter.

12.2.4 *Effect of Tempering on Strength*

The hardness and tensile strength of fully bainitic microstructures decrease during tempering, the rate of change being larger for lower bainite, which has a higher starting hardness. As is to be expected, it is the highest strength steels which undergo the largest changes in strength during tempering (Bush and Kelly, 1971). This behaviour is also found during tempering of martensite (Leslie, 1982) and is a reflection of the fact that the low strength steels are in any case rather close to the strength of the fully tempered microstructure.

It has been shown that the strength at any stage of tempering correlates well with the interparticle spacing, irrespective of the thermal history of the bainite (Deep and Williams, 1975). These results could be taken to imply that the strength depends mainly on carbide dispersion strengthening, but unfortunately, the grain size, particle size and distribution and dislocation density are not independent parameters. For example, studies using very low carbon bainitic steels have established that the combined

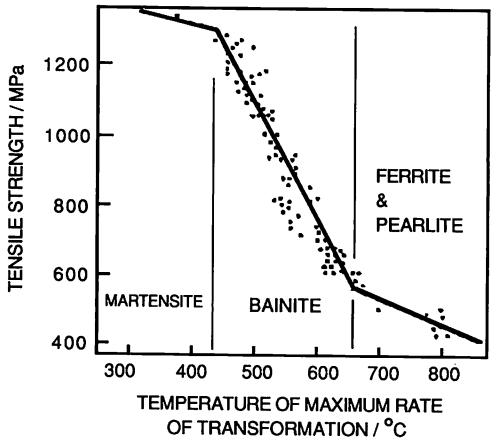

Fig. 12.4 *Variation in the tensile strength of bainitic steels as a function of the temperature at which the rate of transformation is largest during continuous cooling heat treatment (Irvine* et al., *1957).*

strengthening effects of dislocation density and the ultrafine bainitic ferrite grain size are very substantial (McEvily and Magee, 1968). In bainitic steels containing retained austenite, the yield strength is found to be low due to the relative softness of the austenite. Tempering these steels at temperatures as high as 540°C does not lead to a reduction in yield strength, the general softening of the microstructure being compensated by the removal of the soft austenite which decomposes diffusionally into a harder mixture of ferrite and carbides (Kalish *et al.*, 1965).

There are some interesting empirical relationships between strength and transformation characteristics, particularly for low carbon, low alloy, fully bainitic steels. Irvine *et al.* 1957 found a negative linear correlation between tensile strength and the 'temperature of maximum rate of transformation', indicating that the alloying element effect on strength can be rationalised simply on the basis of transformation kinetics (Fig. 12.4). For similar steels, the tensile strength is also found to correlate with the B_S temperature (Coldren *et al.*, 1969). These results may be explained qualitatively: the bainite obtained at lower transformation temperatures should have a finer plate size and a larger dislocation density.

12.2.5 The Strength Differential Effect

It is an established effect in metals that plastic deformation becomes easier when the sense of the deformation is suddenly reversed. Thus, when the loading is changed from compression to tension (or vice versa), the deformation occurs more easily than would have been the case had it continued

in the compressive mode. This is called the *Bauschinger effect*. A simplistic explanation for it is that deformation creates reversible features such as dislocation pile-ups, which relax and hence aid deformation in the reverse direction when the sense of the load is changed. The effect before becomes less prominent as the total plastic strain increases, since the general build up in defect density makes it difficult for relaxation to occur.

Careful experiments on steels containing either martensite, bainite or Widmanstätten ferrite show that they have a higher yield stress in compression than in tension. This *strength differential effect* (Rauch and Leslie, 1972), persists even at large plastic strains, is independent of the starting sense of the deformation, and it is not influenced by cyclic prestraining. It is believed to be associated with microstructures containing a high density of dislocations. It is not, for example, found in annealed ferrite or in ferrite–pearlite mixtures (Leslie, 1982). It has been shown to be inconsistent with an internally induced Bauschinger effect. Since the elastic modulus is found to be similar in both tension and compression, the results cannot be explained in terms of the opening of microcracks during tension but not in compression (Rauch and Leslie, 1972).

There does not seem to be any complete explanation for the phenomenon (Kennon, 1974), but then it may be related to the presence of a nonlinear elastic interaction between dislocations and interstitial carbon atoms, the interaction being asymmetric in tension and compression (Hirth and Cohen, 1970). But it is not clear why the effect should be confined to microstructures with large dislocation densities.

12.3 Ratio of Proof Stress to Ultimate Tensile Strength

If a material does not exhibit a sharp yield strength then a proof stress may be defined as the uniaxial stress needed to produce a specified amount of plastic strain (usually 0.2%). The strain rate involved in the measurement should strictly also be defined, but for steels there is only a 10% increase in the flow stress with an order of magnitude change in strain rate (Knott, 1981). Sharp yield points are not observed in stress–strain curves of bainite and it is usual to specify the yield strength in terms of a proof stress. As dislocation motion becomes more difficult at low temperatures, the proof-stress to UTS ratio increases, typically from about 0.67–0.80 over the range 300–70 K (Krishnadev and Ghosh, 1979).

In high strength steels, it is desirable to have a proof stress to ultimate tensile strength (UTS) ratio (r_1) which is less than about 0.8. This helps to ensure that there is substantial plastic deformation prior to ductile fracture, and a low value of r_1 in many cases correlates with good fatigue resistance. On the other hand, it is also a disadvantage to have a very low value of r_1, because it indicates a low proof stress which makes for

uneconomical engineering design. Unfortunately, many bainitic steels, particularly those with high strengths, have r_1 values much lower than 0.8 even though the UTS may be very large (Irvine and Pickering, 1965). It is believed that internal stresses caused by the displacive mode of transformation, and the existence of many mobile dislocations, has the effect of lowering the proof stress. This is confirmed by the fact that a low temperature (400°C, 1hr) tempering treatment, which has only a minor effect on the microstructure, reduces the internal stresses and raises r_1 without any loss of strength. Such tempering treatments are the whole only effective for bainite produced by transformation at relatively low temperatures, since that produced at higher temperatures is in any case annealed during transformation.

Residual stress is not a complete explanation of the absence of sudden yielding during tensile tests. Gradual yielding is found to persist even after stress relief heat treatments. The microstructure of bainite is inhomogeneous and includes fine particles of relatively hard phases such as cementite, which by acting as stress concentrators with different potencies, induce a gradual yielding behaviour. In bainite, there is also an irregular distribution of obstacles (solute atoms, precipitates of different sizes, boundaries) to the motion of dislocations, obstacles whose 'strength' is variable. There will therefore exist obstacle free areas into which dislocations can penetrate at low stresses, thus giving rise to a gradual deviation from elastic deformation (Kettunen and Kocks, 1972; Kettunen and Lepistö, 1976).[2]

Another scale of microstructural heterogeneity can arise when a large volume fraction of a phase harder or softer than bainite is included in the sample (Hehemann *et al.*, 1957). Much of the deformation is initially concentrated in the softer phase and this has the effect of reducing the yield stress of the softer phase (see for example, Tomota *et al.*, 1976). The hard phase commences to deform after the softer phase has strain hardened and is able to transfer some of the load. Some of the early work which indicated rather low values of r_1 for bainite, can be explained by the fact that it was based on mechanically inhomogeneous microstructures of martensite, retained austenite and bainite, instead of fully bainitic samples (Coldren *et al.*, 1969). In high silicon steels, where it is generally

2 The deformation behaviour of a microstructure as complex as that of bainite seems qualitatively consistent with the statistical theory of slip (Kocks, 1966). In this, a crystal is assumed to contain a random distribution of obstacles of differing strength. Dislocations have a finite probability of overcoming obstacles even when the applied stress σ is below the macroscopic yield stress σ_y. The mean free slip area A_S for dislocation glide varies with σ/σ_y and when dislocations can sweep right across the specimen, $\sigma=\sigma_y$.

possible to obtain large amounts of retained austenite in association with bainite, the softer austenite has been shown to lead to a reduction in the yield stress of the microstructure (Kalish *et al.*, 1965). More recent research confirms this, since low values of r_1 are found to correlate with the existence of large amounts of retained austenite in the microstructure (Sandvik and Nevalainen, 1981). The austenite can be partly transformed into martensite by refrigeration in liquid nitrogen, or by tempering the steel to induce the austenite to decompose into ferrite and carbides. The reduction in retained austenite content leads to an increase in yield strength after both of these thermal treatments. The ultimate tensile strength is hardly affected, because the retained austenite in any case decomposes by stress induced martensitic transformation during the early stages of deformation in a tensile test (Kalish *et al.*, 1965).

Gradual yielding is advantageous in forming operations where it helps to avoid the 'stretcher strains' which represent fronts between yielded and unyielded metal (Luders fronts). Dual phase steels are designed to take advantage of the gradual yielding associated with mechanically inhomogeneous microstructures. They consist of a mixture of soft proeutectoid ferrite and a hard phase which may be bainite, martensite or indeed, a mixture of both phases (e.g., Bhadeshia and Edmonds, 1980b). However, recent reports indicate that after intercritical annealing to produce a mixture of allotriomorphic ferrite and austenite, quenching to a temperature below B_S to isothermally transform the austenite to bainite, can lead to difficulties with respect to the yielding behaviour (Choi *et al.*, 1988). The heat treatment below B_S causes quench ageing in the allotriomorphic ferrite, thereby giving discontinuous yielding behaviour during tensile tests. The ageing occurs because of the difference in the solubility of interstitials, between the intercritical annealing temperature and the bainite transformation temperature. It may therefore be possible to avoid quench ageing by generating the required microstructure using continuous cooling heat treatment, which would provide an opportunity for the interstitials to equilibrate during cooling.

Choi *et al.* have also shown that discontinuous yielding can be avoided if the hard phase is a mixture of bainite and martensite. This is because the latter forms during cooling from the isothermal transformation temperature and generates fresh interstitial-free dislocations so that the gradual yielding behaviour is recovered.

It is not surprising that bainitic dual phase steels are weaker than those containing martensite. Because of their lower strength, the ratio of the proof stress to UTS tends to be larger. Bainitic dual phase steels have nevertheless been demonstrated to possess better formability and fatigue strength (Sudo *et al.*, 1982, 1983). It follows that in this instance, r_1 is not a reliable indicator of fatigue performance.

The required magnitude of the proof stress/UTS ratio must be assessed for each application. For example, in the case of pipe line alloys (low carbon bainitic steels) used for the conveyance of oil or gas under pressure, the fabricated line has to undergo a preservice hydrotest in which it is pressurised to 125% of the planned operating pressure. If the value of r_1 is too low, there is a possibility of gross plastic deformation and hence, pipe failure during hydrotesting. It is then common to specify a minimum value of r_1 which is in the range 0.85–0.90 (Jones and Johnson, 1983). On the other hand, steel columns used in the construction of steel buildings in earthquake areas are required to absorb energy without failure; a low r_1 value is then an advantage.

12.4 Ductility

It was noticed as early as 1957 by Irvine and Pickering, that low carbon bainitic or martensitic steels always show superior tensile ductility when compared with their high carbon counterparts, even when the comparison is made at identical strength. Their subsequent work (1965) confirmed that ductility can be improved by reducing the carbon concentration of a fully bainitic microstructure while maintaining its strength using substitutional solid solution strengthening.

Ductile fracture in good quality commercial steels which do not contain many nonmetallic inclusions propagates via the nucleation, growth and coalescence of voids. Macroscopic fracture occurs when the voids link on a large enough scale. If the number density of voids is large, then their mean separation is reduced and coalescence occurs rapidly, giving a minimal amount of plastic deformation before fracture, and reducing the

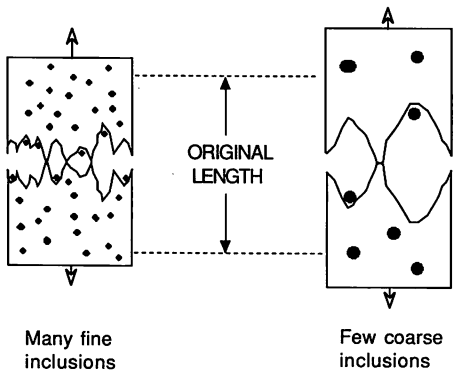

Fig. 12.5 *An illustration of how a large density of void nucleating particles can result in fracture with a low overall ductility, even though the material fails by gross plastic deformation on a microscopic scale.*

overall ductility (Fig. 12.5). The number of carbide particles per unit volume increases with the carbon concentration of bainitic steels (Pickering, 1958). It is these carbides which are responsible for void nucleation in clean steels, so it follows that ductility must decrease with increasing carbon concentration even if the strength remains constant.[3]

In steels which do not transform completely to bainite, voiding during ductile deformation has also been observed at the hard regions of untempered martensite which form on the transformation of carbon enriched residual austenite (McCutcheon *et al.*, 1976). Presumably, the brittle failure of martensite provides the nuclei for void growth. This also explains why the elongation of fully bainitic low carbon steels is always better than that of tempered martensite of the same strength, whereas the situation reverses when the comparison is made at high carbon concentrations (Irvine and Pickering, 1965). It is probably more difficult to obtain fully bainitic microstructures (without the untempered martensite) when the carbon concentration is large.

The linking of voids during ductile deformation begins with internal necking between adjacent voids (*see* for example, Knott, 1973, p. 211). Since the necking instability depends on the ability of the material to work harden, ductility should decrease if the work hardening rate is small. Experimental results do not bear this out. Deep and Williams (1975) have shown that tempered upper bainite strain hardens more rapidly than tempered lower bainite. Both microstructures were found to have identical ductilities even though comparisons were made at identical values of interparticle spacing and mean carbide size. Thus, the effect of work hardening, and indeed of the yield stress, on ductile failure of bainitic steels is not yet understood.

The ductility (as measured by elongation) of fully bainitic, low carbon steels is found to be better than that of quenched and tempered martensitic steels of equal strength (Irvine and Pickering, 1965) but the situation reverses at higher carbon concentrations. The ductility as measured by reduction of area is on the other hand always worse for bainitic steels. These results are also not easily explained. A further difficulty is that the ductility trends indicated by elongation data are inconsistent with those suggested by reduction of area measurements. Martensitic steels almost always have larger reductions of area in tensile tests against comparable bainitic steels.

3 The term *clean* implies the absence of nonmetallic inclusions of a size larger than cementite particles. High carbon steels, where the cementite particle size may be expected to be large, can be air melted, and yet be classified as clean. For low carbon bainitic steels, significant differences in toughness are obtained for the air melted and vacuum refined conditions (McEvily and Magee, 1968), so that only the latter can be considered clean.

12.4.1 Ductility: The Role of Retained Austenite

Both the total elongation, and its uniform component, reach an optimum peak value as a function of the volume fraction of retained austenite, when the amount of austenite is varied by altering the degree of isothermal transformation to bainitic ferrite (Sandvik and Nevalainen, 1981). The difference between the uniform and total elongation decreases as the optimum volume of retained austenite is reached. Further increases in retained austenite content are associated with tensile failure which occurs before the necking instability, so that the difference between uniform and total elongation vanishes.

The best elongation behaviour is observed when the retained austenite is present mainly in the form of films between the sub-units of bainite, rather than as blocky regions between the sheaves of bainite (Sandvik and Nevalainen, 1981). Hence, the optimum retained austenite content increases as the transformation temperature decreases, because the sub-unit thickness decreases, permitting more of the austenite to be in the film morphology for a given volume fraction of transformation to bainite. For the same reason, the elongation becomes less sensitive to retained austenite content as the transformation temperature is reduced. While mechanically unstable austenite, i.e. the austenite which decomposes to deformation induced martensite, is recognised to cause a deterioration in toughness for bainitic steels (Horn and Ritchie, 1978; Bhadeshia and Edmonds, 1983a, b), this is not the case for ductility, presumably because of the TRIP effect and the lower strain rates involved in conventional tensile tests.

It must be emphasised that all these results are very difficult to interpret quantitatively. Changes in retained austenite content cannot easily be made without altering other factors such as the tensile strength and the distribution of the austenite. For example, Miihkinen and Edmonds (1987b) have reported a monotonic increase in uniform and total ductility with retained austenite content. The latter was varied by altering the transformation temperature, so that the strength increased as the austenite content decreased.

12.5 Impact Toughness

Impact toughness is generally characterised by a Charpy test in which a square sectioned, notched bar is fractured under given conditions and the energy absorbed in the process is taken as a measure of toughness. The purpose of the blunt notch is to concentrate the stress in such a way that it increases the degree of constraint in the vicinity of the notch. The yield stress for plastic flow is therefore raised, making brittle fracture more

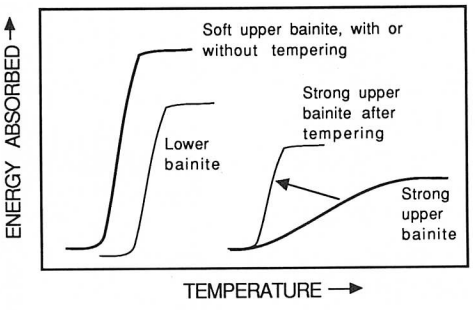

(a)

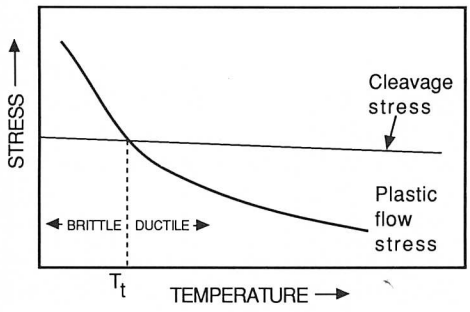

(b)

Fig. 12.6 *Schematic illustration of impact transition curves (a) and of the cause of the ductile–brittle transition temperature. (b).*

likely. The tests are conducted over a range of temperatures, and a plot of the impact toughness versus temperature is called an impact transition curve, which generally has a sigmoidal shape (Fig. 12.6a). The flat region of the curve at high temperatures is called the *upper shelf* and represents ductile failure. The corresponding flat region at lower temperatures is called the *lower shelf* and represents cleavage failure. In the transition region fracture occurs as a mixture of cleavage and ductile failure. The impact transition temperature (T_t) is usually defined as the temperature at which fracture surface shows 50% cleavage fracture.

The impact test is undoubtedly an empirical test in the sense that it does not give information of direct use in design since the results vary with sample size and geometry. It is nevertheless widely used in quality control and in development work; minimum values of impact toughness are often specified in official standards and safety assessments.

The transition temperature is a concept unique to BCC metals whose cleavage stress is insensitive to temperature, but whose plastic flow stress rises rapidly as the temperature decreases (Fig. 12.6b). The rapid increase in plastic flow stress is partly a consequence of the large Peierls–Nabarro

barrier to dislocation motion and partly a consequence of the ubiquitous presence of traces of interstitial elements, which interact strongly with dislocation motion. At the transition temperature the curves representing cleavage and flow stress cross on a plot of stress versus temperature. Below T_t, cleavage is easier than plastic flow and vice versa. Any effect which raises the plastic yield stress (such as physical constraint caused by a notch) without influencing the nucleation or growth of cleavage cracks inevitably leads to an increase in T_t. In general, cleavage fracture is fast, occurs with little warning, absorbs minimal energy and is undesirable so that a low transition temperature is an important aim in safe design.

12.5.1 Fully Bainitic Structures

Irvine and Pickering (1963) conducted a major study of the Charpy impact properties of normalised low-carbon bainitic steels (typical composition Fe–0.003B–0.5Mn–0.5Mo–0.1C wt%). Their results are important and simple to interpret because the samples studied were free of proeutectoid ferrite and almost free of martensite.[4]

The impact properties of relatively soft upper bainite formed at high temperatures were not found to be significantly affected by tempering treatments at temperatures as high as 925K for 1h, as long as the plate morphology of the ferrite was unaltered by the heat treatment. Any bainite that grows at a high temperature is expected to undergo some tempering during transformation so it is not surprising that few changes occur when further tempering is carried out. The effect is analogous to the *autotempering* which is associated with martensite which has a high M_S temperature.

For strong upper bainite obtained by continuous cooling transformation at lower temperatures, the impact transition temperature T_t increases as expected, but the upper shelf energy also decreases. Furthermore, the ductile–brittle transition becomes less well defined, the region of the impact curve between the upper and lower shelves extending over a larger temperature range (Fig. 12.6a). This temperature range becomes narrower, and T_t and σ_y decrease, on tempering. The larger sensitivity to tempering is consistent with the lower degree of autotempering expected in bainite generated by transformation at low temperatures.

Even higher strength can be obtained by transforming to lower bainite, which then exhibits good impact transition temperatures comparable to

4 It is the combination of low carbon and low substitutional alloy concentration, the ease of cementite precipitation in these steels, and the continuous cooling heat treatment which allow the bainite reaction to consume all of the austenite (i.e., avoid the incomplete reaction phenomenon).

those of low strength upper bainite. The cementite particles in lower bainite are much finer than in upper bainite. Cementite is intrinsically brittle and tends to crack under the influence of the stress which accumulates as its blocks an active slip band. At a sufficiently low temperature, or when the strain rate is large, the crack in the cementite can then propagate into the ferrite. When the carbide particles fracture, they do so in their thickness directions; for finer carbides, these cracks are in turn smaller and do not propagate as readily into the matrix, thus explaining the higher toughness of lower bainite.

If the microcrack nucleus is treated as a through thickness Griffith crack of length c, then the fracture stress for the propagation of cleavage, σ_F, is given (McMahon and Cohen, 1965) by

$$\sigma_F = [4E\sigma_p/\pi(1-\nu^2)c]^{0.5} \tag{12.2}$$

where E is the Young's Modulus for ferrite, ν is Poisson's ratio for ferrite and σ_p is the plastic work of fracture per unit area of crack surface (i.e., an effective surface energy). If c is now set equal to the carbide particle thickness c_O, then the fracture stress is found to vary as $(c_O)^{-0.5}$. The details of this relationship must of course vary with the shape of carbide particles but the general relationship between σ_F and c remains the same; for example, when considering mixtures of ferrite and spheroidal carbides, the stress σ_F necessary to propagate cleavage fracture through the ferrite has been shown (Curry and Knott, 1978) to be given by

$$\sigma_F = [\pi E\sigma_p/(1-\nu^2)c_d]^{0.5} \tag{12.3}$$

where c_d is the diameter of the penny shaped crack resulting from the cleavage of the spheroidal carbide particle.

The identification of the crack length c with the carbide particle thickness c_O is a vital assumption which can be justified experimentally for mild steels containing a microstructure of equiaxed ferrite and cementite particles. This is a carbide controlled fracture mechanism, but the alternative possibility is a grain size controlled fracture mechanism, in which the fracture stress is the stress required to propagate cleavage across grains. In that case, the parameter c must be identified with a grain size dimension, and in the case of bainite, with a packet size. Brozzo *et al.* (1977) have demonstrated that for very low carbon bainitic steels (containing 0.025–0.50 C wt%) the convariant bainite packet size is the microstructural unit controlling cleavage resistance.

It may however be the case that for higher carbon bainitic steels, it is the carbide particle size which controls cleavage fracture. For these alloys, bainitic microstructures are found to be more brittle when compared with martensitic structures of equal strength (Irvine and Pickering, 1965). This is probably because the inter-plate carbides are much coarser in bainite

than in martensite. This has hindered the use of high carbon bainitic steels in applications where toughness is crucial. The problem is discussed in more detail in the next section.

12.6 Fracture Mechanics Approach to Toughness

Most bainitic steels are used in high strength applications and failure is not usually accompanied by a large amount of plasticity; they are in this sense 'brittle' materials. It is therefore a good approximation to use elasticity theory to represent the stresses in the vicinity of a sharp crack, even though cleavage crack propagation in metals always involves a degree of plastic deformation at the crack tip. Making the further assumption of *linear* elasticity, we have the linear elastic fracture mechanics (LEFM) approximation. One definition of a sharp crack is that the inevitable plastic zone that exists at the crack tip is small enough to permit the LEFM approximation.

A fracture mechanics approach to toughness is much more reliable than impact testing in the sense that a properly conducted test gives a toughness value which is a material property, on the whole independent of specimen geometry effects. The pre-cracked test samples and the conditions (e.g., strain rate) during the test are similar to the conditions experienced during service, and the results can be used quantitatively to predict whether a structure is likely to fail catastrophically under the influence of the design stress. There are excellent books and reviews on the subject (e.g., Knott, 1973) but a brief introduction is necessary for an adequate discussion of the work on bainite.

Using LEFM, it is possible to show that under the influence of an uniaxial applied tensile stress σ (i.e., in mode I loading), the stress σ_r at a distance r ahead of the sharp crack tip is given by

$$\sigma_r = K_I (2\pi r)^{-0.5} \tag{12.4}$$

where K_I is a stress intensification factor in mode I loading. K_I is a function of the applied stress σ and of the specimen geometry

$$K_I = \sigma Y\{c/W\}, \tag{12.5}$$

where Y is a compliance function which depends on the crack length c and on the specimen width W. For a body of infinite extent, containing a central through thickness crack of length $2c$, normal to σ, $Y=(\pi c)^{0.5}$. For 'brittle' materials, K_I at fracture takes a unique *critical* value K_{IC}. The value of K_{IC} is then independent of W or any other specimen variables; it is a material constant and can, with the help of appropriate compliance functions, be used to design against catastrophic failure in service.

12.6.1 Microstructural Interpretation of K_{IC}

In considering the role of microstructure in fracture, it is in general necessary to distinguish between 'large' and 'small' particles, in the sense that for small particles, the phenomenon controlling fracture is the propagation of particle sized microcracks into the surrounding ferrite matrix. For larger particles the cracking of the particle represents the critical event, with propagation into the matrix and across the grain boundaries following automatically (Gibson, 1988; Burdekin, 1990). For the most part, high strength steels such as bainitic or martensitic alloys should, if manufactured properly, lie in the small particle regime so that the discussion below focuses on that specific issue.

It is sometimes possible to relate the K_{IC} values to microstructural and micromechanistic parameters. It can be argued that the critical value of stress intensity which leads to failure must be associated with corresponding critical values of stress σ_C and distance r_C (Knott and Cottrell, 1963; Knott, 1966; Ritchie *et al.*, 1973; Knott, 1981)

$$K_{IC} = \sigma_C (2\pi r_C)^{0.5} \tag{12.6}$$

where σ_C is usually identified with σ_F (equation 12.1), the local stress necessary to propagate a microcrack nucleus. σ_F varies with carbide thickness, or more generally, with the size of the microcrack nuclei resulting from the fracture of any brittle phase in the steel; it is however, relatively independent of temperature.

The interpretation of the distance r_C is rather less straightforward. The sample used in a fracture toughness test contains a machined notch, but to make the specimen more representative of failure during service, it is initially fatigue loaded. A fatigue crack then propagates slowly from the notch root and the fatigue loading is stopped as soon as a uniform crack front is established. The specimen is then ready for toughness testing. The fatigue crack tip is relatively sharp but not as sharp as the tip of a cleavage crack. It does not therefore propagate when the specimen is tensile loaded for the K_{IC} test. Instead, it is alleged that the stress field extending from the fatigue crack tip causes carbide particles, or other brittle phases, within a distance r_C of the crack tip to fracture. The resulting microcrack nuclei are atomically sharp and propagate into the matrix if the stress σ_C is exceeded. The cleavage cracks then link up with the original fatigue crack and failure occurs rapidly across the specimen section. It is emphasised that both r_C and σ_C are for most materials, statistically averaged quantities, since carbide particles and other microstructural features exhibit variations in size, shape and distribution. If the carbide particle size and spatial distribution is bimodal, due perhaps to the presence of a mixture of microstructures then a large degree of scatter can be expected in

experimental determinations of K_{IC}. The stress field extending from the crack tip in effect samples a finite volume and it is the microstructure of that volume which determines toughness. Hence, Bowen *et al.* (1986) found that K_{IC} values determined for mixed microstructures of upper and lower bainite (the former containing in general coarser cementite) exhibited a large degree of scatter when compared with a microstructure of just upper bainite or just martensite.

The microstructural interpretation of a K_{IC} value thus requires a knowledge of a local tensile stress and a microstructural distance. This approach has been successful in explaining the toughness of mild steels with a microstructure of ferrite and grain boundary cementite (McMahon and Cohen, 1965; Smith, 1966, Knott, 1981) and to a limited extent of low alloy steel weld deposits which have complex microstructures containing non-metallic inclusions which initiate failure (Tweed and Knott, 1983; McRobie and Knott, 1985). In some of these cases, the critical microstructural features controlling cleavage fracture resistance have been identified directly, giving considerable faith in the r_C concept. Difficulties arise when attempts are made to rationalise similarly the toughness of clean bainitic or martensitic structures. A major difficulty is that the carbides particles which may be responsible for microcrack initiation are very fine, making a direct identification of r_C impossible.

If, in these circumstances, the fracture stress σ_F can nevertheless be measured and shown to be constant, then σ_F itself can be used as a measure of 'toughness' (Bowen *et al.*, 1986), although it is not clear how possible variations in r_C can be accounted for in this assessment of toughness. This would also establish that the critical step in the fracture process is the propagation of a microcrack under the action of a tensile stress, and the distance c of equation (12.1) can then be equated to the size of a microstructural feature (such as carbide thickness).

Bowen *et al.* used this approach, together with K_{IC} studies to explain the toughness of tempered martensites and bainite in a low-alloy steel. In all cases, K_{IC} values were found to increase with the test temperature over the range 77–300K. Over the same temperature range, the proof stress was found to decrease with increasing temperature. For a given proof stress, the toughness of bainite was always considerably lower than that of tempered martensite (Fig. 12.7). The fracture stress σ_F was in all cases found to be virtually independent of test temperature, but was again much lower for bainitic than martensitic structures. The results were explained in terms of measured cementite particle size distributions (Fig. 12.7). They showed that it is not the mean carbide particle size which determines toughness, but the coarsest particles to be found in the microstructure and indeed, a plot of σ_F versus the reciprocal square root of the coarsest carbide thickness gave a straight line as predicted by the

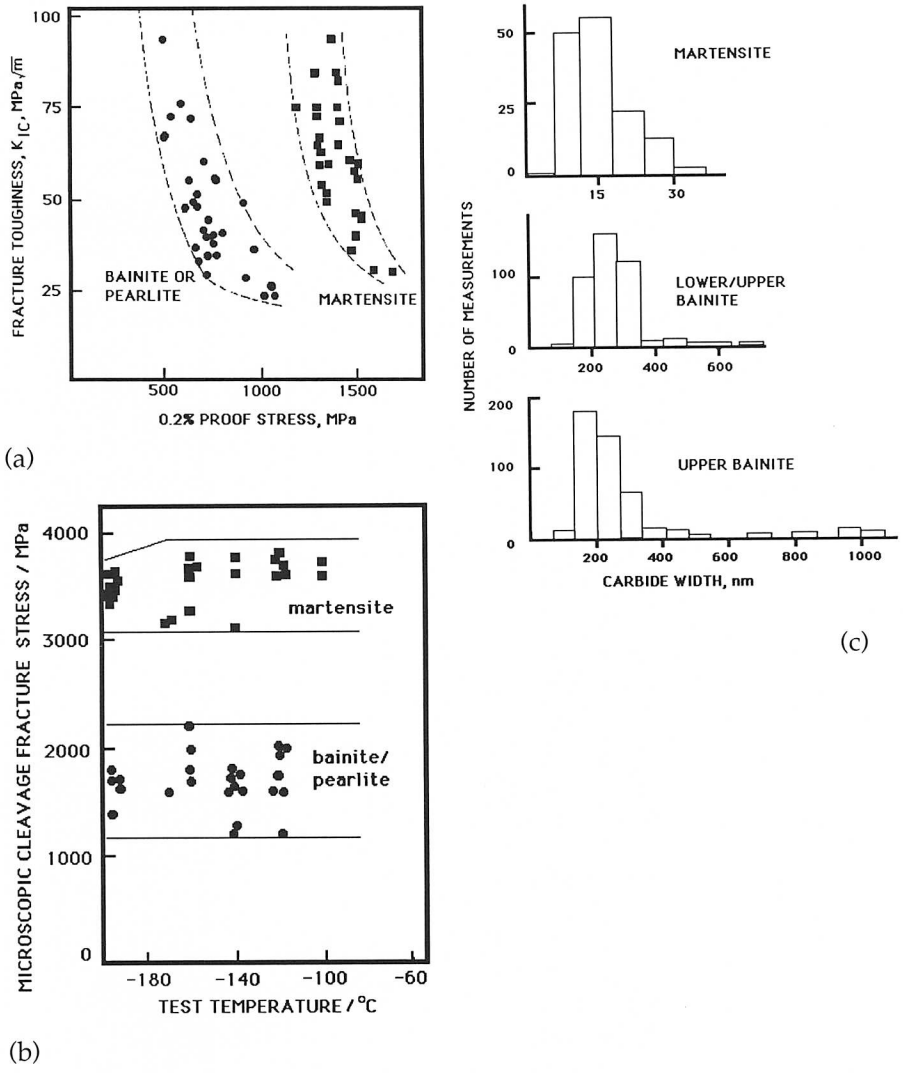

Fig. 12.7 *(a)* K_{IC} *values plotted against corresponding values of the 0.2% proof stress. (b)* σ_F *values plotted against test temperatures. (c) Carbide size distributions obtained from martensitic and bainitic microstructures. (After Bowen* et al.*)*

modified Griffith equation (equation 12.1); deviations from this equation occurred at very small particle sizes. On this basis, for a given proof stress, the toughness is expected (and found) to increase in the order upper bainite, lower bainite and tempered martensite. Trends like these are also very important in the design of welding processes and materials,

and there are many qualitative results which confirm that the toughness increases in that order for microstuctures in the heat affected zones and steel welds (Inagaki and Hiroyuki, 1984; Harrison and Farrar, 1989).

The reason why the modified Griffith equation fails at very small particle sizes is not clear but it means that σ_F becomes relatively insensitive to carbide thickness when the latter is less than about 450 nm.

It must not be assumed that these results spell doom for bainitic microstructures; they need not always have poor toughness relative to tempered martensie. The size of bainitic carbides can be controlled using suitable alloying additions. Indeed, they can be eliminated completely by adding sufficient Si or Al to the steel. The results are also only valid for clean steels in which the fracture mechanism is carbide nucleated and growth controlled. That the coarseness of carbides controls the toughness of bainite in clean steels is emphasised by the fact that in fully bainitic steels, lower bainite with its finer carbides and higher strength nevertheless has a better toughness than the relatively weak upper bainite (e.g. Pickering, 1967). All other things being equal, toughness is expected to improve as the strength falls (i.e., as plastic deformation becomes easier).

We have seen that the micromechanistic model for the toughness of bainite contains the terms σ_C and r_C, the former defining the stress to propagate a microcrack in a cementite particle, and the latter defining the distance over which the stress is sufficiently large to cause carbide cracking. The distance r_C is expected to be very small in comparison with the width of a bainite sheaf, so that the toughness of bainite or martensite should not be dependent on the austenite grain size or the bainite packet size. This prediction has been demonstrated to be the case for tempered martensite (Bowen *et al.*) but contradictory results exist for bainite. Naylor and Krahe (1974) using notched bar impact tests have shown that a refinement in the bainite packet size leads to an improvement in toughness. The impact transition temperature of bainitic steels is also found to decrease as the austenite grain size decreases (Fig. 12.8), although this might simply reflect the fact that the bainite packet size is expected to decrease with austenite grain size. The austenite grain size in Irvine and Pickering's experiments was varied by controlling the temperature at which hot rolling finished, or by reheating into the austenite phase field, before the steel was continuously cooled to give a bainitic structure.

The fracture stress σ_F and the critical distance r_C do not vary significantly with temperature, although K_{IC} for bainite is found experimentally to increase as the test temperature rises. This apparent contradiction arises because of the LEFM approximation. In practice, the effect of temperature is to change the yield stress of the material. At higher temperatures the yield stress is also low, and there is a greater degree of stress

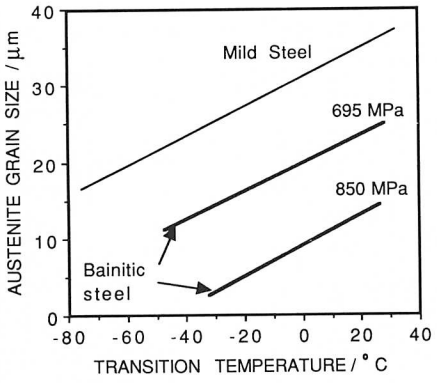

Fig. 12.8 *Variation in the impact transition temperature as a function of the austenite grain size. (After Irvine and Pickering, 1963.)*

intensification in the vicinity of the crack tip. It follows that the size of the plastic zone at the crack tip also increases and consequently, more work is done as the crack propagates, leading to an increase in K_{IC} (Ritchie *et al.*, 1973).

Finally, it is worth noting that the austenite grain size cannot always be varied independently. Some carbides may not dissolve if low austenitising temperatures are used to control the grain size, and these carbides can be detrimental to toughness. There is certainly an increase in toughness as the carbides dissolve when the austenitising temperature is raised (Tom, 1973). As the carbide solubility increases with austenitising temperature, so does the average carbon concentration in the austenite; this in turn causes more of the austenite to be retained to ambient temperature after partial transformation to martensite or bainite (Mendiratta *et al.*, 1972; Kar *et al.*, 1979). Variations in austenite grain size also influence hardenability, so that a fine grain structure can be detrimental if it causes the formation of transformation products such as allotriomorphic ferrite during cooling in a high strength steel (Parker and Zackay, 1975).

12.6.2 Cleavage Fracture Path

Microstructural observations have demonstrated that during cleavage failure, the cracks propagate virtually undeviated across individual sheaves of bainite in low carbon, low alloy steels (Pickering, 1967). Similar results have been reported for low carbon, low alloy steel weld deposits, where qualitative evidence suggests that the cleavage cracks propagate undeflected across packets of bainite platelets but have to be reinitiated on encountering bainite sheaf boundaries (Chandel *et al.*, 1985).

In such steels, the platelets within the sheaves either touch each other at low angle grain boundaries, or are in contact with inter-plate (brittle) cementite. Substantial crack deflections are only found to occur when the cracks encounter sheaf boundaries or prior austenite grain boundaries. The size of cleavage facets obtained by brittle fracture is found to correlate well with the width of the bainite sheaves, i.e., the packet size (Naylor and Krahe, 1974), although there are also many results which indicate that the *unit crack path* is approximately 1.5 times larger than the width of bainite sheaves (Ohmori *et al.*, 1974; Brozzo *et al.*, 1977). The unit crack path is defined simply as the region within which the crack propagates in a nearly straight fashion (Matsuda *et al.*, 1968, 1972). The reason why the path length tends to be somewhat larger than the sheaf width may have something to do with the fact that adjacent sheaves, which are different variants of the Kurdjumov–Sachs orientation relationship with austenite, may have their cleavage planes fairly parallel (Brozzo *et al.*, 1977). Thus, any discrepancy between the packet size and unit crack path length does not weaken the basic argument that having a set of parallel ferrite plates in identical orientation is bad for toughness. Instead, it leads to a more general condition that groups of plates with a common cleavage plane should be avoided. These concepts also extend to martensitic microstructures in low alloy steels, where fractographic measurements indicate that the dominant microstructural feature in the cleavage fracture of martensite is the size of the martensite packet (Roberts, 1970).

Naylor and Krahe (1975) reported some high resolution fractographic experiments on bainitic steels, but unfortunately did not manage to examine fracture in bainitic regions, since the thin foils they prepared always turned out to be the small regions of martensite within the steels. They nevertheless established that the cleavage crack path can lie on {110}, {100}, {112} or {123} ferrite planes.

It was emphasised earlier, that the observations establishing the correlation between the cleavage facet size and the bainite sheaf width, were for low carbon, low alloy steels. In these steels, the volume fraction of bainitic ferrite that forms is large, so that the amount of any residual phases (such as cementite, martensite or retained austenite) between the platelets of bainitic ferrite within a given sheaf tends to be small. Hence, the platelets may touch each other over large areas at low misorientation boundaries, thus giving the crystallographic continuity essential for undeviated cleavage crack propagation. On the other hand, in many more heavily alloyed steels, relatively thick layers of ductile retained austenite can be found between the platelets within a given sheaf. It has yet to be established whether cleavage cracks can propagate undeviated across individual sheaves in these circumstances.

12.7 Temper Embrittlement

There has been relatively little work on temper embrittlement phenomena associated with bainitic microstructures, presumably because most bainitic steels have not been used for applications requiring high strength, where tempered martensitic steels dominate, and where such embrittlement effects are most common. Perhaps the toughness of many common steels in their bainitic condition is so bad as to mask any impurity induced embrittlement.

There are three kinds of embrittlement phenomena associated with quenched and tempered steels, each of which leads either to a minimum in the toughness versus tempering temperature curve, or to a reduction in the rate at which toughness rises with tempering temperature:

(i) *650°C Reversible Temper Embrittlement*: In this, tempering at around 650°C facilitates the segregation of impurity elements such as phosphorous to the prior austenite grain boundaries, leading to intergranular failure along these boundaries. The reversibility arises because the impurity atmospheres at the grain boundaries can be 'evaporated' by tempering at a higher temperature (below the eutectoid temperature). Quenching from the higher temperature avoids the resegregation of the impurities while cooling past 650°C, so that the embrittlement effect can be eliminated.

In fact, one of the tests for the susceptibility of bainite microstructure to impurity controlled embrittlement involves a comparison of the toughness of samples which are water quenched from a high tempering temperature (680°C) with those which are slowly cooled to provide an opportunity for the impurities to segregate during cooling (Bodnar *et al.*, 1989).

Studies of the bainitic steels used in creep resistant applications reveal that phosphorus and tin, and to a lesser extent manganese and silicon, are detrimental as far as temper embrittlement is concerned (Bodnar *et al.*, 1989). The manganese effect is consistent with other work which suggests that it reduces the intergranular fracture strength (Grabke *et al.*, 1987). Silicon on the other hand, is known to promote the segregation of phosphorus to the austenite grain boundaries (Smith, 1980), and can itself cosegregate with nickel to the grain surfaces (Olefjord, 1978). There are also smaller effects due to arsenic, antimony and sulphur. The tendency for embrittlement seems to correlate strongly with an empirical 'J' factor

$$J = \text{Mn} + \text{Si} + 10^4(\text{P} + \text{Sn}) \tag{12.7}$$

where the concentrations of elements are in weight percent (Fig. 12.9).

To summarise, the impurity controlled temper embrittlement phenomenon for bainitic steels essentially replicates the behaviour of quenched

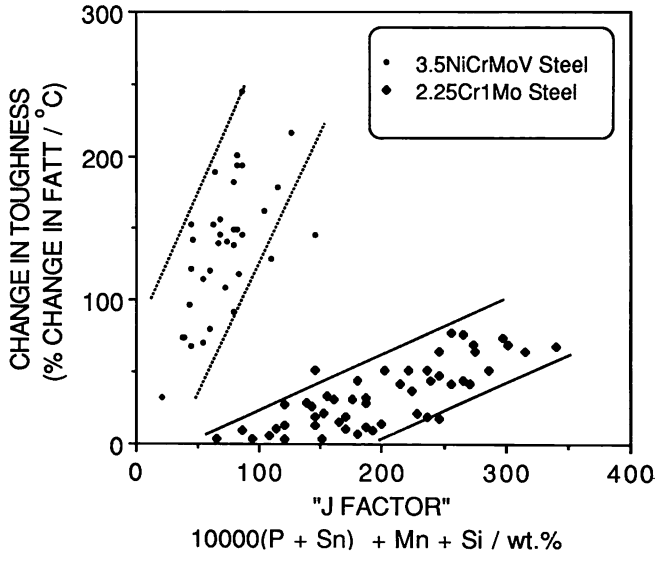

Fig. 12.9 *Correlation between the tendency to undergo temper embrittlement and an empirical 'J' factor which is a function of chemical composition (Watanbe and Murakami, 1981; Bodnar* et al., *1989).*

and tempered martensitic steels, a result which is not unexpected since the growth of both products is confined to individual austenite grains. This means that the original structure of the austenite grain surfaces although modified, is not really disrupted by transformation as far as segregation effects are concerned. By comparison, reconstructive transformations products such as allotriomorphic ferrite, can grow across the austenite grain surfaces, so that failure along the prior austenite grain boundaries becomes impossible.

Finally, it is noteworthy that although the science of the embrittlement effects is fairly well established, most commercial steels contain more impurities than would be desirable in ideal circumstances. With the exception of Mn and Si, all the other impurity elements are very difficult to control for commercial steels, and there is considerable effort involved during the steelmaking process and in the choice of scrap and raw material inputs.

(ii) *300→350°C Temper Embrittlement*: Fracture is again intergranular with respect to the prior austenite grain boundaries where coarse cementite particles precipitate during tempering. At the same time, the grain boundaries are weakened by impurity segregation. The cementite particles crack under the influence of the applied stress and hence concentrate stress at the weakened boundaries. These factors combine to cause an embrittlement effect.

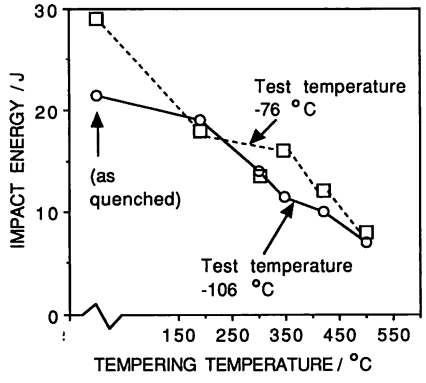

Fig. 12.10 *Plot of toughness versus tempering temperature for a high purity martensitic steel, illustrating that the toughness is reduced even though the strength decreases on tempering (Bhadeshia and Edmonds, 1979b).*

(iii) *300→350°C Tempered Martensite Embrittlement*: This effect is common in very clean steels, with fracture occurring transgranularly with respect to the prior austenite grain boundaries. It is attributed to the formation of cementite particles at the martensite lath boundaries and within the laths. During tempering, the particles coarsen and become large enough to crack, thus providing crack nuclei which may then propagate into the matrix. As a consequence of this effect, untempered low carbon martensitic steels sometimes have a better toughness than when they are tempered, even though the tempering reduces strength (Fig. 12.10). The cementite in effect acts in the manner of undesirable inclusions.

Both of the impurity controlled embrittlement phenomena (i) and (ii) can be minimised, particularly by adding up to 0.5 wt% molybdenum to the steel. The Mo associates with phosphorus atoms in the lattice so that their tendency to segregate to boundaries is reduced along with their mobility. Higher molybdenum concentrations are often not useful because some of the molybdenum then precipitates in the form of carbides. Clean steels do not suffer from such temper embrittlement.

In many bainitic microstructures, tempering even at temperatures as high as 550°C has a relatively small effect on cementite particle size and morphology. Consequently, the low temperature embrittlement phenomena are not found in conventional bainitic microstructures (Ohmori *et al.*, 1974).

When bainite in carbon containing iron alloys is free from carbide particles, its microstructure consists of bainitic ferrite and the residual phase martensite and carbon enriched retained austenite, there is a special 'embrittlement' effect associated with the decomposition of the

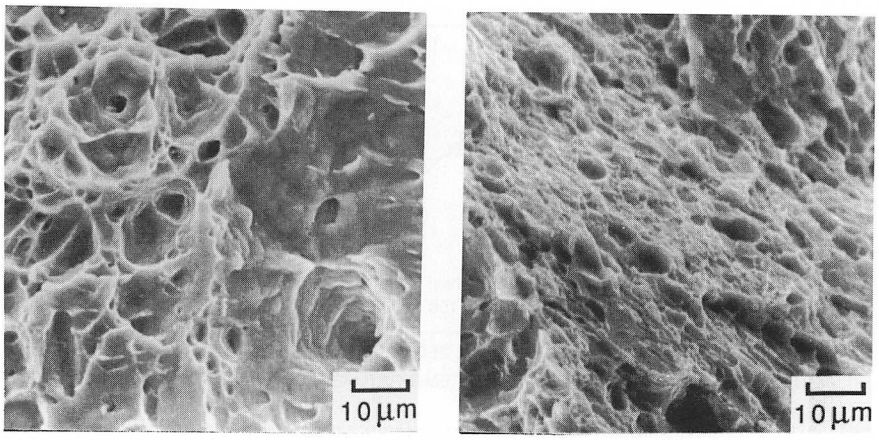

(a) (b)

Fig. 12.11 *Scanning electron micrographs of the fracture surfaces of untempered (a) and tempered (b) samples, showing the much reduced dimple size in the latter sample which contains numerous carbide particles which help nucleate voids.*

austenite during tempering (Bhadeshia and Edmonds, 1983a, b). The effect is specific to clean steels and is associated with a large reduction in the work of fracture even though the failure mode is ductile. Ductile failure occurs by the nucleation and linkage and microvoids. In the absence of carbide particles, the number of voids nucleated is small, so that the total plastic strain before the voids link is large since they are widely spaced (Fig. 12.5). When the austenite decomposes to a mixture of carbides and ferrite, the carbides enhance the void nucleation rate. The resulting smaller spacing between the voids leads to a reduction in the plastic strain prior to failure, even though the strength of the bainite drops on tempering. The effect is obvious from an examination of fracture surfaces: those from untempered bainite exhibit much larger 'dimples', indicative of widely spaced nucleation sites (Fig. 12.11). Similar reductions in the ductility and toughness have been correlated versus the decomposition of austenite to carbides in high silicon bainitic cast irons (Dubensky *et al.*, 1985). Recent work has indicated that even the presence of carbides within the lower bainitic ferrite can impair toughness (Miihkenen and Edmonds, 1987c).

12.8 The Fatigue Resistance of Bainite Steels

There are relatively few studies of fatigue phenomena in bainitic steels, partly because the steels have only recently been considered seriously as

high strength alternatives to the generally superior quenched and tempered martensitic steels, in structural applications where toughness is of prime importance. Notable exceptions are the alloys used in the power generation industry, where thermal fatigue resistance is important in plant designed for intermittent operation, although even there, creep resistance is in most cases the prime factor determining service life. Fatigue crack propagation in hydrogen containing environments (such as chemical or coal conversion plant and a variety of pressure vessel applications) can be life limiting and has been studied in detail for bainitic steels. Good fatigue resistance is also important in bainitic rail steels, where contact stresses due to the repeated passage of train wheels, combined with severe wear problems can limit the service life of rails.

12.8.1 Fatigue of Smooth Samples

Fatigue tests on smooth samples give information on the sensitivity of the specimen to fatigue crack initiation, especially if the material involved is 'clean'. The results are usually expressed in the form of an *S–N* curve, which is a plot of $\ln\{\sigma_a\}$ versus $\ln\{N\}$, where σ_a is the alternating stress amplitude used in any particular test, and N is the corresponding number of cycles to failure (Fig. 12.12).

Materials which strain-age show a 'fatigue limit', which is a value of the alternating stress amplitude below which fatigue failure does not occur. The fatigue limit is the stress below which fatigue cracking never develops, and is usually ascribed to dynamic strain aging in which the mobile dislocations are pinned by interstitials. Recent evidence has on the other hand, emphasised the need for plasticity to spread across grain boundaries for the successful propagation of fatigue cracks (Wilson and Oates, 1964; Mintz and Wilson, 1965; Petch, 1990). Fatigue cracks are said not to develop when plasticity is confined to the surface regions of the

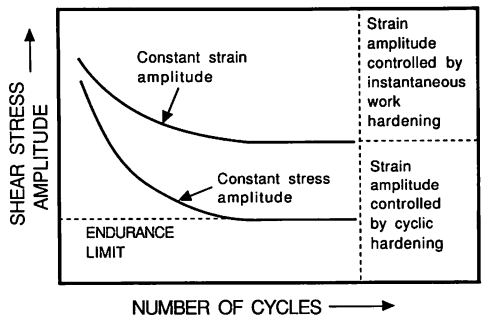

Fig. 12.12 *Schematic S–N curves for fatigue.*

samples. This alternative explanation is supported by the fact that a fatigue limit can be found even when the test temperature is so low that interstitials can hardly be mobile enough to enable dynamic strain aging. At the same time, the role of interstitials is recognised as an additional factor since the fatigue limit actually rises as the temperature is raised to a point where aging becomes possible (Petch, 1990).

Mild steels with a microstructure of equiaxed proeutectoid ferrite exhibit a fatigue limit. For other materials, an endurance limit is defined as the value of the stress amplitude corresponding to a fatigue life of say $N = 10^8$. It is worth noting that the fatigue stresses are in practice less than half the ultimate tensile strength of the steel, so that the plastic strain per cycle can be very small.

Fatigue tests on smooth samples can be carried out with the stress amplitude maintained constant for all cycles, or with the plastic strain amplitude fixed for each cycle (Fig. 12.13). The test chosen depends on the nature of the application, but the two kinds of experiments can reveal different information on the relationship between microstructure and fatigue properties. Clearly, when the strain per cycle is a fixed quantity, the alternating stress amplitude needed to maintain a constant plastic strain increases with the number of cycles since the material *fatigue hardens* as the test proceeds. The hardening eventually reaches a saturation level after many cycles and the stress σ_a does not then vary with N (Fig. 12.13). During each half cycle σ_a has to be raised to the instantaneous flow stress σ_{iy} which can be determined experimentally by interrupting the test at any stage. As the test proceeds, σ_{iy} can be expected to increase as instantaneous work hardening occurs. If σ_s is the value of σ_{iy} at saturation, the ratio $r_2 = \sigma_a/\sigma_s$ is always expected to be close to unity because the applied stress σ_a has to rise to the value of σ_{iy} (Kettunen and Kocks, 1967).

For a test in which the alternating stress amplitude is kept constant, the plastic strain per cycle decreases as the material *cyclically hardens*, until it eventually reaches an approximately constant value. In cyclic hardening, σ_a is constant but σ_{iy} rises, whereas in fatigue hardening $\sigma_a \approx \sigma_{iy}$

Fig. 12.13 *Schematic illustration of constant plastic strain and constant stress fatigue tests (after Kettunen and Kocks, 1967).*

(Kettunen and Kocks, 1972). During the test, σ_{iy} increases due to cyclic hardening as the mean free slip area for dislocations (A_S) decreases. σ_{iy} eventually reaches the saturation value σ_S and at that stage, A_S remains approximately constant with N.

The area A_S at saturation may be larger than the mean slip area per obstacle in which case the to and fro movement of dislocations causes an accumulation of damage which eventually may cause fatigue failure. However, if A_S is of the order of the mean free slip area per obstacle, because σ_a is low, then the motion of dislocations simply involves bowing between obstacles, a process which leads to energy dissipation but not to damage accumulation. The applied stress σ_a at which this happens is the endurance limit and fatigue failure does not then occur for many millions of cycles. For cyclic stressing, the ratio r_2 varies with σ_a, but its value corresponding to the endurance limit (i.e., r_e) is predicted to be $\approx$ 0.65–0.75 for single crystal specimens (Kocks, 1967); for polycrystalline specimens of lower bainite, $r_e \approx$ 0.51–0.55, depending on the way in which the saturation flow stress σ_s, is defined. Bainite yields gradually so that a saturation *proof* stress has to be substituted for σ_s, and the proof stress has to be measured after an arbitrary (though small) plastic strain. Kettunen and Lepistö (1976) found that the saturation proof stress defined at a strain of 0.02 gives the best agreement with theory. Note that the *saturation* proof stress was measured by testing specimens which had first been fatigue cycled to about 20% of their fatigue life to be sure that the specimens are in a state of saturation. In fact, for lower bainite it is a good approximation to take $r_2=(\sigma_a/\sigma_y)$ where σ_y is the proof stress obtained from an ordinary uniaxial tensile test, even though the microstructure is then not in the saturated condition (Kettunen and Lepistö, 1976).

Cyclic hardening is known to correlate with the rate of work hardening in monotonic tensile tests. The rate at which work hardening occurs decreases during both fatigue tests and during monotonic tensile testing. The endurance limit can be identified with the onset of a critical (low) value of the rate of work hardening, associated with the approach to saturation in the context discussed above. Since the ultimate tensile strength is also determined by the point at which a reduced rate of work hardening cannot keep up with increasing stress due to reduction of area, the endurance limit should correlate well with the UTS, and this is experimentally found to be the case (Kettunen and Kocks, 1967, 1972). This correlation should remain valid as long as the failure mode is ductile.

12.8.2 Fatigue Crack Growth Rates

For many engineering applications, the steels used can be assumed to contain subcritical cracks, in which case the initiation of cracks is not a

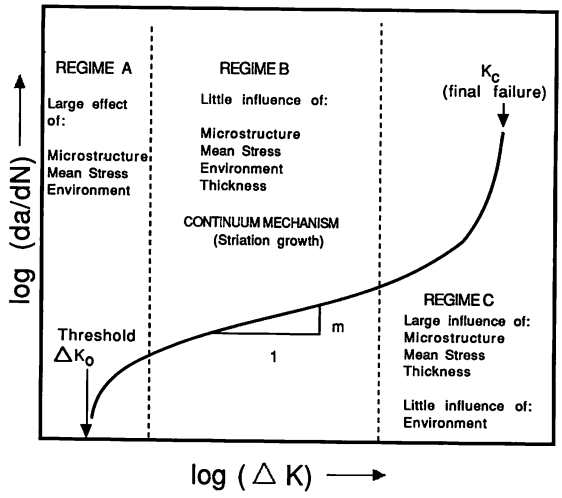

Fig. 12.14 *Schematic illustration of the variation in fatigue crack growth rate as a function of the stress intensity range. (After Ritchie, 1979.)*

controlling feature of fatigue life. The lifetime of the component then depends on the rate at which these subcritical cracks can grow slowly to a critical size where final failure may occur catastrophically. If the plastic zone at the crack tip is small when compared with the characteristic dimensions of the specimen, then most of the material surrounding the tip behaves elastically, and linear elastic fracture mechanics can be used to estimate the stress intensity range ΔK felt at the crack tip due to the alternating applied stress. The stress intensity range can be related to the crack growth rate da/dN, which is the average distance advanced by the crack front per cycle.

Experiments indicate that there is a minimum threshold value of ΔK below which subcritical cracks do not propagate (Fig. 12.14). For many applications, the majority of fatigue life is spent at near threshold levels of stress intensity since the crack growth rates there can be incredibly small, the average advance of the crack front sometimes being less than an interatomic spacing per cycle. Beyond the threshold regime, the crack growth rate increases with ΔK, until the 'Paris Law' regime is reached (Fig. 12.14) the relationship between the stress intensity range and the crack growth rate is empirically found to be of the form

$$da/dN = C_4(\Delta K)^m \tag{12.8}$$

where C_4 is a constant and m is called the Paris constant.

The crack growth rates in regime A where the stress intensity range is near the threshold value are found to be most sensitive to microstructure,

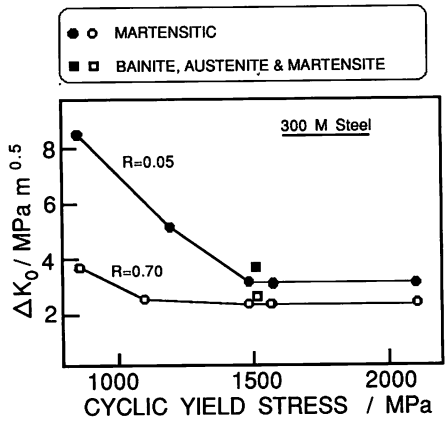

Fig. 12.15 *Correlation of the threshold stress intensity range for fatigue crack propagation versus the cyclic yield stress for fully martensitic, and mixed microstructures at two values of R, which is the ratio of the minimum to maximum stress intensity (Ritchie, 1977a).*

mean stress and environment (Ritchie, 1979). The threshold region is of practical significance because many cracked components spend a good proportion of their fatigue life in that region. The threshold value of ΔK (i.e., ΔK_0) correlates directly with the 'cyclic yield strength' (Fig. 12.15) which is in general less than the yield strength as measured in a uniaxial tensile test (Ritchie, 1979). The sensitivity of ΔK_0 to strength decreases as the mean stress amplitude rises.[5] This correlation is not unexpected since the plastic zone at the fatigue crack tip is subject to alternating stresses, so that the effects of cyclic deformation can be expected to be different from those encountered during monotonic strain hardening. Cyclic softening in quenched and tempered martensitic steels is usually attributed to rearrangements of the dislocation substructure and to a reduction in the dislocation density with alternating load. The softening occurs also because some of the plastic strain is reversible, a phenomenon analogous to the Bauschinger effect.

With some microstructures, the cyclic yield strength is found to be larger than the ordinary yield strength. In lightly tempered martensitic steels, the cyclic hardening is believed to occur due to dynamic strain

5 This behaviour contrasts with the fatigue or endurance limit for steels, which increases with strength since it becomes more dificult to initiate cracks in smooth samples as the strength increases. The threshold value of ΔK on the other hand, depends on the ability of existing long cracks to grow, an ability which is enhanced by an increase in strength.

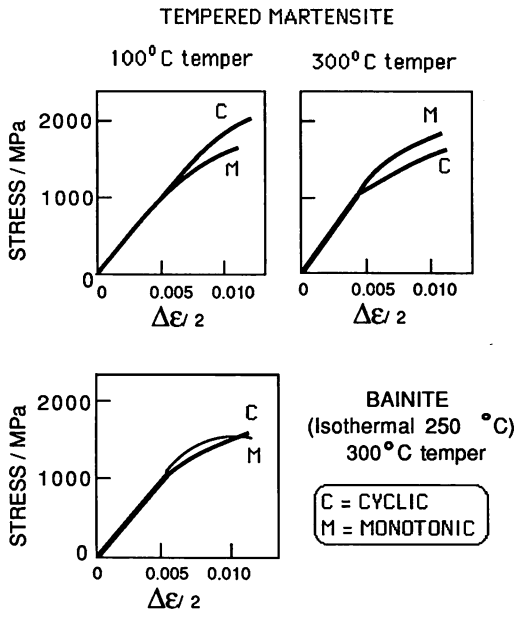

Fig. 12.16 *Data illustrating the differences between the cyclic and monotonic yield behaviours for tempered martensite and bainite in 300 M steel (Ritchie, 1977a).*

aging (Thielen *et al.*, 1976). For a high strength steel transformed isothermally to a mixed microstructure of bainite, martensite and retained austenite, Ritchie (1977a) found that the deformation induced transformation of retained austenite to martensite reduced the reversibility of plastic strain during cyclic deformation, causing the cyclic yield strength to exceed the ordinary yield strength and consequently leading to a low value of the ΔK_o (Fig. 12.16). Cyclic softening is therefore regarded as being beneficial to improving the near threshold fatigue crack growth resistance as long as the overall tensile strength is not reduced by a modification of the microstructure. Consistent with this, it is found that in a Fe–0.5Cr–0.5Mo–0.25V wt% steel, coarse grained precipitation hardened ferritic microstructures show significantly lower fatigue crack growth rates near ΔK_o, than higher strength bainitic or martensitic microstructures in the same alloy (Benson and Edmonds, 1978). In all cases, the crack path was found to be predominantly transgranular, with the bainite or martensite lath boundaries bearing no obvious relationship with the fracture surface.

A major reason why the threshold region is microstructure sensitive is that at higher stress intensities, the plastic zone size at the crack tip can be many times greater than the grain size or other microstructural

feature. Benson and Edmonds showed that in the threshold region, the maximum plastic zone size was about 3–5 times the ferrite grain size, and comparable with the austenite grain size in the case of the bainitic and martensitic microstructures (i.e., a few times larger than the lath or packet size).

In the Paris Law regime (regime B, Fig. 12.14), the material behaves essentially as a continuum with little demonstrable influence of microstructure or mean stress. For ductile materials, the crack advances by a striation mechanism although other modes of fracture might occur at the same time in embrittled materials, giving values of m which are much larger than the m=2 value expected theoretically. As the crack continues to grow at increasing ΔK, the maximum stress intensity begins to approach the critical value K_{IC} characteristic of final failure. The growth rate then becomes microstructurally sensitive, the dependency on microstructure reflecting its relationship with toughness. Thus, the austenite associated with bainitic microstructures can be beneficial to fatigue in Regime C (Fig. 12.14). The fracture modes in this regime replicate those found in static fracture, such as cleavage or intergranular failure.

12.8.3 Fatigue and Retained Austenite

There are now considerable data on the influence of austenite on fatigue properties, especially for martensitic steels including the TRIP variety; the picture that is emerging is that retained austenite is not a panacea for all the unresolved issues in the field of high strength steels, as was once believed.

Fatigue crack propagation can be considered to result from the accumulation of damage caused by the strain cycling of the material at the crack tip. It is natural to expect metastable austenite in the vicinity of the crack tip to transform into martensite, leading effectively to an increase in the strain hardening rate. According to Cotterell (1965), a high strain hardening rate leads to a relatively large crack propagation rate, presumably because the ability of the material to accommodate plastic strain then becomes exhausted more readily. The formation of martensite in a ductile matrix also appears to decrease the strain required to cause fracture. However, work by Chanani *et al.* (1972) shows that these detrimental factors can sometimes be offset by the energy absorbing effects of the strain induced martensitic transformation. It is likely that on balance, a small quantity of fairly stable austenite should lead to an improvement in the fatigue properties of bainitic steels, by virtue of the larger ductility of the austenite. Clear experiments are difficult to design because of the almost inevitable presence of high carbon martensite in association with the austenite in bainitic steels.

12.8.4 Corrosion fatigue

Although data do not seem to be available specifically for bainitic microstructures, it is well established that environmental effects can greatly enhance fatigue crack propagation rates, via a conjoint action of stress and corrosion. Many of the effects are attributable to hydrogen embrittlement. The fresh fracture surfaces created as the crack propagates are very vulnerable to environmental attack, as long as there is sufficient time available for the hydrogen to diffuse into the region ahead of the crack front. Consequently, corrosion fatigue is less detrimental at high frequencies of cyclic loading.

Corrosion during fatigue also leads to a reduction in the threshold stress intensity (below which normal fatigue crack growth does not occur), to a value designated K_{CRIT}. The reduction may be so drastic as to make K_{CRIT} of little use as a design parameter, since the section sizes necessary to reduce the design stresses to a level at which fatigue crack propagation does not occur may be unrealistically large. In such circumstances, the components are assigned service lives calculated using known corrosion fatigue data.

Although it is intuitively reasonable that corrosion should, by chemical degradation, enhance the crack growth rate, there are complications which sometimes lead to an overall reduction in the rate of crack propagation

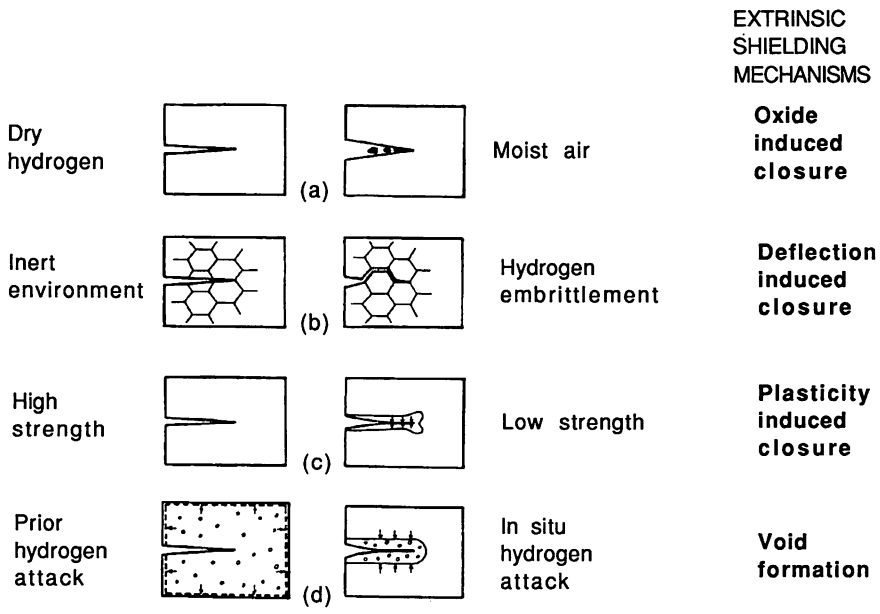

Fig. 12.17 *An illustration of the micromechanisms of crack tip shielding, as discussed in the text. (After Dauskardt and Ritchie, 1986.)*

(Dauskardt and Ritchie, 1986). When the stress intensity range and mean stress is low, any corrosion products that form can isolate the crack tip from its environment. Thus, fatigue crack growth in a moist environment can occur at a lower rate than in dry hydrogen (Ritchie *et al.*, 1980; Suresh *et al.*, 1981). Specimens which have been damaged by hydrogen bubble formation prior to fatigue testing can fail more rapidly relative to those in which the hydrogen bubbles form in the vicinity of the crack front during testing. The expansion associated with bubble formation then induces crack tip closure (Fig. 12.17). All other factors being equal, lower strength steels have a higher crack growth resistance because plasticity at the crack tip again leads to crack tip closure. Similarly, hydrogen embrittlement which causes failure at the austenite grain surfaces (rather than undeflected transgranular fracture) causes the crack path to deviate along those surfaces, giving a net increase in the work of fracture. All these effects are of lesser importance when the mean stress is large, because the crack opening is then correspondingly bigger, so that any crack tip shielding effects are relatively small.

12.9 Stress Corrosion Resistance

We have seen that cleavage fracture occurs when a critical stress is exceeded over a region ahead of the crack tip, which can propagate a preexisting microcrack. This critical stress can be reduced by environmental effects, and in the case of high strength steels, by hydrogen embrittlement resulting directly from the infusion of hydrogen during corrosion reactions. Cleavage fracture thus occurs at a critical stress intensity K_{ISCC} which is generally much smaller than the limit K_{IC}. The exact fracture path depends to some extent on the distribution of hydrogen traps; for example, failure can be intergranular if carbide precipitates decorate the grain boundaries.

For steels, K_{ISCC} is usually found to be about a third of K_{IC}, so that stress corrosion can severely limit their effective use. For high strength steels, the effect of corrosion manifests itself primarily via hydrogen embrittlement, the hydrogen being generated by cathodic reaction at the crack surface. It then diffuses to regions of highest dilatation ahead of the crack tip, leading to a reduction in the cohesive strength (Pfeil, 1926; Troiano, 1960; Oriani and Josephic, 1974).

It is difficult to comment on the relationship of K_{ISCC} with microstructure (and very few data exist for bainitic microstructures) but it appears that the presence of retained austenite reduces the stress corrosion crack growth rates, by hindering the diffusion of hydrogen to the sites of triaxial tension ahead of the advancing crack front (Parker, 1977; Ritchie *et al.*, 1978). The bulk diffusivity of hydrogen through austenite can be many

orders of magnitude smaller than that in ferrite (Shively *et al.*, 1966). Comparative experiments on tempered martensite and on a mixed microstructure of lower bainite, martensite and retained austenite (of the same yield strengths as the tempered martensite) revealed that the sample containing the larger quantity of austenite exhibited better stress corrosion resistance in a NaCl solution (Ritchie *et al.*, 1978). While both samples showed intragranular failure with respect to the prior austenite grain surfaces, a greater proportion of ductile tearing was found at those surfaces for the bainitic samples. This was attributed to the ability of the retained austenite to act as sinks for impurities (Marschall *et al.*, 1962), thereby leading to a lower degree of embrittlement at the grain boundaries. It is well established that prior austenite grain boundary embrittlement effects lead to higher stress corrosion crack growth rates (Ritchie, 1977b).

Whilst the above investigations emphasise the role of retained austenite in enhancing stress corrosion resistance, some recent very detailed investigations (Solana *et al.*, 1987; Kerr *et al.*, 1987) have established that there are restricted conditions under which the austenite can be beneficial. For example, the austenite has to continuously surround the plates of ferrite if it is to significantly hinder the difusion of hydrogen. The role of austenite also does not appear to be as prominent as has been suggested by earlier investigations. Other microstructural modifications which led to a high density of innocuous hydrogen traps (e.g., interfaces between cementite and ferrite) were often found to cause larger improvements in stress corrosion resistance.

In fact, Kerr *et al.*, and Solana *et al.*, studied a wide range of microstructures in high strength steels and were able to establish some general principles relating them to stress corrosion resistance (SCR). The sensitivity to microstructure was largest at yield strengths less than about 1000 MPa, and when failure occurred by a transgranular mechanism. Furthermore, the largest improvements obtained did not correlate with the presence of retained austenite. For reasons which are not clear, twinned martensite was deleterious to SCR. This may have something to do with the fact that in the steels studied, twinned martensite is usually a high carbon martensite (and hence more brittle), the twins themselves being inconsequential to the SCR problem. Mixtures of ferrite and martensite were found to be better, correlating with extensive crack branching due to the numerous interphase interfaces. The presence of lower bainite also led to improved SCR, but the effect could not be separated from any effect due to the associated drop in yield strength. All other factors being equal, reductions in yield strength correlated strongly with improved SCR (Fig. 12.18). Alloy specific effects were also observed, and attributed to differences in the density of innocuous traps for hydrogen.

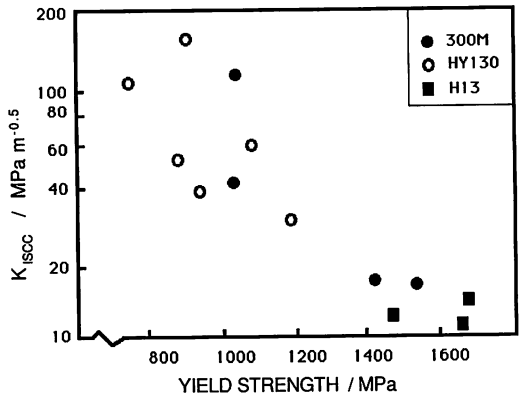

Fig. 12.18 *The correlation of stress corrosion cracking resistance versus the yield strength for a variety of steels (Solana et al., 1987).*

Indeed, any feature of the microstructure which enables the hydrogen to be well dispersed, or which promotes crack branching, seems to lead to improved SCR in steels where the role of hydrogen is crucial.

12.10 The Creep Resistance of Bainitic Steels

The vast majority of creep resisting steels used in power plant or in the petrochemical industry, are based on low carbon, low alloy steels containing chromium, molybdenum or vanadium as the significant alloying additions. The steels are used very widely, but their major applications are in the fabrication of pressure vessels, boiler steam pipes, steam generating and handling equipment, high pressure tubes with thick walls, turbine rotors, superheater tubes, coal to methane conversion plants, petrochemical reactors for the treatment of heavy oils and tar sands bitumen, etc. They are designed for service at elevated temperatures where creep resistance, and to some extent, oxidation and hot corrosion resistance in environments containing hydrogen and sulphur are of prime importance. For large scale coal liquefaction and gasification plant, the pressure vessels constructed using these steels have to contain mixtures of hydrogen and hydrogen sulphide at pressures up to 20 MPa at 550°C. Typical creep resistant bainitic steels also have good formability and weldability, and are relatively cheap.

Given that the steels are likely to be in service at high temperatures over very long periods of time, their microstructures also have to be resistant to other phenomena, such as graphitisation, which are not directly related to creep strength. Protection against graphitisation is one of the reasons why the aluminium concentration is usually limited to less

than 0.015 wt%, and why chromium and molybdenum are used together as alloying additions, since molybdenum on its own promotes the tendency to graphitisation (Hrivnak, 1987). Ambient temperature properties are also relevant, since any fabricated component must be safe during periods where its operation is interrupted. Resistance to fatigue, for both wrought and weld metals, is an important factor, but it appears that there is little difficulty in restricting fatigue crack growth to negligible proportions by suitable design. Most failures seem to occur when calculated design stresses or other design factors are unreliable (Griffiths and Oates, 1977). The required service life is usually of the order of a few decades.

The steels might typically be used within the temperature range 480–565°C, the service stresses being of the order of 15–30 MPa. In power plant, the stresses normally originate from a combination of internal steam pressure and the dead weight of the components in large assemblies. The most important property requirement is creep resistance, and not just because increased creep strength can prolong service life. There are many advantages to be achieved by using the extra strength to reduce the component wall thickness. The components in an electricity generating power plant can be very large in size, and ancillary structures have to be designed to retain them in position during service. Thus, the supporting structures have to be much more formidable for steam pipes made from low alloy ferritic steels, where the wall thickness can be typically 120 mm. A higher creep strength can permit a reduction of thickness, and corresponding reductions in the support structure. Indeed, the hoop stresses generated by the pressurised steam can be comparable to the stress arising from the weight of the steam pipes, providing a further incentive for weight reduction. Higher alloy steels can be used without additional expense, if they have a higher creep strength. Furthermore, welding becomes simpler and cheaper for smaller section sizes. Thermal stresses induced by temperature differences between the inner and outer surfaces of any component are smaller with section size, thereby mitigating any thermal fatigue problems associated with the irregular use of the power plant, due for example to variations in electricity demand. Such flexibility can make enormous differences to the economic performance of such plant.

Some typical chemical compositions of bainitic steels used for their creep resistance are given below; higher alloy steels are also used but these have microstructures based on tempered martensite and are not discussed further. The newer steels tend to contain less manganese, in order to reduce their susceptibility to temper embrittlement and banding. To maintain hardenability, the reduction in manganese concentration is usually compensated for by an increased concentration of other elements such as nickel.

Table 12.1 Typical compositions (wt%) of creep resistant steels used in the power generation and petrochemical industries. The range of compositions stated lie within the technical specifications, but are really intended to reflect the variations observed in practice. The sulphur concentration is usually within the range 0.005–0.02 wt%, and that of phosphorus within the range 0.005–0.025 wt%

Nominal designation	C	Si	Mn	Ni	Mo	Cr	V	Ti	B
0.25CrMoV	0.15	0.25	0.50	0.05	0.50	0.30	0.25	–	–
0.25CrMoV Specification	<0.18	0.10–0.60	0.40–0.65	–	0.45–0.65	0.25–0.35	0.20–0.30	–	–
1CrMoV	0.25	0.25	0.75	0.70	1.00	1.10	0.35	–	–
1CrMoV Specification	0.24–0.31	0.17–0.27	0.74–0.81	0.60–0.76	0.65–1.08	0.98–1.15	0.27–0.36	–	–
2.25Cr1Mo	0.15	0.25	0.50	0.10	1.00	2.30	0.00	–	–
2.25Cr1Mo Specification	<0.16	<0.5	0.3–0.6	–	0.9–1.1	2.0–2.5	–	–	–
'Modified 2.25Cr1Mo'	0.1	0.05	0.5	0.16	1.00	2.30	0.25	0.03	0.0024
3.0Cr1.5Mo	0.1	0.2	1.0	0.1	1.5	3.0	0.1	–	–
5.0Cr0.5Mo Specification	<0.16	<0.5	0.30–0.60	–	0.45–0.65	4.0–6.0	–	–	
3.5NiCrMoV	0.24	0.01	0.20	3.50	0.45	1.70	0.10	–	–
3.5NiCrMoV Specification	<0.29	<0.11	0.20–0.60	3.25–4.00	0.25–0.60	1.25–2.00	0.05–0.15	–	–

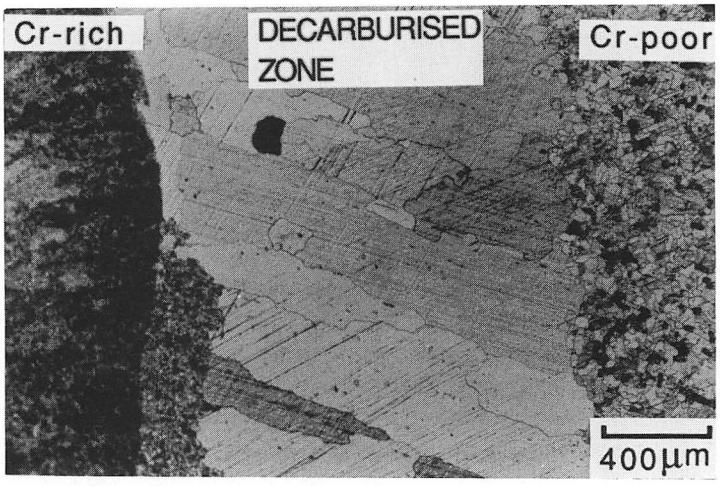

Fig. 12.19 *Optical micrograph of a junction between mild steel and a 2.25Cr–1Mo alloy, showing the development of a decarburised zone in the mild steel side of the joint after tempering (After Race, 1990).*

The actual chemistry can in practice vary significantly from the typical composition. The specified composition range is generally not very tight from a metallurgical point of view (Table 12.1). Indeed, the American Society for Testing Materials has at least twelve standards for the 2.25Cr–1Mo steel for different applications (Lundin *et al.*, 1986). It is unfortunate that many publications refer only to the nominal designation, and sometimes do not even mention the carbon concentration of the steel concerned.

An interesting reason for keeping the carbon concentration as low as possible, it that it is often necessary to join these steels to stainless steels (or other more heavily alloyed steels). There is then a carbon chemical potential gradient which exists at the junction, which causes the carbon to migrate during service at high temperatures (Fig. 12.19). The migration usually occurs from the low alloy to the high alloy steel, causing a decarburised layer to develop in the former, the layer then becoming extremely susceptible to creep failure (Klueh, 1974a, Lundin *et al.*, 1982). On the other hand, too small a carbon concentration leads to inferior creep properties since the steels rely on alloy carbides for their resistance to creep (Klueh, 1974a, b). In view of this well known effect, it is amazing that many of the standards only state an upper limit to the carbon concentration of the steel.

The standard alloys sometimes contain trace additions of boron and titanium (e.g., Collins, 1989), presumably added to enhance the bainitic hardenability in the manner discussed in Chapter 6. Other unintentional

trace impurities such as tin and antimony are also known to have disproportionate effects on creep strength for reasons which are not well understood (Collins, 1989). The alloys are usually fabricated by welding, and the filler material used is often chemically different from the parent plate; the Cr–Mo–V steels are usually welded with 2.25Cr–1Mo fillers in order to ensure good creep properties in the weld metal.

12.10.1 Heat Treatment

For power plant applications, the steels are usually air cooled ('normalised') after austenitisation; the specimen thicknesses may vary from 12–75 mm. The times specified for all the heat treatments depend on the component thickness, ostensibly to allow the steels to reach a uniform temperature. On the other hand, heat flow considerations alone indicate that the periods specified are excessive (Greenwell, 1989). The temperature to which the steels are heated for austenitisation is usually about 1000°C above the Ae_3 temperature (or 50°C above the Ac_3 temperature when the heating rate is about 1K min^{-1}), and hence depends on the steel composition. Lower temperatures lead to correspondingly smaller austenite grain sizes, a factor which can be beneficial to mechanical properties. This is in spite of the fact that the steels are destined for creep resistant applications, since the creep mechanism involved at service temperatures does not rely on grain boundary diffusion or sliding.

Given that it is impossible to achieve uniform cooling throughout the thick samples typical in industry, the heat treatments conceal a wide range of cooling rates. For a typical range of chemical compositions encountered within the '2.25Cr–1Mo' designation, the normalised microstructures consist of mixtures of allotriomorphic ferrite and bainite, can include between 0.34–0.94 volume fraction of bainite (Murphy and Branch, 1971). The effect on the mechanical properties, of such large variations in microstructure, is very pronounced during the early stages of service, but after long periods at elevated temperatures, the differences in creep strength become insignificant (Murphy and Branch, 1971). Before service, the normalised steels are usually given a stress relief treatment which involves tempering at 660–700°C for time periods ranging from one hour to several hours, depending on application. Welding under conditions of severe structural restraint requires a post weld stress relief heat treatment for several hours at 700°C. The temperature during service ranges from 550–570°C with occasional excursions to temperatures higher than 600°C.

The use of steels in the normalised condition, rather than a quenched and tempered martensitic condition, seems to be based on the fact that the allotriomorphic ferrite and bainite microstructure is more creep resistant than the martensitic microstructure, even though after tempering, the

martensitic steel usually has a higher hardness. A continuous cooling heat treatment is also more convenient for large components. Steels in power plant can be required in very large sections; uniformly martensitic microstructures are then difficult to produce using commercial heat treatments. For example, the 2.25Cr–1Mo alloy can be austenitised and water quenched in thicknesses up to 20 cm and still be bainitic throughout the entire thickness (Wada and Eldis, 1982; Lundin *et al.*, 1986). The cooling conditions are often characterised in industry, by quoting the time interval Δt taken for the sample to cool between 800 and 500°C. It has been reported that a fully bainitic microstructure is obtained during cooling from austenite, for Δt ranging from 20–500 s (Wada and Eldis, 1982). In fact, one of the most important properties of the 2.25Cr–1Mo steel is its high bainitic hardenability, which allows allotriomorphic ferrite growth to be avoided during cooling, making it suitable for heavy section applications.

12.10.2 2.25Cr–1Mo Type Steels

The main factor responsible for the good creep resistance of the low alloy steels used in the power generation industry is the formation of fine and highly stable dispersions of alloy carbides, although a significant contribution also comes from solid solution strengthening by substitutional solutes (Lundin *et al.*, 1986). The solid solution strengthening component becomes more important after prolonged service at elevated temperatures, as the microstructural contribution to strengthening diminishes due to annealing effects. Molybdenum is found to be particularly effective as a solid solution strengthening element (Lundin *et al.*, 1982). A good reason for keeping the carbon concentration as low as possible, is to avoid tying up too much of the molybdenum in the form of carbides. Low carbon concentrations are also desirable in situations where decarburisation can be a problem. The carbon concentration should not be less than about 0.1 wt% since not only does the creep strength then deteriorate, but the required alloy hardenability is also not achieved.

The heat treatments given to the steels, prior to service are usually so severe that the precipitates are in an overaged condition (Pilling and Ridley, 1982), so that the microstructures can be particularly stable during service. A detailed microstructural investigation has suggested that the better creep resistance of the ferrite/bainite microstructure in the 2.25Cr–1Mo steel arises because during service, the carbide M_2C, which is replaced by thermodynamically more stable carbides during service at elevated temperatures, persists for shorter times in the martensitic microstructure (Baker and Nutting, 1959). In the mixed microstructure, the M_2C in the ferrite regions was found to persist for much longer periods

than that in the bainite regions or in the martensitic steel. Murphy and Branch later confirmed these microstructural observations, and they also pointed out that when mixed ferrite/bainite microstructures are aged, any decrease in hardness due to aging is due primarily to the relatively rapid decline in the hardness of the initially stronger bainite. Thus, the overall softening of the alloy is a function of the bainite content, the steels containing the highest initial volume fraction of bainite showing the most softening.

Although the correlation of the higher stability of the M_2C in the normalised steel with better creep resistance appears to be justified, the relationship has yet to be established quantitatively and in terms of the detailed mechanisms by which M_2C imparts creep resistance. The hypothesis also implies that a fully bainitic microstructure should not have better creep properties when compared with a fully martensitic microstructure. In this respect, comparative experiments with the more heavily alloyed 5Cr–0.5Mo steels, which also transforms to a mixture of bainitic ferrite and residual phases (retained austenite and martensite) could be revealing, since these alloys should yield a higher ratio of martensite to bainitic ferrite relative to the 2.25Cr–1Mo steels.

12.10.3 1Cr–Mo–V Type Steels

1Cr–Mo–V steels are usually austenitised at temperatures within the range 950–1000°C for 1–14 h, and air cooled or furnace cooled to give a fully bainitic microstructure (Myres *et al.*, 1968). Since commercial alloys in this general category have a wide span of composition, a corresponding variety of ferrite and bainite mixtures can also be obtained (Murphy and Branch, 1969). Isothermal transformation tends to give an incomplete transformation to bainite and is not used commercially. Before service, the microstructure is usually tempered at about 690°C for 20 hr; the microstructure then consists of a fine dispersion of V_4C_3 particles (particle diameter $\approx$ 12 nm) in a matrix of ferrite. When the vanadium and carbon concentrations are not stoichiometrically balanced, other carbides such as M_3C and $M_{23}C_6$ are also found. These tend to be coarser and are located mainly at prior austenite grain boundaries or ferrite grain boundaries. Note that the V_4C_3 carbide in these alloys usually contains some iron, manganese molybdenum and chromium in solid solution, although vanadium is by far the major carbide forming constituent (Senior, 1988).

Quenching 1Cr–Mo–V steels yields a martensitic microstructure which after tempering at 690°C for 20 h consists mainly of a fine dispersion of V_4C_3 (particle radius $\approx$ 50 nm) in a matrix of ferrite (Myers *et al.*, 1968). The reason why the V_4C_3 particles are coarser in tempered martensite when compared with tempered bainite has not been investigated. The

creep strength of 1Cr–Mo–V steels in the tempered bainite condition is found to be higher than when the steels are in the tempered martensite condition. This could be attributed to the finer V_4C_3 particles in the former (Buchi *et al.*, 1965), but it has been argued that the rather high experimentally observed value for the activation free energy for creep is inconsistent with the cross-slip or climb of dislocations and that the spacing between particles is too close to allow dislocation bowing (Myres *et al.*, 1968). They suggest instead that it is solute (dissolved V)/dislocation interactions which control creep deformation. The higher creep strength of tempered bainitic microstructure which has smaller V_4C_3 particles is attributed to an increased solubility of vanadium due to the Gibbs–Thompson capillarity effect. A higher concentration of vanadium in solid solution implies a smaller distance between solute pinning points for dislocations. Myers *et al.* (1968) presented a quantitative model for solute/dislocation interactions and capillarity effects which is consistent with their experimental data. It appears therefore that in 1Cr–Mo–V steels it is the vanadium in solid solution which controls creep deformation; the fine dispersions of particles must however contribute significantly since it is unlikely that Fe–V solid solutions would have good creep properties in their own right.

It has been observed that in vanadium containing creep resistant steels, the uniformity of the V_4C_3 dispersion depends on the form of M_3C present (Buchi *et al.*, 1965). In stoichiometric steels, where M_3C is virtually absent after tempering, the V_4C_3 dispersions are found to be extremely uniform. Otherwise, the regions around M_3C particles are usually free of V_4C_3 (again, the reason for this has not been investigated). The M_3C particles are usually located at prior austenite or ferrite/ferrite boundaries, and their presence there causes the formation of a zone which is free of V_4C_3. It is established that the creep properties are worse for situations where the V_4C_3 is nonuniformly dispersed (Buchi *et al.*, 1965; Murphy and Branch, 1969).

12.10.4 0.25Cr–Mo–V Type Steels

0.25Cr–Mo–V steels have a relatively low hardenability and on normalising tend to transform to mixtures of mainly allotriomorphic ferrite with a small quantity of pearlite. On tempering, fine V_4C_3 dispersions form in the ferrite and to a lesser extent in the pearlite regions. These steels have a higher creep ductility than the 1Cr–Mo–V alloys for a slightly lower creep strength. The higher ductility has been attributed to the observation that in the 1Cr–Mo–V steels, creep cavitation occurs at both the ferrite/ferrite and ferrite/bainite boundaries, whereas ferrite/pearlite boundaries presumably are not as susceptible to cavitation (Murphy and Branch, 1969).

There are also indications that in steels containing a predominantly bainitic microstructure, but with some allotriomorphic ferrite, the creep crack growth rate increases with the volume fraction of bainite. This is because the presence of the softer ferrite permits a greater relaxation of stresses, thereby inhibiting cavity nucleation and growth (Jones and Pilkington, 1978). An apparently contradictory result is that in the Cr and Mo containing power plant steels, microstructures containing larger amounts of bainite perform better in stress-rupture tests[6] when the applied stress is large (i.e., for 'short' times to failure, typically 10^{-5} hours in power plant conditions). However, for small applied stresses and prolonged service, the ferrite/pearlite mixtures exhibit the best creep properties (Viswanathan, 1974). There does not seem to be an explanation for this effect.

12.10.5 Enhanced Cr–Mo Bainitic Steels

Many attempts have been made to improve on the properties of the creep resistant steels discussed above, especially for pressure vessel applications at elevated temperatures and in hydrogen environments. The use of a higher concentration of alloy carbide forming elements can reduce the stability of cementite, which apparently is more prone to hydrogen problems in severe conditions (Ritchie *et al.*, 1984; George *et al.*, e985). It appears that in the lower alloy content steels the relatively unstable carbides such as cementite and Mo_2C tend to react with ingressed hydrogen, leading to decarburisation, cavitation and on occasions to the formation of methane bubbles at interfaces. Damage by hydrogen is thought to occur in three stages (Vagarali and Odette, 1981; Shewmon, 1976). The first stage, during which the microstructure and macroscopic mechanical properties are largely unaffected, involves the nucleation and growth of bubbles. This is followed by rapid attack as methane bubbles grow and coalesce into fissures at the grain boundaries, leading to swelling and a deterioration of mechanical properties. The final stage involves extensive decarburisation involving the gross dissolution of carbides as the system attempts to maintain an equilibrium carbon concentration in the ferrite.

In certain applications, such as coal conversion plant, plate thickness of 300–400 mm are required, and conventional steels do not in those cases have adequate hardenability to confer a uniformly bainitic microstructure after continuous cooling heat treatments.

6 A stress rupture test is often used to characterise creep properties. It is sometimes regarded as an accelerated creep test, and involves the measurement of the time to failure as a function of applied stress and temperature. The stresses applied are usually higher than those encountered in service.

Attention has been focused on the popular bainitic 2.25Cr–1Mo steel, the main objective being to extend the temperature range (and hence the thermodynamic efficiency of power plant) over which the alloy can be utilised, while maintaining the bainitic microstructure. Modifications include microalloying additions to improve elevated temperature strength, enhanced concentrations of chromium for improved resistance to hydrogen embrittlement, carbide stabilising additions such as vanadium and niobium, and nickel, boron and carbon additions for improved bainitic hardenability (Wada and Eldis, 1982; Wada and Cox, 1982, 1984; Ishiguro *et al.*, 1982, 1984; Kozasu *et al.*, 1984; Parker *et al.*, 1984; Klueh and Swindeman, 1986). Relatively high concentrations of chromium also seem to accelerate tempering kinetics so that the formation of $M_{23}C_6$ carbide is accelerated, and the carbide is obtained during the stress relief heat treatment at 700°C (Ritchie *et al.*, 1984; Spencer *et al.*, 1989); the significance of this with respect to properties other than hydrogen effects is not clear.

Ishiguro *et al.* (1982) developed an alloy which differs from the classic 2.25Cr–1Mo steel in that it has a negligible silicon concentration, a lower carbon concentration (0.1 wt%), and the additional solutes 0.25V–0.02Ti–0.002B wt%. It is designated the 'Modified 2.25Cr–1Mo' steel, and is found to exhibit an improved creep strength and impact toughness and was also claimed to be more resistant to temper embrittlement. The titanium was added to combine with any nitrogen, thereby permitting the boron (which forms less stable nitrides) to remain in solid solution and enhance the alloy hardenability, making it possible to obtain bainitic microstructures at slower cooling rates. The enhanced creep resistance was later demonstrated to be due to the precipitation of fine vanadium carbides which make the bainitic microstructure more resistant to tempering (Klueh and Swindeman, 1986).

An alloy which is receiving a lot of attention is Fe–3Cr–1.5Mo–0.1V–1Mn–0.1C wt% compositions developed by Wada and co-workers (1982, 1984). After austenitisation at about 1000°C for two hours and air cooling, the alloy has a microstructure which is essentially a mixture of bainitic ferrite and austenite/martensite, of the kind normally associated with the 2.25Cr–1Mo steel discussed earlier. The extra alloying elements add to solution hardening, an important factor determining the creep strength, especially over long time periods when the microstructure may othersise have coarsened.

As already pointed out, a further advantage of the higher chromium concentration is that during the preservice tempering treatment at 700°C, the cementite is more rapidly replaced by carbides such as M_7C_3, $M_{23}C_6$ and M_6C, thus rendering the microstructure less susceptible to severe hydrogen attack. An interesting consequence of this is that bainitic microstructures in high chromium containing steels become less susceptible to ingressed hydrogen. Chung *et al.* (1982) demonstrated that in 2.25Cr–1Mo

steels, a bainitic microstructure is far more sensitive to a high pressure hydrogen embrittlement treatment than a tempered martensitic microstructure. This is because the bainitic microstructure which forms during cooling from the austenite phase field contains substantial quantities of carbon enriched retained austenite, which on tempering decomposes into regions containing intense precipitation of cementite which are highly susceptible to reaction with hydrogen. In a tempered martensitic microstructure, any cementite precipitation is more or less uniformly distributed. An increase in the chromium concentration causes the cementite precipitates in the tempered bainitic microstructure to be replaced by more stable carbides during the tempering treatment, so that its toughness becomes far less sensitive to hydrogen exposure (George *et al.*, 1985).

Manganese and silicon as alloying additions are known to lead to a deterioration in mechanical properties via temper embrittlement effects (Bodnar *et al.*, 1989). A high hardenability steel with low concentrations of these elements, which transforms to a fully bainitic microstructure during continuous cooling at rates consistent with the usual industrial practices, is the 3.5Ni–3Cr–Mo–V steel, which has been demonstrated to be insensitive to hydrogen and temper embrittlement effects when compared with the classical 2.25Cr–1Mo type alloys (Ritchie *et al.*, 1984). A part of the reason why the alloy appears to be resistant to hydrogen embrittlement is believed to be associated with the higher content of carbide forming elements, which leads to the rapid replacement of cementite by more stable carbides during the preservice tempering heat treatment at 700°C. Hydrogen sometimes reacts with any carbon in solid solution in the ferrite, to generate gaseous products such as methane, products which manifest themselves as optically visible bubbles in the microstructure under conditions of severe hydrogen attack. Cementite and Mo_2C dissolve rapidly to sustain the equilibrium ferrite carbon concentration as the hydrogen reaction proceeds (Shewmon, 1985).

The nickel serves primarily to enhance toughness and the hardenability (so that the alloy can in principle be used in sections as thick as 0.4 m, and yet have a fully bainitic microstructure). It also lowers the Ae_3 temperature of the alloy, thereby permitting the use of lower austenitisation temperatures and the better properties associated with austenite grain size refinement. Several steels with lower nickel concentrations have also been investigated and found to possess better properties over the conventional 2.25Cr–1Mo alloy (Spencer *et al.*, 1989).

12.10.6 Regenerative Heat Treatments

Cavitation and other similar irreversible creep damage does not occur to a significant extent during much of the service life of the creep resistant

steels described above. During that period, any loss in properties is due largely to microstructural changes such as carbide coarsening, changes in the configuration of any dislocations, and in the general approach of the microstructure towards equilibrium. These microstructural changes can in principle be reversed by regenerating the original microstructure by heating the component back into the austenite phase field, a process which is not often desirable due to the high temperatures involved.

A possible alternative is to regenerate just the carbides, by annealing the steel at a temperature above the service temperature ($\approx$ 700°C), but below that at which austenite can form (Senior, 1988). The aim of such a heat treatment would be to dissolve some of the carbides, and reprecipitate them by aging at a lower temperature, thereby regenerating a fine carbide dispersion. The work reported by Senior on a 1Cr–Mo–V steel indicates, however, that 700°C is not high enough to allow a substantial amount of carbide to dissolve, the annealing in fact leading to a further deterioration in the microstructure by accelerating its approach towards equilibrium. For example, in the 1Cr–Mo–V steel, the beneficial V_4C_3 carbide increases in volume fraction but also coarsens rapidly.

12.10.7 Transition Metal Joints

In steam turbine assemblies it is sometimes necessary to join the low alloy ferritic steels (of the type discussed above) to austenitic steels which are more suited for corrosive environments. The joints are usually between tubular elements although thicker joints are occasionally needed. The welds between these dissimilar steels are then usually made using a filler material which is either an austenitic stainless steel, or a nickel based alloy such as 'Inconel'. The filler material/ferritic steel interface is from a metallographic found to be more abrupt when the nickel based filler is used, even though in all cases, true metallurgical bonds are achieved at all junctions.

The ferritic steel is usually the 2.25Cr–1Mo alloy. It is well established that the chances of such a 'transition metal joint' failing during service are large when compared with other welded joints between similar metals. Nath (1982) has suggested that this is because of the complex stresses arising because of the different creep properties of the filler, the HAZ and the ferritic base plate proper. The stresses are such as to intensify creep damage in the vicinity of the weld/base plate junction.

The microstructure of 2.25Cr–1Mo is usually fully bainitic, but after welding, that of the heat affected zone away from the fusion boundary can contain a substantial amount of allotriomorphic ferrite. In the immediate proximity of the fusion boundary, the coarser austenite grain structure leads to an increase in hardenability; the HAZ microstructure there is then fully bainitic. The allotriomorphic ferrite containing region is during

the early stages of creep relatively weak, and is in effect sandwiched between two stronger regions, the optimised parent plate microstructure far from the fusion boundary, and the fully bainitic region near the fusion boundary. This combined with the fully austenitic (or Inconel) filler material which is relatively rigid, leads to the poor properties of transition joints. The joints are sometimes heat treated at 700°C for 30 min after welding for stress relief, but this in itself does not lead to much homogenisation of mechanical properties.

Nath (1984) attempted to overcome these problems by reheating the entire welded joint into the austenite phase field at 950°C for 1 h, followed by air cooling, with the aim of regenerating a fully bainitic microstructure throughout the parent material, including the heat affected zone. Although the treatment was found to be successful in improving the overall creep properties, the properties were still lacking when compared with those of the unwelded base plate microstructure. The reaustenitising heat treatment caused the migration of carbon, which in the case of the ferritic/austenitic joint led to the formation of a decarburised zone on the ferrite side of the dissimilar metal interface, and a corresponding carbon enriched zone in the austenite on the other side. The carbon migration is presumably driven by the chemical potential gradient resulting from the different chemistries of the ferritic and austenitic steels, as happened in the classic Darken experiments on uphill diffusion. The decarburised region due to its lower hardenability contained a mixed microstructure of allotriomorphic ferrite and bainite, so that the desired homogeneous microstructure was not obtained.

12.10.8 Cr–W Steels

Metals often tend to swell during irradiation by neutrons from fusion or fission reactors. The extent of swelling is known to be smaller for ferritic steels when compared with austenitic alloys. Thus, ferritic steels are prime candidate alloys for structural applications in the sensitive regions of fusion reactors, and many Fe–Cr–Mo–C steels of the type used widely in the fossil fuel power stations are currently being investigated.

Irradiation during service can also lead to transmutations in the steel, causing the formation of long life radioactive nuclides, thereby adding to the problems of nuclear waste disposal. Initial research indicates that conventional power plant steels can be modified to substitute elements such as molybdenum and niobium (which transmute to undesirable products) with tungsten without influencing the mechanical properties of the steel (Abe *et al.*, 1990). Tungsten, like C, V, Ta, Ti, Si and Mn interact with the neutron flux to yield radioactive by-products with decay times which are smaller than that of iron.

12.11 Steels with Mixed Microstructures

Mixed microstructures consisting of bainite and martensite are usually a consequence of inadequate heat-treatment or the use of steels with insufficient martensitic hardenability in applications involving heavy sections.

Early research suggested that the presence of bainite in an otherwise martensitic microstructure generally leads to a deterioration in ductility, toughness and strength (Bailey, 1954; Hehemann *et al.*, 1957). The impairment of properties becomes less severe as the bainite forms at lower transformation temperatures, and is related to the difference in strength between martensite and bainite. As the strength difference decreases, so does the reduction in properties. Bainite which forms at low transformation temperatures has a relatively high strength, but if its strength is reduced by annealing then the deterioration of properties in a mixed microstructure is found to be larger; this was established in a unique experiment by Hehemann and co-workers (1957), using a sample transformed partially to bainite with its temperature then being raised to the annealing temperature before quenching to allow the residual austenite to transform to martensite.

These results are consistent with the observation that the impairment of properties becomes less severe as the overall strength level decreases during tempering of the mixed microstructure (Triano and Klinger, 1952; Hehemann *et al.*, 1957). During tempering, the strength of martensite (which contains excess carbon in solid solution) decreases more rapidly than that of bainite, so that the difference in strength between the two phases becomes smaller during annealing. Furthermore, microstructures of lower bainite and martensite are consistently found to perform better than those containing upper bainite and martensite, presumably because the strength of lower bainite is nearer to that of the martensite.

Contrary to these generally pessimistic indications of the properties of mixed microstructures, the first indications that the mixed microstructures can in some circumstances outperform the individual phases began to emerge in 1969, when Edwards observed that after tempering, mixtures of lower bainite and martensite appeared to be tougher than either martensite or bainite. More recent work supports this notion, with considerable data that the presence of bainite in a predominantly martensitic microstructure enhances both strength and toughness relative to the single phase samples (Tomita and Okabayashi, 1983a, b 1985a, b, 1987, 1988). For example, the strength of a mixture of lower bainite and martensite in an isothermally transformed high strength steel (Fe–0.4C–0.15Si–0.66Mn–1.87Ni–0.8Cr–0.2Mo wt%, i.e., AISI 4340 type) is found to go through a maximum as a function of the volume fraction of lower bainite (Fig. 12.20). This goes against intuition in that the overall strength of a

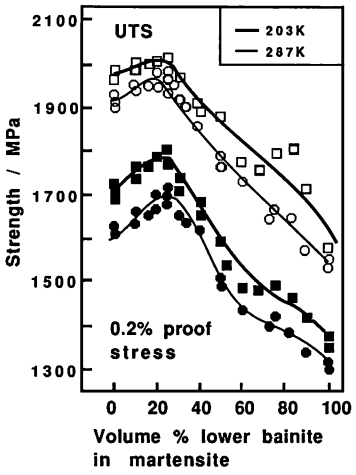

Fig. 12.20 *Variation in the 0.2% proof stress as a function of the volume fraction of lower bainite in a mixed, tempered microstructure of lower bainite and martensite. The different curves represent data collected at the temperatures indicated on the diagram.*

two-phase microstructure may be expected to be between that of the individual phases in isolation. The results were explained using an idea proposed by Mutui *et al.* (1977), that as the lower bainite subdivides regions of austenite, there is in effect a refinement of the austenite grain size and consequently a refinement of the martensite packet size on subsequent transformation of austenite. This leads to a strengthening of the martensite via a Hall–Petch effect. In addition, the strength of the bainite is enhanced by the constraint provided to its deformation by the stronger martensite.

The constraint argument used is however, incomplete; any enhancement in the strength of bainite should at the same time lead to a reduction in that of martensite (see for example, Tomoto *et al.*, 1976). The model also does not account for the effect of bainite formation in increasing the carbon concentration of the residual austenite, and hence the strength of any martensite that forms subsequently. Although sub-zero refrigeration and low temperature (150°C) double tempering treatments were used, it is not established that the samples tested did not contain retained austenite; the austenite can be extremely stable to subzero cooling (Bhadeshia and Edmonds, 1979b) and to tempering at temperatures as high as 200°C for 1 h (Horn, 1976). The strengthening effect of a refinement of the austenite grain structure by lower bainite was taken into account by examining the dependence of the strength of fully martensitic samples on the austenite grain size. It is not clear why this dependence was found to be different for samples with a variety of tempering treatments, given that

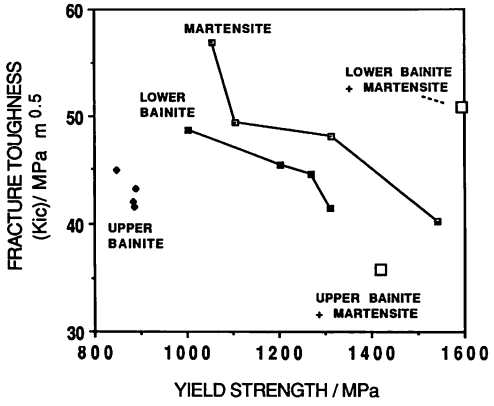

Fig. 12.21 *Plot of toughness versus strength for a variety of microstructures in an ultra-high strength steel. (Data from Tomita, 1988.)*

tempering of the kind studied does not alter the martensite plate or packet size.

Notwithstanding these difficulties in the interpretation of results, the experimental data are clear, that the overall strength of a mixture of lower bainite and martensite can exceed that of the martensite alone, and yet leads to an improvement in toughness (Fig. 12.21). This latter improvement was initially ascribed to the cleavage crack stopping ability of the more ductile lower bainite, but fractography revealed a ductile fracture mechanism rather than regions of quasicleavage where the martensite fractures in a brittle manner, separated by ductile fracture in the lower bainitic areas (Tomita, 1987). The notion that the dispersal of a ductile phase in an otherwise brittle matrix leads in itself to an improvement in properties is most likely an oversimplification, since mixtures of upper bainite and martensite do not lead to any improvement in toughness. Similarly, correlations of fracture facet size against microstructural parameters have not revealed any clear explanation for the change in fracture mode or toughness. Apart from the obvious refinement of martensitic regions in the mixed microstructures, any strength/toughness relationship must include the well-established fact that the bainitic carbide particle size is much smaller in lower bainite when compared with upper bainite.

12.12 Summary

The highly anisotropic, thin plate shape of bainite platelets ensures that the mean free path for slip is comparable to the plate thickness rather than the length. This means that the major microstructural contribution to

strength is via the fine sub-unit size, rather than the sheaf or austenite grain sizes which are of minor importance as far as the strength is concerned. The sub-unit size is so small, that the Hall–Petch relation does not apply; yield is instead controlled by the stress required to expand dislocation loops. This gives a linear relationship between the yield strength and the inverse of the sub-unit size.

Bainitic steels usually exhibit continuous yielding behaviour, with proof stress to UTS ratios which can be much smaller than 0.8. This gradual yielding is a consequence of mobile dislocations, the presence of heterogeneities in the microstructure and residual stresses due to transformation. The ratio can to some extent be improved by annealing at low temperatures, although there is not much response if the bainite transformation temperature is comparable to the annealing temperature.

There is no doubt that higher carbon concentrations lead to a deterioration of ductility, primarily because of the void nucleating tendency of cementite particles. The presence of large regions of untempered martensite in the microstructure can reduce ductility, whereas retained austenite can in some circumstances enhance it.

The impact toughness of upper bainite deteriorates as its strength increases, but that of lower bainite which has much finer carbides is superior at the same strength level. An interpretation in terms of fracture toughness theory has demonstrated that it is the coarsest carbides in the microstructure which control toughness. Consistent with theory, the fracture strength correlates directly with the reciprocal of the square root of the coarsest carbide particle size. The degree of scatter in toughness data increases as the microstructure becomes more heterogeneous; mixed microstructures of bainite and martensite show larger scatter than fully bainitic samples. During cleavage fracture, the cleavage facet dimensions are found to be comparable to those of bainite packets. A refinement of the austenite grain size also reduces the packet size, and consequently leads to an improvement in toughness. All of the normal impurity controlled temper embrittlement phenomena normally associated with martensite, are found in bainitic steels.

The endurance limit during the fatigue testing of smooth samples correlates well with the UTS of bainitic steels. The threshold stress intensity range for fatigue crack growth is reduced by the presence of retained austenite, because its transformation to martensite prevents the reversal of plastic strain during cyclic deformation. Stable austenite on the whole leads to an improvement in fatigue properties via the ductility it confers to the microstructure.

Retained austenite also can enhance the stress corrosion cracking resistance, probably by hindering the diffusion of hydrogen. However,

comparable benefits can be achieved by any method which increases the number density of hydrogen traps in the microstructure.

Creep resistant alloys containing strong carbide forming elements represent one of the most successful industrial applications of bainitic microstructures. They achieve their creep strength via solid solution strengthening and with the help of the fine dispersions of alloy carbides.

Finally, there are now considerable data to suggest that mixed microstructures of bainite and martensite can in some circumstances offer higher strength and toughness than fully martensitic alloys. The mechanism behind this remains to be established.

13 *Advanced Bainitic Steels and Cast Irons*

Steels with yield strengths in excess of 1000 MPa are important in certain applications, but the biggest markets are for lower strength varieties, where the total alloy content rarely exceeds 2 wt%. The alloy design therefore has to be extremely careful, and has its origins in the early work of Irvine and Pickering. Lean steels tend to transform to mixtures of allotriomorphic ferrite and bainite, whereas attempts to improve hardenability usually lead to partially martensitic microstructures. The solution therefore lies in low alloy, low carbon steels, containing small amounts of boron and molybdenum to suppress allotriomorphic ferrite formation. Boron increases the bainitic hardenability. Other solute additions can, in the presence of boron, be kept at sufficiently low concentrations to avoid the formation of martensite. Steels like these (alloy 1, Table 13.1) are found to transform into virtually fully bainitic microstructures with very little martensite using normalising heat treatments.

The other alloys listed in Table 13.1 are examples of some of the latest commercial bainitic steels. A striking feature of the list is that the alloys are all very similar. This similarity is misleading: they have very different mechanical properties, partly because the trace element concentrations are important, but also because the processing routes vary considerably.

The steels developed by Irvine and Pickering exhibited quite reasonable combinations of toughness and strength, but in time proved to be unexciting when compared with the best of quenched and tempered martensitic steels. Nevertheless, the physical metallurgy principles established during their development are now being applied in the metallurgical design of a new generation of bainitic steels, in which the emphasis is on further reductions in carbon and other alloying element concentrations, and on processing designed to refine the microstructure. Hence the terms 'control rolling' and 'microalloying', concepts which revolutionised the application and design of hot rolled steels. This chapter contains a

Table 13.1 Typical compositions of advanced bainitic steels (wt%). Notice that the steels are fairly similar in composition with respect to the major alloying additions, although there are significant differences with respect to carbon and trace element concentrations. The fabrication procedure is also of vital importance in giving a large variation in properties in spite of the similarities of chemical composition.

No.	C	Si	Mn	Ni	Mo	Cr	Nb	Ti	B	Al	N	Others	
1	0.100	0.25	0.50	–	0.55	–	–	–	0.0030	–	–	–	Early bainitic steel
2	0.039	0.20	1.55	0.20	–	–	0.042	0.015	0.0013	0.024	0.0030	–	Rapidly cooled bainitic steel
3	0.081	0.25	1.86	0.20	0.09	–	0.045	0.016	–	0.025	0.0028	–	Rapidly cooled bainitic steel
4	0.110	0.34	1.51	–	–	–	0.029	–	–	–	–	–	Rapidly cooled bainitic steel
5	0.100	0.25	<1.00	–	–	–	–	–	–	–	–	–	Bainitic dual phase steel
6	0.040	–	0.40	–	–	–	–	–	–	0.05	–	–	Triple phase steel
7	0.150	0.35	1.40	–	–	–	0.022	0.011	–	0.035	–	–	Bainitic dual phase steel for buildings
8	0.020	0.20	2.00	0.30	0.30	–	0.050	0.020	0.0010	–	0.0025	–	ULCB steel
9	0.028	0.25	1.75	0.20	–	0.30	0.100	0.015	–	0.030	0.0035	Cu 0.3, Ca 0.004	ULCB steel
10	0.080	0.20	1.40	–	–	–	–	0.012	–	0.002	0.0020		Inoculated acicular ferrite steel
11	0.15	0.80	1.40	–	0.20	–	–	–	–	–	–	V 0.15	Forging steel (high strength)
12	0.09	0.25	1.00	0.50	1.00	–	0.10	0.02	0.002	0.04	0.006	–	Forging steel (100% bainitic)
13	0.09	0.40	1.40	–	–	–	0.07	–	–	0.04	0.010	V 0.06	Forging steel (Nb+V)
14	0.09	0.25	1.40	–	–	–	0.07	0.02	0.002	0.04	0.006	–	Forging steel (Nb+B)
15	0.12	–	1.60	–	–	–	0.08	–	0.004	–	–	–	Cold-heading steel

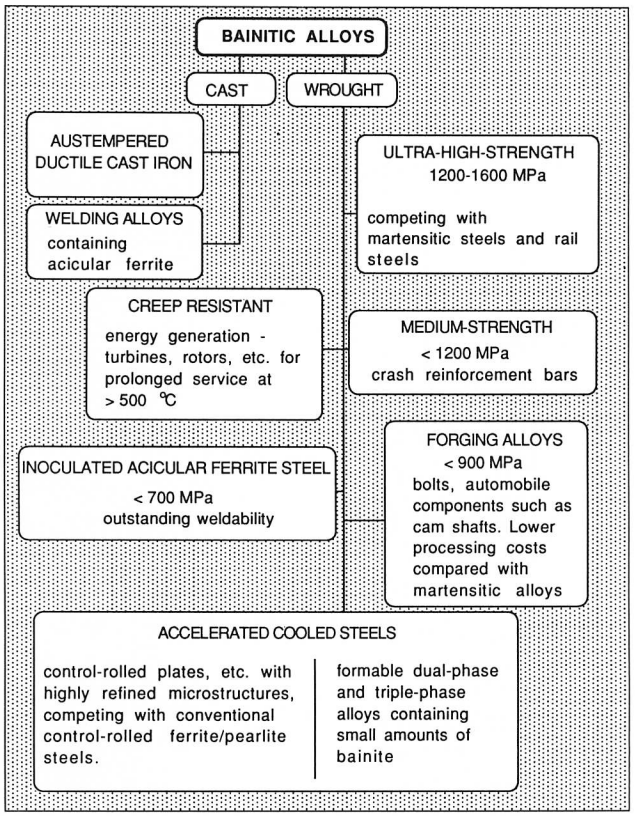

Fig. 13.1 *The range of bainitic alloys currently available on a commercial basis.*

summary of recent developments in high technology steels and cast irons based on bainitic microstructures. Many of the lower alloy content steels are thermomechanically processed prior to their transformation so that it is appropriate to begin with a description of the key industrial processes in the context of bainite. The range of bainitic alloys currently in use is summarised in Fig. 13.1; the 'inoculated' acicular ferrite steels have already been dealt with in Chapter 10.

13.1 Controlled Rolling of Bainitic Steels

The strengthening of iron via a reduction in grain size is a very attractive option because a smaller grain size leads also to an improvement in toughness. This simple fact has led to the development of impressive technology, designed to impart thermomechanical treatments capable of refining the austenite grain structure prior to its transformation to ferrite

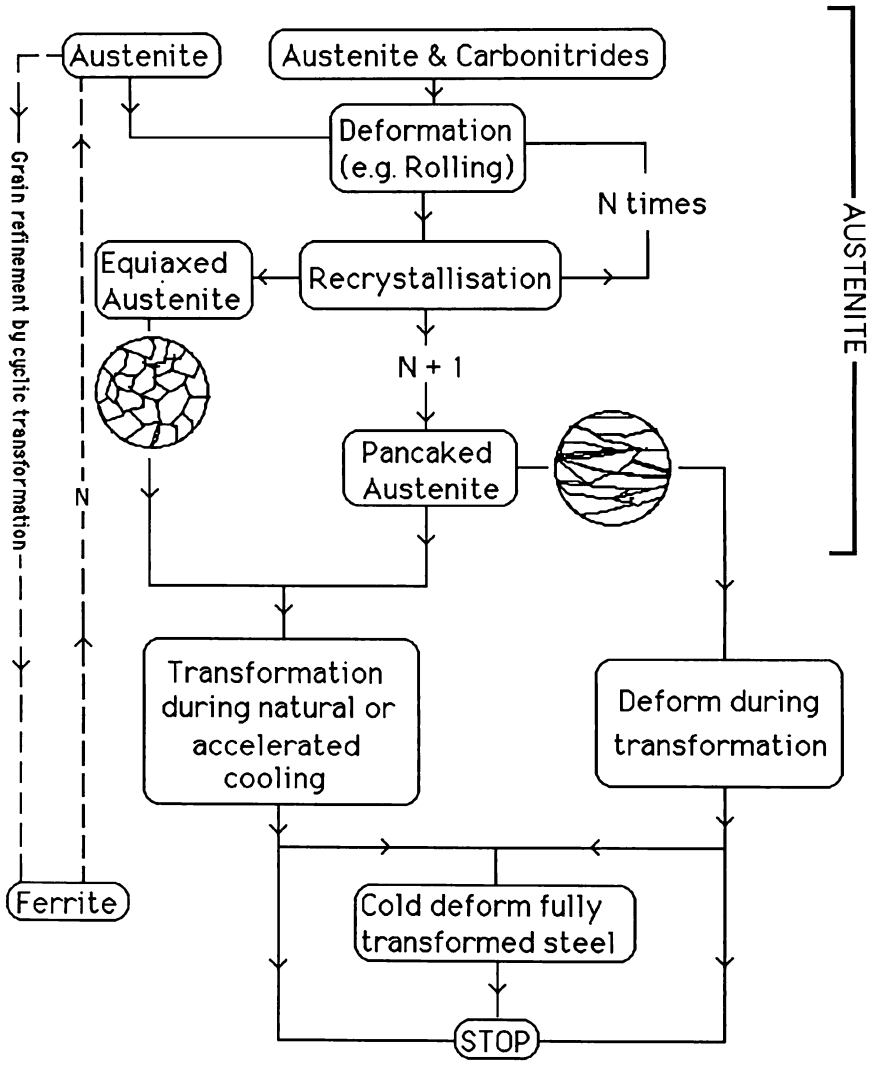

Fig. 13.2 *Flow chart illustrating some of the thermomechanical processing routes available for the manufacture of steels.*

(Fig. 13.2). A fine austenite grain size leads to a correspondingly refined ferrite grain structure. The process involves a sophisticated rolling deformation of austenite, and is called *controlled rolling*. The subject has been reviewed recently by Speich *et al.* (1984), where the complex procedures and the variety of rolling and alloying practices are discussed in detail. The essence of the process is the reduction of ingots by hot rolling in the austenite phase field, such that the austenite is induced to recrystallise

several times before the finish rolling temperature is reached. This gives a very fine recrystallised austenite grain structure. The growth of these grains during the hot rolling process is hindered by the use of microalloying additions such as niobium or titanium. These elements have a low solubility in austenite and are added in small concentrations ($\approx$ 0.03–0.06 wt%) to form stable carbides or carbonitrides which impede austenite grain growth during hot deformation and subsequent cooling. As will be seen later, it can be an advantage if the austenite grain structure before transformation is in flattened (pancaked) form rather than an equiaxed structure, because it adds to the degree of refinement. A typical chemical composition of a steel suitable for control rolling to a ferritic microstructure is Fe–0.08C–0.3Si–1Mn–0.03Nb–0.004N wt%.

Controlled rolling has been used successfully over the past 30 years or so, for steels containing allotriomorphic ferrite and a small amount of pearlite, but has only recently been adapted for bainitic alloys (Nakasugi *et al.*, 1980, 1983). There are two ways in which a bainitic microstructure can be obtained: the first, discussed in the next section, involves an increase in the cooling rate in order to allow the austenite to supercool into the bainite transformation range. The second alternative, discussed here, is to modify the steel hardenability without substantially changing the processing conditions. Alloying elements such as manganese are boosted in order to retard the formation of allotriomorphic ferrite relative to the bainite reaction. Unlike conventional steels for control rolling, TiN particles (of size $\approx$ 0.02 μm) are induced to precipitate during solidification and subsequent cooling to ambient temperature. The precipitation of the fine TiN is stimulated by increasing the cooling rate of the molten steel so that the alloys are best produced by continuous casting. Slabs of the material are then reheated to a relatively low reaustenitisation temperature of 1150°C, the particles inhibiting austenite grain growth. Reductions in grain size are obtained by repeated recrystallisation during control rolling. By inhibiting grain growth, the particles also help to produce a more uniform grain structure than is obtained in conventional control rolling treatments. Finish rolling is carried out at a temperature where recrystallisation does not occur within the time scale of the rolling sequence, so that the austenite grains are pancaked and have a deformed microstructure just before they start to transform. The hardenability of the steels is such that in spite of their small grain size, they transform to a 'uniform and fine' bainitic structure on further cooling. The metallography of these fine microstructures has yet to be properly characterised. In particular, experiments in which the steel is quenched to a partially transformed sample from various stages of the manufacturing process would be very interesting. The observations need to be done using transmission electron microscopy.

Finally, it must be emphasised that the details of the steelmaking process are crucial in determining the final properties of control rolled steels. The higher quality steels are dephosphorised, desulphurised and vacuum degassed prior to casting. Typical concentrations of phosphorous and sulphur after these treatments are 0.015 and 0.0015 wt% respectively. In circumstances where formability and uniform ductility are important, the steel is usually treated with calcium which has the effect of fixing sulphur and of modifying the shape of the sulphide inclusions.

13.1.1 Crystallographic Texture

Polycrystalline materials do not in general contain grains which are randomly oriented; the crystals in fact tend to align themselves in particular orientations determined by the thermomechanical history of the material. This alignment is called 'crystallographic texture' and its most important manifestation is in the development of anisotropic mechanical properties. The anisotropy may be exploited, as in deep drawing steels where the texture is optimised to reduce plastic strain in the thickness direction. It can on the other hand be detrimental if the cleavage planes show a tendency to align because the fracture path can then be continuous across many grains.

In wrought steels, it is deformation, recrystallisation or transformation which can lead to the development of crystallographic texture. All of these processes occur during controlled rolling and the consequent textural effects must be taken into account if the mechanical properties are to be fully interpreted. There are excellent reviews on the subject (Tanaka, 1981; Ray and Jonas, 1990), but the purpose here is to highlight the differences of crystallographic texture which arise between conventional and bainitic control rolled steels.

A convenient (though incomplete) way of representing the type of texture in rolled sheet is by stating the set $\{hkl\}\langle uvw\rangle$, where $\{hkl\}$ are the Miller indices of the planes which lie roughly parallel to the rolling plane, and $\langle uvw\rangle$ the Miller indices of the direction in $\{hkl\}$, which tends to be parallel to the rolling direction. The texture can sometimes be deconvoluted into components

$$\text{texture} = \Sigma \lambda_i \{hkl\}_i\langle uvw\rangle_i \qquad (13.1)$$

where λ represents the weighting given to a particular type of texture. The major components of the deformation texture of austenite are $\{110\}\langle 1\bar{1}2\rangle$ and $\{112\}\langle 11\bar{1}\rangle$, the so-called brass and copper textures respectively. Because ferrite has a specific orientation relationship with the parent austenite, the brass texture gives rise to a $\{332\}\langle 11\bar{3}\rangle$ ferrite texture, and the copper texture to a $\{113\}\langle 1\bar{1}0\rangle$ ferrite component

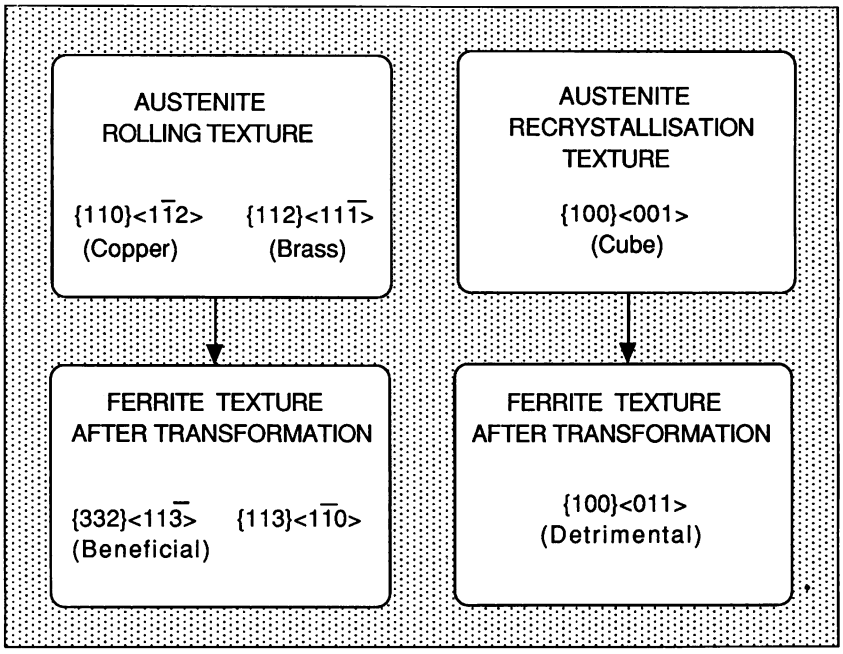

Fig. 13.3 *Summary of crystallographic texture phenomena in wrought steels. (Adapted from Ray and Jonas, 1990.)*

(Fig. 13.3). It is found experimentally that the {332}<113$\bar{}$> ferrite texture is beneficial to the deep drawing qualities of steels and for strength and toughness. Controlled rolling should therefore aim to maximise the brass texture component of austenite.

The texture of steel obtained from recrystallised austenite is made up predominantly of {100}<011> ferrite, originating from the {100}{001} 'cube' recrystallisation texture of the parent austenite. This variety of ferrite texture can in principle be very detrimental to the through thickness mechanical properties of rolled steels, since the {100} ferrite cleavage planes tend to align with the rolling plane. The fraction of {100} normals within 10° of the plate normal tends to increase as the finish rolling temperature decreases, but there does not appear to be any systematic correlation with measures of toughness (Davies *et al.*, 1977). It is possible that the texture is non-uniform on a local scale. A much more dificult but conclusive technique which could resolve this problem measures the misorientation distribution function which permits the orientation relations between adjacent grains to be recorded and studied. In fact, the cleavage process itself is not very well defined with fine microstructures suyh as bainite, where the mode of brittle fracture is more

accurately described as 'quasi-cleavage', involving cleavage planes being frequently disrupted by fibrous fracture at finely spaced plate boundaries. The complete story is therefore likely to be more complex given that inclusions such as MnS also tend to align parallel to the rolling plane. Whatever the detailed explanation, both the texture and inclusions make it easier for the steel to delaminate parallel to the rolling plane. The texture enhances the toughness along the length and width directions at the expense of the through thickness properties. It is important therefore to ensure that the austenite is in a deformed, rather than in its recrystallised state just before it begins to transform.

It is now well established that the transformation textures associated with martensitic or bainitic microstructures (or acicular ferrite) are much more pronounced when compared with the case where the austenite transforms into allotriomorphic ferrite (Fig. 13.4). It is however, difficult to gauge the significance of the observations as far as delamination is concerned, because although the texture increases in intensity when the austenite transforms by a displacive mechanism, all components are strengthened. Any deleterious influence of the {100}<011>

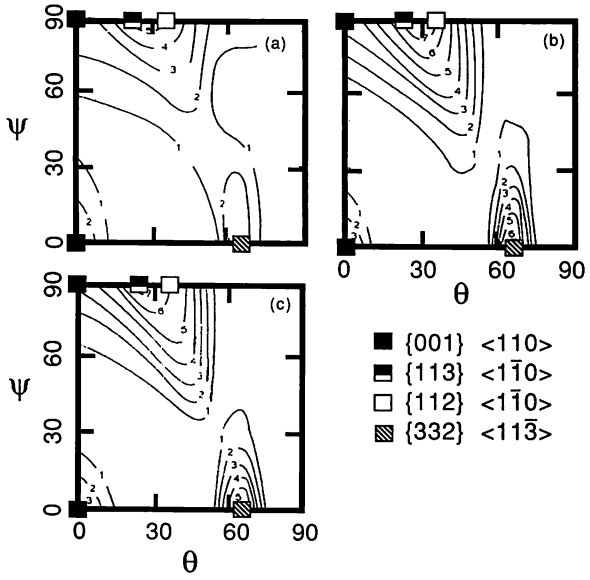

Fig. 13.4 *Sections along φ=45° of the crystal orientation distribution functions showing transformation textures of control rolled steels with a variety of microstructures (Yutori and Ogawa, 1979). For steels the most important features of the orientation distribution function are in the section of Euler space at φ=45° because it contains orientations of the form {100}<uvw> and the fibre textures {hkl}<110> and {111}<uvw>. (a) Allotriomorphic ferrite/pearlite; (b) acicular ferrite; (c) martensite. The points represent the exact textures indicated on the diagrams.*

ferrite component may therefore be masked by the other stronger components, and there do not seem to be any mechanical property data to indicate that bainitic steels which have been control rolled have a greater propensity for delamination. Indeed, results to the contrary have been reported by Tamehiro *et al.* (1985b), who demonstrated that the delamination tendency is greater for conventional control rolled steels, when compared with the more modern accelerated cooled ferrite/bainite steels.

The observed differences in the strength of transformation textures are due to the displacive growth mechanisms of martensite, bainite and acicular ferrite; the experimental data have been critically assessed by Ray and Jonas (1990). It appears to be a general result that when the transformation mechanism is reconstructive, all possible variants of the austenite/ferrite orientation relationship occur during transformation. There is therefore no *variant selection* during reconstructive transformations. On the other hand, attempts at predicting the product texture during displacive transformation, without assuming any variant selection, have not been successful in explaining experimental observations. The stresses and strains due to deformation favour the formation of particular variants in individual grains, by interacting with the shape deformation associated with the transformation.

13.2 Rapidly Cooled Control Rolled Steels

It was suggested in the previous section that bainitic microstructures can be generated in control rolled steel either by increasing the hardenability or by changing the cooling rate during processing. The latter is in fact the preferred route because the weldability deteriorates as the hardenability increases. The technology of rapid cooling during contrilled rolled is not trivial given the speed of production, the kinetics of transformation, the need to avoid distortions and the need to achieve uniform cooling rates. Considerable progress has nevertheless been made and the rapidly cooled steels described here are commercially available. It is worth noting that rapidly cooled steels are often referred to as 'accelerated cooled steels'.

13.2.1 Pipeline and Plate Steels

There is a general demand for a reduction in the wall thickness and an increase in the diameter of pipelines for gas transmission. Thinner walls permit faster and less troublesome girth welding operations, thereby reducing costs. This can be done by increasing the strength of the steels used, as long as toughness and weldability are not sacrificed in the

process. When thickness considerations are not paramount, an increase in strength has the further advantage that the gas can be transmitted more efficiently under increased pressure (≈ 10 MPa).

It is found that if, after thermomechanical processing of the kind associated with the controlled rolling, the steel is cooled from the austenite phase field at a rate which is high enough to reduce the formation of products such as allotriomorphic ferrite, but low enough to avoid substantial quantities of martensite, then a fine grained microstructure which is a mixture of allotriomorphic ferrite and bainite is formed, which is capable of meeting the required properties of increased yield strength without an adverse effect on toughness. The cooling rates involved are higher (10–40°Cs^{-1} over the temperature range 800–500°C) than those appropriate for normal control rolled steel processes. The accelerated cooling is achieved in industrial practice by the use of water spray curtains directed on either side of the hot plate (which could be some 15 mm in thickness) in a manner designed to ensure uniform cooling and to minimise distortion. The rapid cooling of thick plate requires different technology with much more careful control of water pouring in order to cope with the large thickness and width of the plates and the relatively slow rate at which the steel moves through the mill.

The process leads to a more refined microstructure in which the bainite platelets contribute to strength and toughness via their fine grain size. For a given strength level, the properties can therefore be achieved using lower alloying concentrations, with the concomitant advantages of reduced cost and in some cases, increased weldability.

Although most investigations of accelerated cooled steels have relied on light microscopy which lacks the necessary resolution, a detailed investigation (Graf *et al.*, 1985) has demonstrated that the microstructure of these rapidly cooled steels does indeed consist of a mixture of ferrite and bainite. The bainite consists of sheaves of platelets of submicron thickness, as compared with the equiaxed grains of allotriomorphic ferrite of size approximately 5 μm. It is also found to have a much higher dislocation density of 1.7×10^{14} m^{-2}, compared with 0.4×10^{14} m^{-2} of the allotriomorphic ferrite. In fact, the dislocation density of the allotriomorphic ferrite in rapidly cooled steels is known to be about four times larger than in other steels containing ferrite, possibly because of plastic deformation by the bainitic transformation which occurs after the allotriomorphic ferrite (DeArdo, 1988). It is as a consequence of the lower transformation temperatures involved, that the overall microstructure of these steels is found to be more refined relative to the conventional control rolled steels. The volume fraction of bainite can vary from about 0.2→1.0 depending on the alloy chemistry and cooling conditions. Typical compositions for accelerated-cooled alloys are given as alloys 2–4 in Table 13.1. Of these,

alloy 2 is the leanest and can be expected to contain the least quantity of bainite.

The production of the steels is not a continuous process of casting and controlled rolling followed directly by accelerated cooling. Instead, cast ingots are first allowed to cool to ambient temperature and then reheated for the thermomechanical treatment. This ensures that the very coarse austenite grain structure which evolves during ingot cooling is disrupted by transformation to ferrite. Hence, the processing involves the reheating of thick ingots to 1150°C, followed by rolling during cooling of the ingot to 740°C, with the total reduction in thickness being more than 500%, followed by accelerated cooling at 20°Cs^{-1} to around 450°C before allowing natural cooling. This treatment changes the microstructure of the plate from the normal mixture of ferrite and pearlite to a ferrite–bainite microstructure giving a better combination of mechanical properties. The tensile strength achieved is typically 700 MPa which is about 50–70 MPa higher than that of conventional control rolled steels and the Charpy impact toughness can be an impressive 160–200 J at –20°C. The extra strength is attributed to the fine size of bainite plates, although Morikawa *et al.* (1985) have demonstrated that the strength of the allotriomorphic ferrite also increases with the accelerated cooling, probably because of the dislocation density increase described above. The steels also do not exhibit sudden yielding, although the relevance of this to pipeline applications is not clear (Collins *et al.*, 1985).

13.2.2 Process Parameters

There are a number of controllable factors which can significantly influence the properties of the final product (Graf *et al.*, 1985; Tamehiro *et al.*, 1985a; Collins *et al.*, 1985). For example, a high ingot reheating temperature allows more of the niobium carbonitrides to dissolve in the austenite; the niobium carbonitrides may subsequently precipitate during the $\gamma \rightarrow \alpha$ reaction to give fine dispersions within the ferrite ('interphase precipitation'), leading to an enhancement of its strength.

The temperature at which the rolling operation finishes is critical in the sense that it should leave the final austenite grains in an unrecrystallised, pancake shape. This ensures a further degree of refinement of the microstructure obtained after transformation and avoids the undesirable recrystallisation texture of austenite. If the finish rolling temperature is too low (below Ar_3), then the allotriomorphic ferrite which forms as a consequence will itself deform, leading to an increase in strength but at the expense of toughness. For this reason, the deformation should be restricted to the austenite phase. The finish rolling temperature (T_R also influences the variation in mechanical properties through the thickness of

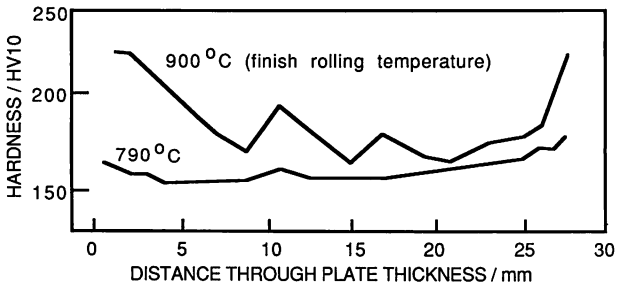

Fig. 13.5 *The effect of the temperature at which rolling is completed, on the variation in hardness of a Fe–0.16C–0.63Mn wt% acelerated cooled steel (Tamukai et al.,* 1981).

heavy gauge plates (Fig. 13.5). The surfaces, where the cooling rates are the largest, tend to be harder when compared with the central regions of the plates. The differences diminish as T_R is reduced because rolling deformation becomes focused at the plate surfaces, which consequently tend to transform more rapidly; this counteracts the effect of the higher surface cooling rates (Tanaka, 1988).

The steels used in the accelerated cooling operations have a hardenability which is high enough to prevent the completion of the bainite reaction during continuous cooling to ambient temperature. Large amounts of martensite are found in the microstructure under some circumstances, leading to a drop in toughness and a significant distortion of the plate product. As a consequence, the cooling has to be arrested by cutting off the water sprays at temperatures ranging between 600→450°C, depending on the steel chemistry and the exact cooling conditions. The subsequent slower cooling rate allows the bainite transformation to proceed to a larger extent, leaving only very small amounts of residual austenite which may transform to martensite on further cooling. Another related problem has been found in alloys with a relatively high hardenability, typically those low alloy steels with more than about 1.4 wt% manganese. When produced using controlled rolling and accelerated cooling, the yield strength decreases even though the tensile strength does not (Fig. 13.6a, Shiga *et al.*, 1983; Amano *et al.*, 1988). This is because martensite replaces bainite as the dominant hard phase, and as in dual phase steels, yielding becomes a gradual process as the stress is raised. Although this has clear advantages for applications involving forming operations, the lowering of yield strength is a disadvantage for pipeline and heavy plate fabrications where the design thickness is calculated using yield criteria.

Assuming that the difficulty can be avoided by limiting the amount of martensite that forms during accelerated cooling, a two-stage accelerated cooling process has been developed to enhance the chances of forming

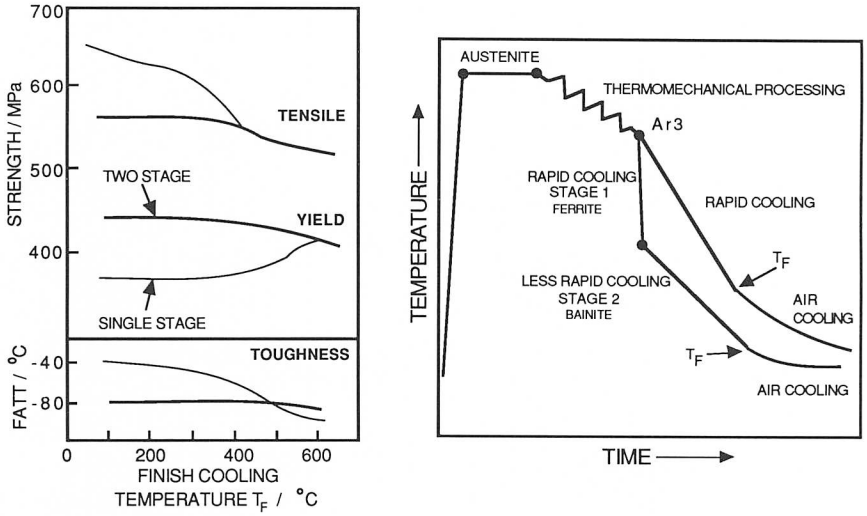

Fig. 13.6 *(a) The relationship between the tensile and yield strength, and toughness of accelerated cooled steels as a function of the temperature at which the forced cooling is stopped, for the single and double stage processes. (b) Schematic illustration of the thermomechanical cycles associated with the two-stage accelerated cooling process (Amano* et al., *1988).*

bainite instead of martensite, while at the same time retaining the high cooling rate required to refine the allotriomorphic ferrite that forms first (Fig. 13.6b). After thermomechanical processing while the steel is in the austenite condition, it is cooled rapidly (25°C s^{-1}) through the ferrite temperature range in order to obtain the fine ferrite grain size, but the cooling rate is then reduced to about 3K s^{-1} over the temperature range where bainite forms, giving a greater opportunity for transformation to proceed before the martensite start temperature is reached. The temperature (T_F) at which the forced cooling is stopped to allow the steel to air cool in the second stage of the process is also important. The mechanical properties are found to be much less sensitive to T_F for the two-stage process presumably because much of the bainitic transformation is completed at a relatively high temperature during the second stage (Fig. 13.6). The process is found to be successful in raising the yield stress of the steel when compared with the conventional accelerated cooling procedure.

Nishioka and Tamehiro (1988) have emphasised that a general problem with the accelerated cooled steels is that the toughness and microstructure are not maintained in the heat affected zones created after welding. On the other hand, the strength of these rapidly cooled steels is some 50 MPa greater than that of conventional control rolled plates. For those applications where this excess strength is not needed, the carbon equivalent of the steel could in principle be reduced further by the removal of alloying

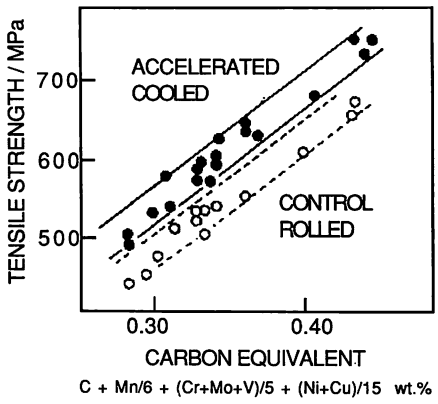

Fig. 13.7 *Relationship between the carbon equivalent and tensile strength for conventionally produced control rolled steels (CR) and accelerated cooled steels (AC); the latter have a mixed microstructure of ferrite and bainite (Tamehiro* et al., *1985a).*

elements, thereby improving the weldability (Fig. 13.7). A further difficulty is that the process is not suitable for heavy gauge plates (20–30 mm thick) since it is then impossible to ensure uniform cooling throughout the depth of the samples (Collins *et al.*, 1985); it is often the case that the central regions of such samples transform instead to a ferrite and pearlite microstructure.

In control rolled steels, heavy gauge plates which are cooled slowly after rolling, have a tendency to develop a coarse ferrite grain structure at the surfaces. This appears to be a consequence of the recrystallisation of ferrite grains deformed by rolling in the ($\alpha + \gamma$) phase field, although the fact that recrystallisation only happens at the surface implies that the deformation must have been inhomogeneous. Accelerated cooling has the added advantage that it inhibits this recrystallisation at the surface (Tamehiro *et al.*, 1985a).

13.2.3 Segregation

A large proportion of control rolled steels originate from the continuous casting process and therefore suffer from pronounced chemical segregation along the mid-thickness of the plate. Microstructural effects which reflect this segregation can be related directly to variations in the manganese concentration, which can reach twice the average concentration along the centre of the plate. Ferrite forms first in the manganese depleted regions and the carbon that it rejects is partitioned into the manganese enriched regions of austenite. This in turn exaggerates the hardenability of the manganese enriched regions which then transform into bands of hard microstructure.

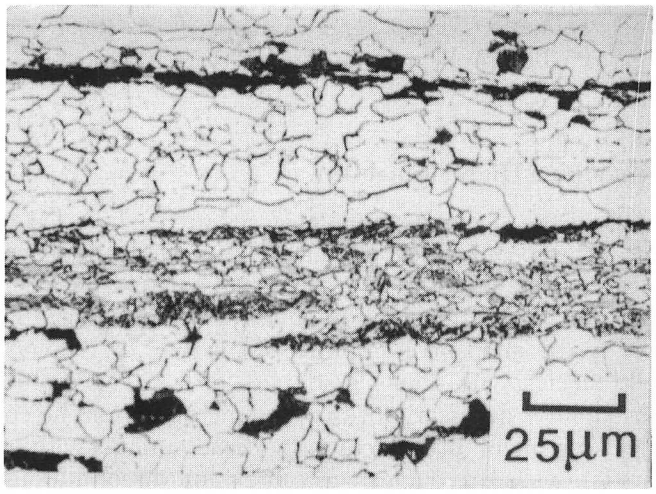

(a)

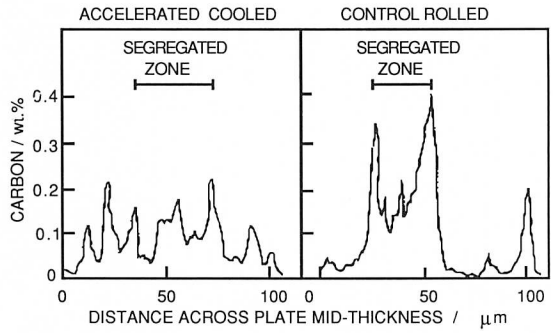

(b)

Fig. 13.8 *(a) A light micrograph illustrating the effect of chemical segregation along the mid-thickness of heavy gauge plate. (b) Distribution of carbon concentration in the segregated zone for conventional control-rolled and rapidly cooled steel plates (Tamehiro* et al. *1985c).*

These bands are highly susceptible to hydrogen induced cracking, the hydrogen being generated through corrosive reactions or other phenomena. An advantage of the accelerated cooled steels is that the resulting microstructure of bainite and ferrite is found experimentally to be less sensitive to solute segregation, when compared with the gross banding effect observed with ferrite–pearlite microstructures (Graf *et al.*, 1985; Tamehiro *et al.*, 1985a). The transformation in rapidly cooled steels is suppressed to lower temperatures, where nucleation is possible in all regions including the solute enriched zones, giving a more uniform distribution of carbon (Fig. 13.8). The resulting lower hardness in the segregated zone makes the steel less susceptible to hydrogen-induced cracking. For the

kind of steels being considered here, Tamehiro *et al.* (1985) find that the cracking ceases to be a problem if the hardness is everywhere is kept below about 250 HV.

13.3 Steels with a High Formability

The oil crisis of the seventies stimulated research which led to the development of the so-called *dual phase* steels, for applications leading to a reduction in the weight of cars in order tn make them more fuel efficient. Prior to this, the conventional automobile type steels consisted either of mixtures of ferrite and small amounts of pearlite, or wholly of ferrite ('dead' mild steels), with a tensile strength of $\approx$ 420 MPa and the high level of formability[1] necessary for the pressing operations so common in automobile component manufacture. A disadvantage with respect to forming operations is that such steels can exhibit discontinuous yielding behaviour, which causes the formation of unsightly 'stretcher strains' on the finished products.

The dual phase steels have a similar composition to the conventional steels, but are heat treated to generate a mixed microstructure of ferrite and martensite. Their mechanical properties are characterised by continuous yielding behaviour, a small yield to tensile strength ratio and a high uniform elongation (Fig. 13.9). The free dislocations associated with the martensite, and induced in the surrounding ferrite as a consequence of martensitic transformation, combine with the large mechanical property difference between the ferrite and martensite, to give the gradual yielding behaviour. Dual phase steels strain harden more rapidly than conventional alloys, leading to a higher tensile strength (500–650 MPa) without a loss in formability. More details on dual phase steels can be found in a review by Owen (1980). A typical dual phase steel would have a chemical composition Fe–0.09C–0.6Si–1.0Mn wt% and would be heat treated to give a mixed microstructure containing about 20% martensite and 80% ferrite. The relatively high silicon concentration is known to enhance formability; alloying elements such as chromium are sometimes added in small concentrations ($\approx$ 0.5 wt%) to enhance the hardenability and solid solution strength. The heat treatment can involve the annealing of strip at a temperature in the two phase ($\alpha+\gamma$) phase field, followed by cooling at a rate which ensures that the austenite transforms to martensite. However, it is commercially less expensive to integrate the heat treatment into the steel production process, by adjusting the conditions to allow the

1 In the context of automobile manufacture, formability includes the effects of operations like deep drawing, bending, stretching, etc. It is also common to spot weld or flash butt weld the finished steel.

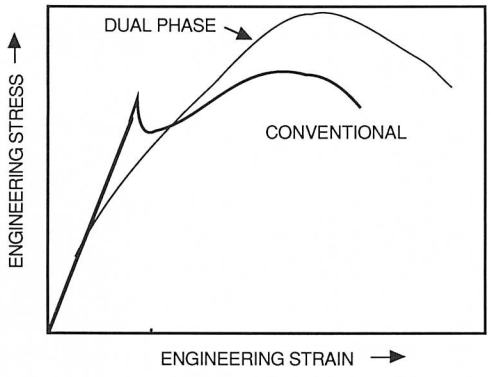

Fig. 13.9 *Schematic stress strain curves illustrating the deformation of dual phase and conventional automobile steels.*

required microstructure to develop immediately after the hot rolling process.

Serious attempts have recently been made to design dual phase steels in which the hard phase is bainite instead of martensite (Esaka *et al.*, 1985). It is claimed that conventional dual phase steels could benefit from a greater degree of stretch flangeability, and that they also suffer from localised necking in the heat affected zones of flash butt welds. To produce the microstructure of martensite and ferrite in a continuous process, the final coiling temperature has to be below the M_S temperature, and this is technically difficult to sustain at high mill speeds. The cooling rate from the austenite phase field also has to be relatively high. In addition, the use of high silicon concentrations and other alloying additions adds to the cost of these dual phase steels, and the silicon gives rise to undesirable scale on the steel surface during the manufacturing stage.

The new dual phase steels usually have a simple alloy chemistry (see for example, alloy 5, Table 13.1). They are hot rolled in the austenite phase field to give a fine austenite grain size, cooled rapidly into the bainite transformation region and coiled in that temperature range to promote the formation of bainite. The allotriomorphic ferrite forms during the cooling operation, and the cooling rate ($40 \rightarrow 100 Ks^{-1}$) determines the volume fraction of bainite (which may vary from 0.2–1.0 depending on the cooling conditions and chemistry). A coiling temperature below the martensite start temperature can lead to the formation of some martensite as well, giving a triple phase steel. The steels have properties which seem to compare well with conventional dual phase alloys, and the ferrite+bainite dual phase steels are claimed to possess better weldability, especially when microalloyed with niobium. The reasons for the improved weldability are not clear, but may have something to do with the fact that

bainite has a lower strength when compared with martensite, so that any hardening in the heat affected zone of the welds should be of lesser consequence. The carbon equivalent of the new steels is lower when compared with conventional dual phase steels since the relatively high hardenability required to induce martensitic transformation is not necessary to generate bainite.

Although conventional dual phase steels have been utilised extensively in automobile manufacture, their application to body panels has not been successful because their formability is not adequate for that purpose. Bainitic dual phase steels on the other hand, are found to exhibit superior formability and toughness during deep drawing operations when set against comparable martensitic dual phase steels. However, the lower strength of bainite means that for the same volume fraction, it is less effective than martensite in eliminating discontinuous yielding and the Luder extension at the yield stress. Since bainitic dual phase steels have the other advantages already discussed, a compromise solution would be the triple phase steel in which the presence of a small amount of martensite (in addition to bainite and ferrite) promotes the gradual yielding behaviour. Using this logic, Sudo and co-workers (1981, 1982) have demonstrated that triple phase steels (alloy 6, Table 13.1) can indeed show the best combination of mechanical properties for press forming applications. Notice that this triple phase steel is in fact leaner in alloy content than the dual phase alloys; the development of the required microstructure therefore depends on more difficult heat treatment practice.

Bainitic dual phase steels have recently been developed for the building industry, specifically to exploit their low yield to tensile strength ratio (Terada *et al.*, 1990). High rise buildings require heavy gauge, high strength, weldable steels. It is also necessary for earthquake resistant design, to ensure that the steel has enough ductility after yielding to sustain localised deformation without collapse. Recent earthquakes have established that steel is the only cost efficient construction material which imparts reliability to structures (Williams, 1991). During an earthquake, the beams and columns of the building framework, which in any case are under axial loads, experience significant bending moments, and the maximum bending moment that the beam can support prior to plastic collapse in these circumstances is lower when the yield ratio is larger. Conventional steels for these applications are quenched to a mixed microstructure of bainite and martensite, which is then tempered; any attempt to increase the yield strength leads to a corresponding detrimental increase in the yield ratio. For reasons already discussed, this is not the case for dual phase steels where the inhomogeneity of microstructure lowers the yield strength but increases the tensile strength. The bainitic dual phase steel developed for building purposes (alloy 7, Table 13.1) has a

yield ratio of about 0.7 compared with the quenched and tempered steel for which the ratio is 0.9. The steel is produced by controlled rolling, and the temperature where the forced cooling cycle commences determines the exact mix of phases in the microstructure, and hence the precise mechanical properties. Typical mechanical properties of plates ranging in thickness from 12–80 mm, are 460 MPa yield strength, 600 MPa tensile strength, 35% elongation and > 200 J of Charpy impact energy at ambient temperature. These properties are not significantly degraded by welding.

13.4 Ultra Low Carbon Bainitic Steels

Ever since the classic experiments of Irvine and Pickering (1957), it has been apparent that good mechanical properties (when compared with martensitic steels) can be obtained in bainitic steels when their carbon concentration is reduced. Otherwise, the coarse cementite particles and relatively large regions of untempered martensite (due to incomplete transformation to bainitic ferrite) have a severe detrimental effect on the toughness of the steel. Very large concentrations of substitutional solutes can also be detrimental if they limit the possible degree of transformation to bainite. Of course, too low an alloy concentration reduces the hardenability of the steel, making the production of bainitic microstructures difficult.

Irvine and Pickering reached a compromise solution, in which the carbon concentration was reduced to $\approx$ 0.1 wt%, and boron and molybdenum additions ensured that the hardenability with respect to bainitic transformation was good while that with respect to martensitic transformation was rather low. Using this method, they were able to produce virtually fully bainitic steels during continuous cooling transformation. Carbon is one of the most effective strengthening elements in steels, but for the same reason, it is also detrimental to weldability, since regions of the heat affected zone of welds then develop unacceptably high hardness levels immediately after welding. Improvements in weldability brought about by reductions in carbon concentration can therefore lead to major economies in fabrication, especially if the welding can be carried out without any preheat.

Recent work has advanced these concepts further, resulting in the development of the so-called *ultra low carbon bainitic* (ULCB) steels (alloys 8 and 9, Table 13.1) with the carbon concentration being limited to the range 0.01–0.03 wt% (Nakasugi *et al.*, 1980, 1983; Hulka *et al.*, 1988). The low carbon concentration ensures the absence of any substantial regions of martensite due to incomplete bainitic transformation, while at the same time the concentration is large enough to react with the niobium microalloying addition to form niobium carbide. The reduction in the volume fraction of martensite with decreasing carbon concentration improves

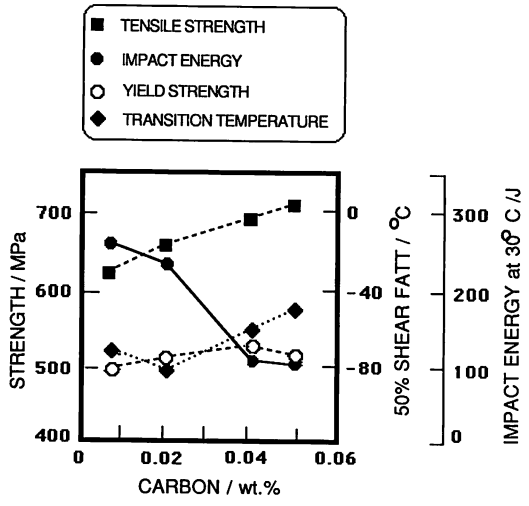

Fig. 13.10 *Variations in mechanical properties as a function of carbon concentration in thermomechanically processed ultra-low carbon steels (Hulka* et al., *1988). Note how the fracture assessed impact transition temperature (FATT), an indicator of the ductile–brittle transition temperature, begins to increase as the carbon concentration falls below about 0.02 wt%.*

toughness without any undue loss of strength (Fig. 13.10). It is important to note that the carbon concentration should not be reduced to <0.01 wt% since niobium carbide cannot then form to the required extent, leading to a decrease in toughness. The niobium carbide and TiN serve to prevent austenite grain growth during controlled rolling operations, which are an additional feature of these steels. The niobium and titanium additions are also known to be effective in suppressing the formation of $Fe_{23}(CB)_6$ during control rolling (Tamehiro *et al.*, 1987a, b). Its formation removes segregated boron from the austenite grain boundaries, thereby negating any hardenability enhancement due to boron, and can be positively detrimental because $Fe_{23}(CB)_6$ can stimulate the nucleation of allotriomorphic ferrite. Nb and Ti combine with the carbon (which also has a tendency to segregate to austenite grain boundaries) and hence prevent it from displacing boron from the grain boundaries. In other respects the steels are similar in concept to the Irvine and Pickering steels; they contain boron and molybdenum or chromium to enhance bainitic hardenability, and the titanium also helps to tie up any dissolved nitrogen which would otherwise combine with the boron and render it ineffective.[2] Although boron

2 It is reckoned that the titanium concentration (wt%) should be about 3.4 times that of nitrogen if the latter is to be fixed.

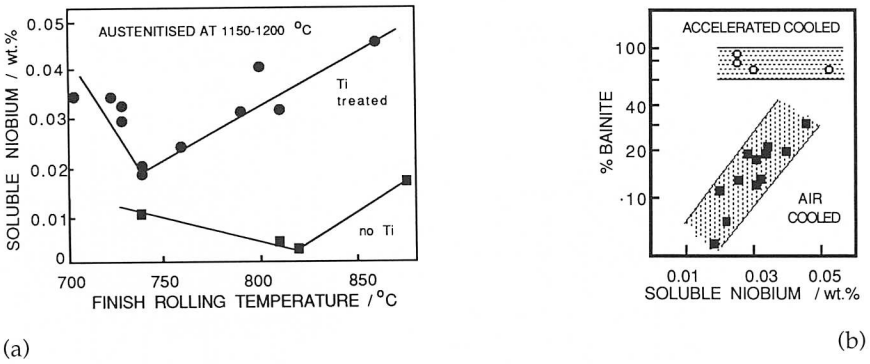

(a) (b)

Fig. 13.11 *Soluble niobium in ULCB steel (Hulka* et al., *1988). (a) Variation in the soluble niobium concentration as a function of the finish roling temperature; (b) variation in microstructure as a function of the finish rolling temperature.*

can in principle lead to an increase in the hardenability and hence the hardness of the heat affected zone, the effect in ULCB steels is far less pronounced because of the very low overall carbon concentrations utilised. Because of the lower carbon concentrations in ULCB steels, the level of manganese and other substitutional elements such as nickel are higher compared with the Irvine and Pickering steels.

In ULCB alloys, the exceptionally small carbon concentration also ensures that a substantial proportion of the total niobium addition remains in solid solution at typical austenitising temperatures and during subsequent processing. The role of niobium in conventional HSLA steels is essentially to form fine austenite grain boundary pinning particles by combining with carbon and nitrogen, elements which are present in relatively large concentrations. The equilibrium solubility of niobium thus tends to be very small in conventional HSLA steels, and the level cannot be increased by raising the overall concentration of niobium, since in typical steels, its solubility limit is about 0.03 wt% in austenite. The situation is different for ULCB steels, which also contain deliberate additions of Ti to tie up as much free nitrogen as possible since it tends to embrittle the steel via strain aging effects. It has been demonstrated that the finish rolling temperature within the austenite phase field during thermomechanical processing has a large influence on the soluble niobium in the final steel (Fig. 13.11a). Less niobium remains in solution as the finish rolling temperature is reduced because there is then a greater opportunity for strain induced precipitation.

The variations in dissolved niobium appear to have a very significant effect on the evolution of microstructure in air cooled ULCB steels, where air cooling corresponds to about $1Ks^{-1}$ over the transformation tempera-

ture range (Fig. 13.11b). It would be surprising if this were to be a purely thermodynamic effect on the austenite to ferrite transformation given the very low concentrations involved, but it is known that niobium strongly retards the formation of allotriomorphic ferrite. Hence, the amount of bainite obtained in the final microstructure is bound to increase with niobium in solid-solution; the effect is however, masked during accelerated cooling (15–20Ks^{-1} over the transformation temperature range) since the cooling rate is then large enough to avoid any substantial transformation to allotriomorphic ferrite (Fig. 13.11b).

The greater tendency to form bainite as the dissolved niobium concentration increases has also been observed by Leber *et al.* (1987) who also found an interesting synergistic effect between niobium and vanadium. Being another carbide forming element, vanadium in solid solution retards the precipitation of niobium, thereby further enhancing the tendency to form bainite.

ULCB steels are found to have extremely good toughness, strength (500–620 MPa depending on thermomechanical processing) and weldability combinations and have been designated for use in high strength line pipe in Arctic or submarine environments. The highest strength values are obtained using low finishing temperatures and accelerated cooling through the transformation temperature range. A small amount of further strengthening can be obtained by retarding cooling below about 550°C, to induce the precipitation of NbC in the ferrite. This can be achieved simply by coiling or stacking the hot product. A possible problem with these steels is in ensuring that the TiN particles which form in the melt are sufficiently small to avoid acting as fracture initiators. The size of the particles can be modified by controlling the cooling rates involved in the solidification process. Sulphide shape control using rare earth or calcium additions is also standard practice and the overall sulphur concentration must be kept below about 10 ppm for pipeline grade steels.

13.5 Bainitic Forging Steels

Forging is a method of fabrication involving the working of metal into the required shape by hot or cold plastic deformation. For very large objects, the metal is deformed into shape using open dies, whereas mass production of more precise shapes can be carried out using closed dies whose internal profile is replicated as the metal flows under the influence of the forge pressure. Forging is attractive from an industrial point of view because it not only reduces or eliminates the machining necessary to achieve the final product shape, but can at the same time enhance the properties along directions consistent with the application. Typical

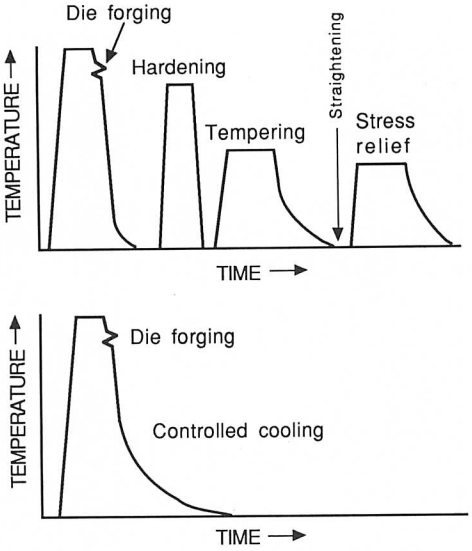

Fig. 13.12 *Schematic illustration of the heat treatment procedures for forging steels (Wright* et al., *1987). (a) Conventional quenched and tempered martensitic steels; (b) microalloyed forging steels.*

components which are forged range from small scale items such as crankshafts, connecting rods, piston shafts, bolts, axles, fasteners, etc., to components which might weigh many tons, such as the rotor shafts in steam turbine generators.

Conventional forging steels, which served the industry very reliably and successfully for many decades, consisted of Fe–C–Mn–Si alloys and were available in two strength ranges, 350–450 MPa ferrite–pearlite alloys, and high strength (>600 MPa) quench and tempered martensitic steels; an excellent review on the subject has been published by Jones *et al.* (1985). To achieve the martensitic microstructure, the forged components have to be austenitised, quenched, tempered, manipulated to remove any distortions resulting from the heat treatment, and finally, stress relieved (Fig. 13.12a). Also, for thick sections, the steels has to be heavily alloyed so that its hardenability is adequate to produce the martensitic microstructure throughout its section. The drive for alloy development comes not from an inability to achieve the required mechanical properties, but from the need to reduce costs by cutting down on alloying elements, and more significantly, to reduce the costs of the post-forging heat treatments. It is often the case that less than half of the final cost is attributable to material and forging expense. In addition to toughness criteria, forged steels also have to satisfy stringent fatigue requirements since many of the components (such as shafts) undergo cyclic stressing during service.

With these goals in mind, modern forging steels are microalloyed to produce either highly-refined ferrite–pearlite microstructures, or are alloyed to give fully bainitic, or predominantly bainitic microstructures. The major gain is that these microstructures can be produced by direct transformation during cooling from the forging temperature, with accompanying savings in heat treatment, handling and other fabrication costs (Fig. 13.12b). Strength levels within the range 500–700 MPa can easily be achieved without loss of toughness and with improvements in fatigue properties, machinability and weldability. There are difficulties at the very high strength levels typical of medium carbon steels (i.e., 1200 MPa), where the toughness does not seem to match that of quenched and tempered martensitic steels, although systematic models capable of optimising the alloy chemistries still need to be developed. There are other special considerations necessary when using directly transformed microalloyed steels; fairly rapid induction heating is often used to heat the stock to forging temperature. The time at the austenitisation temperature has to be long enough to permit the microalloying elements such as niobium to dissolve (Wright *et al.*, 1987). The way in which the finished components are stacked after the final forging operation will determine their cooling rates.

The new alloys also open up the possibility of 'controlled forging', which by analogy with controlled rolling, aims to refine the austenite grain structure prior to transformation (Jones *et al.*, 1987). The forging sequence is then designed so that the final stages of deformation are carried out at relatively low temperatures where the austenite does not recrystallise (i.e., the grains ends up with a pancake shape), or alternatively, recrystallises to a very fine grain size. The disadvantage is that reductions in forging temperature cause an increase in the force required to cause deformation, so that the required forge capacity rises. Furthermore, the increased stress also leads to more rapid die wear. These counterproductive effects must be taken into account into any cost analysis.

Many of the new forging steels contain a variety of carbide forming elements such as Nb, V, Mo, etc. (alloys 11–15, Table 13.1). Tempering heat treatments can then lead to very fine scale precipitation reactions which are important in determining the strength of the final product. It has been demonstrated that the response to tempering is related to the amount of type and bainite present in the as-transformed microstructure in steels containing mixtures of allotriomorphic ferrite, bainite and pearlite (Leber *et al.*, 1988). In this context, the higher dislocation density of bainite rich microstructures leads to a faster rate of hardening as the dislocations help nucleate the carbides. For the same reason, bainite which is obtained by transformation at a lower temperature, and which consequently exhibits a larger dislocation content, also exhibits a stronger hardening response when tempered. Predominantly bainitic micro-

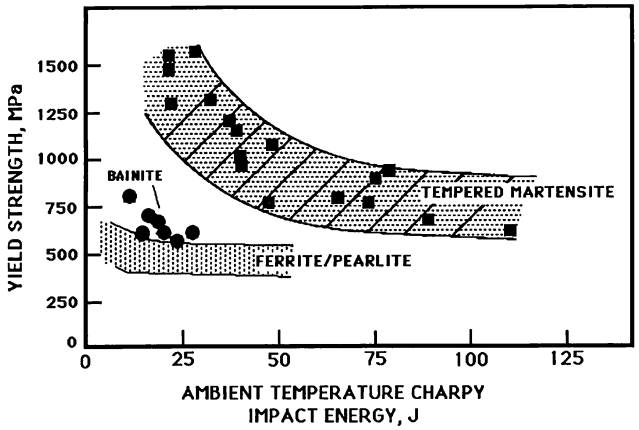

Fig. 13.13 *A comparison of the properties of ferrite–pearlite, bainitic and martensitic forging steels (Grassl* et al., *1989).*

structures are therefore to be preferred over those containing large fractions of allotriomorphic ferrite. In some cases, where niobium and boron additions are used to develop low carbon bainitic microstructures with high work hardening rates (alloy 15, Table 13.1), cold deformation can be used to increase the strength of the final product. A good example is the series of steels developed for the production of high strength bolts by cold heading operations (Heritier *et al.*, 1984).

One class of high-strength bainitic forging steel being developed for applications in the automobile industries are alloys containing high silicon and molybdenum concentrations with typical composition Fe–1.4Mn–0.8Si–0.15V–0.2Mo wt% with 0.1–0.40 wt% C (Heitmann and Babu, 1987; Grassl *et al.*, 1989). These steels are designed to replace current quenched and tempered martensitic alloys. The compositions are chosen to avoid the formation of carbides during bainitic transformation, carbides which can be detrimental to toughness. The toughness is indeed found to be better than that of ferrite–pearlite mixed microstructures at comparable strength levels; at the higher carbon concentrations, comparisons with martensitic microstructures reveal that the latter have superior toughness (Fig. 13.13), although similar comparisons at lower carbon concentrations are not available. Although this might deter against the use of bainitic forging steels, their toughness is still more than adequate for many applications, so that their cost advantage can still be usefully exploited.

13.6 High Strength Bainitic Steels without Carbides

As discussed in Chapters 2 and 3, it is now well established that in many steels, especially those with large concentrations of silicon or aluminium,

carbide precipitation reactions lag far behind the growth of bainitic ferrite. As a consequence, the carbon which is rejected from the bainitic ferrite enriches the residual austenite, thereby stabilising it to martensitic transformation during cooling to ambient temperatures.

The mixture of bainitic ferrite and austenite is in principle an ideal combination from many points of view. Most modern high strength steels are clean in the sense that they are largely free from non-metallic inclusions. Those destined for critical applications are usually vacuum arc refined prior to fabrication and heat treatment. As a consequence, it is the components of the intrinsic microstructure, such as particles of cementite, which are responsible for damage initiation. The upper bainitic ferrite and austenite mixture is however, free from cleavage and void nucleating cementite. The ferrite also has a very low interstitial content, since much of the excess carbon is partitioned into the residual austenite; the toughness of ferrite is known to deteriorate rapidly with an increasing concentration of carbon in solid solution.

The microstructure derives its strength from the ultrafine grain size which results from the displacive mechanism of ferrite growth, giving an effective grain size which is much less than 1 μm. Such a small grain size cannot be achieved by any commercial process other than mechanical alloying (powder metallurgical process). A fine grain structure is an optimum method for improving strength since unlike most other strengthening mechanisms, the improvement in strength is also accompanied by an improvement in toughness. The intimately dispersed and ductile FCC austenite films between the ferrite platelets can be expected at the very least to have a crack blunting effect, and could also increase the work of fracture by undergoing martensitic transformation under the influence of the stress field of the propagating crack (i.e., the TRIP, or transformation induced plasticity effect). The diffusivity of hydrogen in austenite is relatively sluggish, so that its presence can enhance stress corrosion resistance. And all these potential benefits can be achieved by creating a duplex microstructure with the cheapest austenite stabiliser available, carbon, whose concentration in the austenite is enhanced during transformation, so that the average carbon concentration of the steel need not be large.

In spite of all these potential advantages, the bainitic ferrite–austenite microstructure has on many occasions failed to live up to its promise, primarily because of the instability of relatively large or blocky regions of austenite which become trapped between sheaves of bainite (Fig. 8.11). The blocks of austenite tend to transform to high carbon, untempered martensite under the influence of small stresses and consequently have an embrittling effect. The films of austenite that are trapped between the platelets of ferrite in a sheaf are much more stable, partly because of their

higher carbon concentration, but also because of the constraint to transformation from the surrounding plates of ferrite.

If it is assumed that a fraction ϕ of a sheaf consists of films of austenite, then it can be demonstrated that the ratio of the volume fractions of film and blocky austenite (prior to any martensitic transformation) is given by

$$V^{\gamma-F}/V^{\gamma-B} = (\phi V^{\alpha})/(V^{\gamma} - \phi V^{\alpha}) \qquad (13.2)$$

where $V^{\gamma-F}$ and $V^{\gamma-B}$ are the volume fractions of film and blocky type retained austenite respectively, and V^{α} and V^{γ} the total volume fractions of bainitic ferrite and residual austenite respectively. It is found experimentally that high strength and good toughness can be obtained by maintaining the above ratio to a value greater than 0.9 (Bhadeshia and Edmonds, 1983a, b). The question then arises as to the factors which control this ratio. There are in fact three different ways of minimising the volume fraction of blocky austenite, each involving an increase in the volume fraction of bainite (equation 13.2).

Lowering the transformation temperature permits the bainite reaction to proceed to a greater extent but there is a limit to the minimum transformation temperature since the lower bainite and martensite reactions eventually set in. An increase in the extent of reaction can also be achieved by reducing the overall carbon concentration of the steel, so that the austenite reaches its limiting composition at a later stage of the reaction. The T_o curves of the phase diagram, which determine the composition of the austenite at the point where the reaction stops, can also be

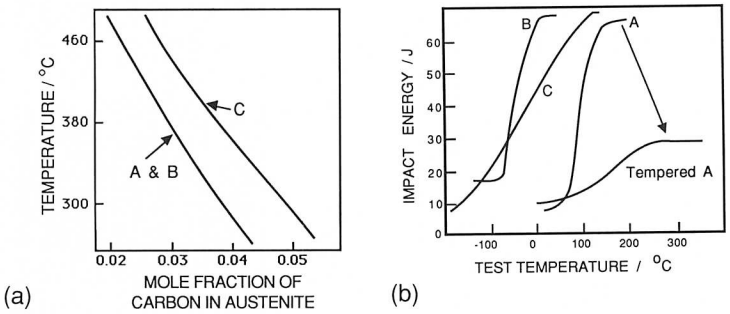

Fig. 13.14 *(a) T_o curves for alloys A, B, and C. (b) Impact transition curves demonstrating how the toughness can be improved, without a loss of strength, simply by minimising the amount of blocky austenite in a mixed microstructure of bainitic ferrite and austenite. Curve A refers to upper bainite in a Fe–0.43C–2Si–3Mn wt% alloy for which $V^{\gamma-F}/V^{\gamma-B}=0.5$. Curve B is for a similar alloy but with about half the carbon concentration. Curve C represents an alloy with the same carbon concentration as A but with the manganese replaced with 4 wt% nickel in order to shift the T_o curve to higher carbon concentrations. $V^{\gamma-F}/V^{\gamma-B}>1.5$ for alloys B and C. After Bhadeshia and Edmonds (1983a,b).*

Table 13.2 Chemical compositions (wt%) of experimental high strength steels with microstructures consisting of mixtures of bainitic ferrite and retained austenite.

C	Si	Mn	Ni
0.22	2.0	3.0	–
0.40	2.0	–	4.0

shifted to higher carbon concentrations by altering the substitutional solute concentration of the steel Fig. 13.14a. The effect on toughness in reducing the amount of blocky austenite is Fig. 13.15b, which shows the large changes in the impact transition temperatures as the ratio of film to blocky austenite is increased in the manner just described. Note that for a duplex $\alpha+\gamma$ microstructure, the strength actually increases as the fraction of bainitic ferrite increases, to that the better toughness is obtained without sacrificing strength.

Typical compositions of high strength steels which show good toughness are given in Table 13.2; Fig. 13.15 shows how the mechanical properties compare with quenched and tempered steels. It is evident that in some cases, the properties match those obtained from much more expensive marageing steels.

The properties of these steels improve only slightly when tempered at temperatures not much higher than the transformation temperature at which the original bainite formed. However, annealing at elevated

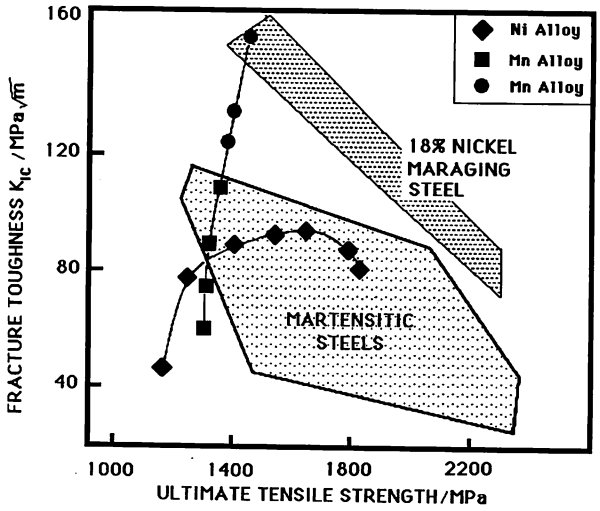

Fig. 13.15 *Comparison of the mechanical properties of mixed microstructures of bainitic ferrite and austenite, versus those of quenched and tempered tmartensitic alloys (Miihkinen and Edmonds, 1987c).*

temperatures or prolonged periods at low temperatures can lead to the decomposition of the austenite into ferrite and carbides, with a simultaneous drop in strength and toughness, especially the upper shelf energy (Fig. 12.11). The latter effect can be attributed directly to the void nucleating propensity of carbide particles in the tempered microstructure, as illustrated by the much smaller void size evident in the fracture surface of the tempered sample (Fig. 12.11).

The mechanical property data on these high silicon steels, especially those steels designed using the phase transformation theory discussed earlier, look extremely promising. It is unlikely that the experimental steels represent the optimum compositions and further development work could lead to even better properties. It is also necessary to carry out a comprehensive assessment of properties such as stress corrosion resistance, fatigue, etc.

13.7 Thermomechanically Processed High Strength Steels

The alloys described here are not in fact terribly useful, but the phenomena they reveal are interesting and certainly add to the general understanding of bainitic transformation.

13.7.1 Ausformed Bainitic Steels

Ausforming involves the deformation of austenite at temperatures well below Ae_3, before any formation of martensite or to bainite. Its main effect is to increase the strength of the steel, usually with a small loss in ductility. The deformation reduces the effective size of the austenite grains, and this in turn leads to a more refined bainitic microstructure on subsequent transformation (Kalish *et al.*, 1965, Duckworth, 1966; Edwards and Kennon, 1974, 1978; Umemoto *et al.*, 1986). In controlled experiments involving tensile deformation (Umemoto *et al.*, 1986), prestraining of the austenite beyond a certain critical plastic strain was found to favour the formation of particular crystallographic variants of bainite, although details about the sense of the alignment or of why a threshold level of plastic strain exists are not understood.

The bainitic ferrite that grows from deformed austenite is known to contain a greater density of dislocations (Irani, 1967; Edwards and Kennon, 1978). This is expected from the displacive mechanism of bainitic transformation; the ferrite can be expected to inherit the dislocations present in the parent austenite. Tsuzaki *et al.* (1989) demonstrated that the bainitic sheaves tend to adopt a much smaller aspect ratio in ausformed samples, in effect leading to a much smaller ferrite grain size. Any cementite particles precipitated during the bainite reaction are also refined, the

Table 13.3 Chemical compositions (wt%) of bainitic steels that have been studied with respect to the ausforming process. The steels are not in some cases custom made for ausforming operations.

C	Si	Mn	Ni	Mo	Cr	V	Cu	W	
0.39	1.00	0.25	–	1.39	5.25	0.54	–	–	Kalish *et al.*, 1965
0.48	0.25	0.86	0.18	0.04	0.98	–	0.09	–	Duckworth, 1966
0.85	–	1.39	–	–	0.59	–	–	0.53	Edwards and Kennon, 1978
0.59	2.01	1.02	–	–	–	–	–	–	Tsuzaki *et al.*, 1989

number density of carbides being higher (at constant volume fraction) in ausformed bainite than in conventional bainite. The refined microstructure and the increased dislocation density seem to be the key factors responsible for the strengthening effect of ausforming on bainitic microstructures (Edwards and Kennon, 1978). As a rough estimate, each one per cent increment of deformation leads to a 5 MPa increase in strength.

Not all steels are suitable for ausforming because the austenite has to be stable to transformation at the ausforming temperature. The steel is usually heavily alloyed with elements which led to the formation of a deep bay in the region of the TTT diagram between the two C curves representing the reconstructive and displacive reactions (Table 13.3). Note that since deformation in general accelerates the rate of bainitic transformation, the bay on the TTT diagram has to be sufficiently deep to avoid this *accelerated* transformation. The relative rates of different transformations can also change. It has been reported that for reasons which are not yet understood, the overall transformation kinetics of allotriomorphic ferrite are accelerated by deforming the austenite prior to transformation, to an extent much greater than that of bainite in a Fe–0.1C–0.39Mo–0.88Mn–0.34Si wt% low alloy steel (Smith and Siebert, 1970). A consequence of this is that it becomes much more difficult to obtain a bainitic microstructure in deformed austenite by continuous cooling transformation.

Some of the alloying elements used for ausforming steels are strong carbide formers and it is suspected that the deformation of austenite enhances the precipitation of fine particles in the austenite, and that this additionally contributes to the strength of ausformed samples (Duckworth *et al.*, 1964, Thomas *et al.*, 1965).

Austenite which is thermomechanically processed at low temperatures during ausforming often does not deform homogeneously. Slip tends instead to concentrate into narrow bands (Schmatz and Zackay, 1959; Evans and O'Neill, 1959; Freiwillig *et al.*, 1976). The austenite in the bands then transforms into a peculiar narrow band of ferrite, whose transformation mechanism and detailed structure are unclear although it is known that such bands act as nucleation sites for bainitic ferrite (Jepson and Thompson, 1949; Freiwillig *et al.*, 1976; Edwards and Kennon, 1978).

Transmission electron microscopy by Freiwillig *et al.* indicates that each band consists of a single crystal of ferrite, whereas Edwards and Kennon demonstrated that they contain parallel laths of ferrite whose long axes lie in the plane of the band, together with some retained austenite. The bands also contain some carbide precipitation, some of which occurs after the formation of the ferrite within the bands. The carbides are believed to assist the further nucleation of ferrite by reducing the carbon supersaturation in the adjacent austenite. These morphological observations, together with the fact that transformation within the bands is faster than the formation of bainite within the rest of the austenite, indicate that the microstructure of the band may simply be some highly refined form of bainite (Edwards and Kennon, 1978).

The tempering behaviour of ausformed bainite is also found to be somewhat different from that of conventional bainite. During tempering at 550°C for 1 h, the dislocations in the ausformed bainite are found to rearrange into cells, whereas those in conventional bainite, which has a lower dislocation density, seem to be unaffected (Edwards and Kennon, 1978).

Ausformed steels have not as yet been very successful in a commercial sense, probably because of the expense of the thermomechanical treatment, which also limits the shape of the components that can be made without subsequent machining operations. With the exception of some low carbon bainitic steels, ausformable alloys tend to be costly since they contain relatively large quantities of alloying elements; a typical ausforming steel which is transformed to bainite might contain 5Cr–2Mo–0.5V–0.3Mn–1.0Si wt%. In general, ausformed martensitic steels exhibit better combinations of toughness and strength when compared with ausformed bainitic steels (Kalish *et al.*, 1965). This is probably related to the relative coarseness of carbides in bainitic microstructures as is confirmed by experiments which show that ausformed low carbon bainitic steels is tougher than martensite in the same alloy (Durbin and Krahe, 1973). There is however, new hope for ausformed bainitic steels containing a relatively large concentration of silicon; research on such steels shows that they respond well to thermomechanical processing because the silicon refines any cementite and hence mitigates any detrimental effects on mechanical properties (Tsusaki *et al.*, 1989).

13.7.2 Strain Tempered Bainitic Steels

Strain tempering involves the deformation of martensitic or bainitic microstructures, followed by an ordinary isothermal tempering heat treatment. The steel compositions are similar to those of ausformed steel. The process leads to large increases in strength, with some loss in ductility

and toughness. The strengthening that is obtained increases with the level of prior deformation, but is not just a reflection of the effects of deformation on the microstructure. The subsequent tempering also causes a significant rise in strength, probably as a consequence of the precipitation of fine carbides on deformation induced defects (Kalish *et al.*, 1965). The strain tempering effect is larger for bainite than for martensite, because the deformation causes the relatively larger amount of retained austenite in the former microstructure to undergo stress induced transformation to harder martensite. Strain tempering is more effective as a method for increasing the yield strength than ausforming, but does lead to lower ductility.

13.7.3 Creep Tempering

It is well established that the recovery and recrystallisation processes associated with the tempering of bainite are accelerated under the influence of creep deformation (Ridal and Quarell, 1962; Murphy and Branch, 1971). For example, during creep testing at elevated temperatures, the unstressed regions of bainitic tensile specimens are found to have a higher hardness than the corresponding stressed regions. Ridal and Quarell have also shown that in Mo containing bainitic steels, the rate of transition from Mo_2C towards the more stable M_6C precipitate during tempering is higher in creep tests. The acceleration was observed to be higher for tests at lower temperatures, for higher creep strain rates and for steels where the kinetics of the $Mo_2C \rightarrow M_6C$ reaction are slow in the absence of creep. The results were explained in terms of enhancement of diffusion processes and nucleation at deformation induced defects. Consistent with experimental data, the effect of any enhancement would be most noticeable at relatively low temperatures, high strain rates and when the reaction rates are intrinsically slow. In the same work, Ridal and Quarell also showed that the $M_7C_3 \rightarrow M_{23}C_6$ reaction during the tempering of Fe–Cr–C martensitic alloys is, if anything, slightly retarded by creep deformation. Hence, the details of the interactions between microstructural changes and creep deformation are not clear.

13.8 Bainite in Rail Steels

Modern railway systems are subjected to intense use, with relatively fast trains and increasing axle loads. Rails must consequently be more wear resistant, and achieve higher standards of straightness and flatness in order to avoid the sort of surface and internal defects which may eventually lead to failure. The shape of the manufactured rail depends to a large extent on the uniformity of thermomechanical processing, so that the

most advanced mills are computer controlled with continuous feedback from the product during manufacture (Fitzgerald, 1991). The tribological and other mechanical properties are a function more of the alloy chemistry and the design of the thermomechanical treatment. It is this metallurgical aspect which is considered below.

13.8.1 Track Materials

Although a variety of different kinds of loadings can adversely affect the life of rails, wear and plastic deformation can lead to unacceptable changes in the rail head profile, changes controlled primarily by a system of rolling contact stresses encountered during service. This system is dependent upon the relative motions of wheel and rail within a small contact zone of about one square centimetre. These motions lead to lateral and longitudinal surface tractions and a spin moment. The rate of rail degradation depends also on the exact location; rail head erosion is at a maximum in regions where the track curves.

Ordinary rail steels usually contain about 0.7wt% of carbon, and give an almost fully pearlitic microstructure during continuous cooling heat treatment from the austenite phase field (Table 13.4). However, special grade steels have been considered for tracks carrying high axle loads or fast trains. Since the steels may be used in continuous welded track, they have to satisfy the weldability criteria, such that any heat affected region regains its original microstructure during cooling to ambient temperature. They must be amenable to being joined by welding to other kinds of low grade rail steels. Conventional welding processes include flash butt

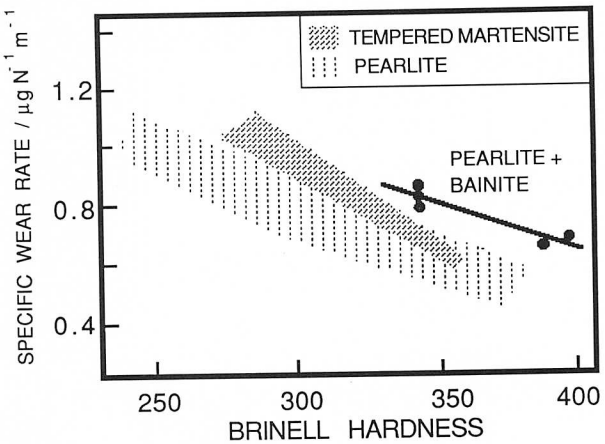

Fig. 13.16 *The correlation of overall hardness with the wear rate for martensitic, bainitic and pearlitic microstructures (Hodgson and Preston, 1988).*

Table 13.4 Compositions (wt%) of typical pearlitic and bainitic rail steels.

No.	C	Si	Mn	Ni	Mo	Cr	V	Nb	B	Al	Ti	Other	
1	0.55	0.25	1.00	–	–	–	–	–	–	–	–	–	Pearlitic rail steel
2	0.80	0.30	1.00	–	–	–	–	–	–	–	–	–	Pearlitic rail steel
3	0.70	1.90	1.50	–	–	–	–	–	–	–	–	–	Pearlitic rail steel
4	0.75	0.70	1.00	–	–	1.0	0.1	–	–	–	–	–	Special grade pearlitic rail steel
5	0.65	0.25	0.70	–	–	–	–	–	–	–	–	–	Pearlitic tyre steel
6	0.04	0.20	0.75	2.0	0.25	2.8	–	–	<0.01	0.03	0.03	–	Best available bainitic rail steel
7	0.09	0.20	1.00	–	0.50	–	–	–	0.003	0.03	0.03	–	Experimental bainitic rail steel
8	0.07	0.30	4.50	–	0.50	–	–	0.1	–	–	–	–	Experimental bainitic rail steel
9	0.10	0.30	0.60	4.0	0.60	1.7	–	–	<0.01	0.03	0.03	–	Experimental bainitic rail steel
10	0.30	0.20	2.00	–	0.50	1.0	–	–	0.003	0.03	0.03	–	Experimental bainitic rail steel
11	0.30	1.00	0.70	–	0.20	2.7	–	0.1	–	–	–	–	Experimental bainitic rail steel
12	0.52	0.25	0.35	1.5	0.25	1.7	–	0.1	<0.01	–	–	–	Experimental bainitic rail steel
13	1.00	0.25	0.25	–	–	1.50	–	–	–	–	–	–	Roller bearing alloy

welding and the thermite process. The Hadfield type cast austenitic manganese steels are excellent for wear resistance but are not weldable to ordinary rail steels (Sawley *et al.*, 1985).

Wear is a system property, not a material property. The relationship between microstructure and wear properties is known to be tenuous. The most prominent correlation is that for the normal sort of eutectoid steels, the wear rate in general decreases monotonically with the hardness of the microstructure Fig. 13.16, although exceptions to this rule have also been reported (Kalousek *et al.*, 1985b). Apart from hardness, Fig. 13.16 also shows that other features of the microstructure must have additional influences on the wear behaviour, albeit to a lesser extent when compared with the sensitivity to hardness. The microstructural effect is emphasised by the established fact that in the context of rails, a refinement of microstructure can prolong the wear-limited rail life (Kalousek and Beynon, 1975).

As pointed out earlier, the vast majority of rail steels are of near eutectoid composition and are pearlitic in microstructure. Pearlite can be refined by reducing the colony size and interlamellar spacing by appropriate heat treatment, but a higher level of refinement can in principle be obtained by transforming the steel to bainite. To date, relatively few experimental bainitic rails have been assessed, and most of the data seem to indicate that bainitic steels do not possess any significant advantage over pearlitic alloys. For example, Ghonem *et al.* (1982) examined the wear and toughness properties of pearlitic rails with that of an experimental bainitic rail. The rail head consisted of a microstructure with about 70% bainite and 30% pearlite. This rail had a composition comparable to a premium quality pearlitic rail (containing Cr and Mo), but with a higher molybdenum concentration by about 0.15–0.2 wt%. The microstructure was found to exhibit relatively poor toughness and, with respect to its hardness, poor gauge face (i.e., rolling–sliding) wear resistance. It was found to offer few or no advantages over the standard and premium fully pearlitic steels investigated. The reasons for this behaviour will only be clarified with more basic research on the relationship between microstructure and wear and with more careful microstructural characterisations than have been reported to date.

Heller and Schweitzer (1980) compared the properties and service performance data from bainitic rail steels (Fe–0.07C–0.3Si–4.5Mn–0.5Mo–0.1Nb, and Fe–0.3C–1.0Si–0.7Mn–2.7Cr–0.2Mo wt%) with those from pearlitic rail steels (Fe–0.75C–0.7Si–1.0Mn–1.0Cr–0.1V wt%). The bainitic steels were found capable of achieving higher tensile and fatigue strength levels and performed well in service. However, there were unspecified problems during welding, and due to their more expensive alloy content, it was concluded that they should be used only in particularly severe

service conditions. Furthermore, service trials subsequently revealed that the bainitic steels wore faster than conventional pearlitic steel rails, when comparisons were made at the same hardness levels (Heller and Schweitzer, 1982). Some work on a low carbon bainitic steel using laboratory tests involving rolling–sliding contact has indicated a wear rate some ten times faster than a pearlitic steel of the same hardness (Ichinose *et al.*, 1982). Other results confirm these general trends and indicate further that mixed microstructures consisting of bainite and pearlite are less wear resistant when compared with fully pearlitic steels, Fig. 13.16, (Kalousek *et al.*, 1985a,b; Mutton, 1985).

In contradiction to these generally gloomy results on bainite, there are other data on bainitic rail steels which look promising. Carbide free low carbon bainitic steels have been tested successfully for railway crossing applications where impact erosion and fatigue of the crossing nose were the major wear problems with conventional pearlitic rail steels (Callender, 1983; Garnham, 1989). An advantatge of using low carbon concentrations is the gain in weldability, enabling the steels to be welded relatively easily to adjoining rails. Other work by Clayton and co-workers (1987) using pure sliding, cooled, pin-ring tests indicates that low carbon bainitic steels might have comparable or superior wear resistance to conventional pearlitic rail steels, Fig. 13.17. Even when the pearlitic and bainitic steels have similar wear characteristics, the lower carbon concentration of bainitic steels can be exploited from the point of view of ductility, toughness and weldability. Clayton *et al.* have also found empirically that alloying with chromium leads to improvements in wear, fatigue, ductility and toughness in bainitic rail steels.

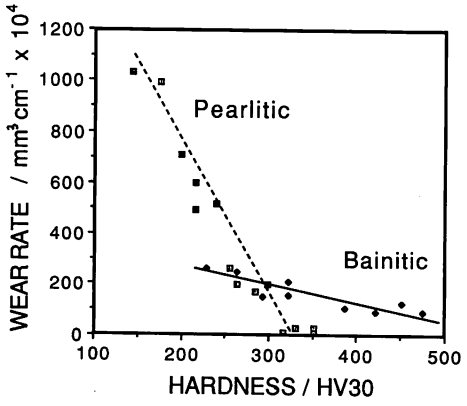

Fig. 13.17 *Pin-ring wear rate versus hardness data for pearlitic and bainitic steels (Clayton* et al., *1987).*

As pointed out by Clayton and co-workers (1987, 1990), most of the pessimistic results on bainitic steels could be challenged on the grounds that the studies did not involve a systematic investigation of the test conditions, and that the microstructural characterisations were not sufficiently detailed. On the other hand, it is also possible that the contradictory observations arise because of the different methods used for testing the wear resistance of rail steels. It could be argued that some of the tests (such as the pin-ring test) are not representative of service conditions, which involve rolling–sliding wear. Using tests designed to stimulate rolling–sliding wear, Garnham (1989) has demonstrated, using a variety of bainitic steels (carbon concentrations 0.04–0.52 wt%) that when the bainitic microstructure was free of carbides, the wear properties were worse relative to pearlite. Although carbide containing bainitic steel was found to show reasonable wear resistance, its use (and that of carbide free bainitic steels), increased the wear of the mating pearlitic railway wheel steel so that the combined wear rates were generally no better than for conventional pearlite–pearlite combinations. It may be concluded from Garnham's work that bainitic steel is not suitable for railway applications where rolling–sliding wear is the major cause of rail or wheel replacement. On the other hand, as discussed later, where thermal damage due to transient temperature excursions into the austenite phase field is the controlling factor, bainitic steels may have a clear advantage over fully pearlitic rail steels (Sawley *et al.*, 1988).

The latest work by Devanathan and Clayton (1990) dispels any doubts that the earlier favourable assessment of bainitic steels by Clayton *et al.* (1987), is an artifact of the test method used. They have confirmed using rolling–sliding tests (rather than the pin-ring method), the potential of bainitic steels for wear resistance, particularly at high contact pressures. Three steels with carbon concentrations ranging from 0.04 to 0.54 wt% (alloys 8, 9 and 12, Table 13.4) were examined in their bainitic condition, and it was found that the lowest carbon steel, which also had the lowest starting hardness, significantly outperformed pearlitic steels at the same hardness level. This was attributed to the ability of the bainitic steel to work harden to a greater degree (as evidenced by hardness changes after wear testing) and its greater ductility compared with pearlitic steels. The medium carbon steel was similar in its wear performance to pearlite, whereas the higher carbon steel was found to be significantly worse. Microstructural observations (Fig. 13.18) revealed that the high carbon steel was heavily segregated, leading to bands of high carbon martensite separated by bainite. Experiments indicated that failure was exacerbated by cracks initiating at the interfaces between the martensitic and bainitic regions (Fig. 13.18).

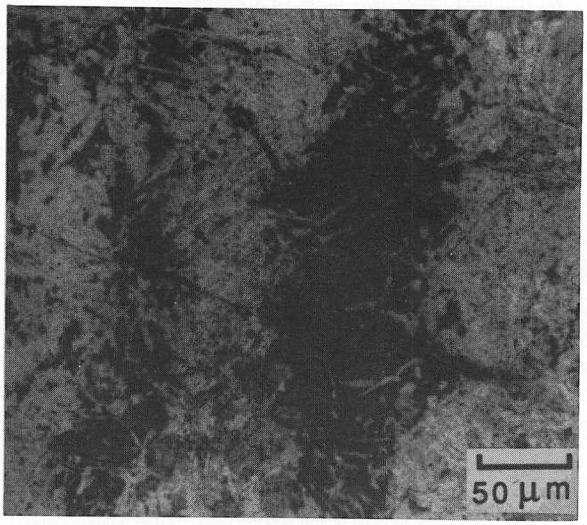

(a)

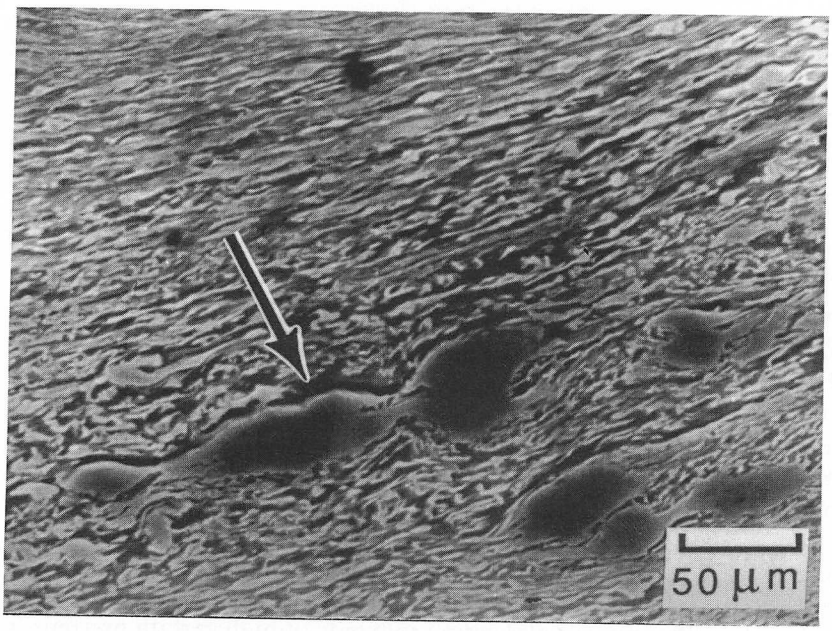

(b)

Fig. 13.18 *(a) Banding apparent in a high carbon bainitic rail steel (alloy 12, Table 13.4); (b) cracking at the interface between a pool of martensite and bainite (after Devanathan and Clayton, 1990).*

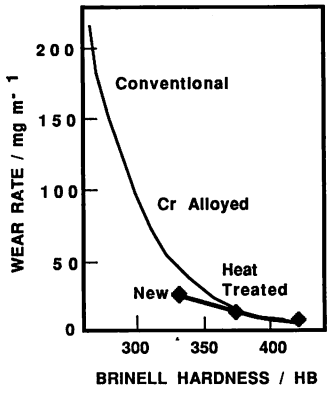

Fig. 13.19 *Comparison of the wear rates and hardness levels of conventional rail steels against the new alloys which have a carbide free microstructure of bainitic ferrite and austenite (Jerath* et al., *1991).*

13.8.2 Carbide free Bainitic Rail Steels

We have seen that rail steels are largely based on high carbon steels of near eutectoid composition and pearlitic microstructures. It is the carbide phase which is crucial in providing the necessary hardness. A novel approach towards the longer term development of wear resistant and much tougher rail steels has been based on medium carbon bainitic alloys without any carbides. Rail steels designed with the bainitic ferrite and austenite duplex microstructure have already demonstrated wear resistance significantly better than conventional alloys, including conventional heat-treated steels (Fig. 13.19). A typical composition for the new steel is Fe–0.5C–1.5Si–2.0Mn wt%, the chemistry being decided using thermodynamic and kinetic theory for bainitic transformations. The hardness in the duplex microstructural condition is about 400 HV. Some of the other measured properties also turn out to be better than currently available rail steels, but the details are at the moment commercially sensitive. Further development work, guided by fundamental research is now in progress to bring this concept to fruition.

13.8.3 Wheels

Bainitic railway wheels are currently under consideration. A particular problem with wheels is that the alloy must be resistant to microstructural change due to 'wheel spin burning'. This can lead to the formation of brittle martensite when material in the vicinity of the surface of a pearlitic steel is momentarily heated to a temperature high enough to cause the

formation of austenite. The same material is then cooled rapidly as the heat is dissipated into the underlying bulk of the wheel, causing the austenite to transform into brittle martensite. This effect can be of greater importance than the rolling sliding wear of the tread (Sawley *et al.*, 1988). Steels containing a lower carbon concentration and a bainitic microstructure have been found to outperform the conventional pearlitic steels in this respect, since their lower hardenability makes the formation of martensite more difficult, and when it does form, the martensite is also less brittle due to its lower carbon concentration and high martensite start temperature and the related autotempering effects.

13.8.4 Bearing Alloys

Although not specifically related to rail steels, roller bearings represent another wear related application in which bainitic microstructures might have an advantage over the traditional alloys which are used in the quenched and tempered condition (Akbasoglu and Edmonds, 1990). The studies to date have focused on altering the microstructure of available alloys, rather than considering the development of specific alloys which might be optimum for bainitic microstructures. The standard bearing alloy is the Fe–1C–1.5Cr wt% steel (alloy 13, Table 13.4), austenitised at 850°C for 20 min, oil quenched and then tempered at 175°C for 1 h. The tempering temperature can be increased to around 250°C in order to improve toughness, but at the expense of hardness. A lower bainitic microstructure can be produced by isothermal transformation below the B_S temperature (a typical heat treatment might consist of 250°C for 40 min).

For roller bearings, the main service parameter to monitor is rolling contact fatigue, a parameter which can be sensitive to the environment (i.e., oil, water etc.) in which the bearing operates. Maximum shear stresses arise under the outer surface of the bearing and can lead to severe spalling. When operating in water based lubricants, hydrogen evolving from electrochemical reactions can cause embrittlement and hence enhance the rate of fatigue crack growth. In these circumstances, bainitic microstructures fare better than the more hydrogen sensitive martensitic microstructures.

13.8.5 Summary

Although there are some contradictory results concerning the advantages of bainitic steels in railway applications, there is now significant evidence that bainitic steels can be developed with wear characteristics which are comparable or better than pearlitic rail steels (Fig. 13.20). They offer the additional advantages of better ductility, toughness and weldability. The

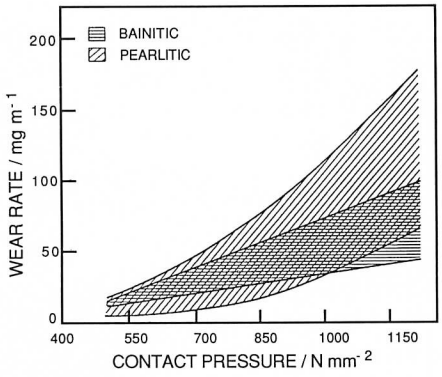

Fig. 13.20 *The latest data on the wear characteristics of bainitic rail steels compared with a range of pearlitic steels (Devanathan and Clayton, 1990).*

role of alloying elements in pearlitic steels is fairly well established; they act to alter the lamellar spacing, influence transformation kinetics and in general influence the overall hardness, which correlates directly with the wear resistance. Systematic work on the relationship between the microstructure and properties of bainitic rail steels is only just beginning to be instituted, so that it is possible that optimum conditions have yet to be established. The alloy chemistry must be such as to produce a reasonably uniform and fully bainitic microstructure during the continuous cooling heat treatment of samples of rail dimensions. Empirical observations indicate that chromium is an element which improves the wear properties, hardenability and hardness at the same time. The indications are that low carbon steels fare better than higher carbon steels, partly because the latter suffer from solidification induced segregation, but also because of an increased tendency to crack at the boundaries between martensite islands and the bainitic regions. It is also clear that within the domain of the bainitic microstructure, wear rate does not correlate with the hardness of the microstructure. Pearlitic rail steels are well established in industrial practice and it will take a large amount of research and development effort before the new bainitic rail and wheel steels can really take a significant share of the market. It is probable, however, that their major contributions will be for difficult situations, such as curved rails or rails which are heavily loaded.

13.9 Bainitic Cast Irons

Cast irons typically contain 2–4 wt% of carbon and frequently have high silicon concentrations and many other impurities when compared with steels. The 'carbon equivalent' (*CE*) of a cast iron is defined in order to

help distinguish those irons which tend to cool to a microstructure containing graphite (grey irons) and those in which the carbon mainly precipitates as cementite (white irons), as follows

$$CE = \text{C, wt\%} + (\text{Si, wt\%} + \text{P, wt\%})/3 \qquad (13.3)$$

A high cooling rate and a low carbon equivalent tends to favour the formation of white cast iron whereas a low cooling rate or a high carbon equivalent favours the formation of grey cast iron.

During solidification, a lot of the carbon precipitates in the form of graphite or cementite. When solidification is just complete, the precipitated phase is embedded in a matrix of austenite which has an equilibrium carbon concentration of about 2 wt%. On further cooling, the carbon concentration of the austenite decreases as more cementite or graphite precipitates from solid solution. For conventional cast irons, the austenite then decomposes into pearlite at the eutectoid temperature. However, in grey cast irons, if the cooling rate through the eutectoid temperature is sufficiently slow, then a completely ferritic matrix is obtained with the excess carbon being deposited on the already existing graphite.

There has recently been considerable interest in modifying the *matrix* of nodular graphite cast irons by heat treatment, to produce a bainitic microstructure, which under certain circumstances gives enhanced ductility and toughness (Dorazil *et al.*, 1962; Blackmore and Harding, 1984; Moore *et al.*, 1985a; Ueda and Takita, 1986; Shea and Ryntz, 1986; Franetovic *et al.*, 1987a,b; Rundman *et al.*, 1988), together with improved abrasion wear resistance (Shepperson and Allen, 1987; Lu and Zhang, 1989). These cast irons, called austempered ductile irons, have a typical composition Fe–4.0C–2.0Si–0.5Mn–0.06Mg wt%, with a carbon equivalent of about 4.5. The nodular iron is prepared by treating the melt with magnesium which alters the flake graphite morphology associated with untreated melts to that of nodular graphite. The solidified iron is then held at 930°C for 12 h followed by slow cooling, to give a structure consisting of graphite nodules in a ferritic matrix.

Subsequent heat treatment consists of austenitisation at around 950°C followed by isothermal transformation of the austenite at temperatures where bainite formation is expected. In the terminology of the cast iron industry, this isothermal transformation is called *austempering*. Because the cast irons have a high silicon concentration, any upper bainite that is formed consists, at the isothermal transformation temperature, of a mixture of bainitic ferrite and carbon enriched residual austenite. Some of the latter phase may decompose to untempered martensite on cooling to ambient temperature (Moore *et al.*, 1985a; Franetovic *et al.*, 1987a). Rundman *et al.* (1988), on the basis of an assumed section of the Fe–Si–C phase

diagram, suggested that the carbon concentration in the austenite after the formation of bainite should be given by the extrapolated Ae_3 phase boundary. This is inconsistent with the fact (Chapter 2) that substitutional solutes are not partitioned during the growth of bainitic ferrite. Furthermore, it is well established that the bainite reaction actually stops when x_γ reaches the T'_o boundary rather than the Ae_3 boundary (Chapters 5, 6). Because this limiting carbon concentration is much less than the equilibrium concentration, explanations based on the Ae_3 curve have had to incorrectly assume a retrograde shape to the $\alpha+\gamma/\gamma$ phase boundary with the extent of the $\alpha+\gamma$ phase field actually decreasing with a reduction in temperature.[3] Other evidence fits the idea that in cast irons, the bainite reaction stops at the T'_o curve of the phase diagram. The limiting carbon concentration does not depend on the starting carbon content of the austenite, which only affects the volume fraction of bainite that forms. Moore *et al.* (1985b) have demonstrated that the maximum carbon concentration reached by the austenite during isothermal transformation is essentially independent of its starting carbon concentration.

Prolonged heat treatment at the isothermal transformation temperature does eventually lead to the diffusional decomposition of the residual austenite into carbides and more ferrite. When the cast iron is isothermally transformed to lower bainite, carbides (such as η) are also found within the bainitic ferrite.

These results are essentially similar to those reported for wrought steels (Hehemann, 1970; Bhadeshia and Edmonds, 1979a; Sandvik, 1982a,b). There is however, an interesting effect of austenitising time, which is unique to cast irons. An increase in austenitising time leads to a greater dissolution of the graphite into the austenite, thereby increasing the austenite carbon concentration to a maximum level consistent with the (γ / γ + graphite) phase boundary (Moore *et al.*, 1987). Consequently, a cast iron isothermally transformed to bainite after holding at the austenitising temperature for a long period gives lower bainite (with η carbides within the bainitic ferrite) whereas the bainite obtained after a short austenitising treatment is upper bainite, free of carbides. This is consistent with the hypothesis that the carbon supersaturation of fresh bainitic ferrite is relieved by two competing processes, the precipitation of carbides within the ferrite, and the diffusion of carbon into the residual austenite.

3 In fact, the use of a vertical section of a ternary equilibrium phase diagram (Rundman *et al.*) to deduce the equilibrium compositions of the phases is incorrect, since the tie lines are not restricted to the plane of the diagram. Note also that for a substitutionally alloyed steel, the equilibrium composition of the austenite as given by the Ae_3 boundary, is not independent of the average carbon concentration of the alloy.

A higher carbon level in the austenite matrix prior to transformation would therefore lead to a transition from upper to lower bainite.

Cast irons need a long time (typically 2 h) at the austenitising temperature to reach equilibrium, when compared with steels (Rouns and Rundman, 1987). This is because the dissolution of graphite otherwise produces carbon concentration gradients in the matrix, leading to an inhomogeneous microstructure. For reasons which are not clear, the ferrite also seems to take longer to dissolve at the austenitising temperature.

Consistent with the lower carbon level expected in the austenite following a low temperature austenitising treatment, the rate of formation of bainite is found to increase with a decrease in the austenitising temperature (Moore *et al.*, 1985a,b). Of course, the austenite grain size also decreases with the austenitising temperature and may contribute to the acceleration of transformation, but the effect of carbon is expected to be the main factor responsible for the increased reaction rate.

A further effect of austenitising temperature that is peculiar to the cast irons is the mechanism by which phosphorous embrittles the austenite grain boundaries (Klug *et al.*, 1985). The phosphorous combines with magnesium to form particles (possibly Mg_3P_2) at the boundaries. The phase begins to redissolve at the grain boundaries if the austenitisation temperature is too high: for a Fe–3.74C–2.4Si–0.19Mn–0.15Mo–0.02P–0.045Mg wt% alloy, the redissolution becomes important at temperatures exceeding $\approx$ 1050°C. The dissolving particles act as a source for free phosphorous which then spreads along the austenite grain. There is then a drop in toughness as fracture occurs preferentially at the embrittled austenite grain boundaries.

As is the case for bainitic steels containing large concentrations of silicon (Chapter 12), austempered nodular graphite cast irons have the highest toughness in the absence of any carbide precipitation, and when the retained austenite is mechanically stable (Moore *et al.*, 1985a; Franetovic *et al.*, 1986). The time at austenitising temperature therefore is important because it determines the matrix austenite carbon concentration, and hence its stability with respect to both carbide precipitation and martensitic decomposition. As noted earlier, a prolonged austenitising treatment causes, for the same isothermal transformation conditions, a transition from the upper to lower bainite transformation (with its accompanying carbides).

The role of carbide precipitation in causing a deterioration in the ductility of bainitic cast irons is not as clear cut as in the wrought alloys. The austempered cast irons contain numerous large graphite particles which should be the main site for failure initiation. It seems unreasonable to suggest that the much smaller carbides associated with bainite can control failure initiation. It is probable that the reduction in austenite volume

fraction and stability caused by carbide precipitation causes the reduced ductility. Fractography could establish this hypothesis.

Common defects in cast irons, such as shrinkage, slag inclusions and films, segregation, and certain eutectic products can negate the benefits achieved by the presence of austenite in the austempered ductile iron (Moore *et al.*, 1987). For example, the brittle interdendritic carbides which form when the molybdenum concentration is greater than 0.5 wt%, make the iron brittle in spite of the austenite. The problems become more severe for larger castings where cooling rate variations might necessitate larger alloy concentrations at the risk of exaggerating segregation. Manganese and molybdenum segregate preferentially into the liquid phase to an extent which is greater than for example, Si, Ni, and Cu which partition preferentially into the solid phase (Hayrynen *et al.*, 1988).

It is a well known result for bainitic steels that the retained austenite occurs in two forms (Chapter 12). There are the films trapped between the platelets of bainitic ferrite, and the coarser blocky regions of austenite trapped between different bainite sheaves. The blocks tend to transform more easily to untempered high carbon martensite which causes embrittlement. Their volume fraction therefore needs to be minimised. Similar results have been obtained for the austempered ductile iron (Moore *et al.*, 1987, Rouns and Rundman, 1987).[4] The ductility decreases as the amount of blocky austenite increases. A smaller fraction of this austenite can be achieved by allowing a longer time t_1 at the austempering temperature assuming that the reaction has not saturated. The difficulty is to ensure that the time t_2, when the residual austenite begins to decompose to carbides is longer than t_1. For example, it has been demonstrated that beyond a certain manganese concentration, t_2 is always found to be smaller than t_1 (Moore *et al.*, 1986, 1987; Rouns and Rundman, 1987). This limiting manganese concentration is expected (and found) to depend on the austenitising temperature since that determines the carbon concentration in the austenite (Moore *et al.*, 1987). Hence, a higher austenitising temperature should lead to more of the blocky austenite. With lower

4 The terminology used to identify the blocky regions is confusing. The regions are designated *untransformed austenite volumes* (UAV), their volume fraction being measured using point counting on a light microscope. However, the films of austenite within the bainite sheaves are not included in this analysis, even though they are also untransformed. Hence, the volume fractions of austenite reported using X-ray diffraction analysis (which includes both films and blocks) are higher than the values reported for the UAV regions. A further difficulty is that the carbon concentration of the UAV regions is assumed to be unchanged by the formation of bainite (Moore *et al.*, 1986); this is incorrect and must lead to an overestimation of carbon in the remaining microstructure, since some of the microstructural parameters are derived using mass conservation conditions.

bainite, the volume fraction of blocky austenite is reduced because some of the carbon is then tied up as carbides in the bainitic ferrite (Moore *et al.*, 1987). However, the higher strength causes a reduction in toughness. Cast irons containing upper bainite generally have a tensile strength in the range 960–1150 MPa with a tensile elongation up to 13%, whereas the corresponding data for lower bainite are 1310–1495 MPa and 5% elongation (Moore *et al.*, 1987).

There are other special effects concerning the bainite transformation in cast irons. In wrought steels, bainite inevitably nucleates at the austenite grain boundaries. In cast irons, the nucleation of bainite is also found to occur at the austenite/graphite interfaces (Moore *et al.*, 1985a). The interface between graphite and iron is weak, and it may in fact be the case that nucleation occurs at the free surface, produced by detachment of the graphite from the matrix. The regions where the nodules of graphite form are in general poorer in alloy concentration, and this might explain their ability to preferentially stimulate the nucleation of bainite (Rouns and Rundman, 1987). Cast irons usually contain chemical segregation which is more pronounced than in steels. Solute concentrations tend to be highest in the interdendritic and intercellular regions, which are the last to solidify (Moore *et al.*, 1985a, b). The problem is made worse by the rather high mean alloy concentration of bainitic cast irons, necessitated by the need for the austenite to have sufficient hardenability to avoid the formation of pearlite, especially for applications where heavy section castings are required (Rundman *et al.*, 1988). The presence of pearlite leads to poor mechanical properties when compared, with bainite (Dorazil *et al.*, 1962; Shiokawa, 1985). The effect of chemical segregation is to give a non-uniform distribution of bainite. Solute rich regions which are unable to transform to bainite during austempering decompose into untempered, high carbon martensite on cooling to ambient temperature and cause a marked decrease in ductility (Moore *et al.*, 1985a; Rundman *et al.*, 1988).

A more uniform distribution of bainite can be obtained in spite of the chemical segregation, by holding for a longer time at the isothermal transformation temperature. The regions rich in austenite stabilising elements then have an opportunity to transform. A difficulty with this approach is that carbides might form in the regions which transform first to bainite (Moore *et al.*, 1985a,b). Another procedure involves ausforming prior to austempering, the rate of transformation to bainite being higher everywhere, in mildly deformed austenite (Moore, 1985a). Ausforming is a specialised treatment involving austenite deformation before transformation and does not seem very practicable for cast irons.

There is an effect of segregation which cannot be eliminated by any of the treatments discussed above. The good properties of austempered ductile irons are because of the stable austenite. A short austempering

time leads to less carbon enrichment in the residual austenite, which consequently suffers from mechanical instability. Longer times, on the other hand, induce carbide precipitation. There is therefore an optimum austempering time which depends on alloy chemistry. Segregation causes this optimum time period to be different in different regions of the sample, making it impossible to obtain stable austenite throughout the sample (Rundman *et al.*, 1988).

We have shown that the physical metallurgy of austempered cast irons may be deduced by analogy with the knowledge available of bainite in silicon rich steels. There is, however, one contradiction which is probably not well founded. Franetovic *et al.*, (1987a) have claimed that the orientation relationship between the bainitic ferrite and austenite in cast irons is the Bain relationship (i.e., $[1\,1\,0]_\gamma \| [0\,1\,0]_\alpha$, $[0\,0\,1]_\gamma \| [0\,0\,1]_\alpha$]). This is unlikely to be correct because the transformation would then cause an intolerable amount of strain. The reported orientation relation is not completely consistent with the published diffraction data; further work is urgently needed.

13.9.1 Wear of Bainitic Cast Irons

Many cast irons are used in situations where resistance to abrasive wear is an important requirement. The mechanical properties (high strength and ductility) of austempered cast irons, together with their cheapness, make them potential candidates for applications involving abrasive wear. Many investigations have now indicated that the austempered ductile cast irons have better abrasive wear resistance when compared with normalised cast irons of the same chemical composition (Lu and Zhang, 1989) or abrasion resistant steels, including the Hadfield manganese steel, of equivalent hardness (Shepperson and Allen, 1987). It appears that the improved wear resistance is at least partly a consequence of the stress induced transformation of austenite into very hard, high carbon martensite, together with the inherent ductility of the microstructure (Shepperson and Allen, 1987). The high work hardening rate usually associated with the transformation induced plasticity may also make a contribution.

13.10 High Strength Steel Welds

The vast majority of weld filler metals have yield strength values which do not exceed 650 MPa. Part of the reason for this is the lack of a suitable microstructure which can resist hydrogen induced cracking, and one which is capable of providing good mechanical properties in multirun welds. This section deals with a novel idea for steel weld deposits, a concept which relies on the ability to generate a microstructure which is

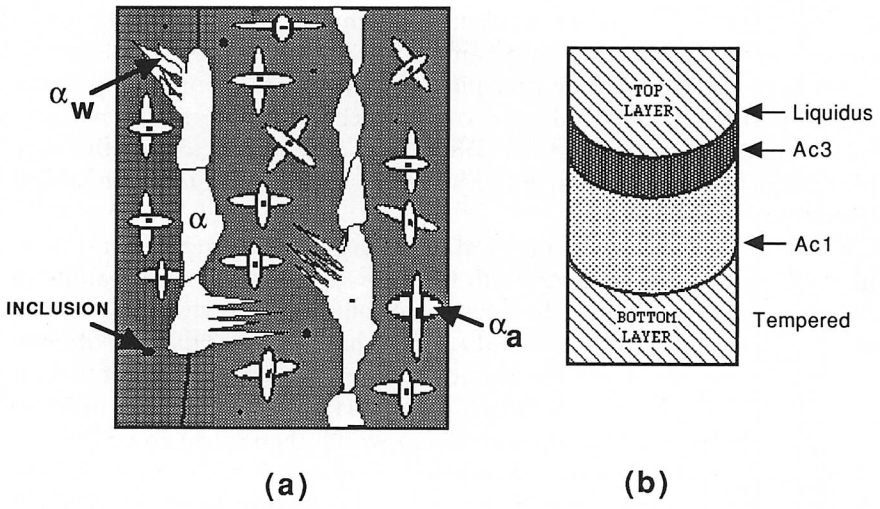

Fig. 13.21 *(a) Schematic illustration of the primary microstructure of a steel weld deposit. Allotriomorphic and Widmanstätten ferrite are seen to grow from the columnar austenite grain boundaries, whereas the acicular ferrite has nucleated intragranularly on non-metallic particles in the weld. (b) Heat affected zone of a weld bead.*

strong and tough, and at the same time insensitive to the austenite grain structure. As will be seen later, intragranularly nucleated bainite (better known as acicular ferrite), meets these specifications and has a tremendous potential for a new generation of very high strength (yield strength > 750 MPa) multirun weld deposits.

The microstructure which evolves when a weld pool solidifies and then cools to ambient temperature is often termed the *as-deposited* or *primary microstructure* of the weld. It may consist typically of a mixture of one or more of the phases allotriomorphic ferrite, Widmanstätten ferrite, acicular ferrite, martensite, retained austenite or degenerate pearlite, contained within the columnar prior austenite grains typical of the solidification structure of low-alloy steel welds (Fig. 13.21).

In multirun welds, the gap between the components to be joined is filled using a sequence of weld passes, each of which fills only a part of the weld gap. The metal deposited is therefore influenced significantly by the additional thermal cycles induced by the deposition of each successive layer. Only the last layer to be deposited can then be expected to exhibit the primary microstructure. The remaining regions of the welds may have undergone transient temperature rises high enough to cause partial or complete transformation into austenite, which on subsequent cooling transforms to a different (less desirable) ferrite microstructure. Those regions which do not revert to austenite are tempered (Fig. 13.21b).

It follows that the microstructure of a multirun weld is expected to be inhomogeneous, with corresponding variations in the mechanical properties. These latter variations are most obviously seen in the hardness profiles of multirun welds.

There is growing evidence that mechanical and microstructural inhomogeneity of the type described above causes *scatter* in mechanical properties (Sugden and Bhadeshia, 1989). For toughness, the lower bound within the scatter has to be accepted for design, leading to a less than optimum exploitation of material properties. The problem can be circumvented in single run welds but the high heat input required leads to poorer quality. Another possibility is to anneal the final weld to such an extent that the differences in strength between the variety of microstructures is reduced. Unfortunately, this has the disadvantage that the general level of strength will drop, perhaps to a level where only solid solution strengthening and the intrinsic strength of pure iron are the main contributors to strength, with the microstructural component more or less wiped out by the tempering. 'Weld refinement' techniques rely on *in situ* tempering during fabrication, using the heat input as each layer is deposited, and can also lead to mechanical homogeneity but at the expense of mean strength. A novel method is described here, designed to produce homogeneous multirun welds of high strength and toughness. Alloys have been manufactured which give an unusual primary microstructure of acicular ferrite and low carbon ductile martensite, a microstructure which

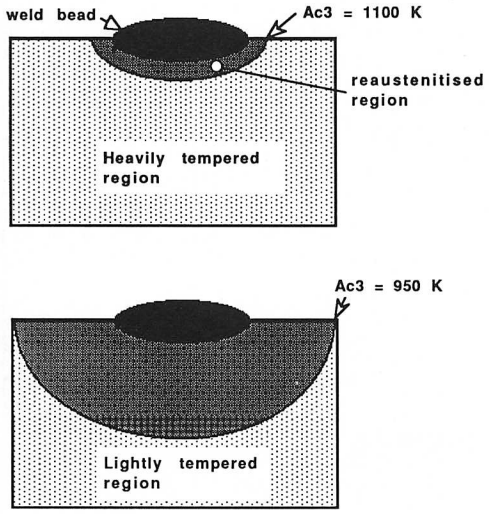

Fig. 13.22 *Schematic illustration of how a lower Ac3 temperature can lead to a greater degree of reaustenitisation in the underlying material, and a smaller region of tempered material.*

persists throughout a multirun weld. This uniformity of microstructure is achieved by simultaneously satisfying four conditions:

1. The Ae_3 temperature of the weld metal is reduced, so that the effect of depositing any new layer is to reaustenitise a large amount of the adjacent substrate, Fig. 13.22 (Bhadeshia and Svensson, 1989c; Reed and Bhadeshia, 1989).

2. The hardenability is adjusted to permit the reaustenitised regions to transform back on cooling, to a microstructure consisting of the required mixture of acicular ferrite and ductile martensite. Acicular ferrite is ideal in this respect, given that the austenite grain size will vary in the heat affected regions of the weld. Since it nucleates intragranularly, it is not sensitive to the austenite grain structure, especially because the alloy has sufficient hardenability to ensure the absence of any grain surface nucleated transformation products (other than a small amount of bainite).

3. A low Ae_3 also ensures that reheated regions which are not reaustenitised, are not excessively tempered (to avoid a loss of strength). The alloy concerned must be designed to be resistant to tempering, primarily by keeping the carbon concentration to a minimum.

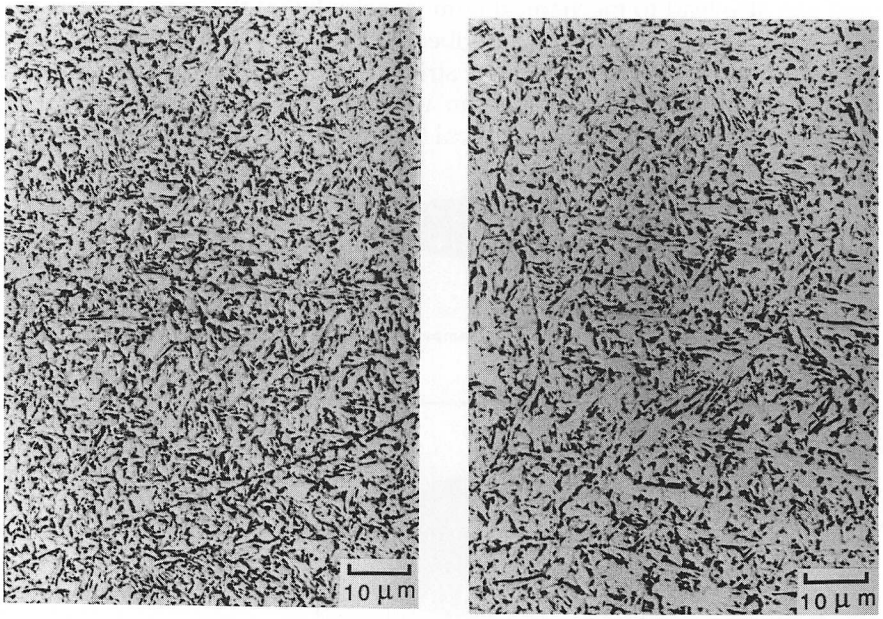

(a) (b)

Fig. 13.23 *Microstructures from the as-deposited weld metal (a) and the heat affected weld metal (b), showing the uniformity of microstructure. The latter contains equiaxed austenite grains whereas the former has columnar austenite grains typical of the solidification microstructure. (After Rees, 1991.)*

4. The strength of acicular ferrite on its own is in fact limited; excluding solid solution strengthening, its microstructure contributes about 400 MPa at most, to the overall yield strength of a 100% acicular ferrite alloy (Sugden and Bhadeshia, 1988). To achieve additional strengthening, some of the acicular ferrite has to be replaced by martensite. A low average carbon concentration is essential to ensure that the martensite remains ductile in all circumstances. Unusually therefore, the fraction of acicular ferrite must be kept small (about 0.5) to prevent the carbon that partitions from the austenite from excessively enriching the residual austenite, which could then transform to brittle martensite.

While successful experimental welding alloys have indeed been designed on these lines (Fig. 13.23), many of the interactions discussed above have not as yet been characterised or established theoretically, so that there is a need for considerable further research to capitalise on the potential of these alloys.

14 *Miscellaneous Aspects of Bainite*

14.1 Bainite in Iron and its Substitutional Alloys

It is sometimes stated that bainite can be distinguished in high purity iron or iron alloys which have an interstitial content less than 0.01 wt%. Experiments using these alloys are difficult because transformation kinetics can be very rapid. The classification of microstructure therefore has to be based on rather limited evidence. The work is nevertheless of interest from a fundamental point of view. For example, it is not clear whether there is, in principle or in practice, any essential difference between martensite and bainite in interstitial free alloys.

Most of the experiments are conducted by monitoring the temperature during rapid cooling. The evolution of latent heat of transformation can cause inflexions in the cooling curves, which give indications of transformation. Continuous cooling experiments on a Fe–14.43Ni wt% alloy which was thought to have a carbon concentration of 0.01 wt% revealed two plateaux in a plot of the thermal arrest temperature versus cooling rate (Wilson *et al.*, 1982). The plateau at the higher temperature was identified with bainitic transformation, the other with the formation of martensite. Microstructural evidence was cited in support of this conclusion: somewhat wider laths were observed due to transformation at the higher temperature, and the boundaries between those laths were wavy. This interpretation is unsatisfactory given that lath widths in any case increase with transformation temperature (Chapter 2). The wavy interfaces were not with austenite, but between ferrite laths. The significance of the wavy character is not known; it is a common feature of martensitic microstructures that the interface with austenite is irregular on a microscopic scale (*see* for example, Maki *et al.*, 1975).

The work to date fails to provide any convincing differentiation between martensite and bainite in interstitial free alloys. This may be

because there is no difference, but fresh ideas and partial transformation experiments are needed to really establish the point.

14.2 The Weldability of Bainitic Steels

The region which is adjacent to the fusion zone of a weld is influenced by heat diffusion from the fusion zone. It is therefore called the *heat affected zone* (HAZ). Its boundaries do not need to be very precisely defined because the definition depends on purpose. The heat dissipated into the HAZ can be detected as the temperature at any point rises to a peak value below the solidus temperature and then drops gently towards the initial temperature of the sample. The severity of the heating or cooling cycles, and the peak temperature, depends on the location within the HAZ (*see* for example, Easterling, 1983; Lancaster, 1986). For steels with a high hardenability, regions of the HAZ which have been austenitised by the heat pulse may during cooling, transform to untempered martensite or to some other hard microstructure. These hard regions are susceptible to cold cracking due to hydrogen embrittlement and other impurity effects.

This is the main reason why hardenable steels are difficult or impossible to weld (Fig. 14.1). The cooling rate can be reduced during welding, do avoid the formation of martensite in the HAZ. This can be done by *preheating* the sample prior to welding. But preheating can lead to severe cost penalties. It has been estimated, for example, that the cost of fabricating an aircraft carrier could be reduced by about £3 million if the number of panels requiring preheat can be reduced by 50% (Cullison, 1991).

On the basis of vast empirical experience, it has been possible to correlate the cold cracking susceptibility with a carbon equivalent (*CE*), which in effect accounts for the influence of alloying additions on hardenability. There are two popular formulae. The first one is a slightly modified

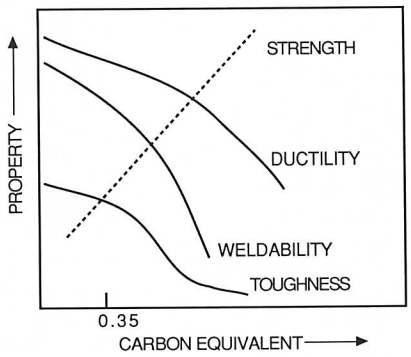

Fig. 14.1 *Variation in mechanical properties of the heat-affected zone as a function of the carbon equivalent.*

version of the equation originally proposed by Dearden and O'Neill, and adopted by the International Institute for Welding. It is usually applied to steels containing less than 0.2 wt% of carbon

$$CE = C + [(SI + Mn)/6) + [(Cu + Ni)/15] + [(Cr + Mo + V)/5] \quad (14.1)$$

where all the concentrations are in wt%, and represent the base metal composition. The other equation, due to Ito and Besseyo is more recent and has been adopted by the Japanese Welding Engineering Society

$$CE = C + (Si/30) + [(Mn + Cu + Cr)]/20 + (Ni/60) + (Mo/15) + (V/10) + 5B \quad (14.2)$$

It is generally accepted that if the carbon equivalent is between 0.35 and 0.55 wt%, then the sample must be preheated prior to welding (the preheat temperature can be as high as 400°C), and when $CE > 0.55$, both preheating and postheating is considered essential to avoid cold cracking and other difficulties.[1] It is however notable that the two equations give very different values of *CE*, the Ito and Besseyo method taking a more conservative account of substitutional alloying additions. In fact, that equation is considered most suitable for low carbon, low alloy steels, and is widely used to assess the weldability of the new ultra low carbon bainitic steels (C ≈ 0.01→0.03wt%, e.g. Nakasugi *et al.*, 1980, Lorenz and Duren, 1983). For these steels, the IIW *CE* is known to give a pessimistic assessment of weldability (an overestimation of hardenability) whereas the Ito and Besseyo equation works well. It has also been demonstrated (Lorenz and Duren, 1983) that for low carbon pipeline steels, the IIW *CE* overestimates the effects of alloying elements like manganese and molybdenum, a more realistic *CE* being given by

$$CE = C + (Si/125) + [(Mn + Cu)/16] + (Cr/20) + (Ni/60) + (Mo/40) + (V/15) \quad (14.3)$$

for weld cooling times of 2–3 seconds over the temperature range 800–500°C (these conditions are typical for girth welds in pipelines).

There are good reasons for supposing that the same *CE* should not apply to medium carbon and very low carbon steels. There is a disproportionate increase in the growth rates of both allotriomorphic and Widmanstätten ferrite as the carbon concentration drops below ≈ 0.06 wt%, when compared with variations in carbon above this value (Bhadeshia *et al.*, 1985; Bhadeshia, 1990). This is because the average carbon concentration of the

1 Note that the carbon equivalent takes no account of the thermal treatment experienced by the steel in the HAZ. Clearly, its use must be restricted to welding conditions used in the original experimental work on which the *CE* formulae are based.

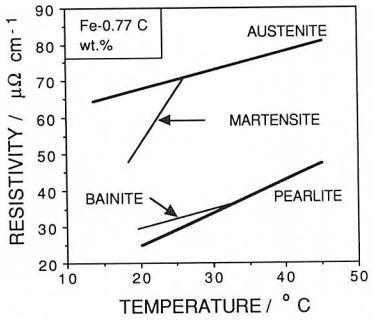

Fig. 14.2 *Electrical resistivity of a variety of microstructures in steels (Radcliffe* et al., *1959).*

alloy approaches the equilibrium solubility of carbon in ferrite. The need to partition carbon into the austenite is thus reduced so that the diffusion controlled velocity rises sharply.

14.3 Electrical Resistance

Bainite can be expected to have a lower electrical resistivity than martensite because in its final state it has less carbon in solid solution and indeed, a lower defect density. On the other hand, its defect density is certainly larger than that of pearlite or allotriomorphic ferrite (Chapter 2). These observations are consistent with the fact that the electrical resistivity of a specimen fully reacted to bainite is always found to be higher than that of pearlite at the same temperature (Radcliffe and Rollason, 1959). In fact, the resistivity decreases in the order austenite, martensite, bainite and pearlite for a given temperature, and for a constant microstructure, decreases with temperature (Fig. 14.2).

14.4 Internal Friction

A material is said to be elastic when it exhibits a stress strain curve which is fully reversible. The removal of stress also removes the strain. The energy stored in the material when it was under stress is fully recovered. If such a material is induced to vibrate, then in a vacuum it can ideally continue vibrating for an indefinite period of time.

Similar vibrations would decay naturally in an *anelastic* solid, since energy is dissipated by some process occurring within the sample during each vibration. The vibrations are said to be damped. An examination of the damping process as a function of temperature and frequency can reveal information about the nature of the dissipative process. 'Internal friction'

measurements like these can be used to detect the onset of transformations, since moving interfaces also lead to the damping of oscillations.

Internal friction measurements conducted during the continuous cooling transformation of a commercial steel to bainite have been interpreted to indicate a *prebainitic* microstructural change before the formation of bainite proper (Jihua *et al.*, 1989). The argument is based on an observed rise in damping during continuous cooling, at temperatures above B_S. These experiments are not backed by any microstructural evidence; nor is there any proof that the damping has anything to do with bainite.

The same experiments have demonstrated that the degree of damping decreases monotonically as the transformation progresses, indicating that the concentration of dissipative units (whatever they may be) varies directly with the extent of reaction. The damping at any instant of time, increases as the temperature is reduced below B_S. This is also expected because the total amount of bainite that can form increases with undercooling below B_S.

14.5 Internal Stress

It has long been recognised that the transformation of austenite to martensite causes the development of residual stresses in the transformed specimen. The stresses are usually attributed to the volume expansion accompanying transformation (Buhler *et al.*, 1932; Buhler and Scheil, 1933; Scheil, 1955; Buhler, 1955; Hildenwall, 1979).

The volume expansion is not unique to martensite; the formation of other products such as allotriomorphic ferrite, pearlite, Widmanstätten ferrite, and bainite is also accompanied by a reduction in density. There are no data for Widmanstätten ferrite, but the formation of bainite certainly gives rise to residual stresses (Radcliffe and Rollason, 1959; Diesburg *et al.*, 1981). As a general rule, X-ray diffraction peaks from transformations which are displacive (martensite, bainite, Widmanstätten ferrite) are found to be more diffuse than those from reconstructive reactions (allotriomorphic ferrite, pearlite). For example, Radcliffe and Rollason demonstrated a larger lattice strain with martensite and bainite than with pearlite. These results can be understood if it is accepted that diffusion during reconstructive transformation can help accommodate the volume change without causing stress.

Because ferrite has a smaller expansion coefficient than austenite, the volume change becomes smaller as the transformation temperature rises. Elements in solid solution have different effects on the lattice parameters of austenite and ferrite, and therefore alter the volume change of transformation.

The residual stresses develop primarily because transformation does not usually occur uniformly in all regions of the sample. This can be exploited for case hardened components, where it is advantageous to have a compressive stress on the surface of the component. The compressive stress prolongs the fatigue life and makes the component more resistant to surface initiated fracture. In steels which are surface carburised and then quenched, the lower carbon core transforms to martensite at a higher temperature. The accompanying core volume expansion puts the still austenitic surface regions into tension, the tensile stress to some extent being relieved plastically. When the surface region eventually transforms to martensite on further cooling, its volume expansion causes stress reversal, so that the surface ends up in compression relative to the core (Koistinen, 1958).

Because of the smaller volume expansion that accompanies the transformation to bainite, and because plastic relaxation of stresses is easier at relatively high temperatures, a bainitic case is not as effective as a martensitic case (Diesburg *et al.*, 1981). Samples containing bainite within the case are found to have lower levels of compressive residual surface stresses. Thus, the performance of case hardened samples can be enhanced by the addition of alloying elements, such as molybdenum, which enhance martensite hardenability at the expense of bainite.

Similar results have been reported by Jones and Alberry (1978), who measured the stress that develops during the cooling of a constrained sample from the austenite phase field (Fig. 8.12). The stress was observed to fall to zero during the austenite to bainite transformation, whereas a compressive stress developed during martensitic transformation. These results can at least partly be explained because the volume change during martensitic transformation is larger than during bainitic transformation (Goldak *et al.*, 1985).[2]

14.6 Bainite in Iron–Nitrogen Alloys

Both nitrogen and carbon exist in interstitial sites in iron and their respective binary phase diagrams with iron both exhibit a eutectoid reaction in which austenite decomposes into a mixture of ferrite and carbide or ferrite and nitride (Fe_4N). It is therefore reasonable to expect similar sorts of phase transformations to occur in both systems. It is well established that martensite can form in both systems, but the first report of the existence of a bainitic transformation in an Fe–N alloy was by Bell and Farnell (1969).

2 If the highest carbon regions of the surface do not transform sufficiently to martensite, then the region of maximum compressive stress is expected to be located somewhere below the component surface.

A Fe–1.8N wt% alloy when transformed isothermally at 350°C was observed using light microscopy to exhibit mixtures of ferrite and Fe_4N whose appearance was similar to that of upper bainite in Fe–C alloys. Furthermore, the transformation products were stifled in their growth by the presence of austenite twin boundaries, implying that the growth process involves a coordinated movement of atoms.

Whilst there is a strong possibility for the existence of a bainite reaction in Fe–N alloys, there is a need for greater microstructural characterisation, thermodynamic analysis and detailed crystallographic experiments including the study of surface relief.

15 *The Transformations in Steel*

Probably the most interesting revelations are made when all of the decomposition reactions of austenite are examined together. And the most awkward question seeks to discover the difference between the variety of transformation products. This chapter is indended to be a brief review of these transformations on the basis of the work presented in the earlier part of the book. Various dificulties of interpretation have already been highlighted so it is not intended to dwell on the problems, but rather to provide a clear view which is consistent with the available experimental and theoretical data (Fig. 15.1).

There is ample evidence that the different forms of ferrite can be categorised into those which are displacive, and the others which involve a reconstructive transformation mechanism. Amongst the displacive transformations are Widmanstätten ferrite, bainite (including acicular ferrite) and martensite, all of them uniquely characterised by their plate or lath shapes and the invariant plane strain surface relief (which has a large shear component). Substitutional solutes are not partitioned, although this may not be an exclusive characteristic of displacive transformations.

Widmanstätten ferrite grows at high temperatures by a paraequilibrium mechanism in which the plates lengthen at a rate controlled by the diffusion of carbon in austenite. This diffusion does not contradict its displacive character because interstitials can move about without affecting the shape change, the substitutional lattice still being displaced into its new structure. The transformation occurs at small driving forces, so that the shape change consists of two adjacent invariant plane strains which tend to mutually accommodate and hence reduce the strain energy.

The nucleation of both Widmanstätten ferrite and bainite occurs with the diffusion of carbon, and probably involves the displacive growth of preexisting embryos. This follows from the observation that the activation energy for nucleation is directly proportional to the driving force, rather

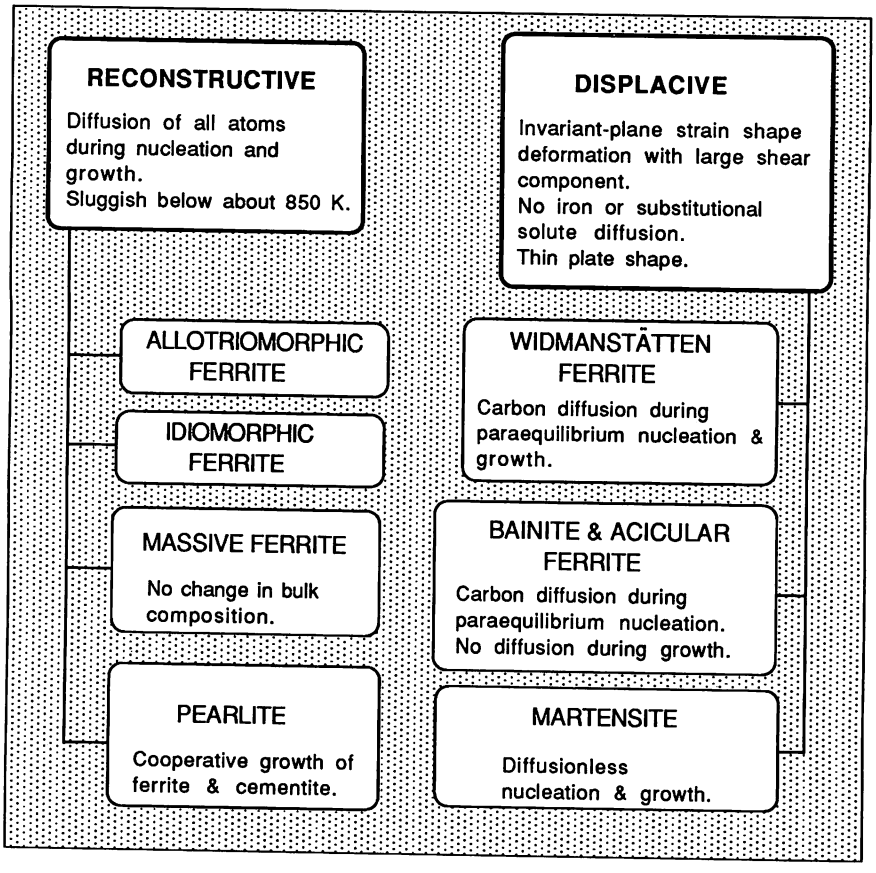

Fig. 15.1 *Flowchart summarising the characteristics of transformations in steels.*

than the inverse square relationship implied by the classical heterophase fluctuation model of nucleation. It appears that the nucleus for both transformations is identical, but it develops into bainite if diffusionless growth is possible at the temperature where substantial nucleation becomes possible. The nucleus otherwise evolves into Widmanstätten ferrite.

Bainite probably grows without any diffusion, although at the temperatures involved, any excess carbon in the ferrite is, soon after transformation, rejected into the residual austenite where it may precipitate carbides, giving the classical upper bainitic microstructure. At somewhat lower transformation temperatures, some of the excess carbon has the opportunity to precipitate inside the bainitic ferrite as the partitioning of carbon into austenite becomes slower. This leads to the lower bainitic microstructure.

Bainite forms at temperatures where the austenite is relatively weak and unable to elastically support large deformations. Platelets (sub-units) of bainite grow to a limiting size which is smaller than the austenite grain size. This is because the debris created as the shape change is plastically accommodated, stifles the interface. Further transformation requires the nucleation of new sub-units, and the chances of this happening are largest at the tips of existing sub-units. This gives rise to the sheaves of bainite, which are clusters of parallel sub-units with identical crystallographic orientation, habit plane and size. Acicular ferrite is an alternative, more chaotic morphology of bainite in which the plates are intragranularly nucleated on nonmetallic inclusions and hence grow in many different directions from the nucleation site.

The possibility remains that the transition from Widmanstätten ferrite to bainite involves a gradual increase in carbon supersaturation, rather than a sudden change from paraequilibrium to diffusionless growth respectively.

Martensitic transformation is diffusionless, both during nucleation and during growth.

The reconstructive transformations include allotriomorphic and idiomorphic ferrite, and pearlite in its various forms. It is important to appreciate that all elements, including iron, must diffuse during reconstructive transformation in order to achieve the structural change without the strain energy characteristic of displacive reactions. It goes without saying that an IPS shape deformation is not found with any of these transformation products. In spite of the need for diffusion, it is in principle possible to achieve paraequilibrium, and indeed, negligible partitioning local equilibrium; there need not therefore be any bulk partitioning of substitutional solutes during reconstructive transformation. A prominent feature of the eutectoid decomposition reaction which leads to the formation of pearlite is that the ferrite and carbide phases grow with a common transformation front with the austenite. They are said to grow cooperatively.

15.1 Notes

Nucleation and growth reactions are of first order in the Ehrenfest classification; in all such reactions, the parent and product phases can coexist, and are separated by well-defined interfaces. Martensitic transformations, because they can be very rapid in steels, are sometimes incorrectly stated not to involve a nucleation and growth process.

It is significant that all the ferrite crystals which grow in the form of plates have an invariant plane shape change with an appreciable shear component accompanying transformation. Pearlitic ferrite does not have a plate morphology, since within an apparently lamellar colony, the ferrite regions are all interconnected in space.

Key Characteristics of Transformations in Steels

The table below indicates the key characteristics of phase transformations in steels; it may be regarded as a working hypothesis which seems most consistent with the available experimental data. The nomenclature used for the transformation products is as follows: martensite (α'), lower bainite (α_{lb}), upper bainite (α_{ub}), acicular ferrite (α_a), Widmanstätten ferrite (α_w), allotriomorphic ferrite (α), idiomorphic ferrite (α_i), pearlite (P), substitutional alloying elements (X). Consistency of a comment with the transformation concerned is indicated by (=), inconsistency by ($\neq$); cases where the comment is only sometimes consistent with the transformation are indicated by ($\otimes$). The term *parent* γ implies the γ grain in which the product phase grows. Note that it is not justified to distinguish massive ferrite from α.

Table

Comment	α'	α_{lb}	α_{ub}	α_a	α_w	α	α_i	P
Nucleation and growth reaction	=	=	=	=	=	=	=	=
Plate morphology	=	=	=	=	=	≠	≠	≠
IPS shape change with shear component	=	=	=	=	=	≠	≠	≠
Diffusionless nucleation	=	≠	≠	≠	≠	≠	≠	≠
Only carbon diffuses during nucleation	≠	=	=	=	=	≠	≠	≠
Reconstructive diffusion during nucleation	≠	≠	≠	≠	≠	=	=	=
Often nucleates intragranularly on defects	=	≠	≠	=	≠	≠	=	≠
Diffusionless growth	=	=	=	=	≠	≠	≠	≠
Reconstructive diffusion during growth	≠	≠	≠	≠	≠	=	=	=
Atomic correspondence (all atoms) during growth	=	=	=	=	≠	≠	≠	≠
Atomic correspondence, during growth, for atoms in substitutional sites	=	=	=	=	=	≠	≠	≠
Bulk redistribution of X atoms during growth	≠	≠	≠	≠	≠	⊗	⊗	⊗
Local equilibrium at interface during growth	≠	≠	≠	≠	≠	⊗	⊗	⊗
Local paraequilibrium at interface during growth	≠	≠	≠	≠	=	⊗	⊗	≠
Diffusion of carbon during transformation	≠	≠	≠	≠	=	=	=	=
Carbon diffusion controlled growth	≠	≠	≠	≠	=	⊗	⊗	⊗
Cooperative growth of ferrite and cementite	≠	≠	≠	≠	≠	≠	≠	=
High dislocation density	=	=	=	=	⊗	≠	≠	≠
Incomplete reaction phenomenon	≠	=	=	=	≠	≠	≠	≠
Necessarily has a glissile interface	=	=	=	=	=	≠	≠	≠
Always has an orientation within the Bain region	=	=	=	=	=	≠	≠	≠
Grows across austenite grain boundaries	≠	≠	≠	≠	≠	=	=	=
High interface mobility at low temperatures	=	=	=	=	=	≠	≠	≠
Displacive transformation mechanism	=	=	=	=	=	≠	≠	≠
Reconstructive transformation mechanism	≠	≠	≠	≠	≠	=	=	=

Reconstructive diffusion is the flow of matter necessary during diffusional transformation, in order to ensure the absence of the sort of shape deformations which accompany the formation of martensite. A diffusional transformation may be regarded as a combination of a lattice change and a recrystallisation of the product phase, reconstructive diffusion being the flow necessary for the recrystallisation process.

In diffusionless transformations, it is possible to specify (in a localised region at least) how particular vectors, planes and unit cells of one structure (defined by an imaginary labelling of the individual atoms) are derived from *corresponding* vectors, planes and unit cells of the other structure. This is termed a lattice correspondence and it defines a pure lattice deformation which carries the original lattice points, or some fraction of these points into points of the new lattice. When interstitial atoms are present, they may move over large distances during transformation without affecting the lattice correspondence; this is sometimes loosely expressed by stating that there is an atomic correspondence for the solvent and substitutional solute atoms but not for the interstitial atoms. A further relaxation of the condition is to allow the solvent and substitutional solute atoms to be displaced during transformation among the sites specified by the lattice correspondence, but not to create new sites or to destroy any specified sites; in this way the lattice correspondence is preserved but there is no longer an atomic correspondence. Note that in the classification presented above, the single atomic jumps of interstitial atoms needed to destroy Zener ordering (which is produced automatically by the Bain correspondence) are not taken into account.

Even though two crystals may have an identical *bulk* composition, it may not be concluded that their compositions at the transformation interface are identical. There are modes of transformation (e.g., negligible partitioning local equilibrium) where the bulk compositions are predicted to be identical, but in the vicinity of the transformation interface the two phases differ in composition.

For plain carbon steels, there is no difference between equilibrium and paraequilibrium.

The incomplete reaction phenomenon implies that when a reaction can be studied in isolation, it stops before the phases reach their equilibrium or paraequilibrium compositions when stored energy terms have been accounted for.

An orientation within the Bain region means a reproducible relation which may be irrational but is close to the rational NW or KS relations.

Massive ferrite is not classified as a separate morphology since it can be included within allotriomorphic or idiomorphic ferrite.

16 *References*

Aaronson, H.I., *The Decomposition of Austenite by Diffusional Processes*, (ed. V.F. Zackay and H.I. Aaronson), Interscience Publishers, New York, 1962, 387–546.

Aaronson, H.I., Domian, H.A. and Pound, G.M., Trans. Met. Soc. AIME **236**, 1966a, 753–767.

Aaronson, H.I., Domian, H.A. and Pound, G.M., Trans. Met. Soc. AIME **236**, 1966b, 768–780.

Aaronson, H.I., Domian, H.A., Trans. Met. Soc. AIME **236**, 1966, 781–796.

Aaronson, H.I., *The Mechanism of Phase Transformations in Crystalline Solids*, The Institute of Metals, London, 1969, 270–281.

Aaronson, H.I. and Wells, C., Trans. AIME **206**, 1956, 1216–1223.

Aaronson, H.I., Laird, C. and Kinsman, K.R., *Phase Transformations*, ASM, Metals Park, Ohio, 1970, 313–396.

Aaronson, H.I., Hall, M.G., Barnett, D.M. and Kinsman, K.R., *Scripta Metall.* **9**, 1975, 705.

Aaronson, H.I., Plichta, H.R., Franti, G.W. and Russell, K.C., *Metall. Trans.* **9A**, 1978, 363.

Aaronson, H.I., Enomoto, M. and Reynolds, W.T., *Advances in Phase Transitions*, (ed. J.D. Embury and G.R. Purdy), Pergamon Press, Oxford, 1988, 20–36.

Abe, F., Araki, H. and Noda, T., *Mater. Sci and Technol.* **6**, 1990, 714–723.

Abson, D.J., Welding Institute Research Report 7931.01/86/544.3, The Welding Institute Abington, Cambridge, 1986, pp. 1–30.

Abson, D.J., *Nonmetallic inclusions in ferritic steel weld metals — a review*, International Institute for Welding, Document IX–1486–87, 1987.

Abson, D.J. and Pargeter, R.J., *Int. Met. Rev.* **31**, 1986, 141–194.

Adcock, J.N., *J. Iron Steel Inst.* **200**, 1962, 909–913.

Afrouz, A., Collins, M.J. and Pilkington, R., *Metals Technol.* **10**, 1983, 461.

Agren, J., *Acta Metall.* **37**, 1989, 181–189.

Akbasoglu, F.C. and Edmonds, D.V., *Metall. Trans. A*, **21A**, 1990, 889–893.

Alberry, P.J. and Jones, W.K.C., *Metals Technol.* **11**, 1977, 557–566.

Alberry, P.J. and Jones, W.K.C., CEGB internal report R/M/R282, April 1979 Central Electricity Research Laboratories, Leatherhead, UK.

Alberry, P.J., Brunnstrom, R.R.L. and Jones, K.E., *Metals Technol.* **10**, 1983, 28.

Al-Salman, S.A. and Ridley, N., *Scripta Metall.* **18**, 1984, 789–791.
Ali, A., Ph.D. Thesis, University of Cambridge, 1990.
Ali, A. and Bhadeshia, H.K.D.H., *Mater. Sci. and Technol.* **5**, 1989, 398–402.
Ali, A. and Bhadeshia, H.K.D.H., *Mater. Sci. and Technol.* **6**, 1990, 781–784.
Ali, A. and Bhadeshia, H.K.D.H., *Mater. Sci. and Technol.* **7**, 1991, 895–903.
Allen, N.P. and Pfeil, L.B., Iron Steel Inst. Special Rep. 24, London pp. 369–390, 1939.
Allen, N.P., Pfeil, L.B. and Griffiths, W.T., 2nd Report, Alloy Steels Research Comm., Iron and Steel Inst., London, 1939, p. 369.
Allten, A.G., Discussion to Owen, 1954.
Allten, A.G. and Payson, P., *Trans. ASM* **45**, 1953, 498.
Amano, K., Karomura, T., Shiga, C., Enami, T. and Tanaka, T., *Accelerated Cooling of Rolled Steel*, (eds G.E. Ruddle and A.F. Crawley), Pergamon Press, Oxford, UK., 1988, 43–56.
American Society for Metals, *Atlas of Isothermal and Cooling Transformation Diagrams*, ASM, Ohio, 1977, 28.
American Society for Testing Materials, Special Technical Publication 155, 1955.
Andrews, K.W., *Acta Metall.* **11**, 1963, 939–946.
Antia, D.P., Fletcher, A. and Cohen, M. *Trans. ASM.* **32**, 1944, 290.
Ashby, M.F., *Proc. Roy. Soc.* **A322**, 1987, 393–407.
Ashby, M.F. and Easterling, K.E., *Acta Metall.* **30**, 1982, 1969–1978.
Atkinson, C., Acta Metall. **15**, 1967, 1207–1211.
Austin, A.E. and Schwartz, C.M., *Proc. ASTM.* **52**, 1952, 592–596.
Austin, A.E. and Schwartz, C.M., *Proc. ASTM.* **55**, 1955, 523–625.
Avrami, M., *J. Chem. Phys.* **7**, 1939, 1103.
Avrami, M., *J. Chem. Phys.* **8**, 1940, 212.
Azevedo, T.A.L. and Galvao–da–Silva, E., *Scripta Metall.* **12**, 1978, 113–117.
Aziz, M.J., *J. Appl. Phys.* **53**, 1982, 1158–1168.
Aziz, M.J., *Appl. Phys. Lett.* **43**, 1983, 552–554.
Babu, B.N.P., Bhat, M.S., Parker, E.R. and Zackay, V.F., *Metall. Trans. A.* **7A**, 1976, 17–22.
Babu, S.S. and Bhadeshia, H.K.D.H., *Mater. Sci. Technol.* **6**, 1990, 1005–1020.
Babu, S.S., Bhadeshia, H.K.D.H., and L.–E. Svensson, *J. Mater. Sci. Lett.* **10**, 1991, 142–144.
Bach, P.W., Beyer, J. and Verbraak, C.A., *Scripta Metall.* **14**, 1980, 205–210.
Bagaryatski, Y.A., *Dokl. Akad. Nauk. SSSR* **73**, 1950, 1161.
Bailey, E.F., *Trans. ASM.* **46**, 1954, 830–854.
Bain, E.C., *Chem. Met. Eng.* **25**, 1921, 657–664.
Bain, E.C., *Trans. AIMME.* **70**, 1924, 25–46.
Bain, E.C., *Trans. AIMME.* **100**, 1932. 13.
Bain, E.C., *Alloying Elements in Steel*, ASM., Cleveland, OH., 1939.
Bain, E.C., *Sorby Centennial Symposium on the History of Metallurgy*, (ed. C.S. Smith), Gordon Breach Publisher, NY, 1963, 121.
Baker, J.C. and Cahn, J.W., *Acta Metall.* **17**, 1969, 575–578.
Baker, J.C. and Cahn, J.W., *Solidification*, ASM, Metals Park, OH., 1971, 23–54.
Baker, R.G. and Nutting, J., *J. Iron Steel Inst.* **192**, 1959, 257–268.
Bannova, M.I., *Fiz. Metal. Metlloved.* **41**, 1976, 1104–1106.

Barbaro, F.J., Edwards, R.H. and Easterling, K.E., *7th National Conference of the Australian X-Ray Analysis Association (AXAA–88)*, University of Western Australia, August 1988, 1–14.
Barbaro, F.J., Krauklis, P. and Easterling, K.E., *Mater. Sci. Technol.* **5**, 1989, 1057–1068.
Barford, J., *J. Iron Steel Inst.* **204**, 1966, 609–614.
Barford, J. and Owen, W.S., *J. Iron Steel Inst.* **197**, 1961, 146.
Barnard, S.J., Smith, G.D.W., Garratt-Reed, A.J. and Vander Sande, J., *Advances in the Physical Metallurgy and Applications of Steels*, Metals Society, London, 1981, 33–38.
Barnard, S.J., Smith, G.D.W., Garratt-Reed, A.J. and Vander Sande, J., *Solid→Solid Phase Transformations*, TMS of AIME, Warrendale, PA, 1982, 881–885.
Barnard, S.J., Smith, G.D.W., Sarikaya, M. and Thomas, G., *Scripta Metall.* **15**, 1981, 387.
Barritte, G.S., Ph.D. Thesis, University of Cambridge, 1982.
Barritte, G.S., Ricks, R.A. and Howell, P.R., *Quantitative Microanalysis with High Spatial Resolution*, The Metals Society, London, 1982, 112–118.
Bastien, P.G., *J. Iron Steel Inst.* **187**, 1957, 281–291.
Benjamin, J.S., *Metall. Trans.* **1**, 1970, 2943–2951.
Bhattacharyya, S. and Kehl, G.L., *Trans. ASM* **47**, 1955, 351–379.
Bee, J.V. and Honeycombe, R.W.K., *Metall. Trans.* **9A**, 1978, 587.
Bell, T. and Farnell, B.C., *The Mechanism of Phase Transformations in Crystalline Solids*, Institute of Metals, London, 1969, 282.
Benson, J.P. and Edmonds, D.V., *Metal Sci.* **12**, 1978, 223–232.
Bhadeshia, H.K.D.H., *Acta Metall.* **28**, 1980a, 1103–1114.
Bhadeshia, H.K.D.H., *Scripta Metall.* **14**, 1980b, 821–824.
Bhadeshia, H.K.D.H., *Acta Metall.* **29**, 1981a, 1117–1130.
Bhadeshia, H.K.D.H., International Conference on Solid→Solid Phase Transformations, (eds H.I. Aaronson *et al.*), TMS of AIME, Warrendale, PA, 1981b, 1041–1048.
Bhadeshia, H.K.D.H., *Metal Sci.* **15**, 1981c, 175–177.
Bhadeshia, H.K.D.H., *Metal Sci.* **15**, 1981d, 178–180.
Bhadeshia, H.K.D.H., *J. Mater. Sci.* **17**, 1982a, 383–386.
Bhadeshia, H.K.D.H., *J. de Physique* **43**, 1982b, C4–437–441.
Bhadeshia, H.K.D.H., *Metal Sci.* **16**, 1982c, 167–169.
Bhadeshia, H.K.D.H., *J. Mater. Sci.* **18**, 1983a, 1473–1481.
Bhadeshia, H.K.D.H., *Metal Sci.* **17** 1983b, 151–152.
Bhadeshia, H.K.D.H., Int. Conf. on Phase Transformations in Ferrous Alloys, (eds Marder A.R. and Goldstein, J.I.), ASM., Cleveland, OH., 1984, 335–340.
Bhadeshia, H.K.D.H., *Mater. Sci. Technol.* **1**, 1985a, 497–504.
Bhadeshia, H.K.D.H., *Progress Mater. Sci.* **29**, 1985b, 321–386.
Bhadeshia, H.K.D.H., *Scripta Metall.* Software Survey Section **22**, 1988a, I–IV.
Bhadeshia, H.K.D.H., *Proc. of Int. Conf. on Solid→Solid Phase Transformations*, Cambridge, (ed. G.W. Lorimer), Institute of Metals, London, 1988b, 309–314.
Bhadeshia, H.K.D.H., *Mater. Sci. Technol.* **5**, 1989, 131–137.
Bhadeshia, H.K.D.H., *Metallurgy, Welding, and Qualification of Microalloyed (HSLA) Steel Weldments*, (eds J.T. Hickey, D.G. Howden and M.D. Randall), American Welding Society, Florida, USA, 1990, 34–69.

Bhadeshia, H.K.D.H. and Edmonds, *Metall. Trans.* **10A**, 1979a, 895–907.
Bhadeshia, H.K.D.H. and Edmonds, *Metal Sci.* **13**, 1979b, 325–334.
Bhadeshia, H.K.D.H. and Edmonds, D.V., *Acta Metall.* **28**, 1980a, 1265–1273.
Bhadeshia, H.K.D.H. and Edmonds, D.V., *Metal Sci.* **14**, 1980b, 41–49.
Bhadeshia, H.K.D.H. and Waugh, A.R., *Proc. of Int. Conf. on Solid→Solid Phase Transformations*, Pittsburgh, ASM., Metals Park, OH., 1981, 993–998.
Bhadeshia, H.K.D.H. and Waugh, A.R., *Acta Metall.* **30**, 1982, 775–784.
Bhadeshia, H.K.D.H. and Edmonds, D.V., *Metal Sci.* **17**, 1983a, 411–419.
Bhadeshia, H.K.D.H. and Edmonds, D.V., *Metal Sci.* **17**, 1983b, 420–425.
Bhadeshia, H.K.D.H., Svensson, L.E. and Gretoft, B., *Acta Metall.* **33**, 1985, 1271–1283.
Bhadeshia, H.K.D.H., Svensson, L.E. and Gretoft, B., *J. Mater. Sci.* **21**, 1986a, 3947–3951.
Bhadeshia, H.K.D.H., Svensson, L.E. and Gretoft, B., *Proc. 4th Scand. Symp. Materials Science*, University of Trodhiem, Norwegian Inst. of Technol., Trondheim, Norway, 1986b, 153–157.
Bhadeshia, H.K.D.H., Svensson, L.E. and Gretoft, B., *Welding Metallurgy of Structural Steels*, (ed. J.Y. Koo), AIME, Warrendale, PA, 1987, 517–530.
Bhadeshia, H.K.D.H. and Svensson, L.E., *Joining and Mater.* **2**, 1989a, 182R–187R.
Bhadeshia, H.K.D.H. and Svensson, L.E., *Joining and Mater.* **2**, 1989b, 236R–238R.
Bhadeshia, H.K.D.H. and Svensson, L.E., *J. Mater. Sci.* **24**, 1989c, 3180–3188.
Bhadeshia, H.K.D.H. and Christian, J.W., *Metall. Trans.* A **21A**, 1990, 767–7 7.
Bhadeshia, H.K.D.H., David, S.A., Vitek, J.M. and Reed, R.W., *Mater. Sci. and Technol.*, **7**, 1991, 686–698.
Bhat, M.S., Ph.D. Thesis, *Microstructure and Mechanical Properties of AISI 4340 Steel modified with Al and Si*, 1977, Lawrence Berkley Laboratories, CA.
Bilby, B.A. and Christian, J.W., *The Mechanism of Phase Transformations in Crystalline Solids, Institute of Metals*, London, Monograph No. 18, 1956, 121–171.
BISRA, *Atlas of Isothermal Transformation Diagrams of BS En Steels*, Special Report 56, 2nd edn, 1956, Iron and Steel Inst., London.
Blackmore, P.A. and Harding, R.A., *Proc. 1st Int. Conf. Austempered Ductile Iron*, American Soc. for Metals, Metals Park, OH., 1984, 117.
Bodnar, R.L., Ohhashi, T. and Jaffe, R.I., *Metall. Trans.* A **20A** 1989, 1445–1460.
Bondt, De M. and Deruyttere, A., *Acta Metall.* **15**, 1967, 993.
Bowen, P. and Knott, J.F., *Metall. Trans.* A **17A**, 1986, 231.
Bowen, P., Druce, S.G. and Knott, J.F., *Acta Metall.* **34**, 1986, 1121–1131.
Bowles, J.S. and MacKenzie, J.K., *Acta Metall.* **2**, 1954, 129–234.
Bowles, J.S. and Kennon, N.F., *J. Aust. Iron Steel Inst.* **5**, 1960, 106–113.
Bowles, J.S. and Wayman, C.M., *Acta Metall.* **27**, 1979, 833.
Bradley, J.R., Rigsbee, J.M. and Aaronson, H.I., *Metall. Trans.* A **8A**, 1977, 323–333.
Bramfitt, B.L., *Metall. Trans.* **1**, 1970, 1987–1995.
Bramfitt, B.L. and Marder, A.R., *Metall. Trans.* **4**, 1973, 2291.
Brown, G.T. and James, B.A., *Metals Technol.* **7**, 1980, 261–268.
Brown, P.W. and D.J. Mack, *Metall. Trans.* **4**, 1973a, 2639–2643.
Brown, P.W. and D.J. Mack, *Metall. Trans.* **4**, 1973, 2850–2851.
Brownrigg, A., *Scripta Metall.* **7**, 1973, 1139–1142.
Brozzo, P., Buzzichelli, G., Mascanzoni, A. and Mirabile, M., *Metal Sci.* **11**, 1977, 123–129.
Buchi, G.J.P., Page, J.H.R. and Sidey, M.P., *J. Iron Steel Inst.* **203**, 1965, 291–298.

Buerger, M.J., *Phase Transformations in Solids*, Wiley, NY., 1951, 183.
Buhler, H., Buchholz, H. and Schulz, E.H., *Arch Eisenhuttenwes.* **5**, 1932, 413.
Buhler, H. and Scheil, E., *Arch. Eisenhuttenwes.* **6**, 1933, 293.
Buhler, H., *Arch. Eisenhuttenwes.* **26**, 1955, 51.
Bunshah, R.F. and Mehl, R.F., *Trans AIME.* **193**, 1953, 1251–1258.
Burdekin, F.M., *Advances in Physical Metallurgy*, (eds J.A. Charles and G.C. Smith), Institute of Metals, London, 1990, 27–45.
Burgess, P.B. and Kennon, N.F., *Metals Forum* **4**, 1978, 185–190.
Bush, M.E. and Kelly, P.M., *Acta Metall.* **19**, 1971, 1363–1371.
Cahn, J.W., *Acta Metall.* **4**, 1956, 572.
Callender, W.R., Ph.D. Thesis, University of Sheffield, 1983.
Cameron, J.A., *J. Iron Steel Inst.* **194**, 1956, 260–267.
Cane, B.J. and Townsend, R.D., Central Electricity Generating Board Report No. TPRD/L/2674/N84, 1984, Leatherhead, UK.
Carlson, M.F., Rao, B.V.N. and Thomas, G., *Metall. Trans.* A **10A**, 1979, 1273–1284.
Carruthers, R.B. and Collins, M.J., *Quantitative Microanalysis with High Spatial Resolution*, p. 108, 1981, Institute of Metals, London.
Carruthers, R.B. and Collins, M.J., *Met. Technol.* **10**, 1983, 461.
Chance, J. and Ridley, N., *Metall. Trans.* A **12**, 1981, 1205.
Chandel, R.S., Orr, R.F., Gianetto, J.A., McGrath, J.T., Patchett, B.M. and Bicknell, A.C., *The Microstructure and Mechanical Properties of Narrow Gap Welds in 2.25Cr–1Mo Steel*, Report ERP/PMRL 85–16(OP–J) of the Physical Metallurgy Research Laboratories, CANMET, Energy, Mines and Resources Canada, Ottawa, Canada, 1985.
Chanani, G.R., Antolovich, S.D. and Gerberich, W.W., *Metall. Trans.* **3**, 1972, 2661–2672.
Chart, T.G., Counsell, J.F., Jones, G.P., Slough, W. and Spencer, P.J., *Int. Metall. Rev.* **20**, 1975, 57–82.
Chevenard, P. and Portevin, A., *Rev. Met.* **28**, 1931, 417.
Chijiiwa, R., Tamehiro, H., Hirai, M., Matsuda, H. and Mimura, H., *Offshore Mechanics and Arctic Engineering (OMAE)*, Houston, TX., 1988, 1–8.
Chilton, J.M., Barton, C.J. and Speich, G.R., *J. Iron Steel Inst.* **208**, 1970, 184–193.
Choi, B.Y., Krauss, G. and Matlock, D.K., *Scripta Metall.* **22**, 1988, 1575–1580.
Christian, J.W., *Acta Metall.* **6**, 1958, 377–379.
Christian, J.W., *The Decomposition of Austenite by Diffusional Processes*, (eds V.F. Zackay and H.I. Aaronson), Interscience Publishers, NY, 1962, 387–546.
Christian, J.W., *Physical Properties of Martensite and Bainite*, Iron Steel Inst. Spec. Rep. No. 93, 1965a, 1–19.
Christian, J.W., *Theory of Transformations in Metals and Alloys*, Pergamon Press, Oxford, 1965b.
Christian, J.W., *The Mechanism of Phase Transformations in Crystalline Solids*, Monogr. Ser. Inst. Metals **33**, 1969, 129.
Christian, J.W., *Strengthening Methods in Crystals*, (eds. A. Kelly and R. Nicholson), Elsevier, North Holland, 1971, 261–329.
Christian, J.W., *Theory of Transformations in Metals and Alloys*, Part 1, 2nd. edn. Pergamon Press, Oxford, 1975.
Christian, J.W., *Phase Transformations* Vol. 1, No. 1, series 3, 1–11, Institute of Metallurgists, London, 1979a.

Christian, J.W., *ICOMAT 79*, International conference on martensitic transformations, Cambridge, Massachusetts, 220–234, 1979b.
Christian, J.W. and Crocker, A.G., *Dislocations in Solids*, (ed. F.R.N. Nabarro), vol. 3, North–Holland, Amsterdam, 1980.
Christian, J.W., *Metall. Trans.* A **13A**, 1982, 509–538.
Christian, J.W., *Metall. Trans.* A 14A, 1983, 1237.
Christian, J.W., *Encyclopedia of Materials Science and Engineering*, Pergamon Press, Oxford, 1986, 2741–2743.
Christian, J.W., *Metall. Trans.* A **21A**, 1990a, 799–803.
Christian, J.W., *Mater. Sci. Eng.* **A127**, 1990b, 215–227.
Christian, J.W. and Edmonds, D.W., *Int. Conf. Phase Transformations in Ferrous Alloys*, (eds. Marder, A.R. and Goldstein, J.I.), ASM., Cleveland, OH, 1984, 293–326.
Chung, D.W., Todd, J.A., Youngs, J.K. and Parker, E.R., *Advanced materials for pressure vessel service with hydrogen at high temperatures and pressures, (ed. M. Semchyshen), MPC–18*, 1982, 25.
Clark, H.M. and Wayman, C.M., *Phase Transformations*, ASM, Metals Park, OH, 1970, 59–114.
Clayton, P., Sawley, K.J., Bolton, P.J. and Bell, G.M., *Wear of Materials*, 9th International Conference, Houston, TX, 1987, publ. *Wear* **120**, 1987, 199–220.
Coates, D.E., *Metall. Trans.* **3**, 1972, 1203–1212.
Coates, D.E., *Metall. Trans.* **4**, 1973a, 1077–1086.
Coates, D.E., *Metall. Trans.* **4**, 1973b, 2313–2325.
Cohen, M., *Trans. ASM* **28**, 1940, 537.
Cohen, M., Discussion to Troiano and Greninger, 1946.
Cohen, M., Machlin, E.S. and Paranjpe, V.G., *Thermodynamics in Physical Metallurgy*, ASM., Cleveland, OH, 1950.
Coheur, P. and Habraken, L., *Rev. Univ. Min.* **94**, 1951, 107.
Coldren, A.P., Cryderman, R.L., Semchysen, M., *Steel Strengthening Mechanisms*, Climax Molybdenum, Ann Arbor, USA., 1969, 17.
Collins, L.E., Knight, R.F., Ruddle, G.E. and Boyd, J.D., *Accelerated Cooling of Steel*, (ed. P.D. Southwick), *TMS–AIME*, 1985, 261–282.
Collins, M., *Mater. Sci. and Technol.* **5**, 1989, 323–327.
Conrad, H., *J. Metals*, July 1964, 582.
Cotterell, B., *Trans. ASME, J. Basic, Eng.* **87**, 1965, 230.
Cottrell, A.H., *J. Iron Steel Inst.* **151**, 1945, 93P–104P.
Cottrell, S.A. and Ko, T., *J. Iron Steel Inst.* **173**, 1953, 225.
Crosky, A., McDougall, P.G. and Bowles, J.S., *Acta Metall.* **28**, 1980, 1495–1504.
Cullison, A., *Amer. Weld. J.* **70**, 1991, 80–82.
Curry, D.A. and Knott, J.F., *Met. Sci.* **12**, 1978, 511.
Dadian, M., *Advances in Welding Science and Technology*, (ed. S.A. David), ASM, Metals Park, OH, 1987, 101–117.
Daigne, J., Guttmann, M. and Naylor, J.P., *Mat. Sci. and Eng.* **56**, 1982, 1–10.
Dallum, C.B. and Olson, D.L., *Amer. Weld. J.* 1989, 198s–205s.
Dan, T. and Gunji, K., *Trans. Nat. Res. Inst. Met., Japan* **26**, 1984, 8.
Darken, L.S., *Trans. AIME* **180**, 1949, 430–438.
Dauskardt, R.H. and Ritchie, R.O., *ASME PVP* Vol. 114/MPC Vol. 27, Amer. Soc. Mechan. Eng., NY, 1986, 17–28.

Davenport, A.T., *The Crystallography of Upper Bainite*, Republic Steel Research Rep. on Project 12051, February 1974, 1–35.
Davenport, A.T., *The Hot Deformation of Austenite*, (ed. J.B. Ballance, *TMS–AIME*, NY, 1977, 517–536.
Davenport, E.S. and Bain, E.C., *Trans. Met. Soc. AIME* **90**, 1930, 117–154. (Also in *Metall. Trans.* A **–1**, 1970, 3501–3530 as a 'Metallurgical Classic', with commentary by H.W. Paxton.)
Davenport, E.S., *Trans. ASM.* **27**, 1939, 837–886.
Davies, G.J. and Garland, J.G., *Int. Metals Rev.* **20**, 1975, 83–106.
Davies, G.J., Kallend, J.S. and Morris, P.P., *The Hot Deformation of Austenite*, (ed. J.B. Ballance, TMS–AIME, NY, 1977, 599–626.
Davies, R.G. and Magee, C.L., Proc. 2nd Int. Conf. on Strength of Metals and Alloys, ASM, 1970a, 817.
Davies, R.G. and Magee, C.L., *Metall. Trans.* **1**, 1970b, 2927–2931.
Davies, R.G. and Magee, C.L., *Metall. Trans.* **2**, 1971, 1939–1947.
Dearden, J. and O'Neill, H., *Trans. Inst. Weld.* **3**, 1940, 203.
DeArdo, A.J., *Accelerated Cooling of Rolled Steel*, (eds G.E. Ruddle and A.F. Crawley), Pergamon Press, Oxford, UK., 1988, 3–27.
Deep, G. and Williams, W.M., *Canadian Metall. Quart.* **14**, 1975, 85–96.
Degang, Y., Dajun, C., Jinghong, Z., Yirong, H.E. and Fufa, S., *Acta Metallurgica Sinica* **2**, 1989, 161–167.
DeHoff, R.T. and Rhines, F.N., eds, *Quantitative Microscopy*, McGraw-Hill Book Company, NY, 1968.
Delacy, L. and Warlimont, H., *'Shape Memory Effects in Alloys'*, J. Perkins Editor, TMS–AIME, Plenum Press, New York, NY, 1975, 89–114.
Deliry, J., Mem. *Sci. Rev. Metall.* **62**, 1965, 527–550.
Denis, S., Gautier, E., Simon, A. and Beck, G., *Mater. Sci. Technol.* **1**, 1985, 805–814.
Devanathan, R. and Clayton, P., Rolling/Sliding Wear Behaviour of Three Bainitic Steels, Private communication, 1990.
Diesburg, D.E., Kim, C. and Fairhurst, W., *Heat Treatment 81*, 15–16 September 1981, The Institute of Metals, London, 178.
Dionne, S., Krishnadev, M.R., Collins, L.E. and Boyd, J.D., *Accelerated Cooling of Rolled Steel*, (eds. G.E. Ruddle and A.F. Crawley), Pergamon Press, Oxford, 1988, 71–84.
Dorazil, E., Barta, B., Munsterova, E., Stransky, L. and Huvar, A., *AFS Int. Cast Met. J.*, June 1962, 52–62.
Dorazil, E. and Svejcar,J., *Arch Eisenhuttenaves* **50**, 1979, 293–298.
Dorn, J.E., *Dislocation Dynamics*, (eds. A.R. Rosenfield, G.T. Hahn, A.L. Bement and R.I. Jaffee), McGraw-Hill, NY, 1968, 27.
Dowling, J.M., Corbett, J.M. and Kerr, H.W., *Metall. trans. A* **17A**, 1986, 1611.
Drozdov, B. Ya., Kogan, L.I. and Entin, R.I., *Fiz. Metal. Metalloved.* **13** (No. 5), 1962, 776–779; English translation in *Phys. of Met. and Metall.* **13** (No. 5), 1962, 135–138.
Dubé, C.A., Ph.D. Thesis, Carnegie Institute of Technology, 1948.
Dubé, C.A., Aaronson, H.I. and Mehl, R.F., *Rev. Met.* **55**, 1958, 201.
Dubensky, W.J. and Rundman, K.B., *AFS Transactions* **93**, 1985, 389–394.
Dubrov, V.A., *Fiz. Metal. Metalloved.* **28** (No. 2), 1969, 309–314; English translation in *Phys. of Met. and Metall.* **28**, (No. 2), 1969, 126–131.

Duckworth, W.E., *J. Met.* **18**, 1966, 915.
Duckworth, W.E., Taylor, P.R. and Leak, D.A., *J. Iron Steel Inst.* **202**, 1964, 135.
Durbin, M. and Krahe, P.R., *Processing and Properties of low-Carbon Steel*, AIME, Warrendale, PA, 1973, 109–31.
Easterling, K.E., *Introduction to the Physical Metallurgy of Welding*, Butterworths, London, 1983.
Edwards, D.P., *J. Iron Steel Inst.* **207**, 1969, 1494–1502.
Edwards, R.H. and Kennon, N.F., *J. Aust. Inst. Met.* **19**, 1974, 45.
Edwards, R.H. and Kennon, N.F., *Metall. Trans.* **9A**, 1978, 1801.
Ehrenfest, P., *Proc. Acad. Sci.* Amsterdam **36**, 1933, 153.
Entin, R., *Decomposition of Austenite by Diffusional Processes*, Interscience, New York, 1962, 295–311.
Ericsson, C.E., Bhat, M.S., Parker, E.R. and Zackay, V.F., *Metall. Trans. A* **7A**, 1976, 1800–1803.
Es-Souni, M. and Beaven, P.A., *Microanalysis of inclusion/matrix interfaces in weld metals*, International Institute of Welding Document II–A–815–90, 1990.
Esaka, K., Koyama, K., Matsumura, Y. and Tashiro, M., *HSLA Steels: Metallurgy and Applications*, (eds. J.M. Gray, T. Ko, Z. Shouhua, W. Baorong and X. Xishan), 1985, Beijing, China, publ. by ASM International, 959–968.
Eterashvili, T.V., Utevsky, L.M. and Spasskiy, M.N., *Phys. Met. Metall.* **48**, (No. 4), 1979, 113–121.
Evans, G.M., International Institute of Welding Document II–A–666–86, 1986.
Evans, G.M., International Institute of Welding Document II–A–739–86, 1988.
Evans, P.R.V. and O'Neill, H., *J. Iron Steel Inst.* **191**, 1959, 34.
Evans, G.M., *The effect of aluminium in shielded metal-arc C–Mn steel multi-run deposits*, International Institute of Welding Document II–1146–90 (sub commission II–A–796–90), 1990, 1–14.
Farrar, R.A. and Harrison, P.L., *J. Mat. Sci.* **22**, 1987, 3812–3820.
Fisher, J.C., *Met. Trans.* **185**, 1949, 688–700.
Fisher, J.C., *Thermodynamics in Physical Metallurgy*, ASM., Cleveland, OH, 1950.
Fisher, R.M., Proc. Int. Conf. on Electron Microscopy, Springer Verlag OHG, Berlin, 1958, pp. 579–588.
Fitzgerald, F., *Met. and Mater.* **7**, 1991, 378–387.
Fleck, N.A., Grong, O., Edwards, G.R. and Matlock, D.K., Welding Res. Supp. to the *Welding Journal*, 1986, 113s–121s.
Fondekar, M.K., Rao, A.M. and Mallik, A.K., *Metall. Trans.* **1**, 1970, 885–890.
Forster, F. and Scheil, E., *Z. Metallkunde* **28**, 1936, 245–247.
Forster, F. and Scheil, E., *Naturwissenschaften* **25**, 1937, 439.
Forster, F. and Scheil, E., *Z. Metallkunde* **32**, 1940, 165.
Fowler, R.H. and Guggenhiem, E. A., *Statistical Thermodynamics*, Cambridge University Press, NY, 1939, 442.
Franetovic, V., Sachdev, A.K. and Ryntz, E.F. *Metallography* **20**, 1987a, 15–37.
Franetovic, V., Shea, M.M. and Ryntz, E.F., *Mater. Sci. and Eng.* **96**, 1987b, 231–245.
Franklin, A.G., *J. Iron Steel Inst.* **207**, 1969, 181–186.
Franti, G.W., Williams, J.C. and Aaronson, H.I., *Metall. Trans.* **9A**, 1978, 1641.
Freiwillig, R., Kudrman, J. and Chraska, P., *Metall. Trans.* **7A**, 1976, 1091.
Fridberg, J., Torndahl, L.–E. and Hillert, M., *Jernkont. Ann.* **153**, 1969, 263–273.

Fullman, R.L., *Trans. AIMME.* **197**, 1953, 477, 1267.
Gadgil, V.J., Swens, J.J. and Kolster, B.H., *Colloque de Physique* (supplement to *J. de Physique*) **50**, 1989, C8–361–364.
Garnham, J., University of Leicester, private communication, 1989.
Garwood, R.D., *J. Inst. Met.* **83**, 1954–55, 64–68.
George, T., Parker, E.R. and Ritchie, R.O., *Mater. Sci. Technol.* **1**, 1985, 198–208.
Ghonem, H., Kalousek, J. and Stone, D., *Specialty Steels and Hard Materials* Pretoria, South Africa, Pergamon Press, Oxford, 1982, 259.
Gibson, G.B., *Review of cleavage fracture mechanisms in ferritic steels*, UKAEA Report R13227, Harwell, Oxon, 1988; referred to by Burdekin 1990.
Gladman, T., Private communication to Honeycombe and Pickering, 1972.
Gladman, T., Dulieu, D. and McIvor, I.D., *Proc. Conf. Microalloying 1975*, Washington, 1–3 October 1975.
Glicksman, M.E., Schaefer, R.J. and Ayres, J.D., *Metall. Trans. A* **7A**, 1976, 1747–1759.
Goldak, J., Patel, B., Bibby, M. and Moore, J., Computational Weld Mechanics, June 1985, Carelton University, Canada, private communication.
Goldman, L.M. and Aziz, M.J., *J. Mater. Res.* **2**, 1987, 524–527.
Goodenow, R.H., and Hehemann, R.F., Discussion to Speich, 1962.
Goodenow, R.H., Matas, S.J. and Hehemann, R.F., *Trans. AIMME.* **227**, 1963, 651–658.
Goodenow, R.H., Hehemann, R.F., *Trans. AIMME.* **233**, 1965, 1777.
Goodenow, R.H., Barkalow, R.H. and Hehemann, R.F., *Iron Steel Inst. Spec. Rep.* 93, London, 1969, 135–141.
Gorbach, V.G., Jelenkowski, J. and Filipiuk, J., *Mater. Sci. Technol.* **5**, 1989, 36–39.
Gordine, J. and Codd, I., *J. Iron Steel Inst.* **207.1**, 1969, 461–467.
Grabke, H.J., Hennesen, K., Moller, R. and Wei, W., *Scripta Metall.* **21**, 1987, 1329–1334.
Graham, L.W. and Axon, H. *J. Iron Steel Inst.* **191**, 1959, 361.
Graf, M.K., Hillenbrand, H.G., Pe4ters, P.A., *Accelerated Cooling of Steel*, (ed. P.D. Southwick), *TMS–AIME*, 1985, 349–366.
Grange, R.A., *Metall. Trans.* **2**, 1971, 417.
Grong, O., Kluken, A.O. and Bjornbakk, B., *Joining and Mater.*, 1988, 164–169.
Grassl, K., Thompson, S.W. and Krauss, G., *New Options for Steel Selection for Automotive Applications*, Soc. Automotive Engrs., Warrendale, PA, Technical Paper 890508, March 1989, 1–13.
Greenwell, B., NEI Parsons, Ltd., Newcastle, UK, private communication, 1989.
Greenwood, G.W., *Acta Metall.* **4**, 1956, 243.
Gregory, E. and Simmons, E.N., *The Structure of Steel*, Blackie and Son Ltd. London, 1947.
Greninger, A.B. and Troianao, A.R., *Trans. AIMME.* **140**, 1940, 307–336.
Griffiths, J.R. and Oates, G., *Met. Sci.* **11**, 1977, 285–292.
Grong. O. and matlock, D.K., *Int. Met. Rev.* **31**, 1986, 27–48.
Grube, W.L. and Rouze, S.R., *High Temperature-High Resolution Metallography*, Gordon and Breach, NY, 1967, 313.
Grujicic, M., Olson, G.B. and Owen, W.S., *Metall. Trans. A* **16A**, 1985a, 1713–1722.
Grujicic, M., Olson, G.B. and Owen, W.S., *Metall. Trans. A* **16A**,1985b, 1723–1734.

Grujicic, M., Olson, G.B. and Owen, W.S., *Metall. Trans. A* 16A, 1985c, 1735–1745.
Gulyaev, A.P., *Metallurg* **15**, 1940, 43.
Habraken, L.J., *Rev. Met.* **53**, 1956, 930.
Habraken, L.J., *Compt. Rend.* **19**, 1957, 126.
Habraken, L.J., *Proc. 4th Int. Conf. on Electron Microscopy*, Springer-Verlag, Berlin, 1958, 621–628.
Habraken, L., *Physical Properties of Martensite and Bainite*, Special Report 93, Iron Steel Inst. (London), 1965, 147.
Habraken, L.J. and Economopolus, M., *Transformation and Hardenability in Steels*, Climax Molybdenum, Ann Arbor, MI, 1967, 69–107.
Habu, R., *Trans. Iron Steel Inst. Japan* **18**, 1978, 492.
Hägg, G., *Z. Kristallogr.* **89**, 1934, 92.
Haezebrouck, D.M., Ph.D. Thesis, *Nucleation and Growth of a Single Martensitic Particle*, Massachusetts Inst. Technol., June 1987.
Hall, D.J., Self, P.G. and Stobbs, W.M., *J. Microscopy* **130**, 1983, 215–224.
Hannemann, H., Hofmann, W. and Wiester, H.J., *Arch, Eisenhuttewesen* **6**, 1932–1933, 199.Harrison, P.L. and Farrar, R.A., *J. Mat. Sci.* **16**, 1981, 2218–2226.
Harrison, P.L. and Farrar, R.A., *Int. Mater. Rev.* **34**, 1989, 35–51.
Hayrynen, K.L., Moore, D.J. and Rundman, K.B., presented at the 1988 American Foundry Society Conference, private communication to H.K.D.H. Bhadeshia, 1988, 1–13.
Hawkins, M.J. and Barford, J., *J. Iron Steel Inst.* **210**, 1972, 97–105.
Heckel, R.W. and Paxton, H.W., *Trans. ASM.* **53**, 1961, 539.
Hehemann, R.F., Luhan, V.J. and Troiano, A.R., *Trans. ASM.* **49**, 1957, 409–426.
Hehemann, R.F., *Phase Transformations*, ASM, Metals Park, OH, 1970, 397–432.
Hehemann, R.F., Kinsman, K.R. and Aaronson, H.I., *Metall. Trans.* **3**, 1972, 1077.
Heitmann, W.F. and babu, F.B., *Fundamentals of Microalloying Forging Steels*, (eds G. Krauss and S.K. Banerji), Metallurgical Soc of AIME., Warrendale, PA, 1987, 55–72.
Heller, W. and Schweitzer, R., *Railway Gazette International*, October 1980, 855–857.
Heller, W. and Schweitzer, R., *2nd Int. Conf. Heavy Haul Railways*, Colorado, USA, 1982, 282–286.
Heritier, B. *et al.*, *HSLA Steels — Technology and Applications*, ASM Int., OH, 1984, 981–990.
Hildenwall, B., *Prediction of the Residual Stresses created during Quenching*, PhD. Thesis, Linkoping University, Sweden, 1979.
Hillert, M., *Jernkontorets Ann.* **136**, 1952, 25–37.
Hillert, M., *Paraequilibrium*, Internal Report, Swedish Inst. Met. Res., Stockholm, Sweden, 1953.
Hillert, M., *Jernkontorets Ann.* **141**, 1957, 757–764.
Hillert, M., *The Growth of Ferrite, Bainite and Martensite*, Internal Report, Swedish Inst. Met. Res., Stockholm, Sweden, 1960.
Hillert, M., *'Decomposition of Austenite by Diffusional Processes'*, (eds. V.F. Zackay and H.I. Aaronson, Interscience, NY, 1962, 197–247.
Hillert, M., *Metall. Trans. A* **6A**, 1975a, 5–19.
Hillert, M., *Lectures on the Theory of Phase Transformations*, (ed. H.I. Aaronson), Amer. Inst. Mining, Metallurgical and Petroleum Engrs, NY, 1975b, 1–44.

Hillert, M., *Solid→Solid Phase Transformations*, TMS–AIME, Warrendale, PA, 1982, 789–806.
Hillert, M. and Sundman, B., *Acta Metall.* **24**, 1976, 731–743.
Hirotsu, K.C.S. and Nagakura, S., *Acta Metall.* **20**, 1972, 645–655.
Hirth, J.P. and Cohen, M., *Metall. Trans.* **1**, 1970, 3.
Hobbs, R.M., Lorimer, G.W. and Ridley, N., *J. Iron Steel Inst.* **210.2**, 1972, 757.
Hodgson, W.H. and Preston, R.R., *Bulletin Canadian Inst. Met. (CIM Bull.)*, October 1988, 95–101.
Hoekstra, S., *Acta Metall.* **28**, 1980, 507–517.
Hoekstra, S., Lelie, H.M.M.V.D. and Verbraak, C.A., *Acta Metall.* **26**, 1978a, 1517–1527.
Hoekstra, S., Ohm, R.K. and Verbraak, C.A., *Acta Metall.* **26**, 1978b, 1505–1516.
Hofer, W.E., Cohn, E.M. and Peebles, W.C. *J. Amer. Chem. Soc.* **71**, 1949, 189.
Hollomon, J.H. and Jaffe, L.D., *Trans. TMS–AIME* **162**, 1945, 223–249.
Homma, H., Ohkita, S., Matsuda, S. and Yammamoto, K., *Amer. Weld. J.*, October 1987, 301s–309s.
Honeycombe, R.W.K., *Phase Transformations in Ferrous Alloys*, (ed. A.R. Marder and J.I. Goldstein), The Metallurgical Society of the AIME, Warrendale, PA, 1984, 259–280.
Honeycombe, R.W.K. and Pickering, F.B., *Metall. Trans.* **3**, 1972, 1099–1112.
Honeycombe, R.W.K., *Steels*, Edward Arnold, London, 1981.
Horii, Y., Ohkita, S., Wakabayashi, M. and Namura, M., *Nippon Steel Technical Report*, Nippon Steel Company, Japan, 1986, 1–9.
Horri, Y., Wakabayashi, M., Ohkita, S. and Namura, M., *Nippon Steel Technical Report* No. 37, April, 1988, Nippon Steel Company, Japan, 1–9.
Horn, R., Ph.D. Thesis, University of California, 1976.
Horn, R.M. and Ritchie, R.O., *Metall. Trans. A* **9A**, 1978, 1039–1053.
Houdremont, E., Koch, E. and Wiester, H.-J., *Arch. Eisenhuttenwesen* **18**, 1945, 147.
Houillier, R. Le, Begin, G. and Dubè, *Metall. Trans.* **2A**, 1971, 2645–2653.
Howard, R.T. and Cohen, M., Trans. AIMME. **176**, 1948, 384–400.
Hrivnak, I., *Guide to the welding and weldability of Cr–Mo and Cr–Mo–V heat resistant steels*, International Institute for Welding Document IX–G–319/c–87, 1987, 1–61.
Hsu, T.Y., *Metall. Trans. A* **21A**, 1990, 811–816.
Hsu, T.Y., and Yiwen, M., *Acta Metall.* **32**, 1984, 1469–1481.
Huang, D.H. and Thomas, G., *Metall. Trans.* **8A**, 1977, 1661.
Hulka, K., Heisterkamp, F. and Nachtel, L., *Processing, Microstructure and Properties of HSLA Steels*, (ed. A.J. DeArdo), Miner. Met. Mater. Soc., Warrendale, PA, 1988, 153–167.
Hull, D., *Bulletin Institute of Metals* **2**, 1954, 134–139.
Hultgren, A., *Trans. ASM.* **39**, 1947, 915–1005.
Hultgren, A., *Jernkontorets Ann.* **135**, 1951, 403.
Hultgren, A., *Kungl. Ver. Akad. Handl.* **4**, 1953, 1.
Hume-Rothery, W., *The Structures of Alloys of Iron*, Pergamon Press, Oxford, 1966, 240–253.
Hume-Rothery, W., Raynor, G.V. and Little, A.T., *Arch Eisenhuttenwesen* **145**, 1942, 143.
Ichinose, H., Takehara, J. and Ueda, M., *1st Int. Conf. On Heavy Haul Railways*, Pearth, Australia, 1978.

Ichinose, H., Takehara, J. and Ueda, M., *2nd Int. Conf. on Heavy Haul Railways*, Colorado Springs, USA, 1982, 178–186.
Imagumbai, M., Chijiiwa, R., Aikawa, N., Nagumo, M. Homma, H., Matsuda, S. and Mimura, H., *HSLA Steels: Metallurgy and Applications*, (eds. J.M. Gray, T. Ko, Z. Shouhua, W. Baorong and X. Xishan), ASM Int. OH, 1985, 557–566.
Inagaki, M. and Hiroyuki, M., *Quality and reliability in welding*, Hangzhou, China, Sept. 1984, Weld Inst. of Chinese Mech. Eng. Soc.
Ion, J.C., Easterling, K.E. and Ashby, M.F., *Acta Metall.* **32**, 1984, 1949–1962.
Irani, J.J., British Iron Steel Res. Assoc. Report No. MG/A/60/67, BSIRA, London, 1967.
Irvine, K.J. and Pickering, F.B., *J. Iron Steel Inst.* **187**, 1957, 292–309.
Irvine, K.J., Pickering, F.B., Heselwood, W.C. and Atkins, M., *J. Iron Steel Inst.* **195**, 1957, 54–67.
Irvine, K.J. and Pickering, F.B., *J. Iron Steel Inst.* **188**, 1958, 101.
Irvine, K.J., Llewellyn, D.T. and Pickering, F.B., *J. Iron Steel Inst.* **199**, 1961, 153.
Irvine, K.J. and Pickering, F.B., *J. Iron Steel Inst.* **201**, 1963, 518–531.
Irvine, K.J. and Pickering, F.B., *Iron Steel Inst. Spec. Rep. 93*, London, 1965, 110–125.
Isaichev, I.V., *Zhur Tekhn. Fiziki. 17*, 1947, 835.
Ishiguro, T., Murakami, Y., Ohnishi, K. and Watanbe, J., *ASTM-STP* **755**, Amer. Soc. for Testing Mater., Philadelphia, 1982, 129–147.
Ishiguro, T., Ohnishi, K., Murakami, Y., Mima, S. and Watanabe, J., Research on Chrome-Moly Steels, MPC–21, ASME, NY, 1984, 43–52.
Ito, Y. and Bessyo, K., *Int. Inst. Weld.* Document IX–576–68, 1968.
Ito, Y. and Nakanishi, M., *Int. Inst. Weld.* Document XII–113–75, 1975.
Ito, Y. and Nakanishi, M., *Sumitomo Search* **15**, 1976, 42–62.
Ito, Y., Nakanishi, M. and Komizo, Y., *Met. Constr.* **14**, 1982, 472.
Ivantsov, G.P., Dokl. *Akad. Nauk. SSSR* **58**, 1947, 567.
Jack, K.H., *Acta Cryst.* **3**, 1950, 392.
Jack, K.H., *J. Iron Steel Inst.* **169**, 1951, 26–36.
Jana, S. and Wayman, C.M., *Metall. Trans.* **1**, 1970, 2825.
Jellinghaus, W., *Arch. Eisenhuttenwesen* **23**, 1952, 459.
Jellinghaus, W., *Arch. Eisenhuttenwesen* 28, 1957, 469.
Jellinghaus, W. and Friedewold, H., *Arch Eisenhuttenwesen* **31**, 1960, 309.
Jepson, M.D. and Thompson, F.C., *J. Iron Steel Inst.* **162**, 1949, 49–56.
Jerath, V., Mistry, K., Bird, P. and Preston, R.R., British Steel Report on a collaborative research project between the University of Cambridge (H. Bhadeshia and BSC), Report SL/RS/R/S/1975/1/91A, 1991, 1–43.
Jihua, Z., Shuchuan, C. and Hsu, T.Y., *Acta Metall.* **37**, 1989, 241–246.
Jingsheng, Y., Zongsen, Y. and Chengjian, W., *J. of Met.* **40**, 1988, 26–31.
Jones, W.K.C. and Alberry, P.J., *'Ferritic Steels for Fast Reactor Steam Generators'*, British Nuclear Engineering Society Conference, London, June 1977, paper 78, 1–4.
Jones, W.K.C. and Alberry, P.J., *Residual Stresses in Welded Construction and Their Effects*, London, Nov. 1978, 15–25.
Jones, B.L. and Johnson, D.L., *Steels for Line-Pipe and Pipeline Fittings*, Metal. Soc., London, 1983, 14.

Jones, B.L., DeArdo, A.J., Garcia, C.I., Hulka, K. and Luthy, H., *HSLA Steels: Metallurgy and Applications*, Proc. of Int. Conf. on HSLA Steels '85, China, (eds. J.M. Gray, T. Ko, Z. Shouhua, W. Barong and X. Xishan, ASM Int., OH, 1985, 875–884.

Jones, C.L. and Pilkington, R., *Metall. Trans. A* **9A**, 1978, 865.

Jones, W.K.C., and Alberry, P.J., *'Ferritic Steels for Fast Reactor Steam Generators'*, British Nuclear Engineering Society, London, 1977a, 1–4.

Jones, W.K.C. and Alberry, P.J., *'Residual Stresses in Welded Constructions'*, Welding Institute, Cambridge, 1977b, paper 2.

Josefsson, B., *Microscopy and Microanalysis of Bainitic Weld Metal*, Licentiate Thesis, Chalmers University, Sweden, 1989.

Joseffson, B., Kvist, A. and Andren, H.O., *J. de Physique* (Colloque C6) **48**, 1987, C6–435–440.

Josefsson, B. and Andren, H.O., *Proc. of the 35th Int. Field Emission Symp.*, Oak Ridge, TN, July 1988, 18–22.

Josefsson, B. and Andren, H.O., *Recent Trends in Welding Science and Technology*, (eds. S.A. David and J. Vitek), ASM Int., OH, 1989, 243–247.

Judson, P. and McKeown, D., Advances in the Control of Weld Metal Toughness, Weld Inst, Abington, Cambridge, 1982.

Kalish, D., Kulin, S.A. and Cohen, M., *J. Met.*, Feb., 1965, 157.

Kalish, D. and Cohen, M., *Mater. Sci. and Eng.* **6**, 1970, 156–166.

Kalousek, J. and Beynon, G., *Rail Metallurgy*, Canadian Pacific Technical Reports, No. S497–75, 1975.

Kalousek, J., Fegredo, D.M. and Laufer, E.E., *Wear* **105**, 1985a, 199–222.

Kalousek, J., Fegredo, D.M. and Laufer, E.E., *Wear of Mater.*, (ed. K.C. Ludema), ASME, NY, 1985b, 212–231.

Kamada, A., Koshizuka, N. and Funakoshi, T., *Trans. Iron Steel Inst.* **16**, 1976, 407.

Kang, M.K., Sun, J.L. and Yang. Q.M., *Metall. Trans. A* **21A**, 1990, 853–858.

Kapadia, B.M., *Hardenability Concepts with Applications to Steel*, (ed. D.V. Doane and J.S. Kirkaldy), Metall. Soc. of AIME., Warrendale, PA, USA, 1978, 448–480.

Kar. R.J., Horn, R.M. and Zackay, V.F., *Metall. Trans. A* **10A**, 1979, 1711–1717.

Kar, R.J. and Todd, J.A., Discussion on Transformation Characteristics, ASTM STP 755, Amer. Soc. for Testing Mater., 1982, 361–362.

Kaufman, L. and Cohen, M., *Prog. in Met. Phys.* **7**, 1958, 165–246.

Kaufman, L. and Radcliffe, S.V., *Decomposition of Austenite by Diffusional Processes*, (eds. V.F. Zackay and H.I. Aaronson), Interscience, NY, 1962, 313–351.

Keh, A.S. and Leslie, W.C., *Mater. Sci. Res.* **1**, Plenum Press, NY, 1963, 208.

Keh, A.S. and Weissmann, S., *Electron Microscopy and the Strength of Crystals*, (eds. G. Thomas and J. Washburn), Interscience, NY, 1963, 231–300.

Kehoe, M. and Kelly, P.W., *Scripta Metall.* **4**, 1970, 473–476.

Kelly, P.M. and Nutting, *J., Proc. Roy. Soc. London A259*, 1960, 45–58.

Kennon, N.F., *J. Aust. Iron Steel Inst.* **19**, 1974, 3.

Kennon, N.F., *Metall. Trans.* **9A**, 1978, 57.

Kennon, N.F. and Kaye, N.A., *Metall. Trans.* **13A**, 1982, 975.

Keown, S.R., Smaill, J.S. and Erasmus, L.A., *Met. Technol.* **3**, 1976, 194.

Kerr, R., Solana, F., Bernstein, I.M. and Thompson, A.W., *Metall. Trans. A* **18A**, 1987, 1011–1022.

Kessler, H. and Pitsch, W., *Acta Metall.* **13**, 1965, 871–874.
Kettunen, P.O. and Kocks, U.F., *Scr. Metall.* **1** (1967), 13–17.
Kettunen, P.O. and Kocks, U.F., *Acta Metall.* **20**, 1972, 95–103.
Kettunen, P.O. and Lepistö, T., *Trans. Japan Inst Mat.* **17**, 1976, 63.
Khan, S.A. and Bhadeshia, H.K.D.H., *Metall. Trans. A* **21A**, 1990a, 859–875.
Khan, S.A. and Bhadeshia, H.K.D.H., *Mater. Sci. Eng.*, **A129**, 1990, 257–272.
Kimmins, S.T. and Gooch, D. *J., Met. Sci.* **17**, 1983, 519–532.
King, A.D. and Bell, T., *Metall. Trans. A* **6A**, 1975, 1419.
King, J.F., David, S.A., Sims, J.E. and Nasreldin, A.M., *Weld. J.*, July 1986, 39–47.
Kinsman, K.R. and Aaronson, H.I., Discussion to Oblak and Hehemann, 1967.
Kinsman, K.R. and Aaronson, H.I., *Metall. Trans.* **1**, 1970, 1485–1488.
Kinsman, K.R., Eichen, E. and Aaronson, H.I., *Metall. Trans.* **2**, 1971, 346–348.
Kinsman, K.R. and Aaronson, H.I., *Metall. Trans.* **4**, 1973, 959–967.
Kinsman, K.R., Eichen, E. and Aaronson, H.I., *Metall. Trans.* **6**, 1975, 303.
Kinsman, K.R., Richman, R.H. and Verhoeven, J.D., *Mater. Sci. Symp. Abst.*, ASM, 1974.
Kirkaldy, J.S., *Can. J. Phys.* **36**, 1958, 899–925.
Kirkaldy, J.S., Forstmann, V.D. and Brigham, R.J., *Can. Metall. Quart.* **1**, 1962, 59–81.
Klier, E.P. and Lyman, T., *Trans. AIMME.* **158**, 1944, 394–422.
Klueh, R.L., *J. Nuclear Mater.* **54**, 1974a, 41–54.
Klueh, R.L., *J. Nuclear Mater.* **54**, 1974b, 55–63.
Klueh, R.L. and Nasreldin, A.M., *Metall. Trans. A* **18A**, 1987, 1279–1290.
Klueh, R.L. and Swindeman, R.W., *Metall. Trans. A* **17A**, 1986, 1027–1034.
Klug, R.C., Hintz, M.B. and Rundman, K.B., *Metall. Trans. A* **16A**, 1985, 797–805.
Kluken, A.O. and Grong, O., *Metall. Trans. A* **20A**, 1989a, 1335–1349.
Kluken, A.O. and Grong, O., *Recent Trends in Welding Science and Technology*, (eds. S.A. David and J. Vitek), ASM Int., OH, 1989b, 781–786.
Kluken, A.O., O. Grong and G. Rorvik, *Metall. Trans. A* **21A**, 1990, 2047–2058.
Kluken, A.O., O. Grong and J. Hjelen, *Metall. Trans. A* **22A**, 1991, 657–663.
Knott, J.F., *J. Iron Steel Inst.* **204**, 1966, 104.
Knott, J.F., *Fundamentals of Fracture Mechanics*, Butterworths, London, 1973.
Knott, J.F., *Advances in the Physical Metallurgy and Applications of Steels*, Met. Soc., London, 1981, 181.
Knott, J.F. and Cottrell, A.H., *J. Iron Steel Inst.* **201**, 1963, 249–260.
Knowles, K.M. and Smith, D.A., *Acta Crystall.* **A38**, 1982, 34–40.
Koistinen, P.P. and Marburger, R.E., *Acta Metall.* **7**, 1959, 59–60.
Konoval, G., Zwell, L., Gorman, L.A. and Leslie, W.C., *Nature* **184**, 1959, 1862–1863.
Ko, T., *J. Iron Steel Inst.* **175**, 1953, 16–18.
Ko, T. and Cottrell, S.A., *J. Iron Steel Inst.* **172**, 1952, 307–313.
Kocks, U.F., *Phil. Mag.* **13**, 1966, 541.
Kocks, U.F., *Can. J. Phys.* **45**, 1967, 737.
Kocks, U.F., Argon, A.S. and Ashby, M.F., *Prog. Mater. Sci.* **19**, 1975, 1.
Koistinen, D.P., *Trans. ASM.* **50**, 1958, 227.
Korenko, M.K., Ph.D. thesis *Martensitic Transformations in High Magnetic Fields*, Massachusetts Inst. Technol., 1973.
Kostic, M.M., Hawbolt, E.B. and Brown, L.C., *Metall. Trans.* **7A**, 1976, 1643.

Kostic, M.M., Hawbolt, E.B. and Brown, L.C., *Metall. Trans.* **10A**, 1979, 165.
Kozasu, I., Suzuki, H., Yamada, M. and Tagawa, H., Research on Chrome–Moly Steels, MPC–21, ASME, NY, 1984, 53–76.
Kriesement, O. and Wever, F., *Mechanism of Phase Trans. in Met.*, Institute of Metals, Monograph and Rep. Ser. No. 18, London, 1956, 253.
Krishnadev, M.R. and Ghosh, R., *Metall. Trans. A* **10A**, 1979, 1941–1944.
Kubaschewski, O. and Evans, E. Li., *Metallurgical Thermochemistry*, Pergamon Press, Oxford, 1950.
Kunitake, T., Reactor Steel Studies, Cr–Mo Steels Research in Japan, (ed. K. Ono, 1971). Quoted in Lundin *et al.*, 1982.
Kunitake, T., Terasaki, F., Ohmori, Y. and Ohtani, H., *Iron and Steel*, December 1972, 647–643.
Kurdjumov, G.V., *Trans. AIMME* (Iron and Steel Div.) **105**, 1933, 253–255.
Kurdjumov, G.V. and Sachs, G., *Z. Phys.* **64**, 1930, 325.
Lacher, J.R., *Proc. Cambridge Phil. Soc.* **33**, 1937, 518.
Lai, G.Y., *Metall. Trans. A* **6A**, 1975, 1469.
Lancaster, J.F., *Metallurgy of Welding*, 4th edn, Allen and Unwin, London, 1986.
Lange, H. and Mathieu, K., Mitt, K.W.I. *Eisenforchung* **20**, 1938, 125.
Langer, E.W., *Met. Sci J.* **2**, 1968, 59.
Langer, J.S. and Müller–Krumbhaar, *Acta Metall.* **26**, 1978, 1681–1687.
Langford, G. and Cohen, M., *Trans. A. S. M.* **62**, 1969, 625.
Langford, G. and Cohen, M., *Metall. Trans.* **1**, 1970, 1478.
Langford, G. and Cohen, M., *Metall. Trans. A* **6A**, 1975, 901.
Lau, T.W., Sadowsky, M.M., North, T.H. and Weatherly, G.C., *Welding Metallurgy of Structural Steels*, (ed. J.Y. Koo), TMS–AIME, Warrendale, PA, 1987, 349–365.
Lau, T.W., Sadowsky, M.M., North, T.H. and Weatherly, G.C., Mater Sci Technol. **4**, 1988, 52–61.
Laverroux, M. and Pineau, A., *Scripta Metall.* **8**, 1974, 351–356.
Law, N. and Edmonds, D.V., *Metall. Trans. A* **11A**, 1980, 33.
Leber, H., Luthy, H. and Form, W., *Fundamentals of Microalloying Forging Steels*, (eds. G. Krauss and S.K. Banerji), Metall. Soc. of AIME, Warrendale, PA, 1987, 189–206.
Leber, H.J., Garcia, C.I., Palmiere, E.J. and DeArdo, A.J., *Processing, Microstructure and Properties of HSLA Steels*, (ed. A.J. DeArdo), Miner., Met. and Mater. Soc., Warrendale, PA, 1988, 425–437.
Lee, Y.J., *Assessment of Creep Damage in Weldments of 1Cr–0.5Mo Steel*, Ph.D. Thesis, 1989, Monash University, Clayton, Victoria, Australia.
Lee, H.J., Spanos, G., Shiflet, G.J. and Aaronson, H.I., *Acta Metall.* **36**, 1129–1140, 1988.
Leont'yev, B.A. and Kovalevskaya, G.V., *Fiz. Metall. Metalloved.* **38**, 1974, 1050.
Leslie, W.C., *Physical Metallurgy of Steels*, McGraw–Hill Kogakusha, Tokyo, Japan, 1982.
Lewis, D., J. Iron Steel Inst. **119**, 1929, 427.
Li, C.Y., Blakely, J.M. and Feingold, A.H., *Acta Metall.* **14**, 1966, 1397.
Lifshitz, I.H. and Slyozov, V.Z., *Phys. Chem. Sols.* **19**, 1961, 35.
Lin, M., Research Proposal for Ph.D. Thesis *Autocatalytic Kinetics of Martensitic Transformations*, Massachusetts Institute of Technology, 1987, private communication G.B. Olson.

Llopis, A.M., Ph.D. Thesis, referred to in E.R. Parker, *Metall. Trans.* **8a**, 1977, 1025.
Lonsdale, D. and Flewitt, P.E.J., *Metall. Trans. A* **9A**, 1978, 1619–1623.
Lorenz, K. and Duren, C., *Steels for line pipe and pipeline fittings*, Metals Society, London, 1983, 322.
Lu, G.–Z., Zhang, H., *Wear of Materials*, (ed. K.C. Ludema), ASME, NY, 1989, 225–231.
Lundin, C.D., Kruse, B.J. and Pendley, M.R., Bulletin 277 of Weld. Res. Council, United Engineering Center, NY, May 1982, 1–27.
Lundin, C.D., Kelly, S.C., Menon, R. and Kruse, B.J., Bulletin 315 of the Weld. Res. Council, United Engineering Center, NY, June 1986, 1–66.
Lyman, T. and Troiano. A.R., *Trans. AIME* **162**, 1945, 196.
Lyman, T. and Troiano, A.R., *Trans. ASM.* **37**, 1946, 402–448.
Mack, C., *Proc. Cambridge Phil. Soc.* **52**, 1956, 246.
Magee, C.L., *Phase Transformations*, ASM., Metals Park, OH, 1970, 115–156.
Magee, C.L., *Metall. Trans.* **2**, 1971, 2419–2430.
Maki, R., Shimooka, S., Arimoto, T. and Tamura, I., *Trans. Japan Inst. Met.* **14**, 1973, 62–67.
Maki, T., Shimooka, S., Fujiwara, S. and Tamura, I., *Trans. Japan Inst. Met.* **16**, 1975, 36–41.
Maki, T. and Tamura, I., *Proc. Int. Conf. on Martensitic Transformations, ICOMAT 86*, Kyoto, Japan Inst. Met., 1986, 963–970.
Malecki, P., Private Communication on a paper published in Procs. of 8th Int. Conf. on Metallography, Leoben, Austria, 1990.
Marder, A.R. and Krauss, G., *Trans. ASM.* **60**, 1967, 651.
Marschall, C.W., Hehemann, R.F. and Troiano, A.R., *Trans. ASM* **55**, 1962, 135.
Matas, S.J. and Hehemann, R.F., *Nature* **187**, 1960, 685–686.
Matas, S.J. and Hehemann, R.F., *Trans. Met. Soc. AIME.* **221**, 1961, 179–185.
Matsuda, A., *Tetsu-to-Hagane*, **56**, 1970, 1428.
Matsueda, S., Inoue, T. and Ogasaswara, M., *Trans. Japan Inst. Met.* **9**, 1968, 343.
Matsuda, S., Inoue, T. and Ogasaswara, M., *Trans. Iron Steel Inst. Jpn.* **12**, 1972, 325.
Matsuda, S. and Okumara, N., *Trans. Iron Steel Inst. Jpn.* **18**, 1978, 198–205.
McCutcheon, D.B., Trumper, T.W. and Embury, J.D., *Revue de Metallurgie*, Feb. 1976, 143–174.
McEvily, A.J. and Magee, C.L., *Low Alloy Steels*, Iron and Steel Institute, London, 1968, 111–117.
McGrath, J.T., Chandel, R.S., Orr, R.F. and Gianetto, J.A., *Canadian Metall. Quart.* **28**, 1989, 75–83.
McLellan, R.B. and Dunn, W.W., *J. Phys. Chem. Solids*, **30**, 1969, 2631–2637.
McMahon Jnr., C.J., Cohen, M., *Acta Metall.* **13**, 1965, 591.
McRobie, D.E. and Knott, J.F., *Mater, Sci. Technol.* **1**, 1985, 137.
Mehl, R.F., *Hardenability of Alloy Steels*, ASM, Cleveland, OH, 1939, 1.
Mehl, R.F., *J. Iron Steel Inst.* **159**, 1948, 113–129.
Mendiratta, M.G., Sasser, J. and Krauss, G., *Metall. Trans. A* **3**, 1972, 351–353.
Miihkinen, V.T.T. and Edmonds, D.V., *Mater. Sci. and Technol.* **3**, 1987a, 422–431.
Miihkinen, V.T.T. and Edmonds, D.V., *Mater. Sci. and Technol.* **3**, 1987b, 432–440.
Miihkinen, V.T.T. and Edmonds, D.V., *Mater. Sci. and Technol.* **3**, 1987c, 441–449.
Miller, R.F., Benz, W.G. and Unverzagt, W.E., *Proc. ASTM.* **40**, 1940, 771–781.

Mills, A.R., Thewlis, G. and Whiteman, J.A., *Mater. Sci. and Technol.* **3**, 1987, 1051–1061.
Mintz, B., and Wilson, D.V., *Acta Metall.* **13**, 1965, 947.
Moore, D.J., Rouns, T.N. and Rundman, K.B., *J. Heat Treating* **4**, 1985a, 7.
Moore, D.J., Rouns, T.N. and Rundman, K.B., *AFS Trans.* **93**, 1985b, 705–718.
Moore, D.J., Rouns, T.N. and Rundman, K.B., *AFS Trans.* **94**, 1986, 255–264.
Moore, D.J., Rouns, T.N. and Rundman, K.B., *AFS Trans.* **95**, 1987, 765–773.
Morgan, E.R., Dancy, T.E. and Korchynsky, M., *Blast Furnace and Steel Plant* **53**, 1965, 921–929.
Mori, N., Homma, H., Okita, S. and Wakabayashi, M., Int. Inst. Weld., Document IX–1196–81, 1981.
Morikawa, H. and Hasegawa, T., *Accelerated Cooling of Steel*, (ed. P.D. Southwick), TMS–AIME, 1985, pp. 83–96.
Morniroli, J., Grosse, E. and Gantois, M., *Phil. Mag. A* **48**, 1983, 311.
Mostert, R.J. and van Rooyen, G.T., *Specialty Steels and Hard Materials*, Pretoria, S.A. Pergamon Press, Oxford, 1982, 229.
Mou, Y. and Hsu, T.Y., *Metall. Trans. A* **19A**, 1988, 1695–1701.
Mujahid, S.A. and Bhadeshia, H.K.D.H., *Acta Metall. et Mater.* **40**, 1992, 389–396.
Murakami, T. and Imai, Y., *Sci. Rep. Res. Inst.* Tohoku Univ., Series A **1**, 1949, 87–92.
Murphy, M.C. and Branch, G.D., *J. Iron Steel Inst.* **206**, 1969, 1347–1364.
Murphy, M.C. and Branch, G.D., *J. Iron Steel Inst.* **209**, 1971, 546–561.
Mutiu, T.A., Kinderman, A.J. and Bernstein, I.M., *The Hot Deformation of Austenite*, (ed. J.B. Ballance), TMS.–AIME., NY, 1977, 410–427.
Mutton, P.J., M. App. S. Thesis, University of Melbourne, 1985. Referred to by Sawley *et al.*, 1987.
Myers, E.J., *Proc. First Int. Cong. in Stereology*, Vienna Medical Academy, 1953, 15/1, 15/7.
Myers, J., Willoughy, G. and Ham, R.K., Central Electricity Research Laboratories Report RD/L/R 1514, 1968, Leatherhead, Surrey, UK.
Nabarro, F.R.N., *Proc. Roy. Soc.* **A381**, 1982, 285.
Nagakura, S., Suzuki, T. and Kusunoki, M., *Trans. Japan Inst. Met.* **22**, 1981, 699–709.
Nagakura, S., Kirotsu, Y., Kusunoki, M., Suzuki, T. and Nakamura, Y., *Metall. Trans. A* **14**, 1983, 1025–1031.
Nakamura, T., Mikami, T. and Nagakura, S., *Trans. Japan Inst. Met.* **26**, 1985, 876–885.
Nakamura, T. and Nagakura, S., *International Conference on Martensitic Transformations ICOMAT 86*, Japan Inst. Met., 1986, 386–391.
Nakasugi, H., Matsuda, H. and Tamehiro, H., *Alloys for the 1980's*, Climax Molybdenum, Ann Arbor, MI, 1980, 213.
Nakasugi, H., Matsuda, H. and Tamehiro, H., *Steels for line pipe and pipeline fittings*, *Met. Soc.* London, 1983, 90.
Nath, B., *Int. Conf. on Welding Technology of Energy Applications*, (ed. S.A. David and G.M. Slaughter, Oak Ridge National Labs, TN, USA, 1982, 1–25.
Nath, B., *2nd Int. Conf. on Creep and Fracture of Engineering Materials and Structures* Pineridge Press Ltd., Swansea, 1984, 827–838.

Naylor, J.P., *Metall. Trans. A* **10**, 1979, 861.
Naylor, J.P. and Krahe, P.R., *Metall. Trans.* **5**, 1974, 1699–1701.
Naylor, J.P. and Krahe, P.R., *Metall. Trans.* **6A**, 1975, 594–598.
Nehrenberg, A.E., *J. Met.* **188**, 1950, 162–180.
Nemoto, M., *High Voltage Electron Microscopy*, Academic Press, New York, 1974, 230, 234.
Nilan, T.G., *Trans. Met. Soc. AIME.* **239**, 1967, 898–909.
Nishiyama, Z., *Sci. Rep. Tohoku Univ.* **23**, 1934, 325.
Nishioka, K. and Tamehiro, H., *Microalloying '88: Int. Symp. on Applications of HSLA Steel*, Chicago, IL, September 1988, 1–9.
Norström, L.–A., Scandinavian *J. Metall.* **5**, 1976, 159–165.
North, T.H., X. Mao and H. Nakagawa, *The Metallurgy, Welding and Qualification of Microalloyed (HSLA) Steel Weldments*, eds. J.T. Hickey, D.G. Howden and M.D. Randall, Amer. Weld. Soc., 1990, 219–247.
Oblak, J.M., Goodenow, R.H. and Hehemann, R.F., *Trans. AIME.* **230**, 1964, 258–259.
Oblak, J.M. and Hehemann, R.F., *Transformations and Hardenability in Steels*, Climax Moly., Ann Arbor, MI, 1967, 15–30.
Ochi, T., Takahashi, T. and Takada, H., *Proc. 30th Mechanical Working and Steel Processing Conference*, Iron and Steel Society, Warrendale, PA, Oct. 1988.
Ohmori, T., Trans. *Iron Steel Inst Jpn.* **11**, 1971a, 95–101.
Ohmori, Y., Trans. *Iron Steel Inst Jpn.* **11**, 1971b, 249.
Ohmori, Y., *Proc. Int. Conf. on Martensitic Transformations, ICOMAT '86*, Japan Inst. Met., 587–594.
Ohmori, Y., *Mater. Trans. (Japan Inst. Met.)* **30**, 1989, 487–497.
Ohmori, Y. and Honeycombe, R.W.K., Proc. ICSTIS, *Suppl. Trans. Iron Steel Inst. Jpn.* **11**, 1971, 1160–1164.
Ohmori, Y., Ohtani, H. and Kunitake, T., *Trans. Iron Steel Inst. Jpn.* **11**, 1971, 250–259.
Ohmori, Y., Ohtani, H. and Kunitake, T., *Met. Sci.* **8**, 1974, 357–366.
Oka, M. and Okamoto, H., *Proc. Int. Conf. on Martensitic Transformations, ICOMAT '86*, Japan Inst. of Met., 271–275.
Oka, M. and Okamoto, H., *Metall. Trans. A* **19A**, 1988, 447.
Okabe, R., Koshizuka, N., Tanaka, M., Katamine, A. and San-Nomiya, Y., *Trans. Iron Steel Inst. Jpn.* **23**, 1983, 390.
Okamoto, H. and Oka, M., *Metall. Trans. A* **17A**, 1986, 1113–1120.
Oldland, R.B., *Australian Welding Research*, 1985, 31.
Olefjord, I., *Int. Metals. Rev.* **23**, 1978, 149–163.
Olson, G.B., Unpublished research, Northwestern University, Chicago, 1984.
Olson, G.B., *Scripta Metall.* **21**, 1987, 1023–1028.
Olson, G.B. and Cohen, M., *Metall. Trans.* **7A**, 1976a, 1897–1904.
Olson, G.B. and Cohen, M., *Metall. Trans.* **7A**, 1976b, 1905–1914.
Olson, G.B. and Cohen, M., *Metall. Trans.* **7A**, 1976c, 1915–1923.
Olson, G.B. and owen, W.S., *New Aspects of Martensitic Transformations*, Tokyo, Japan Inst. of Met., 1976, 105–110.
Olson, G.B. and Cohen, M., *Scripta Metall.* **11**, 1977, 345–347.
Olson, G.B. and Cohen, M., *Acta Metall.* **27**, 1979, 1907–1918.
Olson, G.B. and Cohen, M., *Ann. Rev. Mater. Sci.*, (eds R.A. Huggins, R.H. Bube and D.A. Vermilyea), Annual Reviews Inc., CA, 1981, 1–30.

Olson, G.B. and Cohen, M., *Metall. Trans. A* **14A**, 1983, 1057–1065.
Olson, G.B. and Cohen, M., *Dislocations in Solids*, (ed. F.R.N. Nabarro), **7**, 1986, 297.
Olson, G.B., Bhadeshia, H.K.D.H. and Cohen, M., *Proc. Int. Conf. Solid→Solid Phase Transformations*, (ed. G.W. Lorimer), Institute of Metals, London, 1988, 322–325.
Olson, G.B., Bhadeshia, H.K.D.H. and Cohen, M., *Acta Metall.* **37**, 1989, 381–389.
Olson G.B., Bhadeshia, H.K.D.H. and Cohen, M., *Metall. Trans. A* **21A**, 1990, 805–809.
Oriani, R.A. and Jopsephic, P.H., *Acta Metall.* **22**, 1974, 1065–1074.
Owen, W.S., *Trans. ASM* **46**, 1954, 812–829.
Owen, W.S., *Met. Technol.* **14**, 1980, 1–13.
Owen, W.S., Wilson, E.A. and Bell, T., *High Strength Materials*, (ed. V.F. Zackay), Wiley, New York, 1964, 167–212.
Oriani, R.A. and Josephic, P.H., *Acta Metall.* **22**, 1974, 1065–1074.
Padmanabhan, R. and Wood, W.E., *Mater. Sci. Eng.* **66**, 1984, 1–11.
Parker, E.R. and Zackay, V.F., *Eng. Fract. Mechan.* **7**, 1975, 371–375.
Parker, E.R., *Metall. Trans.* **8A**, 1977, 1025–1042.
Parker, E.R., Ritchie, R.O., Todd, J.A. and Spencer, P.N., *Research on Chrome–Moly Steels*, MPC–21, ASME, NY, 1984, 109–116.
Patel, J.R. and Cohen, M., *Acta Metall.* **1**, 1953, 531.
Pati, S.R. and Cohen, M., *Acta Metall.* **19**, 1971, 1327–1332.
Paxton, H.W., *Metall. Trans.* **1**, 1970, 3479–3500.
Paxton, H.W., *Metall. Trans.* **3**, 1972, 1035–1042.
Perovic, P., Purdy, G.R. and Brown, L., *Scripta Metall.* **15**, 1981, 217–221.
Petch, N.J., *Advances in Physical Metallurgy*, (eds J.A. Charles and G.C. Smith), Institute of Metals, London, 1990, 11–25.
Pfeil, L.B., *Proc. Roy. Soc.* **112**, 1926, 182–195.
Pickering, F.B., *Int. Conf. on Electron Microscopy*, Springer Verlag OHG, Berlin, 1958, 628–637.
Pickering, F.B., *Transformations and Hardenability in Steels*, Climax Moly., Ann Arbor, MI, 1967, 109–132.
Pickering, F.B., *Physical Metallurgy and the Design of Steels*, Applied Science Publishers, Essex, UK, 1978, 104.
Pickering, F.B., *Phase Transformations*, Inst. Metallurgists, London, April 1979, series 3, No. 11, Vol. 2k, VI 7–13.
Pilling, J. and Ridley, N., *Metall. Trans. A* **13A**, 1982, 557–563.
Pippard, A.B., *Classical Thermodynamics*, Cambridge University Press, 1981.
Pitsch, W., *Acta Metall.* **10**, 1962, 897.
Pomey, J. Mem. *Sci. Rev. Metall.* **63**, 1966, 507–532.
Porter, L.E. and Rosenthal, P.C., *Acta Metall.* **7**, 1959, 504–514.
Portevin, A. and Chevenard, P., *Compt. Rend.* **204**, 1937, 772.
Portevin, A. and Jolivet, H., *Annales de l'Academie des Sciences Techniques à Varsorie* **4**, 1937, 177.
Portevin, A. and Jolivet, H., *Compt. Rend.* **207**, 1938, 1412.
Prado, J., J. Mat. Sci. Lett. **5**, 1986, 1075–1076.
Prado, J., Catalan, J.J. and Marsal, M., *J. Mater. Sci.* **25**, 1990, 1939–1946.
Purdy, G.R. and Hillert, M., *Acta Metall.* **32**, 1984, 823–828.
Purdy, G.R., Weichert, D.H. and Kirkaldy, J.S., *TMS–AIME* **230**, 1964, 1025–1034.

Race, J., Private communication, University of Cambridge, 1990.
Radcliffe, S.V. and Rollason, E.C., *J. Iron Steel Inst.* **191**, 1959, 56–65.
Radcliffe, S.V., Schatz, M. and Kulin, S.A., *J. Iron Steel Inst.* **201**, 1963, 143–153.
Ragha van, V. and Entwistle, A.R., *Physical Properties of Martensite and Bainite*, Special Rep. 93, Iron Steel Inst., London, 1965, pp. 30–37.
Raghavan, V. and Cohen, M., *Metall. Trans.* **2**, 1971, 2409.
Rao, B.V.N. and Thomas, G., *Int. Conf. on Martensitic Transformations, ICOMAT 79*, Massachusetts Inst. Technol., 1979, 12.
Rao, B.V.N. and Thomas, G., *Metall. Trans. A* **11A**, 1980, 441–457.
Rao, M.M. and Winchell, P.G., *Trans. Met. Soc. AIME.* **239**, 1967, 956–960.
Rauch, G.C. and Leslie, W.C., *Metall. Trans.* **3**, 1972, 373.
Ray, R.K. and Jonas, J.J., *Int. Mater. Rev.* **35**, 1990, 1–36.
Reed, R. and Bhadeshia, H.K.D.H., *Recent Trends in Welding Science and Technology*, (eds. S.A. David and J. Vitek), ASM International, OH, 1989, 205–210.
Rees, G., Ph.D. Thesis, University of Cambridge, 1991.
Reisdorf, B.G., *TMS–AIME* **227**, 1963, 1334.
Ricks, R.A., Howell, P.R. and Barritte, G.S., *J. Mater. Sci.* **17**, 1982, 732–740.
Ridal, K.A. and Quarrell, A.G., *J. Iron Steel Inst.* **200**, 1962, 366–373.
Ridal, K.A. and McCann, J., *Physical Properties of Martensite and Bainite*, Special Report 93, Iron Steel Inst., London, 1965, 147–148.
Ridley, N., *Phase Transformations in Ferrous Alloys*, TMS–AIME, Warrendale, PA, 1984, 210–236.
Rigsbee, J.M. and Aaronson, H.I., *Acta Metall.* **27**, 1979, 351.
Rigsbee, J.M. and Aaronson, H.I., *Acta Metall.* **27**, 1979, 365.
Ringer, S.R. Barbaro, F., Krauklis, P. and Easterling, K.E., *Microstructure Control to Achieve Properties In Modern Steels*, Inst. Met. and Mater. Australasia, Melbourne, 1990, 1–6.
Ritchie, R.O., *J. Eng. Mater. Technol. (Trans. ASME., H)* **99**, 1977a, 195–204.
Ritchie, R.O., *Met. Sci.* **11**, 1977b, 368–381.
Ritchie, R.O., Castro, M.H.C., Zackay, V.F. and Parker, E.R., *Metall. Trans. A.* **9A**, 1978, 35–40.
Ritchie, R.O., *Int. Met. Rev.*, 1979, 205–230.
Ritchie, R.O., Knott, J.F. and Rice, J.R., *J. Mech. Phys. Sol.* **21**, 1973, 395–400.
Ritchie, R.O., Moss, C.M. and Suresh, S., *J. Eng. Mater. Technol. (Trans. ASME, H)* **102**, 1980, 293.
Ritchie, R.O., Parker, E.R., Spencer, P.N. and Todd, J.A., *J. Mater. for Energy Systems* **6**, 1984, 151–162.
Roberts, C.S., Averbach, B.L. and Cohen, M., *Trans. ASM* **45**, 1957, 576.
Roberts. M.J., *Metall. Trans.* **1**, 1970, 3287–3294.
Robertsonn J.M., *J. Iron Steel Inst.* **119**, 1929, 391–426.
Rouns, T.N. and Rundman, K.B., *AFS Trans.* **95**, 1987, 851–874.
Rudberg, E. *Jernkontorets Ann.* **136**, 1952, 91.
Rundman, K.B., Moore, D.J., Hayrynen, K.L., Dubensky, W.J. and Rouns, T.N., *J. Heat Treating* **5**, 1988, 79.
Russell, K.C., *Metall. Trans.* **2**, 1971, 5-12.
Sachs, K., Ralph, B. and Salter, J., *Heat Treatment '79*, Metals Society, London, 1980, 141–146.

Sadovskii, V.D., *Probl. Mettaloverskie Term Obrab*, 1956, 31–52, Central Electricity Generating Board Translation 7648.
Saeki, M., Kurosawa, F. and Matsuo, M., *Trans. Iron Steel Inst. Jpn.* **26**, 1986, 1017–1035.
Sandvik, B.P.J. and Nevalainen, H.P., *Met. Tech.* **15**, 1981, 213–220.
Sandvik, B.P.J., *Metall. Trans. A* **13**, 1982a, 777–787.
Sandvik, B.P.J., *Metall. Trans. A* **13**, 1982b, 789–800.
Sandvik, B.P.J. and Wayman, C.M., *Metall. Trans. A* **14A**, 1983, 809–822.
Sarikaya, M., Tokushige, H. and Thomas, G., *International Conference on Martensitic Transformations 'ICOMAT 86'*, Japan Inst. of Metals, Tokyo, Japan, 1986, 613–618.
Sawley, K.J., Preston, R.R. and Pendleton, R., Abstracts of the conference on Bainite, Institute of Metals, London, 25 April 1985.
Sawley, K.J., Bolton, P.J. and Pell, G.M., *Wear of Materials*, (ed. K.C. Ludema), Amer. Soc. Mech. Engrs., New York, 1987, 133–143.
Sawley, K.J., Benyon, J.A. and Jones, E.G., *9th International Wheelset Congress*, September 1988, Quebec, Canada, Paper 2–6, 1–12.
Schaaber, O., *J. Met.* **7**, 1955, 559–560.
Schanck, J.L., *Industrial Heating*, September 1969, 1664.
Scheil, E., *Arch. Eisenhuttenwesen* **12**, 1935, 565.
Scheil, E., *Hart.–Tech. Mitt.* **7**, 1955, 9.
Schissler, J.M., Arnould, J. and Metauer, G., *Mem. Sci. Rev. Metallurgie* **6**, 1975, 779–793.
Schmatz, D.J. and Zackay, V.F., *Trans. ASM.* **51**, 1959, 476.
Schrader, A. and Wever, F., *Arch. Eisenhuttenwesen* **23**, 1952, 489–495.
Self, P., Bhadeshia, H.K.D.H. and Stobbs, W.M., *Ultramicroscopy* **6**, 1981, 29.
Senior, B.A., *The Effects of Retempering on the Microstructure of Ferritic Steels*, Central Electricity Generating Board Report TPRD/L/3220/R87, 1988.
Shackleton, D.N. and Kelly, P.M., *Acta Metall.* **15**, 1967, 979–992.
Shackleton, D.N. and Kelly, P.M., *Iron Steel Inst. Special Rep.* 93, London, pp. 126–134, 1965.
Sharma, R.C. and Purdy, G.R., *Metall. Trans.* **4**, 1973, 2303–2311.
Shea, M.M. and Ryntz, E.F., *Trans. Am. Foundrymen's Soc.* **94**, 1986, 683.
Shepperson, S. and Allen, C., *Wear of Materials*, (ed. K.C. Ludema), Amer. Soc. Mech. Engrs., New York, 1987, 572–583.
Shewmon, P., *Metall. Trans. A* **7A**, 1976, 279.
Shewmon, P., *Mater. Sci. Technol.* **1**, 1985, 2.
Shiflet, G.J., BraTley, J.R. and Aaronson, H.I., *Metall. Trans.* **9**, 1978, 999–1008.
Shiga, C., Amano, K., Enami, T., Tanaka, M., Tarui, R. and Kushuhara, Y., *Technology and Applications of High Strength Low Alloy (HSLA) Steels*, ASM International, 1983, 643–654.
Shih, C.H., Averbach, B.L. and Cohen, M., *Trans. AIME.* **203**, 1955, 183–187.
Shimizu, K. and Nishiyama, Z., *Mem. Inst. Sci. Ind. Res.*, Osaka University, **20**, 1963, 42.
Shimizu, K., Ko, T. and Nishiyama, Z. *Trans. Japan Inst. Met.* **5**, 1964, 223–228.
Shiokawa, T., Unpublished research quoted in Moore, 1985.
Shively, J.H., Hehemann, R.F. and Troiano, A.R., *Corrosion* **22**, 1966, 253–256.

Simonen, E.P., Aaronson, H.I. and Trivedi, R., *Metall. Trans.* **4**, 1973, 1239–1245.
Siriwardene, P.P.L.G., Ph.D. Thesis, University of Cambridge, 1955.
Smirenskaya, N.A., Kogan, L.I. and Entin, R.I., *Fiz. Metal. Metalloved.* **41**, 1976, 1019–1028.
Smith, C.S., *A History of Metallography*, University of Chicago Press, 1960, 225.
Smith, E., *Physical Basis of Yield and Fracture, Inst. of Phys. and Phys. Soc.*, Oxford, 1966, 36.
Smith, G.M., Ph.D. Thesis on *The Microstructure and Yielding behaviour of some Ti Steels*, University of Cambridge, 1984.
Smith, G.V. and Mehl, R.F., *Trans. AIMME.* **150**, 1942, 211–226.
Smith, M.F., Speich, G.R. and Cohen, M., *Trans. Met. Soc. AIME.* **215**, 1959, 528–530.
Smith, Y.E. and Siebert, C.A., *Amer. Soc. for Testing and Mater., Special Tech. Publ.* **480**, 1970, 131–151.
Smith, J.F., *Acta Metall.* **28**, 1980, 1555–1564.
Snieder, G. and Kerr, H.W., *Canadian Metall. Quart.* **23**, 1984, 315–325.
Solana, F., Takamadate, C., Bernstein, I.M. and Thompson, A.W., *Metall. Trans. A.* **18A**, 1987, 1023–1028.
Speich, G.R., *Decomposition of Austenite by Diffusional Processes*, Interscience, New York, 1962, 353–369.
Speich, G.R., *Trans. AIME.* **245**, 1969, 2553–2564.
Speich, G.R., *Innovations in Ultrahigh-Strength Steel Technology*, (eds G.B. Olson, M. Azrin and E.S. Wright), 34th Sagamore Army Mater. Conf., Watertown, MA, 1987, 89–112.
Speich, G.R. and Cohen, M., *Trans. Met. Soc. AIME.* **218**, 1960, 1050–1059.
Speich, G.R. and Warlimont, H., *J. Iron Steel Inst.* **206**, 1968, 385–392.
Speich, G.R., Cuddy, L.J., Gordon, C.R. and DeArdo, A.K., *Int. Conf. on Phase Transformations in Ferrous Alloys*, (eds Marder, A.R. and Goldstein, J.I.), ASM. Cleveland, OH, 1984, 341–392.
Spencer, P.N., Dauskardt, R.H., Parker, E.R. and Ritchie, R.O., *High Temperature Technol.* **7**, 1989, 17–26.
Srinivasan, G.R. and Wayman, C.M., *Trans. Met. Soc. AIME.* **242**, 1968a, 79–81.
Srinivasan, G.R. and Wayman, C.M., *Acta Metall.* **16**, 1968b, 609–620.
Srinivasan, G.R. and Wayman, C.M., *Acta Metall.* **16**, 1968c, 621–636.
Stark, I. and Smith, G.D.W., *Journal de Physique* **48** C6, 1987, 447–452.
Stark, I., Smith, G.D.W. and Bhadeshia, H.K.D.H., *Solid→Solid Phase Transformations*, Institute of Metals, London, 1988, 211–215.
Stark, I., Smith, G.D.W. and Bhadeshia, H.K.D.H., *Metall. Trans. A* **21A**, 1990, 847–845.
Steven, W. and Haynes, A.J., *J. Iron Steel Inst.* **183**, 1956, 349–359.
Stickels, C.A., *Metall. Trans.* **5**, 1974, 865–874.
Strangwood, M., Ph.D. Thesis, University of Cambridge, 1987.
Strangwood, M. and Bhadeshia, H.K.D.H., *Advances in Welding Science and Technology*, (ed. S.A. David), ASM, Metals park, OH, 1987, 209–213.
Strangwood, M. and Bhadeshia, H.K.D.H., *Solid→Solid Phase Transformations*, (ed. G.W. Lorimer), Institute of Metals, London, 1988, 466–470.
Sudo, M., Higashi, M., Hori, H., Iwai, T., Kambe, S. and Shibata, Z., *Trans. Iron Steel Inst. Jpn.* **21**, 1981, 820–827.

Sudo, M., Tsukatani, I. and Shibata, Z., *Metallurgy of Continuously Annealed Sheet Steel*, (eds B.L. Bramfitt and P.L. Mangonon Jr.), TMS–AIME, Warrendale, PA, 1982, 301–319.
Sudo, M. and Iwai, T., *Trans. Iron Steel Inst. of Jpn.* **23**, 1983, 294.
Sugden, A.A.B. and Bhadeshia, H.K.D.H., *Metall. Trans. A* **19A**, 1988, 669–674.
Sugden, A.A.B. and Bhadeshia, H.K.D.H., *Metall. Trans. A* **20A**, 1989, 1597–1602.
Suresh, S., Zamiski, G.F. and Ritchie, R.O., *Metall. Trans. A* **12A**, 1981, 1435.
Svensson, L.–E. and Bhadeshia, H.K.D.H., *J. Mater. Sci.* **24**, 1989, 3180–3188.
Takahashi, M. and Bhadeshia, H.K.D.H., *J. of Materials Science Letters* **8**, 1989, 477–478.
Takahashi, M. and Bhadeshia, H.K.D.H., *Mater. Sci. Technol.* **6**, 1990, 592–603.
Takezawa, K. and Sato, S., *International Conference on Martensitic Transformations, ICOMAT-86*, Japan Inst. Met., 1986, 625–630.
Tamehiro, H., Habu, R., Yamada, N., Matsuda, H. and Nagumo, M., *Accelerated Cooling of Steel*, (ed. P.D. Southwick), TMS–AIME, 1985a, 401–414.
Tamehiro, H., Yamada, N. and Matsuda, H., *Trans. Iron Steel Inst. Jpn.* **25**, 1985b, 55–61.
Tamehiro, H., Takeda, T., Matsuda, S., Yamamoto, K. and Okumura, N., *Trans. Iron Steel Inst. Jpn.* **25**, 1985c, 982–988.
Tamehiro, H., Murata, M., Habu, R. and Nagumo, M., *Trans. Iron Steel Inst. Jpn.* **27**, 1987a, 120–129.
Tamehiro, H., Murata, M., Habu, R. and Nagumo, M., *Trans. Iron Steel Inst. Jpn.* **27**, 1987b, 130–138.
Tamehiro, H., Nishioka, K., Murata, M., Habu, R. and Kawada, Y., *Symp. on Accelerated Cooling of Rolled Steel*, Winnepeg, Canada, August 1987, 1–8.
Tamukai, S., Onoe, Y., Nakajima, H., Umeno, M., Iwanaga, K. and Sasaji, S., *Tetsu-to-Hagane* **67**, 1981, 1344.
Tanaka, T. *Int. Metals Reviews*, No. 4, 1981, 185–212.
Tanaka, T., *Accelerated Cooling of Rolled Steel*, (eds G.E. Ruddle and A.F. Crawley), Pergamon Press, Oxford, 1988, 187–208.
Terada, Y., Chijiiwa, R., Tamehiro, H., Kikuma, T. and Kazuo, F., *1st Int. Conf. on New Manufacturing Technology* (World Techno-Fair in Chiba '90) Chiba, Japan, 1990. Reprint available from the Nippon Steel Corporation, Japan.
Thelning, K.–A., *Scand. J. Metall.* **7**, 1978, 252.
Thewlis, G., *Joining and Mater.*, January 1989a, 25–32.
Thewlis, G., *Joining and Mater.*, March 1989b, 125–129.
Thewlis, G., *Transformation Kinetics of Submerged Arc Weld Metal*, British Steel internal report IXJ–165–90, May 1990, 1–11.
Thielen, P.N., Fine, M.E. and Fournelle, R.A., *Acta Metall.* **24**, 1976, 1–10.
Thomas, G., Schmatz, D. and Gerberich, W., *High Strength Materials*, (ed. V.F. Zackay, 263), J. Wiley and Sons, New York, 1965.
Tom, T., D. Eng. Thesis, University of California, Berkely, 1973, quoted in Zackay and Parker, 1975.
Tomita, Y. and Okabayashi, K., *Metall. Trans. A* **14A**, 1983a, 485–492.
Tomita, Y. and Okabayashi, K., *Metall. Trans. A* **14A**, 1983b, 2387–2393.
Tomita, Y. and Okabayashi, K., *Metall. Trans. A* **16A**, 1985a, 73–82.
Tomita, Y. and Okabayashi, K., *Metall. Trans. A* **16A**, 1985b, 83–91.

Tomita, Y., *Metall. Trans. A* **18A**, 1987, 1495–1501.
Tomita, Y., *Metall. Trans. A* **19A**, 1988, 2513–2521.
Thomson, R., University of Cambridge, Private Communication, 1990.
Thompson, S.W., Colvin, D.J. and Krauss, G., *Scripta Metall.* **22**, 1988, 1069–1074.
Tomota, Y., Kuroki, K., Mori, T. and Tamura, I., *Mater. Sci. Eng.* **24**, 1976, 85.
Townsend, R. and Kirkaldy, J.S., *Trans. ASM.* **61**, 1968, 605.
Trivedi, R., *Metall. Trans.* **1**, 1970, 921–927.
Troiano, A.R., *Trans. ASM.* **52**, 1960, 54–80.
Troiano, A.R. and Greninger, A.B., *Met. Prog.* **50**, 1946, 303.
Troiano, A.R. and Klinger, L.J., *Trans. ASM.* **44**, 1952, 775–802.
Tsivinsky, S.V., Kogan, L.I. and Entin, R.I., *Problems of Metallography and the Physics of Metals*, (ed B. Ya Lybubov), State Scientific Press, Moscow, 1955. Trans. publ. by Consultants Bureau Inc., New York, 1959, 185–199.
Tsuya, K., *J. Mech. Lab. Japan* **2**, 1956, 20.
Tsuzaki, K., Yamaguchi, K., Maki, T. and Tamura, I., *Tetsu–tó-Hagane (J. Iron Steel Inst. Jpn)* **74**, 1988, 234–241.
Tsuzaki, K., Ueda, T., Fujiwara, K. and Maki, T., *New Materials and Processes for the Future*, Proc. 1st Japan Int SAMPE Symp. and Exhib., Soc. for Advancement of Mater. and Process Eng., Chiba, Japan, 1989, 699–704.
Turnbull, D., *Metall. Trans. A* **12A**, 1981, 695.
Tweed, J.T.H. and Knott, J.F., *Met. Sci.* **17**, 1983, 45.
Ueda, Y. and Takita, M., Proc. *2nd. Int. Conf. on Austempered Ductile Iron*, ASM, Metals Park, OH, 1986, 141.
Ueshima, Y., Isobe, H., Mizoguchi, S., Maeda, H. and Kajioka, H., *Tetsu–to-Hagane* **75**, 1989, 501–508.
Umemoto, M., Horiuchi, K. and Tamura, I., *Trans Iron Steel Inst. of Japan* **22**, 1982, 854.
Umemoto, M., Bando, S. and Tamura, I., *Proc. Int. Conf. on Martensitic Transformations (ICOMAT '86)*, Japan Inst. Met., 1986a, 595–600.
Umemoto, M., Furuhara, T. and Tamura, I., *Acta Metall.* **34**, 1986b, 2235–2245.
Umemoto, M., Horiuchi, K. and Tamura, I., *Tetsu-to-Hagane* **66**, 1980, 400.
Vagarali, S.S. and Odette, G.R., *Metall. Trans. A* **12A**, 1981, 2071.
Vandermeer, R.A., *A dilatometric investigation of phase transformation kinetics in HP 9–4–20 steel*, Report Y/DV–315, October 1983, Oak Ridge National Laboratories (Y12), TN, 1–28.
Vasudevan, P., Graham, L.W. and Axon, H.J. *J. Iron Steel Inst.* **190**, 1958, 386–391.
Venugopalan, D. and Kirkaldy, J.S., *Hardenability Concepts with Applications to Steels*, (eds D.V. Doane and J.S. Kirkaldy), TMS–AIME., 1977, 249–268.
Vilella, J.R., Guellich, G.E. and Baine, E.C., *Trans. ASM.* **24**, 1936, 225–261.
Vilella, J.R., *Trans. AIME.* **140**, 1940, 332.
Vitek, J.M., Packan, N.H. and David, S.A., *Advances in Welding Science and Technology* Proc. Int. Conf. on Trends in Welding Research, 1986, (ed S.A. David), ASM International, OH, 203–208.
Vlad, C.M., *Accelerated Cooling of Steel*, (ed. P.D. Southwick), TMS–AIME, 1985, 435–448.
Vyhnal, R.F. and Radcliffe, S.V., *Acta Metall.* **15**, 1967, 1475–1488.
Viswanathan, R., *Met. Technol.* **8**, 1974, 284–294.

Wada, T. and Eldis, G.T., *Transformation characteristics of 2.25Cr–1Mo Steel*, Application of 2.25Cr–1Mo Steel for Thick-Wall Pressure Vessels, ASTM STP 755, Amer. Soc. for Testing Mater., 1982, 343–362.
Wada, T. and Cox, T.B., *Advanced Materials for Pressure Vessel Service with Hydrogen at High Temperatures and Pressures*, (ed. M. Semchyshen), MPC–18, Amer. Soc. Mech. Engrs., New York, 1982, 111–121.
Wada, T. and Cox, T.B., *Research on Chrome–Moly Steels*, MPC–21, Amer. Soc. Mech. Engrs., New York, 1984, 77–93.
Wagner, C., *Zeit fur Electrochem* **65**, 1961, 581.
Wakasa, K. and Wayman, C.M., *Acta Metall.* **29**, 1981, 991–1011.
Watanbe, J. and Murakami, Y., Amer. Petroleum Inst., preprint no. 28–81, 1981, 216–224, quoted by Bodnar *et al.*, 1989.
Watson, J.D. and McDougall, P.G., *Acta Metall.* **21**, 1973, 961.
Wayman, C.M., *Introduction to the Crystallography of Martensitic Transformations*, MacMillan, New York, 1964, 168.
Wechsler, M.S., Lieberman, D.S. and Reed, T.A., *Trans. AIMME.* **197**, 1953, 1503–1515.
Wever, F., *Z. Metallkunde* **24**, 1932, 270.
Wever, F. and Jellinghaus, W., *Mitt. Kaiser-Wilhelm-Inst. Eisenforsch.* **14**, 1932, 85.
Wever, F. and lange, H., *Mitt. Kaiser-Wilhelm-Inst. Eisenforsch.* **14**, 1932, 71.
Wever, F. and Hensel, H., *Mitt. Kaiser-Wilhelm-Inst. Eisenforsch.* **19**, 1937, 47.
Wever, F. and Mathieu, K., *Mitt. Kaiser-Wilhelm-Inst. Eisenforsch.* **22**, 1940, 9.
White, J.S. and Owen, W., *J. Iron Steel Inst.* **197**, 1961, 241–243.
Wiester, H.J., *Z. Metallkunde* **24**, 1932, 276.
Williams, W.F., *World Steel Rev.* **1**, 1991, 18–22.
Wilson, A.D., *Microalloyed HSLA Steels*, ASM, Metals Park, OH, 1988, 259–275.
Wilson, D.V. and Oates, G., *Acta Metall.* **12**, 1964, 21.
Wilson, E.A., *Scripta Metall.* **12**, 1978, 961.
Wilson, E.A., Allen, S.P. and Butler, J., *Met. Sci.* **16**, 1982, 539.
Wilson, A.D., Hamburg, E.G., Colvin, D.J., Thompson, S.W. and Krauss, G., *Microalloyed HSLA Steels*, ASM International, 1988, 259–275.
Wilson, P.W., Ph.D. Thesis, University of Cambridge, 1991.
Winchell, P.G. and Cohen, M., *Trans. ASM* **55**, 1962, 347.
Winterton, K., *J. Iron Steel Inst.* **151**, 1945, 79.
Woodhead, J.H. and Quarell, A.G., *J. Iron Steel Inst.* **203**, 1965, 605–620.
Wright, P.H., Harrington, T.L., Szilva, W.A. and White, T.R., *Fundamentals of Microalloying Forging Steels*, (eds G. Krauss and S.K. Banerji), Metall. Soc. of AIME. Warrendale, PA, 1987, 541–566.
Wu, M.H. and Wayman, C.M., *International Conference on Martensitic Transformations*, ICOMAT-86, Japan Inst. Met., 1986, 619–624.
Yakel, H.C., *Int. Met. Rev.* **30**, 1985, 17–40.
Yamamoto, K., Matsuda, S., Haze, T., Chijiiwa, R. and Mimura, H., *Residual and Unspecified Elements in Steel*, ASM Int., OH, November 1987, 1–24.
Yang, J.R. and Bhadeshia, H.K.D.H., *Advances in Welding Science and Technology*, (ed. S.A. David), ASM, Metals Park, OH, 1986, 187–191.
Yang, J.R. and Bhadeshia, H.K.D.H., *Proc. Int. Conf. Welding Metallurgy of Structural Steels*, TMS–AIME, Warrendale, PA, 1987, 549–563.

Yang, J.R. and Bhadeshia, H.K.D.H., *Proc. of Int. Conf. Phase Tranformations '87*, (ed. G.W. Lorimer), Institute of Metals, London, 1988, 203–206.
Yang, J.R. and Bhadeshia, H.K.D.H., *Mater. Sci. and Technol.* **5**, 1989a, 93–97.
Yang, J.R. and Bhadeshia, H.K.D.H., *Mater. Sci. Eng.* **A118**, 1989b, 155–170.
Yang, J.R. and Bhadeshia, H.K.D.H., *Amer. Welding J.* **69**, 1990, 305s–309s.
Yu, J., *Metall. Trans. A* **20A**, 1989, 1561–1564.
Yutori, T. and Ogawa, R., *Tetsu-to-Hagane* **61**, 1979, 991–1011.
Zener, C., *Trans. AIME.* **167**, 1946, 550–595.
Zener, C., *J. Applied Phys.* **20**, 1949, 950.

Author Index

Subject Index